Department of Environment and Heritage

Air Quality Forecasting

For Australia's Major Cities

Final Report

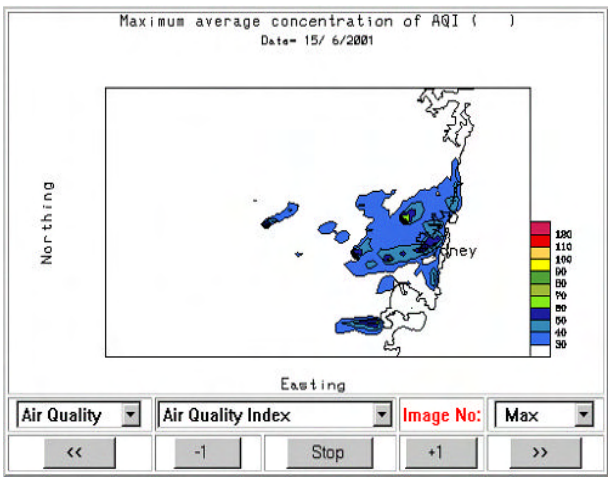

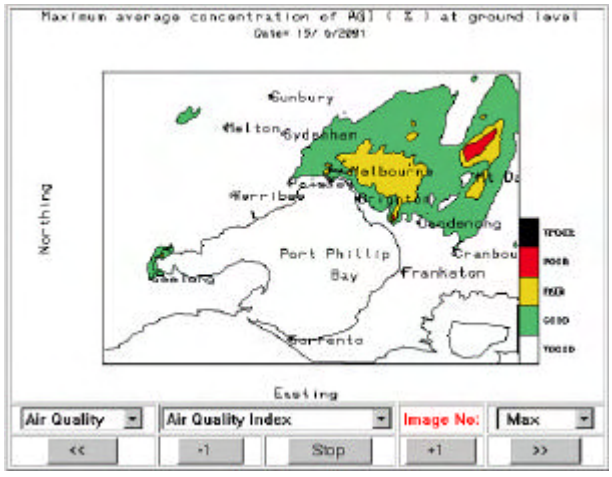

Natural Heritage Trust
Helping Communities Helping Australia
A Commonwealth Government Initiative

EPA VICTORIA

BMRC Bureau of Meteorology Research Centre

Environment Australia

CSIRO

NSW EPA

Department of the Environment and Heritage

Air Quality Forecasting for Australia's Major Cities
Final Report

Prepared by Project Management Committee

Contact: peter.manins@dar.csiro.au

CSIRO Atmospheric Research
PMB 1 Aspendale 3195
Australia

November 2001 PSS : dh79A

Air quality forecasting for Australia's major cities :
final report.

Bibliography.
Includes index.
ISBN 0 643 06648 9.

1. Air quality - Australia - Forecasting. 2. Air -
Pollution - Australia - Forecasting. I. CSIRO. Division of
Atmospheric Research. II. Australia. Dept. of the
Environment and Heritage. III. Australian Air Quality
Forecasting System Management Committee .

363.73920994

List of contributors to the Study

Bureau of Meteorology
(LAPS meteorological model and modelling system operation)
Dr Kamal Puri (k.puri@bom.gov.au)
Mr Terry Hart
Dr Dale Hess
Dr Kevin Tory

CSIRO Atmospheric Research
(Chemical transport model, Web operation and reporting)
Dr Martin Cope (martin.cope@dar.csiro.au)
Mr Russell Howden
Dr Sunhee Lee
Ms Julie Penn

CSIRO Energy Technology
(Specialist vehicle emissions, biogenics emissions and GRS model)
Dr Peter Nelson (peter.nelson@det.csiro.au)
Dr Merched Azzi
Dr John Carras
Mr Bill Lilley

EPA Victoria
(Provision of air quality, meteorological and emissions data, emissions inventory development, forecasting assessment)
Dr Neil Wong (neil.wong@epa.vic.gov.au)
Dr Piya Dewundege
Dr Yuk Leung Ng
Mr Sean Walsh

EPA New South Wales
(Provision of air quality, meteorological and emissions data, forecasting assessment)
Ms Margaret Young (YoungM@epa.nsw.gov.au)
Ms Loredana Angri
Dr Hiep Duc
Mr Michael Johnson
Ms Susan Quigley

Project Manager
Dr Peter Manins, CSIRO Atmospheric Research (peter.manins@dar.csiro.au)

Acknowledgements

The Project Team is particularly grateful for the insightful assistance of Dr Michael Manton, Chief of Bureau of Meteorology Research Centre, and for the guidance and support of Mr Paul Kesby, Christine Schweizer, Sandra Doolan and Emma Campbell of Environment Australia.

CONTENTS

page

Notation

AAQFS	Australian Air Quality Forecasting System
ADMS	Atmospheric Dispersion Modelling System (from Cambridge Environmental Research Consultants)
AMDAR	Meteorological data as reported by commercial aircraft
AQI	Air Quality Index – defined by EPAs as a measure of air quality
AQS	Air Quality Standard
B_f	Fractional bias, a performance measure – see Eq (2) on page 38
BoM	Bureau of Meteorology
CAR	CSIRO Atmospheric Research
CB99	Carbon Bond 99 – a complex atmospheric chemistry reaction scheme
CB-IV	Carbon Bond IV – a complex atmospheric chemistry reaction scheme (older than CB99)
CO	Carbon monoxide
CSIRO	Commonwealth Scientific and Industrial Research Organisation (of Australia)
CTM	Chemical Transport Module (Model) – the pollution component of AAQFS
E_f	Fractional gross error, a performance measure – see Eq (3) on page 38
EIM	Emissions Inventory Module (Model) – the emissions inventory system responsive to weather forcing in AAQFS
EPA	Environment Protection Authority
EPA Victoria	Environment Protection Authority of Victoria
False Alarm Rate	The ratio of the number of incorrectly predicted to total number of predicted pollution events
ftp	File Transfer Protocol – a computer file transfer convention
GRS	Generic Reaction Set – a highly simplified photochemical chemical reaction scheme for urban smog
GRS2	Second generation of the GRS
GUI	Graphical User Interface – the computer display system that accepts and responds to user information
LAPS	Limited Area Prediction System of BoM
METAR/SYNOP	BoM meteorological reporting stations
NEPM	National Environment Protection Measure – here, the Air Measure setting air quality standards for Australia
NetCDF	Network Common Data Form – a unified data file format for exchanging and managing large data sets
NH_3	Ammonia
NMHC	Non-methanic hydrocarbons – closely similar to ROC
NO	Nitric oxide
NO_2	Nitrogen dioxide
NO_x	Nitrogen oxides – the sum of nitric oxide and nitrogen dioxide
NO_y	Reactive odd nitrogen species – includes NO_x and secondary nitrogen species

NSW	New South Wales
NSW EPA	New South Wales Environment Protection Authority
NWP	Numerical Weather Prediction system – also, the meteorological model component of AAQFS
O_3	Ozone
OBS	Observed – refers to observed data as compared with model predictions
PBL	Planetary boundary layer – the layer of the atmosphere influenced directly by the underlying ground surface
Persistence Forecast	A forecast that says that "the pollution levels for the next hour (day) are the same as for the present hour (day)"
PM1	Airborne particulate matter with an aerodynamic diameter of 1 μm or less
PM10	Airborne particulate matter with an aerodynamic diameter of 10 μm or less
PM2.5	Airborne particulate matter with an aerodynamic diameter of 2.5 μm or less
Probability of Detection	The ratio of the number of correctly predicted to total number of observed pollution events
ROC	Reactive Organic Compounds – carbon-based compounds that in the presence of strong sunlight react with nitrogen oxides to make ozone
SO_2	Sulfur dioxide
SP	see *Probability of Detection*
SR	The ratio of the number of realised predicted pollution events compared with the total number of predicted events
(1 - *SR*)	see *False Alarm Rate*
TAPM	The Air Pollution Model (from CSIRO Atmospheric Research)
TSP	Total Suspended Particulate matter – includes all PM fractions
UAM	Urban Airshed Model – a detailed (old) urban air pollution model
UTC	Universal Time Coordinate – same as Greenwich Mean Time
VOC	Volatile Organic Carbon – closely similar to ROC

Executive Guide and Recommendations

With Natural Heritage Trust funding designated to improve urban air quality, the Australian Air Quality Forecasting System (AAQFS) has been a joint project between CSIRO Atmospheric Research, CSIRO Energy Technology, the Bureau of Meteorology (BoM), the Environment Protection Authority of Victoria (EPA Victoria) and the New South Wales Environment Protection Authority (NSW EPA) to develop a high-resolution air quality forecasting system. Currently, twice-daily 24–36 hour, numerical air quality forecasts are made (1 km resolution) for two regions of Australia: the airshed of Melbourne and Geelong in Victoria and the airshed of Sydney in NSW. Forecasts at a lower resolution (5 km) are carried out for most of Victoria and much of NSW.

The principal AAQFS goal is to issue numerical forecasts to State EPAs in time for guidance and reference against current air quality forecasting procedures.

In keeping with the AAQFS goal, the primary objective has been the development of a state-of-the-art, flexible numerical system, able to forecast air quality for multiple pollutants over spatial scales ranging from intra-suburb to inter-regional (1–500 km). A secondary objective is the generation of a 'green' air quality forecast (with, for example, a 25% reduction in motor vehicle emissions), in addition to the 'business-as-usual' forecast, to demonstrate the impact of a concerted public response to a forecast of potentially poor air quality.

A description of the full Demonstration System and the activities undertaken for the project are presented in **Chapter 1** of this Report. The Chapter also presents a summary of the outcomes of the project, including

- a review of the technical performance of the System as delivered to the Commonwealth that shows it is performing very well in most respects but requires further attention with respect to predictions of fine particle concentrations;
- a review of the System in the international context showing that it is world-leading: it is a reference for several other systems now under development;
- discussion of the uptake of the System by EPAs—NSW and Victoria are presently reviewing the implications of the System on their activities, and other States, Tasmania in particular, are discussing with the Commonwealth application to their regions.

Other Chapters of the Report develop the aspects noted in **Chapter 1** in more detail. **Chapter 2** reviews the System in depth and presents verifications of its statistical performance. The other important means used to develop and verify the System was by use of case studies. The performance of the System in three important case studies is presented later, in **Chapter 7**. Since it is such an important aspect of the System, the emissions inventory component is discussed next, in **Chapter 3**. AAQFS is extremely demanding of the emissions inventory and several ways of improving the emissions inventories and the modelling of emissions are canvassed in the Chapter. **Chapter 4** describes the outputs from AAQFS, including the data packets that can be used later to rerun important events, the Web display components, and the visualisation tools that are available to users. Several important options have been developed for AAQFS including, a new fast chemistry that obviates several inadequacies of the implemented chemical scheme in the System, and an alternative model to describe emissions from vehicles that is responsive to road conditions. These are described in **Chapter 5**, as are other options, *viz.* the handling of wildfires and the provision of the alternative 'green' forecast. **Chapter 6** reports the experiences of EPA Victoria and NSW EPA as users of the System. Their involvement has been critical to the success of the System

overall, and for the delivery of outputs that are useful for their operational needs. **Chapter 8** attempts to assess for a potential user what the demands and commitments by them would be in becoming a partner in the ongoing operation of the System. Then **Chapter 9** presents some conclusions from the Project and lists recommendations. These are repeated below.

Much more detail of several aspects of the Project is given in a series of Appendices, numbered to correspond with the relevant Chapter and Section of the main Report. For example, full documentation of the necessary formats for the emissions inventory data to be supplied to the System is presented in **Appendix 3.4**. A demonstration of a 'green' scenario (in the form of a new Conference Paper) is presented in **Appendix 5.2**. **Appendix 5.4** documents the power-based motor vehicle emissions model, the option for the description of emissions from roads mentioned above. **Appendix 7** (**7.1**, **7.2**, **7.3** and **7.3a**) thoroughly discuss the performance of the Demonstration System for three important case studies, including photochemical smog episodes in Melbourne and Sydney, and an interregional transport event of smoke from fires on King Island to Melbourne.

Conclusions and Recommendations from the Report

All contractual obligations to Environment Australia have been fully met with the proviso that public demonstration of the System has been entirely in the control of the two participating EPAs, since they explicitly retain the emissions inventory data.

The Demonstration System's performance during the various trials has been extremely encouraging. The trials have enabled documentation of the strengths of the System, and the areas in which the System has needed improvement. Performance has been assessed for the prediction of hourly and daily peaks each day, and for the prediction of weekly, monthly and seasonal trends. Various statistical measures have been used including comparisons against a persistence model ("the pollution levels for the next hour are the same as for the present hour"). A second method of assessing System performance is through detailed examination of case studies of extreme events. Extensive use is made of visualisations in time and space of the meteorological and air quality fields, which are compared with observations.

Airshed-Wide Pollution Performance: The System has shown good potential for forecasting extreme ozone concentrations. When considering a 7-day ozone episode in Sydney (21–27 January 2001), the System went from forecasting near-background concentrations of ozone prior to and after the episode to forecasting concentrations of over 160 ppb during the course of the episode. The probability of detection over the airshed for O_3 was 100% for thresholds in the range 60–100 ppb, and the false alarm rates were between zero and 25%. While the forecast probability of detection was the same as that for persistence (which also achieved a 100% hit rate), the false alarm rates were generally significantly better than those based on persistence. The System has achieved a probability of detection for the 1-hour daily peak of oxides of nitrogen over the Sydney airshed of 98% at a 60 ppb exceedence threshold, and a false alarm rate of 4%. The forecast probability of detection and the false alarm rate were better than persistence forecasts. These results are very good by comparison with international expectations.

Similarly, the System has been able to capture a three-day high ozone episode, observed in Melbourne (7–9 March 2001). Peak concentrations were observed to reach about 80 ppb and were reproduced with excellent skill by the System. The probability of detection over the airshed for O_3 was 100% at a 60 ppb threshold, and the false alarm rate was 25%. Both the

probability of detection and the false alarm rate were significantly better than achieved by persistence forecasts. The System achieved a probability of detection for the 1-hour daily peak of NO_y over the Melbourne airshed of 100% at a 60 ppb exceedence threshold, and a false alarm rate of 16%. The probability of detection was better than for persistence forecasts, but the false alarm rate was about the same as persistence. These results are also very good by comparison with international findings, which suggest detection rates above 50% and false alarm rates below 50% are good.

Station-Level Performance: Correct predictions at the station level are vastly more taxing than airshed-wide predictions. The System was able to reproduce the spatial distribution of peak O_3 with good skill in Melbourne for all days of the 3-day event, and for a majority of days in the Sydney 7-day event. This is reflected in the station-level skill scores of O_3, where, for Melbourne, the System achieved a detection probability of 70% at a 60 ppb exceedence threshold for O_3, and a false alarm rate of about 50%. In Sydney the skill scores for O_3 prediction (60 ppb threshold) were 70% and 13% for the detection probability and false alarm rate, respectively. At higher exceedence thresholds, the detection rates were less favourable than persistence while the false alarm rates were generally substantially better. Since the persistence results are dominated by a contiguous 7-day event, the performance of AAQFS would have to be rated as good.

Recommendation 1: Modifications to the System, based on findings from recent trials, need to be fully implemented and should be evaluated further during the next photo-chemical oxidant season and next year's winter particle season.

To help gauge the value of the System and to keep the public informed, on 3 September 2001 EPA Victoria began showing the hour-by hour forecasts for Victoria and Melbourne on their Web site at http://www.epa.vic.gov.au/Air/AAQFS. (A subset of pollutants is shown. No validation information is included at this stage.) Initial public interest has been very strong. NSW EPA has not made a similar commitment, arguing that the System output requires interpretation and is hence considered unsuitable for routine public release.

Recommendation 2: The Australian Air Quality Forecasting System should continue to be supported by the Commonwealth and be adopted by Jurisdictions.

Recommendation 3: The interested public should be given the opportunity to learn about the forecasts and make their own judgements about their utility.

Statistical performance of the meteorological component of AAQFS is very good by comparison with wind data from the Bureau of Meteorology network. There is the possibility that there are local flows not resolved by this network that are important for air pollution dispersion. The model may not resolve these flows either.

The most severe test of System performance is predicting the spatial distribution of pollutants as measured at EPA monitoring stations. The pollutant levels at more remote sites (outer suburbs of Melbourne, Sydney) are mostly a result of transport by the wind (*trajectories* of parcels of pollutants are most important), so the quality of the predicted meteorology is vital.

Recommendation 4: Caution is needed in interpreting the overall performance of the System compared with results from EPA monitoring stations. This may particularly be true in the northwest of the Sydney Basin.

Recommendation 5: To better resolve local winds in the AAQFS, BoM and CSIRO should develop and implement a hybrid dynamic interpolation scheme in the chemical transport model component.

Recommendation 6: BoM should improve the initialisation of the meteorological model for AAQFS applications.

Recommendation 7: BoM needs to examine the boundary-layer physics in the meteorological model, and the impact on low wind speeds, boundary-layer height, and turbulent mixing. This is particularly an issue in the Sydney region.

As shown by case studies, the performance of the System, particularly the meteorological component, is impressive in resolving features and pollution consequences of the sea-bay breeze in Port Phillip Bay, and the interaction of fronts with the geography of the East Coast.

Recommendation 8: Performance of the System should continue to be judged against case studies of important air pollution episodes in preference to, but not to the exclusion of, statistical tests.

AAQFS is showing good potential for forecasting extreme ozone concentrations. For example, when considering a 7-day ozone episode in Sydney, the System went from forecasting near-background concentrations of ozone prior to and after the episode to forecasting concentrations of over 160 ppb during the course of the episode. This is an excellent outcome. It did not always perform well in predicting the correct spatial distribution of the ozone field. This led to a relatively poor reflection of the System's performance in the forecasting skill scores at the station level.

System forecasting performance in Sydney is reduced compared to Melbourne. Frequency distributions of reactive nitrogen species (NO_y) for Sydney show a larger station-to-station variation in performance than was observed in Melbourne. To some degree this may be a natural outcome of evaluating System performance at a greater number of stations. On the other hand, it may indicate shortcomings in the prediction of local meteorological conditions or shortcomings in the emissions inventory.

Recommendation 9: Although complex meteorology (some features of which were possibly unresolved by the meteorological model) was primarily responsible for spatial errors in the forecast ozone fields for the 7-day event, there does appear to be a systematic problem with the prediction of ozone peaks at the northwestern stations in the Sydney region. This needs to be investigated further as the System continues to evolve (see Recommendation 4).

The System is very sensitive to the quality of the supplied emissions inventory, highlighting the need for sound emissions data. In particular, the Project has been the most comprehensive particle modelling exercise undertaken in Australia to date, and this has led to some issues with the emissions estimation methodologies. These issues have been exposed through the daily forecasts from the AAQFS.

Recommendation 10: AAQFS makes a valuable contribution to identifying significant emission inventory issues that need to be addressed. The benefit is not only to the quality of the forecasts, but extends to other uses of inventories in policy and reporting.

Recommendation 11: AAQFS and the National Pollutant Inventory can mutually benefit from the other's outcomes.

The prediction of primary gaseous pollutants such as NO_y and CO has continued to improve throughout the study period, with 1-hour NO_y currently the best-predicted primary pollutant.

Recommendation 12: Further improvements in the prediction of daily peak concentrations (and skill scores) of these pollutants may require the implementation of an improved, interactive urban canopy model in the System.

The System has not been able to reproduce the correct seasonal variation for particles. Upon going from the warmer months into winter, the System has systematically over-predicted the concentrations of both PM2.5 and PM10. This is currently the most challenging issue for AAQFS forecasting in Melbourne and Sydney. Wintertime aerosol concentrations are currently over-predicted. It is believed that outdated emissions factors in the domestic wood-burning model is one cause, but other factors include a too-low nocturnal mixing height over the city. In summer, the role of secondary aerosol seems to be a substantial issue not yet well understood.

Recommendation 13: As a matter of priority the emission factors, assumptions and data streams of the wood-fire emissions sub-system need to be carefully reviewed. (EPA Victoria has made some progress here already, leading to the next recommendation.)

Recommendation 14: AAQFS should conduct a trial of new particle emission factors arising from new information on firewood sources in Victoria.

Recommendation 15: There is a clear need to review the emission and treatment of other aerosol sources within the System. Application to new regions may be hampered by the present poor understanding embodied in AAQFS.

Recommendation 16: AAQFS should implement a description of wind-blown dust.

In the Sydney region, the forecasts of PM10 appear to be deleteriously affected by emissions estimates for a number of significant point sources of aerosol (some of the emissions estimates for these sources also affect forecasts of NO_y and SO_2). As part of its work plan NSW EPA is looking to update its inventory. It is envisaged that this will occur progressively, and any improved estimates will be implemented in AAQFS as they become available.

Recommendation 17: The emissions estimates for major point sources need to be reviewed by NSW EPA, and their treatment of these sources within AAQFS also needs to be revisited.

Recommendation 18: The AAQFS should be used to provide feedback to EPAs about issues regarding the emissions inventories to aid emission inventory development. This feedback on significant issues should also be made available more widely, for example to the Air Managers Forum.

In the course of the Project, we have developed some options to the point of showing important potential, ready for adoption and testing by AAQFS with the view to operational implementation.

Recommendation 19: AAQFS should implement and trial the power-based near-road motor-vehicle emissions option.

Recommendation 20: AAQFS should implement and trial the upgraded simplified chemical mechanism (GRS2), and explore the application of a comprehensive chemical mechanism (CB99) for testing and validation purposes.

Recommendation 21: The relevant jurisdictions should explore with fire management agencies the inclusion of burn data into the AAQFS emissions option for better forecasts of the impacts of such events.

During the Demonstration Period the emissions inventory model has been run twice daily as part of the full System. This may be an avoidable substantial overhead. Further, the output from the meteorological model has been used to run the chemical transport model offline. Combining these models into one model (online) will give higher temporal and spatial resolution for the air quality transport and dispersion calculations.

Recommendation 22: AAQFS should explore improving the effective speed of the emissions inventory model by incorporating daily (but probably not seasonal) variations of emissions into the chemical transport model. This should include motor vehicle emissions, which would then be more responsive in the model to forecast temperatures.

Recommendation 23: The option to implement the chemical transport model within the meteorological model should be investigated for its suitability as the ultimate configuration of the fully implemented system.

EPA Victoria and NSW EPA have yet to fully decide to employ the AAQFS in an operational mode. The System has been shown to be capable of producing high-quality forecasts under a variety of conditions, including highly complex meteorological situations. Airshed-wide performance for tracer pollutants and ozone is very good. However the same cannot be yet said for aerosol. At the station-by-station level, performance is encouraging, but needs improvement. Thus there continue to be questions about the quality of the emissions data and the reliability of forecasts. The EPAs will be examining the sections on the System performance contained in this Report. This will provide the information that is needed to base a decision on the short-term applications of the AAQFS.

Recommendation 24: At this stage of its development, AAQFS should be used as an additional source of information to assist EPAs in formulating an air quality forecast.

*Recommendation 25: The System should be re-evaluated after the coming photo-chemical oxidant season, and next year's winter particle season (*cf., *Recommendation 1*).

Recommendation 26: The System should next be extended to Tasmania and begin to forecast particles in the Launceston region in winter.

Recommendation 27: AAQFS needs to facilitate EPAs to realise the potential of the System for use in predicting regional impacts of significant new emission sources or of land use changes.

Recommendation 28: The substantial effort required to archive adequate forecast data for scenario model runs needs to be recognised.

Accepting the problems exposed in the trials, the AAQFS is an international leader, in particular because:

- The system runs as a collaboration between the national meteorological agency (the Bureau of Meteorology) and the environment protection agencies, which are responsible for informing the public.
- A twice-daily exchange of air pollution monitoring data and air pollution predictions occurs between the agencies.
- The predictions are subjected to an hour-by-hour daily routine station-level verification of criteria pollutant concentrations, reported to participants on the Web.
- By comparison with some other systems internationally, the meteorological forecast is undertaken at a comparable resolution to the air pollution forecast—at a scale that is useful in resolving suburb-scale variations hour by hour.
- The emissions inputs to the forecasts depend on the predicted meteorology—for example, vehicle evaporative emissions and biogenic emissions both depend on the forecast hour-by-hour temperature, and woodheater emissions depend on the forecast daily average temperature. Sea-salt emissions depend on the forecast local wind strength.
- A high-speed photochemistry is used; its performance is adequate for screening and for forecasts of an alternative 'green' scenario for high pollution days.

Chapter 1—Introduction and Summary

In announcing the Natural Heritage Trust Projects to Improve Urban Air Quality in May 1998, the Minister for the Environment, Senator Robert Hill, described the need for a forecasting system as follows:

> "Changes to community behaviour, which affect air quality, are assisted by timely and accurate information. A reliable and accessible pollution forecasting system would be invaluable for "at risk" members of the community, enable industry to participate in actively reducing urban pollution peak loads, and provide encouragement to the public to modify their contributing activities."

This need would be met by a new project: the Air Quality Forecasting System for Australia's Major Cities Project, which would

> "Develop a full air quality forecasting model integrating new high resolution weather and photochemical smog forecasting and using real-time emissions inventory techniques. Applicable to metropolitan areas of Australia, with a demonstration project to be implemented in a major city. The system will provide detailed three-dimensional, high resolution objective forecasts of major weather and air quality constituents on a daily basis to suburb levels."

1.1 Primary Objectives

The primary objective of the familiarly known Australian Air Quality Forecasting System (AAQFS) Project was to set up, validate, and trial for a four month demonstration period, a real time software system capable of providing accurate air quality forecasts to the public for the purpose of "*preventing, combating, or rectifying*" the level of air pollution, particularly on forecast high pollution days.

After the Australian Air Quality Forecasting System (AAQFS) had been demonstrated in Sydney and Melbourne, the Commonwealth would be the custodian of the System in Australia for Air Quality Forecasting and would have a non-exclusive right to use the System overseas for the same purpose.

The System had to be completed and demonstrated to the public in Sydney [subject to agreement by NSW EPA[∇]] in time to provide air quality forecasts for the 2000 Olympic Games. The demonstrations in Sydney and Melbourne need not necessarily have been run simultaneously.

1.2 The AAQFS Project

The Project has involved several teams: project leadership and pollution science from CSIRO Atmospheric Research, meteorology science from Bureau of Meteorology (BoM) Research Centre, pollutant emission science and user involvement from Environment Protection Authority of Victoria (EPA Victoria), air chemistry and emission science from CSIRO Energy Technology, and data and user involvement from NSW EPA.

[∇] NSW EPA has been a partner in the project and as such has had, through their provision of the emissions inventory data, complete control over the issuing of any material to the public in that jurisdiction. The same situation is true in Victoria for partner EPA Victoria.

The AAQFS consists of five major components: a numerical weather prediction (NWP) system, an emissions inventory module (EIM), a chemical transport model (CTM) for air quality modelling, an evaluation module, and a data archiving and display module (data package).

The BoM's operational NWP system, LAPS (Limited Area Prediction System; Puri *et al.*, 1998), has been adapted for the AAQFS. State-of-the-art numerics and physics packages are included with special attention paid to the resolution and treatment of surface processes. The horizontal resolution is an unprecedented 0.05° (approximately 5 km).

During the Demonstration Period the output from LAPS has been used to run the CTM offline. Ultimately the emissions and air quality modelling will be incorporated within the LAPS NWP component. Combining these models into one model (online) will give higher temporal and spatial resolution for the air quality transport and dispersion calculations. This option will be investigated for its suitability as the ultimate configuration of the fully implemented system.

EPA Victoria and CSIRO, with support from NSW EPA, have undertaken emission inventory development specifically for the AAQFS. The resulting hybrid offline/online EIM estimates emission fluxes for 60 chemical species from man-made, biogenic and natural sources and uses size-fractionated and speciated particle emissions. Area sources are gridded to 0.01° over the densely populated regions and meteorologically dependent emissions are generated based on LAPS predictions. New data on biogenic emissions have been obtained and incorporated into the System. A power-based vehicle emissions model has been developed and is available as an option. It is used to generate road-specific vehicle emission fluxes for the purpose of near-road impact modelling in Sydney, with application to other centres at a later date.

The CTM has been custom built for the project using well established, state-of-the-art methodologies (Cope *et al.*, 1998). It generates air quality forecasts for 25 pollutants (including PM1, PM2.5, PM10, photochemical oxidants, formaldehyde, butadiene and benzene) on a horizontal grid spacing of 0.01° for the urban areas and 0.05° for the non-urban areas. The CTM has been designed to run in either offline mode (downstream of the LAPS forecast), or in online mode (as an interface, which is called within the time-marching loop of LAPS). A notable inclusion to the CTM is the Generic Reaction Set (GRS) photochemical mechanism (Azzi *et al.*, 1992), a highly condensed (seven species and seven reactions) photochemical transformation mechanism featuring minimal computational overhead. Particle transformations are modelled by a sectional particle scheme. The transport fields are updated every 60 minutes in the offline system (would be every six minutes in an online system).

Both the meteorological and air quality forecasts are the subject of on-going daily and case-specific validation. This is done through comparison of LAPS meteorological fields with METAR/SYNOP (near-surface) and AMDAR (vertical profile from commercial aircraft) data and meteorological observations from the EPA monitoring networks. Air quality forecasts are compared to 1-hour EPA observations for NO_x (both as NO and NO_2) and O_3. This has been expanded to include SO_2, PM10, PM2.5, CO and, where available, non-methanic hydrocarbons. Critical to the validation process has been the availability of EPA datasets by the end of each forecast period, enabling the on-going validation to be substantially automated.

Data archiving uses unified NetCDF data packets (NetCDF was already used in the case of LAPS), which are accessible via GUI-driven Q&A software. Sufficient information is available in a data packet to enable the CTM to be run offline at a later time. The EPAs have access to the daily forecasts via the AAQFS Web Site and are responsible for managing the extent to which the forecasts are used and disseminated.

1.3 Outcomes of the Project

The major activities undertaken by the Project participants are summarised in Table 1, and are reported in greater depth in the rest of this Report.

Activities included several presentations to international Conferences including Clean Air Society Conferences in 1998 and 2000, press interviews (radio, television and print media), a journal publication (AMOS Bulletin 2000), with several more presently in preparation. The Project Team briefed Environment Australia on progress on several occasions, including a detailed presentation in Canberra and, in cooperation with Environment Australia, ran a comprehensive workshop involving representatives from all Australian jurisdictions where the outcomes of the Project were presented and discussed. The highlight was the launch of the System at EPA Victoria by Senator Robert Hill on 3 September 2001, organised by the Project team, Environment Australia and the Minister's Office.

Table 1. Major activities undertaken during the AAQFS Project

Major Events	Date
Announcement of Project by Senator Hill	May 1998
Component test system for AAQFS trialled	March 1999
First Phase Progress Report to EA	July 1999
The prototype system commenced trials	August 1999
Second Phase Progress Report to EA	September 1999
Real-time inventories in place, power-based vehicle emissions model progressed, GRS chemistry working, and prototype system commenced trials in Sydney	January 2000
Presentation to Air Managers' Forum, Brisbane	January 2000
Presentation to EA in Canberra by AAQFS Team	8 February 2000
Third Phase Progress Report to EA	February 2000
Real-time Demonstration System nearly completed and Web site for forecasts running (slowly)	May 2000
Fourth Phase Progress Report to EA	June 2000
Demonstration System running in time for the Olympic Games in Sydney.	7 August 2000
Demonstration System running throughout the Olympic and Para-Olympic Games — the Demonstration Period	7 August–4 December 2000
'The Australian Air Quality Forecasting System' by Hess *et al*., 2000b, AMOS Bulletin **13**, 67–73	August 2000
Invited presentations to WMO GURME air pollution forecasting workshop in Kuching, Malaysia	August 2000
Fifth and Sixth Phases' Progress Report to EA	September 2000

Team commitment to run the System throughout the summer smog season of 2000–01	October 2000
Report on the performance of the Demonstration System for the period 13–27 November 2000	January 2001
Workshop on the AAQFS, its status, results, on-going applications — representatives from all jurisdictions.	15 June 2001
Commence transfer of Web and model components from CSIRO to Bureau of Meteorology	July 2001
Launch of AAQFS at EPA Victoria by Senator Robert Hill and Victorian Minister for Environment Sherryl Garbutt.	3 September 2001
EPA Victoria website for AAQFS open to public at www.epa.vic.gov.au/air/aaqfs.	3 September 2001
Final Report on AAQFS	November 2001

1.3.1 Trialling of the System in Melbourne

Because of the ready availability of emissions data, monitoring data and infrastructure support provided by EPA Victoria, Melbourne was used as the initial and ongoing centre for trials throughout the development of the Project.

As summarised in **Section 1.3.4 Review of the AAQFS Technical Performance** and discussed in detail in **Section 2.4 CTM performance in Melbourne and Geelong**, these trials have proved invaluable for probing for weaknesses in the System.

These trials have shown that the System is performing well for important gaseous pollutants and in particular in its ability to forecast summer ozone events, but is less successful for particles in some winter conditions.

1.3.2 The Responsive Emissions Inventory

A significant objective of the Project has been the development of an Emissions Inventory Model (EIM) that is responsive to seasonal, weather and event forecasts. It is described in **Chapter 3—The Emissions Inventory Model**. The objective has been achieved, though a component dealing with wood-fuel heaters has been overestimating their emissions, is presently undergoing alterations, but requires further work by relevant jurisdictions.

The EIM includes relationships based on observations of motor vehicle emissions varying with season, weekday, Saturday, Sunday, and time of day. The model also responds to forecast temperature by varying motor vehicle emissions of several species, in particular petrol vapour.

Temperature is a dominant factor in the wood-smoke model, and also influences strongly the emissions from biogenic sources in the System.

Application of a power-based motor vehicle emissions model in Sydney for the AAQFS has allowed demonstration of the response vehicle emissions have to road network conditions, including terrain slope and traffic intersections. There is the potential to incorporate models of

traffic numbers by developing relationships from intersection traffic count data obtained automatically.

Special event days (usually, public holidays) are handled by their treatment as a Sunday.

There is facility to accommodate forecast burn-offs and persistent wildfires and to have their emissions estimated hourly according to their fuel loads and fire sizes. There is also a facility to include additional tracers for special applications.

Sea-salt spray is incorporated so that it responds to the forecast wind; wind-blown dust from open areas is yet to be included.

1.3.3 Timeliness of Meeting the Objective of Forecasting for the Olympic Games

The Demonstration System was in full operation well in time for the Olympic Games in Sydney. Indeed, it was run throughout the Games and the Para-Olympics. Special emission sources at each of the Olympic venues were included in the runs and dispersion from these sources was tracked each day of the Olympics.

The single biggest problem in achieving this objective was getting the Web reporting system to work in a usable manner. What looked useful to the Team proved in practice to be far too slow and failed to meet the needs of our users. Following a lot of feedback from EPA Victoria users and NSW EPA, the Web displays were simplified and prioritised to give the most important information first. Automatic e-mailing of the summary results to users also greatly improved the dissemination of the forecasts. These issues are discussed in **Chapter 4—Outputs from AAQFS**.

1.3.4 Review of the AAQFS Technical Performance

The System has been extensively trialled and refined by application to the Melbourne and Sydney airsheds. These trials are discussed in some detail in **Chapter 2—The AAQFS** and **Chapter 7—Case Studies with AAQFS**. We present here a summary of the System performance and the findings from the trials.

- A demonstration forecasting System has been developed. The System operates on two large supercomputers and a number of workstations.
- The System generates twice-daily forecasts of air pollution for four grids: Victoria, Melbourne, NSW and Sydney. During the Demonstration Period the System met the critical 3 pm deadline 79–86% of the time. (Recently the number of computer processors has been increased and this performance has markedly improved.)
- Twice-daily output from the System is summarised into a series of images that are delivered to the EPAs *via* e-mail, ftp and web servers.
- The System has continued to be upgraded throughout the Demonstration Period in response to issues that were identified during this time. The statistical trials were performed after the System had stabilised in March; case studies were re-run using the stabilised System.
- System performance for the prediction of meteorology and air quality is routinely verified using a number of procedures based on comparisons with monitoring data, both at the regional scale and at the level of individual stations.

- Performance is assessed for the prediction of hourly and daily peaks, and for the prediction of weekly, monthly and seasonal trends. Various statistical measures are used to quantify the System performance.
- A second method of assessing System performance is though detailed examination of case studies of extreme events. Extensive use is made of visualisations in time and space of the meteorological and air quality fields, which are compared with observations.
- Both the statistical approach and the case-study approach have been very encouraging, indicating that the System is capable of producing high-quality forecasts under a variety of conditions, including highly complex meteorological situations.
- In Melbourne, the System has demonstrated an ability to reproduce the key meteorological patterns that are associated with conditions of poor air quality. For example, the System is able to reproduce the kind of mesoscale circulations (*e.g.*, the Melbourne Eddy, the bay breeze, the sea breeze) and their interaction with the larger scale synoptic forcing, which play an important role during photochemical smog episodes.
- In Sydney, the System is able to reproduce the complex interplay between drainage flows, sea breezes, and synoptic-scale flows such as southerly wind changes (*e.g.*, the Southerly Buster) that characterise the meteorology of photochemical episodes in this region.
- The System has shown good potential for forecasting extreme ozone concentrations. When considering a 7-day ozone episode in Sydney (21–27 January 2001), the System went from forecasting near-background concentrations of ozone prior to and after the episode to forecasting concentrations of over 160 ppb during the course of the episode. The probability of detection over the airshed for O_3 was 100% for thresholds in the range 60–100 ppb, and the false alarm rates were between zero and 25%. While the forecast probability of detection was the same as that for persistence (which also achieved a 100% hit rate), the false alarm rates were generally significantly better than those based on persistence. These are excellent outcomes, and represent an enormous improvement compared to continual forecasts of near-background ozone concentration as were being made when the Demonstration System was first implemented.
- The System achieved a probability of detection for the 1-hour daily peak of reactive odd nitrogen species (NO_y) over the Sydney airshed of 98% at a 60 ppb exceedence threshold, and a false alarm rate of 4%. The forecast probability of detection and the false alarm rate were better than persistence forecasts.
- Similarly, the System was able to capture a three-day ozone episode, observed in Melbourne (7–9 March 2001). Peak concentrations were observed to reach about 80 ppb and were reproduced with excellent skill by the System. The probability of detection over the airshed for O_3 was 100% at a 60 ppb threshold, and the false alarm rate was 25%. Both the probability of detection and the false alarm rate were significantly better than achieved by persistence forecasts.
- The System achieved a probability of detection for the 1-hour daily peak of NO_y (reactive odd nitrogen species) over the Melbourne airshed of 100% at a 60 ppb exceedence threshold, and a false alarm rate of 16%. The probability of detection was better than for persistence forecasts, but the false alarm rate was about the same as persistence.
- The System was able to simulate inter-regional transport of pollutants, outside the region currently monitored by the EPA networks. These simulations appear to be able to explain previously mysterious observed nocturnal ozone peaks found at Canberra. Using the

System, we are also able to show the impact of pollutant transport into the study region, such as the impact on 11 January 2001 of the King Island bushfire on Melbourne.

- At the station level, the System was able to reproduce the spatial distribution of peak O_3 with good skill in Melbourne for all days of the 3-day event, and for a majority of days in the Sydney 7-day event. This is reflected in the station-level skill scores of O_3, where, for Melbourne, the System achieved a detection probability of 70% at a 60 ppb exceedence threshold for O_3, and a false alarm rate of about 50%. In Sydney the skill scores for O_3 prediction (60 ppb threshold) were 70% and 13% for the detection probability and false alarm rate, respectively. At higher exceedence thresholds, the detection rates were less favourable than persistence while the false alarm rates were substantially better.
- Station-level performance for primary pollutants such as NO_y and CO showed substantial improvement over the course of the three-month evaluation period. For example, in Melbourne the fractional bias of the daily peak for NO_y went from -0.33 to 0.14 and the fractional bias for CO went from -0.14 to 0.38; in Sydney the fractional bias for NO_y went from -1.08 to -0.44 and for CO went from -0.88 to 0.24.
- System performance for the prediction of particle concentrations indicated a tendency for under-prediction during the summer months. A primary cause of this under-prediction has been identified as the absence of wind-blown dust in the model. A module for wind-blown dust emissions will be implemented in the near future.
- The System has not been able to reproduce the correct seasonal variation for particles (although it has done this with excellent skill for the other pollutants). Upon going from the warmer months into winter, the System has systematically over-predicted the concentrations of both PM2.5 and PM10. It is believed that outdated emission factors in the wood-combustion emissions model may be the cause of the over-prediction. A study underway by EPA Victoria is finding that recent scientific evidence indicates that the emission factors should be reduced to 60% of their current values, on the average, and that the emission factor for open fires should be reduced to 30% of the current value. A trial using these new emission factors has commenced.

In summary, the System's performance during the trials, in general, has been extremely encouraging. The trials have been valuable in that they have enabled us to document the strengths of the System, and the areas in which the System has needed to be improved. Modifications to the System, based on these findings, are currently being implemented, and should be ready before the next photochemical oxidant season.

1.4 Standing of AAQFS in the International Context

Forecasting air quality is a relatively new concept. However there are a number of groups around the world providing such air quality forecasts. How does the Australian Air Quality Forecasting System (AAQFS) compare to these other systems?

- The most common ozone forecasting systems are based on statistical regression with predictants such as screen temperature, mean sea-level pressure, solar radiation, wind speed, and boundary-layer height. Examples of groups practicing this method include EPA Victoria, NSW EPA, and the University of Maryland, which forecasts for Washington, DC, Baltimore, MD, Philadelphia, PA and Virginia. There are many other groups using this technique around the world.

- The next level of complexity is a box-model forecast. The UK Department of Environment, Transport and the Regions uses this methodology to forecast for ozone, nitrogen dioxide, sulfur dioxide, carbon monoxide and PM10.
- The Cambridge Environmental Research Consultants use the UK Meteorological Office's wind fields, a Gaussian dispersion model that they have refined (ADMS), and the condensed chemistry developed by CSIRO (GRS) to produce suburban-scale forecasts for York, Leicester, South Gloucestershire, Bristol, north Somerset, Bath and north-east Somerset.
- GMD FIRST performs forecasts for Berlin using a simplified meteorological model called REGOZON. The model is restricted to fair weather, stagnant air flow, and relatively flat terrain without strong orographic features or strong horizontal temperature gradients (no land/sea breezes). It uses a comprehensive chemistry, CB-IV, and has about 2 km horizontal resolution.
- The Air Resources Laboratory performs (unverified) forecasts for ozone for the Eastern half of the United States and for the region near Houston, Texas. They employ a hybrid Lagrangian puff model and a comprehensive chemistry, CB-IV, with 50 km horizontal resolution. The wind fields are calculated by Eulerian models from the US National Weather Service.
- The Danish Atmospheric Chemistry Forecast System model computes backward trajectories from receptor points, and then retraces the paths using a comprehensive chemistry EMEP MSC-W. It has 50 km horizontal resolution. The wind fields are calculated by the Eulerian model HIRLAM.
- Another Danish system, called DMU-ATMI-THOR uses an Eulerian meteorological model at 25 km horizontal resolution and a comprehensive chemistry, CB-IV. Air quality predictions are made to high resolution, including street canyons, using the same 25 km windfield.
- The North Carolina Supercomputing Center runs a meteorological model called MM5 and an Eulerian chemical model MAQSIP with CB-IV chemistry. They perform (unverified) forecasts for the Eastern half of the United States at 36 km horizontal resolution.
- The Technical University of Madrid has developed a forecasting system called EMMA as a European Union project. It uses a meteorological model called REMEST, based on the MEMO 5.0 and MM5 models, inline with a solver for complex chemistry based on CBM-IV. The resolution of 1 x 1 km is centred over Madrid. Forecasts (unverified) are for ozone and sulfur dioxide, reported as an air quality index since 4 July 2001.
- Project PIONEER is an operational ozone forecasting system developed by Meteo France with the Euler Polytechnical of France and others. Forced by ECMWF or NCEP weather forecasts for Europe at a resolution of 50 km, a nested resolution of 6 or 4 km in three regions of France is achieved by interpolation. Pollution emissions are obtained from the EMEP dataset. The CHIMERE chemical transport model is used to predict ozone concentrations. The unique feature of this system is the extensive analyses of performance, including verification against observations and uncertainty analyses using ensembles of forecasts that was undertaken for a 4.5 months in 2000. Operational forecasts appear to be unverified.
- The Meteorological Service of Canada has been developing an air quality forecasting system for Eastern Canada over the summers of 1999 and 2000, with a full implementation expected for 2001 summer. The chemical model used is the Canadian Hemispheric and Regional Ozone and NOx System (CHRONOS). Current research emphasis is on sizes and chemical composition of atmospheric particles. The model runs

off line with the main weather forecasting system (GEM), both at a 25 km horizontal resolution. MSC has maintained a keen interest in AAQFS.

- The World Meteorological Organization has initiated a project called GURME. The GURME project arose in response to the requests for assistance by many National Meteorological Services dealing with urban issues, and in recognition that the management of urban environments requires special attention. A major need that has been identified is for WMO to assist countries in providing air quality services of high quality, particularly the capabilities to provide meteorological and air quality forecasts of urban environments. This need also entails measurement efforts that support operational and verification aspects of forecasting, and performed in co-operation with appropriate agencies. The status of the program can be found on the Web at http://www.cgrer.uiowa.edu/people/carmichael/GURME/GURME.html. By comparison with all other Systems presented, AAQFS is the leading System, not least because it involves a partnership between environment agencies and the weather service, it includes appropriate physics appropriately implemented, and because it uniquely undergoes daily validation against multi-site monitoring data.
- Air Resources Laboratory, US National Oceanographic and Atmospheric Administration, has initiated a collaboration with the AAQFS Team to better implement a similar System.

1.5 Effectiveness of the Project

The Project has met all its main objectives. The Demonstration System was set up, validated and trialled for far longer than the specified four-month period. It was operating in good time in Sydney for the Olympic Games in September 2000.

The System uniquely combines the expertise and capacity of the national weather service and the principal jurisdiction EPAs to provide prognostic numerical twice-daily forecasts down to 1 km resolution for a suite of air pollutants including photochemical smog. The System uniquely presents the forecasts in tailored graphical formats for each participating EPA in time for their pollution bulletins to meet media deadlines. Uniquely, the System is validated against air pollution monitoring data each day and these results are displayed on a responsive Web site for investigation and confirmation of performance.

The AAQFS is regarded by the Bureau of Meteorology as the most appropriate system for any operational air quality forecasting service that it would provide. While there are still important technical issues to be resolved, particularly about System performance in predicting particle concentrations, these are not a serious impediment to implementing the System. AAQFS will benefit in the longer term from an implementation of the Option components developed as part of the Project, and the refining of solutions to the various issues raised.

1.6 Transferability of the Demonstration System

The application of the AAQFS Demonstration System to Victoria and NSW has shown the critical importance of an accurate base emissions inventory: this may limit its transferability to other jurisdictions. Daily forecasts of air pollution from AAQFS are of such detail that every weakness in the inventory is highlighted. However the System can be used to show which aspects of an inventory require most attention, so a priority schedule can be developed.

The Bureau of Meteorology through its National Meteorological and Oceanographic Centre is planning eventually to extend its operational fine-scale models to other cities. Although there

are resource issues to be overcome, the air quality project should be able to leverage off these developments and we can anticipate that the necessary finer-scale meteorological models will become available to support extensions of the air quality system to some other locations.

The Department of Primary Industries, Water and Environment, Tasmania, is particularly keen in applying AAQFS to Launceston winter particle pollution. Since this application has proved the most challenging in the Demonstration Project, the application to Launceston would permit a strong focus on better describing wood-fire emissions. The application of the EIM to Launceston would likely benefit substantially from the new information being obtained by the Environment Australia project called "Characterisation of Emissions from Solid Fuel Burning Appliances (Woodheaters, Open Fire Places)" presently being undertaken by CSIRO and others.

Chapter 2—The AAQFS

2.1 Description of the Forecasting System

The AAQFS consists of five major components: a numerical weather prediction (NWP) system, an emissions inventory module, a chemical transport module (CTM) for air quality modelling, an evaluation module, and a data archiving and display module (data package). The purpose of the NWP system is to provide accurate, high-resolution (both spatial and temporal) forecasts of the vector wind, temperature, humidity and radiation fields and surface-layer characteristics, *e.g.* stability parameters and surface fluxes. Data from the meteorological forecast and emissions inventory are used by the CTM to drive processes of pollutant transport and deposition and to provide radiation, temperature and humidity fields for the simulation of chemical transformation processes. The resulting concentrations of the air quality species are then distributed to the EPAs and archived, and are also used for evaluation of the forecasts. Figure 2.1.1 summarises the relationship between the components, both at the start of the project (Pilot Scheme) and at present (Current Scheme).

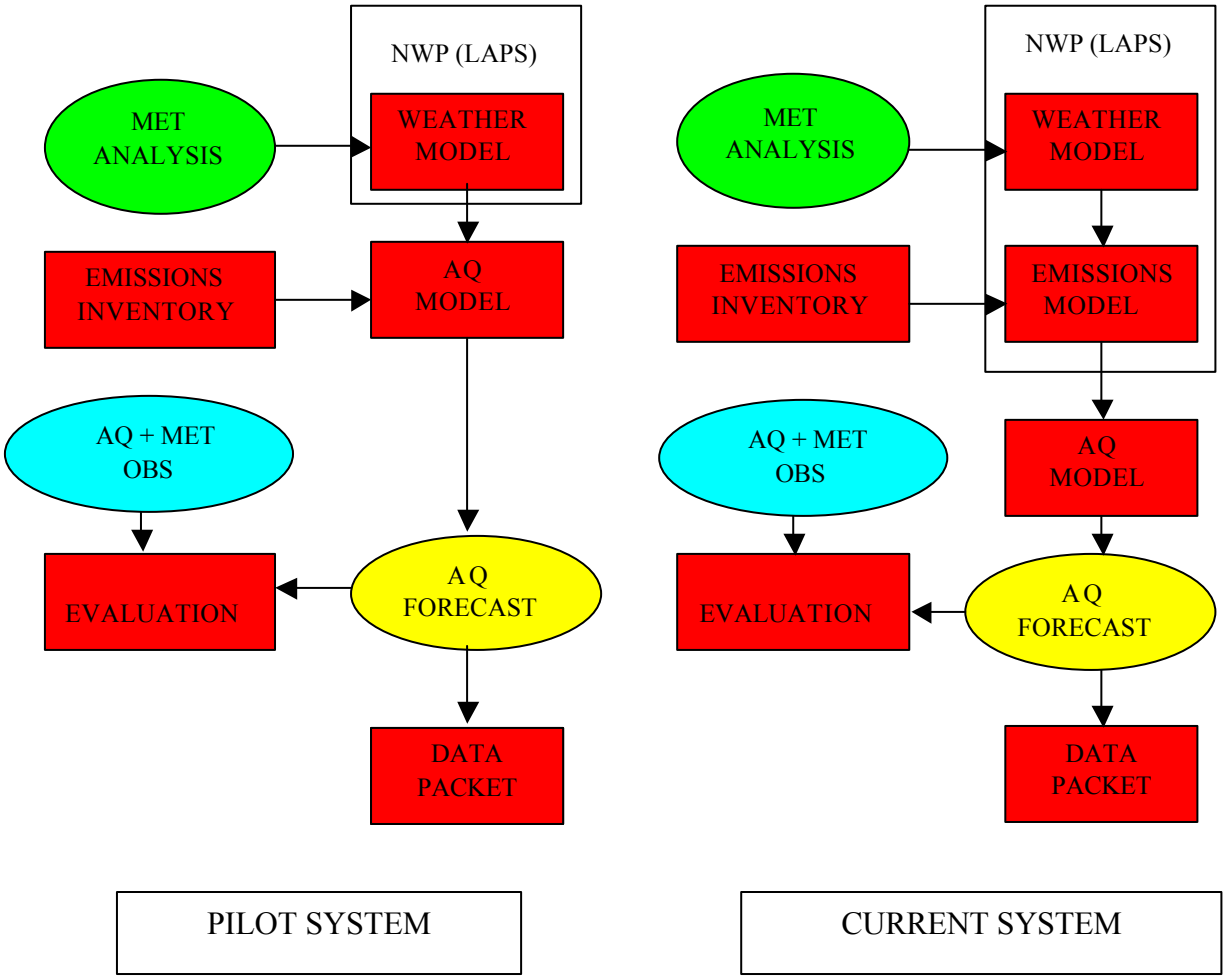

Figure 2.1.1. Schematic diagram for the pilot version and the current version of AAQFS. The system components are shown by red (darkest) rectangles; the ovals show observational data input or forecast output. Some of the emissions depend on meteorological conditions and are now modelled using NWP output.

The meteorological forecasts are generated by the BoM Limited Area Prediction System (LAPS, Puri *et al.*, 1998), a state-of-the-art NWP system. LAPS began operational forecasts in July 1996 at a horizontal grid resolution of 0.75°. The LAPS suite now has several nested domains, starting at 0.375° resolution for broad-scale guidance, and a 0.125° version covering the full Australian continent to portray finer-scale features. The air quality applications operate within two very fine-scale versions of LAPS with a horizontal grid spacing of 0.05° (approximately 5 km). These are run twice daily (commencing at 1100 and 2300 UTC) and generate 36-hour forecasts for two domains, one approximately corresponding to the size of the state of Victoria and the other to NSW (see Figures 2.1.2 and 2.1.3).

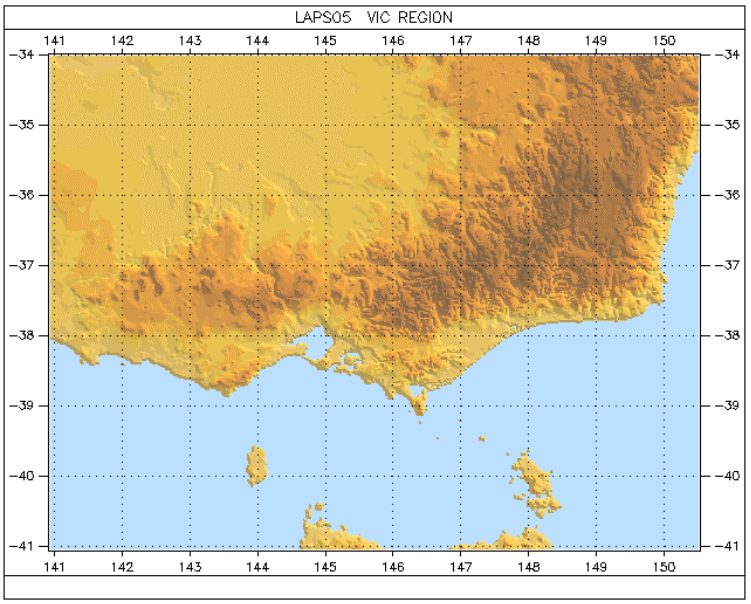

Figure 2.1.2 LAPS domains for Victoria. The topography is indicated by the shading. Melbourne is located at -37.82° latitude, 144.97° longitude.

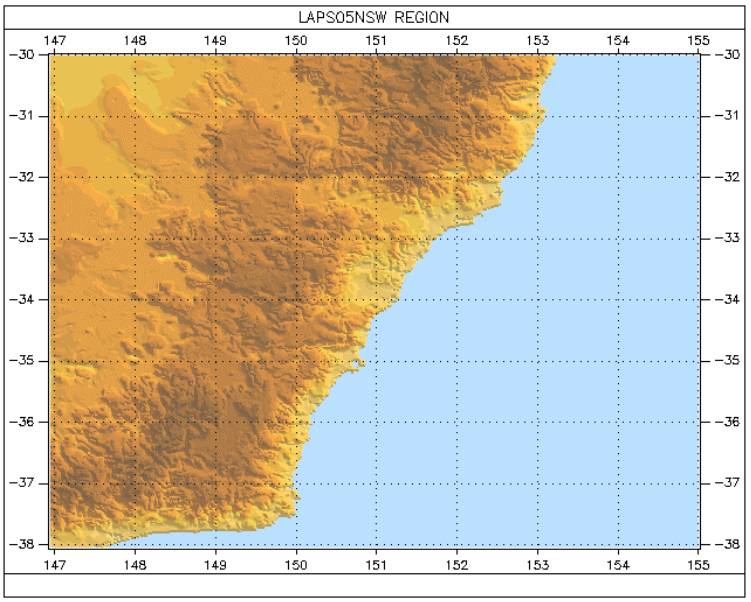

Figure 2.1.3. LAPS domain for NSW. The topography is indicated by the shading. Sydney is located at -33.87° latitude, 151.21° longitude.

LAPS uses a latitude/longitude grid and solves the primitive equations for momentum, mass, temperature, and humidity on a non-staggered Arakawa A grid. Physical processes in the model include direct calculation of the fluxes in the Monin-Obukhov surface layer, stability dependent mixing formulations, an upgraded Viterbo-Beljaars land-surface scheme that includes high-resolution variation of vegetative and soil properties and multi-level diffusion of temperature and moisture in the soil, Tiedtke moist convection and shallow convection parameterisations, and a Fels-Schwartzkopf radiation scheme.

The model is initialised from a limited-area (at 0.375^o resolution) multi-variate statistical interpolation analysis. This analysis uses data comprising available surface pressure observations, radiosondes, radar winds, cloud drift winds, AMDAR (commercial airline winds and temperatures), satellite temperatures and moisture, and METAR/SYNOP (near-surface automatic weather stations) moisture. The analysis is interpolated to 0.05^o resolution. Boundary conditions are obtained by nesting LAPS at 0.05^o resolution in LAPS at 0.375^o resolution. (Currently, computer resources do not allow us to nest LAPS at 0.05^o in LAPS at 0.125^o and still meet the EPA deadlines for receiving the forecasts). The model at 0.375^o resolution has in turn been nested in the BoM global model (GASP).

A significant effort has been made to resolve the vertical structure of the atmosphere near the surface. It is within this region that surface friction, heating and cooling, and moistening and drying have their greatest influence on the flow and consequently on the concentration of pollutants. The surface heat and moisture fluxes are major factors in determining the surface temperature, the land-sea temperature contrast, and the timing and penetration of bay and sea breezes. Details of these enhancements to LAPS are given in **Appendix 2.1a**.

The current LAPS model with the changes we have implemented during the course of this project has led to greatly improved forecasts. We are now able to accurately forecast the occurrence of small-scale flow features, which can have significant impact on air quality like the Melbourne Eddy, the Port Phillip bay breeze, and the sea breeze. We were unable to do this previously. We have also improved our ability to forecast the passage of cold fronts, including the small-scale detail at the leading edge of 'Southerly Buster' fronts. We show examples of our ability to forecast these features in Figures 2.1.4–2.1.9, with illustrations from both Victoria and NSW.

Figure 2.1.4 shows the Melbourne eddy that typically forms during the night in periods of light easterly flow and a stable boundary layer. The air flow is unable to travel over the high topography (the Australian Alps) east of Melbourne and must therefore travel around the topography. This leads to the formation of an eddy over Melbourne. The eddy re-circulates precursors and pollutants from the western industrial suburbs of Melbourne, over the city and then over the bay. These pollutants are trapped vertically by the stable thermal stratification.

Figure 2.1.5 shows the bay breeze, a small-scale wind feature that typically develops in the mid- to late morning, when a land-sea temperature contrast exists. The inland penetration of the bay breeze is particularly sensitive to the background synoptic flow, which can be seen opposing the bay breeze in Figure 2.1.5. A stronger opposing flow will inhibit the formation of the bay breeze altogether. The model's ability to forecast this delicate balance can be crucial to producing an accurate air quality forecast in Melbourne.

The bay breeze tends to be relatively short-lived, since it is usually overpowered by a sea breeze that develops in Bass Strait. Like the bay breeze, the sea breeze is also influenced by

the background synoptic flow. In Figure 2.1.6 we show the sea breeze in Melbourne that replaced the bay breeze; note the opposing synoptic flow.

In Sydney the typical flow pattern leading to air quality events is a little different. During the night a shallow layer of relatively cold air drains from the highlands to the west, bringing precursors and sometimes pollutants from the previous day over the city and out over the sea. Since the coastline is effectively a straight line, there is no bay breeze. In the late morning or in the afternoon, after the temperature contrast between land and sea has become great enough, a sea breeze develops and transports the pollutants back over the land. In this case the synoptic flow may not impose the same direct opposition to the progress of the sea breeze as often happens in Melbourne, although resistance is provided by the topography. The depth of penetration can be determined by examining the planetary boundary-layer height as seen in Figure 2.1.7. The shallow boundary layer height near the coast indicates the region of sea breeze penetration.

Figure 2.1.8 shows the arrival of a Southerly Buster. The Southerly Buster is an acceleration of the cold front in the coastal regions, caused by the interaction of the front with the Great Dividing Range. In the case shown in Figure 2.1.8, a mesoscale pressure trough appeared in the model results that propagated ahead of the main wind change. This produced a shift in the wind direction ahead of the Southerly Buster. Although such a wave may not significantly affect pollution levels, it is an excellent example of the LAPS model's ability to predict small-scale flow features. Waves leading strong Southerly Busters have been extensively documented by Colquhoun (1981) from observations, but this is the first time we have seen such a feature reproduced by our numerical model.

Four hours later, the main wind surge arrived at Sydney (Figure 2.1.9). The arrival of the Southerly Buster and other cold fronts often flush the Sydney Basin clear of ozone and other pollutants, which may have been re-circulating for a period of days. Such flushing by strong (and, occasionally, weak) cold fronts can be a cause of the transport of pollutants up the east coast of Australia (*e.g.*, from Sydney to the lower Hunter Valley) and can therefore be important for predicting air quality.

Further discussion of the modelling of particular ozone events and the meteorology associated with them is given in Cope *et al*. (1998), Hess *et al*. (1999), Cope *et al*. (1999), Hess *et al*. (2000a), Hess *et al*. (2000b) and Tory *et al*. (2000).

When we started the project, the NWP system, emissions inventory and an initial version of the CTM basically comprised AAQFS; the evaluation module and the data packet were very elementary. We recognised from the beginning that significant developmental work on each component of AAQFS would be necessary if we were to achieve a world-class air quality forecasting system. The progress achieved in each of the components is described in Table 2.1.1. Based on public domain components, the current CTM v1.0 is detailed in **Appendix 2.1b**.

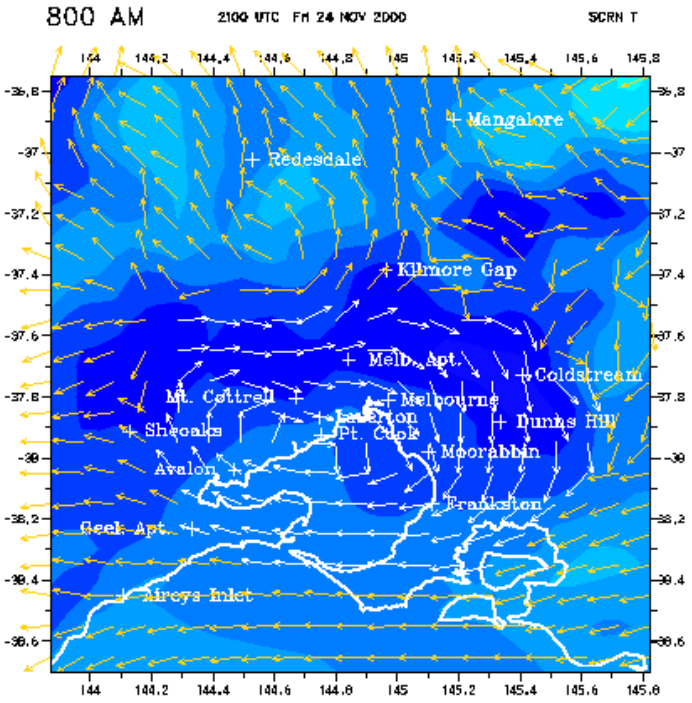

Figure 2.1.4. Forecast of the Melbourne Eddy (white vectors) at 0800 EDT 25 November 2000. The background colour (shading) indicates screen temperature; deeper blue (darker) is cooler.

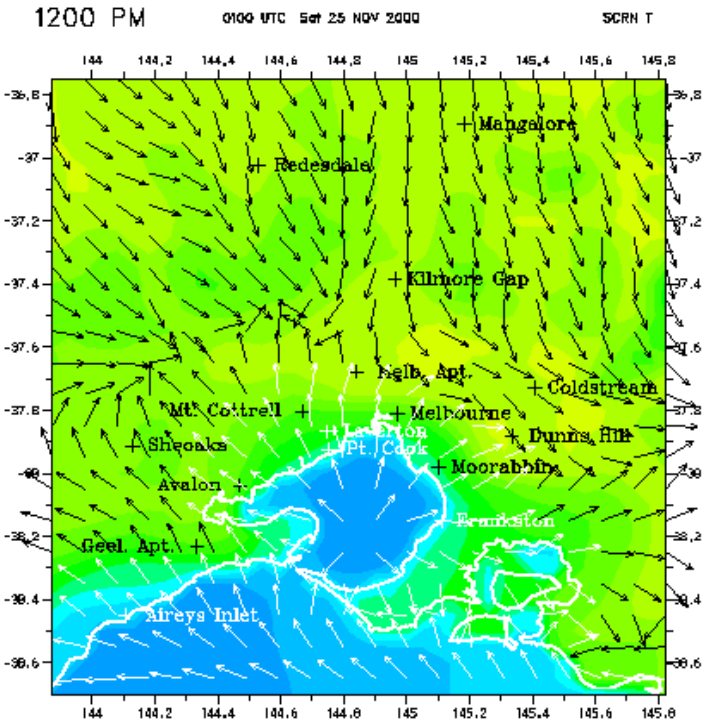

Figure 2.1.5. Forecast of Port Phillip bay breeze (white vectors) at 1200 EDT 25 November 2000. The background colour (shading) indicates the screen temperature: blue (darker) is cool, green-yellow (lighter) is warm.

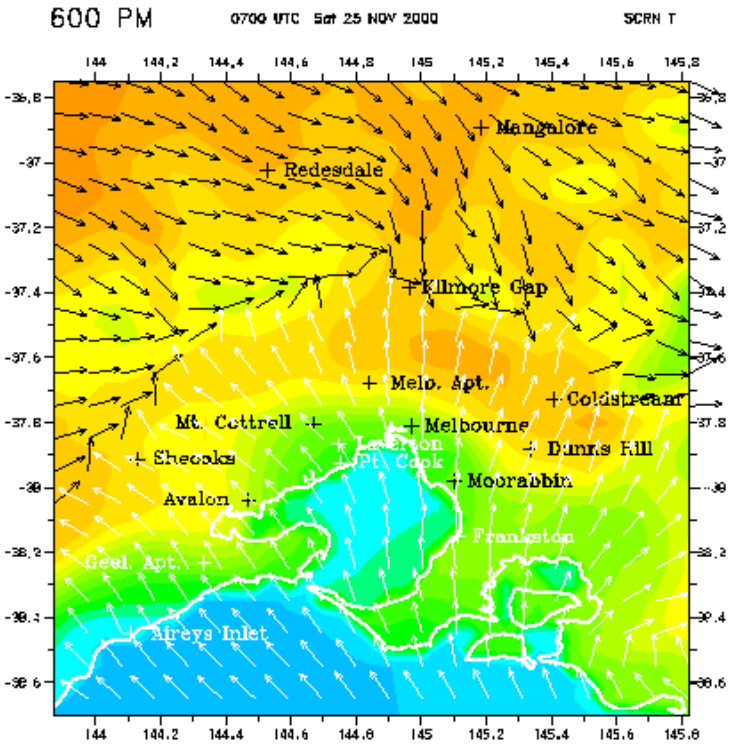

Figure 2.1.6. Forecast of the sea breeze (white vectors) at 1800 EDT on 25 November 2000 in Melbourne showing the opposing synoptic flow. The background colour (shading) indicates screen temperature; blue (darker) is cool, yellow-green (lighter) is warm, orange (darker) is hot.

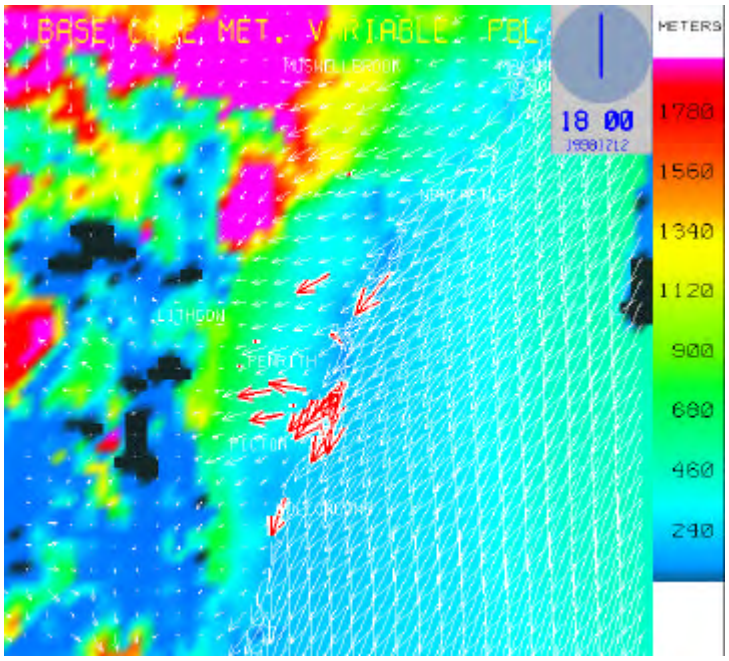

Figure 2.1.7. Forecast of the sea breeze at 1800 EDT on 12 December 1998 in Sydney. The background colour indicates the planetary boundary-layer height. The sea breeze is accompanied by reduced PBL heights. The red (dark) arrows indicate wind observations.

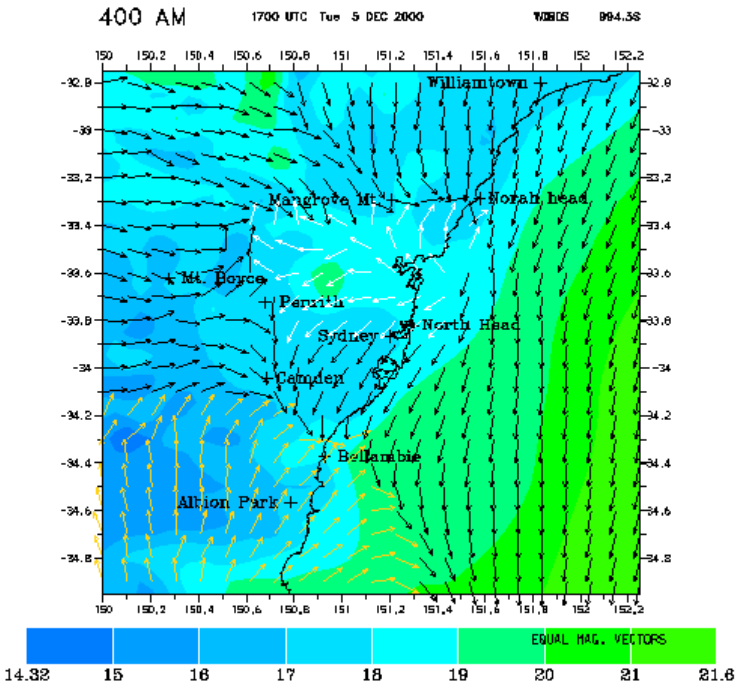

Figure 2.1.8. The Southerly Buster at 0400 EDT on 6 December 2000 with a mesoscale circulation (white vectors) leading the main wind change (yellow [grey] vectors).

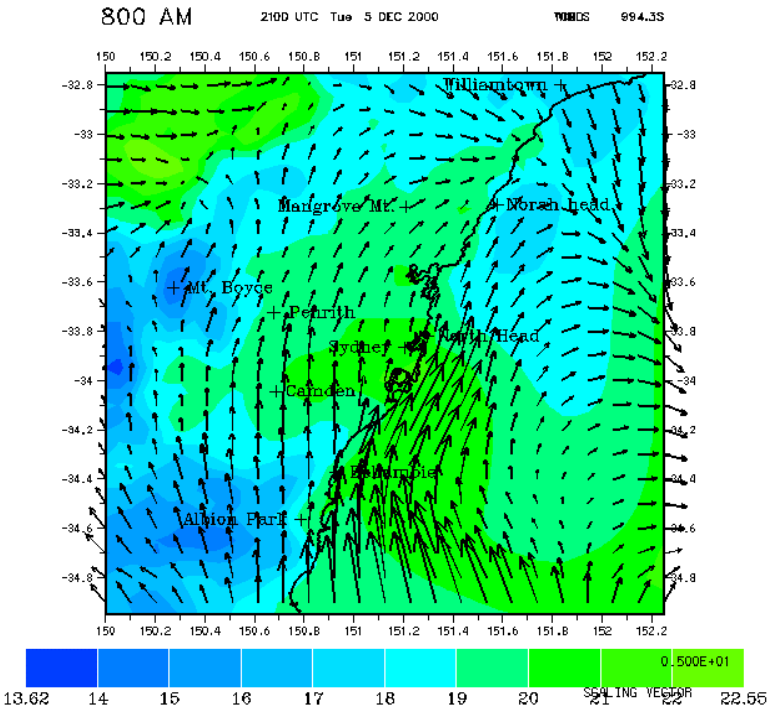

Figure 2.1.9. The Southerly Buster at 0800 EDT on 6 December 2000 showing the coastal wind surge. The background colour (shading) indicates the screen temperature.

Table 2.1.1. Description of AAQFS Components

PILOT SCHEME	CURRENT SCHEME
Numerical Weather Prediction (NWP)	
• Two domains run twice a day	• Two domains run twice a day
• Simple local turbulent mixing scheme	• Non-local turbulent mixing scheme
• Parameterised surface flux scheme	• Direct calculation of surface fluxes
• No vegetation	• Vegetation effects included (32 categories of vegetation/land use, vegetative fraction and leaf-area index at 0.05° resolution)
• Uniform soil properties	• Varying soil properties (7 soil types plus ocean at 0.05° resolution)
• Same roughness for momentum, heat and moisture; constant roughness over land	• Separate roughness lengths for momentum and heat and moisture; roughness length variation determined at 0.05° resolution; vegetative and topographical roughness effects included
• Smooth topography (interpolation from 0.10° grid)	• High-resolution topography (based on 0.008° data)
• Smooth sea-surface temperature (interpolated from 1.0° grid, weekly data)	• Higher-resolution sea-surface temperature (interpolated from 0.25° grid, daily data)
• Model initiated by interpolating an analysis done at 0.75° resolution	• Model initiated by interpolating an analysis done at 0.375° resolution; improved analysis of heating and moistening rates and near-surface moisture
• 0.05° horizontal computational grid with 19 vertical levels	• 0.05° horizontal computation grid with 29 vertical levels
Emissions Inventory (EIM)	
• Victoria: Melbourne Airshed 1990 emissions inventory for NO_x, ROC, SO_2 and TSP	• Victoria: Inventory expanded to cover Victoria and updated to year 1996
• NSW: Metropolitan Air Quality Study (MAQS) 1992 inventory for NO_x, ROC, SO_2 and TSP	• NSW: Inventory extrapolated to year 2000 • Modelled species: NO_x, ROC, SO_2, size-fractionated and speciated particles, CO, NH_3, some air toxics (formaldehyde, benzene, butadiene)
Inventories based on: • 3-km resolution of area sources • Discrimination between weekday/weekend and seasonal variability	
CTM applications simplified the inventories: • Victoria: 3-km grid resolution • NSW: 6-km grid resolution • No discrimination between weekday/weekend and no seasonal variability	• Grid resolution: 0.05° in rural areas; 0.01° in major urban areas for Victoria and NSW • Weekday/weekend discrimination, seasonal variation, public holiday discrimination (Sunday emissions used as surrogate for public holidays)

• Biogenic emissions calculated using 'typical' summer time temperature and radiation fluxes	• Meteorologically dependent emissions modelled—*weak dependence* (wood-burning, motor vehicle evaporatives); *strong dependence* (biogenics, wind-blown dust, sea salt) • Prescribed burns (manual insertion) • Power-based emissions model developed by CSIRO (DCET) to generate road-specific emissions fluxes for selected roads • Biogenic emission factors from a CSIRO measurement program for NSW EPA
Chemical Transport Model (CTM)	
• California Institute of Technology (CIT) photochemical model upgraded and adapted for Australian applications • GRS photochemical mechanism • Scalar transport of PM10 and SO_2 • Melbourne Airshed domain: 3-km resolution and 10 vertical levels; MAQS domain: 6-km resolution and 10 vertical levels • 24-hour forecast using 1100 UTC LAPS meteorology	• New, efficient CTM developed from the CIT model for Australian applications • Extended GRS photochemical mechanism • Comprehensive photochemical mechanism (Carbon Bond IV) available for evaluating performance of GRS mechanism • Size-fractionated particle scheme • Some air toxics (formaldehyde, benzene, butadiene) simulated • Victoria and NSW domains: 0.05^{o} grid resolution with nested regions of 0.01^{o} resolution in major urban areas; 17 vertical levels • 36-hour forecasts using 1100 and 2300 UTC LAPS meteorology • Subgrid-scale module for near-road impacts
Evaluation	
• Comparison of peak-daily air quality concentrations with observations; limited comparison of LAPS winds with observations • Model evaluation done for specific case studies • Some 1-hour observed and modelled time series analysised	• Daily and monthly verification METAR/SYNOP surface observations, rawindsondes, pilot balloons, vertical profilers, AMDAR and EPA meteorological and air quality datasets • Detailed case studies conducted as required • Statistical analysis tools to look at long-term performance trends • Cluster analysis used to test match between observed and modelled 1-hour air quality time series

Data Packets	
• Data archived in native formats of current models (LAPS—NetCDF, CIT—ASCII and FORTRAN binary)	• Data archived in unified NetCDF data packets • Packets distributed via ftp or CD-ROM. Offline CTM simulations possible from archived dataset • Graphics of daily forecasts and verification available to EPAs via website, e-mail, ftp

EPA Victoria and CSIRO, with support from NSW EPA, have undertaken emission inventory development. They have developed the simple emissions inventories of the Pilot Scheme into comprehensive emissions inventories and have updated them for Victoria and NSW. The new inventories use size-fractionated and speciated particle emissions, 0.01° gridded area sources over the densely populated regions, 0.05° gridded area sources in rural areas, and meteorologically dependant emissions are now modelled for each forecast, based on input data from the LAPS predictions. A more detailed description of the emissions inventories is given in **Chapter 3—The Emissions Inventory Model**.

A power-based vehicle-emissions model has been developed at CSIRO to generate road-specific vehicle emission fluxes for the purpose of near-road impact modelling. This module is available to be used in the CTM and has been demonstrated for Sydney. It is now ready for application within the AAQFS system. The details of the model are described in **Section 5.4 Power-Based Motor Vehicle Emissions**.

Based on a public-domain California Institute of Technology model, the CTM has been custom built for the project using well established, state-of-the-art methodologies (Cope *et al.*, 1998). A notable inclusion to the CTM is the Generic Reaction Set (GRS) photochemical mechanism (Azzi *et al.*, 1992), a highly condensed (seven species and seven reactions) photochemical transformation mechanism featuring minimal computational overhead. Particle transformation is modelled by a modal-based particle scheme. The transport fields are updated every 60 minutes. The CTM simulations use a 0.05° outer grid, with nested 0.01° inner grids for major urban areas and have 17 vertical levels. Recently the GRS photochemical mechanism has been updated and enhanced. It now includes 12 species and 14 reactions. Although its mechanism is larger, it is still highly condensed. It is now ready for testing in specific regions within the AAQFS system. Alternative chemistries and their strengths and weaknesses are discussed in **Section 5.1 The Generalized Reaction Scheme (GRS) Options**.

Both the meteorological and air quality forecasts are the subject of on-going and case-specific validation. This is done through comparison of LAPS meteorological fields with METAR/SYNOP (near-surface) and AMDAR (vertical profile from commercial aircraft) data and meteorological observations from the EPA monitoring networks. Air quality forecasts are compared to 1-hour EPA observations for NO_x (both as NO and NO_2) and O_3. This has been expanded to include SO_2, PM10, PM2.5, CO and, if available, non-methanic hydrocarbons. Critical to the validation process has been the availability of EPA datasets by the end of each forecast period, enabling the on-going validation to be substantially automated. Recent examples of the on-going validation for AAQFS are described in the next section; examples of case-specific validation will be given in **Chapter 7—Case Studies with AAQFS**.

Data archiving has evolved from use of native system formats to unified NetCDF data packets (NetCDF was already used in the case of LAPS), which are accessible via GUI-driven Q&A software. Sufficient information is available in a data packet to enable the CTM to be run offline at a later time. The EPAs have access to the daily forecasts via the AAQFS Web Site and manage the dissemination of the forecast data. A detailed discussion of the Web Site, data archives and data dissemination is given in **Chapter 4—Outputs from AAQFS**.

2.2 Verification of Performance of the NWP

We now present statistical verification of the performance of the NWP and CTM. We start with the NWP. We can characterise the performance of the near-surface wind by a single variable called the Wind Index. The Wind Index is essentially the vector root-mean-square (rms) error for the wind at 10 m height. It is calculated by taking the square root of the sum of the squares of the rms errors between the modelled values and the measured values from the METAR/SYNOP network of the wind components u and v. The Wind Index is averaged over all stations in the domain and over 24 hours. Note that here we are not comparing predictions against data from EPA monitoring sites, which have been set up for different purposes to the METAR/SYNOP network. In particular EPA sites may be more subject to local winds such as nocturnal drainage flows. Figure 2.10 shows a plot of the Wind Index for the Victorian domain for the period January to the middle of May, 2001.

Figure 2.2.2 shows the Temperature Index for the Victorian domain. The Temperature Index is a single variable that characterises the performance of the near-surface temperature. It is calculated by taking the square root of the sum of the rms errors between the modelled values and the measured values from the METAR/SYNOP network for the screen temperature and screen dewpoint temperature. It also is averaged over the entire domain and over 24 hours.

The results shown in Figures 2.2.1 and 2.2.2 indicate that, in general, the LAPS model performs very well, and the performance is consistent over the whole period. The performance fluctuates because of the variation of the modelling difficulty with different weather systems, and the variation of errors in the initial conditions. Large excursions from the mean value in the temperature index are associated with the difficulty in forecasting rainfall and initialising the soil moisture. The trend in the Indices is attributable to seasonal changes; the weather is more variable during the summer.

Figure 2.2.3 shows the Wind Index and the Temperature Index for the upper air. In this case the indices represent the errors between the modelled values and the measured values along the three-dimensional flight path of commercial aircraft taking off from Melbourne Airport (AMDAR data). The Wind Index represents the vector wind rms error and the Temperature Index is the rms temperature error; there are no dewpoint temperature measurements available for the flights. The indices are averaged over all heights up to 5,000 m and over 24 hours (but the averages are weighted towards daylight hours; there are few flights overnight).

The results shown in Figure 2.2.3 are similar to those in Figures 2.2.1 and 2.2.2, except that the upper air wind errors are larger than those near the surface. This is expected because the wind speed increases with height. The upper air temperature errors are smaller than those near the surface. There are two reasons for this. Firstly, the upper air Temperature Index does not contain the dewpoint temperature, which is difficult to model. Secondly, the upper air is thermally stably-stratified to a greater extend than the near-surface. Again there is a trend for decreasing rms errors with time, which we attribute to seasonal changes.

The ventilation is displayed in Figure 2.2.4. Ventilation is the product of the height of the planetary boundary layer times the average wind speed within the planetary boundary layer. This variable is an important predictor of air pollution potential. It quantifies the amount of mixing available to dilute pollutant concentrations. Smaller values of ventilation indicate higher pollution potential. The comparison of the modelled and observed values shown in Figure 2.2.4 show the ventilation trends are quite well captured by the model. There is a small bias for the model to over-predict the ventilation because of a slight bias towards dryness in the model.

Figures 2.2.5–2.2.6 are the same as Figures 2.2.1–2.2.4, except for the NSW domain. If we compare Figures 2.2.5–8 with Figures 2.2.1–2.2.4, we see that the errors are less for the NSW domain compared to the Victorian domain. We have observed this feature before. In Victoria the presence of Port Phillip Bay makes the meteorology more complicated compared to the NSW region where the coastline is oriented approximately northeast-southwest over the domain. The consistent performance of the LAPS model is noted. Again we see a slight trend for decreasing errors with time. Of particular interest is the excellent agreement between the predicted and measured ventilation.

A summary of the performance statistics for the NWP component (the LAPS model) is given in Table 2.2.1. The results are similar to those obtained for the two-week validation period in November 2000 (see Manins, 2001).

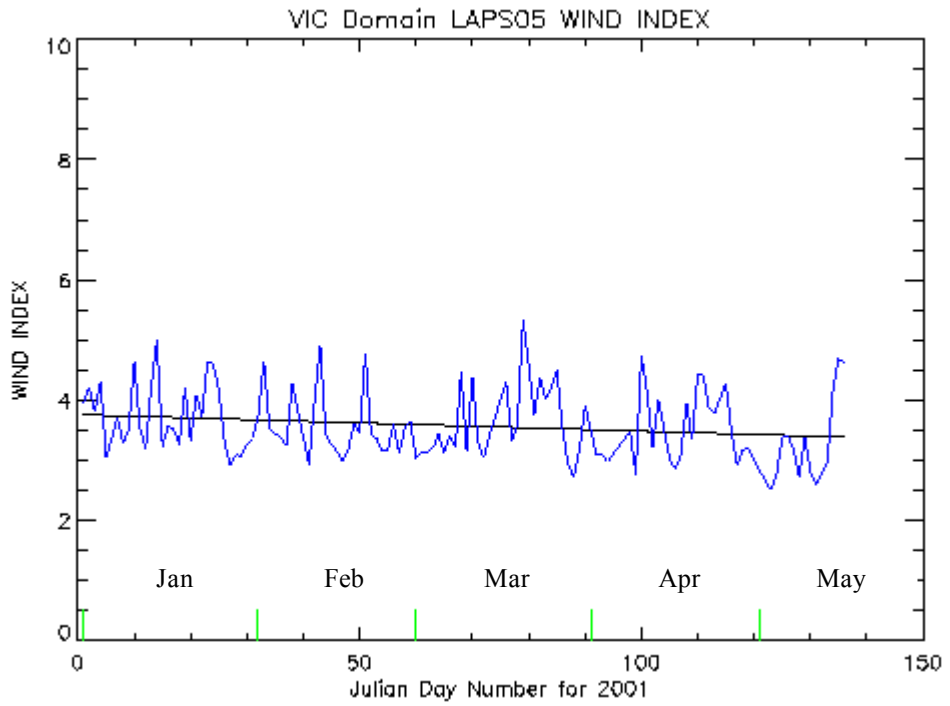

Figure 2.2.1. The Victorian domain Wind Index showing the vector wind rms error at 10 m height as a function of time.

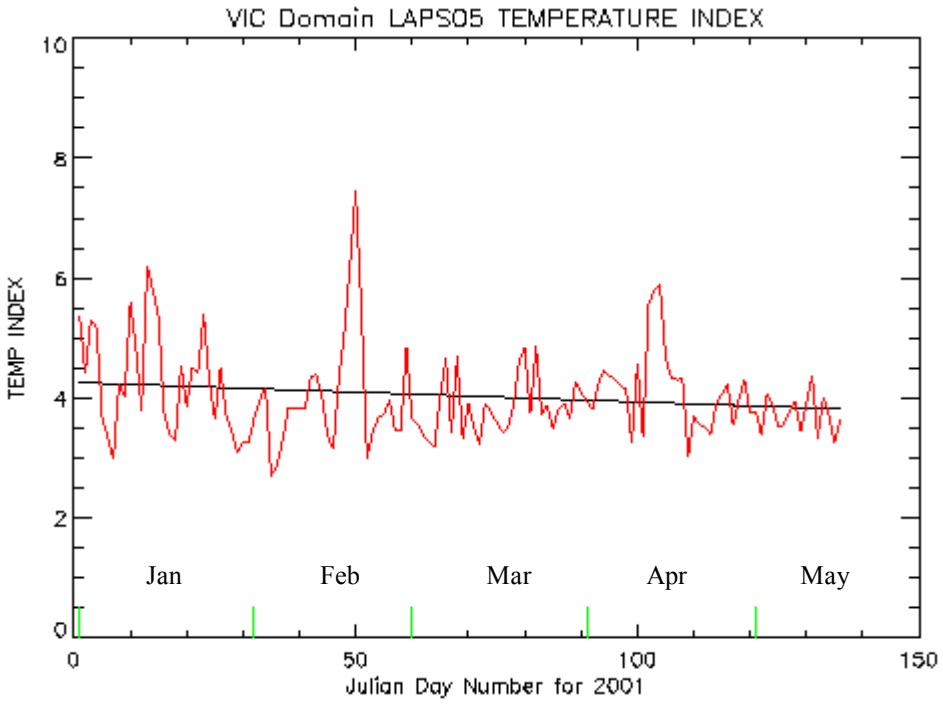

Figure 2.2.2. The Victorian domain Temperature Index showing the rms error for both the screen temperature and screen dewpoint temperature as a function of time.

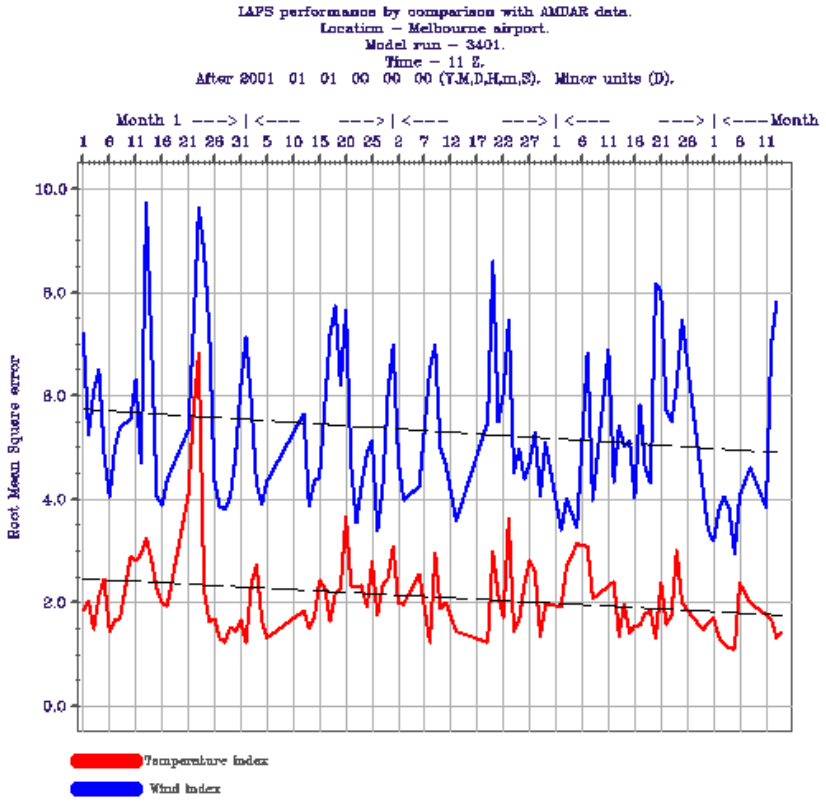

Figure 2.2.3. The Victorian domain Wind and Temperature Indices along the flight paths of commercial aircraft as a function of time.

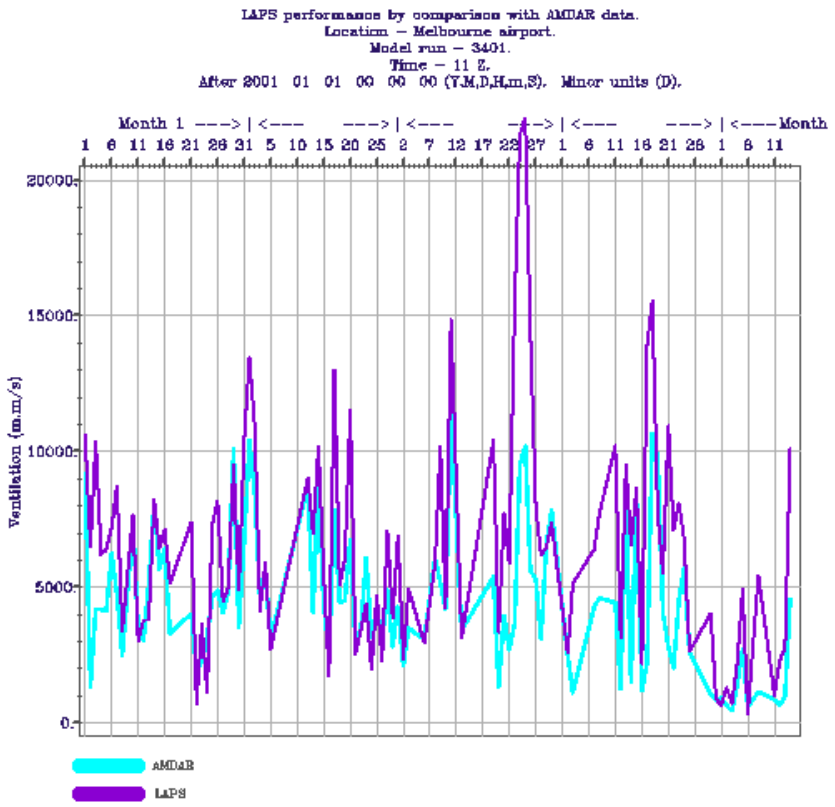

Figure 22.4. Comparison of the Victorian modelled and measured values of ventilation as a function of time.

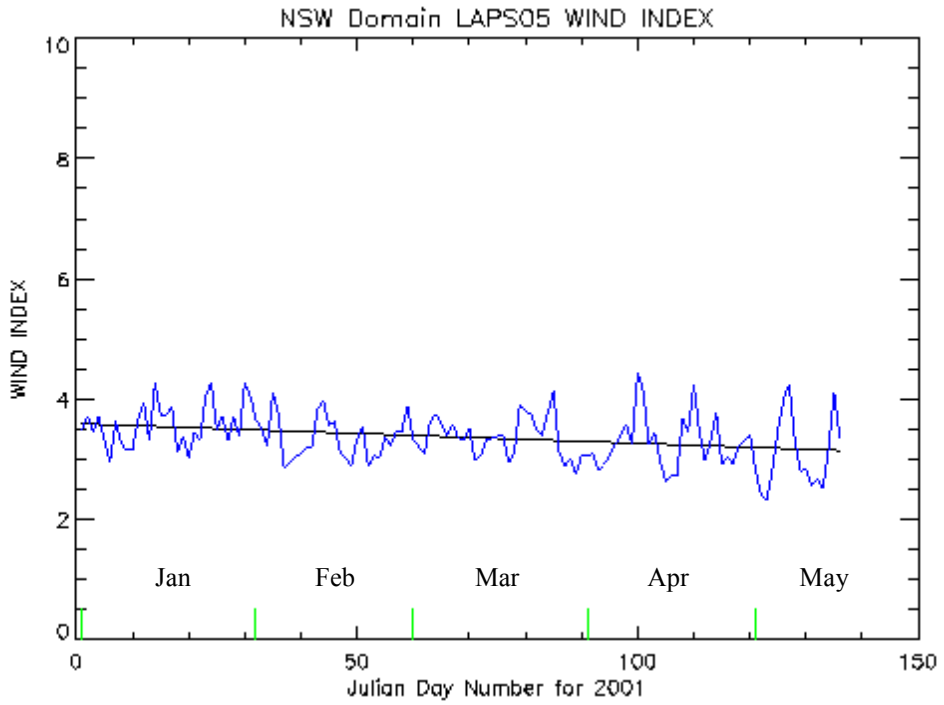

Figure 2.2.5. The NSW domain Wind Index showing the vector wind rms eror at 10-m height as a function of time.

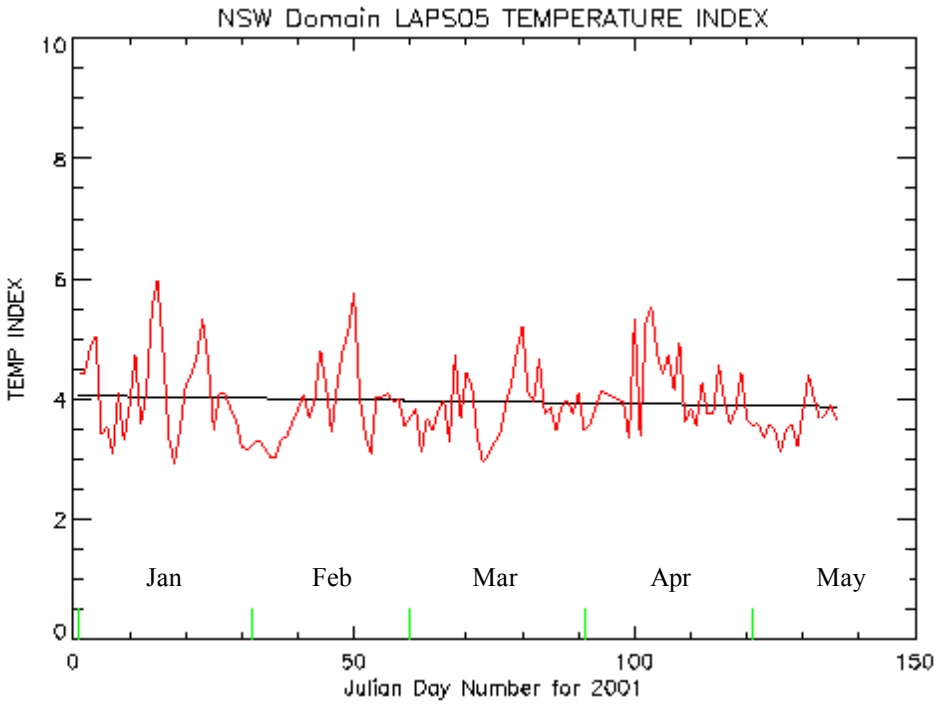

Figure 2.2.6. The NSW domain Temperature Index showing the rms error for both the scre en temperature and screen dewpoint temperature as a function of time.

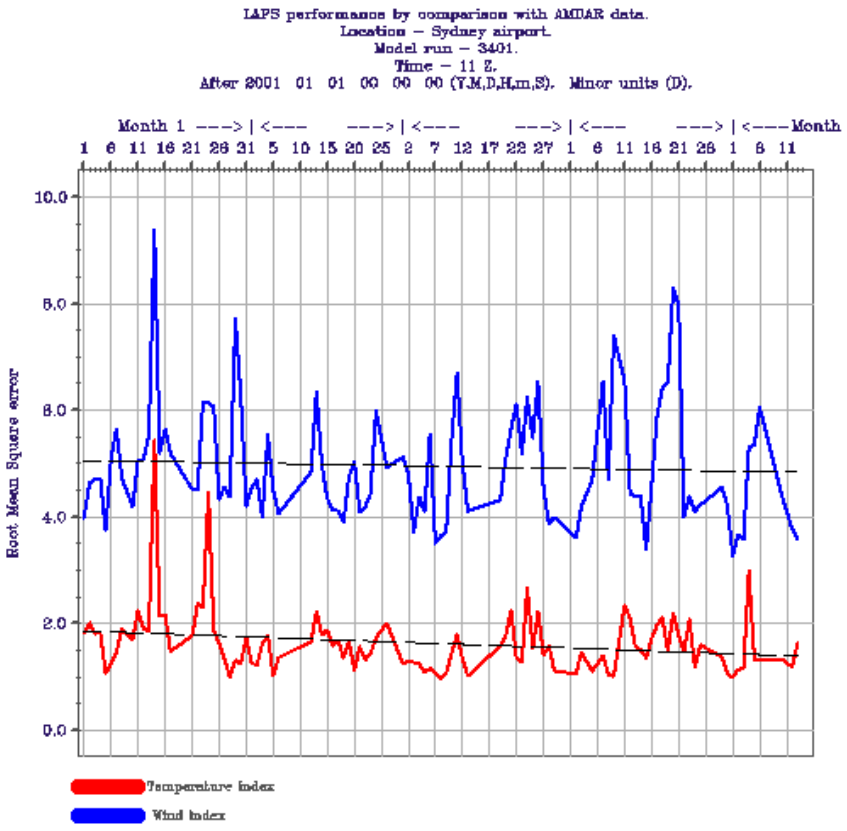

Figure 2.2.7. The NSW domain Wind and Temperature Indices along the flight paths of commercial aircraft as a function of time.

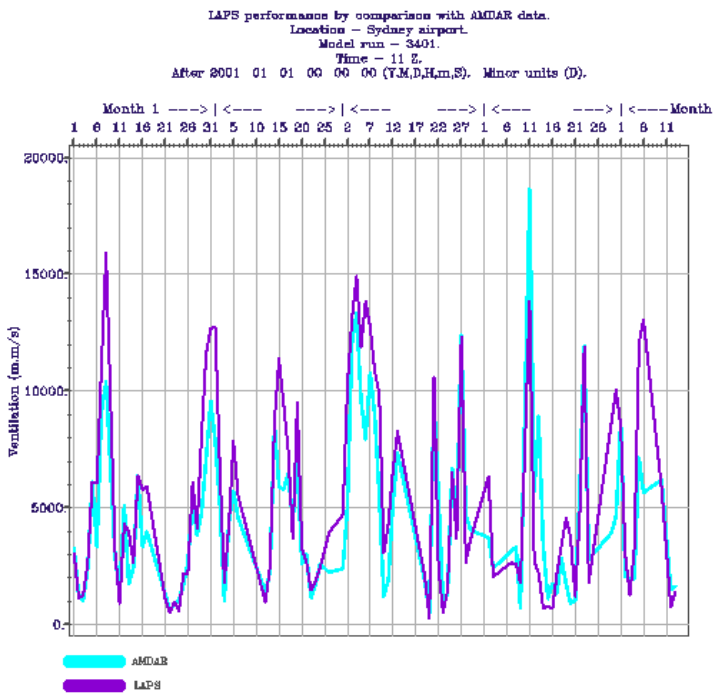

Figure 2.2.8. Comparison of the NSW modelled and measured values of ventilation as a function of time.

Table 2.2.1: Statistical summary of NWP performance

Victoria Statistical Summary (January to the first half of May, 2001)		
Variable	*Mean Bias*	*Mean Correlation*
u-component (m/s) at 10 m	-1.12	0.601
v-component (m/s) at 10 m	0.22	0.587
Screen temperature (^{o}C)	1.11	0.868
Screen dewpoint temperature (^{o}C)	0.24	0.659
	Wind Index (m/s)	*Temperature Index (°C)*
Mean RMS Error (METAR/SYNOP comparison: near-surface data)	3.57	4.04
Mean RMS Error (AMDAR comparison: upper-air data)	5.33	2.12

Table 2.2.1: (continued) Statistical summary of NWP performance

NSW Statistical Summary (January to the first half of May, 2001)		
Variable	*Mean Bias*	*Mean Correlation*
u-component (m/s) at 10 m	-0.27	0.561
v-component (m/s) at 10 m	0.06	0.544
Screen temperature (°C)	1.31	0.894
Screen dewpoint temperature (°C)	-0.11	0.768
	Wind Index (m/s)	*Temperature Index (°C)*
Mean RMS Error (METAR/SYNOP comparison: near-surface data)	3.37	3.96
Mean RMS Error (AMDAR comparison: upper-air data)	4.95	1.65

2.3 Verification of Performance of the CTM

In the next two Sections we assess the performance of AAQFS in forecasting primary and secondary gaseous and aerosol air pollution in Melbourne and Geelong, and then review the performance in the Sydney Region. In a later Section, we draw together the findings for both Melbourne and Sydney and present some conclusions about the current status of the System. This assessment is for the performance of the System as a whole: the coupled inventory-meteorology-chemical transport components of AAQFS.

Before the results of the performance assessment are presented, it should be recalled that the Demonstration System is effectively a new system (even though it is based on a public domain model and some of the individual components have been under development for some time as part of other, ongoing projects). Since the System is new, it is important to use a range of performance indicators, which examine all aspects of system performance (not just forecasting performance). A hierarchical approach has been taken in this regard. At the first level, we have assessed the air pollution forecasts for consistency. This has been undertaken through careful review of the time and spatial distribution of the modelled air pollutant fields and through diagnostic testing in which model inputs are perturbed and outcome gradients reviewed. Inconsistencies have been identified and then examined in detail to determine the responsible component(s) of the system.

The second level of performance evaluation has involved looking at trends in long-term (*i.e.* monthly and seasonal) performance statistics through consideration of observed and modelled cumulative frequency distributions and through the use of daily average bias. Such information has been used to examine systematic differences between forecasts and observations, and to identify underlaying processes that may need improvement or modification.

The third level of evaluation has involved a review of system performance in forecasting 'high-percentile events'. This is after all, one of the primary purposes of the forecasting system. A number of case studies described in **Chapter 7—Case Studies with AAQFS** correspond to some of the significant events that have been observed during the course of the Demonstration Period. We have also examined the ability of the System to forecast cases of less significant but still elevated air pollution concentration.

During the course of the project, results have been reviewed for the period 17–29 November 2000, for March 2001 and for the period 1–30 June and 1–20 July 2001 (hereafter referred to as June–July). The November 2000 period (which is discussed in Manins, 2001) provided an initial indication of performance for the demonstration system following its commencement in August 2000. The March period followed three months of diagnostic evaluation in which system performance for photochemical smog was assessed and a number of important system improvements undertaken. One of the outcomes of this diagnosis and assessment cycle was the identification and elimination of several factors, which in combination initially caused the system to severely under-predict photochemical smog. As will be demonstrated in the following sections, the system now has the capability to accurately predict impending photochemical smog episodes. The June–July period was selected in order to assess system performance for forecasting the concentrations of primary gaseous pollutants under low-ventilation wintertime conditions. This period was also selected in order to examine the impact of aerosol emissions from domestic-sector wood combustion on forecasts of PM2.5 and PM10. We are partway through this current cycle of assessment, with a number of changes made to increase the minium levels of dispersion under low-ventilation conditions. However, as will also be evident, there is currently a chronic problem with the over-prediction of aerosol concentrations during the winter months. This problem appears to be related to the outdated emission factors in the wood combustion emissions model. EPA Victoria has just concluded a study of these factors and found that, from recent scientific evidence, those currently employed should be reduced to 60% of current values on average, and to 30% of current values for open fires. A trial using the new emission factors is underway but is too late to be reported here.

In the next section we investigate system performance for forecasting Melbourne and Geelong regions. A review of AAQFS forecasting performance for the Sydney region then follows.

2.4 CTM performance in Melbourne and Geelong

2.4.1 Primary gaseous pollutants

In this section we review model performance for forecasting the concentrations of primary gaseous pollutants in the Melbourne and Geelong region. The pollutants, under consideration here are nitrogen-based compounds (NO_y = NO_x + other nitrates; NO_x= NO + NO_2), carbon monoxide and sulfur dioxide. Although NO_y is not a 'NEPM criteria pollutant', it is nevertheless a useful species to validate, being (i) quasi-conserved; (ii) a useful tracer for the urban (*i.e.* motor-vehicle dominated) plume; and (iii) a pollutant that is generally the most accurately inventoried. Carbon monoxide (CO) is the second primary gaseous pollutant that we consider here. Carbon monoxide is a criteria pollutant with an air quality standard (AQS) of 9 ppm (9000 ppb) for an 8-hour average. We consider here model performance for both 1-hour and running 8-hour averages. The former is also considered because we are interested in evaluating short-term model dynamics and its impact on the 8-hour averaged CO concentrations. Sulfur dioxide (SO_2) is also a NEPM pollutant with an AQS prescribed for 1-hour, 24-hour and 12-month averaging periods. We restrict consideration here to a 1-hour averaging period.

Time series plots. A useful qualitative indication of system performance may be gained from a consideration of 1-hour concentration time series plots. Plots of NO_y are shown in Figures 2.4.2 and 2.4.3 for Box Hill, Alphington and Brighton monitoring stations for March and June–July 2001. Referring to Figure 2.4.1, it can be seen that the selected monitoring stations are representative of a coastal site (Brighton), an inner northeastern site (Alphington) and an

outer eastern site (Box Hill). Note that the gridded forecast concentrations have been matched to the location of each monitoring site using bilinear interpolation. The impact of sharp gradients within the concentration field is examined through consideration of the concentration range predicted within ± 1 cell (*i.e.* the 9 nearest cells; ± 1½ km) of a monitoring site. Plots of SO_2 are shown in Figure 2.4.4 for Alphington, Paisley and South Geelong monitoring stations (see Figure 2.4.1 for locations). Time series plots for CO are not shown because they are similar to the NO_y plots.

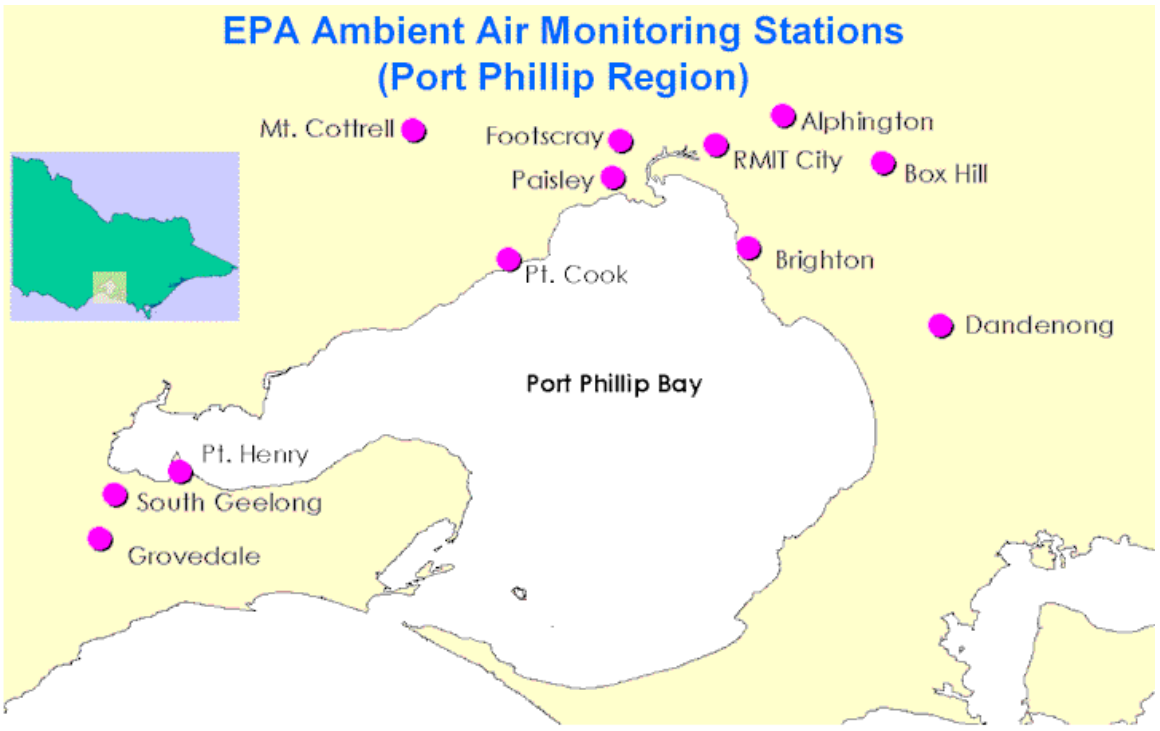

Figure 2.4.1. Location of EPA Victoria monitoring network for Melbourne/Geelong region (EPA Victoria image).

Figure 2.4.2 and Figure 2.4.3 provide qualitative examples of the typical level of skill, which may be expected from a state-of-the-art Eulerian grid model when attempting to match observed concentrations of a primary gaseous pollutant in time and space within an urban environment (Harley *et al.*, 1993; Hedley *et al.*, 1997). In particular, it can be seen that both observed and forecast NO_y time series show a cycle of strong diurnal variation. The System has had good success in matching some of the diurnal peaks (*e.g.*, Figure 2.4.2 – Brighton, hours 1–73), however, it has missed other peaks (*e.g.*, Figure 2.4.3 – Box Hill, hours 673–1067). Superimposed on the diurnal cycle are periods of low concentration extending for one or more days (*i.e.* between hours 241 and 313 in Figure 2.4.2), which correspond to conditions of greater ventilation. These are generally well reproduced by the system. A seasonal cycle is also apparent from a comparison of Figure 2.4.2 and Figure 2.4.3. Conditions of greater stability/lower ventilation in June and July lead to more frequent periods of elevated NO_y in both the observations and the forecast.

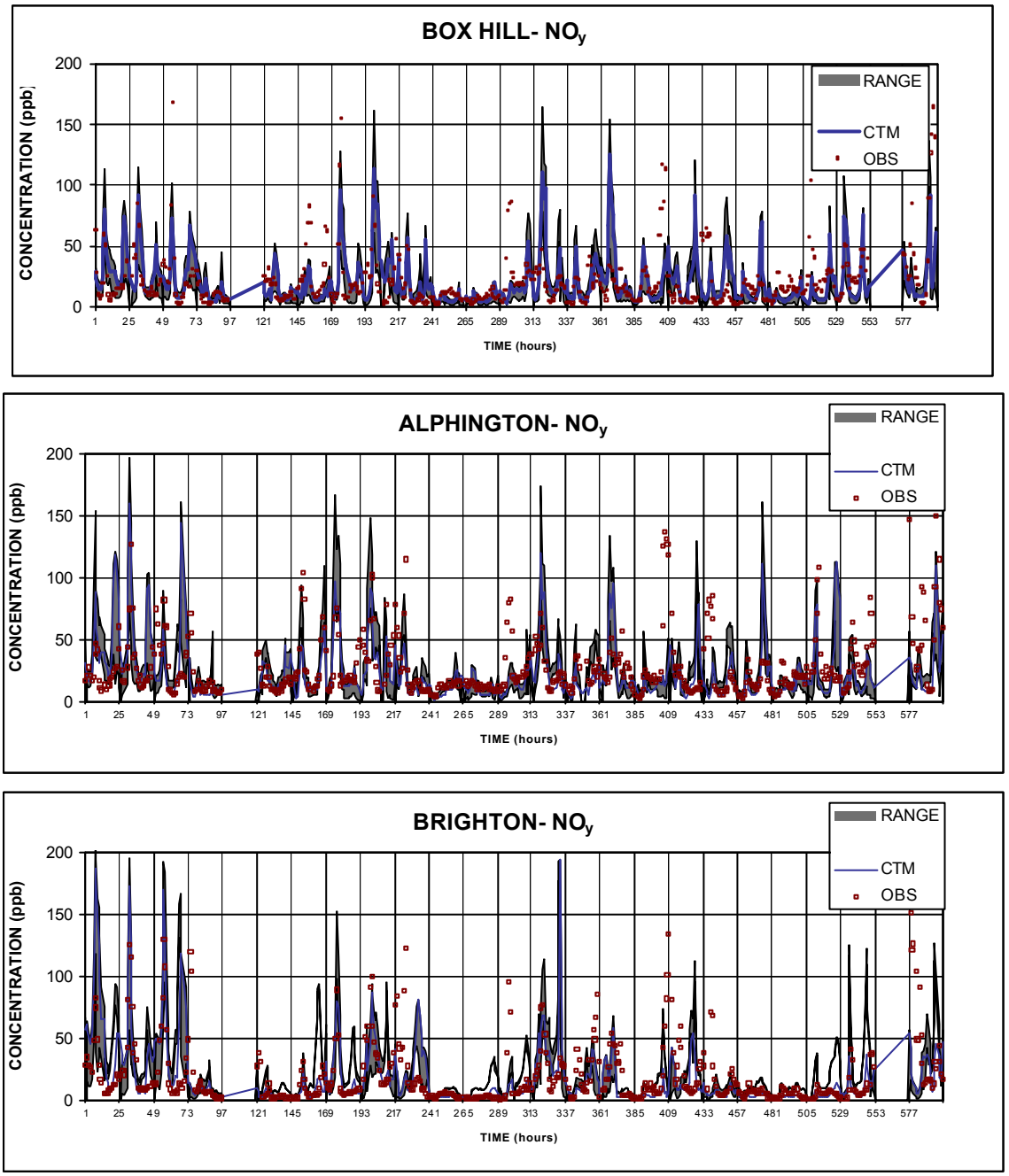

Figure 2.4.2. Observed vs modelled concentration time series of nitrogen compounds (NO_y) for Box Hill, Alphington and Brighton montoring stations March 2001. Forecast concentrations are interpolated to the observation site. Range corresponds to the minimum and maximum forecast concentrations within ± 1½ km of the observation site.

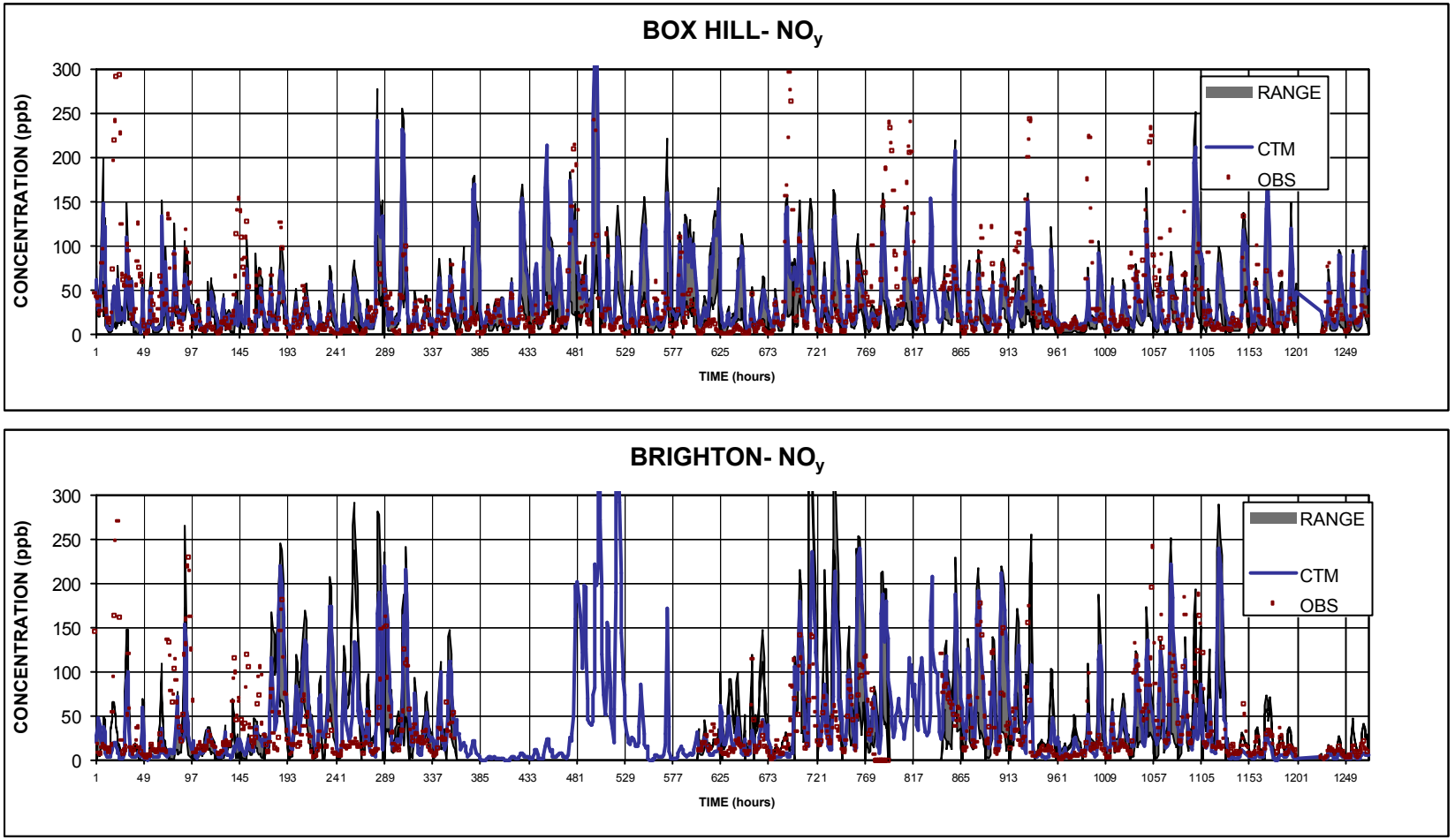

Figure 2.4.3. Observed vs modelled concentration time series of nitrogen compounds (NO_y) for Box Hill and Brighton montoring stations 1–30 June; 1–20 July 2001. Forecast concentrations are interpolated to the observation site. Range corresponds to the minimum and maximum forecast concentrations within ± 1½ km of the observation site.

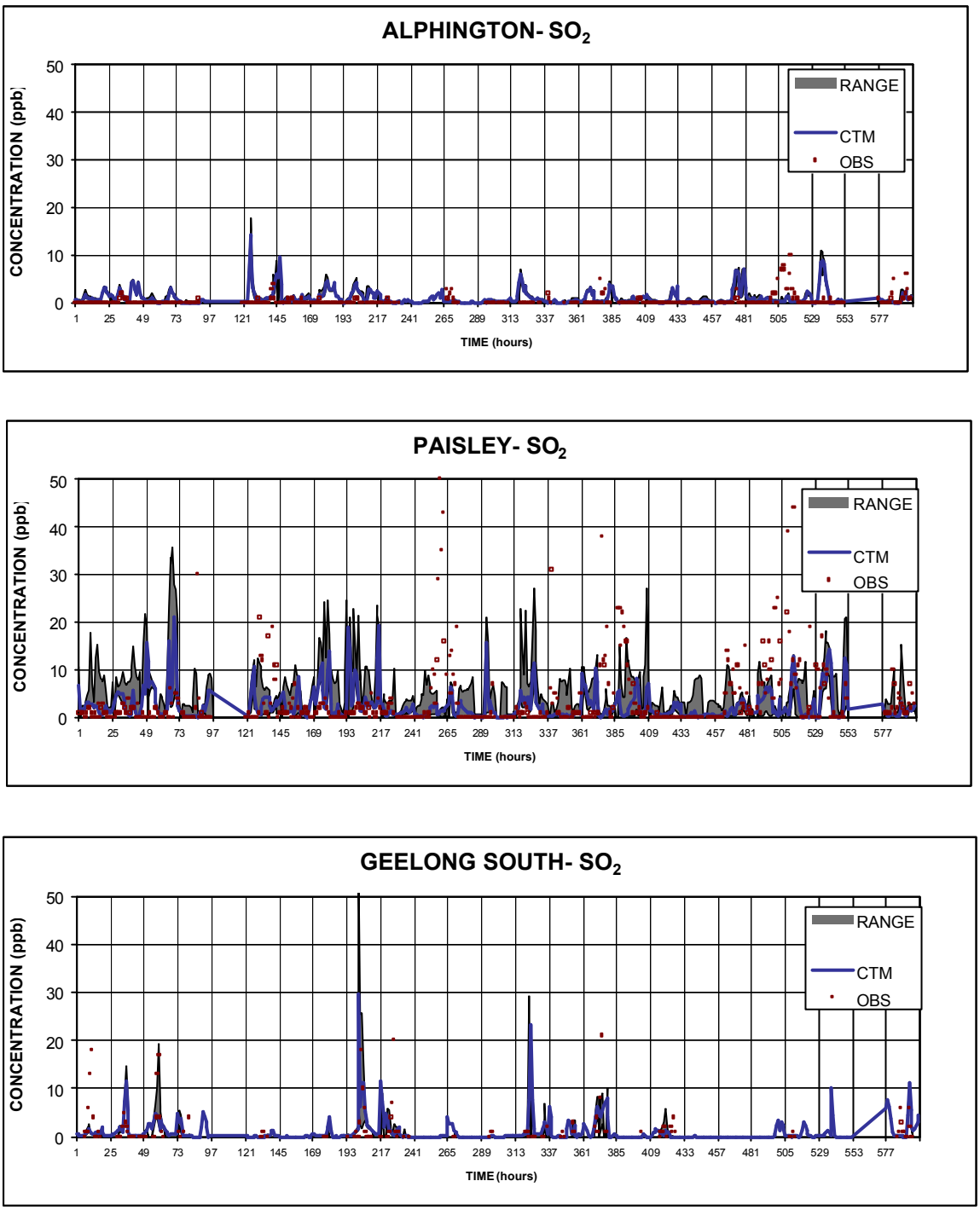

Figure 2.4.4. Observed vs modelled concentration time series of sulfur dioxide (SO_2) for Alphington, Paisley and Geelong South montoring stations March 2001. Forecast concentrations are interpolated to the observation site. Range corresponds to the minimum and maximum forecast concentrations within ±1½ km of the observation site.

The SO_2 time series plot for Alphington (Figure 2.4.4) is indicative of the generally low background SO_2 concentrations that are present in urban Melbourne. On the other hand, Paisley monitoring station, which is located within the vicinity of a large industrial complex occasionally observed 1-hour SO_2 peaks of greater than 50 ppb during the March period. It

can be seen that the system has had difficulties in matching the highest observed SO_2 concentrations. This is because the 1-km AAQFS urban grid cannot adequately resolve the point source SO_2 plumes responsible for the observed peaks. However, the system has had more success in reproducing the (smaller) SO_2 peaks observed at South Geelong. In this case, the monitoring station is in the 'far field' relative to the SO_2 sources in Geelong, Point Henry and Anglesea, and thus the system is better able to represent the characteristics of the more dispersed SO_2 plumes.

Frequency Distributions. When long-term time series of pollutant concentrations are available, it is recommended (Seigneur *et al*., 2000) that frequency distributions of observed and modelled concentration be compared to assess model performance in reproducing observed characteristics such as the mean, mode and variational properties. Given our requirements of forecasting extreme air pollution events, it is of particular interest to ascertain how the system has performed in predicting the upper percentiles (50^{th} to 100^{th} percentiles) of the observed frequency distribution.

An example of the observed and modelled upper percentiles of 1-hour NO_y is given in Figure 2.4.5 for Alphington, Box Hill and Brighton monitoring stations for March 2001 and June–July 2001. The distributions have been generated by ranking, by magnitude, hourly concentrations for the entire time period. Thus the observations and predictions are matched in space (bi-linear interpolation) but not in time. It can be seen that the system has done a very good job at reproducing the observed percentiles. Note how the system has reproduced the observed increase in the concentrations by a factor of two, when going from the autumn conditions in March to the more stable wintertime conditions of June and July. This indicates that the system has been able to successfully reproduce a major inter-seasonal variation of the observed concentration distribution. The results of Figure 2.4.5 are summarised, and expanded to include additional stations in Figure 2.4.6, where observed and modelled 50^{th}, 90^{th}, 95^{th}, 99^{th}, 99.9^{th} and 100^{th} percentile NO_y and CO concentrations are presented as scatter plots. Scatter plots for SO_2 are shown in Figure 2.4.7. The normalised bias is defined as

$$B_n = \frac{P - O}{O} \times 100\% \qquad (1)$$

where P is the modelled concentration and O is the observed concentration. The normalised bias for each pollutant and percentile is given in Table 2.4.1.

With respect to the scatter plots of NO_y percentile, it can be seen that the system has generally been able to reproduce the observed distribution with only a small (< 20%) negative bias for all of the percentile levels. This compares very well with the work of Hurley (2000), who modelled Melbourne's air quality for a one-month period (December 1998) using TAPM driven by analysed meteorological fields rather than forecast fields. He found a bias of the all-station mean observed and predicted 99.9 percentile of -7.8%, and a bias for the maximum NO_y concentration of only -1%. A one-year simulation of air quality in London undertaken by Carruthers *et al*., (1999) using the ADMS-Urban model also yielded similar results with mean biases for the average, 98^{th}, 99^{th} and 100^{th} percentile 1-hour NO_y concentrations lying within the range 1 to -20%. Thus AAQFS when operating in forecast mode has performed similarly to models that have either been driven by 6-hourly meteorological analyses (TAPM), or by meteorological observations.

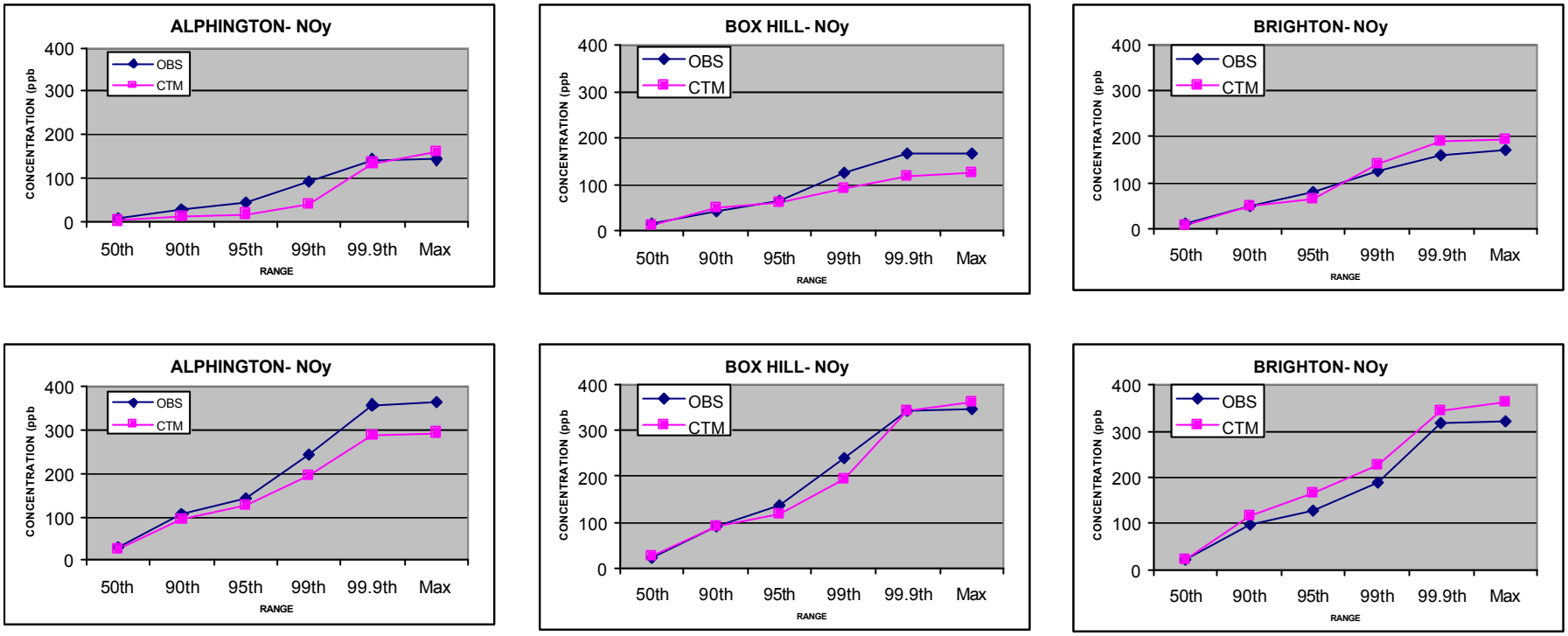

Figure 2.4.5. Observed (OBS) and forecast (CTM) cumulative frequency distributions of 1-hour NO_y for selected monitoring stations for March 2001 (top) and June–July 2001 (bottom). See map - Fig. 1 for station locations.

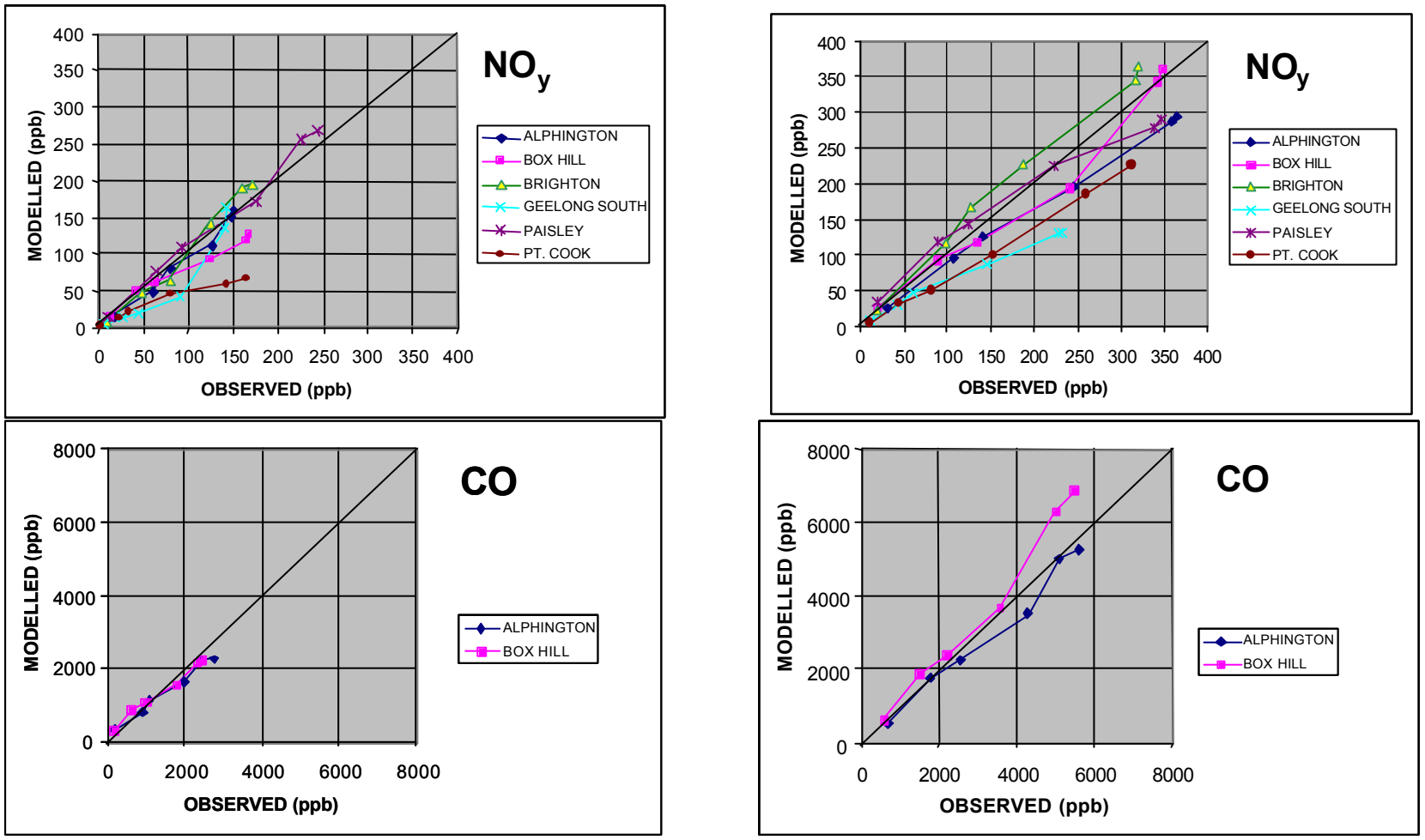

Figure 2.4.6. Plots of observed and forecast percentiles of the NO_y and NO_2 concentration distribution (50^{th}, 90^{th}, 99^{th}, 99.5^{th}, 99.9^{th}, and 100^{th} percentiles) for March 2001 (left) and June–July 2001 (right) – for selected monitoring stations in the Melbourne and Geelong region.

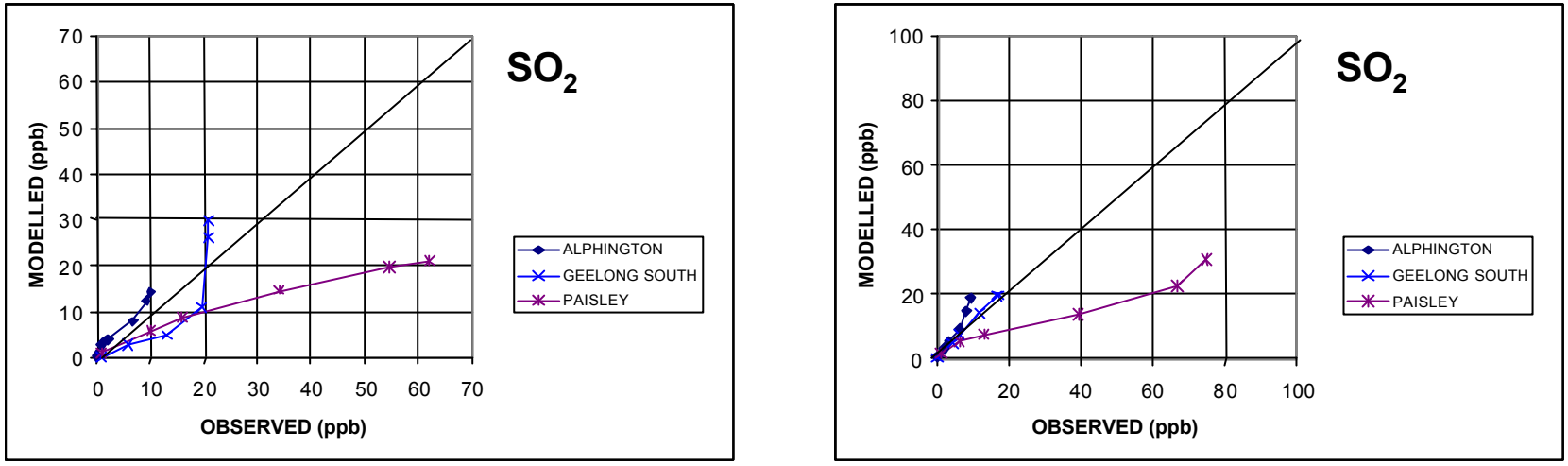

Figure 2.4.7. Plots of observed and forecast percentiles of the SO_2 concentration distribution (50^{th}, 90^{th}, 99^{th}, 99.5^{th}, 99.9^{th}, and 100^{th} percentiles) for March 2001 (left) and June–July 2001 (right) – for selected monitoring stations in the Melbourne and Geelong region.

Table 2.4.1. Percentage normalised bias for NO_y, NO_2, O_3, CO, PM2.5, PM10 and SO_2 for Melbourne— March 2001 and June–July 2001.

	NO_y bias (%)		NO_2 bias (%)	
Percentile	March	June/July	March	June/July
50	-16.4	5.5	6.1	-5.7
90	-9.7	2.5	18.2	-0.5
95	-11.9	-3.0	22.1	5.5
99	-16.8	-14.2	35.0	19.0
99.9	-8.1	-15.0	52.0	41.8
100	-6.8	-13.3	57.0	43.1
	O_3 bias (%)		**CO bias (%)**	
Percentile	March	June/July	March	June/July
50	76.6	16.5	2.3	-8.7
90	19.5	15.4	-14.0	9.4
95	0.3	13.5	-16.2	-2.0
99	3.2	4.7	-25.1	-8.8
99.9	0.6	5.7	-5.6	12.2
100	-1.2	8.8	-5.6	9.2
	PM2.5 bias (%)		**PM10 bias (%)**	
Percentile	March	June/July	March	June/July
50	-75.5	35.3	-39.2	64.4
90	-48.6	157.9	-29.4	200.5
95	-43.5	167.7	-28.0	210.6
99	-1.8	136.2	-14.7	212.6
99.9	28.4	144.3	-29.5	256.6
100	29.6	111.9	-33.9	260.4
	SO_2 bias (%)			
Percentile	March	June/July		
50	N/A	N/A		
90	-18.0	30.4		
95	-34.4	4.8		
99	-34.2	-26.6		
99.9	-24.0	-27.9		
100	-26.5	-22.3		

Scatter plots of observed and modelled CO concentration percentiles also indicate that the system is performing well at reproducing the peak concentrations of this pollutant (Figure 2.4.6, bottom). On the other hand, it can be seen that, as discussed previously, peak 1-hour SO_2 is under-predicted at Paisley monitoring station (Figure 2.4.7).

Residual analysis: Following the recommendations of EPA (1992) and Seigneur *et al.* (2000), quantification of system performance on an hourly and daily basis has been undertaken using the following statistical measures.

The first measure, **fractional bias**, is defined as

$$B_f = \frac{2}{N}\sum_{i=1}^{N}\left(\frac{P_i - O_i}{P_i + O_i}\right), \quad (2)$$

where N is the number of model (P_i), observation (O_i) pairs. Note that B_f varies symmetrically between -2 and 2. Also note that a factor of two difference between observed and modelled values corresponds to a fractional bias of ± 2/3 (0.667), a factor of five difference corresponds to a fractional bias of ± 4/3 (1.333), and a factor of 0.25 corresponds to a fractional bias of ± 2/9 (0.2222).

A second residual analysis statistical measure is the **fractional gross error**, which is defined similarly to B_f, except that the bounds of E_f are 0–2.

$$E_f = \frac{2}{N}\sum_{i=1}^{N}\left|\frac{P_i - O_i}{P_i + O_i}\right|. \quad (3)$$

In addition to these measures, we also report the **coefficient of determination**, which provides an indication of the correlation or degree to which the observations and system follow the same pattern (but not the amplitude).

$$r^2 = \frac{\left[\sum_{i=1}^{N}(P_i - \overline{P})(O_i - \overline{O})\right]^2}{\sum_{i=1}^{N}(P_i - \overline{P})^2 \sum_{i=1}^{N}(O_i - \overline{O})^2}, \quad (4)$$

where $\overline{P}$ is the predicted mean concentration and $\overline{O}$ is the observed mean.

Table 2.4.2. Mean fractional bias, gross error and coefficient of determination for 1-hour concentrations of selected pollutants— March 2001 and 1–30 June, 1–20 July 2001.

	March 2001			June/July 2001		
Species	Fractional bias	Gross Error	Coeff.Det.	Fractional Bias	Gross Error	Coeff. Det.
NO_y	-0.28	0.67	0.40	-0.03	0.71	0.39
NO_2	-0.08	0.58	0.46	-0.05	0.53	0.39
O_3	0.28	0.58	0.31	-0.25	0.89	0.24
CO	-0.32	0.68	0.55	-0.07	0.56	0.03
SO_2	-1.18	1.22	0.48	-0.12	0.76	0.19
PM2.5	-0.69	0.85	0.22	0.24	0.74	0.18
PM10	-0.68	0.82	0.41	0.48	0.78	0.16

Shown in Figure 2.4.8 is the mean (taken across all stations for a given hour) fractional bias for NO_y and CO for March 2001. Also shown is a running 24-hour average of the mean 1-hour fractional bias. A similar plot is provided for June–July in Figure 2.4.9. Note that all of

the statistics presented in this section are for observation/prediction couples that are paired in time and space (and based on one-hour data). The March and the June–July average fractional bias together with the fractional gross error and coefficient of determination are listed in Table 2.4.2.

It can be seen from Figure 2.4.8 that 1-hour NO_y, was, on the average, predicted with little bias at the beginning of March, and with an increasingly negative bias as the month progressed. The mean fractional bias for the month is -0.28 (25–50% under-prediction) and the mean fractional gross error is 0.67. The latter indicates an average variation between modelled and observed of approximately a factor of two. This level of variation, which is in part, caused by small mis-matches in reproducing the timing and magnitude of the observed NO_y concentration, is typical of the performance of air quality models when trying to match short-term near-source concentrations in time and space.

The fractional bias for NO_y is improved for June–July, particularly during the second half of the period (Figure 2.4.9). These improvements followed a number of adjustments that were made to the chemical transport model in order to improve the dispersion predictions under wintertime light-wind stable conditions. The mean fractional bias for June-July was -0.03, which is an excellent result.

It can be seen from Figure 2.4.8 that 1-hour CO was also under-predicted during March (by 20–50%) and that the bias was again reduced for the June–July period to an acceptable -0.069 (±15%). Again the noise level is of the order of two.

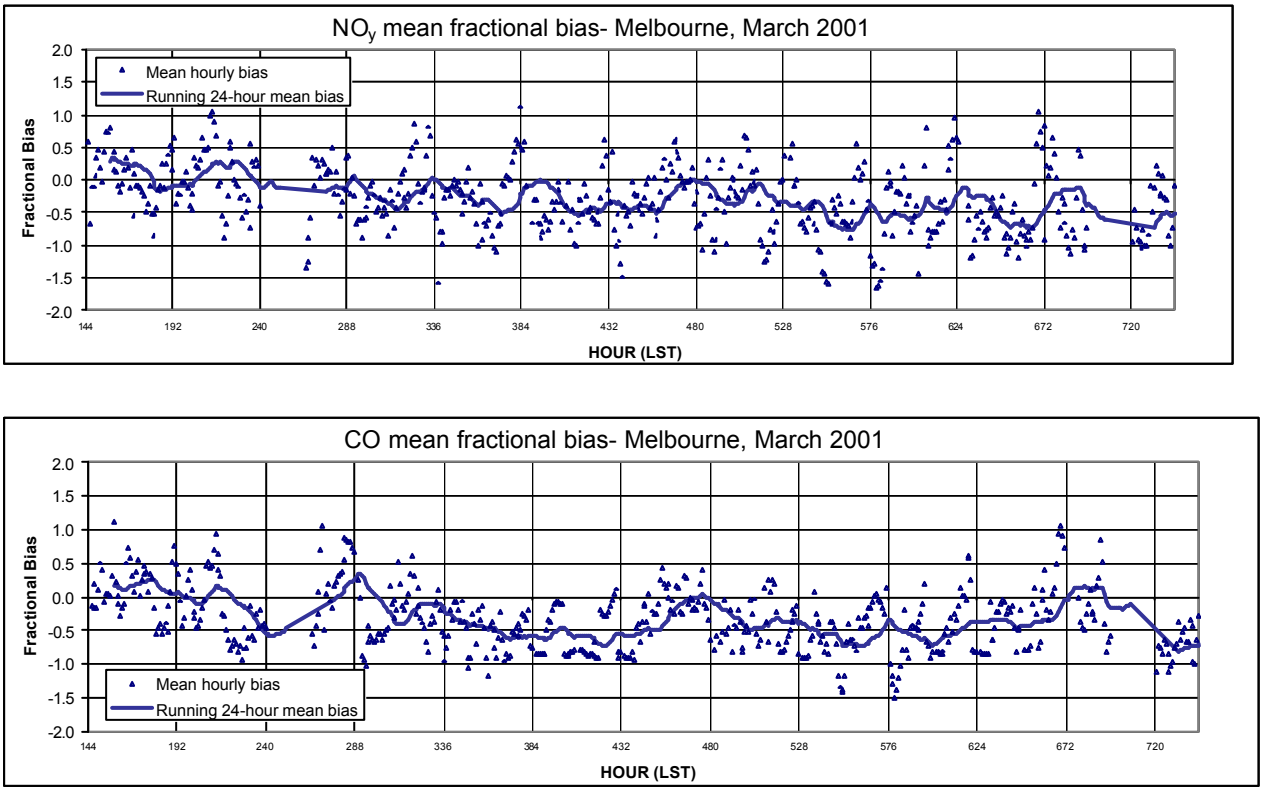

Figure 2.4.8. One-hour and running 24-hour mean of one-hour fractional bias for observed and forecast NO_y, and CO, Melbourne and Geelong monitoring stations, March 2001.

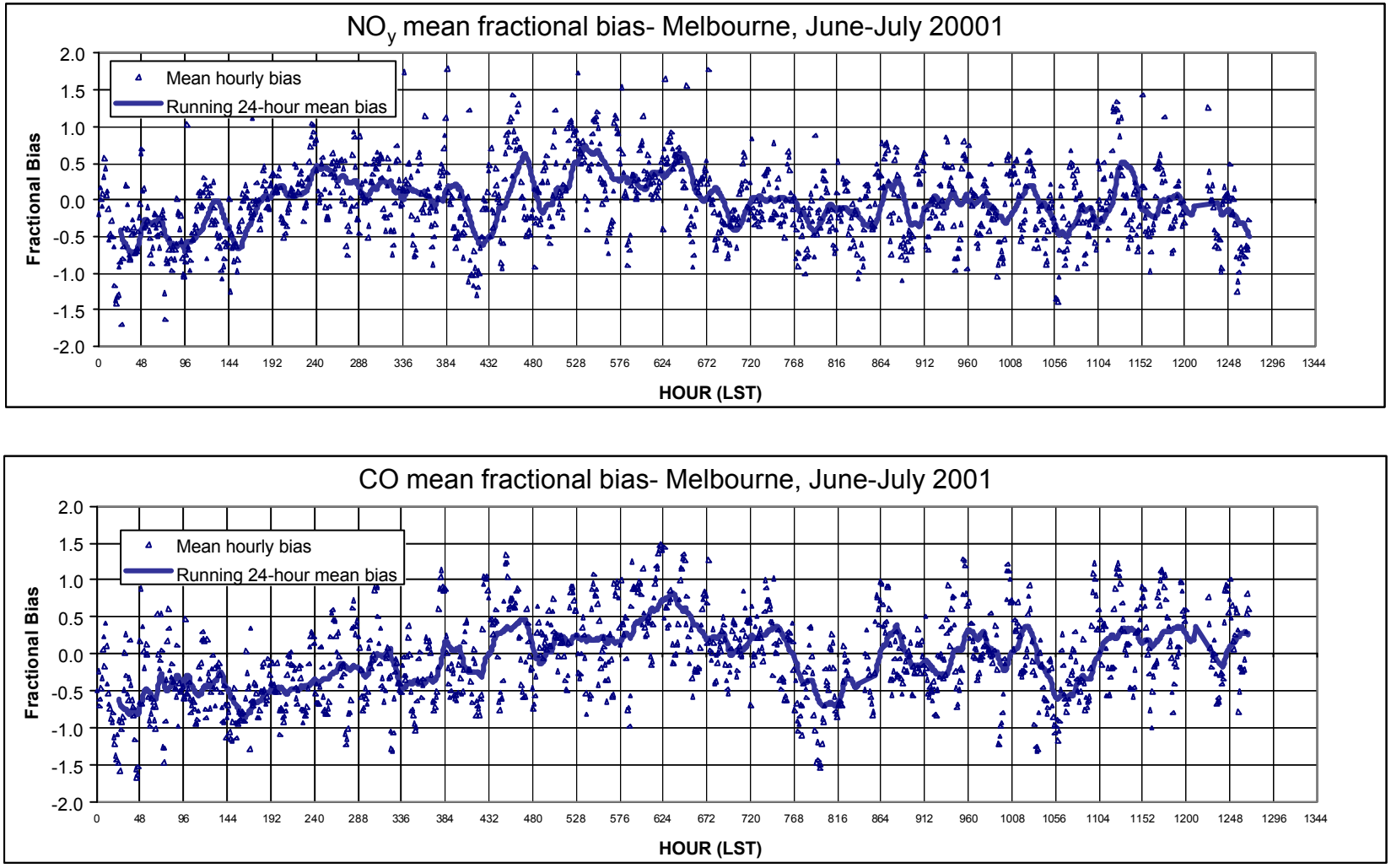

Figure 2.4.9. One-hour and running 24-hour mean of one-hour fractional bias for observed and forecast NO_y and CO, Melbourne and Geelong monitoring stations, June–July 2001.

Forecasting daily maxima. The evaluation presented in the previous Sections was undertaken in order to examine the ability of the System to reproduce the observed daily and monthly cycles of concentration. However, one of the principal aims of the system is to provide forecasts of peak concentrations. We examine here the system's ability to forecast peak daily concentrations of 1-hour NO_y, 8-hour CO (rolling averages) and 1-hour SO_2.

Shown in Figure 2.4.10 are plots of fractional bias of peak daily pollutant concentrations for NO_y, CO and SO_2 for March 2001 and June–July 2001. The mean fractional bias for NO_y is -0.07 (< 25% difference between observed and predicted on the average), which is an excellent result, although it can be seen from Figure 2.4.10 that peak NO_y was under-predicted in March and slightly over-predicted in July, thus leading to a reduced average result. The mean fractional gross error is 0.50 (predictions vary about the observed by about 70% of the observed concentration on the average), which is reduced compared to the fractional gross error of the 1-hour NO_y predictions.

The 8-hour CO fractional bias also shows a trend towards increasing positive bias over the three-month period (mean fractional bias is 0.15), although the mean fractional gross error (0.51) is comparable to NO_y. The fractional bias plot for daily peak 1-hour SO_2 indicates reduced performance for this pollutant. As has been explained in a previous section, the relatively poor performance for this pollutant stems from near-source impacts of SO_2 plumes on Paisley monitoring station.

An additional approach for appraising forecasting performance is through the use of contingency tables. As discussed in De Leeuw (2000), contingency tables are a tabulation of the number of correct and incorrect forecasts made over the course of a forecasting season. For example, shown in Table 2.4.3 is a contingency table of daily 1-hour NO_y forecasts for the March, and June–July periods. The contingency table has been generated by comparing the daily observed and forecast NO_y peaks at individual stations, thus assessing the System's ability to forecast, at a given monitoring station (*i.e.* paired in space), the potential for NO_y to exceed 100 ppb.

Table 2.4.3. Contingency table for the forecast of peak 1-hour NO_y > 100 ppb

	Observed		
Forecast	Yes	No	**Total**
Yes	69	61	130
No	47	135	182
Total	116	196	312

A number of performance measures can be generated from Table 2.4.3. For example, the probability of detection (*SP*) is given by the ratio of correct (Yes, Yes) forecasts to the total number of observed exceedences. Referring to Table 2.4.3 it can be seen that $SP = 69/116 = 0.59$. Thus the system had a 59% probability of forecasting, at a given monitoring station, that a 1-hour NO_y concentration in excess of 100 ppb would occur on the following day. Similarly, the fraction of non-forecast events is given by $1 - SP$, which in this case corresponds to 41% of the time. Furthermore, the fraction of realised events (*i.e.* the number of forecast events that were found to be correct) is given by $SR = 69/130$. Thus a forecast exceedence was likely to be correct on about 53% of occasions. The complement to *SR* (*i.e.*, $1 - SR$) is the false alarm rate, which for the example above corresponds to 47% of occasions.

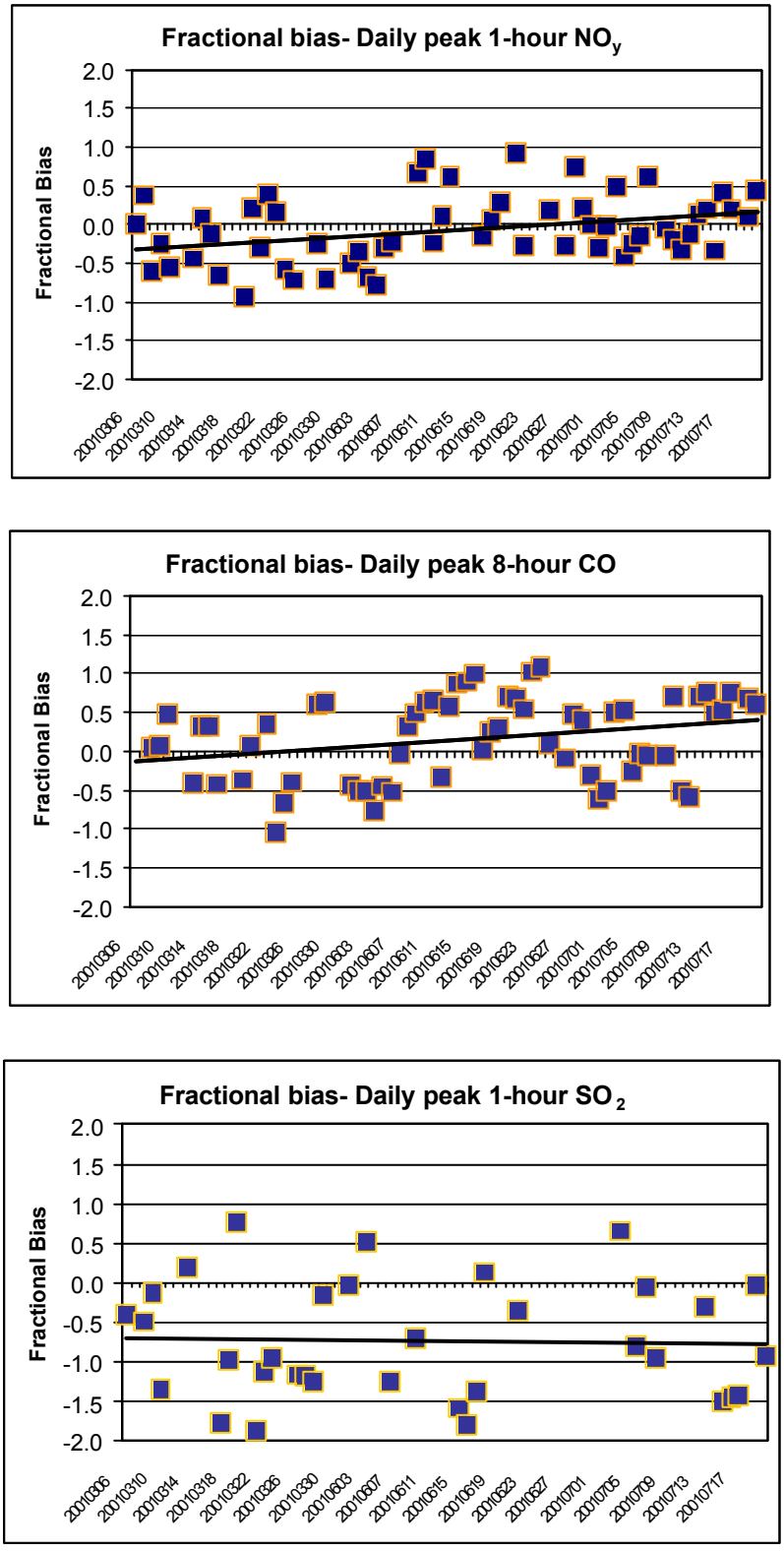

Figure 2.4.10. Fractional bias of peak daily 1-hour NO_y, 8-hour CO and 1-hour SO_2 for Melbourne and Geelong March 2001 and June–July 2001. Least squares regression trend lines are also shown for each pollutant.

A number of additional measures of system performance are also discussed in De Leeuw (2000). Following De Leeuw's recommendation we currently restrict consideration to the use of *SP* and *1 - SR*. Some guidance as to current skill levels of contemporary forecasting systems is also available from De Leeuw. An effective forecast model is expected to score a high detection rate, while maintaining a low false alarm rate. De Leeuw reports detection rates in the range 30–70% for forecasting regional ozone. False alarms fall in the range 15–60%. Dewundege (2001) reported on the development of a new regional ozone and visibility forecasting system for Melbourne. Probability of detection increased from 43% (old system) to 57% (revised system) for regional ozone and from 25% to 62% for regional visibility. De Leeuw also recommends that forecast performance be compared to that of a simple persistence model (*i.e.* the forecast pollutant concentration for day '**i**' is equal to the observed pollutant concentration on day '**i - 1**'). At a minimum, it is necessary to demonstrate that a proposed forecast model be able to provide a superior forecast to the persistence model.

Shown in Figure 2.4.11 are plots of *SP* and *1 - SR* for 24 hour forecasts of peak 1-hour NO_y and peak 8-hour CO. The plots show the response of *SP* and *1 - SR* to varying exceedence levels (50–200 ppb for NO_y and 1000–3000 ppb for CO). Note that 8-hour CO was not observed to exceed the Air Quality Standard of 9000 ppb; thus this level was not included in the analysis. The performance metrics have been plotted for AAQFS forecasts and for a persistence model. The AAQFS forecasts labelled 'Daily Peak' are for space-paired prediction and observation data of peak daily concentration (CTM), and for the maximum forecast AAQFS concentration within ±1 cell of a monitoring site ('CTM-range'). The forecast plots labelled 'Airshed Daily Peak' (only shown for NO_y in Figure 2.4.11) explores the ability of the system to forecast the airshed-wide daily peak concentration.

Considering the probability of detection for peak 1-hour NO_y it can be seen that the AAQFS has an 80% probability of forecasting an exceedence of 50 ppb at any given monitoring site (both at the site and within ± 1 cell of a monitoring site) and a 100% detection probability for the airshed maxima. These are reduced to about 20% (40% for CTM-range) and 75% respectively for an exceedence threshold of 200 ppb. It can be seen that AAQFS does significantly better than persistence for the airshed maxima and for the maxima within ±1 cell of a monitoring site. AAQFS is only marginally better than persistence in the case of full spatial coupling. Nevertheless, the overall result is pleasing, given that our goal is to generate realistic suburb-scale forecasts (*i.e.*, a goal comparable to the CTM-range forecasting ability).

The fraction of false alarms varies in a similar manner for both AAQFS and the persistence model, increasing from 25% at an exceedence threshold of 50 ppb (15% for the airshed maxima) to around 80% (60–70%) at an exceedence threshold of 200 ppb. In the case of the persistence model, an increasing probability of false alarm can be rationalised on the basis of a reducing probability that pairs of day with extreme concentrations of NO_y will be observed. In the case of AAQFS, there are a small number of cases where forecasts in excess of 200 ppb are generated by the system but were not observed. This result forces the fraction of false alarms towards 100% as the number of observations greater than the highest exceedence threshold approaches zero. An analysis of a more extended period is needed to further examine the relationship between false alarms and the maximum exceedence thresholds.

Plots of *SP* and *1 - SR* for daily peak 8-hour CO are also shown in Figure 2.4.11. Plots are shown only for the space-paired and near-space-paired statistics (the statistics for airshed maxima show a level of improvement similar to observed for NO_y). It can be seen that AAQFS and persistence have a similar probability of detection for an exceedence threshold of

1000 ppb, AAQFS does worse than the persistence model for mid-range concentrations, and both models perform comparably at a threshold concentration of 3000 ppb. On the other hand, the persistence model generally has a lower false alarm rate. This results from the tendency of AAQFS to over-predict daily 8-hour CO (*c.f.* Figure 2.4.10). With regard to SO_2, AAQFS performs poorly relative to persistence (not shown). The reason for the poor performance has been discussed previously.

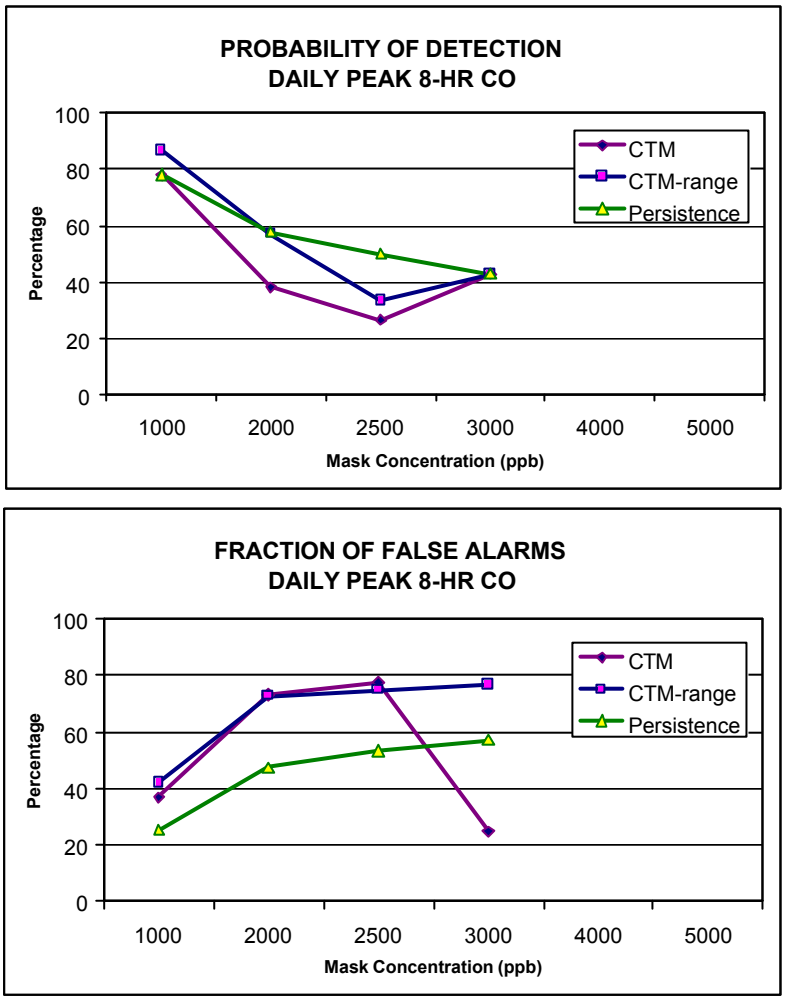

Figure 2.4.11a Contingency table outcomes for daily 8-hour CO. Melbourne - March 2001 and June–July 2001.

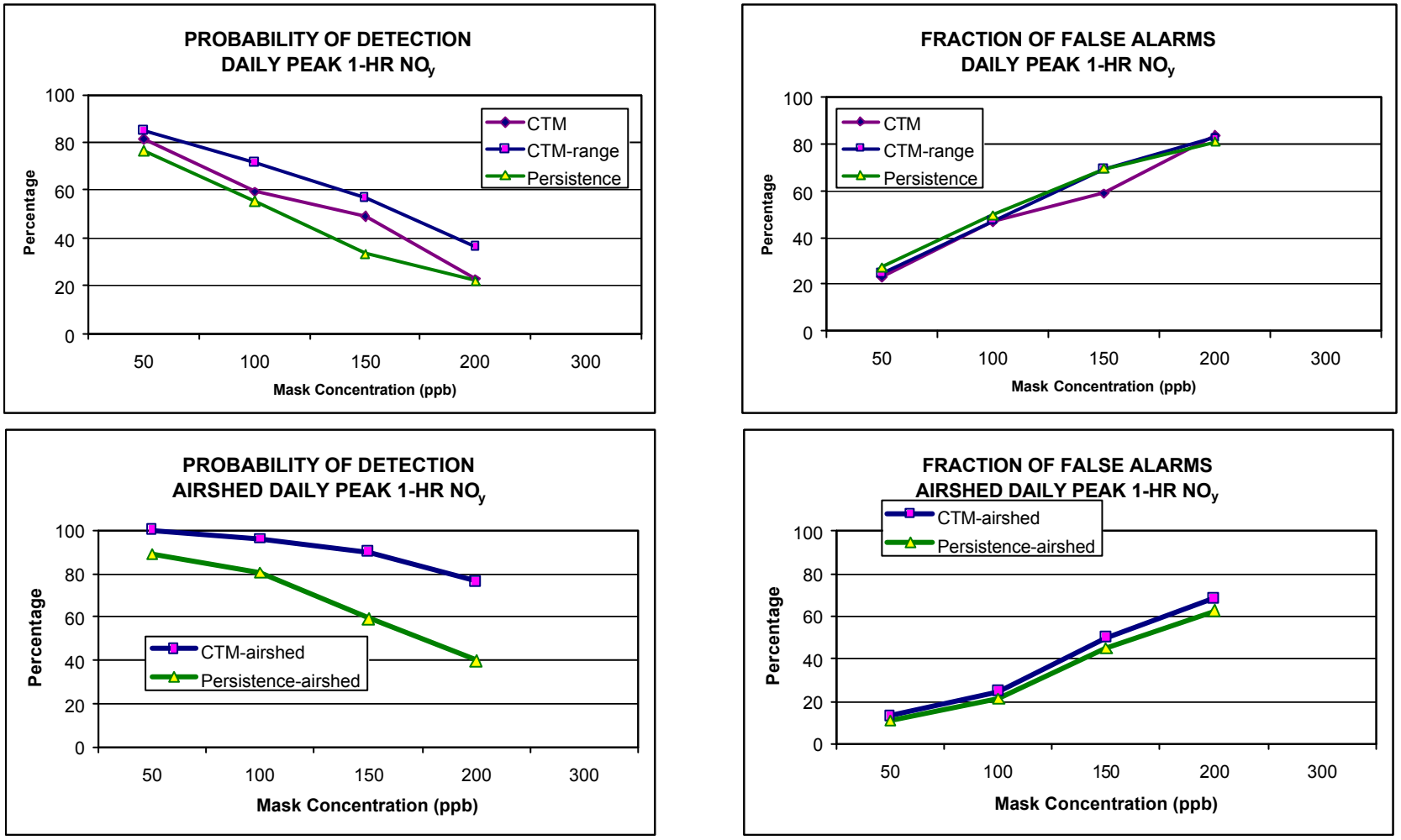

Figure 2.4.11b. Contingency table outcomes for daily 1-hour NO_y. Melbourne - March 2001 and June–July 2001.

2.4.2 Secondary gaseous pollutants.

One of the primary objectives of AAQFS is to forecast extreme photochemical smog events. In this section we review model performance for ozone (O_3) and nitrogen dioxide (NO_2), the two primary components of photochemical smog. Note that NO_2 may be considered both a primary and a secondary pollutant, with, approximately 10% of NO_x from efficient combustion sources being emitted as NO_2. Other important pathways of NO_2 production are the titration of nitric oxide to nitrogen dioxide in the presence of ozone, and during the photochemical generation of ozone. Both pollutants are subject to NEPM air quality standards (AQS) with a 1-hour O_3 AQS of 100 ppb, a 4-hour O_3 AQS of 80 ppb, a 1-hour AQS for NO_2 of 120 ppb and an annual average NO_2 AQS of 30 ppb. Consideration here is restricted to 1-hour average performance.

Time series plots. Plots of observed and forecast 1-hour NO_2 and O_3 are shown in Figure 2.4.12 and Figure 2.4.13 respectively. Note that NO_2 concentrations generally cycle between zero and 20 ppb, with occasional peaks of up to 60 ppb. These peaks lie well below the 1-hour AQS for NO_2. The 0-20 ppb diurnal cycle is a primarily a result of the NO/O_3 titration reaction. The amplitude of the cycle is robustly determined by the background concentration of O_3. Peak NO_2 concentrations in excess of about 30 ppb are photochemically generated. It can be seen that the diurnal cycle is well reproduced (this should be a basic requirement of any state-of-the-art air quality model). However, there is a tendency for the system to over-predict the concentrations of photochemically generated NO_2.

The O_3 time series plots are complementary to the NO_2 plots, with a strong diurnal variation between zero and the background of 20–25 ppb (again due to titration and, to a lesser extent dry deposition), and a number of days in which photochemically generated O_3 concentrations are observed (and forecast) to exceed 40 ppb. Note how the diurnal variation is absent from the Brighton time series for some days (eg. between hours 433 and 529). This is a consequence of Brighton monitoring station's location close to the coast (see Figure 2.4.1). Under conditions of onshore flow, un-titrated ozone, which has also undergone little depositional loss, is advected directly onshore. The background ozone concentrations are over-predicted under these conditions. The reason for this is discussed in the next section.

The period of photochemically generated ozone, present at the beginning of the March period, is shown in more detail in Figure 2.4.14 (note that the expanded view in Figure 2.4.14. includes a pre-event day that is not plotted in Figure 2.4.13). Peak ozone concentrations observed over the period 7–9 March 2001 are among the highest observed in Melbourne and Geelong for the 2000–2001 photochemical smog season and thus it is important to ascertain the system's ability to accurately forecast such an event. Again, when considering the O_3 time series plots, it should first be recalled that some of the agreement between observed and modelled is forced by the diurnal cycle of radiation and the titration of ozone by nitric oxide under stable nocturnal conditions. Thus consideration should be restricted to the (photochemically generated) ozone concentrations in excess of 30–40 ppb. On this basis, it can be seen that the system has been able to forecast the distribution of ozone with good skill over the four-day period, with the only significant discrepancy being the over prediction of pre-sea breeze ozone on 7 March (hours 36–42) at Pt. Cook, Brighton and Paisley. Performance statistics for the 7–9 March ozone event are presented below; a more comprehensive description of the meteorological and chemical transport dynamics of this event is given in **Chapter 7** of this Report.

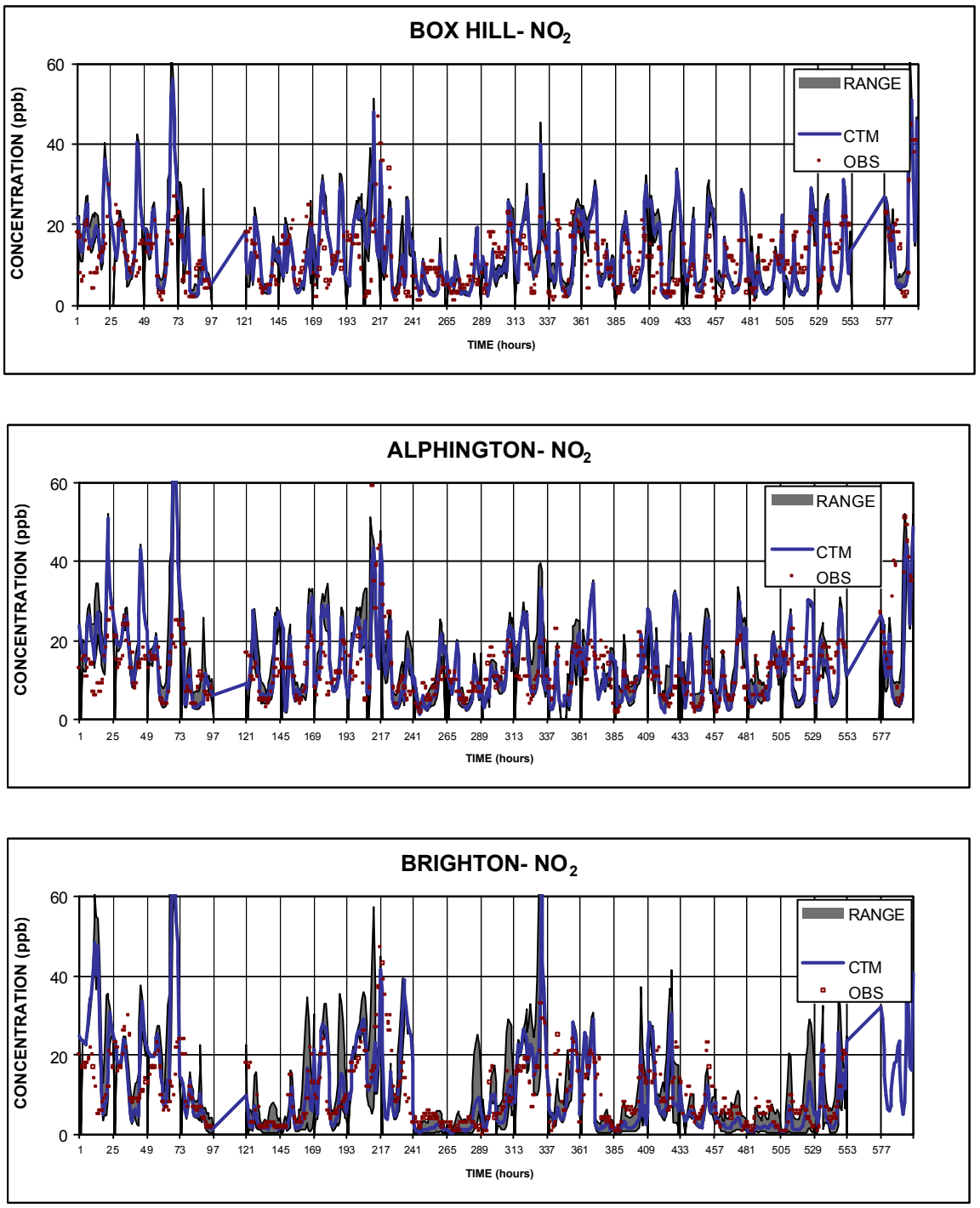

Figure 2.4.12. Observed vs modelled concentration time series of nitrogen dioxide (NO_2) for Box Hill, Alphington and Brighton montoring stations March 2001. Forecast concentrations are interpolated to the observation site. Range corresponds to the minimum and maximum forecast concentrations within ±1½ km of the observ ation site.

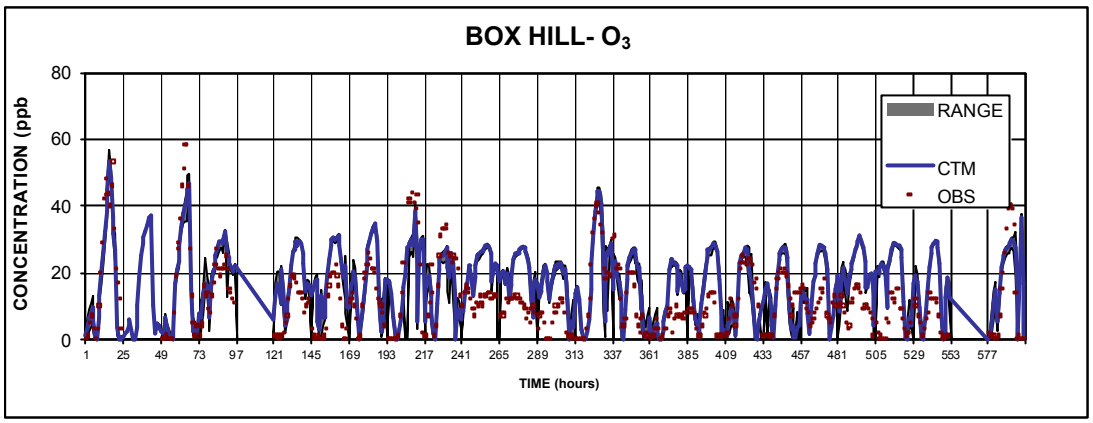

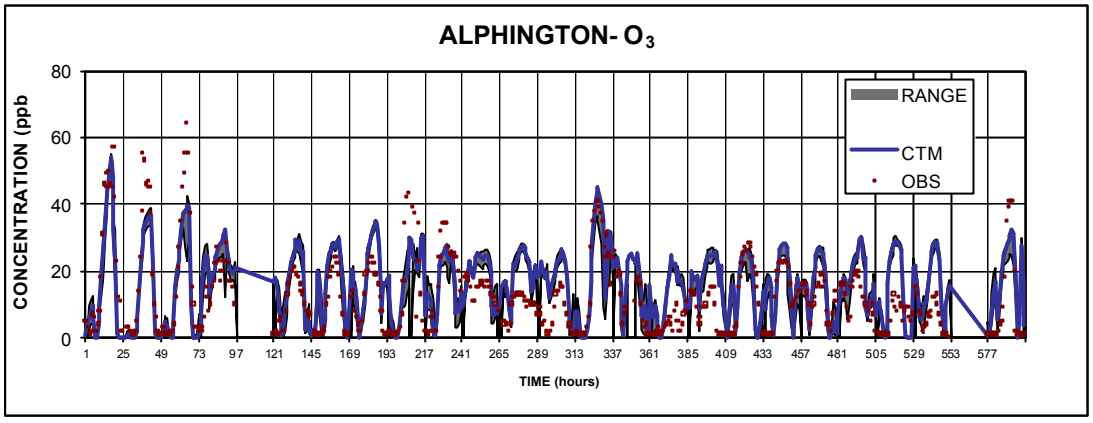

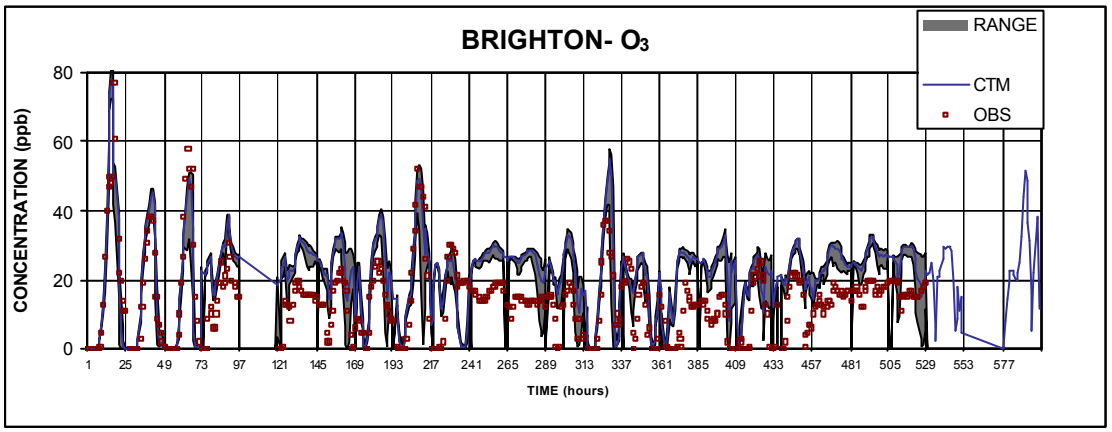

Figure 2.4.13. Observed vs modelled concentration time series of ozone (O_3) for Box Hill, Alphington and Brighton montoring stations March 2001. Forecast concentrations are interpolated to the observation site. Range corresponds to the minimum and maximum forecast concentrations within ±1½ km of the observation site.

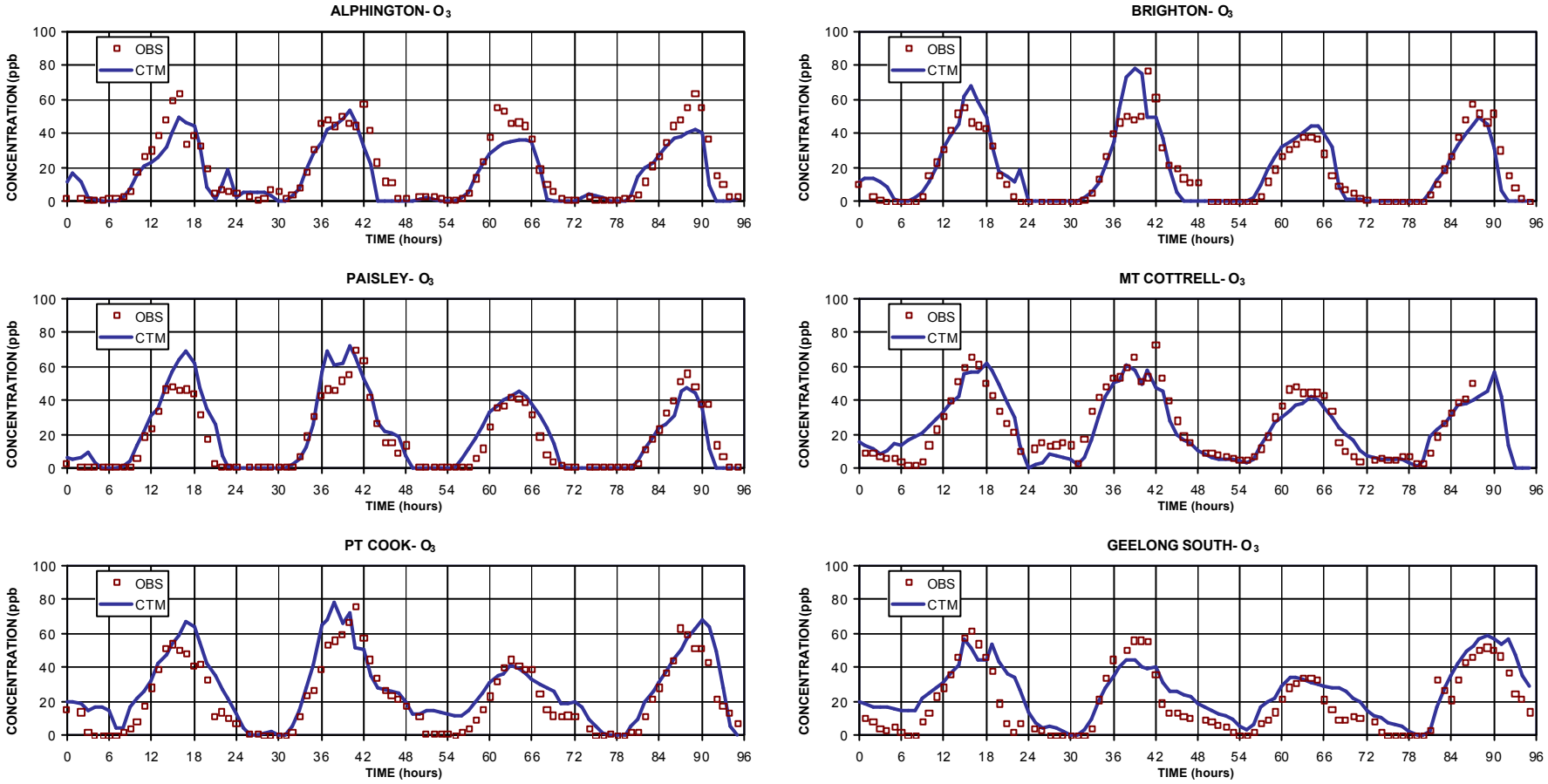

Figure 2.4.14. Observed (obs) and forecast (CTM) 1-hour ozone concentration time series for 7–9 March 2001 — selected EPA Victoria monitoring stations.

Frequency Distributions. Cumulative frequency distributions for NO_2 and O_3 are presented in Figure 2.4.15 for both March 2001 and June–July 2001. Percentile bias statistics were presented in Table 2.4.1. Note how the seasonal variation for these photochemical species is inverted compared to the primary gaseous species (*c.f.* Figure 2.4.6). Referring to Figure 2.4.15 it can be seen that NO_2 is over-predicted at the higher percentiles. This is also apparent from Table 2.4.1, the bias between predicted and observed percentiles increases from 6% at the 50^{th} percentile to 57% for the maximum concentration. This trend was also observed by Carruthers *et al*. (1999), when modelling the London urban plume using ADMS-Urban with GRS photochemistry (annual 1-hour maxima's were over-predicted by 400% on the average in that study). For the Australian modelling, the cause is a systematic over-estimate of the initial reactivity of the urban air mass by the highly condensed GRS photochemical mechanism. This will be rectified when the mechanism is upgraded to GRS2 (see **Section 5.1.2 GRS2 development**) as a part of our on-going development of the system. Considering O_3 and again referring to Figure 2.4.15, it can be seen that the agreement between observed and forecast percentiles is excellent, particularly at the higher percentiles. There is however, a trend to over-predict the observed ozone concentration at the lower percentiles. The primary cause is a 5–10 ppb over prescription of the background O_3 concentration in unpolluted maritime flows (25 ppb vs. 15–20 ppb). The reason again appears to lie with the GRS mechanism — ozone destruction under conditions of low NO_x and high water vapour concentration is not modelled by the mechanism. This has been addressed in GRS2.

Residual analysis. Plots of fractional mean bias for NO_2 and O_3 are given in Figure 2.4.16 for March 2001. Monthly mean statistics for these pollutants were presented in Table 2.4.2. From the Figure it can be seen that NO_2 has a small trend towards under-prediction as the month progresses. Recall that this was also reflected in the NO_y fractional bias. The monthly-average fractional bias is only -0.08 for NO_2, which, although excellent, primarily demonstrates the robustness of forecasting the diurnal variation of NO_2 due to the NO–O_3 titration reaction.

The fractional bias plot for O_3, confirms the outcomes from comparing the observed and modelled percentiles for this pollutant. With the exception of the 7–9 March photochemical smog event (for which the mean bias is close to zero — hours 144–192 in Figure 2.4.16), hourly ozone is biased high. However, as discussed in the previous section, this primarily applies to near-background ozone concentrations, and will be corrected following implementation of the GRS2 mechanism.

Forecasting daily maxima. A plot of the fractional bias for peak daily NO_2 for March 2001 is given in Figure 2.4.17. Fractional bias has been calculated for all days where the observed daily maximum NO_2 exceeded 25 ppb, thus eliminating cases where the NO_2 peaks are generated from the titration of the background O_3 field. It can be seen that daily maximum NO_2 is, on the average, forecast with the least bias of any of the pollutants considered so far, although the highest 1-hour NO_2 concentrations are systematically over-predicted by AAQFS. This is an excellent result and is reflected in the mean fractional bias of 0.07, and a mean fractional gross error of 0.20.

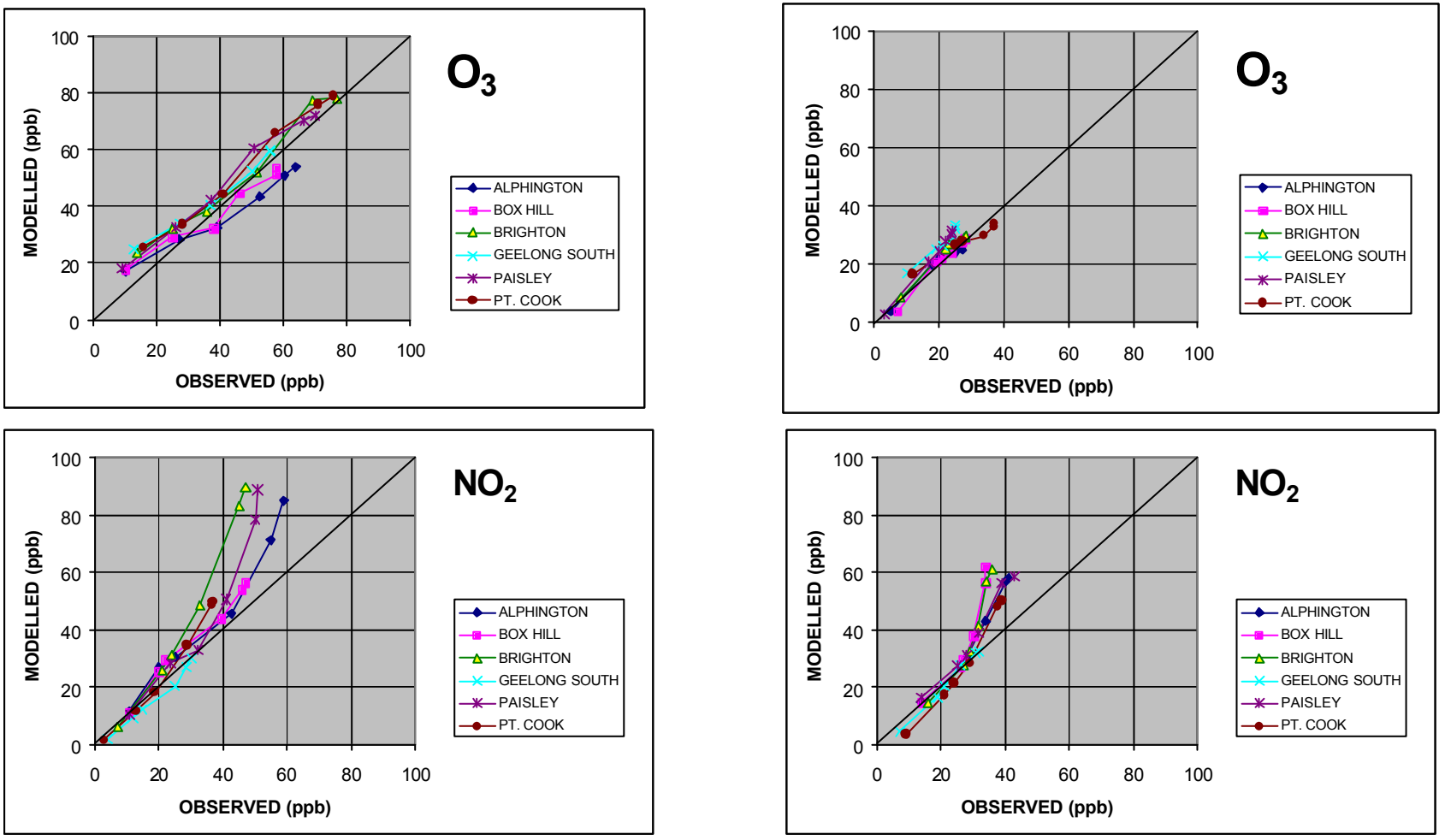

Figure 2.4.15. Plots of observed and forecast percentiles of the O_3 and NO_2 concentration distributions (50th, 90th, 99th, 99.5th, 99.9th, and 100th percentiles) for March 2001 (left) and June–July 2001 (right) — for selected monitoring stations in the Melbourne and Geelong region.

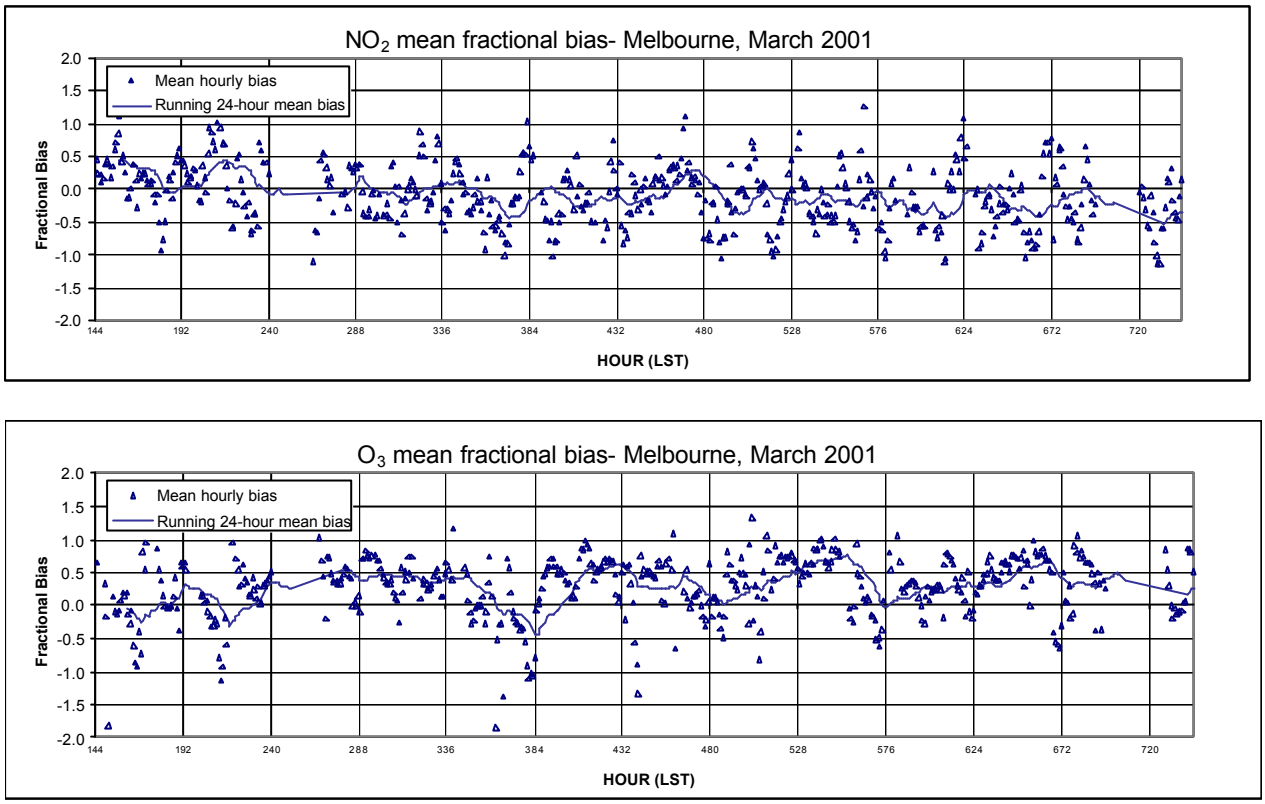

Figure 2.4.16. One-hour and running 24-hour mean of one-hour fractional bias for observed and forecast NO_2 and O_3, Melbourne and Geelong monitoring stations, March 2001.

We have not plotted the daily time series of fractional bias for peak daily ozone because, with the exception of 7–9 March 2001, ozone concentrations were close to background. Instead, presented in Table 2.4.4 are various performance measures for the 3-day period. Guidance as to acceptable model performance for 1-hour ozone is provided in EPA (1991) and references therein. Airshed model performance is deemed to be acceptable if (in addition to a range of diagnostic tests), the magnitude of peak unpaired prediction accuracy, overall bias and gross error statistics fall within the ranges ±15–20%, ±5–15% and ±30–35% respectively. As can be seen from Table 2.4.4, all of these measures of model performance fall within the recommended range, thus indicating that the forecast performance for ozone was excellent for this three-day period.

Plots derived from forecast contingency tables for peak daily NO_2 and O_3 are presented in Figure 2.4.18. It can be seen that the results are, in general, improved compared to both CO and NO_y. In particular, it can be seen that AAQFS maintains a high probability of detection for NO_2 (60–80%) for all observed ranges. On the other hand, the persistence model rapidly loses skill as the exceedence threshold rises above 20 ppb. The prediction of false alarms for NO_2 is not better than that of persistence. This indicates that in part, the high detection probability is due to over-prediction by the System of peak 1-hour NO_2.

Ozone contingency results are shown for both station-level daily peaks and for airshed maxima. It can be seen that the ozone contingency results are very promising. Although the system is yet to be tested for a full range of conditions, it can nevertheless be seen that both the probability of detection and the rate of false alarms for AAQFS are considerably better than that which can be achieved through persistence.

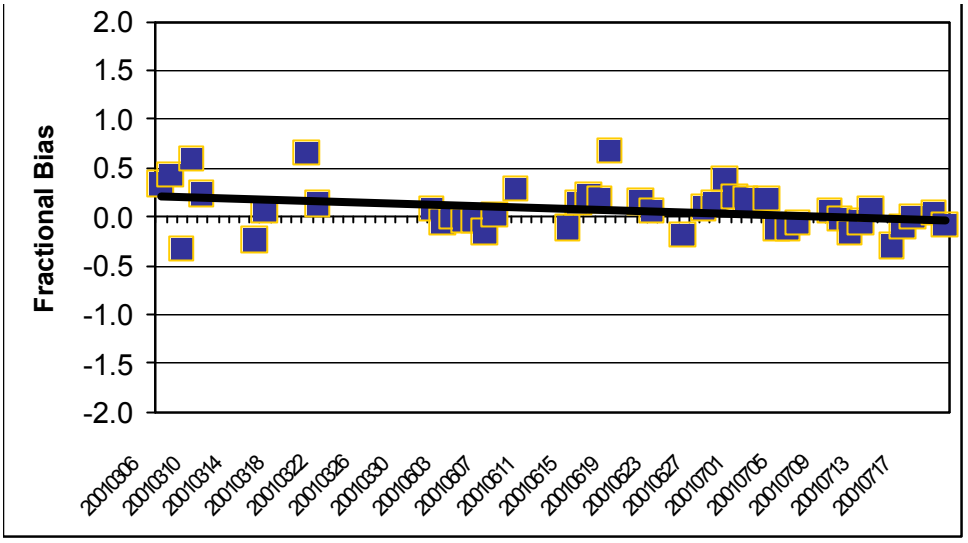

Figure 2.4.17. Fractional bias of peak daily 1-hour NO_2, for Melbourne and Geelong March 2001. A least square regression trend line is also shown.

These results also compare very favourably with other forecast systems. For example, as discussed previously, DeLeeuw (2000) compared the results of three statistical models for a Dutch ozone forecasting system. When forecasting the exceedences of 60 ppb, three alternative models recorded detection probabilities in the range 30–70% and probability of false alarm in the range 14–63%. At a 60 ppb exceedence threshold, AAQFS achieved a detection probability of 70% for local-level forecasts and 100% for the forecast of airshed maxima. The false alarm rates are about 50% and 30% respectively. These results also compare well with those reported by Cardelino *et al.* (2000) for a study in which four numerical methods and a 10 person team were used to forecast 8-hour ozone peaks for the Atlanta region for the 1999 ozone season. Two regression models, persistence and a coupled NWP-CTM, comprised the numerical forecasting methods. Results from the numerical models were then provided to the forecasting team and combined with experience and intuition and a 'team forecast' generated. The numerical models achieved detection probabilities in the range 75–85%, and false alarm rates in the range 16–28%. A statistical regression model provided the most skilful forecast, the persistence model had the lowest probability of detection and the NWP-CTM had the highest number of false alarms. The team performance was comparable to the best model. The NWP-CTM was considered to have the greatest potential for improvement, having the highest systematic error component (as compared to a non-systematic or random error).

Although it is not possible to directly compare AAQFS to the revised EPA Victoria expert forecasting system (Dewundege 2000), it is of interest to recall that that system (regional forecasts for $O_3 > 100$ ppb) has a detection probability of 57%.

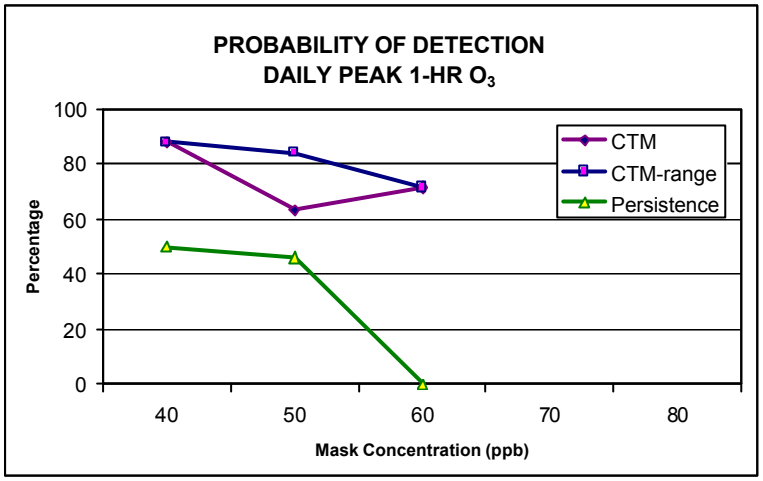

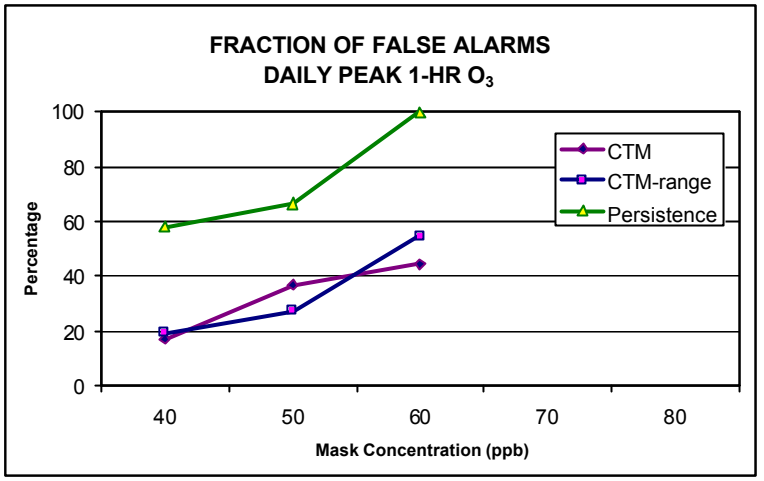

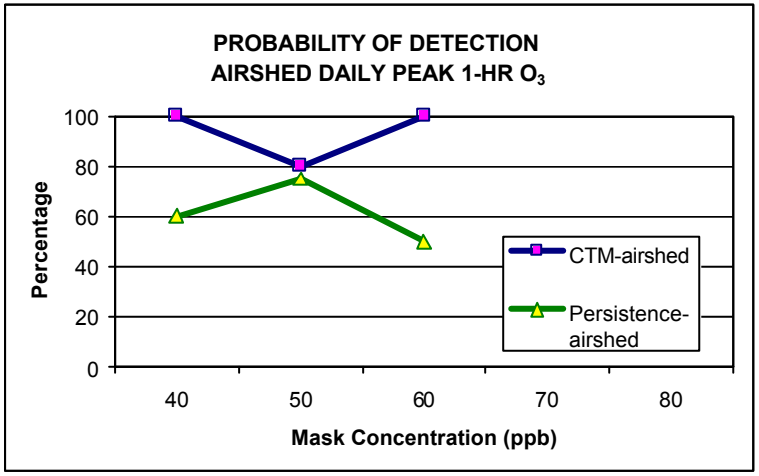

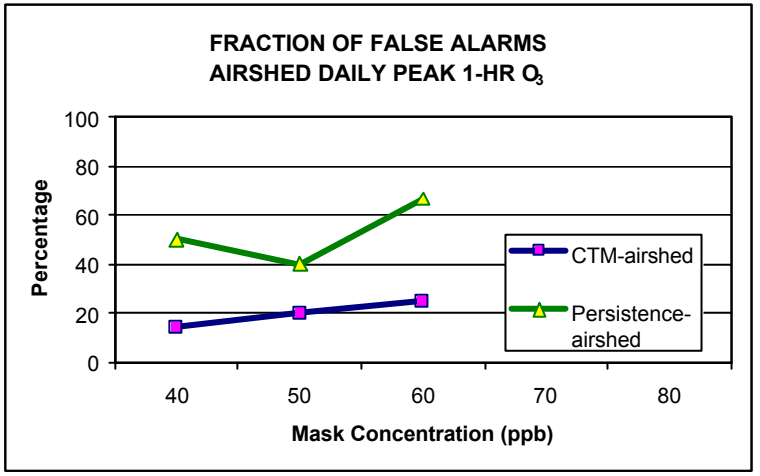

Figure 2.4.18a. Contingency table outcomes for daily 1-hour O_3. Melbourne — March 2001 and June–July 2001.

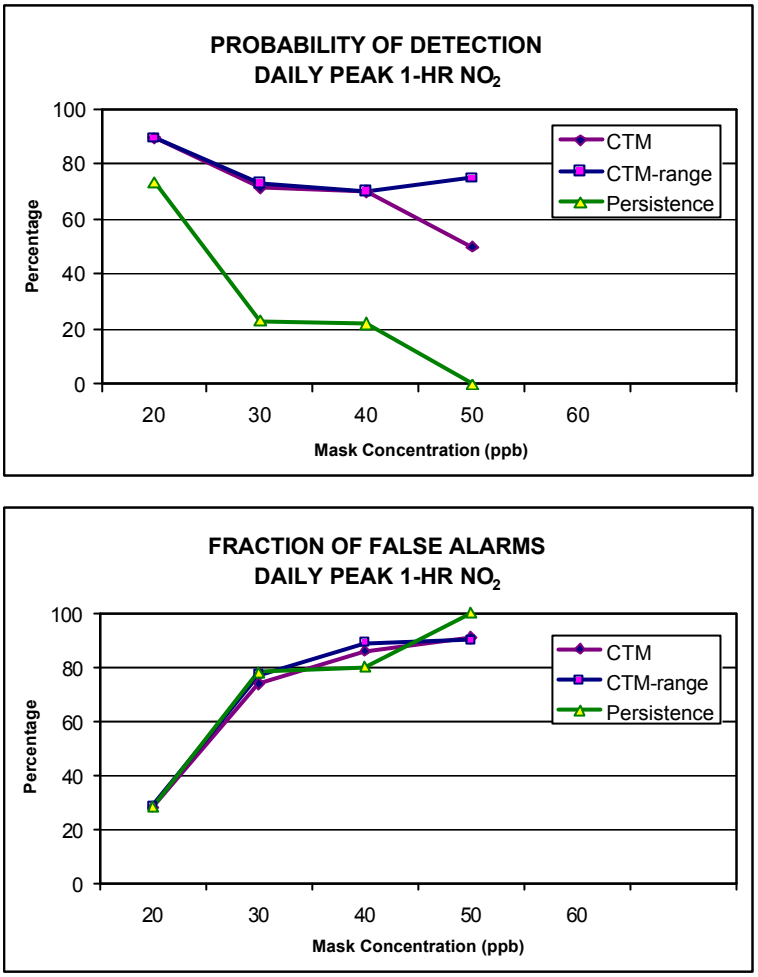

Figure 2.4.18b. Contingency table outcomes for daily 1-hour NO_2. Melbourne — March 2001 and June–July 2001.

Table 2.4.4. Performance measures for O_3 for Melbourne/Geelong monitoring stations for 7–9 March 2001.

STATISTICAL MEASURE	OZONE		
	Day		
	7 Mar 2001	8 Mar 2001	9 Mar 2001
Unpaired highest prediction accuracy (%)	2	-18	8
Bias (ppb)	-1	-6	-6
Normalised Bias (%)	-14	-12	-12
Gross error (ppb)	12	8	12
Normalised gross error (%)	23	17	24

2.4.3 Aerosol

The last pollutant species to be reviewed in this section are PM10 and PM2.5. While the air NEPM includes a 24-hour Standard of 50 $\mu g\ m^{-3}$ for PM10, PM2.5 is not currently a criteria pollutant. However, in the forecast System, 1-hour PM2.5 is used as a surrogate for visibility, using a least squares regression between PM2.5 mass and dry backscatter coefficient.

Time series plots. Shown in Figure 2.4.19 are time series plots of 1-hour PM10 for Box Hill, Alphington and Brighton monitoring stations for March 2001. Similar plots are shown for June–July in Figure 2.4.20. Note that, although the AQS for PM10 is a 24-hour average, we again consider model performance for 1-hour average concentrations. Time series plots of PM2.5 are not displayed here for brevity.

Considering the observed and modelled PM10 time series for March, it can be seen that background concentrations are under-predicted, and also that some of the peak concentrations have been under-predicted, particularly at Box Hill monitoring station. With regard to background concentration, testing has indicated that this may be improved through a revision to the vertical distribution of PM10 (and PM2.5) on the boundaries of the model. Furthermore, the system is currently running without a wind-blown dust emissions module. Both of these issues will be addressed as part of our commitment to on-going maintenance and improvement of the system.

The time series plots of 1-hour PM10 concentration for June–July are very different to those presented for March 2001. Whereas observed PM10 peaks were generally under-predicted during March, Figure 2.4.20 shows that the system has systematically over-predicted PM10 during the months of June and July (due to overestimation of domestic wood-fire emissions—see later). This is also the case for PM2.5 (not shown).

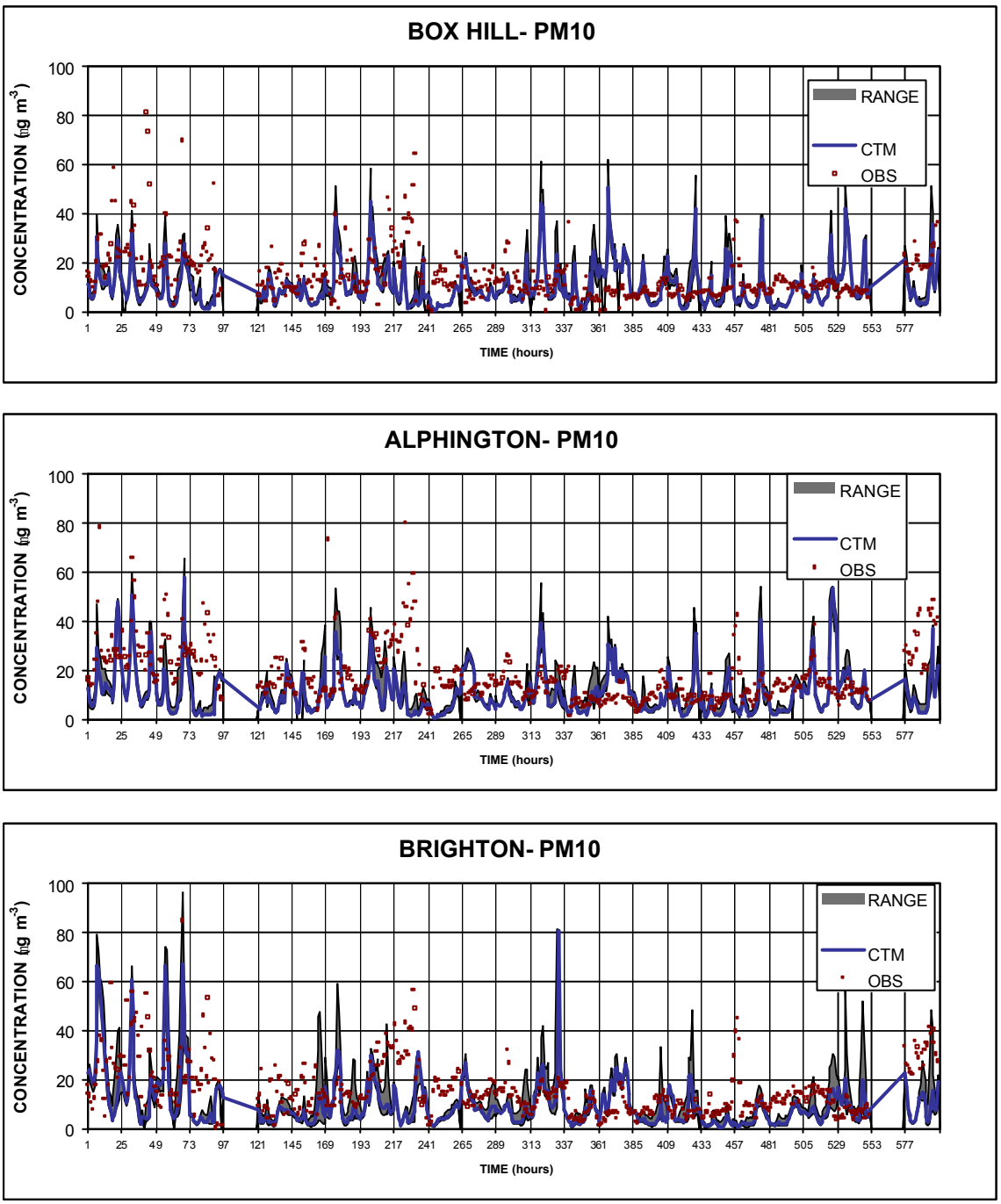

Figure 2.4.19. Observed vs modelled concentration time series of PM10 for Box Hill, Alphington and Brighton montoring stations March 2001. Forecast concentrations are interpolated to the observation site. Range corresponds to the minimum and maximum forecast concentrations within ±1½km of the observation site.

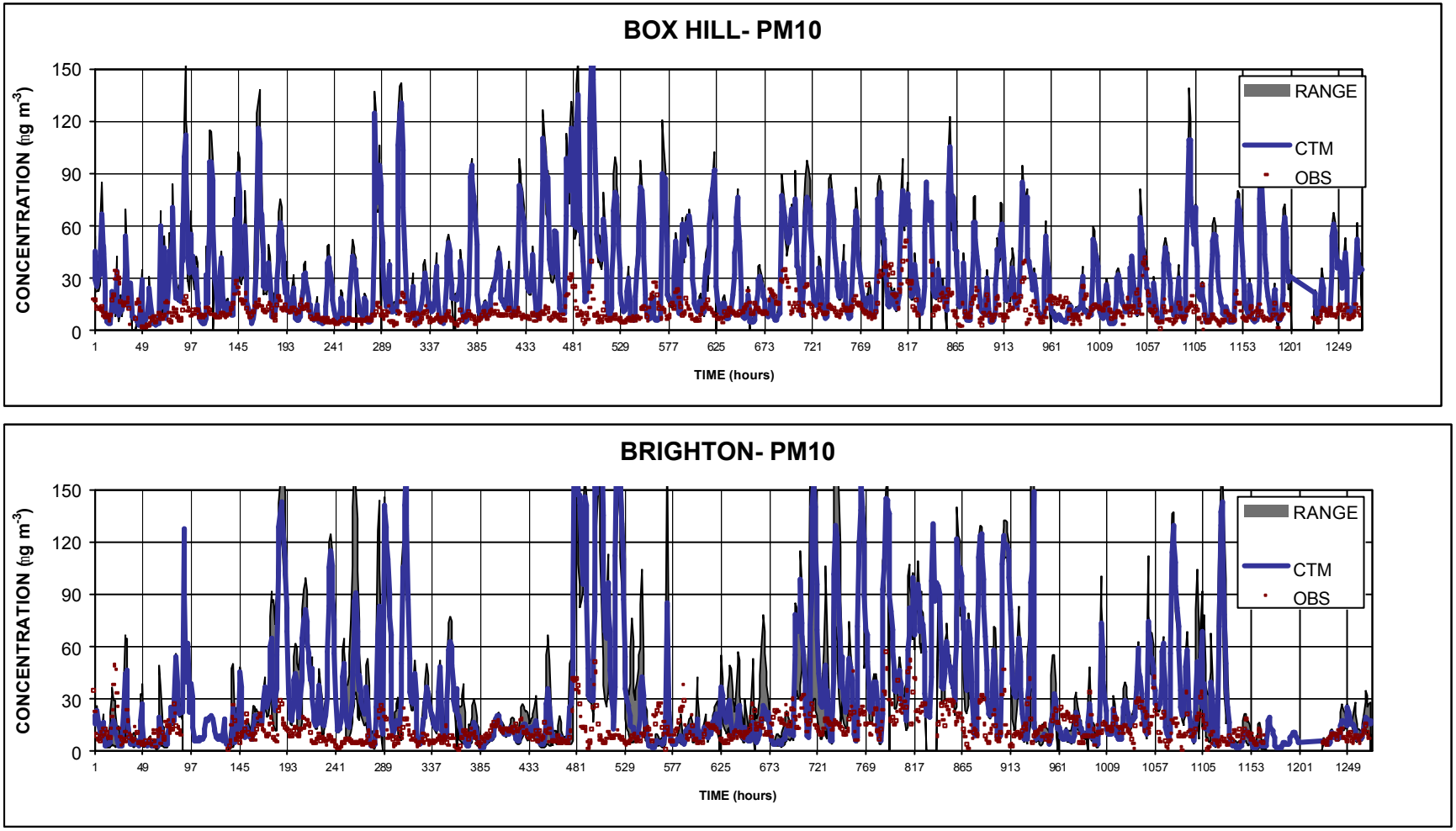

Figure 2.4.20. Observed vs modelled concentration time series of PM10 for Box Hill and Brighton montoring stations 1-30 June, 1–20 July 2001. Forecast concentrations are interpolated to the observation site. Range corresponds to the minimum and maximum forecast concentrations within ±1½ km of the observation site.

Frequency distributions: Observed and predicted percentiles for the cumulative frequency distributions of 1-hour PM2.5 and PM10 for March and for June–July 2001 are shown in Figure 2.4.21. Tabulations of normalised bias were given in Table 2.4.1. Considering the results for March, it can be seen that the observed concentrations of the upper percentiles of PM2.5 are well matched by AAQFS at Alphington monitoring station but over-predicted at Brighton. On the other hand, the observed PM10 percentiles have been well matched at Brighton. Still considering PM10, it can be seen that all observed concentrations are slightly under-predicted by the system for all the percentiles at Alphington and strongly under-predicted at the 99.9 and 100th percentile at Box Hill monitoring station. Interestingly, further investigation of the latter case showed the cause to be an isolated (single pollutant) PM10 one-hour event- likely the result of a short-term, local, un-inventoried source.

Considering the right-hand plots of Figure 2.4.21, it can be seen that that AAQFS has strongly over-predicted the observed concentrations of PM2.5 and PM10 for all levels at, and above the 90th percentile.

At this point it is interesting to note that the ratio of peak observed PM2.5 for June–July to the peak observed in March is about two. This is consistent with the ratio observed for NO_y. In the case of NO_y it was assumed that the principal cause of the variation in peak concentrations was seasonal effects in the controlling meteorology. However, if this is the case, then it implies that either the principal source of PM2.5 is unchanged relative to the March case, or that it has been replaced by a source of similar magnitude. Further to this issue, it can also be seen from Figure 2.4.21 that the peak observed concentrations of PM10 are actually reduced for the June–July period. Again this implies that a source of aerosol is now absent from the airshed. AAQFS on the other hand predicts significantly increased peak concentrations of PM10.

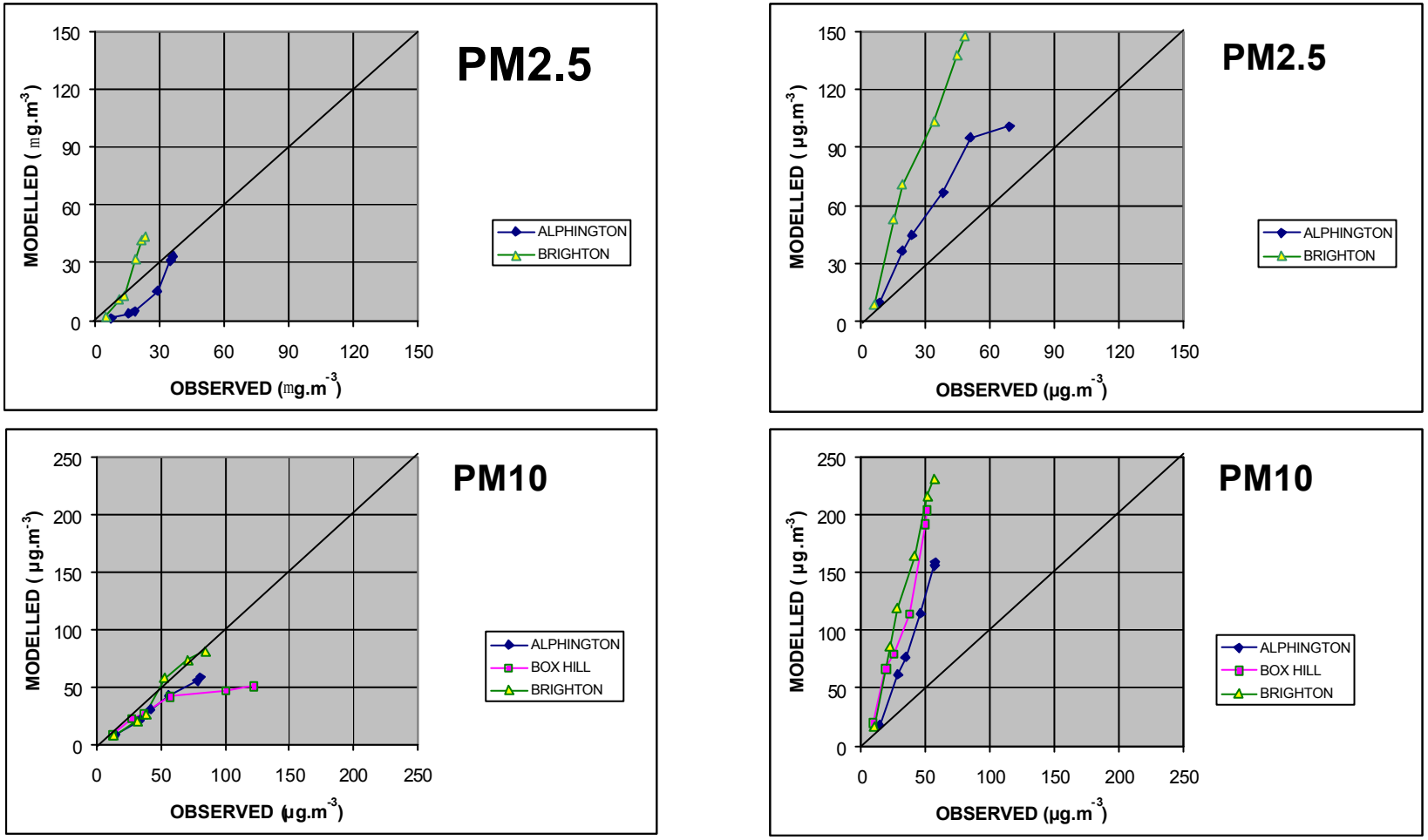

Figure 2.4.21. Plots of observed and forecast percentiles of the PM2.5 and PM10 concentration distributions (50th, 90th, 99th, 99.5th, 99.9th, and 100th percentiles) for March 2001 (left) and June–July 2001 (right) — for selected monitoring stations in the Melbourne region.

Residual analysis. Fraction mean bias plots for PM2.5 and PM10 are displayed in Figure 2.4.22 for March 2001 and in Figure 2.4.23 for June–July. The March fractional bias calculations indicate that the System is systematically under-predicting PM2.5 and PM10 concentrations during the early autumn period. Referring to Table 2.4.2, is can be seen that the particle groups are, on the average, under-predicted by about a factor of two. As previously noted, this is believed to be due to the omission of wind blown dust from the model, and, also due to uncertainties in the vertical distribution of aerosol mass on the boundaries of the model. Both of these issues will be addressed as part of the on-going support of the system.

Fractional bias plots for June–July (Figure 2.4.23) support our previous comments that particle concentrations are strongly over-predicted during this period.

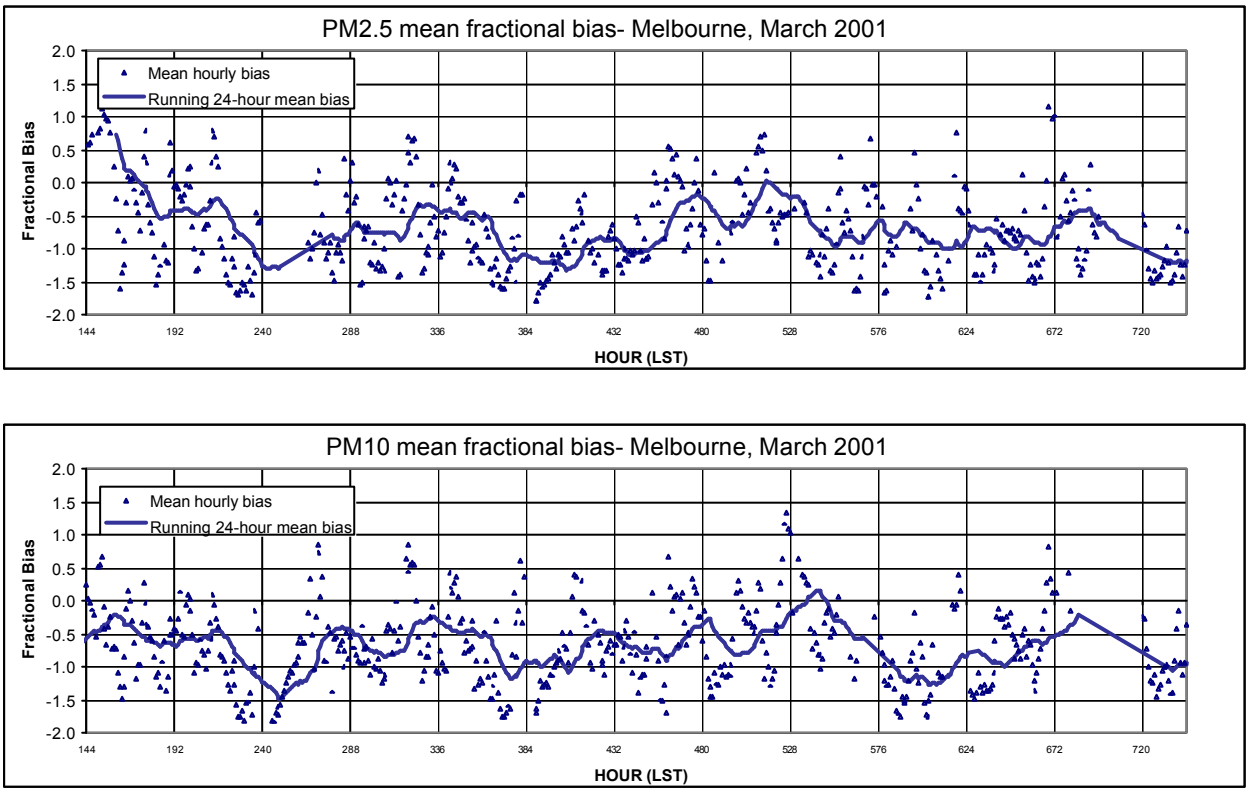

Figure 2.4.22. One-hour and running 24-hour mean of one-hour fractional bias for observed and forecast PM2.5 and PM10. Melbourne and Geelong monitoring stations, March 2001.

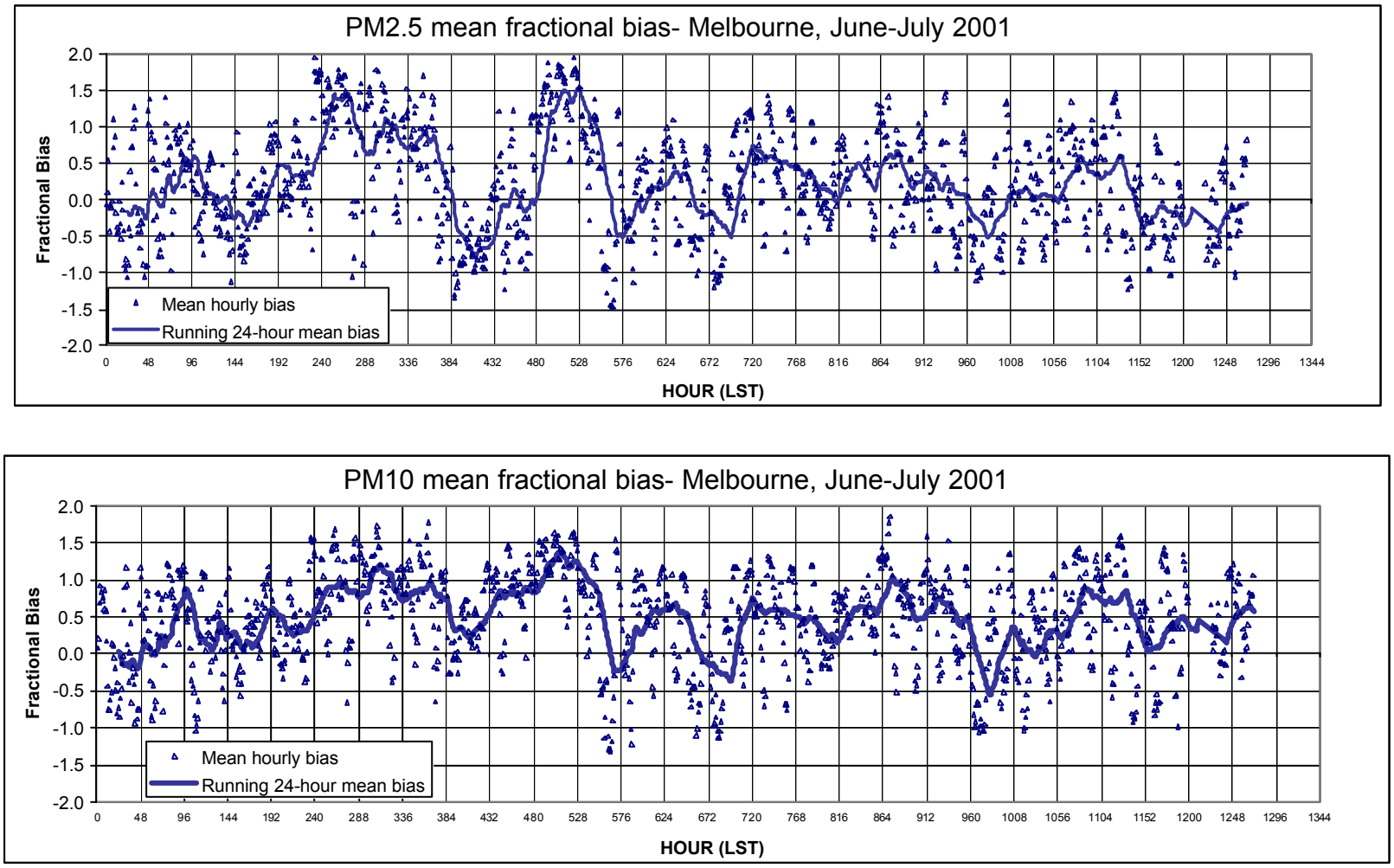

Figure 2.4.23. One-hour and running 24-hour mean of one-hour fractional bias for observed and forecast PM2.5 and PM10, Melbourne and Geelong monitoring stations, June–July 2001.

Forecasting daily maxima. Plots of observed and modelled peak daily 1-hour PM2.5 and running 24-hour PM10 are shown in Figure 2.4.24. It can be seen that peak PM2.5 was forecast with little bias for March 2001 and was over-predicted by about a factor of two during June–July. Peak running 24-hour PM10 was under-predicted during March and over-predicted during June–July.

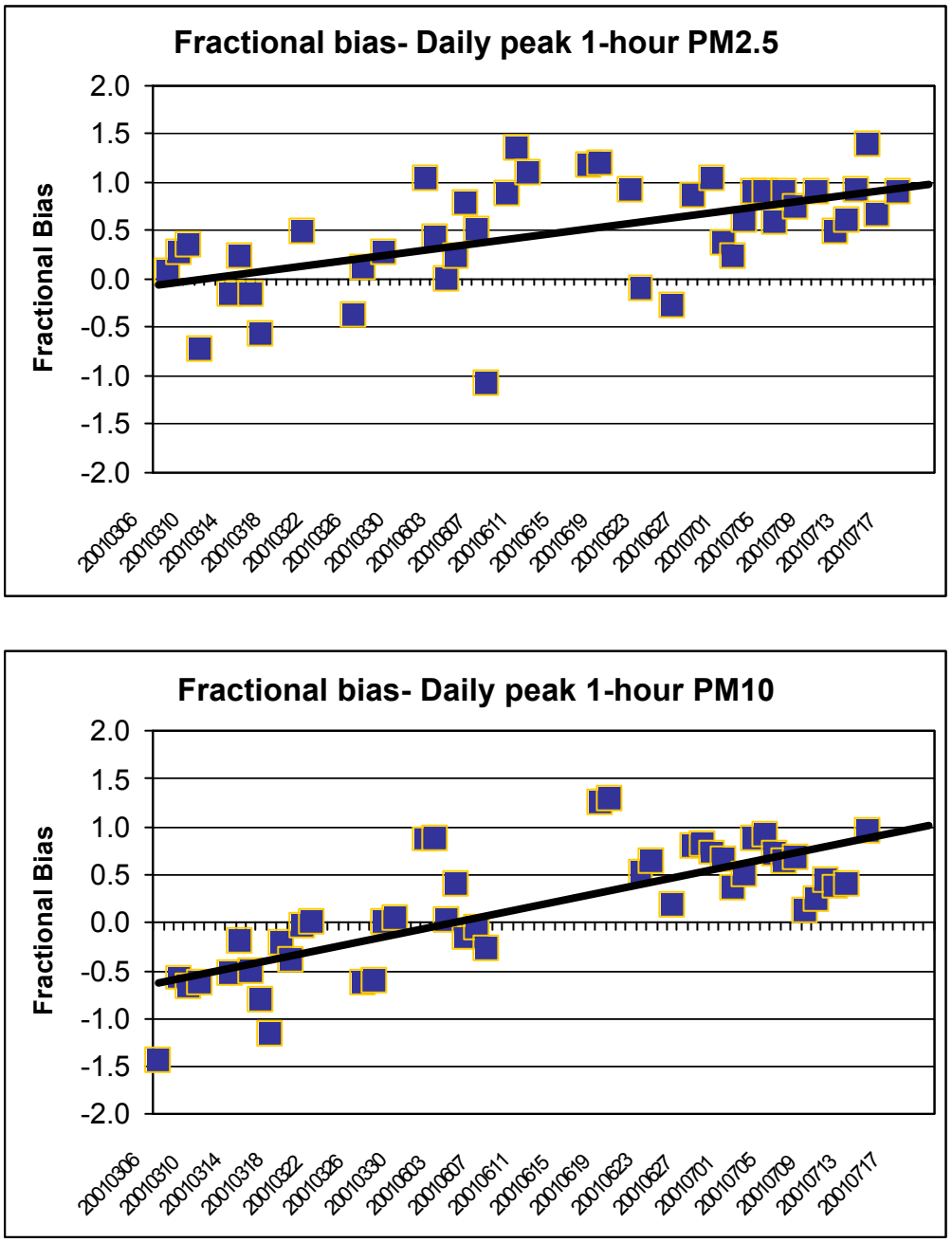

Figure 2.4.24. Fractional bias of peak daily 1-hour PM2.5 and 24-hour PM10 for Melbourne and Geelong for March 2001 and June–July 2001. Least square regression trend lines are also shown for each pollutant

Combined contingency table outcomes for the two study periods are shown in Figure 2.4.25 for PM2.5 and PM10. With the exception of *SP* for daily peak 1-hour PM2.5, AAQFS does considerably worse than persistence.

The poor performance of AAQFS with respect of the forecasting of aerosol concentration in the winter months is the subject of on-going work. An analysis of the PM2.5 and PM10 results and discussions with EPA Victoria suggest that the strong over-predictions of particle concentrations in wintertime is related to the emissions from domestic wood combustion. This is supported by the observations that (i) NO_y is currently predicted with little bias (*e.g.*, see Figure 2.4.9 [top], hours 720–1248). If it is assumed that, NO_x has been correctly inventoried, then the small fractional bias for NO_y indicates that predicted winter ventilation rates are approximately correct. (ii) PM10 and PM2.5 were not systematically over-predicted until June (at which point the wood burning model substantially increased PM10 and PM2.5 emission rates); (iii) in the limit of small ventilation rates, the predicted PM10:NO_y ratios exceed observed ratios by a factor of 2–3.

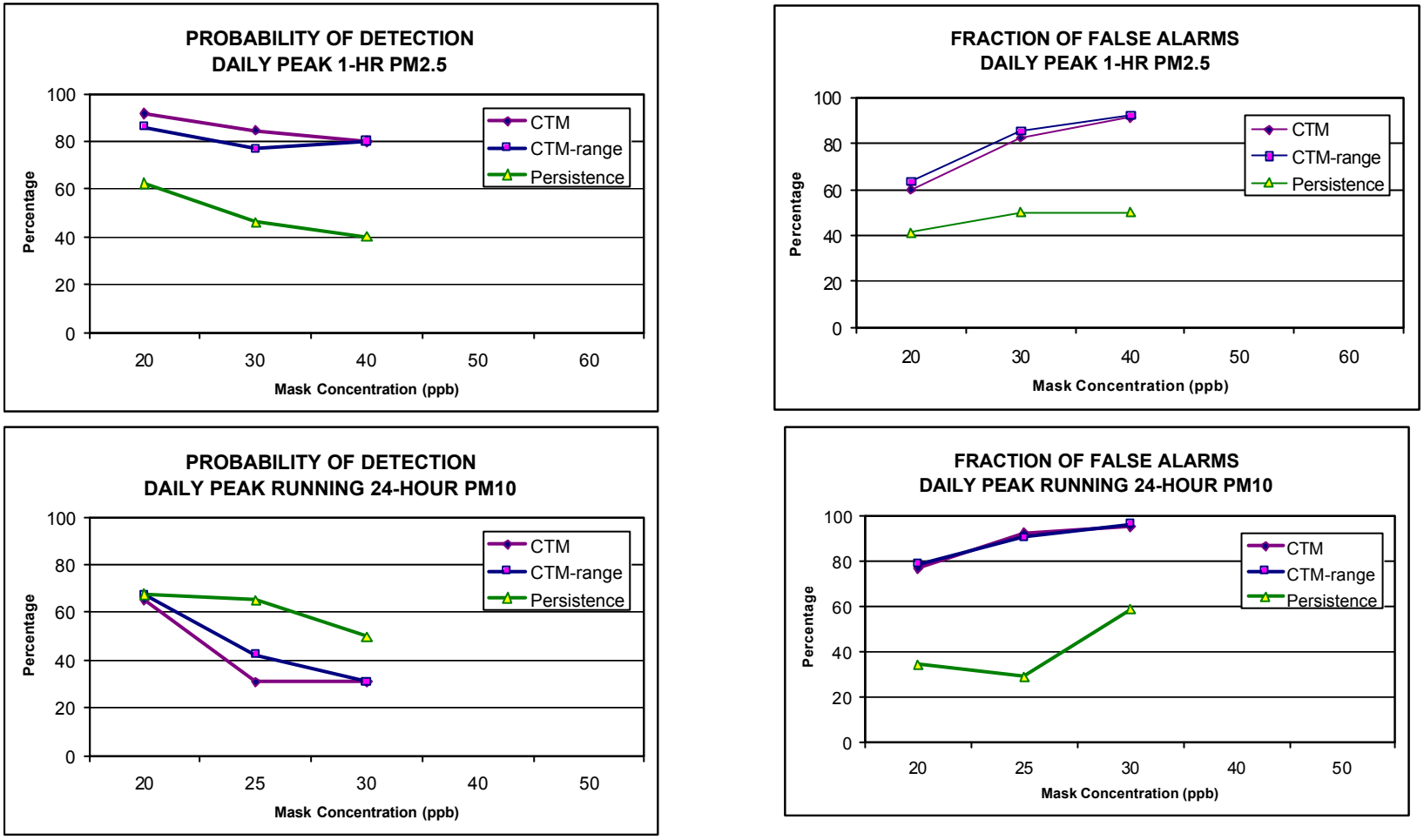

Figure 2.4.25. Contingency table outcomes for daily 1-hour PM2.5 and daily 24-hour PM10. Melbourne — March 2001 and June–July 2001.

2.5 CTM Performance in Sydney

In this section we review the performance of AAQFS for the Sydney region (see Figure 2.51 for a plot of the CTM 1-km Sydney grid and for a list of monitoring station sites). The methodology used to assess system performance is identical to that described in detail for the Melbourne and Geelong region. Because of this, consideration will be given only to the System's ability to predict peak concentrations.

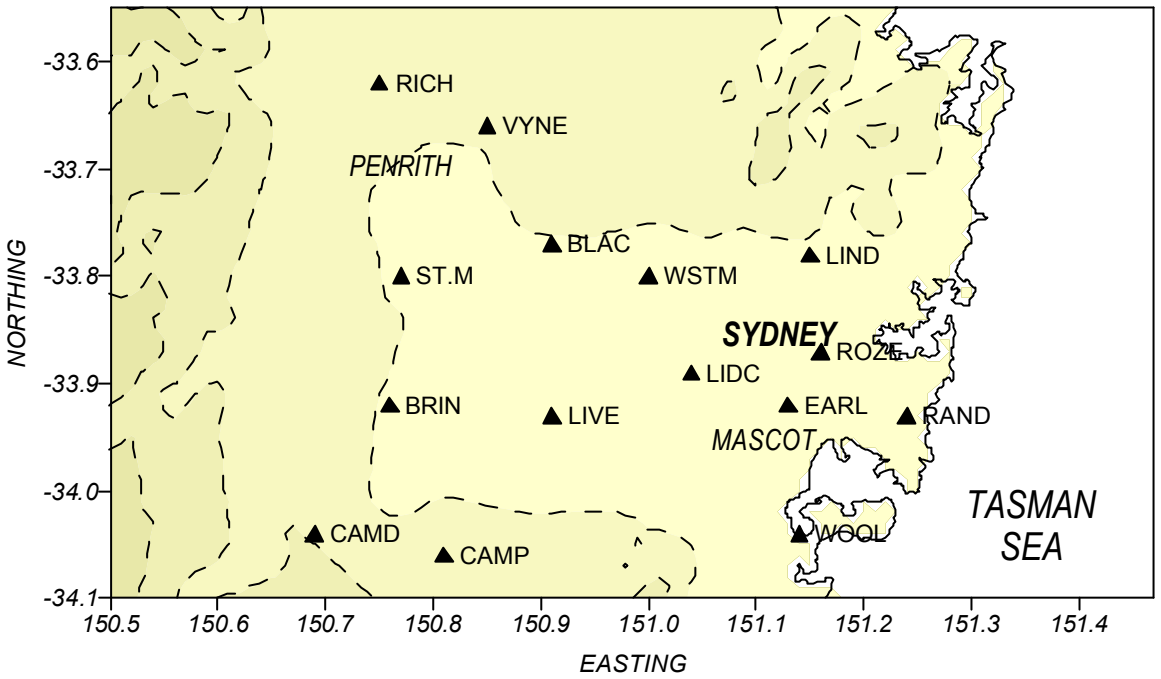

Figure 2.5.1. Location of EPA NSW monitoring network for Sydney region (BLAC-Blacktown, BRIN-Bringelly, CAMD-Camden, CAMP-Campbelltown, EARL-Earlwood, LIDC-Lidcombe, LIND-Lindfield, LIVE-Liverpool, RAND-Randwick, RICH-Richmond, ROZ-Rozelle, ST.M-St. Marys, WOOL-Woolooware, WSTM-Westmead, VYNE-Vineyard.

2.5.1 Primary gaseous pollutants

First we review model performance in forecasting the concentrations of nitrogen compounds (recall from **Section 2.4** that NO_y = NO_x + other nitrates is a semi-conserved tracer), carbon monoxide and sulfur dioxide. We begin by considering model performance in the prediction of the upper percentiles of the frequency distributions for 1-hour average concentrations of these three species.

Frequency Distributions. Shown in Figure 2.5.2 and Figure 2.5.3 are scatter diagrams of upper percentiles (50^{th}, 90^{th}, 99.5^{th}, 99.9^{th} and 100^{th} percentiles) for the observed and modelled 1-hour concentration frequency distributions of NO_y, CO and SO_2 for March and June–July 2001. As noted in **Section 2.4.1,** these plots represent a summary of single-station line plots of the observed and modelled frequency distribution (see Figure 2.4.5). The data are coupled in space (bi-linear interpolation from the CTM grid to each monitoring site) but uncoupled in time. Bias statistics of system performance are given in Table 2.5.1.

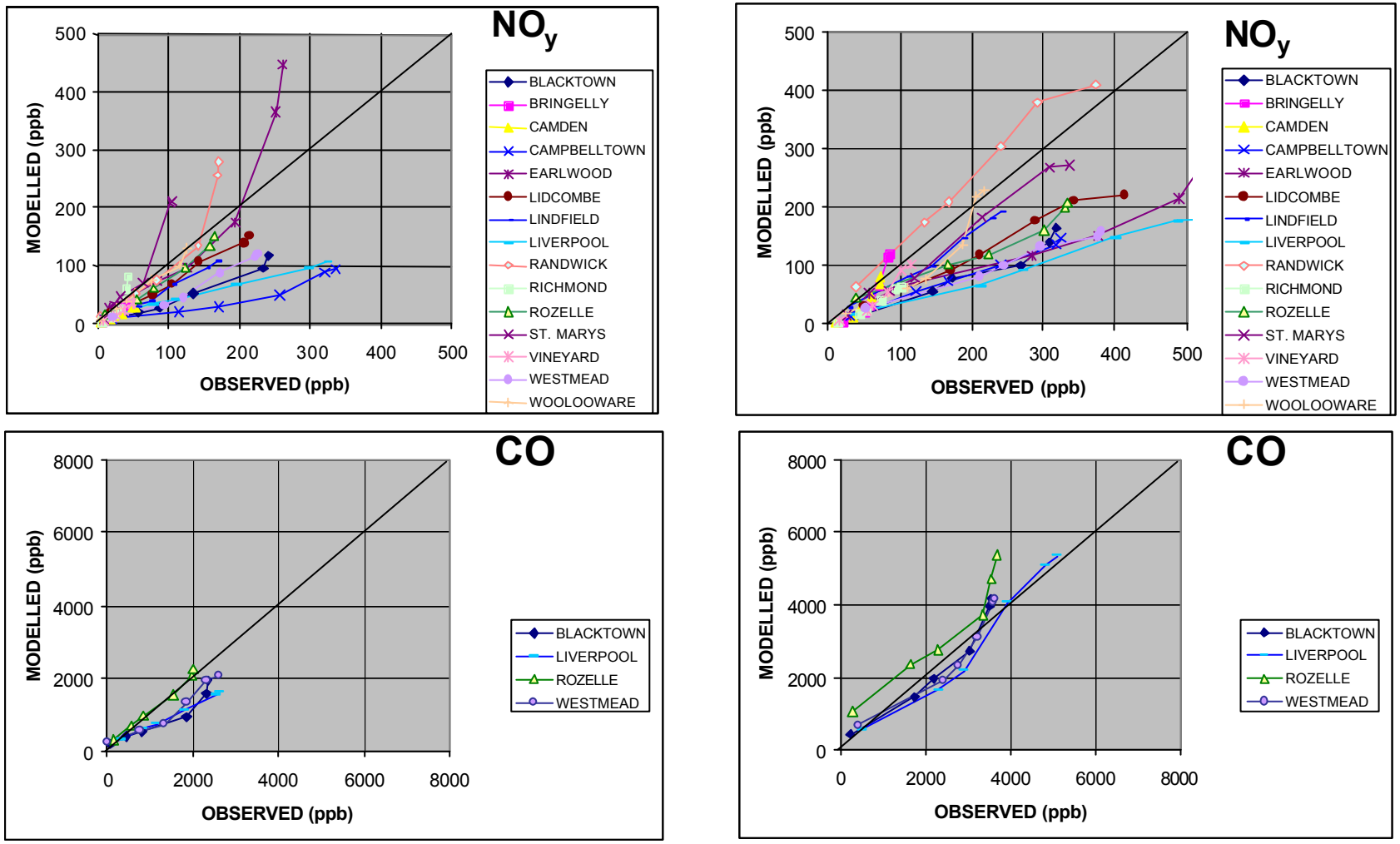

Figure 2.5.2. Plots of observed and forecast percentiles of the NO_y and CO concentration distribution (50th, 90th, 99th, 99.5th, 99.9th, and 100th percentiles) for March 2001 (left) and June–July 2001 (right) — for selected monitoring stations in the Sydney region.

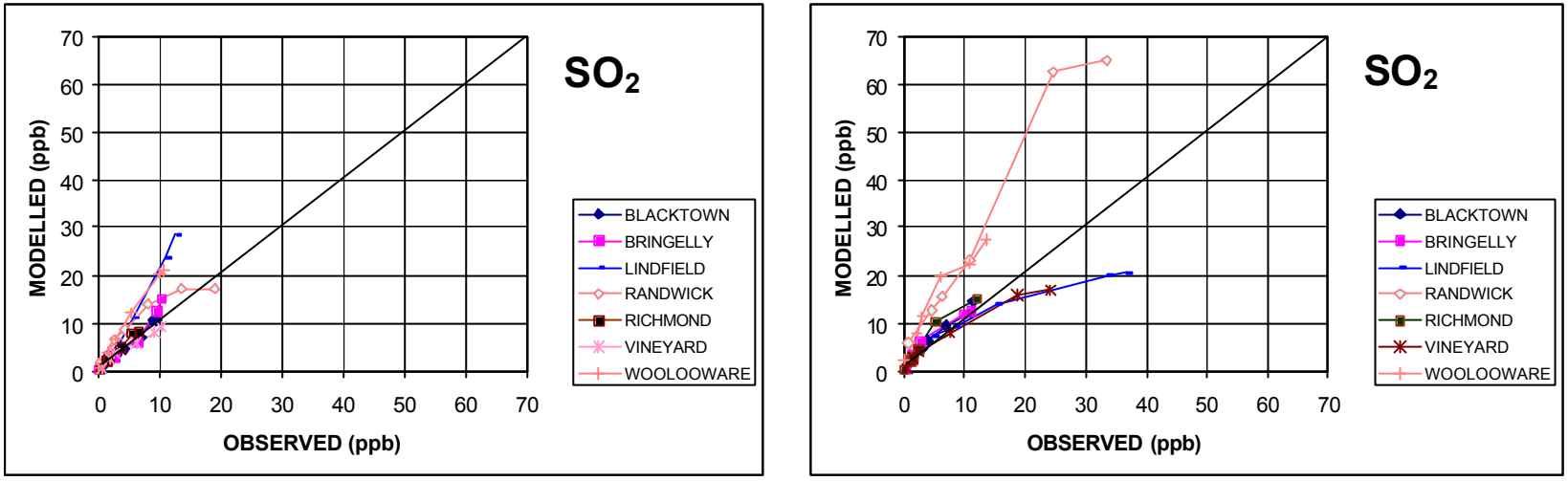

Figure 2.5.3. Plots of observed and forecast percentiles of the SO_2 concentration distribution (50^{th}, 90^{th}, 99^{th}, 99.5^{th}, 99.9^{th}, and 100^{th} percentiles) for March 2001 (left) and June–July 2001 (right) — for selected monitoring stations in the Sydney region.

Table 2.5.1. Percentage normalised bias for NO_y, NO_2, O_3, CO, PM2.5, PM10 and SO_2 for Sydney — March 2001 and June–July 2001.

	NO_y bias (%)		NO_2 bias (%)	
Percentile	March	June/July	March	June/July
50	-20.5	-29.5	-16.6	-16.7
90	-49.9	-47.7	-11.5	2.8
95	-53.6	-46.6	-10.4	10.7
99	-46.4	-40.9	-16.0	30.8
99.9	-32.3	-33.4	-8.8	50.0
100	-24.8	-35.3	-9.7	51.1
	O_3 bias (%)		**CO bias (%)**	
Percentile	Jan/March[1]	June/July	March	June/July
50	53.3	22.0	N/A	N/A
90	-5.8	5.1	-10.9	-9.8
95	-12.6	4.1	-38.7	-9.5
99	-18.5	13.1	-49.3	0.0
99.9	-26.0	23.7	-31.9	14.9
100	-29.2	23.2	-17.5	18.7
	PM2.5 bias (%)		**PM10 bias (%)**	
Percentile	March	June/July	March	June/July
50	5.0	108.4	-39.8	90.4
90	61.6	112.8	-23.1	143.2
95	74.2	142.3	-13.6	176.2
99	90.7	203.6	7.0	224.4
99.9	40.7	290.8	3.2	222.3
100	-0.8	162.4	5.1	188.8
	SO_2 bias (%)			
Percentile	March	June/July		
50	N/A	N/A		
90	40.4	-13.9		
95	13.6	-14.7		
99	-0.7	-25.2		
99.9	26.5	-45.9		
100	32.0	-52.2		

[1]Includes the period 21–27 January 2001.

With respect to system performance for NO_y, it can be seen that that, although AAQFS has correctly reproduced the increase in the observed peak concentrations when going from the warmer to cooler months, the observed percentiles are generally under-predicted by the System (*e.g.* average bias at the 99.9 percentile is -32% for March and -33.4% for June–July). There is also considerable scatter in the results, ranging from systematic over-prediction at Randwick monitoring station to strong under-prediction at Liverpool monitoring station (see Figure 2.5.1 for locations).

It is interesting to contrast these results with those from the Melbourne–Geelong comparison in **Section 2.4**, where both the bias and scatter are reduced (*i.e.* average bias at the 99.9 percentile is -8% and -15% for March and June–July respectively in the Melbourne-Geelong data). Note, however, that the reduction in scatter may also be due to the smaller number of Melbourne-based monitoring stations used in that assessment.

The observed upper percentiles of 1-hour carbon monoxide concentration are better predicted by the System (Figure 2.5.2-bottom) with a bias between the observed and predicted 99.9 percentile of -18% for March 2001 and 19% for June–July 2001.

Scatter plots of observed and modelled SO_2 percentile concentrations are shown in Figure 2.5.3. It can be seen that a good correspondence exists between observed and modelled percentiles for Blacktown, Bringelly and Vineyard. On the other hand, the peak percentile concentrations are over-predicted at Lindfield in March, and over-predicted at Randwick in June–July. This result is similar to that found for the Melbourne analysis, where the general urban concentrations of SO_2 were well reproduced by the system, and the larger SO_2 values resulting from point source industrial plume impacts at particular monitoring stations were more difficult for the System to reproduce.

Forecasting daily maxima. Now we examine the system's ability to forecast peak daily concentrations of 1-hour NO_y, 8-hour CO (rolling averages) and 1-hour SO_2. Shown in Figure 2.5.4 are plots of mean fractional bias (see **Section 2.4.1** for definitions) for daily peak 1-hour NO_y, daily peak 8-hour CO and daily peak 1-hour SO_2. The statistics are derived for the period covering one week in January, all of March, and all of June–July 2001. Note that the comparison has been undertaken for a representative eleven monitoring-station subset (Blacktown, Bringelly, Campbelltown, Lindfield, Lidcombe, St. Mary's, Randwick, Rozelle, Vineyard, Westmead and Wooloowware). In calculating fractional bias, consideration has only been given to days in which pollutant concentrations are substantially above background (NO_y > 100 ppb, CO > 1000 ppb and SO_2 > 10 ppb).

Because O_3 concentrations did not significantly exceed background levels in the Sydney region during March 2001, the analysis has been supplemented to include the period 21–27 January 2001, a high ozone period (see **Section 7.2 Sydney 7-Day Photochemical Smog Event**).

Recalling from **Section 2.4.1**, that a fractional bias of ±0.667 represents a relative error of two, it can be seen that in the study period, peak 1-hour NO_y was initially under-predicted by more than a factor of two by AAQFS. However, it can also be seen that the amount of under-prediction has decreased over the period and that the observed peak daily NO_y was under-predicted by about 50% in July 2001. This can be contrasted with the Melbourne results (*c.f.* Figure 2.4.8 and Figure 2.4.10), where it can be seen that, although a positive trend in fractional error is also evident, initial levels of under-prediction were already only 50%, and this became a 25% over-prediction by the end of the study period. Note that the trend to predict higher peak concentrations of NO_y, in both Melbourne and Sydney was a result of ongoing improvements to the CTM.

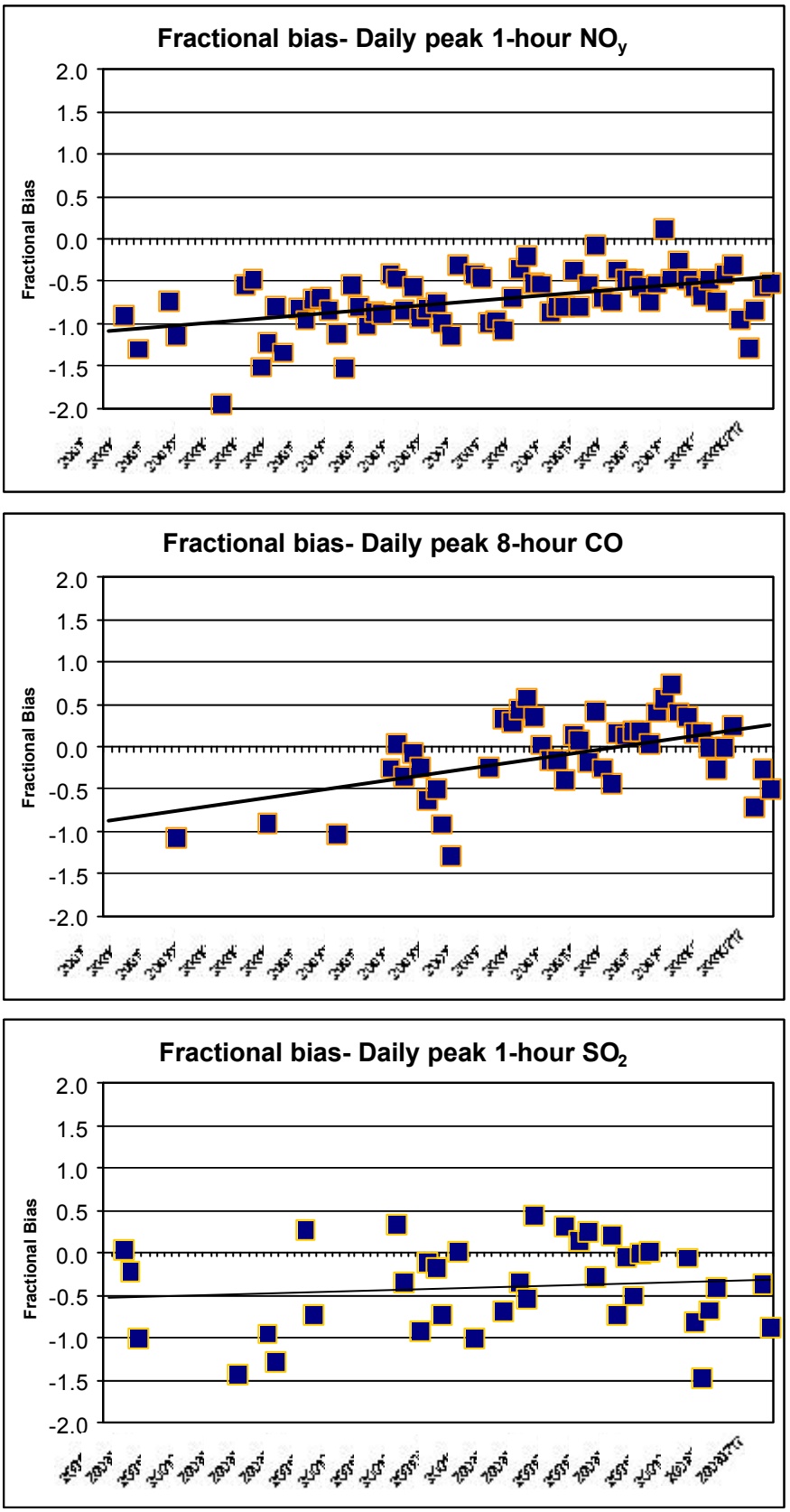

Figure 2.5.4. Fractional bias of peak daily 1-hour NO_y, 8-hour CO and 1-hour SO_2 for Sydney 21–27 January 2001, March 2001 and June–July 2001. Least squares regression trend lines are also shown for each pollutant.

Observed concentrations of daily peak (running) 8-hour CO (Figure 2.5.4 middle plot) display a similar trend to NO_y. However, in this case the system predicts CO with a positive bias towards the end of the study period. Results for the final month of the study period are comparable to those observed in the Melbourne analysis. It is also interesting to note that the fractional gross error (E_f, see **Section 2.4.1** for definitions) is 0.44 (equivalent to a daily average variation between predicted and observed of about 50%), which is slightly improved compared to Melbourne ($E_f = 0.51$).

The mean fractional bias for predicted peak daily 1-hour SO_2 is -0.4 (50% under-prediction), with a fractional gross error of 0.53 (daily average prediction error of about 70%). This is a considerably better result than for Melbourne, where $B_f > 0.7$ and $E_f > 0.9$. This suggests that the sources responsible for peak daily SO_2 in Sydney are in the far field, and are thus easier to resolve than was found to be the case at Paisley monitoring station in Melbourne.

The final component of this section examines the ability of the system to forecast exceedences of prescribed concentration thresholds. This ability may be analysed through the use of contingency tables (De Leeuw 2000). A brief description of contingency tables and related definitions is given in **Section 4.2.1**. An important point to note is that an effective forecast model should have a high probability of detection and a low false alarm rate. Detection rates in the range 30–70 % and false alarm rates in the range 15–60% have been reported in the literature for forecasting regional ozone. Following the recommendations of De Leeuw (2000), we have also generated forecasts using a simple persistence model (*i.e.* the forecast pollutant concentration for day '**i**' is equal to the observed pollutant concentration on day '**i - 1**'). It is desirable to demonstrate that a proposed forecast model be able to provide a superior forecast to the persistence model.

Plots of detection probability (*SP*) and false alarm rates (*1 - SR*) are shown in Figure 2.5.5 for peak daily 1-hour NO_y, and peak daily 8-hour CO. Comparable plots for Melbourne can be seen in Figure 2.4.11. Note that 'CTM' corresponds to a comparison between an observed daily maximum concentration and a predicted concentration that has been interpolated to the location of the monitoring site (prediction and observation are matched in space). 'CTM-range' corresponds to a comparison between the observed concentration and the maximum predicted concentration within ±1 grid cell of the monitoring site. Plots of model performance for forecasting Sydney NO_y maxima are also shown (see plot labelled 'Airshed Daily Peak 1-hr NO_y').

From a consideration of Figure 2.5.5, it can be seen that AAQFS has had difficulty in forecasting daily maximum concentrations of NO_y and CO with more skill than a persistence model at the local scale. This is in contrast to the Melbourne forecasts where it was found that AAQFS had considerably better performance than persistence for NO_y and a comparable performance for CO. In the case of NO_y for Sydney, it can be seen that AAQFS has a lower probability of detection, particularly for an exceedence threshold in the range 100–200 ppb. Paradoxically, AAQFS also generated a higher false alarm rate. Both of these outcomes can be explained on the basis of the frequency distribution plots and fractional bias plots for NO_y (Figure 2.5.2 and Figure 2.5.4). The fractional bias plot demonstrates that peak daily NO_y is, on the average, under-predicted, hence the low probability of detection. The frequency plot demonstrates that NO_y can be strongly over-predicted at some inner-suburban sites—hence the high fraction of false alarms.

On the other hand, it should also be noted that AAQFS has improved performance compared to persistence when forecasting daily maxima for the entire Sydney basin (Figure 2.5.5). In this case it can be seen that AAQFS has both a higher probability of detection and a lower false alarm rate compared to the persistence model.

AAQFS performance for 8-hour CO is generally comparable or improved relative to NO_y for both the local-scale and airshed forecasts (latter not shown). For example, because CO has a smaller negative bias than NO_y in the prediction of daily peak concentrations, the CTM-range forecasts of CO have a superior probability of detection compared to the persistence model.

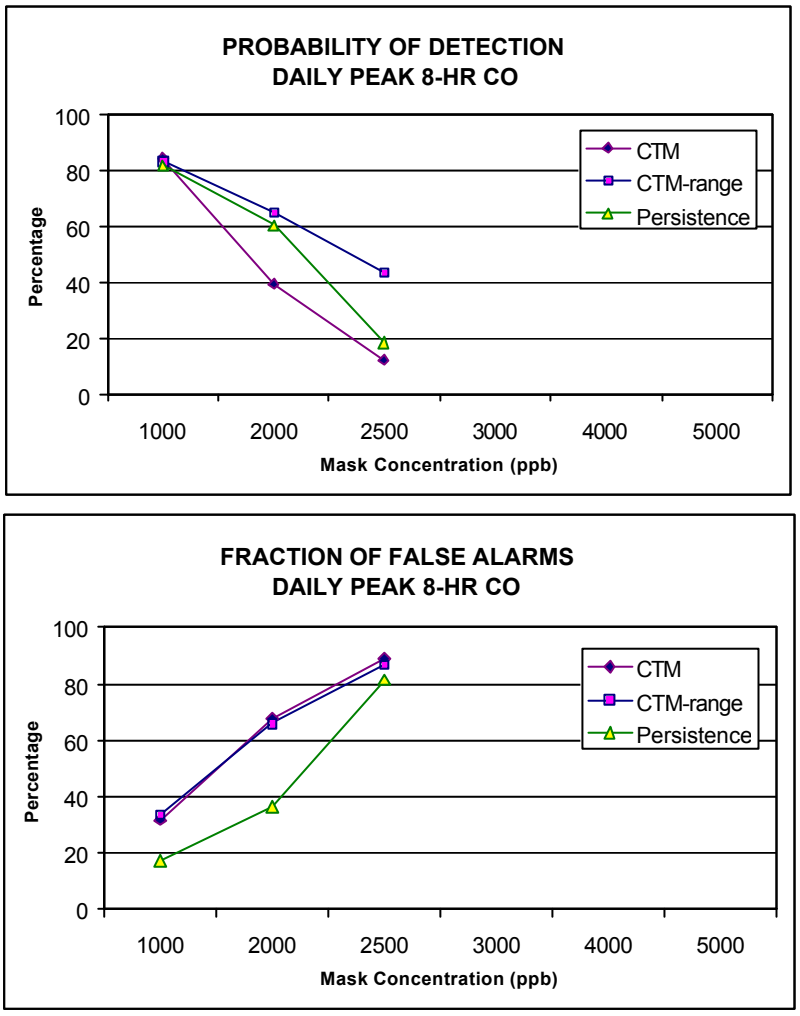

Figure 2.5.5a. Contingency table outcomes for daily 8-hour CO. Sydney — 21–28 January 2001, March 2001 and June–July 2001.

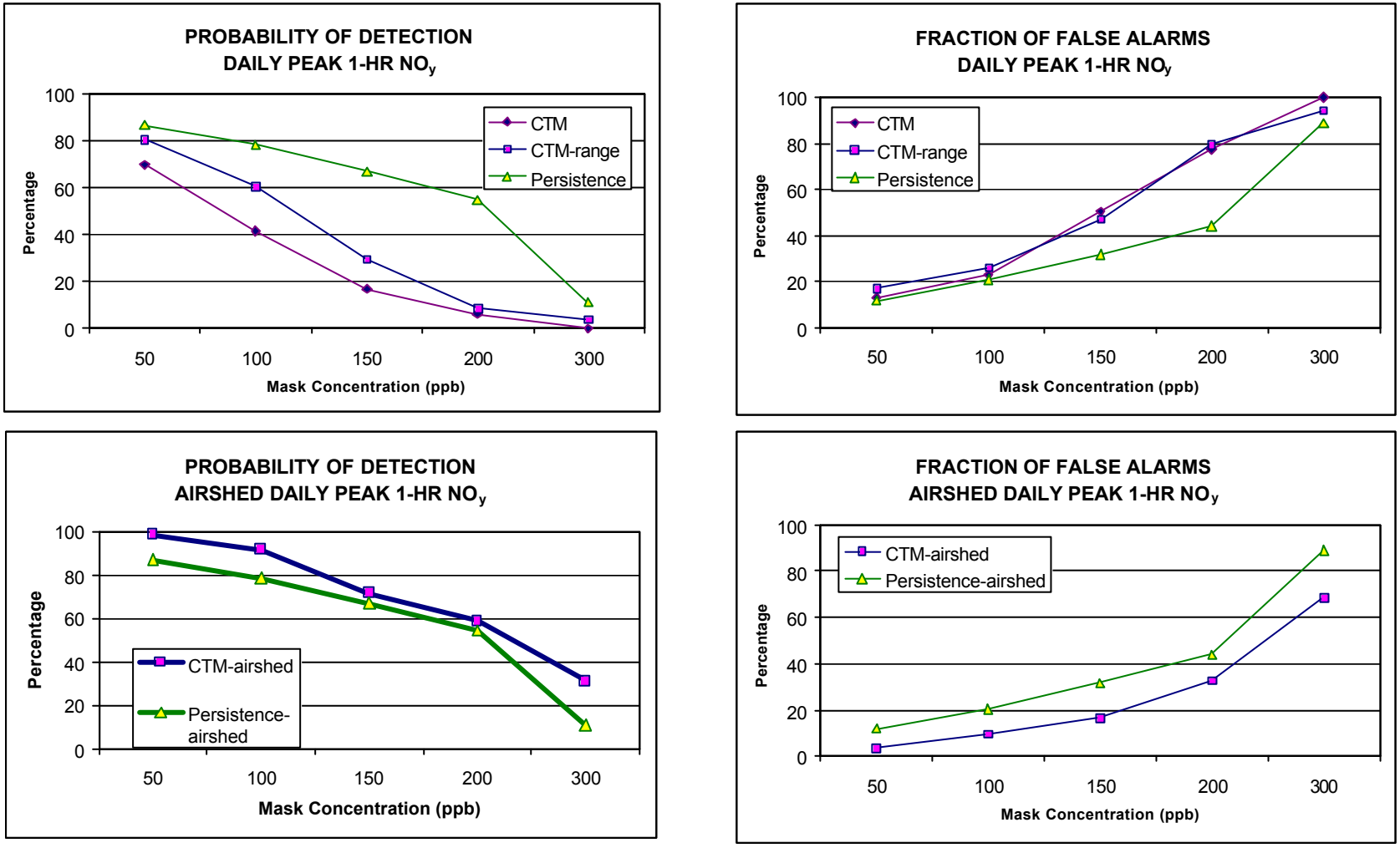

Figure 2.5.5b. Contingency table outcomes for daily 1-hour NO_y. Sydney — 21–28 January 2001, March 2001 and June–July 2001.

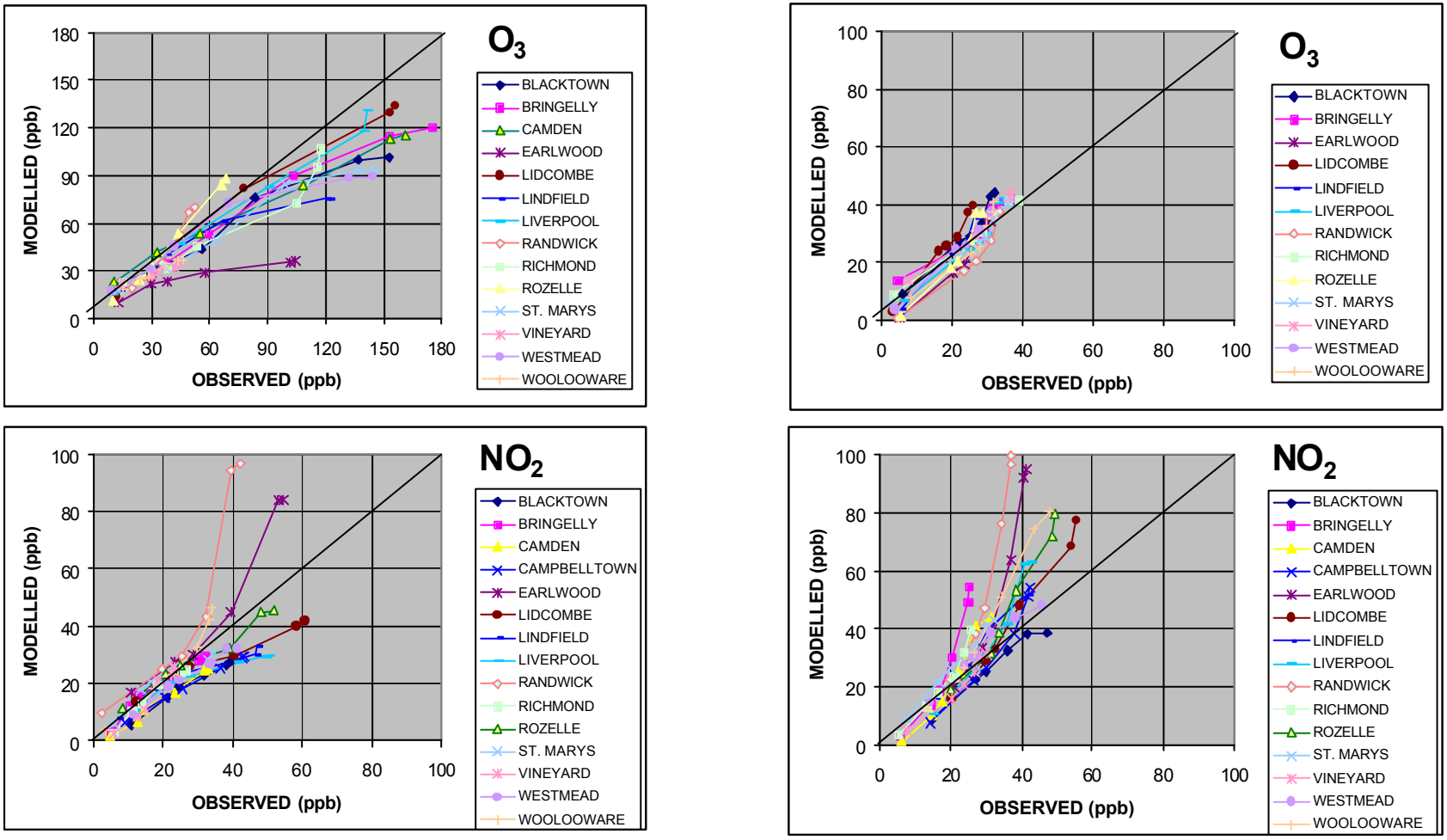

Figure 2.5.6. Plots of observed and forecast percentiles of the O_3 and NO_2 concentration distributions (50^{th}, 90^{th}, 99^{th}, 99.5^{th}, 99.9^{th}, and 100^{th} percentiles) for 21–27 January and March 2001 (left) and June–July 2001 (right) — for selected monitoring stations in the Sydney region.

2.5.2 Secondary gaseous pollutants.

As noted in **Section 2.4.1** the forecasting of extreme photochemical smog events is a primary objective of AAQFS. Consideration is given in this section to the System's ability to forecast peak 1-hour concentrations of ozone and nitrogen dioxide within the Sydney region.

Frequency Distributions. Figure 2.5.6 shows scatter diagrams of observed and modelled percentiles from the concentration distributions of 1-hour O_3 and 1-hour NO_2. Note that the O_3 scatter diagram for March has been extended to include data from 21–27 January 2001, a period during which significant concentrations of O_3 were observed. Normalised bias results are also presented in Table 2.5.1.

Figure 2.5.6 demonstrates that the System has done a reasonable job at predicting the upper range of the O_3 concentration distribution for most sites in the Sydney region for both January/March and for June–July (although the latter primarily consists of near-background concentrations). Peak ozone concentrations are, on average, under-predicted by about 25–30%, which is generally considered a good result for a state-of-the-art chemical transport model. However, it can also be seen from Table 2.5.1, that the 50^{th} percentile ozone concentration is biased high, a probable cause and solution for this problem is discussed in **Section 2.4.2.**

With respect to NO_2, it can be seen that the system is biased towards over-prediction at the higher percentiles. This is particularly apparent during the months of June and July (Figure 2.5.6-bottom). A similar result is also apparent for the Melbourne forecasts (Figure 2.4.15). Again a probable cause and solution for this problem are discussed in **Section 2.4.2**.

Forecasting daily maxima. The daily average fractional bias for peak 1-hour NO_2 is presented in Figure 2.5.7. It can be seen that NO_2 is forecast with the smallest bias of any of the pollutants (B_f = -0.09; E_f = -0.29). Again it can be seen that the magnitude of the fractional bias has been reduced during the course of the study. Part of the reason for the good performance is that NO_2 is created from titration of nitric oxide with the background ozone field. In the presence of excess nitric oxide, peak concentrations of NO_2 are determined by the background ozone concentration plus the small component of NO_2 in NO_x emissions (typically about 10%) plus photochemical production. Even though we have set a lower-bound threshold of 30 ppb for the comparison of observed and modelled daily peak NO_2, it is likely that our results may still be dominated by NO_2 production through the easily modelled process of titration.

Because peak daily ozone exceeded background concentrations for only a small number of days in the study period, it is not useful to present results for daily ozone maxima. Instead, presented in Figure 2.5.8 are time series plots of observed and modelled 1-hour ozone concentration for the period 21–27 January 2001. The time series plots indicate that the system has generally been able to reproduce the gradient of increasing ozone concentrations with distance inland from the coast. It can also be seen that the system has done well at reproducing peak concentrations to the southwest on the third day of this high-ozone event (*i.e.* at Liverpool and Campbelltown). However, the model has had difficulty in reproducing the large concentrations of ozone observed at the northwestern stations (*e.g.* St. Mary's), and also in reproducing the significant ozone concentrations observed at all inland monitoring stations on the fourth day of the event. The reasons for this are discussed in **Appendix 7.2 Sydney 7-Day Photochemical Smog Event**.

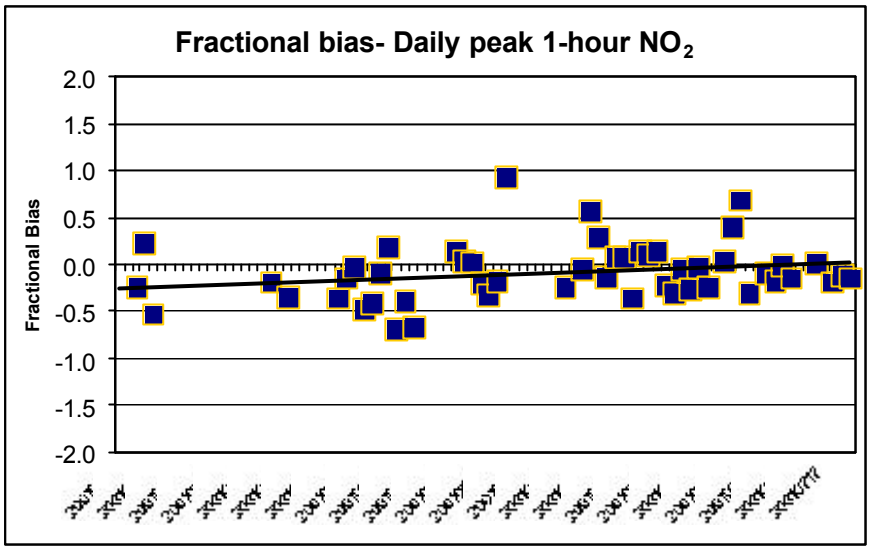

Figure 2.5.7. Fractional bias of peak daily 1-hour NO_2, for Sydney — 21–27 January 2001, March 2001, June–July 2001. A least square regression trend line is also shown.

Table 2.5.2. Performance measures for O_3 for Sydney monitoring stations for 21–27 January 2001.

STATISTICAL MEASURE	OZONE							BENCH MARK
	Day							
	21	22	23	24	25	26	27	
Unpaired highest prediction accuracy (%)	-7	-30	-3	-24	74	24	64	±15–20
Bias (ppb)	-10	-19	-18	-27	-20	11	1	
Normalised Bias (%)	-15	-26	-17	-29	-22	21	5	±5–15
Gross error (ppb)	13	20	26	29	30	16	14	
Normalised gross error (%)	20	29	29	33	44	29	27	±30–35

Various performance measures for the 7-day period in January 2001 are presented in Table 2.5.2. A discussion regarding the performance of the system in reproducing both the meteorological and air quality aspects of this event is given in **Section 7.2 Sydney 7-Day Photochemical Smog Event** of this Report. A preliminary indication of system performance may be obtained through comparing the statistics in Table 2.5.2 with the indicated benchmarks, namely, the magnitude of peak unpaired prediction accuracy, overall bias and gross error statistics should fall within the ranges ±15–20%, ±5–15% and ±30–35% respectively. As can be seen from Table 2.5.2, AAQFS achieves the first and second measures on two of the seven days, and achieves the third measure on six of the seven days. An inability to achieve all of the measures is a direct result of the difficulty in modelling an extremely complex cycle and interaction of mesoscale and synoptic scale meteorological processes, which occurred during the seven-day period.

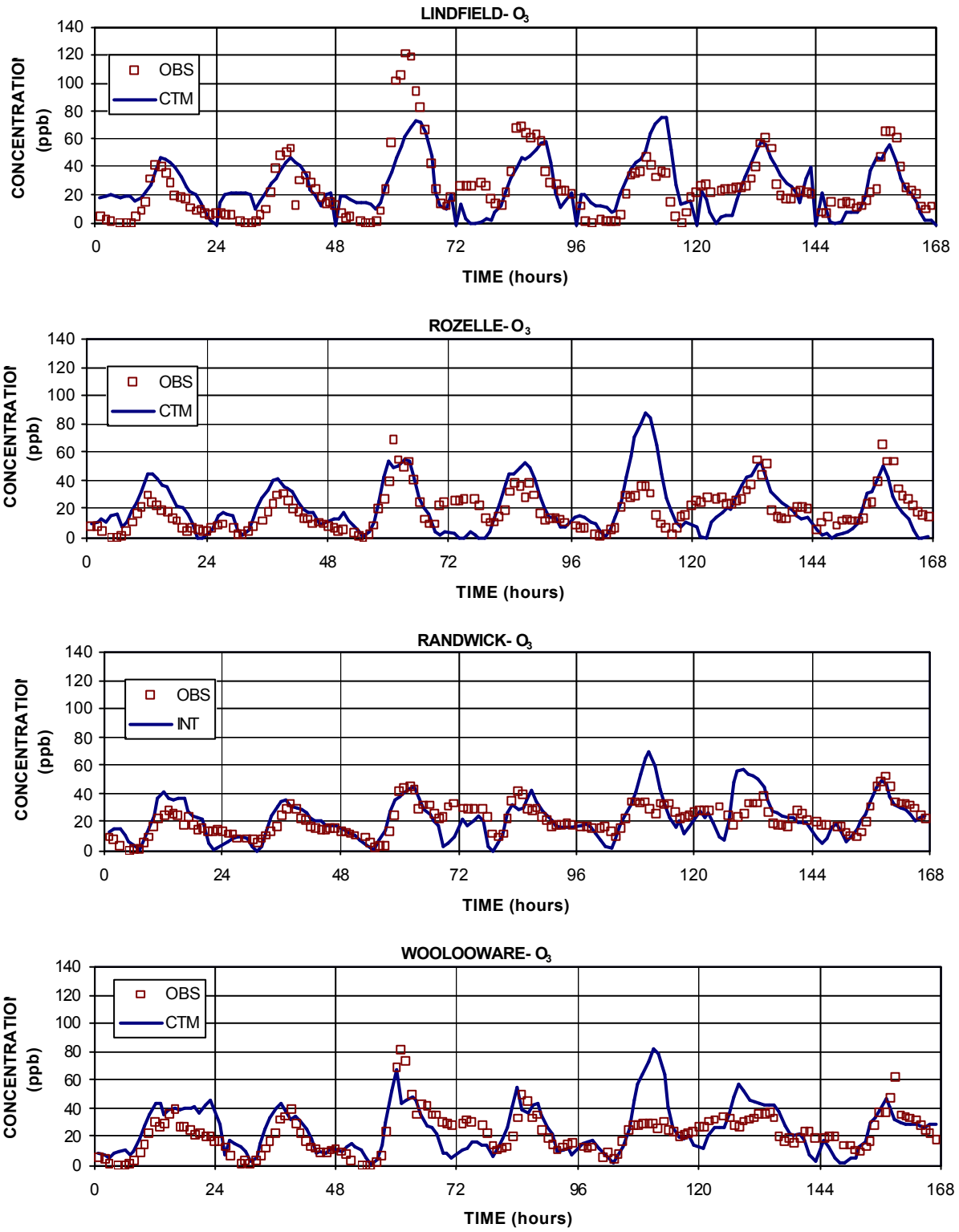

Figure 2.5.8a. Observed (obs) and forecast (CTM) 1-hour ozone concentration time series for 21–27 January 2001 — selected NSW EPA coastal/eastern suburb monitoring stations.

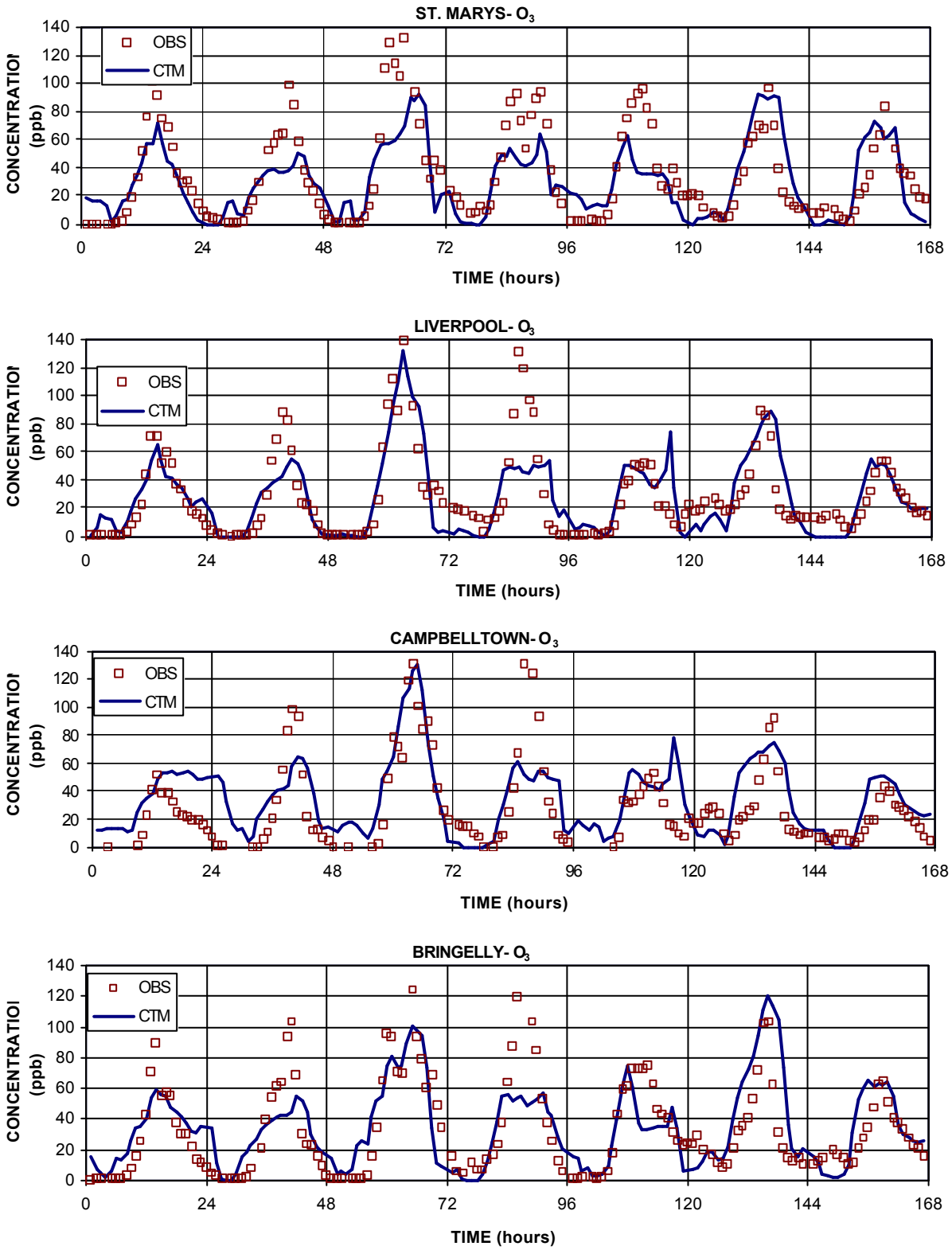

Figure 2.5.8b: Observed (obs) and forecast (CTM) 1-hour ozone concentration time series for 21–27 January 2001 — selected NSW EPA inland monitoring stations

Plots from contingency tables of system performance for daily peak 1-hour NO_2 and O_3 are presented in Figure 2.5.9. As was done for Melbourne, we have included a plot of model performance for forecasting the airshed O_3 maxima. With respect to NO_2 it can be seen that AAQFS performance is comparable to the persistence model until NO_2 exceeds 50 ppb. AAQFS then performs better than persistence, although the probability of detection is low. AAQFS has a higher fraction of false alarms compared to persistence, an outcome that is a result of the over-prediction of NO_2 (particularly during the winter months) by AAQFS.

AAQFS performance in forecasting peak 1-hour ozone is mixed. Note that these results are dominated by the System performance for the period 21–27 January 2001. Because ozone concentrations in excess of 80 ppb were observed on all days of the event, the persistence model was able to generate very favourable performance statistics. On the other hand, although AAQFS has been able to forecast the presence of extreme ozone concentrations within the airshed (see discussion in **Section 7.2**), the complexity of the meteorological fields during the seven-day period has occasionally led to difficulties in correctly predicting the spatial distribution of the ozone plume. Thus, when consideration is given to the space-paired (in the case of CTM) and near-space paired (in the case of CTM-range) prediction/observed pairs, small relative errors in plume location have degraded the accuracy of the local-scale forecasts from AAQFS. This can be seen from Figure 2.5.9, where, for peak daily ozone concentrations in the range 60–90 ppb, the persistence model was able to maintain detection probabilities of 60–70%, while AAQFS detection probabilities were in the range 30–70%. However, although the AAQFS detection probabilities are reduced compared to persistence, the false alarm rate for persistence is higher.

Furthermore, when consideration is restricted to the forecasting of airshed maxima, it can be seen that the persistence model and AAQFS had comparable performance with respect to detection probability, and that AAQFS generally has a considerably lower false alarm rate.

2.5.3 Aerosol

As noted in **Chapter 1,** one of the objectives of AAQFS is to generate forecasts of PM2.5 and PM10. Performance of the System in forecasting these components has been examined in detail for Melbourne and Geelong in Victoria in **Section 2.4.3.** It was found that aerosol was under-predicted during March and over-predicted during June and July. It was suggested that under-prediction of aerosol mass during the warmer dryer months might be primarily caused by the lack of a wind-blown dust component in the system and through uncertainties in boundary conditions. Both of these issues are currently being remedied. During the winter months, strong over-prediction of aerosol mass appears to be a result of over-prediction of domestic wood-burning emissions. The emissions factors are currently under review.

Shown in Figure 2.5.10 are scatter plots of observed and predicted percentiles for PM2.5 and PM10 for the March and June-July study periods. Bias statistics are presented in Table 2.5.1. A comparison of the seasonal variation in peak concentration for either pollutant demonstrates the impact of the wood-burning algorithm (**Section 3.2.2** and **Appendix 3.2**), with peak predicted concentrations increasing by a factor of 2–3 for some sites. This is consistent with the results presented for Melbourne. However, where the Sydney results differ from Melbourne is in the prediction of PM10 for March 2001. In the case of Melbourne, PM10 was generally predicted with a negative bias. However, for Sydney, there are a number of sites where the System exhibits a strong positive bias (*i.e.* Randwick and St. Mary's). Visual inspection of the spatial PM10 concentrations generated by AAQFS indicate that both of these

site are downwind of significant local sources of PM10. This would suggest that the source of over-prediction, for these sites at least, might be resolved through a careful inspection and revision of the Sydney emissions inventory for aerosol.

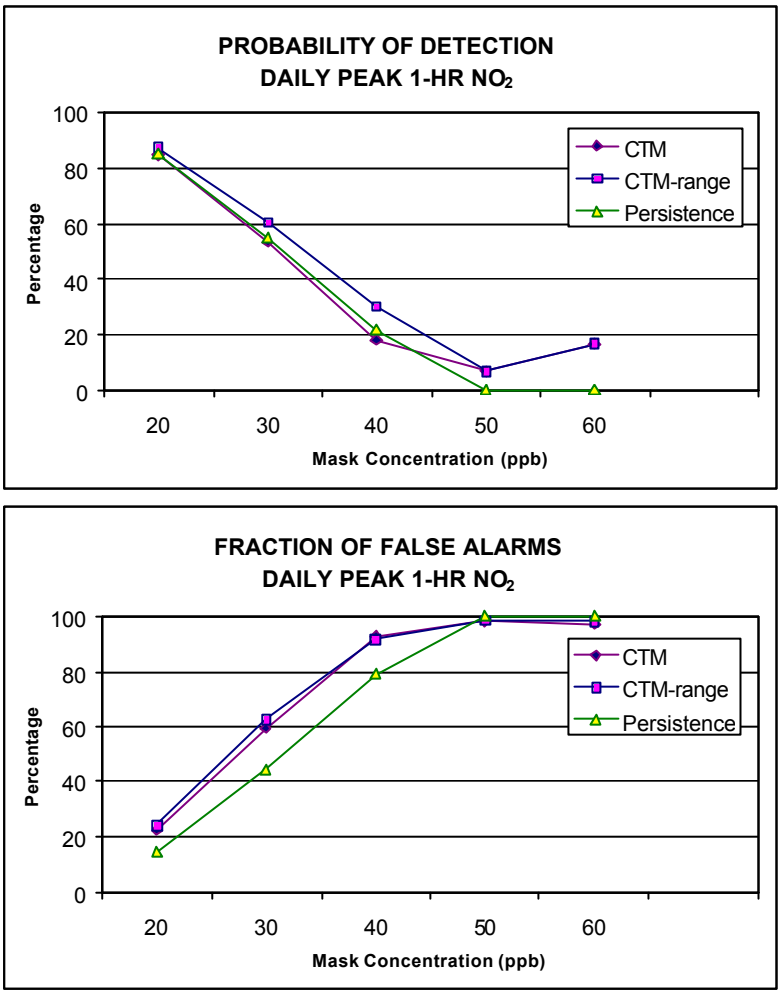

Figure 2.5.9a: Contingency table outcomes for daily 1-hour NO_2 — Sydney 21–27 January, March 2001 and June–July 2001.

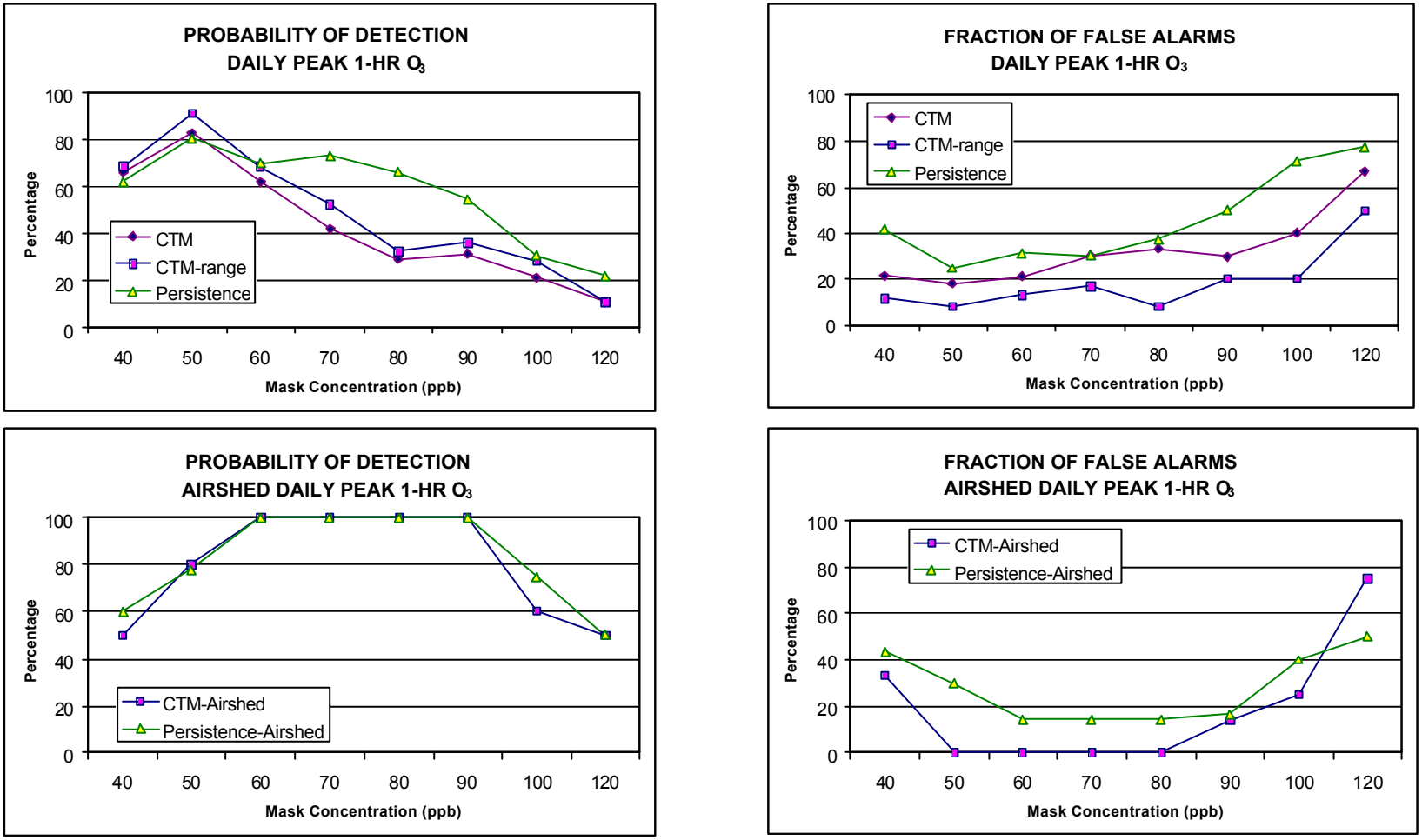

Figure 2.5.9b. Contingency table outcomes for daily 1-hour O_3 — Sydney 21–27 January, March 2001 and June–July 2001.

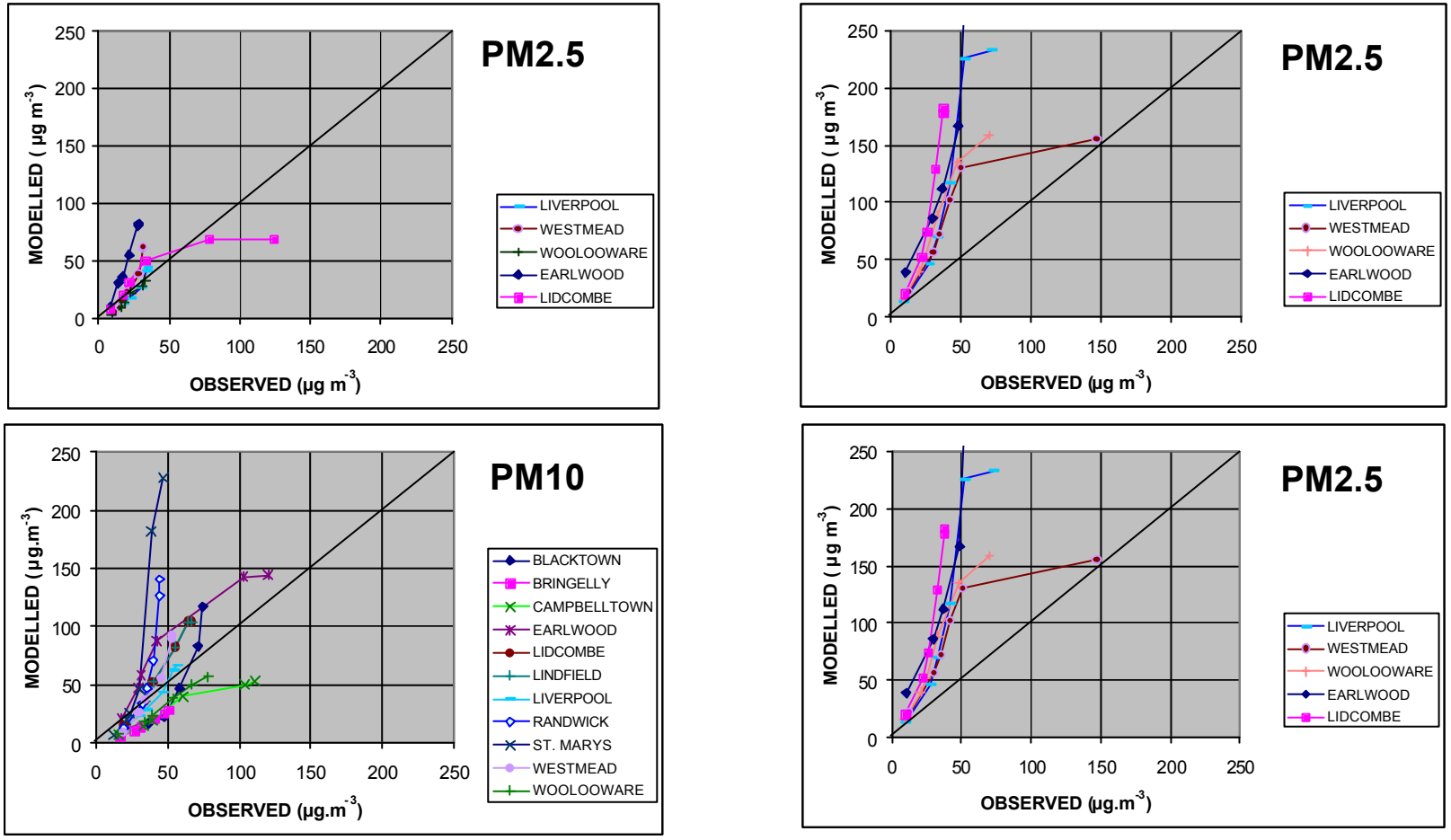

Figure 2.5.10. Plots of observed and forecast percentiles of the PM2.5 and PM10 concentration distributions (50th, 90th, 99th, 99.5th, 99.9th, and 100th percentiles) for March 2001 (left) and June–July 2001 (right) — for selected monitoring stations in the Sydney region. Note different scales used for the PM10 plots.

2.6 Operational Performance of AAQFS

The ability to model the air quality over large domains on the scale of a few kilometres is made possible by the HPCCC supercomputers jointly owned by CSIRO and BoM. The actual computers used in AAQFS also include work stations in addition to the NEC-SX5 supercomputers, 'florey' (16 processors) and 'russell' (8 processors). The capabilities of the System are changed and upgraded from time to time, so the configuration of the System continues to evolve to keep up with these changes. The current configuration is shown in Figure 2.6.1 in simplified form. (On 15 August 2001 'russell' was upgraded to 16 processors.)

The BoM global meteorological model (GASP) is run first on 'florey'. The meteorological data analysis, pre-processing, and post-processing components are not shown in Figure 2.6.1. LAPS at 0.375^{o} horizontal grid resolution is nested within GASP. Once LAPS375 is run, its output is used to provide initial conditions and boundary conditions for the LAPS05 domains for Victoria and NSW. (We had been running a further nesting step by nesting the LAPS125 within the LAPS375 model, and also using the screen temperature output from LAPS125 as input for the emissions models. However to speed up the operation of the System we are now by-passing this step, and using the screen temperature output from LAPS375 for emissions modelling.) The above models, GASP, LAPS375 and LAPS125, are run on 'florey'.

Recently the LAPS05 models for Victoria and NSW were moved to 'russell' to avoid congestion on 'florey' and to improve the times of completion of the forecasts. As the number of processors increases on 'russell', more of the System will be run there. The output from the LAPS05 model runs is transferred to 'florey' and used to drive the CTMs for Victoria and NSW. The CTM pre-processor (part of the CTM diagram) includes the emissions model and the emissions inventory, based on data provided by the EPAs.

Output from the LAPS05 models and the CTM models are post-processed on 'florey'. Data files are generated for plotting, archiving, and for verification of the forecasts. In addition some files are generated for direct transfer to the EPAs via the ftp sites. Plots are displayed on the AAQFS web site and also sent to the EPAs via e-mail. Data from the EPAs are used in verification of the CTM. The verification results are displayed on the AAQFS web site. The near-surface concentrations are archived along with the initial and boundary conditions for the CTM and the entire model output of the LAPS05 models. This allows the CTM to be re-run at a later time, if required.

It is critically important that the System be able to generate and disseminate the forecasts in time to provide input into the EPAs' daily forecasting process. In the case of both the NSW and Victorian EPA, this currently requires that (1) images of peak ground-level pollutant concentration and air quality index be e-mailed directly to each EPA, and (2) the images of the hourly variation of ground-level pollutant concentrations and air quality index be available for download from the AAQFS web site (see **Chapter 4—Outputs from AAQFS**). Both sets of information must be delivered to each EPA before 3 pm each day, and the results of a confirmation forecast must be available by 9 am the following morning.

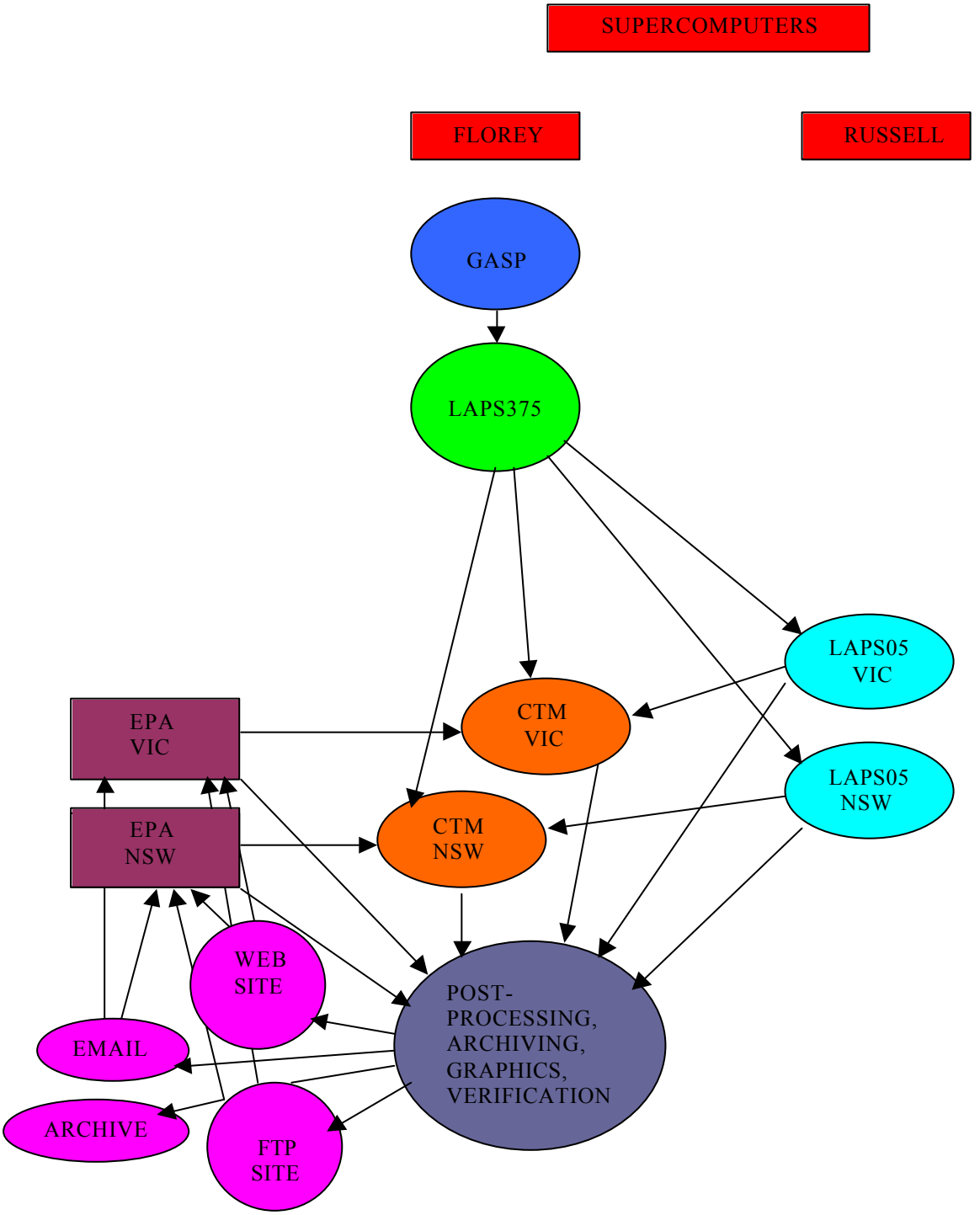

Figure 2.6.1. Simplified schematic flow diagram of the computing showing the two supercomputers, 'florey' and 'russell', and where the EPAs' data inputs enter into the System, and where data outputs go to the EPAs.

Experience has shown that the 3pm deadline is the more difficult to achieve because it requires that the System be run during a period of peak demand on the NEC-SX5 supercomputers (*i.e.* between 11 am and 2 pm). System performance for achieving the 3 pm deadline is summarised in Figures 2.6.2–2.6.4. In Figure 2.6.2 we have plotted the commencement and completion times for the pre-processing, CTM integration, and post-processing stages for the NSW and Victorian pm forecasts. In Figure 2.6.3 we show time series of elapsed time (wall clock time, not CPU time) for completing pre-, post-processing and CTM stages, and in Figure 2.6.4 we present the cumulative frequency distribution of delivery times. All plots are for the period 23 October 2000 to 31 March 2001. Note that the commencement time corresponds to the time at which data files become available from the LAPS05 36-hour forecast (thus the elapsed time doesn't include the time taken to run the numerical weather prediction System).

In comparing the Victorian and NSW delivery performance it should be noted that the Victorian pm forecasts are for a period of 24 hours while the NSW forecasts are for 36 hours. Even though a shorter integration period is used for the Victorian forecast, the System typically takes about 90 minutes to complete the forecast—60% longer than the NSW forecasts, which on the average takes about 55 minutes to complete. In part this is because the Victorian domain is 30% larger (353,000 vs. 241,000 grid points), but also stems from the fact that the emissions inventory model (EIM) of the pre-processor stage can take up to four times longer than NSW for the larger and more comprehensive Victorian emission data base.

The performance of the EIM may be able to be dramatically improved, following experience in running TAPM for EPA VIC's Air Quality Improvement Plan (see EPAV 2001). That work suggests it should be possible to run the EIM only a few times a month instead of twice a day. All the temporal variations on shorter time scales can be incorporated into the CTM since these variations are in practice in the EIM as currently developed for AAQFS, all algorithmically-driven and these algorithms can be much more efficiently done in the CTM. See **Section 3.3.9 Improving the effective speed of the EIM in the AAQFS**.

As may be deduced from the Figures, the pre-processor stage typically takes about 6 minutes to complete for the NSW domains (11% of the total System time), and about 24 minutes for the Victorian domains (34% of total System time). The CTM integration stage takes about 21 minutes to complete for NSW (37% of total time) and about 20 minutes (21%) for Victoria. It is also interesting to note the variability in elapsed times for the CTM integration (Figure 2.6.3) with minimum and maximum times of 13 and 79 minutes respectively for NSW and 11 and 45 minutes for Victoria. In part this variation is due to the use of adaptive integration algorithms (integration time steps vary with meteorological conditions and chemical loading), but primarily it may be expected that the variation is due to changes in machine loading. Post-processing (the supercomputer-based plot file generation) takes about four minutes (7%) for NSW and two minutes (3%) for Victoria. Approximately 650 plots are generated in the post-processing stage, which are then converted to GIF format and copied to the web server. Prior to optimisation, the conversion and copying process took about 30 minutes. The time taken to complete this process has since been reduced to 20 minutes.

The frequency and cumulative frequencies of forecast delivery times are presented in Figure 2.6.4 for the NSW and Victorian pm forecasts for the analysed period. Note that forecasts were actually delivered on 150 (NSW) and 149 (Victoria) days of the 159-day period. Thus a failure somewhere in the System led to a missed forecast on 6% of the forecast days. Of the 94% of days on which a forecast was issued, Figure 2.6.4 indicates that 21% of

the forecasts were delivered before 2 pm, 55–60% of the forecasts were delivered before 2:30 pm, and 79–86% were delivered before 3 pm. This number increases to greater than 90% for a 3:30 pm delivery time. The majority of forecasts were delivered in the period 2–3 pm. The earliest delivery of a forecast was at 1:11 pm for NSW and at 1:07 pm for Victoria. The latest delivery was 4:58 pm for NSW and 5:52 pm for Victoria. These occurred after an operating system upgrade and during a period when the supercomputer was under extremely heavy load. On the average, the NSW forecast was delivered at 2:36 pm and the Victorian forecast at 2:29 pm. Delivery performance was superior for Victoria because this forecast is generally run ahead of the NSW forecast.

Bearing in mind that the pre-, post-processing and CTM components of AAQFS do not have full operational status and sometimes have to compete with other major projects, we have nevertheless been able to demonstrate that the System can be operated with a high degree of reliability. Moreover, improvements are continuing to be made to the scheduling of the System on the supercomputer. It is anticipated that still further improvements in reliability and forecast delivery times will be achieved once the Demonstration System software has been handed over to the Bureau of Meteorology's operational forecasting group and full operational forecasting status is achieved.

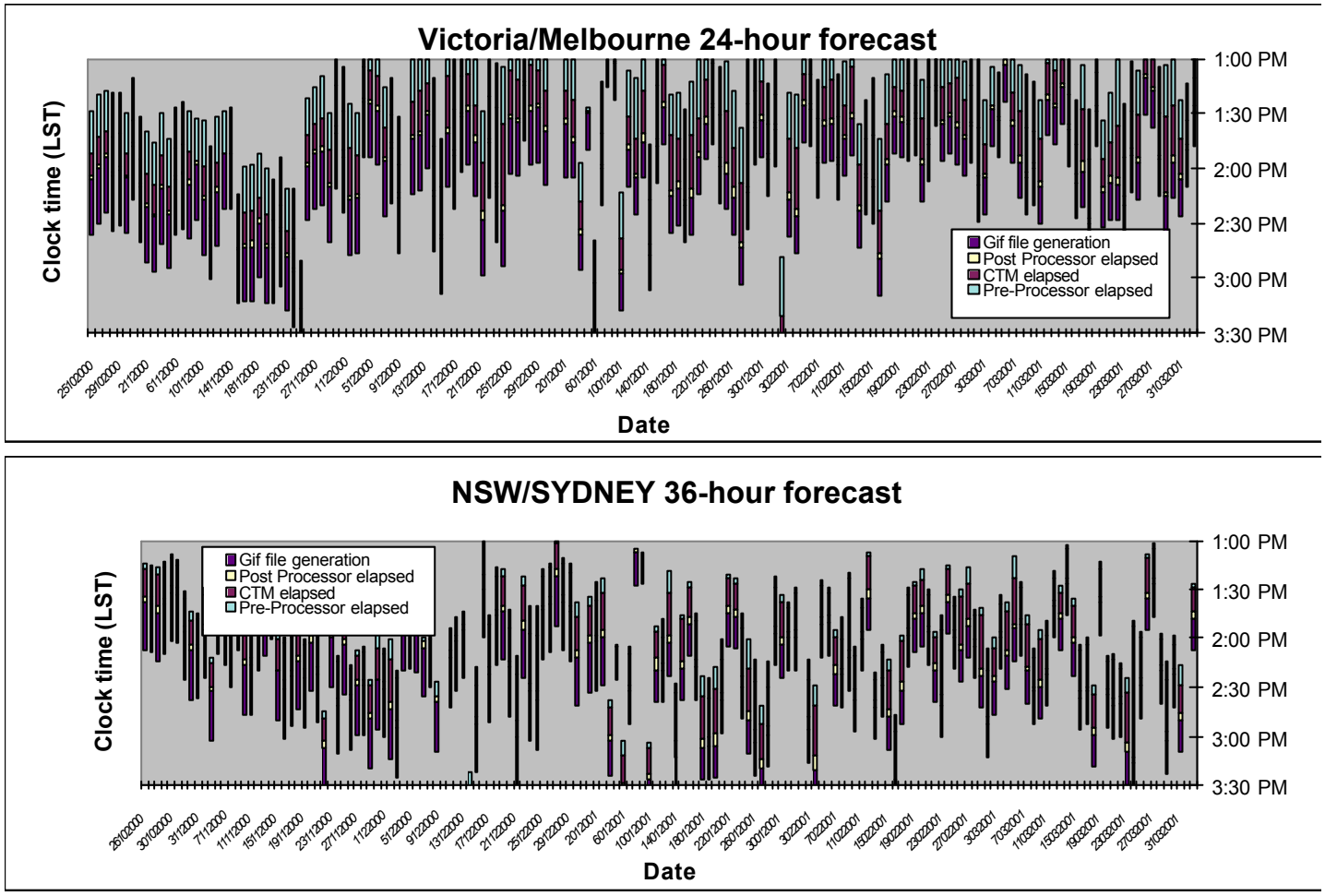

Figure 2.6.2. Performance data for run times and delivery times of the pre-processing, post-processing and AAQFS chemical transport integration for the 3 pm Victorian (top) and NSW (bottom) air quality forecasts.

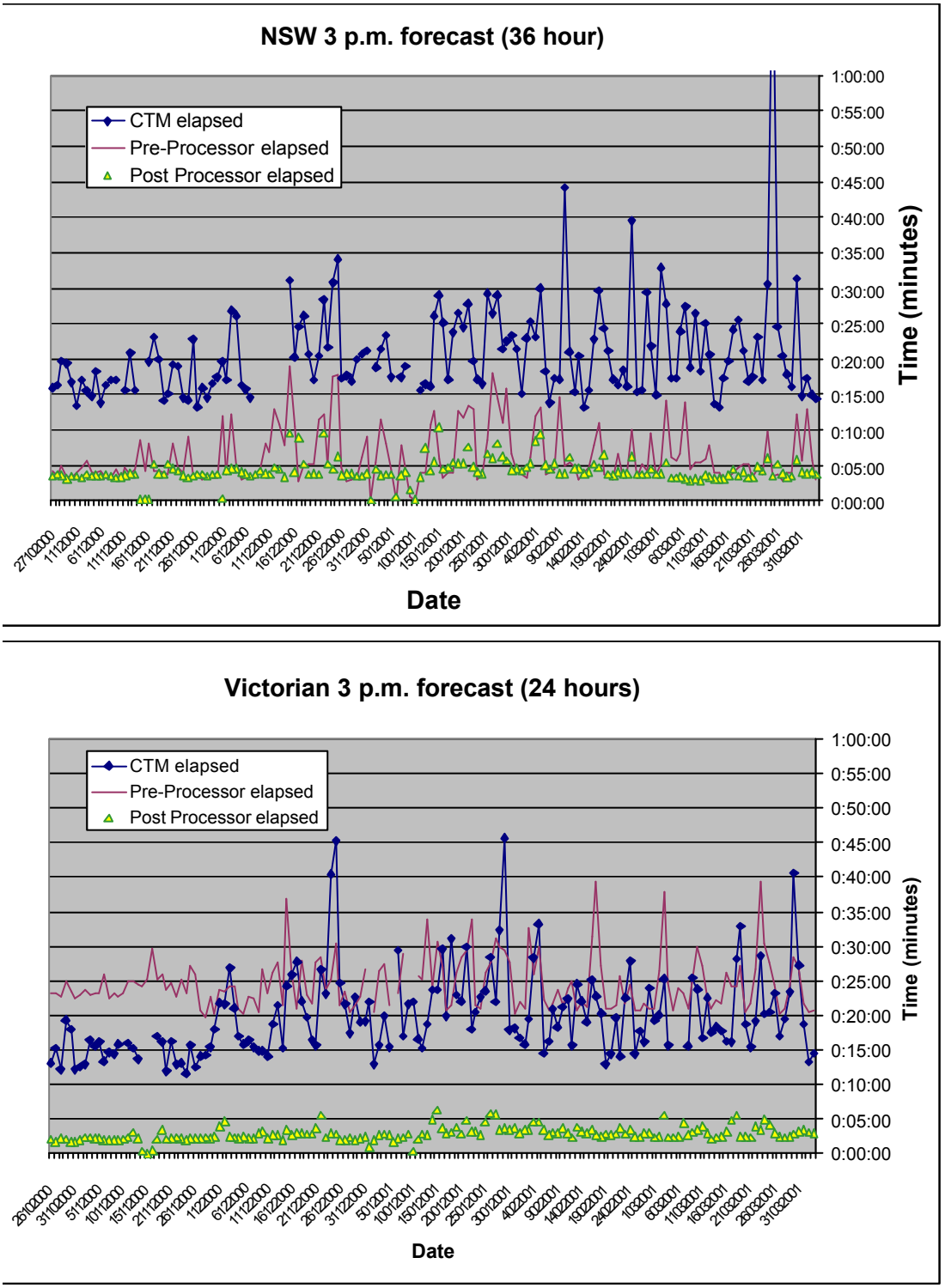

Figure 2.6.3. Time series of elapsed time for the completion of pre-processing, post-processing and chemical/transport modelling components of the air quality forecast. NSW (top) and Victoria (bottom).

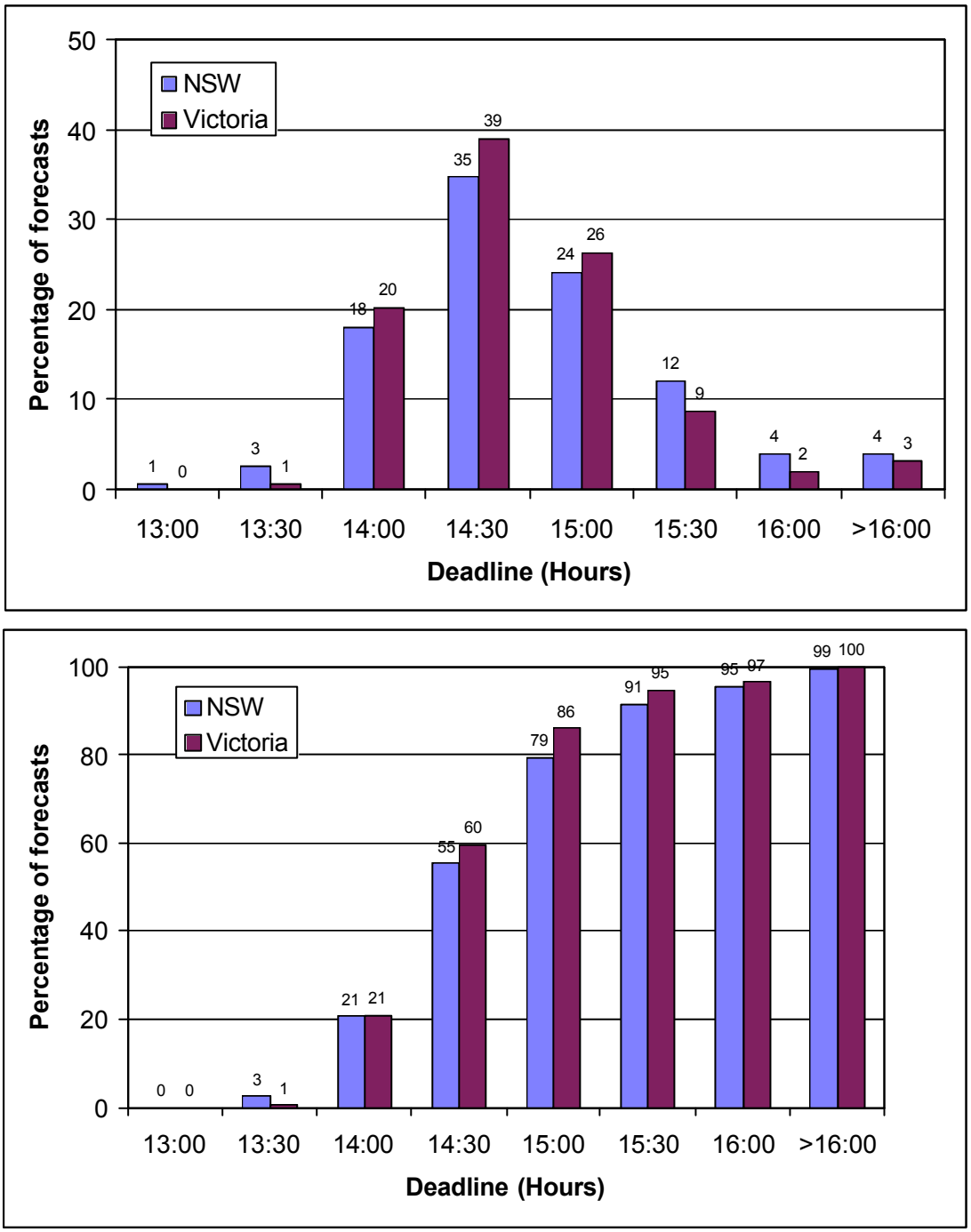

Figure 2.6.4. Frequency and cumulative frequency distributions of delivery times for the period 23 October 2000 to 31 March 2001 for NSW and Victorian 3 pm forecasts.

Chapter 3—The Emissions Inventory Model

3.1 Introduction

The emissions inventory is one of the major components of the Australian Air Quality Forecasting System (AAQFS). The development of the emissions inventory proceeded in two phases, in concert with the AAQFS: 1) construction and operation of a Pilot System using components that were available at the time of study inception; and 2) development of the Demonstration System, through the enhancement of components in the Pilot System, and where necessary, through the construction of new modules.

The Pilot System used a cut-down version of the 1992 Metropolitan Air Quality Study (MAQS) emissions inventory (Carnovale *et al*., 1996) for NSW, and the 1990 Port Phillip Control Region emissions inventory (EPAV 1991) for Victoria. All emissions processing for the Pilot System was undertaken offline with no allowance made for weekday/weekend or seasonal/local meteorological dependencies. Biogenic emissions were calculated using typical summertime temperatures and radiation fluxes.

The Demonstration System's Emission Inventory Model (EIM) has to meet several challenges. One is to estimate daily emissions, allowing for weekday/weekend, monthly or seasonal, and meteorological dependencies. Also the emissions must be generated for a 36-hour period, rather than 24 hours as in a traditional emission model. Special events or scenarios, such as minimal motor-vehicle usage, need to be considered in the model.

Another challenge is to verify performance of the emissions data obtained from the power-based vehicle emissions model developed by CSIRO (based on Williams *et al*., 1994), in the EIM. These emissions are road-specific, so are quite different from the traditional forms of emissions that are based on points or grid cells. The power-based vehicle model is discussed further in **Section 5.4 Power-Based Motor Vehicle Emissions** and **Appendix 5.4 Power-Based Motor Vehicle Emissions**.

Currently, the AAQFS uses an emissions inventory for NSW that is projected to year 2000 from the 1992 MAQS emissions inventory. The Victorian emissions inventory is based on the 1996 Port Phillip Region emissions inventory (EPAV 1998), extended to cover the whole of Victoria.

As part of its work plan NSW EPA is looking to update its inventory. It is envisaged that this will occur progressively, and any improved estimates will be implemented in AAQFS as they become available.

3.2 Overview of the Emission Inventory Model

3.2.1 System Design

The EIM provides forecasts of emissions for a range of air pollutants including carbon monoxide (CO), oxides of nitrogen (NOx), fine particles (PM10), sulfur dioxide (SO_2), volatile organic compounds (VOC), ammonia, benzene, 1,3-butadiene and formaldehyde. Particles are speciated into discrete compounds and size fractions, and VOC are speciated into individual Carbon Bond IV (CB-IV) species (Gery *et al*., 1989). The EIM accepts data for any grid size, cell size and coordinate system although latitudes and longitudes are used for the AAQFS.

The model is very powerful and flexible, being essentially gridless, and permitting very many possible variations of emissions as a function of hour, day, and season. This power comes at a cost of considerable runtime and disk space (see **Section 2.6 Operational Performance of AAQFS**).

Every effort has been made to ensure that it uses the minimum necessary time and disk space to run. In order to reduce the time to run the model, static data, *i.e.* data which do not have temporal dependency, such as spatial data, are preprocessed and put on the System. To reduce the use of disk space, the size of datasets are kept to the minimum. For example, instead of storing a large dataset of area source gridded emissions, these emissions are generated in the model by distributing the annual emissions by spatial data, such as population.

3.2.2 Model Components

The emissions model consists of seven submodels: point-source model, area-source model, motor-vehicle model, biogenics model, prescribed-burning and wildfires model, sea-salt model and wind-blown-dust model. The power-based vehicle emissions model is an option in the motor-vehicle model. Although available, some of these models are currently bypassed for algorithms incorporated in the CTM (see below).

The emissions forecast is improved through the use of day-specific variations in source groups subject to meteorological influences.

- Day-specific emissions from each individual point source, individual area source or motor vehicles are estimated from a set of temporal factors, which are different for each month, day and hour. A public holiday is treated as a Sunday. For an event or a scenario, an event factor is used instead of the daily temporal factor.
- Emissions from domestic wood combustion are adjusted linearly according to the predicted daily average temperature using an algorithm developed by Ng and Minchin (2000).
- Exhaust and evaporative emissions from motor vehicles are estimated according to the predicted temperature of each grid cell and hour using emission factors derived from MOBILE5a (USEPA 1995) and confirmed by tests for Melbourne (EPAV 1998). The evaporative emission factor for petrol-fuelled motor vehicles is also adjusted for Reid Vapour Pressure, which may differ for different periods in a year.
- Biogenic emissions are calculated for each day on the basis of predicted solar flux and diurnal temperature.
- Emissions from wildfires and prescribed burns are estimated based on reported or planned fires on the day. The hourly evolution of emission is estimated based on an algorithm adapted from Ferguson *et al*. (1998).
- Sea-salt emission is determined for each grid cell and hour using predicted wind speed at 10 m above sea level.

The point-source model, area-source model, motor-vehicle model and prescribed-burns and wildfires model are described in detail in **Appendix 3.1 Emissions Model for AAQFS** and **Appendix 3.4 Australian Air Quality Forecasting System Emissions Inventory Model System Document**. Note that the material in **Appendix 3.4** supersedes that in **Appendix 3.1**. Some of the meteorologically-dependent models are also described there also. However, they

have not been activated in the current EIM. Instead simpler models for biogenic emissions and sea-salt aerosol are implemented directly in the CTM and are described in **Appendix 3.3 Specific Meteorologically-Dependent Emissions in AAQFS**. The wind-blown-dust model is still being developed by the CSIRO.

To improve the biogenic emission factors, and as a contribution to the Project, NSW EPA funded an investigation of biogenic emissions from trees and grasses. This is summarised in **Appendix 3.5 Biogenic Emissions from Trees and Grasses**.

The power-based model of motor vehicle emissions has been incorporated into the EIM as an option. See **Appendix 3.1 Emissions Model for AAQFS** and **Appendix 3.4 Australian Air Quality Forecasting System Emissions Inventory Model System Document**. (Note that the material in **Appendix 3.4** supersedes that in Appendix 3.1.) However, at present data are only available for Sydney. See **Appendix 5.4 Power-Based Motor Vehicle Emissions**.

Each of the models is a subroutine that can be called from the Chemical Transport Model (CTM) preprocessor. Each subroutine supplies spatially discrete, hourly, speciated emissions to the CTM preprocessor for a given grid domain and forecasting time period. Since the models are called directly from the CTM preprocessor, no disk space is required to store the speciated emission data from each model.

3.3 Future Development of the EIM

Although the EIM is generally running well, with the exception of winter wood-smoke (see **Chapter 2** and below), further development can be done to improve the useability, accuracy and speed of the model.

3.3.1 Development of an Emission Modelling and Data Management System

For the AAQFS to extend to other jurisdictions, each jurisdiction needs to provide emissions inventory data in the format required by the EIM. For jurisdictions that do not have much experience in modelling, it might be difficult to understand the set-up and requirements of the EIM datasets. Therefore it would be useful to develop a database application to assist each jurisdiction to prepare the emissions inventory data, and to output the data in the required format for the EIM.

3.3.2 Development of a National Motor-Vehicle Emission Factor System

Each jurisdiction is required to supply the emission factors for estimating motor vehicle emissions in the EIM. Developing motor vehicle emission factors is often the most difficult task in preparing an emissions inventory. To assist jurisdictions, it would be helpful to develop an application to estimate these emission factors. Such applications already exist in other countries, such as the USA (USEPA 1998) and New Zealand (MOT 1998). The application would make use of the latest Australian vehicle test data, such as from the Diesel NEPM Study (NEPC 2001), and overseas emission factors, such as those from MOBILE6 (USEPA 1998).

3.3.3 Improving Estimation of Motor Vehicle Emissions at Different Temperatures

In the current EIM, motor vehicle emission factors for different temperatures are obtained from a lookup table, which lists emission factor against temperature. It would be more convenient to convert these emission factors at different temperatures to adjustment factors with respect to a standard temperature, such as 20°C. A jurisdiction would then only be

required to supply the emission factors at the standard temperature, and those at different temperature would be derived in the EIM using the temperature adjustment factors. These adjustment factors can also be used for the power-based motor vehicle emission factors, as they are not derived for different temperatures.

3.3.4 Improving Speciation Processing

In the current EIM, VOC are speciated into individual CB-IV species and particles are speciated into discrete compounds and size fractions. However, in the CTM, the CB-IV species are lumped into a single, reactivity-weighted VOC class as required by the Generic Reaction Set (GRS) mechanism. Also, the particle species are lumped into eight size fractions regardless of chemical nature.

The creation of individual CB-IV species (nine species) and particle species of discrete compounds and size fractions (32 species) in the EIM gives modellers the flexibility to develop the CTM as the System evolves. However, the creation of so many species, which are not all used in the CTM, uses a lot of memory and slows down the processing in the EIM.

The memory requirement and speed of the EIM can be improved by streamlining the speciation processing such that it produces one VOC species and eight particle species as presently required by the CTM.

3.3.5 Improving Speciation Profiles

In the current EIM, speciation profiles are based on those from EMS-95. These profiles need to be updated with the release of EMS-2001 (Janssen 2001), which uses speciation data from the new USEPA program — Speciate 3.0. However, the speciation profiles in EMS-2001 are mostly based on studies in the USA. Local speciation profiles, such as motor vehicles and cutback bitumen, are available and can be used to replace some of the speciation profiles in EMS-2001.

3.3.6 Improving System Integration

There are currently two copies of EIM on the System, the original copy is maintained by EPA Victoria and the other copy, which is modified to integrate with the CTM, has been maintained by CSIRO. Any change to the original copy would require changing the other copy.

This practice is acceptable in the initial phase of development as both parties may not understand each other's requirements exactly. However, it makes the maintenance of the System harder in the long run.

It will improve the maintenance of the EIM by keeping one copy of the software. Also, there may be opportunity to streamline the processing of the EIM once the developers understand the requirements of the CTM.

3.3.7 Improving Biogenic Model

In the current EIM, biogenic emissions are estimated by a model that was developed for airshed modelling studies in NSW and Western Australia (Carnovale *et al.*, 1996; Cope and Ischtwan 1995). The emission estimates may be improved by further interpretation of the measurements reported in **Appendix 3.5 Biogenic Emissions from Trees and Grasses**, new measurement work presently underway by CSIRO for the NSW Environment Trust, and

adapting the BEIS3 (Yarwood *et al.*, 1999) algorithm in the EIM, which uses a revised leaf energy balance to adjust radiation levels for sunlit and shaded leaves as a function of height in the canopy. Emission estimates can also be improved by using different foliage density covers for different seasons.

3.3.8 Improving Wildfire and Prescribed Burning Model

The current wildfire and prescribed burning model uses a simplified algorithm, which is adapted from the Emissions Production Model developed by Ferguson *et al.* (1998), to estimate the hourly evolution of emissions. The emission estimates can be improved by including wind speed, humidity, precipitation and ambient temperature in the estimation.

Providing data for this model is a major challenge, especially in those States where the fire management agencies are not well coordinated. For example, under current arrangements, NSW EPA does not have information about planned hazard reduction events routinely available for incorporation into the model. Clearly this limits the performance of the forecast on days when such burning makes significant contribution to the particle load in the region. The NSW EPA plans to investigate the feasibility of obtaining sufficiently detailed and timely information for incorporation into the model.

3.3.9 Improving the effective speed of the EIM in the AAQFS

The effective performance of the EIM may be able to be dramatically improved, following experience in running TAPM for EPA Victoria's Air Quality Improvement Plan (EPAV 2001). That work suggests it should be possible to run the EIM only a few times a month instead of twice a day. Except for the case of special events (including wildfires and prescribed burns), all the temporal variations on shorter time scales can be incorporated into the CTM since these variations are in practice in the EIM as currently developed for AAQFS, and are all algorithmically-driven; these algorithms can be much more efficiently done in the CTM since the latter is better optimised for the computer environment.

In the TAPM applications, outputs from the AAQFS emission inventory software for the Port Phillip Control Region covering Melbourne and Geelong were processed by new software to convert this information into a form that TAPM could use for a week-long period (weekday, Saturday and Sunday emissions). The emissions consisted of point sources (including Latrobe Valley Power stations) and Port Phillip Control region gridded surface emissions for area sources, wood heater emissions, vehicle exhaust emissions (petrol, diesel and LPG fuel types), vehicle evaporative emissions (petrol fuel type) and biogenic emissions. The last six of these sources were provided to TAPM at constant temperature, with temperature variations accounted for using TAPM temperatures as the model ran. Extra monthly varying emission factors for vehicles of ~3% were ignored, and wood heater seasonal adjustments were chosen for Spring which has ~22% of annual emissions (note that soon after this study, the AAQFS was changed to eliminate this seasonal adjustment, which means that all seasons would use ~25% of annual emissions, approximately consistent with this work).

These simplifications allowed TAPM to be run for every day of a year with only emissions data characterising a week-long period. In a possible development for AAQFS, the EIM could be run a few times a month to provide the seasonal information. The temperature variation of emissions from motor vehicles could, as done for TAPM, be incorporated into the CTM. Biogenic emissions variations are already done this way.

Chapter 4—Outputs from AAQFS

This Chapter describes the data-archiving and display procedures and products for the Demonstration System of AAQFS. The procedures are likely to change for the operational version of the System, since CSIRO would not then be involved in the day-to-day running of the System.

4.1 Data Packet and Archiving System

In the Demonstration Project, the AAQFS Chemical Transport Model (CTM) produces multilevel output for both the NSW and Victorian airsheds. The size of the output files amounts to seven gigabytes, daily. For archiving, visualization, web display and further analysis of CTM output, a more compact set of surface-level data files is generated from the multilevel CTM output files.

The naming convention for a surface-level data file begins with the case scenario, airshed, grid, date and run time start. For example, basecase_vic_grid1_2001061200_ctm.nc and greencase_nsw_ grid2_2001061210_ctm.nc represent a morning operational forecast run for the Victoria outer grid, and an afternoon green scenario run for the NSW inner grid, for 21 June 2000, respectively. The daily surface-level data files total 180 and 220 megabytes for Victoria and NSW, respectively. They contain

(1) spatial information, such as the latitude and longitude of the gridpoints, terrain, coastline, and suburb location,

(2) temporal information such as the date, the starting time of forecast and the time difference between local standard time and UTC,

(3) boundary and initial conditions,

(4) emission values of 35 chemical species from industrial source, commercial/domestic and motor vehicle emissions,

(5) 12 meteorological fields including wind, temperature, pressure,

(6) concentrations of 13 air pollutants at each grid point and other variables used in data display system.

Inland temperature files that provide hourly temperature profiles for motor vehicle emissions and daily average temperature for commercial /domestic emission are archived. Temperature profiles are generated from LAPS375 output of screen temperature and land-sea mask. These files are about 100 kilobytes for each airshed per day. The naming convention is similar to the surface-level CTM file name. It contains the date, forecast time, and airshed name. For example, 2001061200_victemp.nc and 2001061210_sydtemp.nc contain inland hourly temperatures on 12 June 2001 for the Victorian outer grid morning run, and for the NSW inner grid afternoon run, respectively. The previous day's observed air quality data from the EPAs, and observed meteorological data from the BoM, are also archived for model verification purposes, once a day.

All of these files are stored in Network Common Date Form (netCDF) to facilitate easy data transfer between computing platforms without conversion. At present, these files are regularly transferred to CAR's local machine and copied to CD for future analysis.

4.2 Web Display System

From surface-level CTM output, graphic meta files of daily maximum and hourly forecast of 11 air pollutants are generated from the BoM/CSIRO supercomputer, florey. These files are transferred to CAR's local Unix machine where they are processed into compressed GIF images. First the gmeta files are converted to X Windows system window dump files, then to portable pixmap format then finally to compressed GIF format. For each airshed, there are about 1600 GIF images generated per day. Each image is about 3–5 kbytes.

Before updating the AAQFS web sites, images of air quality index (AQI) and the chemical species used for its calculation are e-mailed to EPA Victoria and NSW EPA to ensure timely delivery of air quality forecasts. Note that different methods are used for the NSW and Victorian AQI calculations. For the Victorian AQI calculation, nitrogen dioxide, ozone, sulfur dioxide, carbon monoxide, PM2.5, and PM10 species are used. Note that an 8-hour running average of the carbon monoxide concentrations and a 24 hours average (not a running average) of the PM10 concentrations are used to comply with EPA Victoria's definition of AQI. For the NSW regional pollution index (RPI) calculation, nitrogen dioxide, PM2.5 and ozone are used. (The important point is that any required Index can be generated by AAQFS.)

Figure 4.1 shows the structure of the CAR–AAQFS web site. Each part is described next.

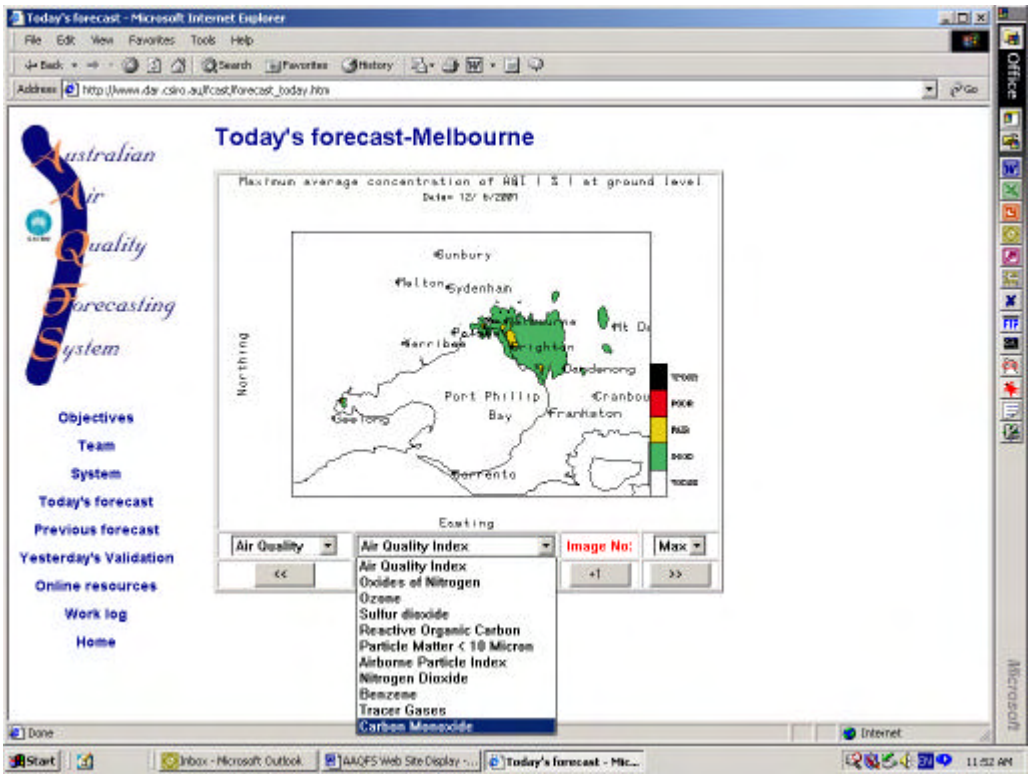

Figure 4.1. The CAR-AAQFS website showing *today's forecast* page for Melbourne grid.

The **Objectives** page lists the AAQFS objectives.

The **Team** page lists the AAQFS participants and their URL links.

The **System** page describes the AAQFS numerical weather prediction model, emission model and chemical transport model

The **Today's forecast** page has an option of four grids, Victoria, Melbourne, NSW and Sydney. This page displays current forecasts of air quality and meteorological fields. For air quality forecasts, there are 11 pollutants species, Air Quality Index, oxides of nitrogen, ozone, sulfur dioxide, reactive organic carbon, PM10, Airborne Particle Index, nitrogen dioxide, benzene, trace gases and carbon monoxide. Each pollutant has a daily maximum image and hourly forecast images. For the Victorian airshed, PM10 displays are for a 24-hour running average and the carbon monoxide display is for an 8-hour running average. Due to the formula we use to calculate AQI for the Victorian airshed, the AQI display has 24 hourly images instead of 36 images. For the afternoon forecast in Victoria, the CTM is run for 24 hours from 10 pm to the next day 10 pm, due to the large grids (98×98 for the outer grid and 130×96 for the inner grid). Thus the Web display is 24 hourly images for all species. For the NSW airshed (98×98 outer grid and 98×56 inner grid), both the morning and afternoon forecasts have 36 hourly images.

The **Previous forecast** page shows the previous forecast for each grid. For morning forecasts, previous forecast page holds the previous day's afternoon forecast, for afternoon forecasts, it holds the same day's morning forecast images.

For **Yesterday's Validation** page for each grid, surface wind and potential temperature are compared with observed measurements. CTM forecasts of eight species are compared to the EPA's observed AQ data, as well as ratios of particulate matter, ozone to oxides of nitrogen, and nitrogen dioxide to oxides of nitrogen. AQI forecasts are also compared with the EPA observations. Note that for the validation web page, Victoria's observed AQI and modelled AQI are calculated with NSW-EPA's RPI formula for simplicity. This avoids computing a running average, and allows a comparison with NSW's RPI validation. Figure 4.2 shows a validation using observed AQ data from Blacktown monitoring station on 14 June 2001. A square box represents observed AQ and a solid line the best model fit.

The **Online resources** page gives access to relevant reports and papers about the AAQFS, including all Progress Reports.

The **Work log** page describes the current work status.

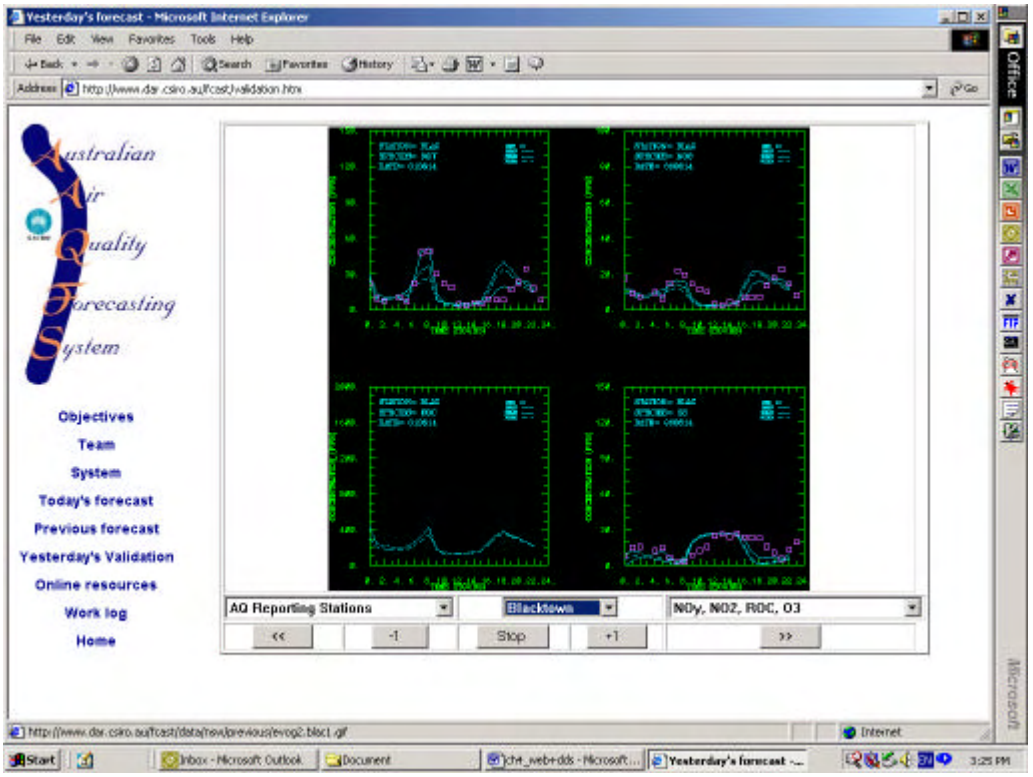

Figure 4.2. The CAR-AAQFS website showing *yesterday's validation* page for Sydney grid.

4.3 2-Dimensional Data Display System

A two-dimensional data display system (DDS) has been developed for post-analysis of meteorological and AQ forecasts on Win 32 platforms, and has been provided to each participating EPA. The 2D-DDS is built using the Lahey Fortran95 Compiler and Winteracter/Open_GL software. It uses surface-level CTM output files, and has options to visualise 13 air pollutants species: oxides of nitrogen, nitrogen dioxide, reactive organic carbon, ozone, sulfur dioxide, carbon monoxide, PM1, PM2.5, PM10, butadiene, benzene, formaldehyde, and trace gases. It also has options to display six meteorological fields: pressure, ambient temperature, friction velocity, mixing ratio and the planetary boundary-layer height with or without overlaying wind vectors. Distributions of concentrations of chemical species can be displayed with other pollutants or meteorological fields. Other options include: multiple windows, different output formats and a variable range for the contour levels. Figure 4.3 shows a typical DDS image that displays two different pollutant species, one with overlaying wind arrows.

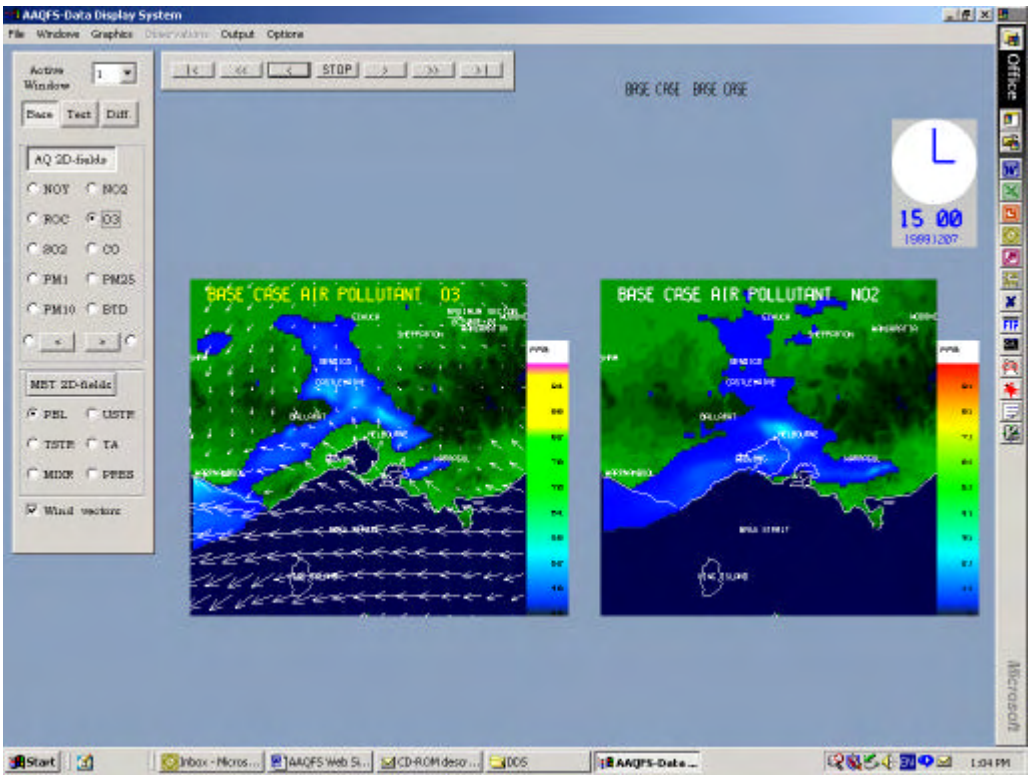

Figure 4.3. A typical of 2D-DDS image showing distribution of two air pollutants for Victoria grid at 3 pm 7 December 1999.

For a better understanding of the underlying meteorological conditions, one can select a meteorological field and compare it with a pollutant field, as shown in Figure 4.4.

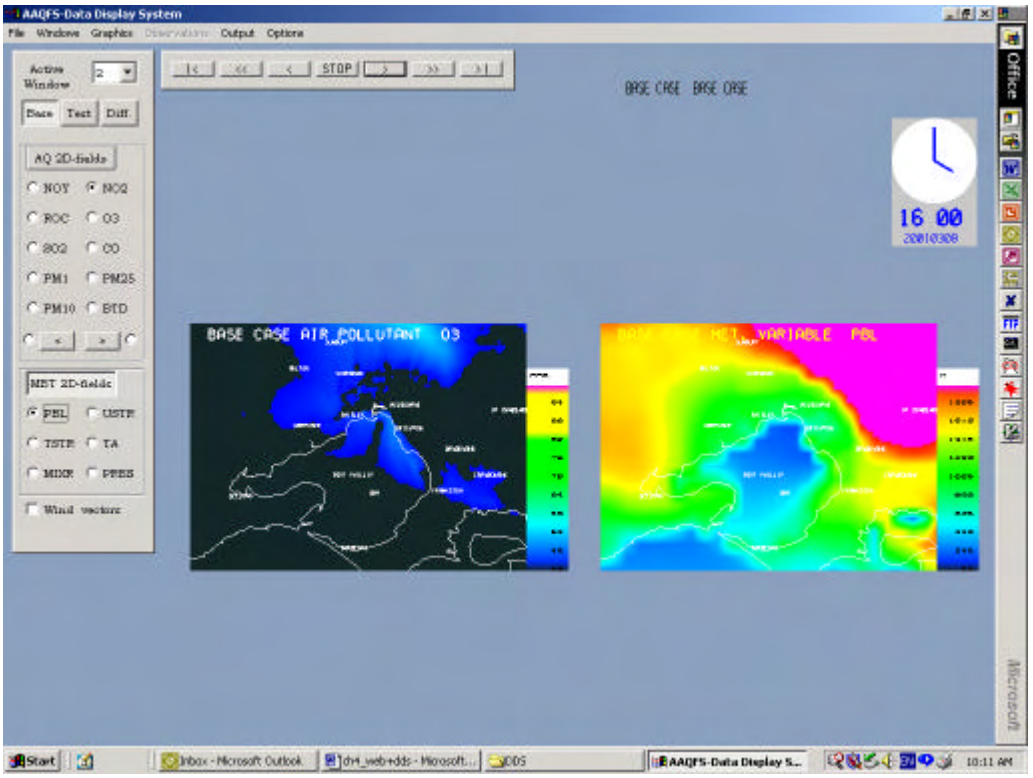

Figure 4.4. A typical 2D-DDS image showing ozone concentration with planetary boundary layer depth for Melbourne grid at 4 pm 8 March 2001.

The 2D-DDS also has a capability to display the difference between two CTM outputs. Figure 4.5 shows the difference in ROC and PM10 for a business-as-usual scenario and a 'green' scenario with motor vehicle emission reduced by 25%. There is also an option to display a time series of observed AQ data at any given monitoring station.

4.4 3-Dimensional Data Display System

A prototype Graphical User Interface (GUI) software package has been developed to visualize meteorological and air quality forecast data produced by the AAQFS. It is capable of displaying simultaneously: contoured meteorological data; wind vectors or barbs; shaded relative humidity (to represent cloud); and chemical species, shaded by concentration. It can be used in a horizontal or vertical mode to build up a comprehensive 3-D picture in the user's mind. In both modes the user can loop forward or backward in time to gain an understanding of the time evolution of the event, and in the horizontal mode the user can loop up or down from level to level. In vertical mode, a vertical slice, in any direction through the model domain, can be chosen by specifying the start and finish grid coordinates. This is particularly useful when viewing a linear feature (such as a sea-breeze front parallel to the NSW coastline) that is not oriented north-south or east-west. Features such as: contour labels; border ticks and tick labels; wind barb and vector frequency, size and scaling; chemical species concentration, shading intensity and colour; and label fonts and sizes, can all be edited 'on the fly'.

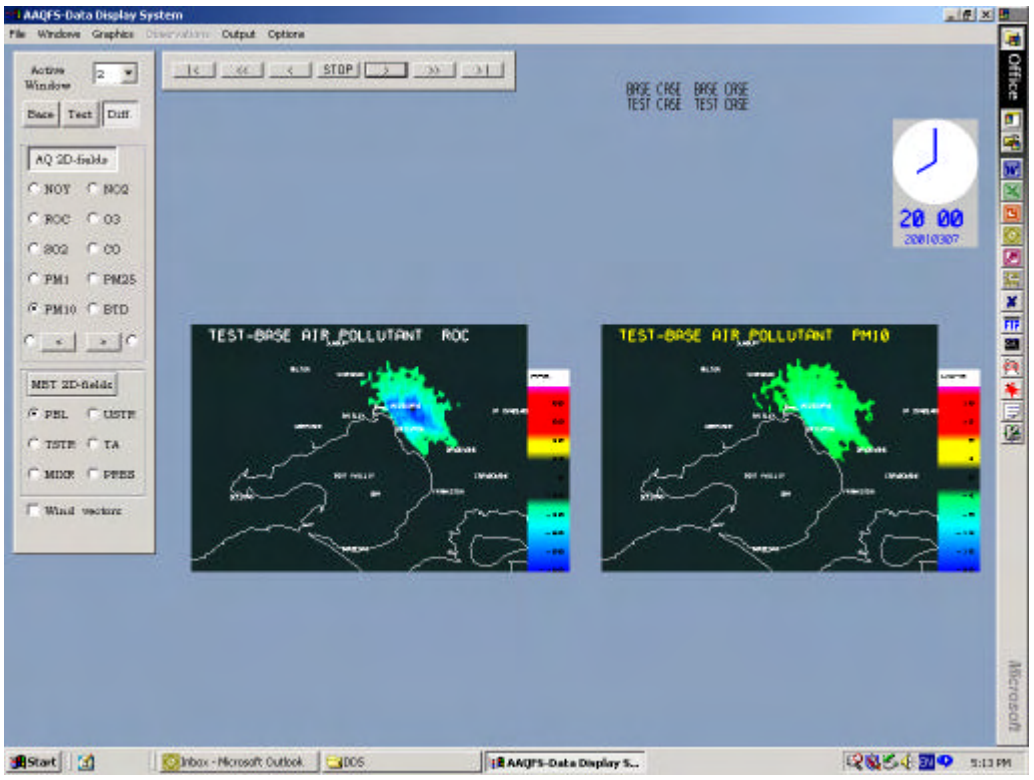

Figure 4.5. 2D-DDS display showing the difference between a business-as-usual scenario and a 'green' scenario with 25% reduction in motor vehicle emissions at 8 pm 8 March 2001.

Two examples in horizontal mode, from a Sydney ozone event, are presented in Figure 4.6. By looping between levels, the user can quickly identify ozone advected inland by a sea breeze at low levels (Figure 4.6a) and ozone advected offshore by the sea-breeze return flow at higher levels (Figure 4.6b). A vertical cross-section further illustrates the changing structure with height. Figure 4.7 shows a vertical cross-section that runs from the left to right edges of Figures 4.6, at latitudes of -32.65° and -35.85° respectively. The vertical structure of the sea-breeze cold air mass is clearly evident. The inland penetration of the sea breeze is resisted by the topography and the opposing offshore synoptic flow. Ozone is concentrated in the convergent zone at the sea-breeze leading edge, and it is advected inland then upwards and back out to sea in the sea-breeze return flow.

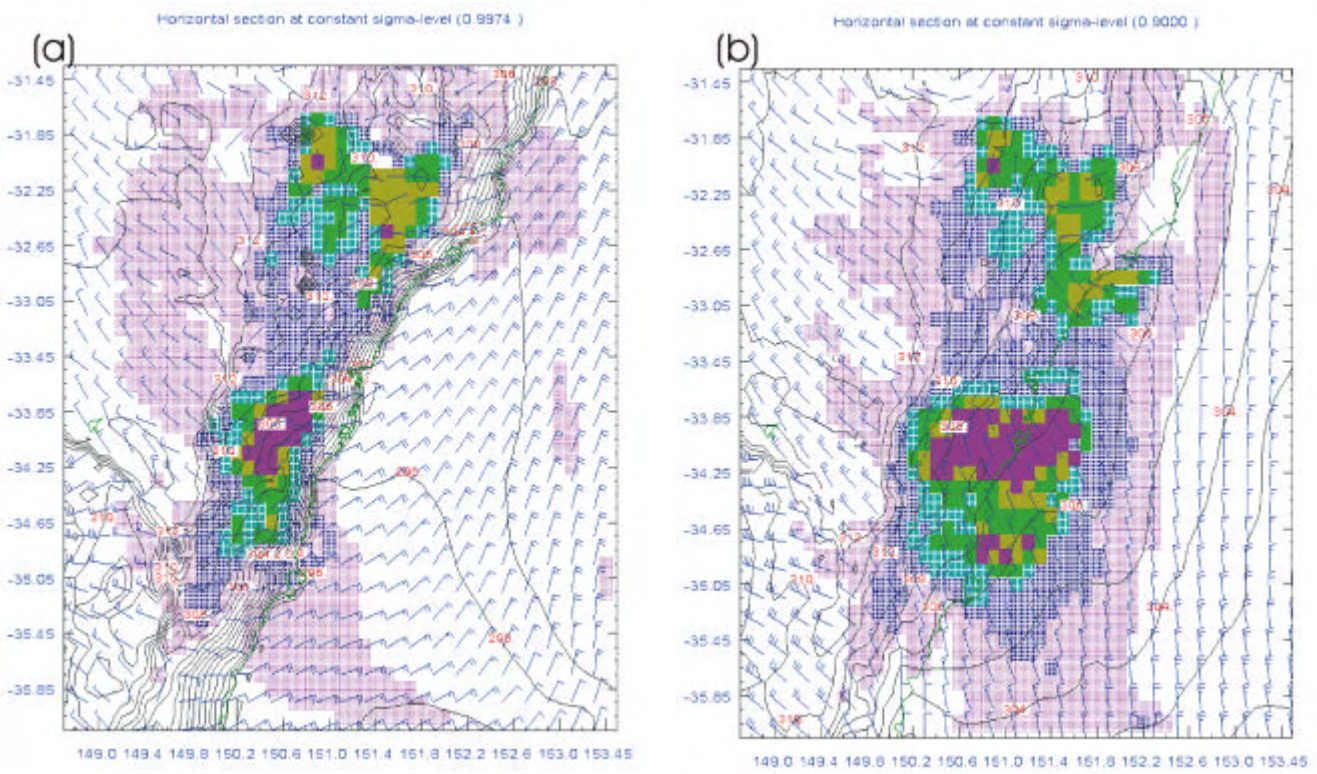

Figure 4.6. Ozone (shaded), potential temperature (contoured) and horizontal winds (barbs) at 5 pm 26 January 2001 at (a) the surface, and (b) 1000 m above the surface. These images show ozone advected inland by the sea breeze near the surface in (a) and ozone being advected back over the sea in the sea-breeze return flow (b).

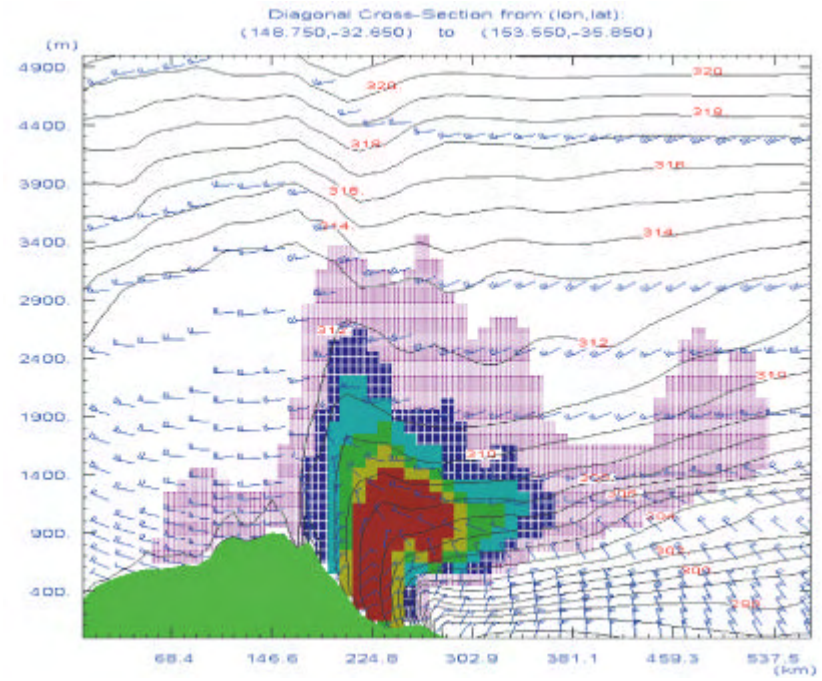

Figure 4.7. Vertical cross-section of ozone (shaded), potential temperature (contoured) and horizontal winds (barbs) at 5 pm 26 January 2001. Downward (upward) pointing barbs represent flow out of (into) the page. This image when combined with Figure 4.6, gives a comprehensive picture of the sea breeze dynamics, and the ozone transported within the sea breeze. The inland penetration of colder marine air is hampered by the topography and the opposing offshore synoptic flow.

Chapter 5—AAQFS Options

The Demonstration System of AAQFS employs the Generic Reaction Set chemistry in the Chemical Transport Model (**Chapter 2**) because preliminary investigations indicated that it adequately described the transformation of species in Sydney and Melbourne. It is a very much faster chemistry than those usually employed for detailed air pollution assessments. However, as the System will be applied to other regions, there is a need to extend the chemistry to conditions of lower concentrations of VOCs and NO_x and to lower ratios of these constituents. As part of the Demonstration Project, we have developed an extension to GRS that appears to be able to perform well in these conditions—GRS2. However, this new chemistry has yet to be tested thoroughly and is offered as an alternative. These two chemistries are discussed here in **Section 5.1**.

In **Section 5.2**, there is a discussion of the alternative 'green' Forecast, **Section 5.3** summarises the option of including wildfires and prescribed burning in the Emissions Inventory Module, and **Section 5.4** describes the power-based motor vehicle emissions option that has been developed for the Sydney region in AAQFS.

5.1 The Generalized Reaction Scheme (GRS) Options

5.1.1 The GRS version 1 (GRS) mechanism

The air chemistry approach employed in the AAQFS Demonstration Project was developed by Johnson, Azzi and co-workers at CSIRO and is based on semi-empirical techniques. Using smog chamber experiments a set of reactions was developed (the Generic Reaction Set, or GRS) to predict ozone formation and NO disappearance in chamber experiments.

From here on called the Generalised Reaction Scheme, this Version 1 mechanism (Azzi *et al*, 1992) is a simplified chemical scheme for predicting the rate of photochemical smog formation. It was developed from smog chamber data and has been used extensively as a model for screening calculations. The major advantages of the model are:

- it is based on experimental data
- it requires far less computer run time and chemical detail than do other more explicit chemical schemes.

The GRS model consists of seven reactions among seven species. These are:

ROC+hν	?	ROC+RP	(1)
RP+NO	?	NO_2	(2)
NO_2	?	NO+O_3	(3)
NO+O_3	?	NO_2	(4)
RP+RP	?	RP	(5)
RP+NO_2	?	Stable Gaseous Nitrogen (SGN)	(6)
RP+NO_2	?	Stable non Gaseous Nitrogen (SNGN)	(7)

where ROC are reactive organic compounds and RP are reactive products. The GRS mechanism was introduced as a reduced reaction scheme to describe photochemical smog formation in contrast to the more detailed chemical kinetics of the Carbon Bond IV (CB-IV) model. Consequently reactions 1, 2, 5, 6 and 7 are descriptive in nature whereas reactions 3 and 4 refer to fundamental chemical processes.

The GRS model has been tested in three ways namely by

- comparison with outdoor smog chamber data
- comparison with estimates from more detailed photochemical mechanisms; and
- incorporation into urban airshed models (UAM and CIT) and applications to different oxidant episodes from different locations.

5.1.2 GRS2 development

In an attempt to overcome various limitations of GRS as discussed in **Appendix 5.1 The Generalized Reaction Scheme (GRS) Model**, an explicit treatment of key radical species has been added as well as direct ozone photolysis. The expanded model is referred to as the GRS2 model and consists of the reactions listed in Table 5.1.

The GRS2 model includes the main reactions for daytime ozone formation and the formation of OH radicals. The production of organic peroxy radicals RO_2, can be achieved by the oxidation reaction of hydrocarbons by OH. The product RO_2 would react with NO to produce NO_2, HO_2 and lower carbon hydrocarbons represented by RCHO.

Unlike the treatment of radical species in GRS where all radicals were lumped into one single radical named "RP", the GRS2 has distinguished between the following major radical species OH, HO_2 and RO_2. The photolysis reaction of NO_2 to produce O_3 and NO and the titration reaction of O_3 by NO were unchanged. New reactions have been added to include ozone photolysis to produce OH radicals. These reactions that treat background ozone and OH are of great importance in rural conditions.

The AAQFS provides forecasts of the atmospheric concentrations of 1,3-butadiene based on the emissions inventory; hence inclusion of the relatively rapid reactions of this compound with OH and O_3 are essential to enable the atmospheric reactivity of 1,3-butadiene to be allowed for.

Atmospheric oxidation of sulfur dioxide is also important in predicting the concentrations of this criteria pollutant. Sulfur dioxide also plays an important role in secondary particle formation in the atmosphere, ultimately affecting PM10 and PM2.5 concentrations. A reaction was included to calculate the homogeneous oxidation of SO_2. This reaction proceeds by reaction of SO_2 with OH. It is recognised that atmospheric SO_2 oxidation is a more complex process than represented by the reaction in Table 5.1.1, involving both homogeneous and heterogeneous processes, but at least the reaction allows an estimate of the homogeneous pathway.

5.1.3 Results and Recommendations

To evaluate the GRS2 model performance, a series of outdoor smog chamber experiments were selected to cover a wide range of urban atmospheric conditions. These experiments were performed in the CSIRO Outdoor Smog Chamber Facility at North Ryde. Details of the experiments have been reported elsewhere (Hess *et al* 1992; Johnson 1993).

Although the detailed results are reported in **Appendix 5.1 The Generalized Reaction Scheme (GRS) Model**, the main findings are:

In general GRS2 provides reasonable predictions for NO, NO_2, and O_3 when compared to the measurements made for the smog chamber experiments and to the predictions made for selected species by the complex CB-IV chemistry. For O_3, the major indicator species for photochemical smog, peak concentrations calculated by GRS2 are within ±10-20% of measured concentrations when high concentrations of O_3 (~0.2–0.5 ppm) are formed. For lower O_3 concentrations of 0.1–0.2 ppm, GRS2 predictions are only within ± 40% or so of the measurements.

Table 5.1.1. GRS2 kinetic parameters (cm ^{3} molecule $^{-1}$ s $^{-1}$ units)

#	Reaction	A (units depend on order)	Ea/R	k_{298}	Comments
1	ROC + hv = HO2 + RO2 + ROC	k_6*FTT*tivity*2			Complex function derived from smog chamber experiments
2	RO2 + NO = NO2 + 0.1*HO2 + 0.5*RCHO	5.30E-12	-360	1.77389E-11	CB-IV_99; reaction rate for C2O3 + NO = NO2 + XO2 + HCHO + HO2; fitted values for HO2 and RCHO co-efficients
3	HO2 + NO = NO2 + OH	3.70E-12	-242	8.33458E-12	CBIV
4	ROC + OH = RO2	1.00E-11		1E-11	CBIV
5	RCHO + OH = C2O3	1.68E-11	559	2.5742E-12	Rate taken from Seinfeld (1986) for RH + OH + RO2 + H2O
6	NO2 + hv = NO + O3	radiation dependent			
7	NO + O3 = NO2	2.00E-12	1400	1.82272E-14	CB-IV 99
8	O3 + hv = O(1D)	radiation dependent			
9	O(1D)+ H2O = OH + OH	2.20E-10		2.20E-10	CB-IV
10	O3 + HO2 = OH	1.10E-14	580	1.5708E-15	CB-IV
11	C2O3 + NO2 = PERNIT	2.63E-12	-380	9.41356E-12	CB-IV; Rate for PERNIT=PAN
12	PERNIT = NO2 + C2O3	2.00E+16	13500	0.000423268	CB-IV; Rate for PERNIT=PAN
13	OH + NO2 = HNO3	1.00E-12	-713	1.09421E-11	CB-IV
14	HO2 + HO2 = H2O2	5.90E-14	-1150	2.79783E-12	CB-IV
15	O(1D) = O	1.92E-11	-126	2.93E-11	CB-IV
16	O=O3	6.0E-34 * $((1/T)^{2.3})$			CBIV
17	H2O2=2OH	radiation dependent			
18	OH+H2O2=HO2	2.90E-12	160	1.70E-12	CBIV
19	RO2+HO2=ROOH	5.60E-12			Seinfield (1986)
20	C4H6+OH=P1	1.48E-11	-448	6.66E-11	
21	C4H6+O3=P2	1.34E-14	2283	6.31E-18	
22	SO2+OH=HOSO2	9.00E-13		9.00E-13	DeMore et al (1997)

The performance of GRS2 appears to be reasonable for a wide range of ROC/NO_x ratios.

Performance with respect to some of the other species is not so encouraging. Compared to CB-IV, concentrations of OH, HO_2, and H_2O_2 can be over- or under-predicted by wide margins, suggesting that more work is required to refine the mechanism.

Further refinements of computationally efficient mechanisms for smog modelling are probably better pursued using a rigorous approach to mechanism reduction.

5.2 Alternative 'Green' Forecast

In addition to the daily forecast of air quality the AAQFS produces, an option for an alternative forecast has been developed as part of the emissions inventory model. It was anticipated that the alternative forecast would produce lower concentrations of air pollutants than the daily forecast and therefore be labelled as a 'green' forecast. The functionality was

developed to be used as an educational tool that can be disseminated to the public to demonstrate that their individual choices can have an impact on air quality. For example, two feasible alternatives are: reducing motor vehicle usage in summer smog conditions, or reducing wood-fire usage (switching to gas/electric heating) during high-particle concentration days in the colder months.

An EPA can choose to change the emissions inventory for the area source, motor vehicle or industrial sources. The alternative source emissions are processed in the CTM to produce the alternative forecast. The data required for the alternative forecast is a simple scaling factor: that is, by what amount the source of the current daily emissions should be changed. Note that the emissions can be either decreased or increased.

The alternative forecast option may also be of interest to EPAs for running scenarios, for example, the effect a policy initiative will have on air quality. This type of forecast would be typically run on the off-line version of the AAQFS.

To illustrate a 'Green' Forecast we show results from the case study of 7–9 March 2001, introduced in **Section 2.4 CTM performance in Melbourne and Geelong**, and discussed in detail in **Section 7.1 Melbourne 3-Day Photochemical Smog Event**. Here we give an extract from a paper presented in September 2001 (Cope *et al.*, 2001); the paper is reproduced in full in **Appendix 5.2 Demonstration of a Green Scenario**.

The objective is to demonstrate some benefits of a hypothetical 25% reduction in motor vehicle usage (the 'green' forecast scenario), following a concerted move by the commuting population away from single-occupant motor vehicle use in response to forecasts of deleterious air pollutant levels on 7–9 March 2001.

One way to present the results is to consider the cumulative impact of reduced motor vehicle usage on a commuter travelling each day from a home base in Geelong to a work place in Melbourne's CBD (Figure 5.2.1). In a 'business-as-usual' scenario, the commuter is assumed to spend 12 hours per day at home, three hours commuting by motor vehicle and nine hours at work. Due allowance is made for in-car *vs*. near-road pollutant concentrations for vehicle-produced pollutants (Duffy and Nelson, 1997).

Forecasts of the commuter's running 24-hour average PM10 concentration, and PM10 cumulative dosage over the period 7–9 March are shown in Figure 5.2.1b and Figure 5.2.1c respectively for 'business-as-usual'; a 'green' scenario, but still including motor vehicle transport; and a 'green' scenario and non-motor vehicle transport (*e.g.* train travel). In the 'business-as-usual' forecast, the commuter's running 24-hour PM10 concentration approached the air quality standard of 50 $\mu g\ m^{-3}$ and the cumulative PM10 dosage reached 27000 $\mu g\ m^{-3}$ hr by the end of the third day. Under the 'green' scenario (but still travelling to work by motor vehicle), the commuter's peak 24-hour PM10 concentration was reduced by 20%, and the cumulative PM10 dosage by 23%. Replacing the motor vehicle by train as the transport mode results in even larger reductions in pollutant exposure: the peak 24-hour PM10 is reduced by 47% and the cumulative dosage by 33% relative to the 'business-as-usual' scenario.

The challenge is to present these 'green' scenario results to the public in a way that leads to positive action to *change* the base forecast.

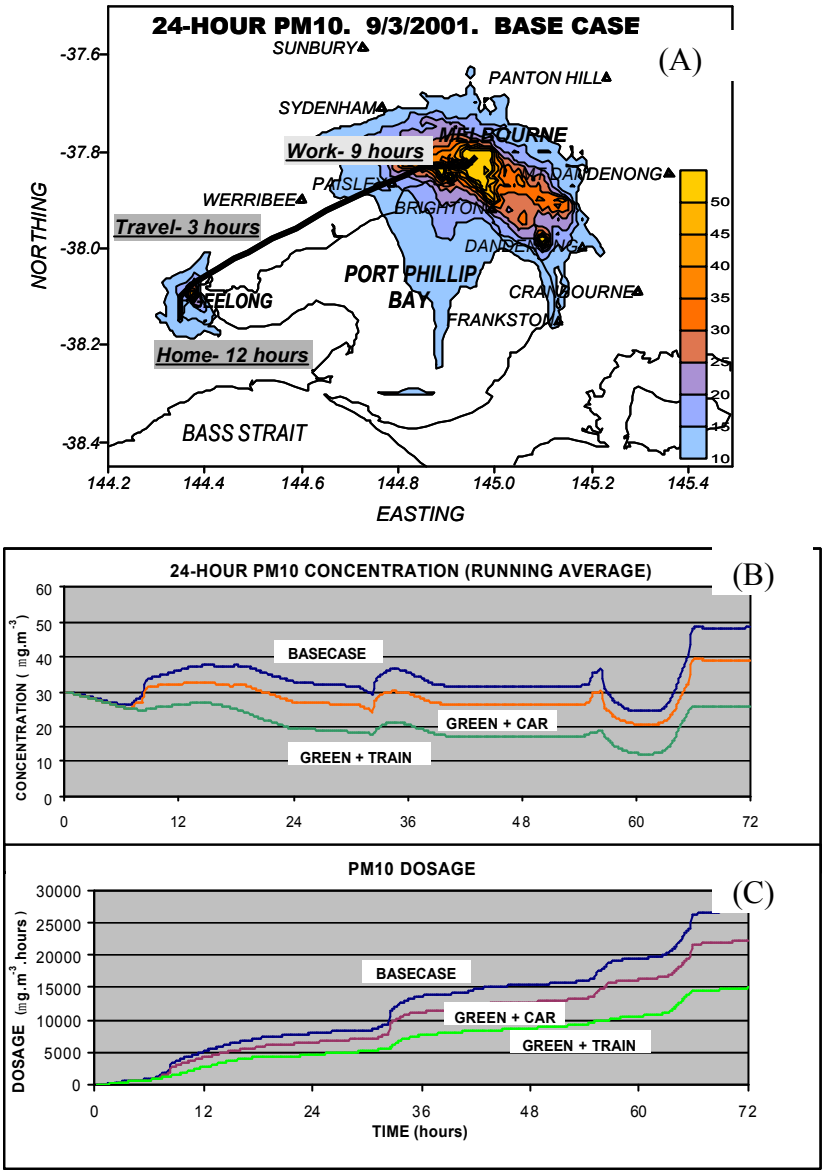

Figure 5.2.1. Example of a 'green' scenario forecast for 7–9 March 2001. (A) Forecast 24-hour PM10 concentration for 9 March 2001 and pathway taken by a person who daily commutes 70 km from Geelong to Melbourne. (B) Forecast 24-hour PM10 concentration (running average) and (C) forecast dosage experienced by the commuter for 3 scenarios ¾ 'business-as-usual' (base case), 25% reduction in motor vehicle emissions and commuter travels by car (green+car), 25% reduction in motor vehicle emissions and commuter travels by train (green+train).

5.3 Emissions for Wildfires and Prescribed Burning

The EIM contains a model for calculating the emissions from fires (**Chapter 3 — The Emissions Inventory Model** and **Appendix 3.1 Emissions Model for AAQFS** presents a description of the fires module).

The input of the fire data on a daily basis requires coordination with the relevant authorities. The ideal system would be that the fire-data agency provides the data in the AAQFS format in an electronic file, which aims to make the System run independently of human intervention.

There are issues regarding the data supplied from fire authorities. These issues have to be weighed up with not including fire emissions in the daily forecast. The issues that may arise from using the fires module are:

- during a wildfire, often limited information is available regarding the geographic location and size of the fire, and other parameters describing the intensity of the fire and emissions;
- for prescribed burns, it is common for scheduled fires to be cancelled, leading to incorrect emissions inputs and hence incorrect forecasts.

5.4 Power-Based Motor Vehicle Emissions

Since emissions from motor vehicles are the major source for smog and secondary particles in major urban regions, the Demonstration Project for AAQFS has included the development of an alternative means of estimating vehicle emissions to that which divides annual VKT by diurnal, daily and seasonal factors — one that could eventually be responsive to real-time traffic data, from traffic-light sensors for example.

The use of VKT as a means of calculating emissions from motor vehicles has a number of limitations. Key among these is the inability to take into account in a detailed way, factors such as road grade, acceleration and deceleration and behaviour of vehicles at intersections. Vehicle emissions using instantaneous vehicle power as the independent variable, can in principle provide the flexibility required. However, power-based modelling has largely been untried in the Australian context.

As a demonstration of its veracity, the power-based model of motor vehicle emissions has been explored and applied to a reduced set of Sydney major roads. The emissions take into account road grade and the presence of intersections as well as the traffic flow rates. While simplifications and generalisations have been required, the work presents the first application of power based modelling to a city road network in Australia.

The need for a vast amount of data, while recognised at the outset, has nevertheless been highlighted by the application of the model to Sydney. Many of the data required for such modelling are simply not available in sufficient detail. Many assumptions have been required.

The work described is based on the synthesis of a large amount of data describing petrol and diesel vehicle emissions, vehicle fleet mixes, road traffic statistics, road networks and vehicle behaviour in free stream traffic and at intersections. Much of the data, particularly the emissions data and the driver behaviour data, show large variations from vehicle to vehicle. This highlights the need for continuing research and data for

- pollutant emission rates from motor vehicles
- traffic flow data
- driver and vehicle behaviour, particularly at intersections.

These data are essential for approaches based on power modelling to be able to provide a more detailed and accurate motor vehicle emissions modelling inventory.

The implementation of the power-based emissions model into AAQFS has been discussed in **Chapter 3—The Emissions Inventory Model** (see also **Appendix 3.4**).

Chapter 6—EPAs' Experiences with AAQFS

Introduction

The quality of the air quality forecast from the AAQFS is dependent on three major factors, the emissions inventory, the meteorological forecast and the chemical transport model. The quality of the emissions inventory is an issue that will directly affect the air quality forecasts. EPAs using the System should aim to provide the best quality emissions inventory data that are available.

6.1 Quality of the Emissions Inventory

The quality of the emissions inventory for the Melbourne region in general is high. The current Melbourne inventory was developed in 1998–1999 for EPA Victoria's Air Quality Improvement Plan.

EPA Victoria estimated the emission for the areas outside the Port Phillip area for AAQFS. This was the first attempt at producing an emissions inventory for the whole State. Emissions inventories for biogenic, motor vehicle and area sources were estimated. The quality of these emissions is low with the exception of the Latrobe Valley where a recent detailed emissions inventory has been undertaken. EPA Victoria is currently compiling an emissions inventory for the Bendigo region that will be updated on the AAQFS datasets. As part of the Victorian inventory, only the power-station emissions were estimated in the industrial sector.

NSW EPA had to draw on a MAQS inventory based on 1992 data. Some modifications were made to provide an updated year 2000 inventory: industrial emissions were scaled on the basis of energy consumption to provide an estimate of year 2000 emissions; updated vehicle kilometre travelled (VKT) information was incorporated, and population data from the 1996 census was used to estimate the area source emissions distributed by population. However, these adjustments were rudimentary in nature.

Also of significance to forecast accuracy, particularly during the cooler months, were the estimates of particulate emissions. The MAQS 1992 inventory provided estimates of total suspended particulates (TSP) emissions and only limited information on emissions of PM_{10}. For the AAQFS project a PM_{10} inventory was produced using standard TSP:PM_{10} ratios for different source categories.

During the demonstration period, several issues with the air quality forecasts came to light. Some of the identified issues, such as the overestimation of emissions from wood heaters, occurred as a result of the outdated emission factors used in the emissions module. Such issues continue to be addressed by EPA Victoria.

6.2 Emissions Data Preparation

Here we provide some indication of the effort required to convert an existing emissions inventory into the format required by the AAQFS, and some of the potential issues that will be encountered in the conversion process. The full System documentation is contained in **Appendix 3.4 Australian Air Quality Forecasting System Emissions Inventory Model System Document** and includes the required formats of the AAQFS data files.

There are emissions inventories available for most state jurisdictions. The existing emissions inventory documentation will include reports, files used to compile inventory, databases and a set of input emissions files for a photochemical model. Converting these data into the required AAQFS format is not an onerous task. For an existing emissions inventory that contains detailed documentation, the conversion process should take approximately 1–3 weeks each for the area, biogenic, industrial and motor vehicle for a person with experience in emission inventory development and with software tools relevant to the conversion process available. An extra week per emissions sector for iterations on the emissions from feedback from the AAQFS forecasts should be factored into time allocations.

The following sections examine the issues in the data conversion process for parts of the emission inventory.

6.2.1 Grid Domains and Spatial Data

The grid spacing of the meteorological forecast is 0.05^o (approximately 5×5 km). The emission inventory needs to be at this resolution and to overlap the meteorological grid. An emissions inventory at a higher resolution of 0.01^o (approximately 1×1 km) for the urban areas is required.

Conversion of existing spatial data into the required AAQFS resolutions will be required. The spatial data for biogenic, motor vehicle and area sources can be produced by two methods. The first option in producing the required AAQFS spatial data is to re-grid the existing inventory into the 0.05^o and 0.01^o grid-cell spaced domains. The second method is to create the required AAQFS spatial domain information from the original or new spatial data.

The industrial spatial data are easy to process from the existing inventory, as the required format for these sources is treated in the same way — as discrete points.

6.2.2 Emissions/Emission Factors

The pollutants list for the AAQFS is presented on page 21 of the Emission Inventory Model System Document in **Appendix 3.4 Australian Air Quality Forecasting System Emissions Inventory Model System Document**. Emissions data for some pollutants (eg NH_3) will not be available from the existing inventory; in other cases they can be derived from the existing emission inventory (eg benzene).

The AAQFS emission format of the area and industrial inventories is as annual emissions and should be available from the existing emission inventory documentation.

The emission factors for the existing motor-vehicle inventory will not be in the required format for the AAQFS. The AAQFS motor vehicle emission factors are required to respond to the daily variation in temperature. This type of conversion was required for the Sydney motor vehicle emission factors.

The biogenic emission factors for the existing inventory are similar to those required for the AAQFS.

6.2.3 Temporal Data

The temporal data required for the AAQFS will be available from the existing emissions inventory. The AAQFS temporal data consist of seasonal or monthly data, and weekly, daily and hourly data.

6.2.4 Speciation

The speciation files for the AAQFS can utilise the existing speciation files. These are predominantly from the U.S. We expect that the difficulty for existing emission inventories will be in providing the cross-reference file for linking each emission source to an appropriate speciation file. This problem was encountered when compiling the Sydney data. Using default speciation data may be the only option to overcome data gaps.

6.2.5 AAQFS Providing Feedback for the Emissions Inventory

Since the AAQFS outputs the forecasts twice daily, hot-spot pollution areas that appear in the forecasts may need to be investigated — they may be real, or may point to a problem in the inventory. For example, in Melbourne several industrial facilities of the same sector had hot-spot emissions. The problem was traced back to an overestimate in fugitive emissions due to poor quality emission factors.

6.3 EPA Victoria's use of the AAQFS

EPA Victoria has had two roles in the AAQFS project. The first was the software development of the emission inventory model. The second role is as a user of the System by providing the emissions inventory data files and air monitoring data, and examining the daily air quality forecasts. This section discusses EPAV as a user of the System.

As participants in the AAQFS, EPAV staff are e-mailed the twice-daily forecasts. These are examined by the staff who issue EPAV's operational air quality forecast. The forecast AQI is of most interest. If poor air quality is forecast from the AQI, the other pollutant information attached to the e-mail is examined.

EPA Victoria has not yet decided to employ the AAQFS in an operational mode. There continue to be questions about the quality of some of the emissions data and hence the reliability of forecasts. However, a significant advantage of the AAQFS is that no EPA resources are required to generate the forecasts on a daily basis and EPA Victoria sees several other uses for the results.

An AAQFS validation report for November 2000 (Manins 2001) demonstrated that the System is able to forecast some air quality parameters accurately (CO and NOx) and reasonably well for particles, though not all particle sources were accounted for in the inventory at that time. The AAQFS has undergone modifications since November 2000 — major modifications concluded in March 2001. EPA Victoria will examine the section on the System performance in Melbourne contained in this Report. This will provide the information that is needed to base a decision on the short-term applications of the AAQFS.

To help gauge the value of the System and to keep the public informed, on 3 September 2001 EPA Victoria began showing the hour-by hour forecasts for Victoria and Melbourne on the Web site at www.epa.vic.gov.au/Air/AAQFS. A subset of pollutants is shown. No validation information is included at this stage. Initial public interest has been very strong.

Potential application of the AAQFS by EPA Victoria include;

- use in an operational mode for EPA's air quality forecasts
- 1st step towards a virtual monitoring system to provide information regarding air quality in places between the stations of the air monitoring network

- the model output and associated meteorological data are useful to further understand smog forecasting
- the System can be used to understand the regional transport of emissions across Victoria
- modelling new emissions sources for environmental impacts
- for use in air policy development work
- health studies (eg data mining the validated forecast for use in risk assessments)
- pin-pointing hot-spot emissions for further examination

EPAVictoria is encouraged by the potential of the AAQFS to forecast air quality and the scientific, policy and operational applications the System holds.

6.4 NSW EPA use of the AAQFS

6.4.1 Involvement and Inputs by NSW EPA

The NSW EPA involvement in AAQFS was chiefly as an operational user of the System. To produce daily validations of the forecasts, the Project required access to air quality and meteorological data from the NSW EPA monitoring network. An automatic transfer of files was set up so that electronic data were made available to CSIRO on a daily basis. These data were presented on a site-by-site basis on the Project website as a graphical comparison of the observed and forecast time-series. The validation information was valuable in assessing the performance of the forecast System and in gaining an understanding of the areas of strength and weakness in the forecasts.

6.4.2 Use of AAQFS Operationally

During the demonstration period, the focus has been on identifying issues with the AAQFS and providing feedback on its performance and the products used to deliver the forecast to the EPA. Issues raised by Project Team members (particularly by NSW EPA and EPA Victoria) resulted in several refinements and improvements to the System and as a result a static System was not in place until fairly late in the demonstration period. Given this focus, it cannot be considered that the System has been used in a truly 'operational' sense by NSW EPA.

Despite this NSW EPA has viewed the model output on a daily basis. During the early operation of the System, there were difficulties in accessing the forecasts on the Web, thereby affecting the utility of the forecast. To address this, the Web presentation files were modified by CSIRO to increase the speed of access, allowing routine examination of the output. To further improve accessibility, CSIRO produced summary plots presenting contours of maximum forecast concentrations for each pollutant. On most days examination of the forecast was restricted to the summary plots. Where these indicated conditions of interest, the more detailed hour-by-hour output were examined. Where it was considered reasonable and appropriate, the System output was used as an additional source of information in arriving at the EPA's daily air quality forecast. The Demonstration Period was of most value in allowing officers to gain experience in the use of the System and hence gaining an understanding of which aspects of the forecasts could be relied on.

For much of the Demonstration Period the model was under-predicting the concentration of ozone. This affected the System's ability to capture ozone events. Predictions were improved by revision of the scheme for calculating vertical dispersion rates and the introduction of a revised chemical mechanism. During January 2001 a significant ozone event occurred over several days. This extended event has provided a valuable event for post-event testing and

evaluation of the modified model's performance. (see **Section 7.2 Sydney 7-Day Photochemical Smog Event**).

6.4.3 Future use in Forecasting

NSW EPA found that during the Demonstration Period, when development of and modifications to the model were being carried out, it was difficult to gain skill in interpreting the forecast in a complex environment like Sydney, where a range of different conditions can lead to air pollution episodes. The System was not static until March 2001.

Negotiations are in progress between NSW EPA and the Bureau of Meteorology for continuation of the service for at least a further 12 months. This period will give NSW EPA the opportunity to determine the value of the forecasts in an operational context using a stable System.

NSW EPA will continue to use the AAQFS forecasts as an additional source of information to assist in formulating its air quality forecast. At this stage there are no plans to release graphical material arising from the System to the public or media. The System output requires interpretation and is hence considered unsuitable for routine public release.

6.4.4 Other Applications

NSW EPA sees that perhaps the greatest potential of the System lies in its ability to be run off-line to investigate control scenarios and policy options, and to better understand the physical mechanisms important on pollution events days. The routine operation of the System provides a library of days that can be explored off-line. This provides the opportunity to apply a climatological approach to pollution events, rather than the reliance on detailed airshed modelling. It should be noted that this approach does not necessarily replace airshed modelling, but provides a useful adjunct to it. To date the off-line System has not been available for use by the NSW EPA, so there has been no opportunity to assess such applications of the System.

Chapter 7—Case Studies with AAQFS

We have made several detailed case studies in order to examine the AAQFS performance when forecasting extreme air quality events. The events reported here include:

(1) a 3-day photochemical smog event in Melbourne, 7–9 March 2001,

(2) a 7-day photochemical smog event in Sydney, 21–27 January 2001, and

(3) the King Island bushfire event which had a serious impact on Melbourne's air quality, 11 January 2001.

7.1 Melbourne 3-Day Photochemical Smog Event

For the 3-day photochemical smog event over Melbourne (7–9 March 2001), the ozone cycle depended on the interaction of light synoptic flow and mesoscale bay- and sea-breeze circulations. The AAQFS performed very well in forecasting the ozone cycle on all three days, during which ventilation played an important role in determining the ozone concentrations. Concentrations were greatest (weakest) over the bay and immediate surrounding areas (inland) where the mixed layer was relatively shallow (deep). On the first two days, southerly winds dominated and ozone was advected inland. On the third day the winds were northerly and ozone precursors were advected out over the bay. Ozone that developed over the bay was advected inland with the bay and sea breeze, although the penetration was slightly under-predicted by the model leading to under-predictions of maximum ozone at Alphington and RMIT.

The transport dynamics for the greater Victorian region were more complex than the region immediately surrounding Melbourne. The larger scale ozone transport highlights the considerable distances high concentrations of pollutants, such as ozone and its precursors, can be transported. It shows also that pollution originating in the Melbourne area can be of regional as well as local concern. This example demonstrates that the AAQFS can offer guidance to pollution forecasters outside the current EPA forecast areas, although without monitoring stations the results cannot be verified.

A full description is given in **Appendix 7.1**.

7.2 Sydney 7-Day Photochemical Smog Event

The 7-day Sydney event (21–27 January 2001) demonstrated the ability of AAQFS to forecast situations involving re-circulation of precursors and remnant ozone, fumigation and complex meteorological dynamics, including drainage winds, sea-breeze circulations, mesoscale cyclonic circulations, and southerly wind shifts associated with trough lines, and the inter-actions of these systems. The forecasting System was able to successfully predict high values of ozone, although on some occasions the peak concentrations for the inland stations were underestimated. The dynamics for the Sydney region require a sensitive balance between the synoptic flow and the mesoscale flow. On two occasions the System forecast a synoptic flow that was too strong. This resulted in blocking of the inland advancement of the sea breeze and only partial success in forecasting the correct ozone concentrations on those occasions.

A full description is given in **Appendix 7.2**.

7.3 King Island Bushfire Smoke

On the afternoon and evening of 11 January 2001 a cold front transported smoke from the Winchelsea and King Island bushfires to Melbourne. The meteorology was particularly complex owing to the delicate balance between the bay/sea breeze and the synoptic northerlies, and the effect these small-scale systems can have on the timing and spatial structure of the arriving cold front. Despite these difficulties LAPS produced an excellent forecast of the meteorology, which, when re-run with smoke sources added, showed the AAQFS is capable of producing high quality forecasts of smoke transport from bushfire events.

A full description is given in **Appendix 7.3**.

A new Conference paper based on this case study is reproduced in **Appendix 7.3a**.

Chapter 8—New User Requirements

Here we concentrate on the technical issues as might be seen by a State EPA (called the "target EPA" here) contemplating looking to have access to the Australian Air Quality Forecasting System in their region.

Currently AAQFS is running only in Victoria and eastern New South Wales in a demonstration mode. A fully operational System requires that the Bureau of Meteorology have the internal resources to run the System. Further, the two EPAs have yet to reach full agreement with the Bureau on the long-term operation of the System, and negotiations on this are currently in progress. Operation in a new region of Australia is so expensive that it must be treated as a public good activity by Bureau of Meteorology. No EPA could contemplate paying the running costs for their region. Further, it is not a static system. It will require ongoing development and improvement.

In addition to reaching an agreement with the Bureau of Meteorology, a new User needs to pay close attention to providing a high quality emissions inventory (since the AAQFS will rapidly demonstrate any significant flaws with the inventory), assign resources to providing automatic daily validation data for comparison with the air quality predictions, and staff to use the new information and to provide feedback to Bureau of Meteorology on the System performance.

Because involvement with the AAQFS requires a sharing of data and information, no charge is made by Bureau of Meteorology for the forecasts to the User.

These factors are discussed in more detail here.

8.1 Current Status

We have reviewed the current status of AAQFS in **Chapter 1—Introduction and Summary**. There the status of the overall System and individual components has been covered, as have issues such as data storage, communication, *etc*. The Chapter also includes a discussion of the System as compared with other systems, including some that are being constructed now and for which AAQFS is a reference. The bulk of the Report has dealt with the performance of the System. The System was demonstrated over a four-month period that included the Olympic and Para-Olympic Games and a preliminary evaluation was conducted. In addition to this, we carried out an extensive trial and evaluation of the System, which included the photochemical oxidant season and the winter low-ventilation season. We have shown that the meteorological component is performing very well, but that there are some issues in the areas of the emissions inventories and chemical transport model to be dealt with.

The development of the System has been documented in papers and Progress Reports and these are all accessible on the Web. See:

- Paper entitled: Development of the Australian Air Quality Forecasting System: Current Status (presented at the International Conference on Urban Climatology, 8–12 November 1999) http://www.dar.csiro.au/publications/Cope_1999a.pdf
- Paper entitled: Development and Application of a Numerical Air Quality Forecasting System (presented at the Clean Air & Environment Conference, 18-22 October 1998) http://www.dar.csiro.au/publications/Cope_1998a.pdf

- Air Quality Forecasting for Australia's Major Cities - 1st Progress Report (5361 KB) http://www.dar.csiro.au/publications/Manins_1999a.pdf
- Air Quality Forecasting for Australia's Major Cities - 2nd Progress Report (1.4 MB) http://www.dar.csiro.au/publications/Manins_1999b.pdf
- Air Quality Forecasting for Australia's Major Cities - 4th Progress Report (33 KB with live Contents Page to component reports) http://www.dar.csiro.au/publications/Manins_2000b.pdf
- Air Quality Forecasting for Australia's Major Cities - 5th and 6th Progress Report (1.5 MB) http://www.dar.csiro.au/publications/Manins_2000c.pdf

8.2 Why should a new EPA want access to AAQFS?

AAQFS delivers twice daily, a forecast of air quality hour by hour for the next 24 hours or more for the target region to a resolution of 1 km (*i.e.*, down to suburb scale). The forecast includes predictions of pollutant concentration including locally defined Air Quality Index, oxides of nitrogen (NO_x), ozone (O_3), sulfur dioxide (SO_2), carbon monoxide (CO), reactive organic compounds (ROCs), PM10, PM2.5, nitrogen dioxide (NO_2), benzene, and tracer gases (for special purposes defined by the EPA for that region). The forecast is generated from a detailed dynamic emissions inventory for the region, and high resolution meteorological forecasts, all run by Bureau of Meteorology. The quality of the forecast is expected to further improve in time as more is learnt about the emissions in a region and the factors that govern its dispersion there.

The data are made available across the Web and by e-mail or FTP to the target EPA. It is entirely the target EPA's responsibility to decide what information is issued to the public. For example, EPA Victoria decided to include the daily outputs for Melbourne from AAQFS on their Web site for the public to access from 3 September 2001. A disclaimer indicating that the information is unvalidated is included (see http://www.epa.vic.gov.au/air/aaqfs). The underlying data are archived each day and are available to the target EPA for any subsequent public-good purpose. A provided graphical analysis tool allows detailed investigation of past days using this archived dataset by the target EPA and by the AAQFS team.

Accumulation of archival data should allow the target EPA to undertake many kinds of analysis including long-term exposure assessments, air quality planning studies, and similar studies. There is room in the System to include special purpose emissions tracers (in Sydney, for Olympic venues for example).

Environment Australia is the custodian of the System, with the target EPA having ultimate say over the emissions data and all air pollution products for that target region. These, and other issues such as quality control functions, feedback of problems and needs, medium- and long-term management of the System, capacity for non-routine work including additional runs of the System, will be described in a memorandum of understanding between the Bureau of Meteorology and the target EPA. CSIRO has undertaken to ensure that the chemical transport component of the System continues to be developed and improved, and to work with Bureau of Meteorology and the participating EPAs to develop the overall System, at no charge so long as the Bureau and the EPAs permit CSIRO to access the underlying data and results for research purposes, disclosure of which would be subject to EPA approval.

Any commercial activity involving AAQFS would require agreement between the relevant parties. It would usually require agreement from all of the AAQFS team: EPA Victoria, Bureau of Meteorology and CSIRO, as well as the target EPA.

8.3 Emissions Inventory

The target EPA will need to provide relevant emissions inventory data as input to the chemical transport model. EPA Victoria has developed the current inventories for AAQFS and can assist by advice or contract work as necessary.

Forecasts of photochemical smog and aerosol would require an inventory of the following air pollutant species — NO_x, VOC, SO_2, PM10, CO, NH_3, and some air toxics (formaldehyde, benzene and butadiene).

The Emissions Inventory Module for AAQFS converts the supplied CB-IV species data to ROC and the PM10 data to fractionated particles by employing speciation profiles obtained from EMS-95. The System Document for the Emissions Inventory Module is contained in **Appendix 3.4**.

If the forecasts were to be limited to aerosol only, the inventory would require only PM10 emissions.

These data will need to be provided in electronic gridded form in the format provided by AAQFS. Experience indicates that they should be provided in four separate databases: vehicles, area-based, industrial stacks, and biogenic. Changes required by the target EPA are instigated simply by supplying a new inventory dataset. Note that biogenic emissions are currently estimated in the CTM using the existing land use data in the module. A jurisdiction need not supply biogenic data at this stage.

Other requirements are:

- Grid resolution for area sources—0.05° (~5 km) in rural areas, 0.01° (~1 km) for the major urban areas.
- Weekday, weekend discrimination, seasonal variation, public holiday discrimination. (Sunday emissions are used as a surrogate for public holiday emissions.)
- Hourly variation of emissions from the major source groups, and those industrial sources using stack need to provide adequate information to permit plume rise to be computed.
- Access to real time databases for prescribed burning and wildfires (optional).

If domestic wood burning is significant, then a relationship between wood consumption and average ambient temperature is required (optional). EPA Victoria has developed a relationship that is used in AAQFS, though local knowledge may well give better results. This is discussed in **Appendix 3.2 Allocation of Emissions from Wood Combustion**.

A protocol between the EPA and Bureau of Meteorology would need to be put into place that ensures that the emissions inventory is maintained, reviewed, evaluated and updated regularly. EPA Victoria and CSIRO would need to be involved on an as-needed basis for these updates and evaluations.

AAQFS participants recognise the likely commercial-in-confidence nature of the emissions inventory. The inventory will be used only for operational and research applications. Inventory data will not be released without permission from the relevant EPA.

8.4 Air Quality and Meteorological Data

The target EPA will need to provide air quality and basic physical meteorological data from its network of monitoring stations to support the routine validation and initialisation of the System. The Air NEPM gives the minimum number, mode of operation etc., for the necessary target EPA monitoring network.

Soon after midnight each day, data for each of the previous 24 hours will need to be transmitted to AAQFS via ftp. AAQFS accepts that these data have undergone no quality assurance and hence may include erroneous data.

The validation air quality data includes the following species- NO, NO_2, O_3, SO_2, PM10, PM2.5 (if available), CO (if available), NMHC (if available). If data from specialised measurement studies are available (such as PAN, C_6H_2, CH_2O, C_4H_6), then they will also need to be made available to AAQFS.

The basic meteorological data from each EPA site need to be included with the air quality data.

8.5 Application

The AAQFS involves the operational exchange of data between Bureau of Meteorology and the EPA. As such, each shares a responsibility to check the accuracy and performance of the forecast products and to provide feedback, which can be used to explain any problems that might arise, and which can also be used to improve the quality of the System.

8.6 Resource Commitment

The routine support of AAQFS involvement by the target EPA is in two parts: (1). Ensuring that air quality and meteorological data are supplied to AAQFS in time each day. (2). Using the AAQFS data for air quality forecasting purposes such as advisories to the public. If the latter is a current EPA function, then the use of AAQFS has the potential to save substantial time each day, since the EPA need only scan one set of output from AAQFS such as the Air Quality Index for that region, instead of having to go through some existing forecasting procedure.

The target EPA is the best judge of the resources required to ensure transmittal of the day's monitoring data to AAQFS.

8.7 Costs

As this agreement involves the exchange of in-kind services (that is, there is consideration for the provision of services), it is subject to GST. The GST to be paid must be determined by the consideration received for the services provided. The AAQFS services provided under this agreement would be part of the Bureau of Meteorology's basic operations (provided for the

Australian community free of charge) and are thus considered to be GST free. Similarly the goods and services provided by the EPA to the AAQFS are considered to be part of the services provided by the EPA freely to each state community. Thus the services provided by the members of the AAQFS and the EPA under this agreement are considered to be GST free.

Any fee-for-service applications would likely require payment of GST.

8.8 Timing of AAQFS extensions to other airsheds.

The timing of AAQFS extension to other airsheds in Australia will be conditional on available resources and the policy environment of participating AAQFS organisations.

Chapter 9—Conclusions and Recommendations

All contractual obligations to Environment Australia have been fully met with the proviso that public demonstration of the System has been entirely in the control of the two participating EPAs, since they explicitly retain the emissions inventory data.

The Demonstration System's performance during the various trials has been extremely encouraging. The trials have enabled documentation of the strengths of the System, and the areas in which the System has needed improvement. Performance has been assessed for the prediction of hourly and daily peaks each day, and for the prediction of weekly, monthly and seasonal trends. Various statistical measures have been used including comparisons against a persistence model ("the pollution levels for the next hour are the same as for the present hour"). A second method of assessing System performance is through detailed examination of case studies of extreme events. Extensive use is made of visualisations in time and space of the meteorological and air quality fields, which are compared with observations.

Airshed-Wide Pollution Performance: The System has shown good potential for forecasting extreme ozone concentrations. When considering a 7-day ozone episode in Sydney (21–27 January 2001), the System went from forecasting near-background concentrations of ozone prior to and after the episode to forecasting concentrations of over 160 ppb during the course of the episode. The probability of detection over the airshed for O_3 was 100% for thresholds in the range 60–100 ppb, and the false alarm rates were between zero and 25%. While the forecast probability of detection was the same as that for persistence (which also achieved a 100% hit rate), the false alarm rates were generally significantly better than those based on persistence. The System has achieved a probability of detection for the 1-hour daily peak of oxides of nitrogen over the Sydney airshed of 98% at a 60 ppb exceedence threshold, and a false alarm rate of 4%. The forecast probability of detection and the false alarm rate were better than persistence forecasts. These results are very good by comparison with international expectations.

Similarly, the System has been able to capture a three-day high ozone episode, observed in Melbourne (7–9 March 2001). Peak concentrations were observed to reach about 80 ppb and were reproduced with excellent skill by the System. The probability of detection over the airshed for O_3 was 100% at a 60 ppb threshold, and the false alarm rate was 25%. Both the probability of detection and the false alarm rate were significantly better than achieved by persistence forecasts. The System achieved a probability of detection for the 1-hour daily peak of NO_y over the Melbourne airshed of 100% at a 60 ppb exceedence threshold, and a false alarm rate of 16%. The probability of detection was better than for persistence forecasts, but the false alarm rate was about the same as persistence. These results are also very good by comparison with international findings, which suggest detection rates above 50% and false alarm rates below 50% are good.

Station-Level Performance: Correct predictions at the station level are vastly more taxing than airshed-wide predictions. The System was able to reproduce the spatial distribution of peak O_3 with good skill in Melbourne for all days of the 3-day event, and for a majority of days in the Sydney 7-day event. This is reflected in the station-level skill scores of O_3, where, for Melbourne, the System achieved a detection probability of 70% at a 60 ppb exceedence threshold for O_3, and a false alarm rate of about 50%. In Sydney the skill scores for O_3 prediction (60 ppb threshold) were 70% and 13% for the detection probability and false alarm rate, respectively. At higher exceedence thresholds, the detection rates were less favourable than persistence while the false alarm rates were substantially better. Since the persistence

results are dominated by a contiguous 7-day event, the performance of AAQFS would have to be rated as good.

Recommendation 1: Modifications to the System, based on findings from recent trials, need to be fully implemented and should be evaluated further during the next photochemical oxidant season and next year's winter particle season.

To help gauge the value of the System and to keep the public informed, on 3 September 2001 EPA Victoria began showing the hour-by hour forecasts for Victoria and Melbourne on their Web site at http://www.epa.vic.gov.au/Air/AAQFS. (A subset of pollutants is shown. No validation information is included at this stage.) Initial public interest has been very strong. NSW EPA has not made a similar commitment, arguing that the System output requires interpretation and is hence considered unsuitable for routine public release.

Recommendation 2: The Australian Air Quality Forecasting System should continue to be supported by the Commonwealth and be adopted by Jurisdictions.

Recommendation 3: The interested public should be given the opportunity to learn about the forecasts and make their own judgements about their utility.

Statistical performance of the meteorological component of AAQFS is very good by comparison with wind data from the Bureau of Meteorology network. There is the possibility that there are local flows not resolved by this network that are important for air pollution dispersion. The model may not resolve these flows either.

The most severe test of System performance is predicting the spatial distribution of pollutants as measured at EPA monitoring stations. The pollutant levels at more remote sites (outer suburbs of Melbourne, Sydney) are mostly a result of transport by the wind (*trajectories* of parcels of pollutants are most important), so the quality of the predicted meteorology is vital.

Recommendation 4: Caution is needed in interpreting the overall performance of the System compared with results from EPA monitoring stations. This may particularly be true in the northwest of the Sydney Basin.

Recommendation 5: To better resolve local winds in the AAQFS, BoM and CSIRO should develop and implement a hybrid dynamic interpolation scheme in the chemical transport model component.

Recommendation 6: BoM should improve the initialisation of the meteorological model for AAQFS applications.

Recommendation 7: BoM needs to examine the boundary-layer physics in the meteorological model, and the impact on low wind speeds, boundary-layer height, and turbulent mixing. This is particularly an issue in the Sydney region.

As shown by case studies, the performance of the System, particularly the meteorological component, is impressive in resolving features and pollution consequences of the sea-bay breeze in Port Phillip Bay, and the interaction of fronts with the geography of the East Coast.

Recommendation 8: Performance of the System should continue to be judged against case studies of important air pollution episodes in preference to (but not to the exclusion of) statistical tests.

AAQFS is showing good potential for forecasting extreme ozone concentrations. For example, when considering a 7-day ozone episode in Sydney, the System went from forecasting near-background concentrations of ozone prior to and after the episode to forecasting concentrations of over 160 ppb during the course of the episode. This is an excellent outcome. It did not always perform well in predicting the correct spatial distribution of the ozone field. This led to a relatively poor reflection of the System's performance in the forecasting skill scores at the station level.

System forecasting performance in Sydney is reduced compared to Melbourne. Frequency distributions of reactive nitrogen species (NO_y) for Sydney show a larger station-to-station variation in performance than was observed in Melbourne. To some degree this may be a natural outcome of evaluating System performance at a greater number of stations. On the other hand, it may indicate shortcomings in the prediction of local meteorological conditions or shortcomings in the emissions inventory.

Recommendation 9: Although complex meteorology (some features of which were possibly unresolved by the meteorological model) was primarily responsible for spatial errors in the forecast ozone fields for the 7-day event, there does appear to be a systematic problem with the prediction of ozone peaks at the northwestern stations in the Sydney region. This needs to be investigated further as the System continues to evolve (see Recommendation 4).

The System is very sensitive to the quality of the supplied emissions inventory, highlighting the need for sound emissions data. In particular, the Project has been the most comprehensive particle modelling exercise undertaken in Australia to date, and this has led to some issues with the emissions estimation methodologies. These issues have been exposed through the daily forecasts from the AAQFS.

Recommendation 10: AAQFS makes a valuable contribution to identifying significant emission inventory issues that need to be addressed. The benefit is not only to the quality of the forecasts, but extends to other uses of inventories in policy and reporting.

Recommendation 11: AAQFS and the National Pollutant Inventory can mutually benefit from the other's outcomes.

The prediction of primary gaseous pollutants such as NO_y and CO has continued to improve throughout the study period, with 1-hour NO_y currently the best-predicted primary pollutant.

Recommendation 12: Further improvements in the prediction of daily peak concentrations (and skill scores) of these pollutants may require the implementation of an improved, interactive urban canopy model in the System.

The System has not been able to reproduce the correct seasonal variation for particles Upon going from the warmer months into winter, the System has systematically over-predicted the concentrations of both PM2.5 and PM10. This is currently the most challenging issue for AAQFS forecasting in Melbourne and Sydney. Wintertime aerosol concentrations are currently over-predicted. It is believed that outdated emissions factors in the domestic wood-burning model is one cause, but other factors include a too-low nocturnal mixing height over the city. In summer, the role of secondary aerosol seems to be a substantial issue not yet well understood.

Recommendation 13: As a matter of priority the emission factors, assumptions and data streams of the wood-fire emissions sub-system need to be carefully reviewed. (EPA Victoria has made some progress here already, leading to the next recommendation.)

Recommendation 14: AAQFS should conduct a trial of new particle emission factors arising from new information on firewood sources in Victoria.

Recommendation 15: There is a clear need to review the emission and treatment of other aerosol sources within the System. Application to new regions may be hampered by the present poor understanding embodied in AAQFS.

Recommendation 16: AAQFS should implement a description of wind-blown dust.

In the Sydney region, the forecasts of PM10 appear to be deleteriously affected by emissions estimates for a number of significant point sources of aerosol (some of the emissions estimates for these sources also affect forecasts of NO_y and SO_2). As part of its work plan NSW EPA is looking to update its inventory. It is envisaged that this will occur progressively, and any improved estimates will be implemented in AAQFS as they become available.

Recommendation 17: The emissions estimates for major point sources need to be reviewed by NSW EPA, and their treatment of these sources within AAQFS also needs to be revisited.

Recommendation 18: The AAQFS should be used to provide feedback to EPAs about issues regarding the emissions inventories to aid emission inventory development. This feedback on significant issues should also be made available more widely, for example to the Air Managers Forum.

In the course of the Project, we have developed some options to the point of showing important potential, ready for adoption and testing by AAQFS with the view to operational implementation.

Recommendation 19: AAQFS should implement and trial the power-based near-road motor-vehicle emissions option.

Recommendation 20: AAQFS should implement and trial the upgraded simplified chemical mechanism (GRS2), and explore the application of a comprehensive chemical mechanism (CB99) for testing and validation purposes.

Recommendation 21: The relevant jurisdictions should explore with fire management agencies the inclusion of burn data into the AAQFS emissions option for better forecasts of the impacts of such events.

During the Demonstration Period the emissions inventory model has been run twice daily as part of the full System. This may be an avoidable substantial overhead. Further, the output from the meteorological model has been used to run the chemical transport model offline. Combining these models into one model (online) will give higher temporal and spatial resolution for the air quality transport and dispersion calculations.

Recommendation 22: AAQFS should explore improving the effective speed of the emissions inventory model by incorporating daily (but probably not seasonal) variations of emissions into the chemical transport model. This should include motor vehicle emissions, which would then be more responsive in the model to forecast temperatures.

Recommendation 23: The option to implement the chemical transport model within the meteorological model should be investigated for its suitability as the ultimate configuration of the fully implemented system.

EPA Victoria and NSW EPA have yet to fully decide to employ the AAQFS in an operational mode. The System has been shown to be capable of producing high-quality forecasts under a variety of conditions, including highly complex meteorological situations. Airshed-wide performance for tracer pollutants and ozone is very good. However the same cannot be yet said for aerosol. At the station-by-station level, performance is encouraging, but needs improvement. Thus there continue to be questions about the quality of the emissions data and the reliability of forecasts. The EPAs will be examining the sections on the System performance contained in this Report. This will provide the information that is needed to base a decision on the short-term applications of the AAQFS.

Recommendation 24: At this stage of its development, AAQFS should be used as an additional source of information to assist EPAs in formulating an air quality forecast.

*Recommendation 25: The System should be re-evaluated after the coming photo-chemical oxidant season, and next year's winter particle season (*cf., *Recommendation 1*).

Recommendation 26: The System should next be extended to Tasmania and begin to forecast particles in the Launceston region in winter.

Recommendation 27: AAQFS needs to facilitate EPAs to realise the potential of the System for use in predicting regional impacts of significant new emission sources or of land use changes.

Recommendation 28: The substantial effort required to archive adequate forecast data for scenario model runs needs to be recognised.

Accepting the problems exposed in the trials, the AAQFS is an international leader, in particular because:

- The system runs as a collaboration between the national meteorological agency (the Bureau of Meteorology) and the environment protection agencies which are responsible for informing the public.
- A twice-daily exchange of air pollution monitoring data and air pollution predictions occurs between the agencies.
- The predictions are subjected to an hour-by-hour daily routine station-level verification of criteria pollutant concentrations, reported to participants on the Web.
- By comparison with some other systems internationally, the meteorological forecast is undertaken at a comparable resolution to the air pollution forecast—at a scale that is useful in resolving suburb-scale variations hour by hour.
- The emissions inputs to the forecasts depend on the predicted meteorology—for example, vehicle evaporative emissions and biogenic emissions both depend on the forecast hour-by-hour temperature, and woodheater emissions depend on the forecast daily average temperature. Sea-salt emissions depend on the forecast local wind strength.
- A high-speed photochemistry is used; its performance is adequate for screening and for forecasts of an alternative 'green' scenario for high pollution days.

References

Azzi M. Johnson G.M. and Cope M. (1992) An introduction to the generic reaction set photochemical smog mechanism. In *Proc. 11th Clean Air Conf. & 4th Regional IUAPPA Conf.,* Brisbane, Australia.

Cardelino C., Chang M., St. John J., Murphey B., Cordle J., Ballagas R., Patterson L., Powell K., Stogner J. and Zimmer-Dauphinee S. (2001) Ozone predictions in Atlanta, Georgia: Analysis of the 1999 ozone season. *J. Air & Waste Manage. Assoc.* **51**:1227–1236.

Carnovale, F., Tilly, K., Stuart, A., Carvalho, C., Summers, M. and Eriksen, P. (1996) *Metropolitan Air Quality Study: Air Emissions Inventory*, Final Report prepared by EPA Victoria for Environment Protection Authority of New South Wales, Sydney.

Carruthers, D.J., Edmunds, H.A., Lester, A.E., McHugh, C. A. and Singles, R.J. (2001) Use and Validation of ADMS-Urban in contrasting urban and industrial locations. Int. J. Environment and Pollution. (submitted).

Colquhoun, J. R. (1981) The origin, evolution and structure of some southerly bursters, *Australian Bureau of Meteorology Technical Report 40*, Bureau of Meteorology, Melbourne, 57 pp.

Cope M.E. and Ischtwan J. (1995) *Perth photochemical smog study: Airshed modelling component*, Final report to Western Power and Department of Environment Protection, Perth.

Cope, M., Hess, D., Lee, S., Azzi, M., Carras, J., Wong, N., and Young, M. (1999) Development of the Australian Air Quality Forecasting System: Current Status. *Proc. International Conf. Urban Climatology*, Sydney, 8–12 November 1999.

Cope, M. E., Manins, P., Hess, D., Mills, G., Puri, K., Dewundege, P., Tilly, K. and Johnson, M. (1998) Development and application of a numerical air quality forecasting system, *Proc. 14th International Conf. Clean Air & Environment*, Melbourne, 18–22 October 1998, Clean Air Society of Australia and New Zealand, 353–358.

Cope, M., Hess, D., Lee, S., Manins, P., Puri, K., Tory, K., Wong, N., Carras, J. and Lilley, W. (2001) The Australian Air Quality Forecasting System: Predicting the Impact of Motor Vehicle Emissions. *Proc. 10th International Symposium "Transport and Air Pollution"* 17–19 September 2001: Boulder, Colorado USA

De Leeuw F. (2000) Criteria for evaluation of smog forecast systems. *Environmental Monitoring and Assessment*, **60**, 1–14.

DeMore, W.B., Sander, S.P., Golden, D.M., Hampson, *et al.* (1997) Chemical kinetics and photochemical data for use in stratospheric modelling. Evaluation number 12. NASA panel for data evaluation. *Jet Propulsion Laboratory Report*, 97–104.

Dewundege P. (2001) A semi automated expert system for smog forecasting over Melbourne airshed. *Clean Air (Australia & New Zealand)*, **35**, 35–40.

Duffy and Nelson (1997) Exposure to emissions of 1,3-butadiene and benzene in the cabins of moving motor vehicles and buses in Sydney, Australia. *Atmos. Environ.*, **31**(23) 3877–3885.

EPA (1992) *Protocol for determining the best performing model*. Office of Air Quality Planning and Standards Research Triangle Park, NC 27711. EPA-454/R-92-025.

EPAV (1991) Air emissions inventory, Port Phillip Control Region: Planning for the future, Report No. SRS 91/001, EPA Victoria, Melbourne.

EPAV (1998) *Air emissions inventory, Port Phillip Region,* Publication 632, EPA Victoria, Melbourne.

EPAV (2001) Air Quality Improvement Plan for Port Phillip Bay, Report to be Printed, EPA Victoria, Melbourne.

Ferguson S.A., Sandberg D.V. and Ottmar R. (1998) Wild-land biomass emissions affected by land-use changes, in *Second Symposium on Fire and Forest Meteorology*, 11–16 Jan 1998, Phoenix, AZ, American Meteorological Society, Boston, MA, 71–74.

Fine P.M., Cass G.R. and Simoneit B.R. (2001) Chemical characterization of fine particle emissions from fireplace combustion of woods grown in the northeastern United States', *Environ. Sci. Technol.*, **35**:2665–2675.

Gery M.W., Whitten G.Z., Killus J.P. and Dodge M.C. (1989) A photochemical kinetics mechanism for urban and regional scale computer modeling, *J. Geophys. Res.*, **94**:12925–56.

Harley R.A., Russell A.G., McRae G.J., Cass G.R. and Seinfeld J.H. (1993) Photochemical modeling of the southern California air quality study. *Environ. Sci. Technol.*, **27**, 378–388.

Hedley M., Mclaren R., Jiang W. and Singleton D.L. (1997) Evaluation of an air quality simulation of the lower Fraser Valley- II. Photochemistry. *Atmos. Environ.* **31**, 1617–1630.

Hess G. D., Carnovale F., Cope M., and Johnson G.M. (1992) Evaluation of some photochemical mechanisms – I. Temperature and initial concentration effects. *Atmos. Environ.* **26A**, 625–641

Hess, G. D., Cope, M. E., Lee, S., and Tory, K. (1999) LAPS and the Australian Air Quality Forecasting System. *Abstracts of Presentation at the Eleventh Annual BMRC Modelling Workshop*, 9–11 November 1999, BMRC Report No. 75, Bureau of Meteorology, Melbourne, 35-40.

Hess, G. D., Cope, M. E., Lee, S., Manins, P. C., Mills, G. A., Puri, K., and Tory, K. (2000a) The development of the Australian Air Quality Forecasting System: Current status. *Proc. Millennium NATO/CCMS International Technical Meeting on Air Pollution Modelling and Its Application*, 15–19 May 2000, Boulder CO, American Meteorological Society, 276-283.

Hess, G. D., Cope, M. E., Lee, S., Manins, P. C., Mills, G. A., Puri, K. and Tory, K. (2000b) The Australian Air Quality Forecasting System, *AMOS Bulletin*, **13**, 67–73.

Hurley P. (2000) The Air Pollution Model (TAPM): Summary of some recent verification work in Australia. *Proc. 15th International Clean Air and Environment Conf*. 26–30 November 2000, Sydney Australia, 98–103.

Janssen M. (2001) Incorporation of Speciate 3.0 into EMS-2001, Paper presented to *10th International Emission Inventory Conference*, Denver, Colorado, USA, April–May 2001.

Johnson G.M. (1993) *Compilation of CSIRO Dual Outdoor Smog Chamber Data.* Edition: November, 1993. CSIRO Division of Coal and Energy Technology Investigation Report CET/IR192.

Lee Sunhee, Cope M, Tory K, Hess D and Ng YL (2001) The Australian Air Quality Forecasting System: Modelling of a Severe Smoke Event in Melbourne, Australia. *Proc.*

25th NATO/CCMS International Technical Meeting on Air Pollution Modelling and its Application, 15–19 October 2001, Louvain-la-Neuve, Belgium.

Manins, P. C., (Chair of Committee) (1999a) *Air quality forecasting for Australia's major cities: 1st progress report* [to Department of the Environment and Heritage] / prepared by Project Management Committee: Environment Protection Authority (Victoria), Environment Protection Authority of NSW, Bureau of Meteorology Research Centre, CSIRO Energy Technology and CSIRO Atmospheric Research: SB/1/407. Aspendale, Vic.: CSIRO Atmospheric Research. 29, [27] p.

Manins, P. C., (Chair of Committee) (1999b) *Air quality forecasting for Australia's major cities: 2nd progress report* [to Department of the Environment and Heritage] / prepared by Project Management Committee: Environment Protection Authority (Victoria), Environment Protection Authority of NSW, Bureau of Meteorology Research Centre, CSIRO Energy Technology and CSIRO Atmospheric Research: SB/1/407. Aspendale, Vic.: CSIRO Atmospheric Research. 35, [6], 5, 16 p.

Manins, P. C., (Chair of Committee) (2000a) *Air quality forecasting for Australia's major cities: 3rd progress report* [to Department of the Environment and Heritage] / prepared by Project Management Committee: Environment Protection Authority (Victoria), Environment Protection Authority of NSW, Bureau of Meteorology Research Centre, CSIRO Energy Technology and CSIRO Atmospheric Research: SB/1/407. Aspendale, Vic.: CSIRO Atmospheric Research. 41, [6], 5, 14 p.

Manins, P. C., (Chair of Committee) (2000b) *Air quality forecasting for Australia's major cities: 4th progress report* [to Department of the Environment and Heritage] / prepared by Project Management Committee: Environment Protection Authority (Victoria), Environment Protection Authority of NSW, Bureau of Meteorology Research Centre, CSIRO Energy Technology and CSIRO Atmospheric Research: SB/1/407. Aspendale, Vic.: CSIRO Atmospheric Research. 86 p.

Manins, P. C., (Chair of Committee) (2000c) *Air quality forecasting for Australia's major cities: 5th & 6th progress report* [to Department of the Environment and Heritage] / prepared by Project Management Committee: Environment Protection Authority (Victoria), Environment Protection Authority of NSW, Bureau of Meteorology Research Centre, CSIRO Energy Technology and CSIRO Atmospheric Research: SB/1/407. Aspendale, Vic.: CSIRO Atmospheric Research. 56 p.

Manins, P. C. (Chair of Committee) (2001) *Current Status, Preliminary Validation Study of the Australian Air Quality Forecasting System*. Prepared by the Project Management Committee: Environment Protection Authority (Victoria), Environment Protection Authority of NSW, Bureau of Meteorology Research Centre, CSIRO Energy Technology, CSIRO Atmospheric Research. CSIRO Atmospheric Research, Aspendale, Victoria.

MOT (1998) *Vehicle fleet emissions control strategy: Final report*, Ministry of Transport, New Zealand.

NEPC (2001) *Draft National Environment Protection (Diesel vehicle emissions) Measure*, Public consultation, National Environment Protection Council, Canberra.

Ng Y.L. and Minchin M. (2000) Spatial and temporal allocation of emissions from wood combustion', *Proc. 15th International Clean Air and Environment Conference, Sydney, 2000*, 288–291.

Puri, K., Dietachmayer, G., Mills, G. A., Davidson, N. E., Bowen, R. A. and Logan, L. W., (1998) The new BMRC Limited Area Prediction System, LAPS, *Aust. Met. Mag*., **47**, 203–233.

Seigneur C., Pun B., Pai Pl, Louis J., Solomon P., Emery C., Morris R., Zahniser M., Worsnop D., Koutrakis P., White W., Tombach I. (2000) Guidance for the performance evaluation of three-dimensional air quality modeling systems for particulate matter and visibility. *J. Air and Waste Manage. Assoc*., **50**, 588–599.

Seinfeld J.H. (1986) Atmospheric Chemistry and Physics of Air Pollution, Wiley-Interscience, New York, 738 + xxiii pp.

Tory, K. J., Hess, G. D., Mills, G. A. and Puri, K. (2000) Verification of the meteorological component of the Australian Air Quality Forecasting System *Proc. 15th Clean Air and Environment Conference*, 26–30 November 2000, Brighton Beach, NSW, Clean Air Society of Australia and New Zealand.

USEPA (1995) *User's Guide to MOBILE5,* Report No EPA-AA-TEB-91-01, United States Environmental Protection Agency, Research Triangle Park, North Carolina, USA.

USEPA (1998) MOBILE6, A Revised Model for Estimation of Highway Vehicle Emissions, presented at *Air and Waste Management Association, Eighth Annual Conference on Emission Inventories*, December 1998, New Orleans, Louisiana, Office of Mobile Sources, United States Environmental Protection Agency, Ann Arbor, Michigan, USA.

Williams D.J., Shenouda D.A. and Carras J.N. (1994) Modelling air toxic emissions from motor vehicles, *Proc. Air Toxics Conference, Sydney, 1994,* Clean Air Society of Australia & New Zealand and CSIRO, NSW, Australia.

Yarwood G., Wilson G., Emery C. and Guenther A. (1999) *Final report: Development of GLOBEIS -- A state of the science biogenic emissions modeling system,* prepared for M. Estes, Texas Natural Resource Conservation Commission, Austin, Texas, USA.

Appendices

The following Appendices contain expanded or related material for the Chapter of the same number.

Appendix 2.1a The Numerical Weather Prediction Model

Summary prepared by Dale Hess and Kamal Puri, Bureau of Meteorology Research Centre

The numerical weather prediction (NWP) model used in AAQFS is the Limited Area Prediction System (LAPS) of BoM. LAPS has been the operational, short-range numerical forecasting system for BoM since July 1996. In summary it has the following features:

- model domains for Victoria and New South Wales with $0.05^o \times 0.05^o$ latitude-longitude grids and 29 vertical levels. The lowest model level is at 10-m height; there are 11 levels within the first 1500 m above the surface.
- nesting of the model domains within a version of LAPS with a domain covering all of Australia and run at $0.375^o \times 0.375^o$ resolution. The latter domain, in turn, is nested within the BoM global model (GASP). The boundary conditions are interpolated in time from 3-hourly output fields.
- twice daily, 36-hour forecasts (commencing at 1100 UTC and 2300 UTC)
- hydrostatic primitive-equation dynamics are solved on a non-staggered Arakawa A-grid
- state-of-the-art, high-order numerics
- detailed parameterisation of physical processes
- multivariate statistical interpolation analysis
- use of locally retrieved temperature soundings and cloud-drift winds
- use of AMDAR (measurements from commercial aircraft) temperatures and winds and METAR/SYNOP near-surface moisture
- use of GMS-based heating rates
- use of synthetic moisture and tropical cyclone data

A detailed overview of LAPS is given in Puri, *et al*. (1998).

Recent upgrades to LAPS have focussed on the physical parameterisation mechanisms, which are particularly relevant to air quality applications. In the surface boundary layer the fluxes are now obtained by solving the Monin-Obukhov profile relations by iteration. For the unstable boundary layer ($\zeta = z/L < 0$, where ζ is a stability parameter, z the height, and L the Obukhov length), the nondimensional gradients (Dyer, 1974; Hogstrom, 1988) for the momentum flux (subscript M) and the heat and moisture flux (subscripts H and Q, respectively) are given by:

$$\Phi_M(\zeta) = (1 - 16\,\zeta)^{-1/4} \qquad \Phi_H(\zeta) = \Phi_Q(\zeta) = (1 - 16\,\zeta)^{-1/2}$$

where $L = -u_*^3 / [(kg/T_L)(H_{v0}/\rho C_p)]$, $u_*^2 = \tau/\rho$, τ the surface stress, ρ the air density, g is the acceleration due to gravity, k the von Karman constant (k = 0.4), T_L the lowest model level temperature, H_{v0} the surface virtual heat flux, and C_p the specific heat of air at constant pressure. Integrating the Φ functions gives:

$$U = (u_*/k)\,\{\ln[(z + z_0)/z_0] - \Psi_M(\zeta) + \Psi_M(\zeta_0)\}$$

$$(\Theta - \Theta_0) = (\Theta_*/k)\,\{\ln[(z + z_0)/z_H] - \Psi_H(\zeta) + \Psi_H(\zeta_H)\}$$

where $\Psi_M(\zeta) = \ln[(1 + x)^2 (1 + x^2)] - 2\arctan(x)$, $\Psi_H(\zeta) = \Psi_Q(\zeta) = 2\ln(1 + x^2)$, $x = (1 - 16\zeta)^{1/4}$, $\zeta_0 = z_0/L$ and $\zeta_H = z_H/L$, Θ is the potential temperature and $\Theta_* = -H_0/(\rho C_p u_*)$. The subscript 0 indicates a value at the surface.

There are separate roughness lengths for momentum z_0 and heat z_H. The roughness length for moisture z_q is taken to be the same as for heat over land.

For the stable surface boundary layer ($\zeta > 0$) the nondimensional gradients are given by (Hogstrom, 1988 for momentum, and derived from the Ellison-Turner relation (Turner, 1973, pp. 136–138):

$$\Phi_M = 1 + 5\zeta \qquad \Phi_H = \Phi_Q = (1 + 4\zeta)^2.$$

For the stable case the empirical forms proposed by Beljaars and Holtslag (1991) are used for the profile relations:

$$\Psi_M(\zeta) = -b(\zeta - c/d)\exp(-d\zeta) - a\zeta - bc/d$$

$$\Psi_H(\zeta) = \Psi_Q(\zeta) = -b(\zeta - c/d)\exp(-d\zeta) - (1 + 2a\zeta/3)^{3/2} - bc/d + 1$$

where a = 1, b = 2/3, c = 5, and d = 0.35.

Below the lowest model level, the exchange coefficients are given by

$$K_M = kzu_*/\Phi_M(\zeta) = u_*^2\Delta z/\Delta U \qquad K_H = kzu_*/\Phi_H(\zeta) = u_*\Theta_*\Delta z/\Delta\Theta$$

where Δ indicates the difference between the surface and the lowest model level.

The stability parameter ζ is found from the bulk Richardson number Ri_b:

$$Ri_b = [2g/(\Theta_{v0} + \Theta_{vL})]\, z_L(\Theta_{vL} - \Theta_{v0})/|U|^2$$

where the subscript v indicates virtual, 0 the surface, and L the lowest model level. The value of ζ is found from:

$$Ri_b = \zeta\,\{\ln[(z_L + z_0)/z_H] - \Psi_H[(z_L + z_0)/L] + \Psi_H(z_H/L)\}/$$
$$\{\ln[(z_L + z_0)/z_0] - \Psi_M[(z_L + z_0)/L] + \Psi_M(z_0/L)\}^2$$

The canopy height, h_c, is obtained from a $0.05^o \times 0.05^o$ data set prepared for the Australian continent by Dean Gratz (http://www.eoc.csiro.au; private communication). Over land the momentum roughness length z_0 is assumed to be equal to 0.1 h_c (Garratt, 1992, p. 87). The heat roughness length $z_H = 0.1\ z_0$. Over the sea (Beljaars, 1994),

$$z_0 = a_M\,\nu/u_* + a_C\,u_*^2/g \qquad z_H = a_H\,\nu/u_* \qquad z_Q = a_Q\,\nu/u_*$$

where $a_M = 0.11$, $a_H = 0.40$, $a_Q = 0.62$ and $a_C = 0.018$.

In addition to vegetative roughness, the model also accounts for topographical roughness based on the theory of Wood and Mason (1993). A topographical data set with resolution of $0.008^o \times 0.008^o$ is used to compute the orientation of the principal axis of the topography (in the direction of maximum topographical variation) with respect to the x-axis, θ_{gw}, and the slope of the topography, σ_{gw}, for each grid square (Lott and Miller, 1997):

$$K = (1/2N)\,\Sigma_i\,[(\partial h/\partial x)^2 + (\partial h/\partial y)^2]$$

$$L = (1/2N)\,\Sigma_i\,[(\partial h/\partial x)^2 - (\partial h/\partial y)^2]$$

$$M = (1/N)\,\Sigma_i\,(\partial h/\partial x)(\partial h/\partial y)$$

where the sum is over a grid square and N is the number of topographical points, $\theta_{gw} = \frac{1}{2}\arctan(M/L)$, and $\sigma_{gw}^2 = K + (L^2 + M^2)^{1/2}$.

The slope is scaled to a maximum value of 0.3 to agree with Wood and Mason (1993, Fig. 13) and the effective roughness length is found by a cubic fit to their model results for values of the scaled slope yielding effective roughness lengths z_{0eff} greater than 5 times the vegetation roughness length z_{0veg}.

$$z_{oeff} = a_1 + a_2 s + a_3 s^2 + a_4 s^3$$

where s is the scaled slope, and $a_1 = 1.64$, $a_2 = -50.1$, $a_3 = 414.0$, and $a_4 = 227.0$.

For the region $z_{0veg} < z_{0eff} < 5\ z_{0veg}$, logarithmic interpolation is used. A maximum value of $z_{0eff} = 30$ m is allowed. The influence of the topographical roughness depends on the cosine of the difference between the angle of the wind direction and θ_{gw}. For a wind direction along the ridges, rather than across them, the roughness length obtains its minimum value, z_{0veg}.

Flux transfer at low wind speeds in convective conditions takes account of dry convective downdrafts by defining u_* by the following expression:

$$u_* = k\,(u^2 + v^2 + w_*^2)^{1/2} / \{\ln[(z_L + z_0)/z_0 0] - \Psi_M[(z_L + z_0)/L] + \Psi_M(z_0/L)\}$$

where $w_* = u_* [-z_i/kL]^{1/3}$ and z_i is the height of the inversion capping the boundary layer, assumed to be 1000 m.

For unstable conditions, the turbulent viscosity K_M and the turbulent diffusivity K_H above the lowest layer are given by a formulation based on the work of Troen & Mahrt (1986). In the surface layer ($z_L < z < 0.1\ z_i$) we have:

$$K_M = kzu_* (1 - z/z_i)^2 / \Phi_M \qquad K_H = kzu_* (1 - z/z_i)^2 / \Phi_H$$

and in the mixed layer ($0.1z_i < z < z_i$) we have:

$$K_M = kzw_s (1 - z/z_i)^2 \qquad K_H = kzw_s (1 - z/z_i)^2\ Pr$$

where $Pr = \Phi_M / \Phi_H$, evaluated at the top of the surface layer $z = 0.1\ z_i$, and $w_s = (u_*^3 + 0.6\ w_*^3)^{1/3}$. In these applications the height z_i is calculated from the Θ_v profile (i.e., z_i is the height of the first level k where $\Theta_{vk} > \Theta_{vk+1} + 2(H_{v0}/\rho C_P w_s)$ for k decreasing with height).

At the top of the mixed layer $z = z_i$, the buoyancy flux is assumed to be proportional to the surface buoyancy flux:

$$(H_{vzi}/\rho C_p) = -C_e\,(H_{vo}/\rho C_p)$$

where $C_e = 0.2$. The turbulent diffusivity at the top of the mixed layer can be written as:

$$`K_H = -C_e\,(H_{v0}/\rho C_p)\,(\Delta z/\Delta\Theta_v)$$

At $z = z_i$ we take:

$$`K_H = \max(K_H, K_H).$$

In stable conditions above the first model layer, the exchange coefficients are given as a function of the bulk Richardson number (Louis et al., 1982):

$$K_M = \ell^2\,|\partial U/\partial z|\,/[1 + 2bRi\,/(1 + d\,Ri)^{1/2}\,]$$

$$K_H = \ell^2\,|\partial U/\partial z|\,/[1 + 3bRi(1 + d\,Ri)^{1/2}\,]$$

where $\ell = kz/(1 + kz/\lambda)$, $\lambda = 150$ m, $b = 5$, and $d = 1$.

A computational value of the top of the boundary layer, used to determine the appropriate stability dependence for the turbulent mixing, is found by calculating two height scales: a dynamic height scale, $h_{dyn} = 0.5\ u_*/|f|$, where equator-wards of 20 degrees, the Coriolis parameter $|f|$ is set to 5×10^{-5} s^{-1}; and a convective height scale, $h_{conv,}$, where z first obtains $\Theta > \Theta_L$. The top of the boundary layer is given by the maximum of these two heights.

Above the top of the boundary layer in stable conditions and above the mixed layer height z_i, the exchange coefficients are based on local scaling similarity:

$$K_M = (\ell^2/\Phi_M^2)\,|\partial U/\partial z| \qquad K_H = (\ell^2/\Phi_M\Phi_H)\,|\partial U/\partial z|.$$

The land-surface scheme uses data sets developed by Dean Gratz (http://www.eoc.csiro.au; private communication) at $0.05^o \times 0.05^o$ resolution for the Australian continent. These include 32 vegetation/land-use types, vegetation fraction C_v, leaf-area index L_f and 8 soil types. The soil types were mapped onto the Clapp-Hornberger (1978) classification, thus making the soil hydraulic properties (soil moisture at saturation θ_{sat}, soil moisture at field capacity θ_{cap}, soil moisture at permanent wilting point θ_{pwp}, matric potential at saturation Ψ_{sat}, hydraulic conductivity at saturation γ_{sat} and the Clapp-Hornberger soil parameters *a* and *b*) available at 5-km resolution.

Soil temperature and moisture are calculated at four soil layers (of depth 0.07 m, 0.21 m, 0.72 m, and 1.89 m). These calculations represent all time scales from one day to one year (Viterbo & Beljaars, 1995). Plant roots exist in the upper three layers. Evaporation E is computed as the sum of three components, E_ℓ, E_v and E_g, which are weighted by the fraction covered by an interception reservoir representing the collection of precipitation and dew C_ℓ, the dry vegetation fraction $(1 - C_\ell)\,C_v$, and the dry bare soil fraction $(1 - C_\ell)(1 - C_v)$:

$$E = C_\ell E_\ell + (1 - C_\ell)C_v E_v + (1 - C_\ell)(1 - C_v)E_g.$$

The interception reservoir fraction is given by

$$C_\ell = \min\,(1, W_\ell/W_{\ell mx})$$

where W_ℓ is the water content of the reservoir, $W_{lmx} = [C_v\ L_f + (1 - C_v)\ ]\ W_{max}$, and $W_{max} = 0.0002$ m.

$$E_\ell = (\rho/r_a)\,[q_L - q_{sat}(T_{sk}, P_0)]$$

where the aerodynamic resistance $r_a = \{\ln[(z_L + z_0)/z_0] - \Psi_M[(z_L + z_0)/L] + \Psi_M(z_0/L)\}\{\ln[(z_L + z_0)/z_H] - \Psi_M[(z_L + z_0)/L] + \Psi_M(z_H/L)\}/(k^2\,|U_L|)$, q_L is the specific humidity at the lowest model level, q_{sat} the saturated specific humidity, T_{sk} the skin temperature, and P_0 the surface pressure. The skin temperature is found from surface energy balance:

$$(1 - \alpha)\,R_s + R_T - \varepsilon\sigma T_{sk}^4 + H_0 + LE_0 = \Lambda_{sk}\,(T_{sk} - T_1)$$

where α is the surface albedo, R_s the downward shortwave radiative flux, R_T the downward longwave radiative flux, ε the surface emissivity, σ the Stefan-Boltzmann constant, H_0 the surface heat flux, E_0 the surface evaporative flux, L the latent heat of vaporisation, Λ_{sk} the soil conductivity ($\Lambda_{sk} = 7$ W m^{-2} K^{-1}) and T_1 the temperature at the first soil layer.

The dry vegetation transpires at the rate:

$$E_v = [\rho/(r_a + r_c)][q_L - q_{sat}(T_{sk}, P_0)]$$

where the canopy resistance $r_c = (r_{smin}/L_f)\ f_1(PAR)\ f_2(\theta)$, r_{smin} is the minimum stomatal resistance for a single leaf ($r_{smin} = 240$ s m^{-1}), PAR the photosynthetically active radiation [$PAR = 0.55(1 - \alpha)\ R_s$] and θ the mean soil moisture in the root zone. The dependence of function f_1 on PAR is given by (Sellers, 1985):

$$f_1 = (k_0 L_f)/\{(b_2/d\ PAR)\ [\ \ln\{[d\ \exp(k_0 L_f) + 1]/(d + 1)\} - \ln\ \{[d + \exp(-k_0 L_f)]/(d + 1)\}]$$

where $k_0 = (1 - \omega)^{1/2}$, $\omega = \alpha_c + \tau_c$, $\alpha_c = 0.105$, $\tau_c = 0.070$, $d = (a_2 + b_2 r_{smin})/(r_{rsmin}\ PAR)$, $a_2 = 5000$ J m^{-3}, $b_2 = 10$ W m^{-2}, and

$$f_2^{-1} = \begin{cases} 0 & \theta < \theta_{pwp} \\ (\theta - \theta_{pwp})/(\theta_{cap} - \theta_{pwp}) & \theta_{pwp} < \theta < \theta_{cap} \\ 1 & \theta > \theta_{cap}, \end{cases}$$

and $\theta = R_1\theta_1 + R_2\theta_2 + R_3\theta_3$ where $R_1 = R_2 = R_3 = 0.33$ specifies the vertical distribution of the roots in the soil.

The bare ground evaporation is given by:

$$E_g = (\rho/r_a)[q_L - \alpha\ q_{sat}(T_{sk}, P_0)]$$

where

$$\alpha = \begin{cases} 0.5\ \{1 - \cos\ [(\pi\theta_1)/(1.6\theta_{cap})]\} & \theta_1 < \theta_{cap} \\ 1 & \theta_1 > \theta_{cap}, \end{cases}$$

and θ_1 is the average soil moisture in the first soil layer.

The soil temperatures are found by solving the following diffusion equation:

$$(\rho C)_s\ \partial T/\partial t = (\partial/\partial z)(\lambda_T\ \partial T/\partial z)$$

where $(\rho C)_s$ is the volumetric soil heat capacity, and λ_T the thermal conductivity

$$\lambda_T = \begin{cases} a\ |\Psi_{sat}|^{-1/\ln 10}\ (\theta_{sat}/\theta)^{-b/\ln 10} & \theta > \theta_\lambda \\ \lambda_{min} & \theta < \theta_\lambda, \end{cases}$$

and $\lambda_{min} = 0.171$ W m^{-1} K^{-1}, and θ_λ is the minimum value of soil moisture that ensures continuity of the equations.

The soil moisture is found by solving:

$$\rho_w\ \partial\theta/\partial t = -\partial F/\partial z + \rho_w S_\theta$$

where ρ_w is the water density, S_θ the root extraction source term, and F the water flux in the soil, $F = -\rho_w\ (\lambda\partial\theta/\partial z - \gamma)$, and λ and γ are the hydraulic diffusivity and hydraulic conductivity, respectively, $\lambda = b\ [\gamma_{sat}\ (-\Psi_{sat})/\theta_{sat}]\ (\theta/\theta_{sat})^{b-2}$ and $\gamma = \gamma_{sat}\ (\theta/\theta_{sat})^{2b+3}$.

The water in the interception layer is found by solving:

$$\partial W_\ell/\partial t = (I + C_\ell E_\ell)/\rho_w$$

where I is the water that is intercepted, $I = \min\ [c_i C_v P^*, \rho_w(W_{\ell mx} - W_\ell^{n+1,1})/\Delta t]$, $P^* = P/k^*$ is a modified precipitation flux, P is the precipitation, $k^* = 0.5$ is the fraction of the grid-box covered by precipitation, $c_i = 0.25$ is the coefficient of efficiency of interception of rain and

$W_\ell^{n+1,1}$ the new value of interception reservoir water content after evaporation has been taken into account.

Further details of the boundary-layer and land-surface parameterisations may be found in ECMWF Research Department (1995) and Viterbo and Beljaars (1995).

References

Beljaars, A. C. M. 1994: The parametrization of surface fluxes in large-scale models under free convection. *Quart. J. Roy. Meteorol. Soc*., **121**, 255–270.

Beljaars, A. C. M., and Holtslag, A. A. M. 1991: Flux parametrization over land surfaces for atmospheric models. *J. Appl. Meteor.,* **30**, 327–341.

Clapp, R. B. and Hornberger, G. M. 1978: Empirical equations for some soil hydraulical properties. *Water Resources Res*., **14**, 601–604.

Dyer, A. J. 1974: A review of flux-profile relationships. *Boundary-Layer Meteorol*., **7**, 363–372.

ECMWF Research Department, 1995*: ECWMF Forecast Model: Physical Parametrization*, Fourth Edition. ECMWF, Shinfield Park, UK.

Garratt, J. R. 1992: The Atmospheric Boundary Layer. Cambridge University Press, Cambridge, 316 pp.

Hogstrom, U., 1988: Non-dimensional wind and temperature profiles in the atmospheric surface layer: A re-evaluation. *Boundary-Layer Meteorol*., **42**, 55–78.

Lott, F. and Miller, M. J. 1997: A new subgrid-scale orographic drag parametrization: Its formulation and testing. *Quart. J. Roy. Meteorol. Soc.,* **123**, 101–127.

Louis, J. F., Tiedtke, M. and Geleyn, J. F. 1982: A short history of the operational PBL parametrization at ECMWF. *Workshop on Boundary Layer Parametrization*, November 1981, ECWMF, Shinfield Park , UK.

Puri, K., Dietachmayer, G., Mills, G. A., Davidson, N. E., Bowen, R. A. and Logan, L. W. 1998, The new BMRC Limited Area Prediction System, LAPS, *Aust. Met. Mag*., **47**, 203–233.

Sellers, P. J. 1985: Canopy reflectance, photosynthesis and transpiration. *Int. J. Remote Sensing*, **6**, 1335-1372.

Troen, I. and Mahrt, L., 1986: A simple model of the atmospheric boundary layer: sensitivity to surface evaporation. *Boundary-Layer Meteorol*., **37**, 129–148.

Turner, J. S. 1973: *Buoyancy Effects in Fluids*. Cambridge University Press, Cambridge, 367 pp.

Viterbo, P. and Beljaars, A. C. M. 1995: An improved land surface parameterization scheme in the ECMWF model and its validation. Technical Report 75, Research Department, ECMWF, Shinfield Park, UK.

Wood, N. and Mason, P. 1993: The pressure force induced by neutral, turbulent flow over hills. *Quart. J. Roy. Meteorol. Soc.,* **119**, 1233–1267.

Appendix 2.1b The Chemical Transport Model

Summary prepared by Martin Cope, CSIRO Atmospheric Research

Overview

In the following sections we provide a brief technical summary of version 1.0 of the AAQFS chemical transport model (CTM). Version 1.0 of the model comprises an Eulerian regional-urban photochemical model, with simple extensions to treat the transport, wet/dry deposition of additional non-reactive gaseous species, and a series of size-lumped, non-reactive aerosol species. The CTM can be configured to run with three alternative photochemical reaction mechanisms, ranging in complexity from simple to comprehensive. The aerosol scheme is currently limited to modelling the processes of emission, transport and deposition of primary anthropogenic/natural particle sources. Where gas phase nitrate and sulfate aerosol are products of the photochemical mechanisms, these species are also lumped into an appropriate aerosol bin. The level of complexity of the aerosol scheme in CTM v1.0 is in accordance with the current level of uncertainty embodied in the AAQFS aerosol emission inventory.

Governing equation

The governing equation for the CTM is the semi-empirical advection-diffusion equation for reactive species, written in a scaled form described in Toon *et al*. (1988) in which geometric scaling factors (map factors) are introduced into the governing equation to enable consideration to be given to alternative coordinate systems.

$$\frac{\partial C^*}{\partial t}+\frac{\partial UC^*}{\partial X}+\frac{\partial VC^*}{\partial Y}+\frac{\partial WC^*}{\partial S}= \frac{\partial r^*}{\partial X}K_x\frac{\partial C^*/r^*}{\partial X}+\frac{\partial r^*}{\partial Y}K_y\frac{\partial C^*/r^*}{\partial Y}+\frac{\partial r^*}{\partial S}K_s\frac{\partial C^*/r^*}{\partial S}+(P-L)V_mM_1M_2 \qquad (1)$$

In equation *(1)*, C^* is the scaled concentration (expressed as a mass density), ρ^* is the scaled atmospheric density, U, V and W are scaled velocities in the X, Y and *sigma* directions, K_x and K_y are the horizontal components of the eddy diffusivity, K_s is the vertical eddy diffusivity, P is the rate of change due to chemical production and emission, and L is the chemical loss rate. In CTM v1.0, the horizontal map factors M_1, M_2 are prescribed for a spherical coordinate system, and the vertical map factor V_m is prescribed for a scaled pressure coordinate system, thus matching the coordinate system used in LAPS (Appendix 2.1).

The solution of equation *(1)* is achieved by splitting the multi-dimensional system into a series of one-dimensional systems, according to the method of Marchuk (1974). Thus individual consideration can be given to the processes of horizontal and vertical advection, horizontal diffusion, and the coupled processes of vertical diffusion, chemical/aerosol transformation, wet and dry deposition.

A single time-level, quasi-second order accurate (in time) solution to *(1)* is given by

$$C^*(t+2Dt) = T_XT_YT_S\,M_c\,D_h\,(D_v\,E_s\,C_c)\,(D_v\,E_s\,C_c)\,D_h\,T_S\,T_Y\,T_X\,M_c\,C^*(t). \qquad (2)$$

Here T_i represents the advection operator in the i^{th} coordinate direction, M_c is a mass correction operator, D_h is the horizontal diffusion operator, D_v is the vertical diffusion operator, E_s is the source term, and C_c is the chemical transformation operator.

Advection (T_X, T_Y, T_S)

The processes of horizontal and vertical advection are treated using the Blackman-constrained cubic scheme of Yamartino (1993), a high-order, flux-based scheme that uses spectral conditioning, sub-grid linear interpolation, donor-cell allocation and supplementary non-linear filtering to achieve a positive-definite solution under conditions of strong concentration gradient. This scheme has been specifically developed for use in Eulerian air quality modelling systems and exhibits excellent retention of peak and shape for short wavelength signals.

The scheme presented in Yamartino (1993) is for a uniform grid mesh. We have extended the Yamartino scheme to apply to a non-uniform grid. This version is used to model transport on the non-uniform sigma (vertical) grid.

Mass correction (M_c)

Being couched in the flux form, equation *(1)* assumes that the transport field is mass consistent. However, mass consistency is not guaranteed for numerical weather prediction systems based on the primitive form of the governing equations. Mass errors may also be introduced through the process of spatially and temporally interpolating the transport fields to the CTM grid. The methodology of EPA (1999), and the methodology of Odman and Russell (2000) are used to correct for mass errors in the CTM. As can be seen from equation *(2)*, mass correction is undertaken following each cycle of 3-D transport.

Horizontal diffusion (D_h)

Two processes of sub-grid scale horizontal diffusion are considered in the CTM—that due to distortion or stress in the horizontal transport field (Smagorinsky, 1963), and that due to sub-grid-scale turbulence (which is described in Hess 1989a and references therein). These components are combined to yield a total horizontal diffusion rate, which is then applied within a second-order, explicit treatment (with a dynamic Courant number-limited time step adjustment) of the horizontal diffusion process.

Vertical processes, mass emission, chemical transformation (D_v M_s C_c)

Vertical diffusion, wet and dry deposition, chemical transformation, and emissions are treated as a single coupled process in the CTM. This approach is used because the time scales of each process can be similar (order of minutes or less), and experience has demonstrated that further de-coupling of the system can lead to large time-discretisation errors, particularly when a high-resolution vertical grid mesh is used in the CTM.

Vertical diffusion

Vertical diffusion coefficients are based on the scheme described in Hess (1989) and references therein. Important prescriptive variables for this scheme are the friction velocity,

the Monin-Obukhov length, the convective velocity scale and the mixing height. All of these variables may be taken directly from LAPS, or alternatively, based on *in situ* derivations.

The vertical diffusion equation is discretised into a second-order accurate, explicit scheme, which is then re-arranged into the form of a first order chemical reaction scheme (by defining product and loss terms). Vertical diffusion rates can then be added to the formation and loss terms generated by the photochemical transformation scheme and piped through the photochemical integration scheme (see *Chemical Transformation* section).

Wet and dry deposition

The processes of wet and dry deposition are parameterised according to the methodology described in Draxler and Hess (1997) and references therein. For example, the dry deposition scheme is based on the classical multi-layer resistance analogy, and is a function of friction velocity, Monin Obukhov length and surface characteristics.

Wet and dry deposition rates are also calculated for each particle size category.

Dry deposition is prescribed as the lower boundary condition to the vertical diffusion equation. Wet deposition is prescribed as a loss term in the chemical transformation mechanism.

Chemical transformation

The CTM has been designed to enable alternative photochemical transformation mechanisms to be readily implemented. Three photochemical mechanisms are available for use in CTM v1.0—GRS (Azzi *et al*., 1992); GRS2 (see Appendix 5.1 of the Main Report) and Carbon Bond 99 (Adelman, 1999).

For the simplest mechanism—GRS, the CTM has been configured to treat seven reactive species (six gaseous and one secondary aerosol), five non-reactive gaseous species, five tracer species and eight non-reactive aerosol species. The reactive gaseous species are *nitric oxide, nitrogen dioxide, reactive organic carbon, ozone, reactive product, secondary gaseous nitrates and secondary non-gaseous nitrates*. The non-reactive gaseous species are *formaldehyde, benzene, butadiene* (this is treated as reactive in GRS2), *carbon monoxide* and *sulfur dioxide* (this is treated as a reactive species in GRS2*)*. The aerosol species are lumped on a size basis only, covering the ranges (in μm): 0.04–0.08, 0.08–0.16, 0.16–0.31, 0.31–0.63, 0.63–1.25, 1.25–2.5, 2.5–5 and 5–10.

Photochemical transformation mechanisms require a description of the actinic flux, temperature, pressure and concentration of water, molecular oxygen and molecular nitrogen. These are all derived from the fields of radiation, temperature and pressure generated by LAPS.

Emissions

Both anthropogenic and biogenic emissions are provided as source terms for solution in the coupled vertical diffusion/chemical transformation system. All anthropogenic sources are currently calculated prior to model execution, and are input from a data file. A full description of the anthropogenic inventory system may be found in Environment Australia (2001).

Natural and biogenic emissions are calculated by the CTM at run time. This is done because emissions from these source groups can potentially vary strongly with the local meteorology over time scales of an hour or less.

The non-anthropogenic source groups treated in CTM v1.0 are vegetation (reactive organic carbon), soil (oxides of nitrogen and wind blown dust aerosol) and ocean (oxides of nitrogen and sea salt aerosol).

For example, in the case of vegetation, emissions of isoprene and monoterpenes (as α-pinene) are estimated according to the following

$$E(VOC)^{i}_{LS} = [f_{dg} \cdot q_{dg} + (1 - f_{dg}) \cdot q_{ndg}] \cdot bm^{i}_{LS} \cdot V_f \cdot C_L \cdot C_T \qquad (3)$$

where $E(VOC)^{i}_{LS}$ is biogenic VOC mass emission flux (g m^{-2} s^{-1}) for landscape category i.

Here, q_{dg} is the mass emission rate of the dominant genera per gram of foliage (g g^{-1} s^{-1}) at a standard temperature of 30°C and a photosynthetically active radiation (PAR) flux of 1000 μmol m^{-2} s^{-1}, and q_{ndg} is the mass emission rate of the non-dominant genera per gram of foliage (g g^{-1} s^{-1}) at a temperature of 30°C and a radiation flux of 1000 μmol m^{-2} s^{-1} and bm^{i}_{LS} is the leaf biomass for the defined landscape category (g m^{-2}). Continuing, f_{dg} is the biomass fraction of the landscape category assigned to the dominant genera, V_f is the fractional spatial coverage of the vegetation landscape within a grid cell, and C_L, C_T are functions to correct the standard emission fluxes to other temperatures and radiation fluxes.

Leaf-level emission rates for trees are based on the measurements of Nelson *et al*. (2000), and the emission rates for grasses are based on the measurements of Kirstine *et al*. (1998) and Nelson *et al*. (2000).

Sea salt aerosol emission rates are calculated according to the methodology of Monahan *et al*. (1986). The sea-salt algorithm is driven by the 10 m LAPS wind field.

Aerosol generation from wind blown dust is based on the algorithms described in Lu and Shao (2001) and references therein. Oxides of nitrogen emissions from soil and ocean are based on the recommendations of Carnovale *et al*. (1996) and references therein.

Emissions of aerosol and gaseous species from the anthropogenic and natural source groups form an additional source term in the coupled vertical processes/chemical transformation system. Surface-based area sources are input into the ground-level layer of the computational domain. In the case of point sources with non-zero momentum or buoyancy fluxes, an effective stack height is calculated, using the plume centreline differential equations of Briggs (1975). Column wind speed and potential temperature gradients, required for the plume rise calculations are taken from the LAPS meteorological forecast.

Vertical processes- numerical integration

Integration of the system of equations describing the vertical processes is undertaken using the Young and Boris (1977) second-order predictor, iterated-corrector scheme, with the modifications introduced by McRae *et al*. (1982). This scheme dynamically divides the species into three groups according to whether they are long-lived, short-lived or in pseudo steady state. Tailored predictor corrector algorithms are then applied to each species group.

The scheme features automatic time step determination and automatic corrector iteration length determination. The scheme is self-starting, and makes no *a priori* assumptions about the structure of the photochemical mechanism.

Computational implementation

Written in ANSI-standard, free format FORTRAN-90, the CTM has been designed to run either online or downstream of LAPS. Online operation has been mitigated through a software design which entails only two subroutine calls for complete CTM operation—*setup* and *time-marching/shutdown*.

The CTM has been vectorised and parallelised to run efficiently on a shared-memory vector parallel supercomputer. The system currently runs at about 12 Gflops on 6 processors of an NEC-SX5 with a vector efficiency of 99.6%.

The system has been designed to run with multiple online one-way nesting for an arbitrary number of grid nests. A typical run time configuration is to define a 1-km grid over an urban area; the 1-km grid is then nested within a 5-km grid, encompassing upwind rural sources. Typical grid dimensions are 100 × 100, with 17 non-uniform levels in the vertical. Version 1.0 of the code typically takes about 20 minutes to perform a 24–36 hour air quality forecast with the GRS mechanism.

References

Adelman Z. E. 1999. A reevaluation of the Carbon Bond-IV photochemical mechanism. Master of Science Thesis, Department of Environmental Sciences and Engineering, School of Public Health, University of North Carolina, U.S.A.

Azzi M., Johnson G.J. and Cope M. 1992. An introduction to the Generic Reaction Set Photochemical smog mechanism. *Proc. 11th International Clean Air Conf.*, Brisbane, 5–10 July, 451–462.

Briggs G.A. 1975. Plume rise predictions. In *lectures on air pollution and environmental impact analyses, Workshop proceedings*, Boston, Mass., Sept. 29–Oct. 3, 59–111. American Meteor. Soc., Boston Mass.

Carnovale F., Tilly K., Stuart A., Carvalho C., Summers M. and Eriksen P. 1996. Metropolitan air quality study: Air emissions inventory. Final report to New South Wales Environment Protection Authority.

Draxler R.R. and Hess G.D. 1997. Description of the HYSPLIT_4 modeling system. NOAA Technical Memorandum ERL ARL-224. Air Resources Laboratory Silver Spring, Maryland.

EPA 1999. Science algorithms of the EPA Models-3 community multiscale air quality (CMAQ) modelling system. EPA/600/R-99/030. Office of Research and Development Washington, DC 20460.

Hess G.D. 1989. A photochemical model for air quality assessment: model description and verification. *Atmos. Environ.*, **23**, 643–660.

Kirstine, W., Galbally, I. E., Ye, Y., and Hooper, M. A. (1998). Emissions of volatile organic compounds (primarily oxygenated species) from pasture. *J. Geophys. Res.,* **103** (D9): 10605–10619.

Lu H. and Shao Y. 2001. Toward quantitative prediction of dust storms: an integrated wind erosion modelling system and its applications. *Environmental Modelling and Software* **16**, 233–249.

McRae G.J., Goodin W.R. and Seinfeld J.H. 1982. *Mathematical Modelling of Photochemical Pollution*. EQL Report No. 18, 661 pp. (Environmental Quality Laboratory, California Institute of Technology: Pasadena).

Marchuk G.I. 1974. *Numerical methods in weather prediction*. Academic Press, New York.

Monahan E.C., Spiel D.E. and Davidson K.L., 1986. A model of marine aerosol generation via whitecaps and wave disruption. In Oceanic Whitecaps, edited by E. C. Monahan and G. Mac Niocaill 167-174. D. Reidel, Norwell, Mass. U.S.A.

Nelson P.F., Nancarrow P.C., Halliburton B., Tibbett A.R., Chase D. and Trieu T. 2000. Biogenic emissions from trees and grasses. Final report to EPA of NSW. Investigation Report ET/297, PO Box 136, North Ryde, Australia.

Odman M. and Russell A. 2000. Mass conservative coupling of non-hydrostatic meteorological models with air quality models. In *Air Pollution Modeling and Its Application XIII*, edited by S.-E Gryning and E. Batchvarova, Kluwer Academic/Plenum Publishers.

Smagorinsky J., 1963. General circulation experiments with the primitive equations 1. The basic experiment. *Mon. Weath. Rev*. **91**, 99–164.

Toon O.B., Turco R.P., Westphal D., Malone R. and Liu M.S. 1998. A multidimensional model for aerosols: description of computational analogs. *J. Atmos. Sci.* **45** (15) 2123–2143.

Yamartino R.J. 1993. Nonnegative conserved scalar transport using grid-cell-centred, spectrally constrained Blackman cubics for applications on a variable-thickness mesh. *Mon. Wea. Rev*., **121**, 753–763.

Young T.R. and Boris J.P. 1977. A numerical technique for solving stiff ordinary differential equations associated with the chemical kinetics of reactive flow problems. *J. Phys. Chem*., **81**, 2424–2427.

Appendix 3.1 Emissions Model for AAQFS

Presented at the 15th International Clean Air & Environment Conference. Sydney, Australia, 26–30 November 2000

EMISSIONS MODEL FOR THE AUSTRALIAN AIR QUALITY FORECASTING SYSTEM

Yuk L. Ng, Sean Walsh and Neil Wong
Environment Protection Authority,
GPO Box 4395QQ, Melbourne, VIC 3000, Australia

Summary

The Australian Air Quality Forecasting System produces high-resolution, meteorological and air quality forecasts for the major urban areas of Australia, and is being initially tested in Melbourne and then demonstrated in Sydney during the 2000 Olympics. The emissions model acts as an input to the air quality forecasting model.

The emissions model consists of several submodels dealing with different sources of emissions. Five submodels: point sources, area sources, biogenic sources, motor vehicles, prescribed burning and wildfires will be discussed in this paper. Emissions from motor vehicles are estimated based on vehicle kilometres travelled; however, emissions on some major roads in Sydney are estimated by a power consumption based vehicle emission model.

The emissions model estimates emissions depending on the season (or month), time of day and whether it is a weekday, Saturday or Sunday. The effect of temperature on the emissions from wood burning (part of the area source module) and on motor vehicles, and the effects of temperature and solar radiation on biogenic emissions are considered in the model.

Keywords: emissions model, emissions inventory, forecasting, day-specific emissions, power-based model.

1. Introduction

The Australian Air Quality Forecasting System (AAQFS) is being developed with funding from the Air Pollution in Major Cities Program. The short term goal of the project is to develop, validate and trial an accurate, next day (36 hours) numerical air quality forecasting system for a three-month demonstration period in Sydney, which includes the 2000 Olympics. Currently forecasts are produced in both Melbourne and Sydney. After the Olympics, the AAQFS will be available for forecasting health- and visibility-related air quality metrics in the other major population centres of Australia. Principal project partners are the Bureau of Meteorology, CSIRO, Environment Protection Authority of Victoria and Environment Protection Authority of New South Wales.

The project has a number of specific goals: to provide the ability to generate 36 hour air quality forecasts twice per day; provide forecasts for a range of air pollutants; provide forecasts at a resolution sufficient to consider suburban variations in air quality; and to provide the ability to generate simultaneous forecasts for different emission scenarios such as minimal motor vehicle usage scenario.

The AAQFS consists of five major components: a numerical weather prediction system (LAPS), an emissions inventory module (EIM), a chemical transport module (CTM) for air quality modelling, an evaluation module, and a data archiving and dissemination module. The development of the AAQFS is proceeding in two phases: 1) the construction and operation of a pilot system using components that were available at the time of study inception; and 2) the development of a demonstration system, through the enhancement of components in the pilot system, and where necessary, through the construction of new modules. The principal difference between the pilot and demonstration systems is that significant components of the emission modelling and chemical transport modelling are conducted online, i.e. modules are called directly by LAPS, in the demonstration system. This contrasts with the pilot system, where a meteorological forecast is first completed, stored and post processed prior to the execution of the chemical transport model.

LAPS has been described by Hess et al. (1999) and CTM by Cope et al. (in press). This paper presents an overview of the EIM developed for the demonstration system, emphasising the design and formulations of the model.

2. Overview of the Emissions Model

2.1. General Overview

Traditional emission models usually produce gridded, hourly, speciated emissions on data files, which are then read into an air quality model. These data files are produced for some specific days which are pre-determined by modellers.

The challenge of the EIM is to estimate emissions on a daily basis that allows for weekday/weekend, monthly or seasonal, and meteorological dependencies. Also the emissions must be generated for a 36 hours period, rather than 24 hours as in a traditional emission model. Special events or scenarios, such as minimal motor vehicle usage, need to be considered in the model.

Another challenge of the model is to incorporate the emissions data obtained from a power-based vehicle emissions model, which has been developed by CSIRO, in the EIM. These emissions are road-specific, which are quite different from the traditional forms of emissions that are based on points or grid cells.

The EIM provides forecasts of emissions for a range of air pollutants including carbon monoxide (CO), oxides of nitrogen (NOx), particulates (PM10), sulfur dioxide (SO_2), volatile organic compounds (VOC), ammonia, benzene, 1,3-butadiene and formaldehyde. Particulates are speciated into discrete compounds and size fractions, and VOC is speciated into individual Carbon Bond IV species (Gery et al. 1989). The EIM accepts data for any grid size, cell size and coordinate system although latitudes and longitudes are used for the AAQFS.

The model is designed in such a way that it uses the minimal amount of time and disk space to run. In order to minimise the time to run the model, static data, i.e. data which do not have temporal dependency, such as spatial data, are preprocessed and put on the system. To minimise the use of disk space, the size of data sets are kept to the minimum. For example, instead of storing a large data set of area source gridded emissions, these emissions are generated in the model by distributing the annual emissions by spatial data, such as population.

The emissions model consists of eight submodels: point source model, area source model, motor vehicle model, biogenic model, prescribed burning and wildfires model, sea-salt model, wind-blown dust model and meteorological data model. Only the first five models are considered in details in this paper, the latter three models require tight integration with LAPS and are being developed by CSIRO. The meteorological data model extracts data from LAPS for emissions estimation and will be described briefly in this paper.
Each of the first five models is a subroutine that can be called from the CTM. Each subroutine supplies spatially disaggregated, hourly, speciated emissions to the CTM for a given grid domain and forecasting time period.

2.2 Point Source Model

Figure 1 shows the data flow diagram for the point source model, which illustrates the data sets required for the model and how they are used to generate the hourly emissions and, in turn, speciated hourly emissions for individual point sources.

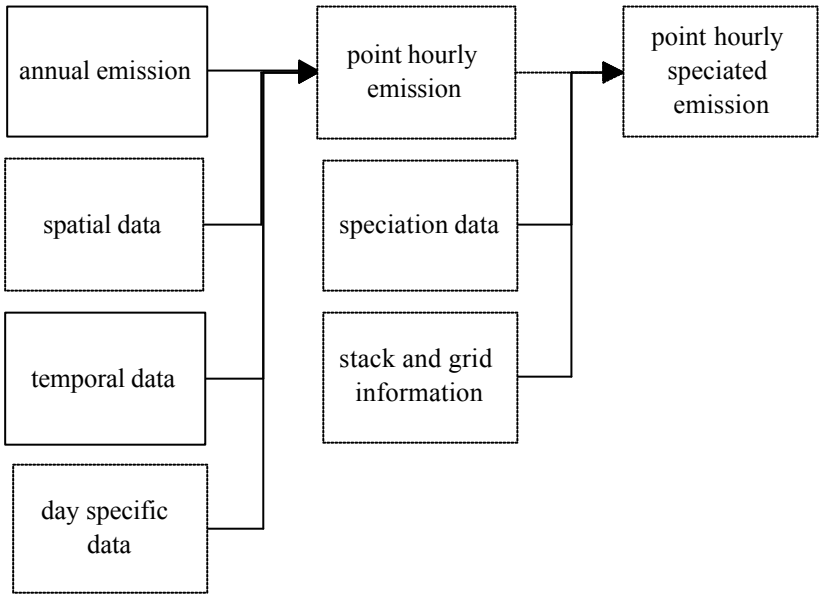

Figure 1 Data flow diagram for point source model

Individual point sources are selected for a given domain based on the information in the spatial data set. The annual emissions are then disaggregated into hourly emissions by applying temporal factors derived from the temporal data set according to the following equation:

$$E_h = A \times M \times D \times H_h / W \qquad (1)$$

where E_h is hourly emission for hour h (kg/hr),
A is annual emission (kg/yr),
M is monthly temporal factor,
W is weekly temporal factor,
D is daily temporal factor, and
H_h is hourly temporal factor for hour h.

The day-specific data contains information on public holidays and special events. For a public holiday, a daily temporal factor for Sunday is used. For an event, an event factor is used instead of the daily temporal factor.

The hourly emissions are speciated using the information in the speciation data set (see Section 2.8) before read into the CTM.

2.3 Area Source Model

Figure 2 shows the data flow diagram for the area source model.

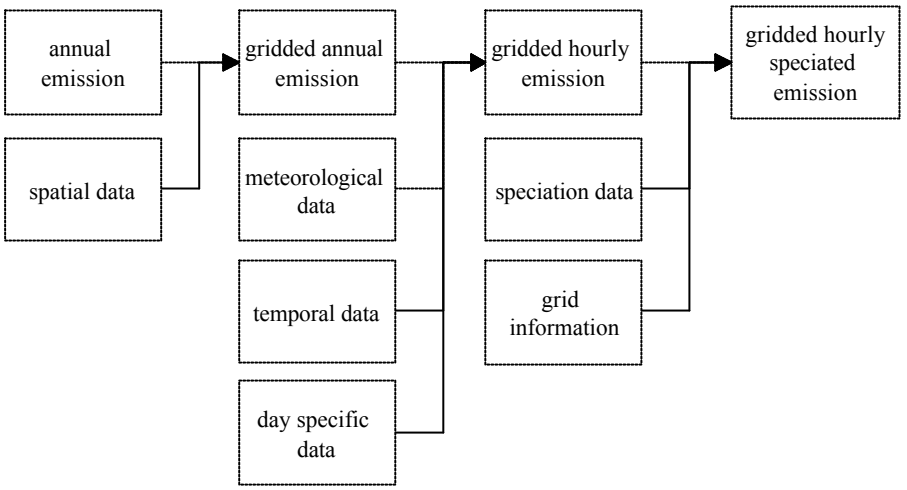

Figure 2 Data flow diagram for area source model

Area source emissions estimates are allocated to grid cells through the application of spatial surrogates, such as population. Each area source (s') which has been assigned to a spatial surrogate (s) can be allocated to grid cells (c) through the application of the following equation:

$$G_{c,s'} = A_{s'} \times R_{c,s} \qquad (2a)$$

where $G_{c,s'}$ is gridded annual emission for an area source s' and grid cell c (kg/yr),
$A_{s'}$ is annual emission for the area source s' over the whole state (kg/yr),
$R_{c,s}$ is gridded surrogate ratio for spatial surrogate s and grid cell c, and

$$\sum_{c} R_{c,s} = 1, \text{ for all spatial surrogates s} \qquad (2b)$$

where the sum is over the whole state.

For wood combustion, emissions depend on daily temperature (Ng & Minchin., 2000) and the following equation is used to find the adjustment factor:

$$f = -0.1539 \times t + 3.0205, \; f > 0 \qquad (3a)$$

where f is the wood burning emission adjustment factor, and
t is the average daily temperature over the modelling grid (°C).

The temperature t needs to be extracted from the LAPS. If the adjustment factor calculated by the above equation is negative, the adjustment factor is set to 0.

The wood burning emission is then obtained by:

$$G' = G \times f \qquad (3b)$$

where G' is the adjusted wood burning emission (kg/yr), and
G is the unadjusted wood burning emission (kg/yr).

After the wood burning emissions are adjusted, the emissions of each area source are temporally allocated by applying temporal factors derived from the temporal data set according to the following equation:

$$E_h = G \times M \times D \times H_h / W \qquad (4)$$

where E_h is the hourly emission for hour h (kg/hr),
G is the gridded annual emission (kg/yr),
M is monthly temporal factor,
W is weekly temporal factor,
D is daily temporal factor, and
H_h is hourly temporal factor for hour h.

The day-specific data contains information on public holidays and special events. For a public holiday, a daily temporal factor for Sunday is used. For an event, an event factor is used instead of the daily temporal factor.

The hourly emissions are speciated using the information in the speciation data set (see Section 2.8) before being passed to the CTM.

2.4. Motor Vehicle Model

There are two submodels for the motor vehicle model: 1) main model and 2) power-based model. To distinguish it from the power-based model developed by CSIRO, the power-based model developed for the EIM will be referred to as 'EIM power-based model'. The CSIRO power-based model does not estimate emissions on a day-by-day basis and is not part of the AAQFS but its results are used as input to the EIM.

The main model estimates gridded, hourly, speciated emissions for domains where the power-based model is not used. If the power-based model is used, the main model provides the background gridded, hourly, speciated emission for the domain. The background emissions are total motor vehicle emissions minus those estimated for the power-based model. The EIM power-based model estimates hourly, speciated emissions for each road link where the power-based model is applied.

Figure 3 shows the data flow diagrams for the two models.

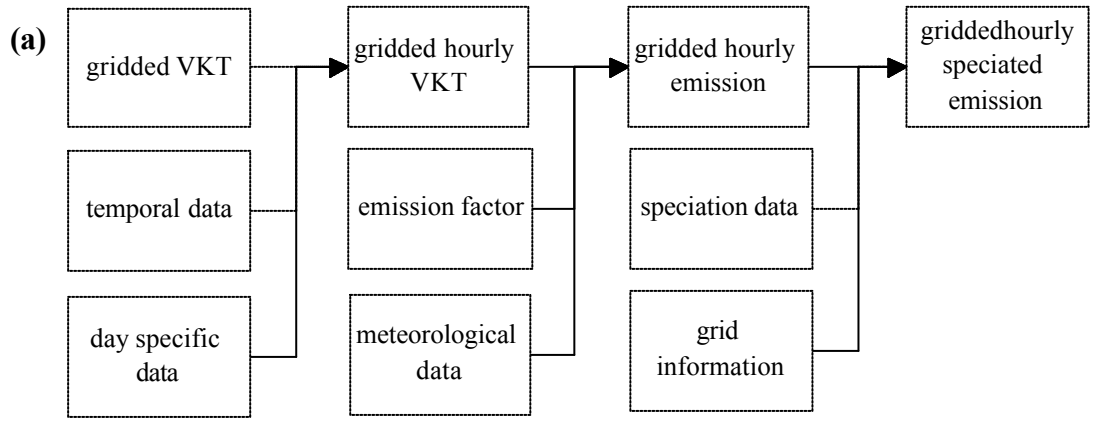

(b)

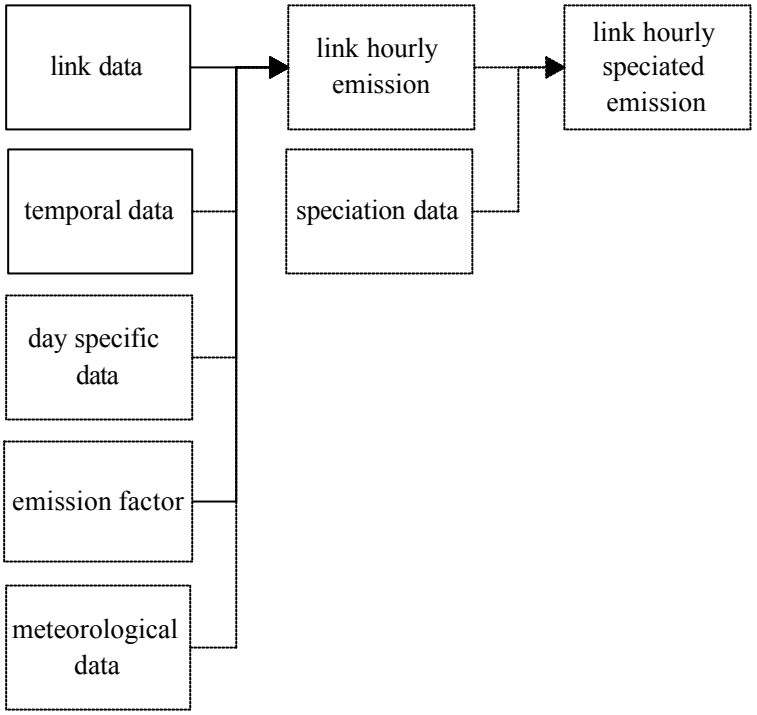

Figure 3 Data flow diagrams for motor vehicle (a) main model and (b) power-based model.

2.4.1 Main model

Prior to computing the motor vehicle emissions estimates, the gridded, hourly vehicle kilometres travelled (VKT) are calculated and the VKT adjusted to the specific modelling day:

$$G_{c,r,h} = V_{c,r} \times M \times D \times H_h \qquad (5)$$

where $G_{c,r,h}$ is VKT for grid cell c, road type r and hour h (km/hr),
$V_{c,r}$ is daily VKT for grid cell c and road type r (km/day),
M is month-specific VKT adjustment factor,
D is the day-specific VKT adjustment factor, and
H_h is the hour-specific VKT fractional profile factor for hour h.

The temporal factors M, D and H_h are supplied through the temporal data set. The day-specific data contains information on public holidays and special events. For a public holiday, the day-specific adjustment factor for Sunday is used. For an event, such as minimal motor vehicle usage, an event factor is used instead of the day-specific adjustment factor.

The model computes day-specific, gridded, hourly motor vehicle emissions estimates of VOC, CO, NOx, PM_{10} and SO_2 according to the following equation:

$$E_{m,t,p} = \sum_r F_{m,t,p,r} \times G_r \qquad (6)$$

where E is gridded, hourly emission (kg/hr),
F is fleet composite emission factor (kg/km),
G is gridded, hourly VKT (km/hr),
m is index for process type (evaporative or exhaust),

t is index for technology type (petrol, diesel, or liquefied petroleum gas),
p is index for pollutant; and
r is road type index.

The emission factors of VOC, CO and NOx depend on temperature, and these emission factors are obtained from a data set which contains emission factors for a range of temperature. The temperature on the day in a specific hour is obtained from the meteorological data model (see Section 2.7). The emission factor closest to this temperature is then chosen for estimating the emission. Note that the emission factor is fleet composite emission factor, ie it has been weighted according to fleet VKT composition.

Evaporative emission factor for petrol-fuelled vehicles is adjusted by an adjustment factor for Reid Vapour Pressure (RVP), which may differ for different periods in a year:

$$F'_r = F_r \times R \qquad (7)$$

where F'_r is adjusted evaporative emission factor (kg/km),
F_r is unadjusted evaporative emission factor (kg/km),
R is RVP adjustment factor for a particular period, and
r is road type index.

Emissions for toxics (benzene, 1,3-butadiene and formaldehyde) are estimated from VOC using speciation fractions.

$$E_{m,t,p} = E_{m,t,voc} \times S_{m,t,p} \qquad (7)$$

where E is gridded, hourly emission (kg/hr),
S is mass fraction of a species in VOC,
m is index for process type,
t is index for technology type, and
p is index for pollutant (benzene, 1,3-butadiene or formaldehyde).

2.4.2 Power-based model

The power-based model as developed by CSIRO (Williams *et al*. 1994) estimates exhaust emissions for CO, NOx and hydrocarbons (HC). These emissions are provided for each hour and road link for an average weekday, Saturday and Sunday in a data file for the EIM power-based model. It is assumed that VOC is equivalent to HC and no conversion factor is used.

The power-based model does not estimate evaporative emission and emissions of other pollutants (PM10, SO_2 and toxics) on roads, so these emissions are estimated by the EIM power-based model using data from the main model.

Evaporative emission and emissions of PM10 and SO_2 on a road link are estimated by the following equation:

$$L_{m,t,p} = F_{m,t,p} \times V \qquad (8)$$

where L is hourly emission on a road link (kg/hr),
F is fleet composite emission factor (kg/km),
V is hourly VKT on the road (km/hr),
m is index for process type,
t is index for technology type, and
p is index for pollutant.

For evaporative emission, the emission factor varies with temperature and hence is different for each grid cell. The emission factor is also adjusted for RVP as in the main model.
Emissions on a road link are adjusted to the specific modelling day according to the following equation:

$$L'_{m,t,p} = L_{m,t,p} \times M \times D \qquad (9)$$

where L' is adjusted hourly emission on a road link (kg/hr),
L is unadjusted hourly emission on a road link (kg/hr),
M is month-specific VKT adjustment factor,
D is event factor if a particular event happens on the day;
m is index for process type,
t is index for technology type, and
p is the index for pollutant (CO, NOx, VOC, PM10 or SO_2).

Emissions for toxics (benzene, 1,3-butadiene and formaldehyde) are estimated from VOC using speciation fractions.

$$L'_{m,t,p} = L'_{m,t,voc} \times S_{m,t,p} \qquad (10)$$

where L' is the hourly emission on a road link (kg/hr),
S is the mass fraction of a species in VOC;
m is the index for process type;
t is the index for technology type, and
p is the index for pollutant (benzene, 1,3-butadiene or formaldehyde).

Emissions are estimated for the EIM power-based model only for some major roads in the metropolitan area. Emissions from other roads are still needed to be included in the model. These 'background' motor vehicle emissions are calculated by gridding and subtracting the emissions estimated for the EIM power-based model from the total gridded emissions.

$$B_{m,t,p} = E_{m,t,p} - L_{m,t,p} \qquad (11)$$

where B is background gridded, hourly emission (kg/hr),
E is the total gridded, hourly emission (kg/hr),
L is the gridded, hourly emission estimated from the EIM power-based model (kg/hr),
m is the index for process type,
t is the index for technology type, and
p is the index for pollutant.

The link data set contains information for the grid cell location of each road link, which is used to grid the link emissions estimated for the EIM power-based model.

2.5 Biogenic Model

Figure 4 shows the data flow diagram for the biogenic model.

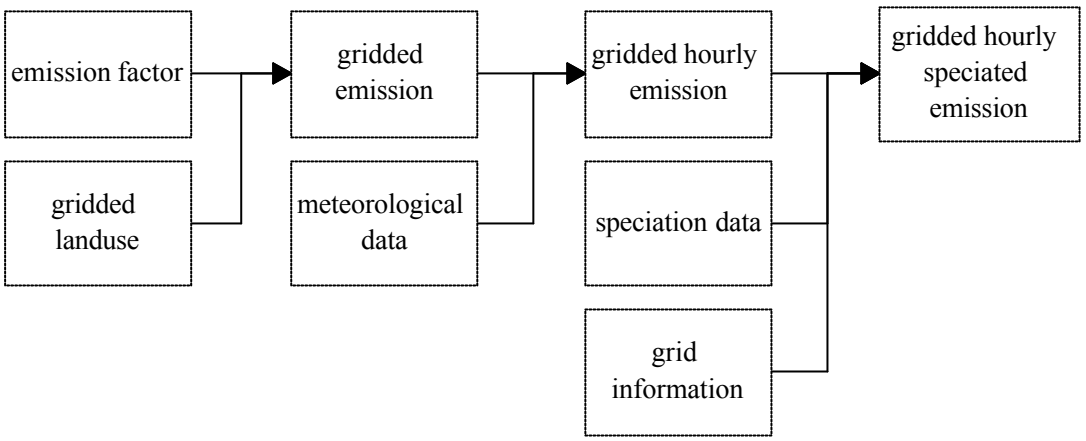

Figure 4 Data flow diagram for biogenic model

The model estimates gridded biogenic emission estimates at a standard condition (30°C and 1000 μE/m²/hr) from the emission fluxes in the emission factor data set and gridded land use data. There are emission fluxes for low, medium and high foliage cover density, which are used for winter, spring or autumn, and summer respectively. The following equation is used to obtain the gridded, standardised biogenic emissions estimates:

$$G_{p,c} = \sum F_{p,u} \times L_{u,c} \qquad (12)$$

where $G_{p,c}$ is gridded biogenic emission of pollutant p in grid cell c (μg/hr),
$F_{p,u}$ is emissions flux of pollutant p for land use type u (μg/ha/hr), and
$L_{u,c}$ is area of land use type u in grid cell c (ha).

The gridded, standardised biogenic emissions are temporally allocated and adjusted using the meteorological data (solar radiation and temperature) supplied from the meteorological data model (see Section 2.7). The following equation is used:

$$E_{p,c,h} = G_{p,c} \times H_{p,c,h} \qquad (13)$$

where $E_{p,c,h}$ is gridded, hourly biogenic emission of pollutant p in grid cell c at hour h (μg/hr),
$G_{p,c}$ is gridded, standardised biogenic emission of pollutant p in grid cell c (μg/hr), and
$H_{p,c,h}$ is biogenic adjustment factor for pollutant p in grid cell c at hour h.

The adjustment factors are based on formulations developed by CSIRO. Emissions are estimated for NOx and VOC.

2.6 Prescribed Burning and Wildfires Model

Figure 5 shows the data flow diagram for the prescribed burning and wildfires model.

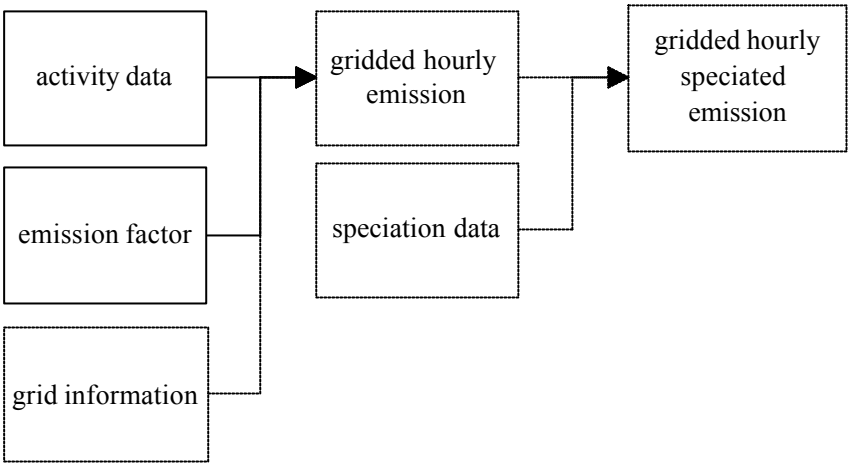

Figure 5 Data flow diagram for prescribed burning and wildfires model

The activity data file contains location and time of fires, fire size and fuel load of the area. The emission factor file contains the emission factors for prescribed burning and wildfires for different pollutants. Because the day and location of these sources vary throughout the year, the model need to find the grid cell location of the fires and select fires occurring on the specific modelling day,

The gridded, hourly emissions are obtained by the following equation:

$$E_{p,c,h} = A_c \times L_c \times F_p / 24 \qquad (14)$$

where $E_{p,c,h}$ is emission of pollutant p from prescribed burning or wildfire in grid cell c at hour h (kg/hr),
A_c is fire size in grid cell c (ha),
L_c is fuel load in grid cell c (t/ha), and
F_p is emission factor for pollutant p (kg/t).

Because the duration of a fire cannot be forecasted, it is assumed that the fire spreads evenly over a 24 hour period.

2.7 Meteorological Data Model

This model extracts meteorological data used in the motor vehicle and biogenic models from LAPS. The data extracted are 1) gridded, hourly solar radiation in μE, and 2) gridded, hourly temperature in °C.

2.8 Speciation

The point, gridded or link, hourly emissions estimated by each model are speciated for NOx, PM10, SO_2 and VOC. NOx is speciated into NO and NO_2, PM10 into discrete compounds (elemental carbon, organic carbon, sulfate and other particles) with eight size fractions, and VOC into individual Carbon Bond IV species. SO_2 is speciated into SO_2 and eight size fractions of sulphate particle. The following equation is used for the speciation:

$$C = E \times S / M \qquad (15)$$

where C is point, gridded or link, hourly, speciated emission (mol/hr),
E is point, gridded or link, hourly emission of the pollutants (g/hr),

S is speciation fraction,
M is molecular weight (g/mol, 1 for VOC and particle species).

3. Conclusion

The AAQFS is evolving from the pilot stage to the demonstration stage. The EIM has been designed to forecast day-specific emissions which vary for weekday/weekend, month/season, and by meteorological conditions. This significantly improves the accuracy of emission estimates provided to the CTM. The power-based model is incorporated in the EIM which generates road-specific vehicle emission fluxes for the purpose of near-road impact modelling.

The EIM can provide forecast for special events or scenarios. The latter may correspond to a minimal motor vehicle usage scenario and will be used to indicate the reduction in population exposure that could result from a concerted public response to a forecast of poor air quality for the next day. In summary, the EIM acts an important channel for inputting scenarios of different policy options to the air quality model, and hence in bridging policy and science.

Acknowledgments

The authors would like to thank the Bureau of Meteorology and CSIRO for granting EPA's access to the NEC-SX supercomputer for development of the emissions model.

References

Birth T.L. and Geron C.D. 1995, *User's Guide to the Personal Computer Version of the Biogenic Emissions Inventory System (PC-BEIS), Version 2.0,* Computer Sciences Corporation and USEPA, Research Triangle Park, North Carolina, USA.

Cope M., Hess D., Lee S., Azzi M., Carras J., Wong N. and Young M., in press, 'Development of the Australian Air Quality Forecasting System', *Proceedings of the International Conference of Urban Climatology, Sydney, 1999*.

Galbally I.E. and Weeks I.A. 1992, *Natural Emissions of Hydrocarbons, Nitrogen Oxides, Carbon Monoxide and Sulfur Gases in the Kooragang Island Region of Newcastle, NSW*, CSIRO Division of Atmospheric Research, Aspendale, Victoria., Australia.

Gery M.W., Whitten G.Z., Killus J.P. and Dodge M.C. 1989. 'A photochemical kinetics mechanism for urban and regional scale computer modeling', *J. Geophys. Res.*, **94**:12925-56.

Hess G.D., Cope M.E., Lee S. and Tory K. 1999, 'LAPS and the Australian Air Quality Forecasting System', in Parallel Computing in Meteorology and Oceanography, BMRC Research Report No. 75, Jasper J.D. and Meighen P.J. (eds), Bureau of Meteorolgy, Australia.

Ng Y.L. and Minchin M., 2000, 'Spatial and temporal allocation of emissions from wood combustion', *Proceedings of the 15th International Clean Air and Environment Conference, Sydney, 2000*, Clean Air Society of Australia & New Zealand, Eastwood, NSW, Australia.

Williams D.J., Shenouda D.A. and Carras J.N. 1994, 'Modelling air toxic emissions from motor vehicles', *Proceedings of the Air Toxics Conference, Sydney, 1994,* Clean Air Society of Australia & New Zealand and CSIRO, NSW, Australia.

Appendix 3.2 Allocation of Emissions from Wood Combustion

Presented at the 15th International Clean Air & Environment Conference. Sydney, Australia, 26–30 November 2000

SPATIAL AND TEMPORAL ALLOCATION OF EMISSIONS FROM WOOD COMBUSTION

Yuk L. Ng and Matthew Minchin
Environment Protection Authority,
GPO Box 4395QQ, Melbourne, VIC 3000, Australia

Summary

Results from a domestic survey for the Port Phillip region were analysed for wood consumption. Spatial analysis was performed to determine regions with similar annual wood consumption. The effects of seasons, weekdays and weekend days, and time of day on wood consumption were also analysed.

In addition to the domestic survey, wood burning diaries were sent out to determine the effect of temperature on wood consumption. An adjustment factor, which is a linear function of daily temperature, was derived to adjust wood consumption based on the average temperature of the day.

Results of the analyses were integrated with an emission modelling system, EMS-95, to estimate, spatially and temporally distribute the emissions.

Keywords: wood combustion, EMS-95, emissions inventory, Port Phillip Region, spatial allocation, temporal allocation

1. Introduction

Emissions inventories from various Australian airsheds show that wood combustion is a significant source of particulate emissions, particularly during winter (EPA 1995, EPA 1996a, EPA 1996b). Emissions from wood combustion for these inventories were usually spatially distributed according to population with an average per capita wood consumption applied over the whole airshed. Although seasonal variation was considered, emissions were estimated for only summer and winter. Also, day-to-day variation of emissions in a season was not considered even if the temperature varied greatly throughout the season.

In order to model emissions from wood combustion more accurately, EPA conducted a general domestic survey and a survey on daily wood use in the Port Phillip Region. The work was carried out as part of the Air Quality Improvement Plan for the Port Phillip Region (EPA 1997).

The general domestic survey obtained responses from more than 1600 households in the study region. It covered solid fuel combustion, lawn mowing, use of pleasure craft, waste incineration and barbecuing; however, only solid fuel (wood) combustion is discussed in this paper. Households were asked for their annual wood consumption, type of heater used,

proportion of wood used in spring, summer, autumn and winter, and time the heater was used on weekdays and weekends.

In the daily wood use survey, households recorded their daily wood use in diaries. The wood burning diaries were completed by 272 households over a 2 week period in spring and another 2-week period in autumn. These periods were chosen as they had a larger variaton of temperature and wood use. The information in these diaries included the times when the fire was lit, the amount of wood used, the type of heater used (open fire, slow combustion etc) and other general household information. The information collected was related to average temperature of the days the woodheater was operated. The temperature data was collected from a number of EPA and Bureau of Meteorology stations in the study region.

The emissions inventory of the Port Phillip Region has been described in the report published by EPA (1998). This paper presents the results obtained from the surveys and explains the implementation of the results in the emissions modelling system EMS-95 (Emigh & Wilkinson 1997).

2. Domestic Survey

The domestic survey was conducted to find out the spatial, seasonal, weekday/weekend day and diurnal variations of wood use in the Port Phillip Region. Spatial analysis needed to be carried out to see whether there were distinct subregions in the study region.

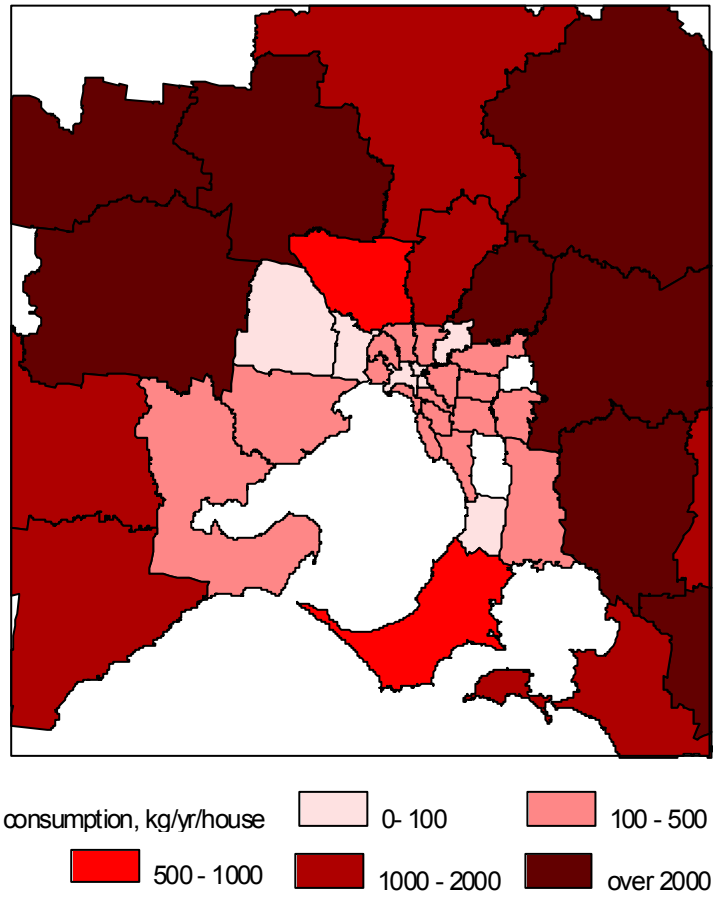

Figure 1 Wood consumption in the local government areas of the Port Phillip Region.

Figure 1 shows the per household wood consumption in the local government areas (LGAs) of the Port Phillip Region. Although LGAs in the metropolitan area usually consumed less wood per household, there is no simple spatial pattern to group these LGAs into subregions. Hence, emissions from wood combustion were estimated on the basis of LGAs rather than subregions. LGAs which did not have enough responses for wood use in the survey, were grouped with the neighbouring LGAs in the analysis.

Figures 2–4 show the seasonal, weekday/weekend day and hourly variation of wood use in the Port Phillip Region obtained from the domestic survey. Nearly 70% of wood was consumed in winter. Note that wood use in spring was slightly higher than that in autumn, indicating that households were still habitually lighting fires in spring. It is a reflection of the transition to winter and people not yet being accustomed to the change in weather. There was little variation in wood use throughout a week, although the consumption on weekends was slightly higher. Through out a day, wood use was the lowest after mid-night and consumption gradually built up during the day and peaked at about 7 pm. The consumption dropped off rapidly after 10 pm.

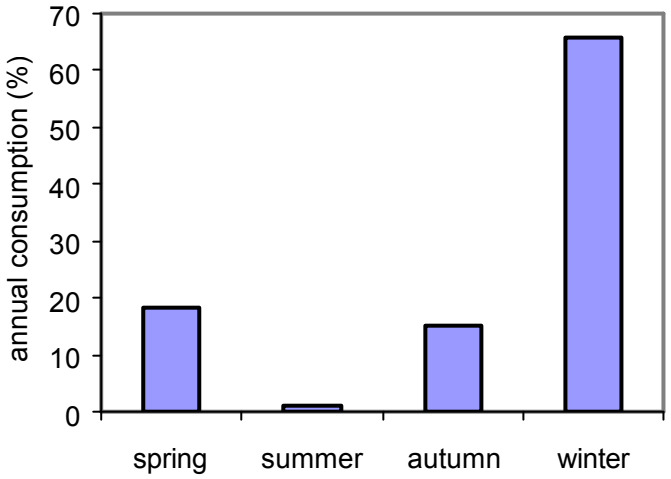

Figure 2 Seasonal variation of wood consumption in the Port Phillip Region.

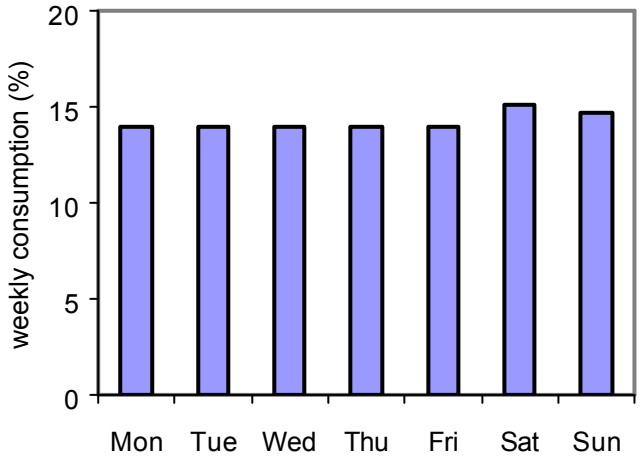

Figure 3 Weekday/weekend day variation of wood consumption in the Port Phillip Region.

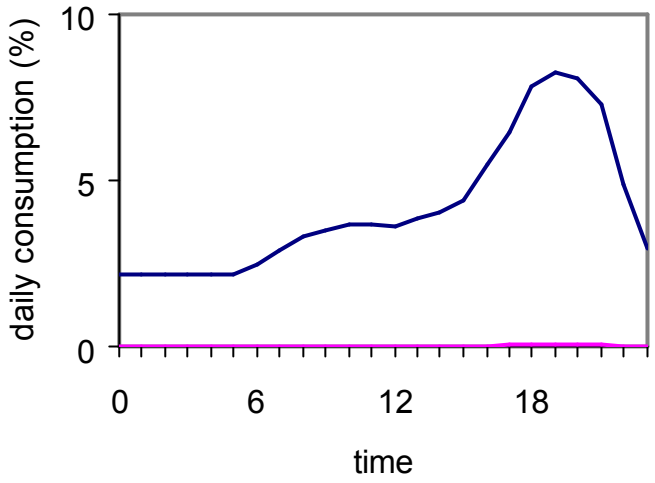

Figure 4 Hourly variation of wood consumption in the Port Phillip Region.

3. Wood Burning Diary

The wood-burning diary was conducted to find out the relationship between wood combustion and temperature. The diary provided information regarding amount of wood used, hours that a fire was lit and proportion of households that lit a fire. Table 1 shows the correlation coefficients between these factors and average daily temperature. Days with less than five responses were excluded from the analysis. The table shows that the proportion of households that lit fires had the strongest relationship with average daily temperature. Wood use and number of hours that a fire was lit had poorer correlation coefficients as these factors were influenced by individual household circumstances as well. Figure 5 shows a plot of proportion of households that lit fires with average daily temperature. The proportion of households that lit fires was therefore chosen as the basis for adjusting emissions with temperature.

Table 1 Correlation coefficients between various factors and average daily temperature.

Factor	Correlation coefficient
wood use	-0.50
number of hours fire was lit	-0.53
proportion of households lit fires	-0.74

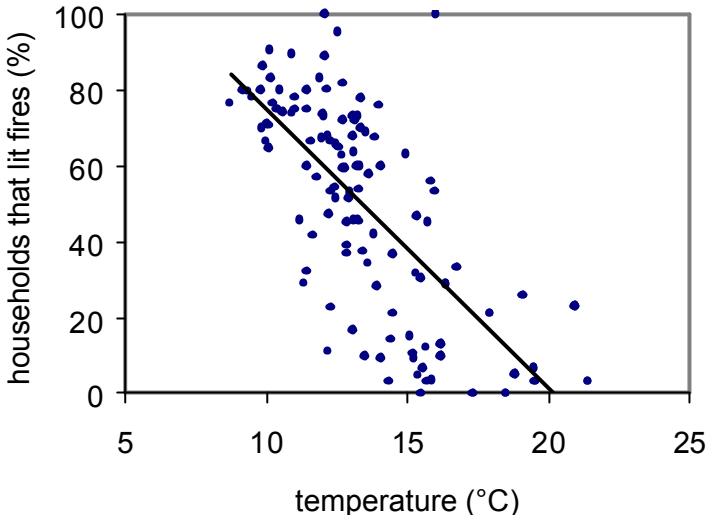

Figure 5 Relationship between proportion of households that lit fires and average daily temperature.

4. Implementation in EMS-95

EMS-95 is a emissions modelling system that spatially and temporally allocates emissions of photochemical and particulate species. The wood consumption that was used in EMS-95 was estimated by multiplying the number of households by the per household wood consumption in each LGA. Emissions were derived by multiplying the wood consumption in each LGA with emission factors (USEPA 1995). The emissions, which were estimated for a year, were allocated spatially to grid cells according to household distribution and temporally according to the following equation:

$$E_h = G \times M \times D \times H_h / W \qquad (1)$$

where E_h is the hourly emission for hour h (kg pollutant/hr),
G is the gridded annual emission (kg pollutant/yr),
M is monthly temporal consumption factor,
W is weekly temporal consumption factor,
D is daily temporal consumption factor, and
H_h is hourly temporal consumption factor for hour h.

The monthly temporal factor was derived by dividing the seasonal consumption factor (see Figure 2) by 3. The weekly temporal consumption factor was the number of days in a month divided by 7. The daily and hourly temporal consumption factors were obtained from Figures 3 and 4 respectively.

Note that the above temporal factors were used for allocating annual emissions to each hour of a day without considering temperature variation. The relationship between the proportion of households that lit fires and average daily temperature as shown in Figure 5 was not a temporal factor and could not be used for allocating emissions. In order to implement the above relationship in EMS-95, it had to be converted into an adjustment factor where the emissions were adjusted up or down according to average daily temperature. An adjustment factor for wood combustion for a particular day could be obtained by dividing the number of

households who lit fires on a particular day by the average number of households who lit fires in spring and autumn. Figure 6 shows the variation of the adjustment factor with the average daily temperature found in the survey.

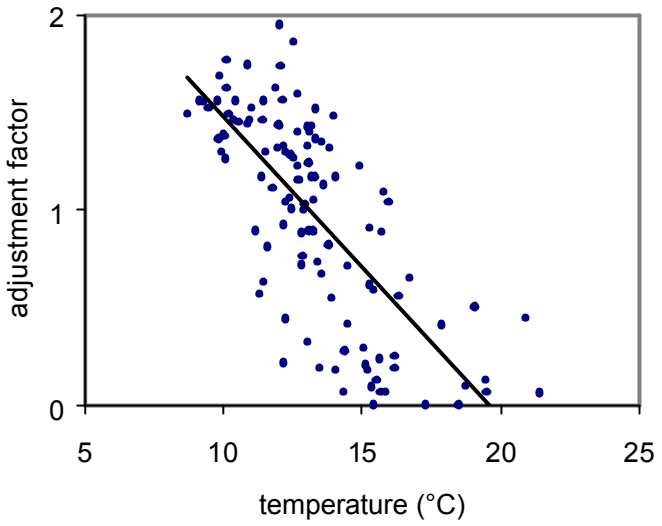

Figure 6 Variation of wood combustion adjustment factor with average daily temperature.

Note that the plot is exactly the same as Figure except that adjustment factor is used instead of household that lit fires. The following linear equation was established from Figure 6 to find the adjustment factor for a given average daily temperature:

$$f = -0.1539 \times t + 3.0205, \quad f > 0 \qquad (2)$$

where f is the wood burning emission adjustment factor, and
t is the average daily temperature in °C.

If the adjustment factor calculated by the above equation was negative, the adjustment factor was set to 0.

The wood burning emission was then obtained by:

$$E_a = E_u \times f \qquad (3)$$

where E_a is the adjusted wood burning emission estimate (kg pollutant/hr), and
E_u is the unadjusted wood burning emission estimate (kg pollutant/hr).

The adjustment factor was applied over the whole study region and should not be used for adjusting emissions due to regional difference in temperature. The proper method to account for regional difference in wood consumption is to conduct a domestic survey in the regions (see Section 2).

Figure 7 shows gridded emissions of PM_{10} (particulates less than 10 μm) in the Port Phillip Region obtained from EMS-95. Although metropolitan areas had lower per household consumption, emissions were still concentrated in them due to the larger number of households in these areas.

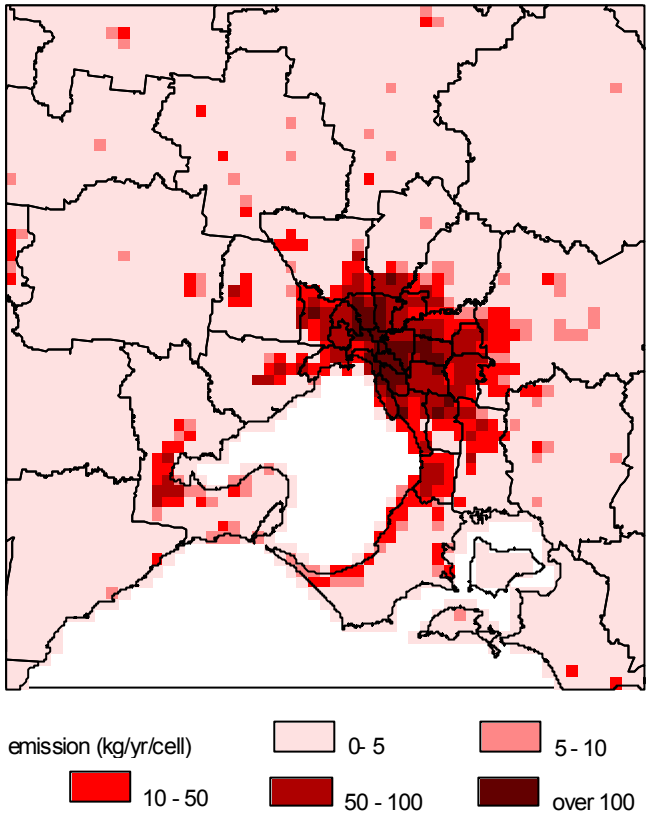

Figure 7 Annual emission of PM10 from wood combustion in the Port Phillip Region

5. Conclusion

Methods and factors were developed and applied successfully for spatially and temporally allocating emissions from wood combustion in the Port Phillip Region using EMS-95. Spatial distribution of emissions was based on different per household consumption in LGAs. Emissions were temporally allocated according to seasons (spring, summer, autumn and winter), weekday/weekend day and hours of the day. Emissions were also adjusted according to the average temperature of the day and this was the first time the effect of temperature was considered in estimating emissions from wood heater use.

The above methods assumed the spatial factor, temporal factors and temperature factor were independent. Investigation of the inter-dependence of these factors would require very large sample sizes for the surveys and was not carried out in this work. Nevertheless, the methods could easily be implemented in EMS-95 and would provide more accurate emission data for use in air quality modelling and air quality management than ever before. The results of this work will be used in the Air Quality Improvement Plan of the Port Phillip Region and the Australian Air Quality Forecasting System (Ng et al.), where different policy options, such as replacement of old heaters with heaters with emission reducing technology, will be tested for their effects on air quality.

Acknowledgments

The authors would like to thank their colleague Dr Piyaratnae Dewundege for providing the temperature data used in this work.

References

Emigh R.A. and Wilkinson J.G. 1997, *The Emission Modeling System (EMS-95) User Guide,* Alpine Geophysics, Colorado, USA.

EPA 1995, *South East Queensland Air Emissions Inventory Consultancy,* Queensland Department of Environment and Heritage, Brisbane.

EPA 1996a, *Metropolitan Air Quality Study, Air Emissions Inventory*, Environment Protection Authority of New South Wales, Sydney.

EPA 1996b, *National Pollutant Inventory: Technical Report on the Air Emissions Trials for the National Pollutant Inventory*, vol. 2, AGPS, Canberra.

EPA 1997, *Taking Stock, A background paper for the Port Phillip region air quality management plan,* Environment Protection Authority of Victoria, Melbourne.

EPA 1998, *Air Emissions Inventory Port Phillip Region,* Publication 632, Environment Protection Authority of Victoria, Melbourne.

Ng Y.L., Walsh S. and Wong N., forthcoming, 'Emissions model for the Australian Air Quality Forecasting System', *Proceedings of the 15th International Clean Air and Environment Conference, Sydney, 2000*, Clean Air Society of Australia & New Zealand, Eastwood, NSW, Australia.

USEPA 1995, *Compilation of Air Pollutant Emission Factors, Vol I. Stationary point and area sources,* AP-42, 5th edn, USEPA, Research Triangle Park, North Carolina, USA.

Appendix 3.3 Specific Meteorologically-Dependent Emissions in AAQFS

Although the Emissions Inventory Model includes meteorologically-dependent emissions, it has proven to be advantageous to include some dependencies in the code of the Chemical Transport Model. AAQFS source groups, which fall into this category, include:

1. Biogenic VOC emissions (*i.e.* isoprene emissions from eucalyptus trees),
2. Emissions of NO_x from soils.
3. Wind-blown dust.
4. Sea-salt aerosol.

1. Biogenic emissions of VOC

The EIM (Appendix 3.1, 3.4) includes a comprehensive, real-time biogenic emissions algorithm, which is based on the BEIS series of models (Birth 1995). The Demonstration System testing has been undertaken using a simpler model, which was developed for airshed modelling studies in NSW and Western Australia (Carnovale *et al*. 1996; Cope and Ischtwan 1995). According to this model, biogenic emissions of isoprene and monoterpenes (as α-pinene) may be estimated as follows:

$$E(VOC)^i_{LS} = [f_{dg} \bullet q_{dg} + (1 - f_{dg}) \bullet q_{ndg}] \bullet bm^i_{LS} \bullet V_f \bullet C_L \bullet C_T \qquad (1)$$

where $E(VOC)^i_{LS}$ is biogenic VOC mass emission flux (g m^{-2} s^{-1}) for landscape category *i*.

Here, q_{dg} is the mass emission rate of the dominant genera per gram of foliage (g g^{-1} s^{-1}) at a standard temperature of 30°C and a photosynthetically active radiation (PAR) flux of 1000 μmol m^{-2} s^{-1}, and q_{ndg} is the mass emission rate of the non-dominant genera per gram of foliage (g g^{-1} s^{-1}) at a temperature of 30°C and a radiation flux of 1000 μmol m^{-2} s^{-1} and bm^i_{LS} is the leaf biomass for the defined landscape category (g m^{-2}). Furthermore, f_{dg} is the biomass fraction of the landscape category assigned to the dominant genera, V_f is the fractional spatial coverage of the vegetation landscape within a grid cell, and C_L, C_T are functions to correct the standard emission fluxes to other temperatures and radiation fluxes.

Further details regarding the form of (1) can be found in the previously cited references. In the AAQFS as implemented, biogenic VOC emissions are estimated on an hourly basis for every land-based grid point, using equation (1) together with a gridded database of landuse category and the LAPS forecasts of leaf-level temperature and radiation. Data on the emissions factors used have come from the study supported by NSW EPA (see **Appendix 3.5 Biogenic Emissions from Trees and Grasses**) An example of the calculated biogenic VOC emission rates is shown in Figure 1 for the Victoria domain, where the 2-D spatial distribution (for hour 12), and a 1-D time series of lumped isoprene and monoterpene emission rate for 6 September 1999 are plotted. Note that the emission rates are relatively small because of the low (12–15°C) ambient temperatures which were present at the time.

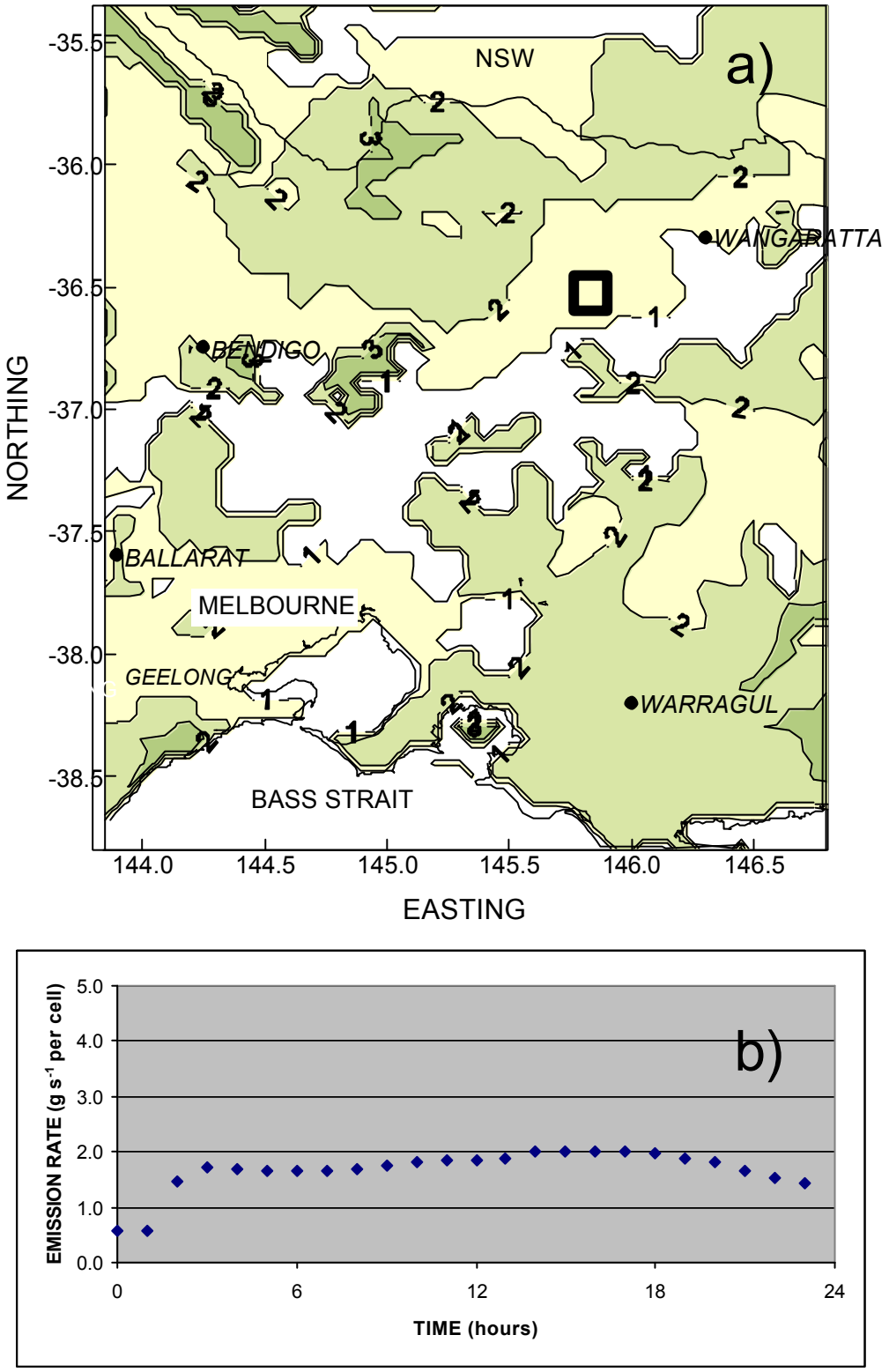

Figure 1: Spatial (a) and temporal (b) distribution of biogenic VOC (isoprene + monoterpenes) emission rates (g s^{-1} per 0.05° ´ 0.05° cell). Emission rates were calculated using the meteorological forecast for 6 September 1999. The time series plot corresponds to the emissions from a cell in the boxed area shown in (a).

2. Emission of sea salt aerosol

The flux of sea-salt aerosol is estimated according to the methodology described in Gong et al. (1997) and references therein. If it is assumed that bubble-bursting is the primary aerosol production method, then a size-segregated emission flux may be parameterised as follows (O'Dowd *et al*., 1997):

$$dF_0/dr = 1.373U_{10}^{3.41}r^{-3}(1+0.057r^{1.05})x10^{1.19e^{-B^2}} \quad (2)$$

where dF_0/dr is the particle density function (particles m^{-2} s^{-1} μm^{-1}), r is the particle radius (μm), U_{10} is the wind speed at 10 m above sea level and $B = (0.380 - \log(r))/0.650$. The cumulative mass emission flux is obtained by integrating (2) over the desired size range (here 0.01–10 μm). In the prototype AAQFS, the flux of sea salt aerosol is determined on an hour-by-hour, cell-by-cell basis (for grid cells located over the ocean) using the LAPS 10 m windspeed forecast.

References

Birth T., 1995. User's Guide to the personal computer version of the Biogenic Emissions Inventory System (PC-BEIS2). EPA-600/R-95-091, Office of Research and Development, U.S. Environmental Protection Agency, Research Triangle Park, NC, 31pp.

Carnovale F., Tilly K., Stuart A., Carvalho C., Summers M. & Eriksen P., 1996, Metropolitan air quality study: Air emissions inventory, Final report to New South Wale Environment Protection Authority, Bankstown, NSW, Australia.

Cope M.E. and Ischtwan J., 1995. Perth photochemical smog study: Airshed modelling component. Final report to Western Power and Department of Environmental Protection.

Gong S.L., Barrie L.A., Blanchet J.P. and Spacek L., 1997. Modelling size-distributed sea salt aerosols in the atmosphere: an application using canadian climate models. Preprints from the 22nd NATO/CCMS International Technical Meeting on Air Pollution Modelling and its Application. June2-6, 1997, Clermont-ferrand, France.

Appendix 3.4 Australian Air Quality Forecasting System Emissions Inventory Model System Document

Australian Air Quality Forecasting System Emission Inventory Model System Document

EPA Victoria

June 2001

Contents

INTRODUCTION

This document describes the directory structure, data files and programs for the Australian Air Quality Forecasting System Emission Inventory Model (EIM). The Emission Inventory Model is composed of six models:

- Point source
- Area source
- Biogenic source
- Motor vehicle
- Wildfire and prescribed burning
- Speciation

The Speciation Model can be considered as part of the other five models. However, the methodology of the speciation is the same for the five models, it will be described as a separate model in discussing its data files and programs.

This document is divided into six major sections: directory structure, data flow diagram, program description. operational procedure, variable cross reference and data dictionary. Directory structure describes the directory structure of the EIM and its organisation. Data flow diagram shows the data files and programs in a model and how they are related in terms of input and output. Program description describes what each program does and the formulae used in the program. Operation procedure describes the procedure to call and run the programs in the EIM. Variable cross reference describes the main variables used in EIM. Data dictionary details the structure of each data file in the system.

DIRECTORY STRUCTURE

The following table shows the directory structure of the Australian Air Quality Forecasting System Emission Inventory Model (EIM).

Environment variable	Directory	Description
FS_HOME	root directory of the EIM	root directory for the EIM
FS_BIN	$FS_HOME/bin	contains all programs for the EIM
FS_SYS	$FS_HOME/sysdata	contains system data that are common to all states, such as speciation data
FS_LOC	$FS_HOME/state	contains state raw data that are common to every grid within a state, such as temporal data
FS_GRD	$FS_HOME/gridspec	contains grid data that can be used for any scenario, such as gridded VKT
FS_RUN	$FS_HOME/scenario	contain files that are specific to a day, such as event.in

DATA FLOW DIAGRAM

Each box in the following diagrams represent one or more data files in a model. Data files that are closely related are put in the same box. Names in dotted boxes are arrays in programs. An arrow represents the flow of data from one set of data files or arrays to another set of data files or arrays. The program which carries out the processing between the two data sets is put alongside the arrow. The details of the programs, arrays and data files will be described in Program Description, Variable Cross Reference and Data Dictionary.

POINT SOURCE MODEL

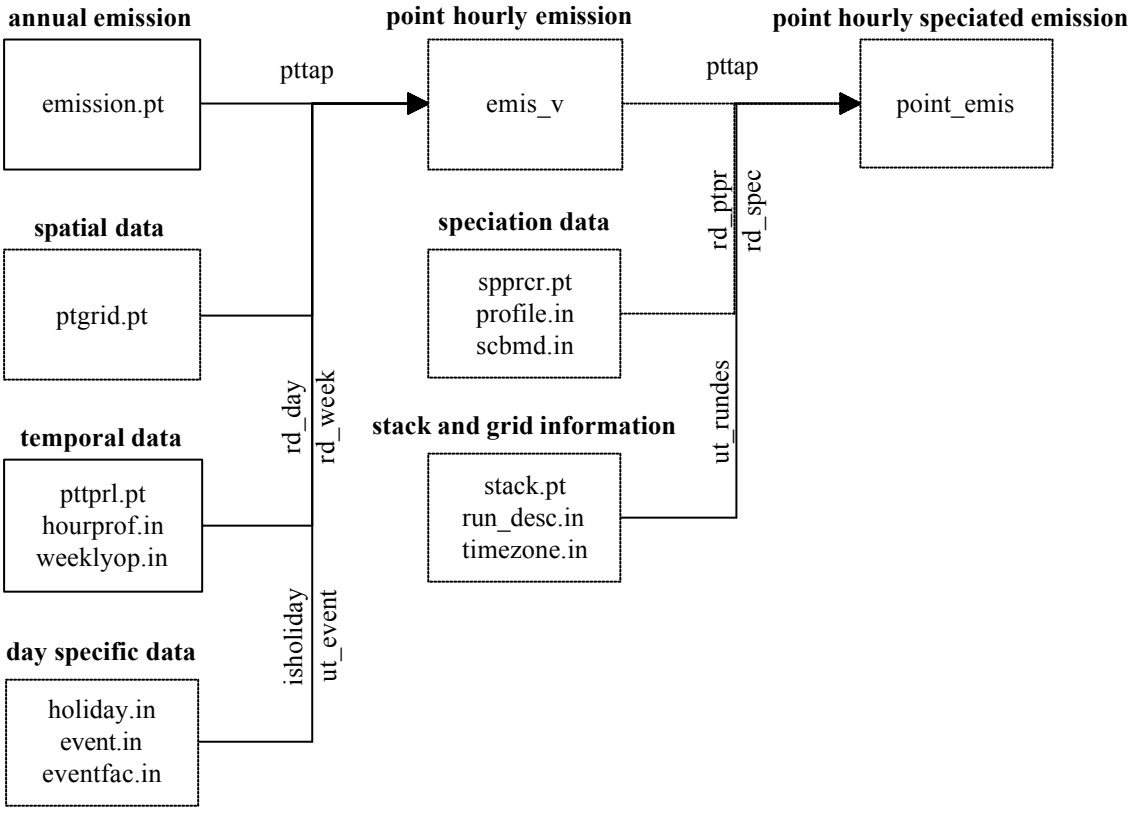

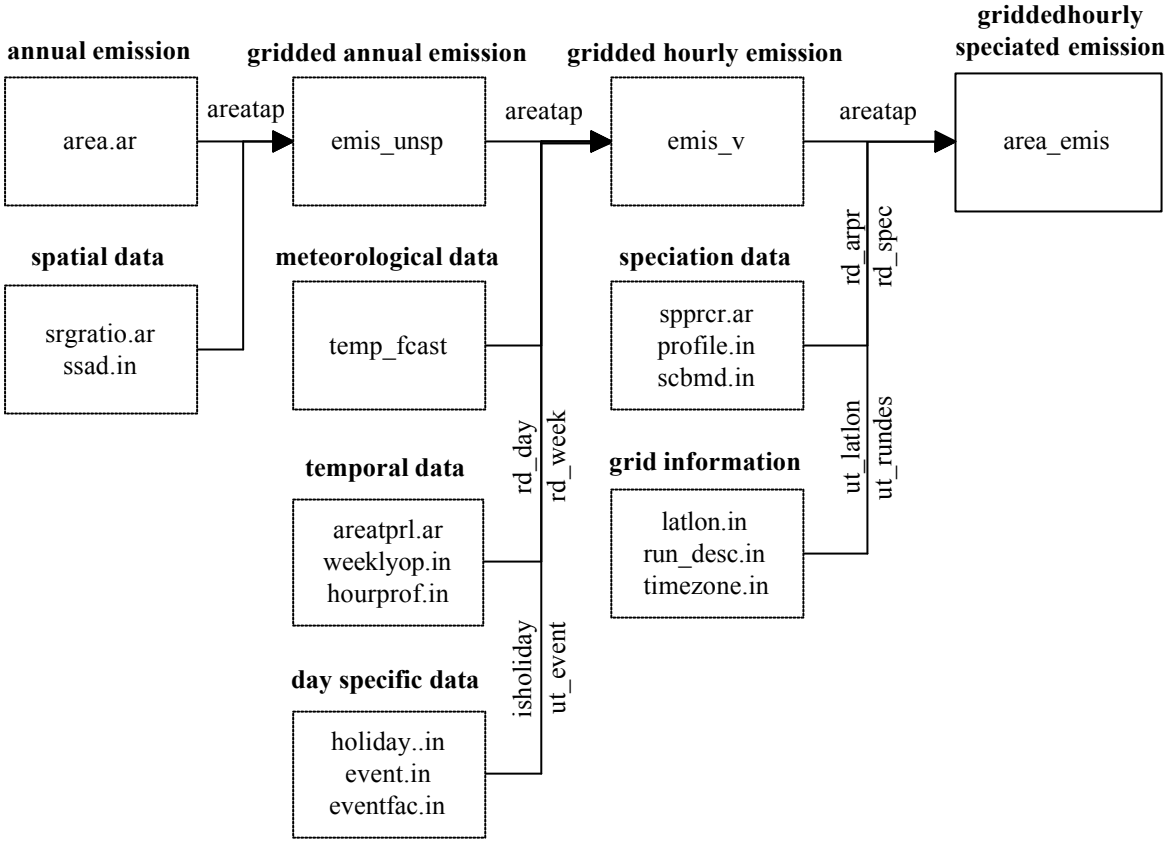

AREA SOURCE MODEL

The scaling program, areascal, does not have to be run in the area source model and is not included in the data flow diagram.

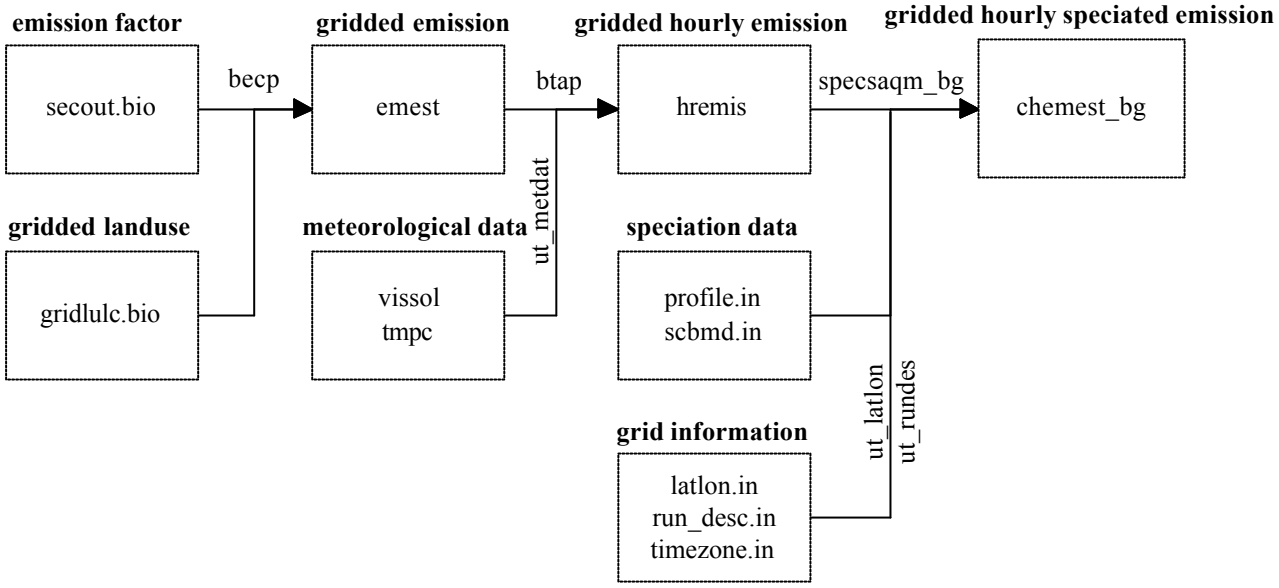

BIOGENIC SOURCE MODEL

MOTOR VEHICLE MODEL

Main Model

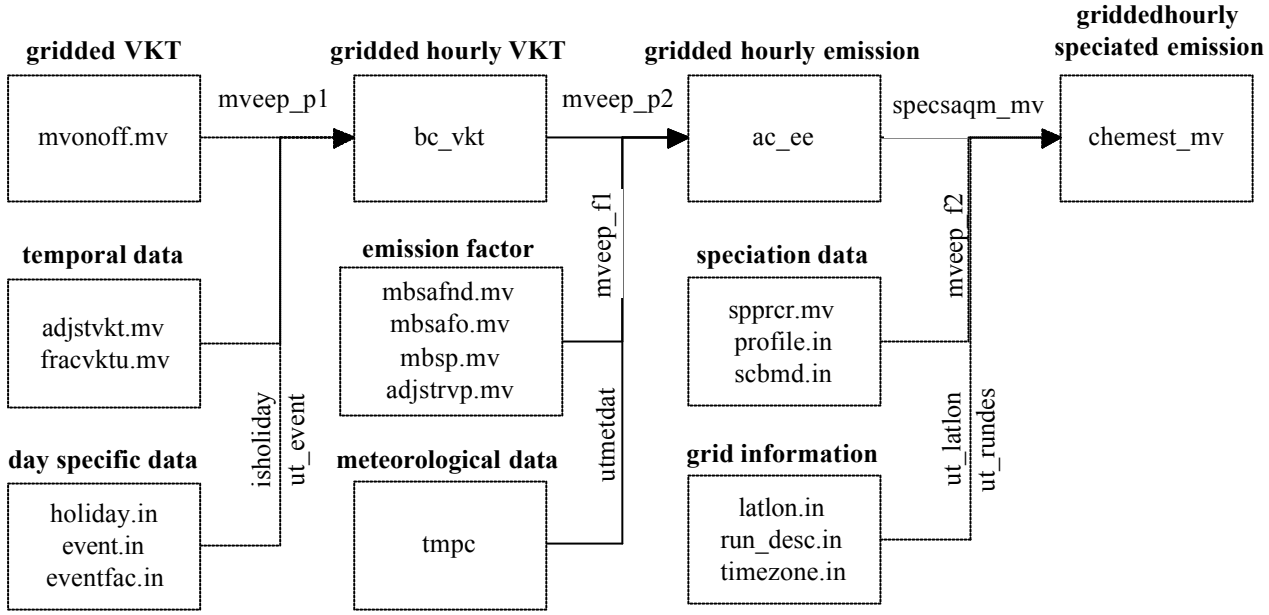

Power-based Model

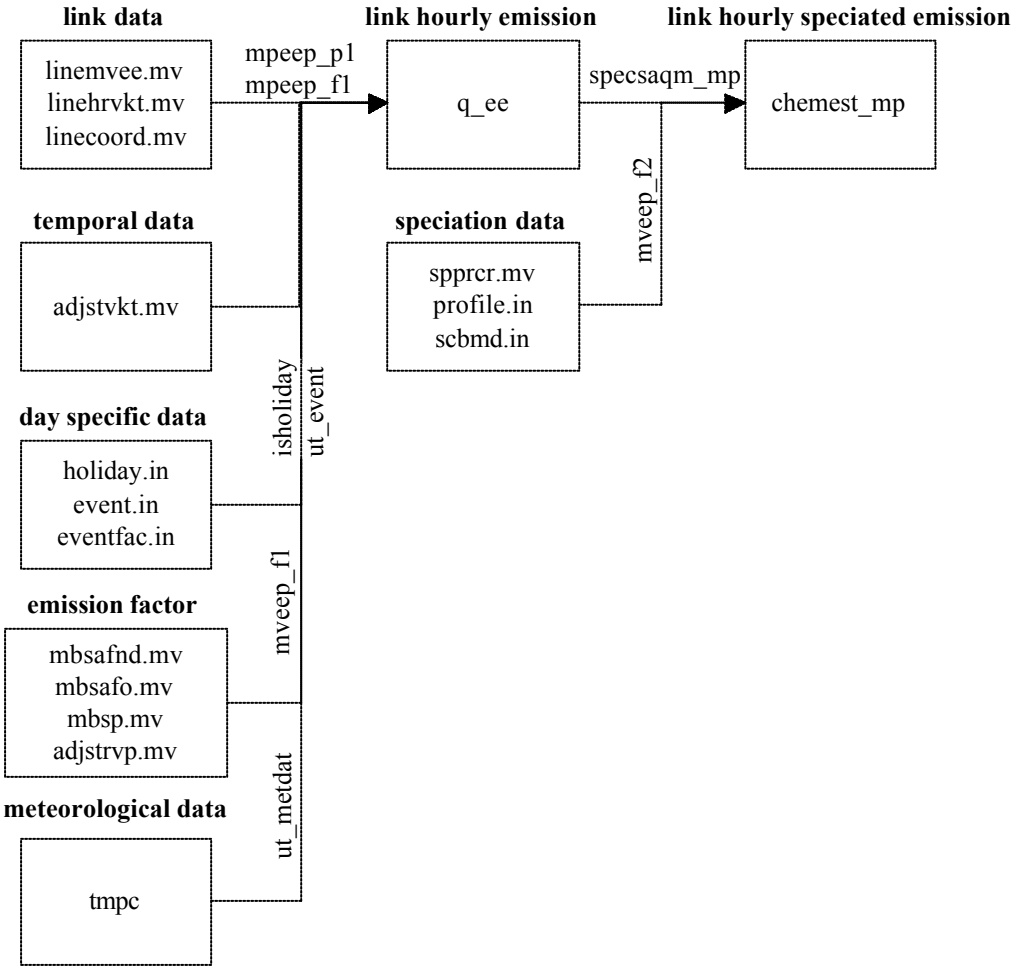

A link is defined as a road segment used in the power-based model.

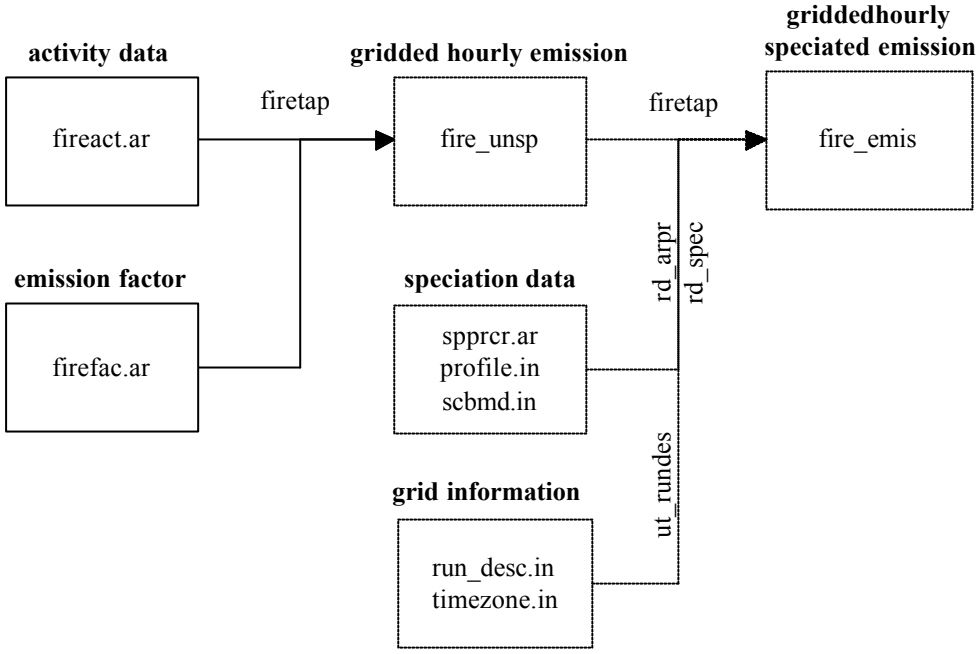

WILDFIRE AND PRESCRIBED BURNING MODEL

PROGRAM DESCRIPTION

This section describes the main programs used in EIM.

point source model

pttap

The program selects point sources in emission.pt from ptgrid.pt and temporally allocates (produces hour-by-hour) emissions estimates based on operating schedule data that are in pttprl.pt. A variety of methods are provided for identifying operating schedule data:

- Monthly throughput fractions (January through December);
- Seasonal throughput fractions (winter, spring, summer and autumn);
- Days per week in operation
- Hours per day in operation

Any, none, or all of the operating schedule data can be supplied. If no operating schedule data are supplied, a default schedule of 24 hours per day, 7 days per week and 12 months per year is used; otherwise, a hierarchy of the operating schedule data is filtered through to determine how to compute the temporal factors:

- Monthly temporal factor;
- Weekly temporal factor;
- Daily temporal factor; and
- 24 hourly temporal factors.

To determine the monthly temporal factor, the following hierarchy is applied:

1. If valid monthly throughputs are available, the monthly temporal factor is set to the monthly throughput value of the month being modelled.
2. If a value is not obtained in Step 1 and valid seasonal throughputs are available, the monthly temporal factor is set to one-third of the seasonal throughput value of the season being modelled.
3. If monthly and seasonal throughtputs are not available, the monthly temporal factor is set to 0.083 (or 1/12 for equal monthly throughputs).

To determine the weekly temporal factor, the number of days in the month being modelled is determined and that value is divided by 7 days per week. For example, in a leap year, there are 29 days in February; therefore, the weekly temporal factor is 4.143 (29 days/month ÷ 7 days/week).

A daily temporal factor is computed through a weekly operation code (Days) in weeklyop.in. If Days cannot be assigned through the method described above, Days is assigned a value of 7. A public holiday is treated as if it is a Sunday. For a specific event, an event factor (from eventfac.in) is used instead of day_fac. If there are more than one event on a day, the last event in the file eventfac.in will be used. If an event happens on a public holiday, the event factor will be used for the day instead of treating it as a Sunday.

An hourly temporal factor is computed through a diurnal operation code (Hours) in hourprof.in. If Hours cannot be assigned through the method described above, Hours is assigned a value of 24.

$$mnth\_fac = mnth_m$$

$$week\_fac = monthday_m / 7$$

$$day\_fac_d = dy\_act_d / \sum_{d=1}^{7} dy\_act_d$$

$$hrprof_h = hr\_act_h / \sum_{h=1}^{24} hr\_act_h$$

where mnth_fac is the monthly temporal factor
week_fac is the weekly temporal factor
day_fac is the day of week temporal factor
hrprof is an array of hourly temporal factors
mnth is an array of relative monthly throughputs ($\sum$mnth(i)=1; for i = 1, 12)
monthday is an array of the number of days in each month
dy_act is an array that contains relative daily activities
hr_act is an array that contains relative hourly activities
m indicates which month of the year is being modelled
d indicates which days per week in operation code (Days) to use
h indicates which hours per day in operation code (Hours) to use

The temporal factors are used to allocate emissions estimates to hourly values.

$$hremis_i = aceekg \times mnth\_fac \times day\_fac \times hrprof_i / week\_fac,\ i = 1, 24$$

where hremis is the array of hourly emissions estimates
aceekg is the emissions estimates

area source model

areatap

This program produces area source gridded hourly emissions.

Area source emissions estimates are allocated to a modelling domain through the application of spatial surrogates. In general, surrogates approximate the value of unknown quantity. For example, population can be used to estimate the number of print shops. A spatial surrogate not only helps estimate the value of an unknown quantity, but a spatial surrogate also helps locate the unknown quantity.

Each area source category (Asct) which has been assigned to a spatial surrogate (k) in ssad.in can be allocated to grid cells (l, m) through the application of the following equation:

$$\text{acee}_{i,j,k',l,m} = \text{acee}_{i,j,k'} \times \text{ratio}_{i,j,k,l,m}$$

where i is the index on states
j is the index on LGA within the states
k is the spatial surrogate index
k' is the area source category index (directly related to k)
l is the x cell index
m is the y cell index
acee is the LGA-wide area source emissions estimate
ratio is the gridded surrogate ratio by state/LGA/surrogate/cell

and

$$\sum_i \sum_j \text{ratio}_{i,j} = 1$$

The program adjusts the wood burning emissions by an average daily temperature and produces gridded hourly emission estimates for each area source category.

The wood burning emission adjustment factor is obtained according to the following equation:

$$\text{adj\_fac} = -0.1539 \times \text{dy\_tmp} + 3.0205, \text{adj\_fac} > 0$$

where adj_fac is the wood burning emission adjustment factor
dy_tmp is the average daily temperature over the modelling grid in °C

If the adjustment factor calculated by the above equation is negative, the adjustment factor is set to 0. The wood burning emission is then obtained by:

$$\text{aceekg}^a = \text{aceekg}^u \times \text{adj\_fac}$$

where aceekg^a is the adjusted wood burning emission estimate
aceekg^u is the unadjusted wood burning emission estimate

After adjusting the wood burning emissions, the program temporally allocates (produces hour-by-hour) emissions estimates based on operating schedule data that are in areatprl.ar. A variety of methods are provided for identifying operating schedule data:

- Monthly throughput fractions (January through December);
- Seasonal throughput fractions (winter, spring, summer and autumn);
- Days per week in operation
- Hours per day in operation

Any, none, or all of the operating schedule data can be supplied. If no operating schedule data are supplied, a default schedule of 24 hours per day, 7 days per week and 12 months per year is used;

otherwise, a hierarchy of the operating schedule data is filtered through to determine how to compute the temporal factors:

- Monthly temporal factor;
- Weekly temporal factor;
- Daily temporal factor; and
- 24 hourly temporal factors.

To determine the monthly temporal factor, the following hierarchy is applied:

1. If valid monthly throughputs are available, the monthly temporal factor is set to the monthly throughput value of the month being modelled.
2. If a value is not obtained in Step 1 and valid seasonal throughputs are available, the monthly temporal factor is set to one-third of the seasonal throughput value of the season being modelled.
3. If monthly and seasonal throughtputs are not available, the monthly temporal factor is set to 0.083 (or 1/12 for equal monthly throughputs).

To determine the weekly temporal factor, the number of days in the month being modelled is determined and that value is divided by 7 days per week. For example, in a leap year, there are 29 days in February; therefore, the weekly temporal factor is 4.143 (29 days/month ÷ 7 days/week).

A daily temporal factor is computed through a weekly operation code (Days) in weeklyop.in. If Days cannot be assigned through the method described above, Days is assigned a value of 7. A public holiday is treated as if it is a Sunday. For a specific event, an event factor (from eventfac.in) is used in instead of day_fac. If there are more than one event on a day, the last event in the file eventfac.in will be used. If an event happens on a public holiday, the event factor will be used for the day instead of treating it as a Sunday.

An hourly temporal factor is computed through a diurnal operation code (Hours) in hourprof.in. If Hours cannot be assigned through the method described above, Hours is assigned a value of 24.

$$\text{mnth\_fac} = \text{mnth}_m$$

$$\text{week\_fac} = \text{monthday}_m / 7$$

$$\text{day\_fac}_d = \text{dy\_act}_d / \sum_{d=1}^{7} \text{dy\_act}_d$$

$$\text{hrprof}_h = \text{hr\_act}_h / \sum_{h=1}^{24} \text{hr\_act}_h$$

where mnth_fac is the monthly temporal factor
week_fac is the weekly temporal factor
day_fac is the day of week temporal factor
hrprof is an array of hourly temporal factors
mnth is an array of relative monthly throughputs ($\sum$mnth(i)=1; for i = 1, 12)
monthday is an array of the number of days in each month
dy_act is an array that contains relative daily activities
hr_act is an array that contains relative hourly activities
m indicates which month of the year is being modelled
d indicates which days per week in operation code (Days) to use
h indicates which hours per day in operation code (Hours) to use

The temporal factors are used to allocate emissions estimates to hourly values.

$$\text{hremis}_i = \text{aceekg} \times \text{mnth\_fac} \times \text{day\_fac} \times \text{hrprof}_i / \text{week\_fac},\ i = 1, 24$$

where hremis is the array of hourly emissions estimates
aceekg is the emissions estimates

areascal

This program allows the scaling of area source emissions by source type (Asct). It applies the scaling factors in arscale.ar to the base area source emissions (area.ar) to create new emissions estimates. Because it overwrites area.ar, it is recommended to back up the original area.ar. The scaling factors can be applied to the base area source emissions estimates by a variety of combinations of state, area source category and pollutant identifiers.

The scaling factor is applied according to the following equation:

$$acee^{s} = acee^{b} \times scal\_fac$$

where $acee^{s}$ is the scaled emission estimate
$acee^{b}$ is the base emission estimate
scal_fac is scaling factor

biogenic source model

becp

The program calculates gridded biogenic emission estimates at standard condition (30°C and 1000 μE/m²/hr) from the emission fluxes in secout.bio and gridded land use data in gridlulc.bio. Depending on the season of the modelling day, the program uses records in secout.bio with foliage cover density L (low) for winter, M (medium) for spring or autumn, and H (high) for summer. The following equation is applied to obtain the gridded, standardised biogenic emissions estimates:

$$\text{emest}_{i,l,m,n} = \sum_{j}\sum_{k}(\text{emflux}_{i,j,k,n} \times \text{luarea}_{i,j,k,l,m})$$

where i is the index on states
j is the index on LGA within the states
k is the land use category index
l is the x cell index
m is the y cell index
n is the pollutant index
luarea is the gridded area of the land use category by state/LGA/land use category/cell (ha)
emest is the gridded biogenic emissions estimate (μg/hr)
emflux is the secondary emissions flux (μg/ha/hr)

btap

The program calculates temporally adjusted emission estimates using the following data:

- bioest.bio – gridded biogenic emission estimates, and
- vissol and tmpc – meteorological data (solar radiation and temperature).

The program is adapted from BEIS2.2 and uses factors in the subroutine HREMIS of BEIS2.2 to adjust the gridded, standardised emissions estimates to day-specific, gridded, hourly biogenic emission estimates. The subroutine HREMIS of BEIS2.2 requires the input of temperature and solar radiation, which is obtained from the subroutine ut_metdat, to calculate the adjustment factors. The adjustment factors are calculated for different canopy types (pines, deciduous, confers, non-forested vegetation) for isoprene and different land use types (grass, forest, wetland, agricultural land) for NO_x. The canopy and land use types are specified in Cantyp of bioest.bio. The following table lists the Cantyp used:

Cantyp	Description
P	pines
D	deciduous
C	confers
N	non-forested vegetation
G	grass
F	forest
W	wetland
A	agricultural land

Note that a canopy type of variable leaf area index (LAI) is not used and so the average LAI (avglai) is not required for input for calculating the adjustment factors.

CO emissions from plants depend on light intensity but the mechanism has not been clearly identified. BEIS2.2 does not calculate CO (and SO_2) emissions. It is assumed that the adjustment factors for CO is the same as those for isoprene in the program. Emissions of SO_2 arise from microbiological processes in soil and water, and depend on soil and water temperature. It is assumed that the adjustment factors for SO_2 is the same as those for NO_x.

The following equation is applied to estimate the hourly emissions from the standardised emissions:

$$\text{hremis}_{i,l,m,n,h} = \text{emest}_{i,l,m,n} \times \text{adjfac}_{l,m,n,h}$$

where i is the index on states
l is the x cell index
m is the y cell index
n is the pollutant index
h is the hour index
hremis is the adjusted gridded hourly biogenic emissions estimate (μg/hr)
emest is the gridded biogenic emissions estimate (μg/hr)
adjfac is the biogenic adjustment factor

motor vehicle model

mveep_p1

Prior to computing the motor vehicle emissions estimates, the gridded, hourly VKT are calculated and the VKT adjusted to the specific modelling day.

$$vkt_{r,i,j,h} = dayvkt_{r,i,j} \times adjday \times adjmonth \times vkt\_prof_{h}$$

where vkt is the gridded, hourly VKT;
dayvkt is the total daily VKT;
adjday is the day-specific VKT adjustment factor supplied through the input file adjstvkt.mv;
adjmonth is the month-specific VKT adjustment factor supplied through the input file adjstvkt.mv;
vkt_prof is the hour-specific VKT fractional profile factor;
r is the road type index;
i is the x cell index;
j is the y cell index; and
h is the hour index.

A public holiday is treated as if it is a Sunday. For a specific event, an event factor (from eventfac.in) is used instead of adjday. If there are more than one event on a day, the last event in the file eventfac.in will be used. If an event happens on a public holiday, the event factor will be used for the day instead of treating it as a Sunday.

mveep_p2

The program computes day-specific, gridded, hourly motor vehicle emissions estimates of VOC, CO, NO_x and other pollutants (PM10 and SO_2). Emissions of VOC, CO and NO_x depend on temperature, the appropriate emission factors have to be used. The file mbsafnd.mv contains emission factors of VOC, CO and NO_x for different road types and temperature. The temperature ranges from 30°F to 110°F in 2°F interval. The temperature on the day in a specific hour is obtained from the subroutine ut_metdat. The emission factor closest to this temperature is then chosen for estimating the emission. Emission factors for other pollutants, which do not depend on temperature, are obtained from the file mbsafo.mv. Note that the emission factor is fleet composite emission factor, ie it has been weighted according to fleet VKT composition.

$$ee_{m,t,p} = 0.001 \sum_{r} ef_{m,t,p,r} \times vkt_{r}$$

where ee is the gridded, hourly emission estimate (kg);
ef is the fleet composite emission factor (g/km);
vkt is the gridded, hourly VKT (km);
m is the index for process type (EV for evaporative, EX for exhaust);
t is the index for technology type (1 for petrol, 2 for diesel, 3 for LPG);
p is the index for pollutant; and
r is the road type index.

Evaporative emission factor for petrol-fuelled vehicles is adjusted by an adjustment factor for Reid Vapour Pressure, which may differ for different periods in a year:

$$ef_{r}^{a} = ef_{r}^{u} \times adjrvp$$

where ef_r^a is the adjusted evaporative emission factor,
ef_r^u is the unadjusted evaporative emission factor
adjrvp is the Reid Vapour Pressure adjustment factor for a particular period
r is the road type index.

Emissions for toxics (benzene, 1,3-butadiene and formaldehyde) are estimated from VOC using speciation fractions.

$$ee_{m,t,p} = ee_{m,t,voc} \times f_{m,t.p}$$

where ee is the gridded, hourly emission estimate (kg);
f is the mass fraction of a species in VOC;
m is the index for process type (EV for evaporative, EX for exhaust);
t is the index for technology type (1 for petrol, 2 for diesel, 3 for LPG); and
p is the index for pollutant (benzene, 1,3-butadiene or formaldehyde).

mpeep_p1

The program reads the VOC, CO and NO_x exhaust-emission data of the power-based model (linemvee.mv), estimates evaporative emission and emissions of PM_{10}, SO_2 and toxics on major roads, and prepare the data for speciation.

Evaporative emission and emissions of PM_{10} and SO_2 on a major road are estimated by the following equation:

$$\mathrm{em}_{m,t,p} = 0.001 \times \mathrm{ef}_{m,t,p} \times \mathrm{vkt}$$

where em is the hourly emission estimate on a major road (kg);
ef is the fleet composite emission factor (g/km);
vkt is the hourly VKT on the road (km);
m is the index for process type (EV for evaporative, EX for exhaust);
t is the index for technology type (1 for petrol, 2 for diesel, 3 for LPG); and
p is the index for pollutant.

For evaporative emission, the emission factor varies with temperature and hence is different for each grid cell. The emission factor is also adjusted for RVP as in mveep_p2.

Emissions on major roads are adjusted to the specific modelling day according to the following equation:

$$\mathrm{em}_{m,t,p} = \mathrm{uem}_{m,t,p} \times \mathrm{adjmonth} \times \mathrm{evf}$$

where em is the adjusted hourly emission estimate on a road link (kg);
uem is the unadjusted hourly emission estimate on a road link (kg);
adjmonth is the month-specific VKT adjustment factor supplied through the input file adjstvkt.mv;
evf is the event factor (from eventfac.mv) if a particular event happens on the day;
m is the index for process type (EV for evaporative, EX for exhaust);
t is the index for technology type (1 for petrol, 2 for diesel, 3 for LPG); and
p is the index for pollutant.

Emissions for toxics (benzene, 1,3-butadiene and formaldehyde) are estimated from VOC using speciation fractions.

$$\mathrm{em}_{m,t,p} = \mathrm{em}_{m,t,\mathrm{voc}} \times \mathrm{f}_{m,t,p}$$

where ep is the hourly emission estimate on a road link (kg);
f is the mass fraction of a species in VOC;
m is the index for process type (EV for evaporative, EX for exhaust);
t is the index for technology type (1 for petrol, 2 for diesel, 3 for LPG); and
p is the index for pollutant (benzene, 1,3-butadiene or formaldehyde).

Background motor vehicle emissions, which include emissions from minor roads, are calculated by gridding and subtracting the emissions on major roads from the total gridded emissions.

$$\mathrm{eb}_{m,t,p} = \mathrm{ee}_{m,t,p} - \mathrm{em}_{m,t,p}$$

where eb is the background gridded, hourly emission estimate (kg);
ee is the total gridded, hourly emission estimate (kg);
em is the gridded, hourly emission estimate from major roads (kg);
m is the index for process type (EV for evaporative, EX for exhaust);
t is the index for technology type (1 for petrol, 2 for diesel, 3 for LPG); and
p is the index for pollutant.

wildfire and prscribed burning model

firetap

This program generates the hourly emissions of wildfire and prescribed burning from each individual fire. The user is expected to enter the fire activity in the file fireact.ar. If the fuel load is not entered, it is assumed to be 25 t/ha. If the firesize is not entered, it is assumed to be 1 ha.

The combustion process is divided into flaming and smouldering phases. For a fire event, the fuel consumed during the two phases are calculated according to the following equations:

$$\text{fcons} = \text{fp} \times \text{firesize} \times \text{fuelload} \qquad \text{flaming}$$

$$\text{scons} = (1 - \text{fp}) \times \text{firesize} \times \text{fuelload} \qquad \text{smouldering}$$

where fcons is fuel consumption in flaming (tonne);
scons is fuel consumption in smouldering (tonne);
fp is the proportion of fuel consumed in flaming;
firesize is area burnt (ha); and
fuelload is fuel load (t/ha).

A constant value of 0.33 is assumed for fp [1].

The fuel consumption rate in the flaming phase is calculated according to the following equations:

$$\text{dcf} = \frac{\text{fcons}}{\text{igndur}} \times \frac{\text{t}}{\text{tflam}} \qquad 0 \le \text{t} \le \text{tflam}$$

$$\text{dcf} = \frac{\text{fcons}}{\text{igndur}} \qquad \text{tflam} < \text{t} < \text{igndur}$$

$$\text{dcf} = \frac{\text{fcons}}{\text{igndur}} \times \frac{\text{igndur} + \text{tflam} - \text{t}}{\text{tflam}} \qquad \text{igndur} \le \text{t} < \text{tflam} + \text{igndur}$$

$$\text{dcf} = 0 \qquad \text{t} \ge \text{tflam} + \text{igndur}$$

where dcf is fuel consumption rate in flaming at time t (tonne/min);
igndur is time required to light the fire (min);
tflam is time from lighting to first smoulder (min); and
t is time (min).

The time from lighting to first smoulder typically takes 30 min [2]. The time required to light a fire depends on area burnt and is estimated by the following equation:

$$\text{igndur} = 3 \times \text{firesize}$$

which assumes ignition of a hectare fire requires 3 min.

The fuel consumption rate in the smouldering phase is calculated according to the following equations:

$$\text{dcs} = \frac{\text{scons}}{\text{igndur}} \times \left\{1 - \exp\left(\frac{\text{tflam} - \text{t}}{\text{edr}}\right)\right\} \qquad 0 \le \text{t} < \text{tflam} + \text{igndur}$$

[1] Compilation of Air Pollutant Emission Factors, Vol I. Stationary point and area sources, AP-42, 5th edn, USEPA, Research Triangle Park, North Carolina, USA, 1995.
[2] Ferguson S.A., Sandberg D.V. and Ottmar R., 'Wild-land biomass emissions affected by land-use changes', in Second Symposium on Fire and Forest Meteorology, 11-16 Jan 1998, Phoenix, AZ, American Meteorological Society, Boston, MA, p. 71-74.

$$dcs = \frac{scons}{igndur} \times \left\{1 - \exp\left(-\frac{igndur}{edr}\right)\right\} \times \exp\left(\frac{igndur + tflam - t}{edr}\right) \quad t \geq tflam + igndur$$

$$dcs = 0 \qquad dcs < 0$$

where dcs is fuel consumption rate in smouldering at time t (tonne/min); and
edr is exponential decay rate constant (min).

The exponential decay rate constant, edr, depends on fuelload and is given by:

$$edr = 1 + 0.192 \times fuelload$$

The heat release rate is calculated by:

$$heat = (dcf + dcs) \times 16867.2$$

where heat is heat release rate at time t (MJ/min).

The emission rate of a pollutant is estimated by:

$$emis = dcf \times emff + dcs \times emfs$$

where emis is emission rate of a pollutant at time t (kg/min);
emff is emission factor of the pollutant for the flaming phase (kg/tonne); and
emfs is emission factor of the pollutant for the smouldering phase (kg/tonne).

Note that the air quality model requires the average heat release rate and emission rates for an hour. That means the above equations need to be integrated analytically or numerically to obtain the total heat release or emissions in an hour and divided by 3600 to arrive at the average heat release rate in MJ/s or emission rates in g/s for that hour.

meteorological data model

utmetdat

This program extracts meteorological data required for the emission model from the LAPS model. The data extracted are:

- gridded, hourly solar radiation in μE, and
- gridded, hourly temperature in °C.

speciation model

The following six programs perform the speciation for various models:

- pttap (point source model)
- areatap (area source model)
- specsaqm_bg (biogenic source model)
- specsaqm_mv (motor vehicle main model),
- specsaqm_mp (motor vehicle power-based model), and
- firetap (wildfire and prescribed burning model).

The programs speciate the point, gridded or link, hourly emissions so that they are ready to be used in the air quality model. The program specsaqm_mv also provides background gridded emissions if the power-based model is used.

The point, gridded or link, hourly emissions estimates are speciated by applying the following equation.

$$\text{chemest} = \text{ee} \times \text{sf} \times \text{mw} / (\text{divisor} \times 3600)$$

where chemest is the point, gridded or link, hourly lumped-model species emissions estimates (grams/second)
ee is the point, gridded or link, hourly emissions estimates of pollutants (grams/hour)
sf is the lumped-model species split factor
mw is molecular weight
divisor is a secondary conversion factor for lumped-model species other than the hydrocarbon-related and particle species.

The following table lists the species and their indices in the arrays point_emis, area_emis, chemest_bg, chemest_mv, chemest_mp or fire_emis. The species and order can be changed in the data file scbmd.in.

Array Index	Species
1	OLE
2	PAR
3	TOL
4	XYL
5	HCHO
6	ALD2
7	ETH
8	ISOP
9	NR
10	NO
11	NO2
12	HONO
13	CO
14	SO2
15	SO3
16	PM2 (PM2.5-10)
17	PM1 (PM2.5)
18	NH3

Array Index	Species
19	BTD (1,3-butadiene)
20	BNZ (benzene)
21	FAD (formaldehyde)[a]
22	EC1 (elemental carbon 0.03906-0.07812 μm)
23	EC2 (elemental carbon 0.07812-0.1562 μm)
24	EC3 (elemental carbon 0.1562-0.3125 μm)
25	EC4 (elemental carbon 0.3125-0.6250 μm)
26	EC5 (elemental carbon 0.6250-1.250 μm)
27	EC6 (elemental carbon 1.250-2.500 μm)
28	EC7 (elemental carbon 2.500-5.000 μm)
29	EC8 (elemental carbon 5.000-10.00 μm)
30	OC1 (organic carbon 0.03906-0.07812 μm)
31	OC2 (organic carbon 0.07812-0.1562 μm)
32	OC3 (organic carbon 0.1562-0.3125 μm)
33	OC4 (organic carbon 0.3125-0.6250 μm)
34	OC5 (organic carbon 0.6250-1.250 μm)
35	OC6 (organic carbon 1.250-2.500 μm)
36	OC7 (organic carbon 2.500-5.000 μm)
37	OC8 (organic carbon 5.000-10.00 μm)
38	OTR1 (other 0.03906-0.07812 μm)
39	OTR2 (other 0.07812-0.1562 μm)
40	OTR3 (other 0.1562-0.3125 μm)
41	OTR4 (other 0.3125-0.6250 μm)
42	OTR5 (other 0.6250-1.250 μm)
43	OTR6 (other 1.250-2.500 μm)
44	OTR7 (other 2.500-5.000 μm)
45	OTR8 (other 5.000-10.00 μm)
46	SO41 (sulphate 0.03906-0.07812 μm)
47	SO42 (sulphate 0.07812-0.1562 μm)
48	SO43 (sulphate 0.1562-0.3125 μm)
49	SO44 (sulphate 0.3125-0.6250 μm)
50	SO45 (sulphate 0.6250-1.250 μm)
51	SO46 (sulphate 1.250-2.500 μm)
52	SO47 (sulphate 2.500-5.000 μm)
53	SO48 (sulphate 5.000-10.00 μm)
54	T1 (tracer 1)
55	T2 (tracer 2)
56	T3 (tracer 3)
57	T4 (tracer 4)
58	T5 (tracer 5)

a) FAD may not be the same as FORM. FAD is estimated directly in inventory whereas FORM is obtained from VOC speciation profile.

OPERATION PROCEDURES

input requirements

The running of the EIM usually do not require any user's input unless the following conditions happen:

1. An event, such as cleaner transport day, happens in the forecasting period. In this case, the user needs to add the event to the file event.in. The file eventdesc.in contains the event codes and their description.
2. A new year starts. In this case, the user needs to update the files holiday.in and timezone.in.

Refer to the Data Dictionary for the format of the files.

set up

The following table lists the setup files and calling programs for the EIM.

File	Description
aqfs.h	include file for parameters used in the EIM
aqfile.h	include file for specifying location of data files
call_pttap.f90	example program to call the point source model
call_areatap.f90	example program to call the area source model
call_mv.f90	example program to call the motor vehicle model
call_mv.f90.m	make file for motor vehicle model
call_firetap.f90	example program to call the wildfire and prescribed burning model

The file aqfs.h contains all the parameters used for the EIM. The parameters, such as the forecasting period MAXHRS, can be changed to accommodate new requirements.

The file aqfile.h specifies the location of data files and need to be change if the system is moved to a new directory.

The programs call_pttap.f90, call_areatap.f90, call_mv.f90 and call_firetap are example programs to call the point source, area source, motor vehicle, and wildfire and prescribed burning models respectively. These programs need to be adapted in the air quality model to call up the various models.

compiling programs

The make file or scripts for compiling various models are shown in the following table.

Model	Make file
point source	link_p
area source	link_a
motor vehicle	call_mv.f90.m
wildfire and prescribed burning	link_f

running programs

The following table shows the typical time and memory requirement of each model when running on the NEC SX-5 computer.

Program	Time, sec	Memory, Mb
call_pttap	30	80
call_areatap	2000	500
call_mv	50	2000
call_firetap	1000	400

VARIABLE CROSS REFERENCE

The following table lists the main variables used in the EIM and variables that have been referenced in the Data Flow Diagram.

Object	Class[a]	Type	Dimensions	Description
system variables				
MAXPOL	P	int		maximum number of pollutants
MAXSP	P	int		maximum number of species
MAXHRS	P	int		number of hours ahead the system is to forecast
MAXSTK	P	int		maximum number of stacks
MAXCOL	P	int		maximum number of grid columns
MAXROW	P	int		maximum number of grid rows
MAXRD	P	int		maximum number of road types
MAXLN	P	int		maximum number of links
MAXAC	P	int		maximum number of combination of Polid, Mvproces and Techtype
MAXFEV	P	int		maximum number of fire events in a forecasting period
point source model				
emis_v	V	real		point hourly emission
point_emis	A	real	MAXSTK, MAXSP, MAXHRS	point hourly, speciated emission
area source model				
emis_unsp	A	real	MAXPOL, MAXCOL, MAXROW	gridded annual emission
emis_v	V	real		gridded, hourly emission
area_emis	A	real	MAXCOL, MAXSP, MAXROW, MAXHRS	gridded, hourly, speciated emission
temp_fcast	A	real	3	average daily temperature for today and the next two days
biogenic source model				
emest	A	real	MAXPOL, MAXCOL, MAXROW	gridded emission at standard conditions
vissol	A	real	MAXCOL, MAXROW, MAXHRS	gridded, hourly solar radiation

Object	Class[a]	Type	Dimensions	Description
tmpc	A	int	MAXCOL, MAXROW, MAXHRS	gridded, hourly temperature
hremis	A	real	MAXPOL, MAXCOL, MAXROW, MAXHRS	gridded, hourly emission
chemest_bg	A	real	MAXCOL, MAXROW, MAXSP, MAXHRS	gridded, hourly, speciated emission
motor vehicle model				
bc_vkt	A	real	MAXRD, MAXCOL, MAXROW. MAXHRS	gridded, hourly VKT
tmpc	A	int	MAXCOL, MAXROW, MAXHRS	gridded, hourly temperature
ac_ee	A	real	MAXAC, MAXCOL, MAXROW, MAXHRS	gridded, hourly emission
chemest_mv	A	real	MAXCOL, MAXROW, MAXSP, MAXHRS	gridded, hourly, speciated emission
q_ee	A	real	MAXAC, MAXLN, MAXHRS	link hourly emission
chemest_mp	A	real	MAXLN, MAXSP, MAXHRS	link hourly, speciated emission
WILDFIRE AND PRSCRIBED BURNING MODEL				
fire_unsp	A	real	MAXFEV, MAXPOL, MAXHRS	gridded, hourly emission
fire_emis	A	real	MAXFEV, MAXSP, MAXHRS	gridded, hourly, speciated emission
heat_rel	A	real	MAXFEV, MAXHRS	gridded, hourly heat release

a) P is parameter, V variable, and A array.

DATA DICTIONARY

The terms 'entity' and 'attribute' are used throughout in the data dictionary, sometimes they are referred as 'table' and 'field' respectively. A 'P' in Key stands for primary key and a 'F' stands for foreign key. An attribute is a primary key if that attribute is unique in an entity. Sometimes, more than one attribute are primary keys in an entity, in this case several attributes taken together is unique in an entity. An attribute is a foreign key if it is not a primary key in an entity but is a primary key in another entity. All files are sorted according to primary keys. If there is more than one primary key in a file, it is first sorted for the first primary key and then the second primary key, etc. A file which contains data for a particular state and/or grid has the extensions {stid} and {gridid} attached, eg latlon.in.2.1 contains the grid cell coordinates for state 2 and grid 1.

system data

Entity	ascd.in.{stid}
Description	area source code and description for every state
Source	EMS-95 or supplied
Destination	none (for reference only)
Location	$FS_SYS

Attribute	Description	Units	Type	Len	Precision	Key	Acceptable values
State	state code		I	2		P	1-8
Asct	area source category		A	15		P	
Desc	description		A	40			

Entity	event.in.{stid}
Description	date of special event
Source	user
Destination	ut_event
Location	$FS_RUN

Attribute	Description	Units	Type	Len	Precision	Key	Acceptable values
Stid	state code		I	2		P	1-8
Eventid	event code		I	2		P	
Date	date of an event	dd/mm/yyyy	A	11		P	

Entity	eventdesc.in
Description	description of special event
Source	user
Destination	none (for reference only)
Location	$FS_SYS

Attribute	Description	Units	Type	Len	Precision	Key	Acceptable values
Eventid	event code		I	2		P	
Desc	description of event		A	50			

Entity	eventfac.in.{stid}
Description	event factors
Source	user
Destination	ut_event
Location	$FS_LOC

Attribute	Description	Units	Type	Len	Precision	Key	Acceptable values
Stid	state code		I	2		P	1-8
Eventid	event code		I	2		P	
Asct[a]	area source category		A	15		P	
Evf	event factor		F	4	2		

a) An Asct of 2200000000 is used for motor vehicles and 2300000000 for industry.

Entity	gridinfo.in.{stid}.{gridid}
Description	Minimum and maximum latitude/longitude of grid domain
Source	EMS-95 or supplied
Destination	Not processed but used for visualisation
Location	$FS_GRD

Attribute	Description	Units	Type	Len	Precision	Key	Acceptable values
Stid	state code		I	2		P	1-8
Gridid	grid ID		I	2		P	
Latmin	Minimum latitude of grid domain (cell centre)	°	F	8	3		
Latmax	Maximum latitude of grid domain (cell centre)	°	F	8	3		
Longmin	Minimum longitude of grid domain (cell centre)	°	F	8	3		
Longmax	Maximum longitude of grid domain (cell centre)	°	F	8	3		

Entity	holiday.in.{stid}
Description	list of public holidays
Source	user
Destination	ut_holiday
Location	$FS_LOC

Attribute	Description	Units	Type	Len	Precision	Key	Acceptable values
Stid	state code		I	2		P	1-8
Date	date of a public holiday	dd/mm/yyyy	A	10		P	

Entity	hourprof.in
Description	hourly profiles
Source	EMS-95 or supplied
Destination	rd_day
Location	$FS_SYS

Attribute	Description	Units	Type	Len	Precision	Key	Acceptable values
Hours	diurnal operation code		I	2		P	1-69
Hr_act(1)	operation profile for hour 0-1		I	3			
Hr_act(2)	operation profile for hour 1-2		I	3			
Hr_act(3)	operation profile for hour 2-3		I	3			
Hr_act(4)	operation profile for hour 3-4		I	3			
Hr_act(5)	operation profile for hour 4-5		I	3			
Hr_act(6)	operation profile for hour 5-6		I	3			
Hr_act(7)	operation profile for hour 6-7		I	3			
Hr_act(8)	operation profile for hour 7-8		I	3			
Hr_act(9)	operation profile for hour 8-9		I	3			
Hr_act(10)	operation profile for hour 9-10		I	3			
Hr_act(11)	operation profile for hour 10-11		I	3			
Hr_act(12)	operation profile for hour 11-12		I	3			
Hr_act(13)	operation profile for hour 12-13		I	3			
Hr_act(14)	operation profile for hour 13-14		I	3			
Hr_act(15)	operation profile for hour 14-15		I	3			
Hr_act(16)	operation profile for hour 15-16		I	3			
Hr_act(17)	operation profile for hour 16-17		I	3			
Hr_act(18)	operation profile for hour 17-18		I	3			
Hr_act(19)	operation profile for hour 18-19		I	3			
Hr_act(20)	operation profile for hour 19-20		I	3			
Hr_act(21)	operation profile for hour 20-21		I	3			
Hr_act(22)	operation profile for hour 21-22		I	3			
Hr_act(23)	operation profile for hour 22-23		I	3			
Hr_act(24)	operation profile for hour 23-24		I	3			

Entity	latlon.in.{stid}.{gridid}
Description	Cross reference of icell and jcell to latitude and longitude
Source	EMS-95 or supplied
Destination	ut_latlon
Location	$FS_GRD

Attribute	Description	Units	Type	Len	Precision	Key	Acceptable values
Stid	state code		I	2		P	1-8
Gridid	grid ID		I	2		P	
Icell	x axis cell index		I	3		P	
Jcell	y axis cell index		I	3		P	
Lat	latitude of cell centre	°	F	8	3		
Long	longitude of cell centre	°	F	8	3		

Entity	profile.in
Description	chemical mechanism speciation profile
Source	EMS-95
Destination	rd_spec, mveep_f2, specsaqm_bg
Location	$FS_SYS

Attribute	Description	Units	Type	Len	Precision	Key	Acceptable values
Inprf	speciation profile number		A	5		P	
Mdlspab	model species abbreviated		A	5		P	
Factor	value to split emissions into class		F	13	6		
Divisor	molecular weight for non-VOC pollutants		I	13			
Polid	pollutant ID		A	5		F	

Entity	rdclass.mv
Description	road type
Source	EMS-95 or supplied
Destination	not used (for documentation purpose only)
Location	$FS_SYS

Attribute	Description	Units	Type	Len	Precision	Key	Acceptable values
Rdtype	road type ID		I	1		P	
Rddesc	road type description		A	50			

Entity	run_desc.in.{stid}.{gridid}
Description	run description file that contains the grid details
Source	user
Destination	utrundes
Location	$FS_SYS

Attribute	Description	Units	Type	Len	Precision	Key	Acceptable values
Stid	state code		I	2		P	1-8
Gridid	grid ID		I	2		P	
Gridnam	grid name		A	8			
Xcells	number of cells in x direction		I	3			1-200
Ycells	number of cells in y direction		I	3			1-200

Entity	scbmd.in
Description	CB-IV model data
Source	EMS-95
Destination	rd_spec, mveep_f2, specsaqm_bg
Location	$FS_SYS

Attribute	Description	Units	Type	Len	Precision	Key	Acceptable values
Mdlspcd	model species code		I	2		P	
Mdlspab	model species abbreviated		A	5			
Mdlspnam	species name		A	30			
Polid	Pollutant ID		A	5			
Mdlspmw	species molecular weight		F	6	2		

Entity	spprcr.ar
Description	Asct to chemical mechanism cross reference for area source
Source	EMS-95
Destination	rd_arpr
Location	$FS_SYS

Attribute	Description	Units	Type	Len	Precision	Key	Acceptable values
Asct	area source category		A	15		P	
Inprf	speciation profile number		A	5		F	

Entity	spprcr.mv
Description	Asct to chemical mechanism cross reference for motor vehicle
Source	EMS-95
Destination	mveep_f2
Location	$FS_SYS

Attribute	Description	Units	Type	Len	Precision	Key	Acceptable values
Mvproces	emission classification for speciation		A	3		P	EX, EV[a]
Techtype	fuel type used in process		I	1		P	1-3[b]
Inprf	speciation profile number		A	5		F	

a) EX – exhaust, EV – evaporative
b) 1 – petrol, 2 – diesel, 3 – LPG

Entity	spprcr.pt
Description	Scc to chemical mechanism cross reference for point source
Source	EMS-95
Destination	rd_ptpr
Location	$FS_SYS

Attribute	Description	Units	Type	Len	Precision	Key	Acceptable values
Scc	source classification code		A	8		P	
Inprf	speciation profile number		A	5		F	

Entity	ssad.in.{stid}
Description	Asct to Ssc cross reference
Source	EMS-95 or supplied
Destination	rd_ssad
Location	$FS_SYS

Attribute	Description	Units	Type	Len	Precision	Key	Acceptable values
Stid	state code		I	2		P	1-8
Asct	area source category		A	15		P	
Ssc	spatial surrogate code		A	3		F	

Entity	timzone.in.{stid}
Description	effective time zone for normal days and days of daylight saving
Source	user
Destination	utrundes
Location	$FS_SYS

Attribute	Description	Units	Type	Len	Precision	Key	Acceptable values
Stid	state code		I	2		P	1-8
Date_start	start date	dd/mm/yyyy	A	10		P	
Date_end	end date	dd/mm/yyyy	A	10		P	
Tmzn	time zone		A	3			

Entity	weeklyop.in
Description	weekly operation codes
Source	EMS-95
Destination	rd_week
Location	$FS_SYS

Attribute	Description	Units	Type	Len	Precision	Key	Acceptable values
Days	weekly operation code		I	2		P	1-23
Dy_act(1)	relative daily activity for Monday		I	3			
Dy_act(2)	relative daily activity for Tuesday		I	3			
Dy_act(3)	relative daily activity for Wednesday		I	3			
Dy_act(4)	relative daily activity for Thursday		I	3			
Dy_act(5)	relative daily activity for Friday		I	3			
Dy_act(6)	relative daily activity for Saturday		I	3			
Dy_act(7)	relative daily activity for Sunday		I	3			

point source model

Entity	emission.pt.{stid}						
Description	point source emissions						
Source	EMS-95 or supplied						
Destination	pttap						
Location	$FS_LOC						
Attribute	Description	Units	Type	Len	Precision	Key	Acceptable values
Stid	state code		I	2		P	1-8
Fcid	facility ID		A	15		P	
Stkid	stack ID		A	12		P	
Polid	pollutant ID		A	5		P	
Acee	actual emission	t/yr	E	13	6		

Entity	ptgrid.pt.{stid}.{gridid}
Description	point sources in the modelling grid
Source	EMS-95 or supplied
Destination	pttap
Location	$FS_GRD

Attribute	Description	Units	Type	Len	Precision	Key	Acceptable values
Stid	state code		I	2		P	1-8
Gridid	grid ID		I	2		P	
Fcid	facility ID		A	15		P	
Stkid	stack ID		A	12		P	

Entity	pttprl.pt.{stid}
Description	point source temporal data
Source	EMS-95 or supplied
Destination	pttap
Location	$FS_LOC

Attribute	Description	Units	Type	Len	Precision	Key	Acceptable values
Stid	state code		I	2		P	1-8
Fcid	facility ID		A	15		P	
Stkid	stack ID		A	12		P	
Mthrput(12)	fractional December throughput		F	5	3		0-1
Mthrput(1)	fractional January throughput		F	5	3		0-1
Mthrput(2)	fractional February throughput		F	5	3		0-1
Mthrput(3)	fractional March throughput		F	5	3		0-1
Mthrput(4)	fractional April throughput		F	5	3		0-1
Mthrput(5)	fractional May throughput		F	5	3		0-1
Mthrput(6)	fractional June throughput		F	5	3		0-1
Mthrput(7)	fractional July throughput		F	5	3		0-1
Mthrput(8)	fractional August throughput		F	5	3		0-1
Mthrput(9)	fractional September throughput		F	5	3		0-1
Mthrput(10)	fractional October throughput		F	5	3		0-1
Mthrput(11)	fractional November throughput		F	5	3		0-1
Sthrput(4)	winter throughput	%	I	3			0-100
Sthrput(1)	spring throughput	%	I	3			0-100
Sthrput(2)	summer throughput	%	I	3			0-100
Sthrput(3)	autumn throughput	%	I	3			0-100
Hours	diurnal operation code		I	2		F	1-69
Days	weekly operation code		I	2		F	

Entity	stack.pt.{stid}
Description	stack data
Source	EMS-95 or supplied
Destination	pttap
Location	$FS_LOC

Attribute	Description	Units	Type	Len	Precision	Key	Acceptable values
Stid	state code		I	2		P	1-8
Fcid	facility ID		A	15		P	
Stkid	stack ID		A	12		P	
Diam	inside stack diameter	m	F	8	4		
Heit	stack height above ground	m	F	7	2		
Temp	exit temperature	°C	F	7	2		
Veloc	exit velocity	m/s	F	10	2		
Lat	stack latitude	°	F	8	3		
Long	stack longitude	°	F	8	3		
Scc	source classification code		A	8		F	

area source model

Entity	area.ar.{stid}
Description	area source emission foundation file
Source	EMS-95 or supplied
Destination	areatap
Location	$FS_LOC

Attribute	Description	Units	Type	Len	Precision	Key	Acceptable values
Stid	state code		I	2		P	1-8
Lgaid	local government area code		I	3		P	
Asct	area source category		A	15		P	
Polid	pollutant ID		A	5		P	
Acee	actual emission	t/yr	E	13	6		

Entity	areatprl.ar.{stid}
Description	area source temporal data
Source	EMS-95 or supplied
Destination	areatap
Location	$FS_LOC

Attribute	Description	Units	Type	Len	Precision	Key	Acceptable values
Stid	state code		I	2		P	1-8
Asct	area source category		A	15		P	
Mthrput(12)	fractional December throughput		F	5	3		0-1
Mthrput(1)	fractional January throughput		F	5	3		0-1
Mthrput(2)	fractional February throughput		F	5	3		0-1
Mthrput(3)	fractional March throughput		F	5	3		0-1
Mthrput(4)	fractional April throughput		F	5	3		0-1
Mthrput(5)	fractional May throughput		F	5	3		0-1
Mthrput(6)	fractional June throughput		F	5	3		0-1
Mthrput(7)	fractional July throughput		F	5	3		0-1
Mthrput(8)	fractional August throughput		F	5	3		0-1
Mthrput(9)	fractional September throughput		F	5	3		0-1
Mthrput(10)	fractional October throughput		F	5	3		0-1
Mthrput(11)	fractional November throughput		F	5	3		0-1
Sthrput(4)	winter throughput	%	I	3			0-100
Sthrput(1)	spring throughput	%	I	3			0-100
Sthrput(2)	summer throughput	%	I	3			0-100
Sthrput(3)	autumn throughput	%	I	3			0-100
Hours	diurnal operation code		I	2		F	1-69
Days	weekly operation code		I	2		F	

Entity	arscale.ar.{stid}
Description	area source scaling factors
Source	user
Destination	areascal
Location	$FS_LOC

Attribute	Description	Units	Type	Len	Precision	Key	Acceptable values
Stid	state code		I	2		P	1-8
Asct	area source category		A	15		P	
Polid	pollutant ID		A	5		P	
Arsf	area source scaling factor		F	4	2		

Entity	srgratio.ar.{stid}.{gridid}
Description	area source spatial surrogate ratio
Source	EMS-95 or supplied
Destination	areatap
Location	$FS_GRD

Attribute	Description	Units	Type	Len	Precision	Key	Acceptable values
Stid	state code		I	2		P	1-8
Gridid	grid ID		I	2		P	
Lgaid	local government area code		I	3		P	
Ssc	spatial surrogate code		A	3		P	
Icell	x axis cell index		I	3		P	
Jcell	y axis cell index		I	3		P	
Ratio	spatial surrogate ratio		E	13	6		0-1

biogenic source model

Entity	gridlulc.bio.{stid}.{gridid}
Description	gridded land use data
Source	EMS-95 or supplied
Destination	becp
Location	$FS_GRD

Attribute	Description	Units	Type	Len	Precision	Key	Acceptable values
Stid	state code		I	2		P	1-8
Gridid	grid ID		I	2		P	
Lgaid	local government area code		I	3		P	
Lucode	land use code		A	3		P	
Icell	x axis cell index		I	3		P	
Jcell	y axis cell index		I	3		P	
Luarea	land use area in the cell	ha	F	11	1		

Entity	secout.bio.{stid}
Description	biogenic emission flux
Source	EMS-95 or supplied
Destination	becp
Location	$FS_LOC

Attribute	Description	Units	Type	Len	Precision	Key	Acceptable values
Folcov	foliage cover density		A	1		P	L, M, H
Stid	state code		I	2		P	1-8
Lgaid	local government area code		I	3		P	
Lucode	land use code		A	3		P	
Polid	pollutant ID		A	5		P	
Cantyp	canopy type		A	1		P	C, D, N, F, G
Emflux	bioemission flux	µg/ha/hr	E	13	6		

motor vehicle model

Entity	adjstrvp.{stid}
Description	RVP adjustment
Source	supplied
Destination	mveep_f1
Location	$FS_LOC

Attribute	Description	Units	Type	Len	Precision	Key	Acceptable values
Stid	state code		I	2		P	1-8
Date_start	start date	dd/mm	A	5		P	
Date_end	end date	dd/mm	A	5		P	
Arvp	RVP adjustment factor		F	4	2		

Entity	adjstvkt.mv.{stid}
Description	seasonal and daily VKT adjustment factors
Source	EMS-95 or supplied
Destination	mveep_p1, mpeep_p1
Location	$FS_LOC

Attribute	Description	Units	Type	Len	Precision	Key	Acceptable values
Stid	state code		I	2		P	1-8
Avktd(1)	VKT adjustment factor for Monday		F	4	2		0-1
Avktd(2)	VKT adjustment factor for Tuesday		F	4	2		0-1
Avktd(3)	VKT adjustment factor for Wednesday		F	4	2		0-1
Avktd(4)	VKT adjustment factor for Thursday		F	4	2		0-1
Avktd(5)	VKT adjustment factor for Friday		F	4	2		0-1
Avktd(6)	VKT adjustment factor for Saturday		F	4	2		0-1
Avktd(7)	VKT adjustment factor for Sunday		F	4	2		0-1
Avktm(1)	VKT adjustment factor for January		F	4	2		0-1
Avktm(2)	VKT adjustment factor for February		F	4	2		0-1
Avktm(3)	VKT adjustment factor for March		F	4	2		0-1
Avktm(4)	VKT adjustment factor for April		F	4	2		0-1
Avktm(5)	VKT adjustment factor for May		F	4	2		0-1
Avktm(6)	VKT adjustment factor for June		F	4	2		0-1
Avktm(7)	VKT adjustment factor for July		F	4	2		0-1
Avktm(8)	VKT adjustment factor for August		F	4	2		0-1
Avktm(9)	VKT adjustment factor for		F	4	2		0-1

	September				
Avktm(10)	VKT adjustment factor for October	F	4	2	0-1
Avktm(11)	VKT adjustment factor for November	F	4	2	0-1
Avktm(12)	VKT adjustment factor for December	F	4	2	0-1

Entity	fracvktu.mv.{stid}
Description	temporal VKT profile
Source	EMS-95 or supplied
Destination	mveep_p1
Location	$FS_LOC

Attribute	Description	Units	Type	Len	Precision	Key	Acceptable values
Stid	state code		I	2		P	1-8
Day	weekday, Saturday or Sunday		I	2		P	1,6,7[a]
Frcvkt(1)	VKT factor for hour 0-1		F	5	3		0-1
Frcvkt(2)	VKT factor for hour 1-2		F	5	3		0-1
Frcvkt(3)	VKT factor for hour 2-3		F	5	3		0-1
Frcvkt(4)	VKT factor for hour 3-4		F	5	3		0-1
Frcvkt(5)	VKT factor for hour 4-5		F	5	3		0-1
Frcvkt(6)	VKT factor for hour 5-6		F	5	3		0-1
Frcvkt(7)	VKT factor for hour 6-7		F	5	3		0-1
Frcvkt(8)	VKT factor for hour 7-8		F	5	3		0-1
Frcvkt(9)	VKT factor for hour 8-9		F	5	3		0-1
Frcvkt(10)	VKT factor for hour 9-10		F	5	3		0-1
Frcvkt(11)	VKT factor for hour 10-11		F	5	3		0-1
Frcvkt(12)	VKT factor for hour 11-12		F	5	3		0-1
Frcvkt(13)	VKT factor for hour 12-13		F	5	3		0-1
Frcvkt(14)	VKT factor for hour 13-14		F	5	3		0-1
Frcvkt(15)	VKT factor for hour 14-15		F	5	3		0-1
Frcvkt(16)	VKT factor for hour 15-16		F	5	3		0-1
Frcvkt(17)	VKT factor for hour 16-17		F	5	3		0-1
Frcvkt(18)	VKT factor for hour 17-18		F	5	3		0-1
Frcvkt(19)	VKT factor for hour 18-19		F	5	3		0-1
Frcvkt(20)	VKT factor for hour 19-20		F	5	3		0-1
Frcvkt(21)	VKT factor for hour 20-21		F	5	3		0-1
Frcvkt(22)	VKT factor for hour 21-22		F	5	3		0-1
Frcvkt(23)	VKT factor for hour 22-23		F	5	3		0-1
Frcvkt(24)	VKT factor for hour 23-24		F	5	3		0-1

a) 1 – weekday, 6 – Saturday, 7 - Sunday

Entity	linecoord.mv.{stid}.{gridid}
Description	coordinates of major roads
Source	supplied
Destination	mpeep_f1
Location	$FS_GRD

Attribute	Description	Units	Type	Len	Precision	Key	Acceptable values
Stid	state code		I	2		P	1-8
Gridid	grid ID		I	2		P	
Linkid	link identifier		I	7		P	
Rdtype [a,b]	road type ID		I	1		P	
Icell	x axis cell index		I	3			
Jcell	y axis cell index		I	3			
Lat_from	latitude of the from-node	°	F	11	6		
Long_from	longitude of the from-node	°	F	11	6		
Lat_to	latitude of the to-node	°	F	11	6		
Long_to	longitude of the to-node	°	F	11	6		

a) For NSW; 1 – freeway, 2 – arterial, 3 –commercial arterial, 4 – commercial highway, 9 –residential
b) For Victoria; 1 – freeway, 2 – arterial, 9 –residential

Entity	linehrvkt.mv.{stid}						
Description	hourly VKT data for major roads						
Source	supplied						
Destination	mpeep_p1						
Location	$FS_LOC						
Attribute	Description	Units	Type	Len	Precision	Key	Acceptable values
Stid	state code		I	2		P	1-8
Linkid	link identifier		I	7		P	
Day	weekday, Saturday or Sunday		I	2		P	1,6,7[a]
Hour	hour		I	2		P	1-24
Vkt	VKT	km/day	E	13	6		

a) 1 – weekday, 6 – Saturday, 7 - Sunday

Entity	linemvee.mv.{stid}
Description	emissions on major roads
Source	supplied
Destination	mpeep_p1
Location	$FS_LOC

Attribute	Description	Units	Type	Len	Precision	Key	Acceptable values
Stid	state code		I	2		P	1-8
Polid	pollutant ID		A	5		P	
Mvproces	emission classification for speciation		A	3		P	EX, EV[b]
Techtype	fuel type used in process		I	1		P	1-3[c]
Linkid	link identifier		I	7		P	
Day	weekday, Saturday or Sunday		I	2		P	1,6,7[a]
Hour	hour		I	2		P	1-24
Ee	emission estimate for an hour	kg	F	9	3		

a) 1 – weekday, 6 – Saturday, 7 - Sunday
b) EX – exhaust, EV – evaporative
c) 1 – petrol, 2 – diesel, 3 – LPG

Entity	mbsafnd.mv.{stid}
Description	emission factors for CO, NOx and VOC
Source	EMS-95 or supplied
Destination	mveep_f1
Location	$FS_LOC

Attribute	Description	Units	Type	Len	Precision	Key	Acceptable values
Stid	state code		I	2		P	1-8
Tempf	temperature	°F	I	8		P	
Polid	pollutant ID		A	5		P	
Mvproces	emission classification for speciation		A	3		P	EX, EV
Techtype	fuel type used in process		I	1		P	1-3
Rdtype	road type ID		I	1		P	
Ef	composite emission factor	g/km	E	13	6		

Entity	mbsafo.mv.{stid}
Description	emission factors for other pollutants
Source	EMS-95 or supplied
Destination	mveep_p2, mpeep_p1
Location	$FS_LOC

Attribute	Description	Units	Type	Len	Precision	Key	Acceptable values
Stid	state code		I	2		P	1-8
Polid	pollutant ID		A	5		P	
Mvproces	emission classification for speciation		A	3		P	EX, EV
Techtype	fuel type used in process		I	1		P	1-3
Rdtype	road type ID		I	1		P	
Ef	composite emission factor	g/km	E	13	6		

Entity	mbsp.mv.{stid}
Description	motor vehicle toxics speciation
Source	EMS-95
Destination	mveep_p2, mpeep_p1
Location	$FS_LOC

Attribute	Description	Units	Type	Len	Precision	Key	Acceptable values
Stid	state code		I	2		P	1-8
Mvproces	emission classification for speciation		A	3		P	EX, EV
Techtype	fuel type used in process		I	1		P	1-3
Species	species		A	5		P	
Fraction	mass fraction		E	13	6		0-1

Entity	mvonoff.mv.{stid}.{gridid}
Description	gridded VKT data
Source	EMS-95 or supplied
Destination	mveep_p1
Location	$FS_GRD

Attribute	Description	Units	Type	Len	Precision	Key	Acceptable values
Stid	state code		I	2		P	1-8
Gridid	grid ID		I	2		P	
Rdtype	road type ID		I	1		P	
Icell	x axis cell index		I	3		P	
Jcell	y axis cell index		I	3		P	
Vkt	VKT	km/day	E	13	6		

wildfire and prescribed burning model

Entity	fireact.ar.{stid}
Description	wildfire or prescribed burning activity data
Source	EMS-95 or supplied
Destination	firesrc
Location	$FS_LOC

Attribute	Description	Units	Type	Len	Precision	Key	Acceptable values
Firekey	unique identifier for a fire event		A	11		P	
Asct	area source code		A	15			2810001000 for wildfire, 2810015000 for prescribed burning
Lat	latitude of fire	°	F	8	3		
Long	longitude of fire	°	F	8	3		
Firesize	area burnt	ha	F	7	1		
Strttime	time the fire starts	hh:mm	A	5			
Strtdate	day the fire starts	dd/mm/yyyy	A	10			
Fuelload	fuel load	t/ha	F	8	3		

Entity	firefac.ar
Description	wildfire or prescribed burning emission factors
Source	EMS-95 or supplied
Destination	firesrc
Location	$FS_SYS

Attribute	Description	Units	Type	Len	Precision	Key	Acceptable values
Asct	area source code		A	15		P	2810001000 for wildfire, 2810015000 for prescribed burning
Phase	phase of burning		A	1		P	F = flaming, S = smouldering
Polid	pollutant ID		A	5		P	
Acef	emission factor	kg/t	E	13	6		

APPENDIX A EMS-95 CONVERSION PROGRAMS

Some of the input files for the Emission Inventory Model are generated from EMS-95. The following table lists the programs that convert the EMS-95 files for the EIM. The programs are written in SAS or ARC/INFO and in the directory $EMS_BIN/forecast on the Unix network of EPA Victoria.

EIM Input Files	EMS-95 Files	Model	Conversion Program
adjstvkt.mv	adjstvmt.ssd01	motor vehicle	aqfs_st.sas
amg.dat	%grid%	wildfire & prescribed burning	aqfs_grd.aml
area.ar	area.ssd01	area source	aqfs_st.sas
areatprl.ar	areatprl.ssd01	area source	aqfs_st.sas
arscale.ar	user-supplied	area source	none
ascd.in	ascd.ssd01	area source	aqfs_st.sas
emission.pt	emission.ssd01	point source	aqfs_st.sas
fireact.ar	fireact.ssd01	wildfire & prescribed burning	aqfs_st.sas
firefac.ar	firefac.ssd01	wildfire & prescribed burning	aqfs_sys.sas
fracvktu.mv	fracvmtd.ssd01	motor vehicle	aqfs_st.sas
fuelload.ar	gridlulc.ssd01	wildfire & prescribed burning	aqfs_grd.sas
griddesc.in[a]	run_desc.ssd01	all models	aqfs_gds.sas
gridlulc.bio	gridlulc.ssd01	biogenic	aqfs_grd.sas
holiday.in	user-supplied	point source, area source and motor vehicle	none
hourprof.in	hourprof.in	point source, area source	none
latlon.in	latlon.dat	area source, biogenic, motor vehicle	aqfs_grd.sas
mbsafnd.mv	m4safnd.ssd01	motor vehicle	aqfs_st.sas
mbsafo.mv	mbsafo.ssd01	motor vehicle	aqfs_st.sas
mbsp.mv	mbsp.ssd01	motor vehicle	aqfs_st.sas
metdata.in	from LAPS	area source, biogenic, motor vehicle	none
mvonoff.mv	mvonoff.ssd01	motor vehicle	aqfs_grd.sas
profile.in	profile.ssd01, profilpm.ssd01[a]	all models	aqfs_sys.sas
ptgrid.pt	ptsorprc.ssd01	point source	aqfs_grd.sas
pttprl.pt	device.ssd01	point source	aqfs_st.sas
rdclass.mv	facclas.ssd01	motor vehicle	aqfs_sys.sas
run_desc.in	user-supplied	all models	none
scbmd.in	scbmd.ssd01, scbmdpm.ssd01[b]	all models	aqfs_sys.sas

EIM Input Files	EMS-95 Files	Model	Conversion Program
secout.bio	secout.ssd01	biogenic	aqfs_bg.sas
spprcr.ar	spprcr.ssd01	area source	aqfs_sys.sas
spprcr.mv	spprcr.ssd01	motor vehicle	aqfs_sys.sas
spprcr.pt	spprcr.ssd01	point source	aqfs_sys.sas
srgratio.ar	srgratio.ssd01	area source	aqfs_grd.sas
ssad.in	ssad.ssd01	area source	aqfs_st.sas
stack.pt	stack.ssd01	point source	aqfs_st.sas
weeklyop.in	weeklyop.in	point source, area source	none

a) Used by aqfs_grd.sas to reference gridid. Note that aqfs_gds.sas should be run before aqfs_grd.sas to generate the cross-reference of gridid and gridnam.

b) Generated from spldpm_fs.sas.

Appendix 3.5 Biogenic Emissions from Trees and Grasses – improvements to emission inventories

Summary prepared by Peter Nelson, CSIRO Energy Technology

Background

Emissions of biogenic organic compounds from vegetation play an important role in photochemical smog formation, and the trace chemistry of the atmosphere. Background concentrations of ozone are directly determined by these emissions, so that an accurate estimate of biogenic fluxes into urban airsheds is an important requirement for an air quality forecasting system.

There is a need to improve emission estimates of isoprene and other non-methane hydrocarbons (NMVOCs) from Australian trees and grasses, and, ultimately, to refine emission inventories for biogenic emissions. The MAQS inventory developed by Carnovale and co-workers recognised that estimates of biogenic emissions for Australian air sheds such as Sydney and Melbourne had large uncertainties as a consequence of the relatively small data set used to derive these estimates.

NSW EPA, as part of its contribution to AAQFS project, supported CSIRO to conduct a scoping study of biogenic emissions from trees and grasses. A summary of the results is given here, and more detail is available in reports by Nelson *et al.* (2000) and Galbally *et al.* (2000). Future work on this important aspect of airshed modelling in Australia will continue through an Environmental Research Trust Grant, administered by the NSWEPA, recently granted to CSIRO.

Emissions from Trees

Scope

Emissions of isoprene and monoterpenes were determined from three Australian eucalypt species. The species were an Argyle Apple (*Eucalyptus cineria*), a Forest Red Gum, (*Eucalyptus tereticornis*) and a Broad-leaved Scribbly Gum (*Eucalyptus haemastoma*).

Measurements were made on large branches of mature trees. The trees had not been grown under controlled conditions, but were "real world" specimens. Two enclosure methods were used: a flexible bag, and a fixed frame chamber (see Figure 1). In both cases the enclosure material was PTFE teflon. The enclosures were ventilated with ambient air to control temperatures to near ambient conditions. Concentrations of CO_2, NO_x, O_3 and NMVOC were monitored continuously with gas analysers. Grab samples were collected for subsequent analysis by GC/MS to determine concentrations of isoprene and various monoterpenes and oxygenated hydrocarbons. Physical parameters such as temperature and photosynthetically active radiation (PAR) were also monitored.

Results

1. Diurnal variations

There is a very close relationship between isoprene, monoterpene and NMVOC emissions from the trees and PAR (illustrated in Figure 2). This is especially apparent for some measurements over a three-day period, which shows that emissions of biogenic species decrease to near zero during the evenings, but reach similar levels during the middle of each day.

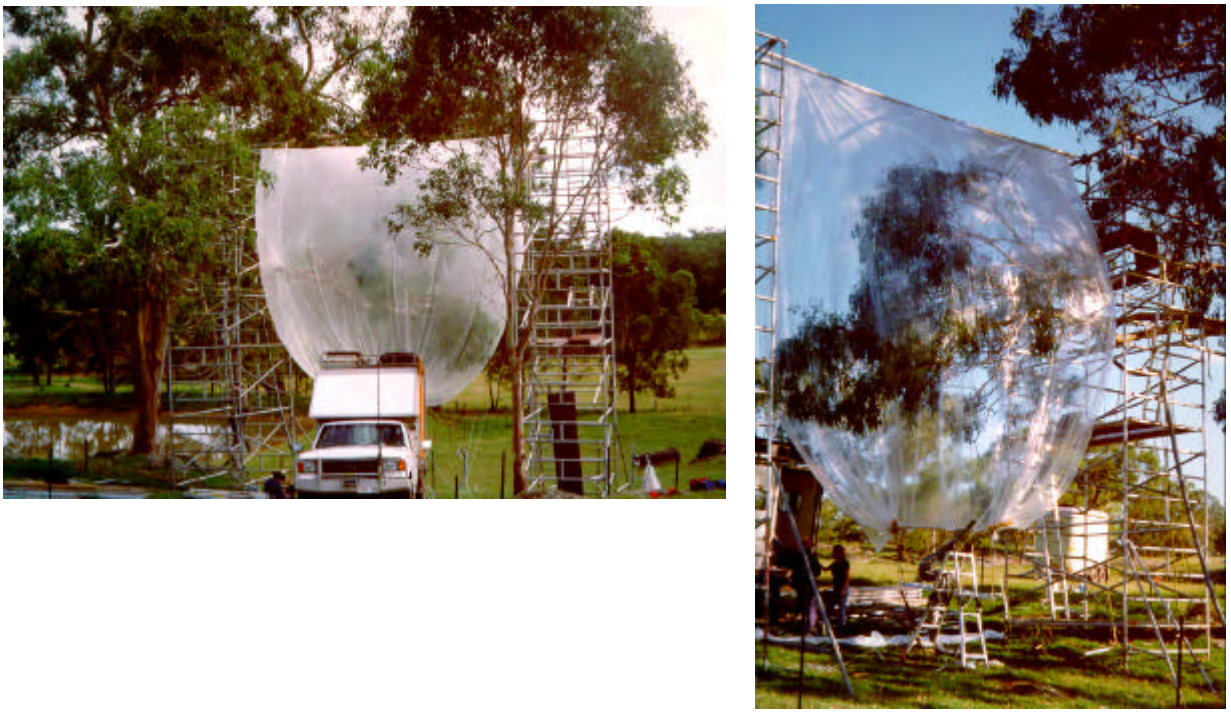

Figure 1: Measuring emissions from eucalypt trees

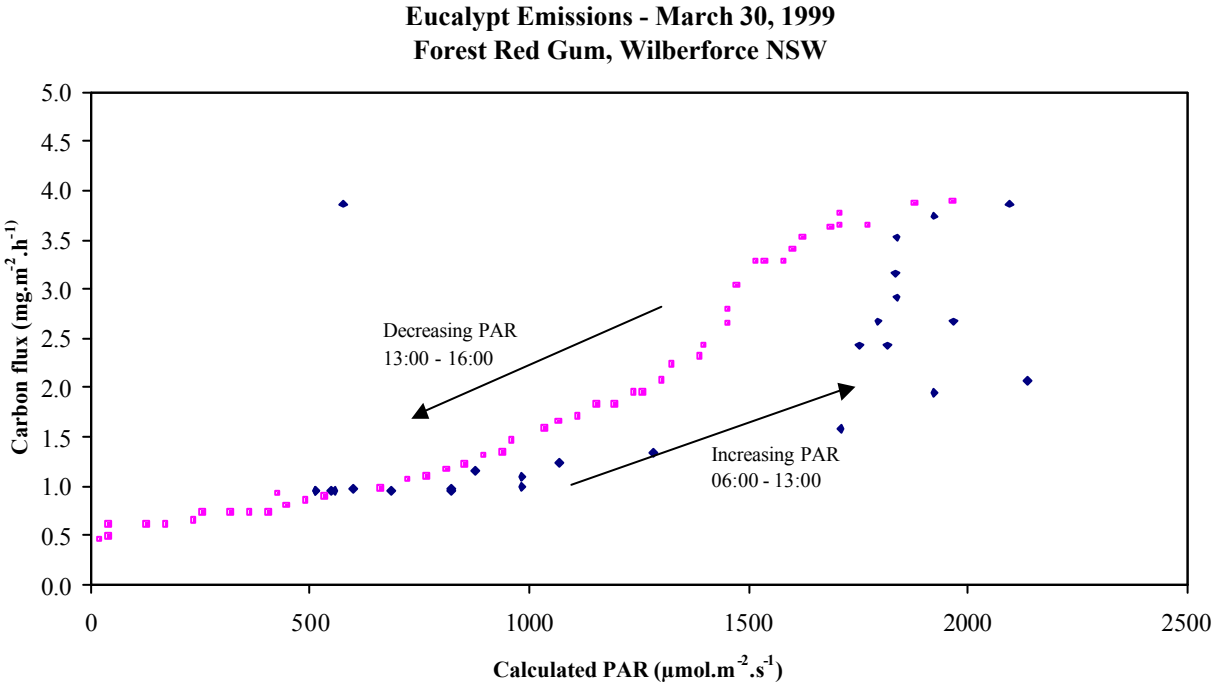

Figure 2: Total non-methanic hydrocarbons emissions and total solar radiation

2. Isoprene and monoterpene compounds observed

Terpenes and oxygenated hydrocarbons detected in emissions from the three tree species are given below. The major compounds (>10% of the non-isoprenoid mass) are underlined. Some oxygenated species were detected in the emissions from *Eucalyptus tereticornis*.

Species	Monoterpenes	Oxygenated hydrocarbons
Eucalyptus cinerea	α-pinene 1,8-cineole (eucalyptol)	
Eucalyptus tereticornis	α-pinene β-pinene cymene β-phellandrene 1,8-cineole β-ocimene δ-terpinene terpinolene	n-octanol acetophenone unknown oxygenate
Eucalyptus haemastoma	α-pinene camphene β-pinene myrcene cymene 1,8-cineole δ-terpinene terpinolene	

There was some variation in the monoterpene composition, apparently related to temperature. The monoterpenes also contributed proportionately more to total biogenic emissions during periods of low PAR (ie early morning and late evening). However, in spite of these variations in the composition and relative emissions of the various monoterpenes, isoprene was always the major contributor to total hydrocarbon fluxes in the middle of the day when total emissions are highest for all species tested. Isoprene contributions to total hydrocarbon fluxes on a mass basis, at times of peak emission during the middle of the day varied from ~85% for Eucalyptus cinerea (Argyle Apple), to 96-99% for Eucalyptus tereticornis (Forest Red Gum), to 88-95% for Eucalyptus haemastoma (Broad-leaved Scribbly Gum).

3. Emission Fluxes

The observed fluxes for isoprene lie in the range from 0.7–3.8 mg m^{-2} h^{-1} (see Figure 2) depending on the species. It is important to note that these emissions are, in a real sense, "real-world emissions", and represent an integration of a large number of leaves of varying age, health and orientation. Previous studies have often used single leaves, or a small number, of cultivated plants and performed measurements under very controlled conditions of temperature and radiation.

These fluxes are broadly consistent with normalised emission fluxes reported in the small number of previous studies of eucalypt species.

Conclusions

The results provide an initial data set for refining inventory estimates of biogenic emissions from Australian vegetation, but, at present, need to be combined with previous data to allow for the effects of temperature and radiation on emissions.

This study also suggests some ideas for future work:

- An increase in the species coverage, perhaps with a simpler enclosure method to allow for screening of a large number of species
- Area-based measurements, using instrumented meteorological towers and rapid response analysers, to determine fluxes.
- Development of a refined emission inventory module for the Sydney region, and other Australian cities

Emissions from Grasses

A brief study of the emission rates of volatile organic compounds (VOCs) from an undisturbed Buffalo grass sward and grass cuttings from mown Buffalo grass was undertaken to examine the importance of these emissions in urban air pollution.

At the commencement of this study, a site at CSIRO Atmospheric Research, Aspendale was instrumented with an automatic flux chamber, three bases set into a well established lawn of buffalo grass, a radiometer, temperature sensors, wind speed and direction anemometer, a total non-methane hydrocarbon (NMHC) analyser and a carbon dioxide analyser operated out of a field laboratory. Figure 3 shows the setup.

Figure 3: Measuring grass emissions

Following a period of exploratory studies in March and April 1999, further work was conducted on volatile organic compounds (VOCs) emitted from the buffalo grass during the period November 1999 to February 2000 inclusive.

The measurements during December 1999 and January 2000 made with the NMHC analyser showed no VOC emissions from the grass. Following this result, emission measurements from undisturbed grass were made by the GC-FID technique on seven separate days. The species measured were

identified by gas chromatography mass spectrometry analysis (GC-MS). An average emission rate of 111 μg (C) m^{-2} h^{-1}, range 24 to 274 μg (C) m^{-2} h^{-1}, was observed. The major species emitted were acetone and furan.

A second experiment conducted in February 2000 consisted of cutting the buffalo grass with a typical domestic lawnmower, and measuring the emissions of VOCs from the cut grass. The emissions from the cut grass far exceeded those from the undisturbed grass being approximately 100 times larger. These emissions from cut grass were tracked using both the NMHC analyser and flask sampling with GC-FID analyses for one or more days after the cutting, in one case for ten days. The integrated emissions over these 10 days were 800 μg (C) per gram dry weight of grass. Seven compounds were identified that account for about two thirds of these emissions.

These observations indicate the importance of VOC emissions from grasses into the urban atmosphere. However the observations are made over a limited time and over only one grass species. Further studies are needed to extend these results.

References

Galbally I.E. et al. (2000) Biogenic volatile organic compound emissions from grasses, Report to the New South Wales Environment Protection Authority, CSIRO Atmospheric Research Aspendale, Victoria, May 2000, 15 pp.

Nelson P.F. Nancarrow P.C. Halliburton B.C. Tibbett A.R. Chase D. and Trieu T. (2000) Biogenic emissions from trees and grasses. Final Report to EPA of New South Wales, June 2000. CSIRO Energy Technology Investigation report ET/IR297, 63 pp.

Appendix 5.1 The Generalized Reaction Scheme (GRS) Model

Photochemical Smog Modelling Using The Generalized Reaction Scheme (GRS) Model

Merched Azzi, Martin Cope and Peter F. Nelson

CSIRO Energy Technology

Introduction

Atmospheric oxidation of volatile or reactive organic compounds (VOCs or ROCs) in the presence of oxides of nitrogen (NO_x) leads to the formation of oxidant species, such as ozone and peroxyacetyl nitrate (PAN). Numerical simulations of the chemical processes occurring in this oxidation are an important component of urban airshed models.

Development of a detailed kinetic model for these processes is challenging due to the large number of VOCs present in polluted atmospheres, and the large number of oxidation pathways and products. All important species should be represented, but the computing time becomes excessive when time-dependent profiles for a large number of species over a fine spatial grid have to be calculated. In the context of the present project, for example, long computing times are not compatible with the use of airshed models in pollutant forecasting.

Some simplification of the chemistry is, therefore, necessary. In the past a number of approaches have been taken to this problem. Moshiri and O'Brien (1984) proposed a simplified mechanism for predicting O_3 formation in photochemical smog systems:

HC + OH	?	$a$$RO_2$ + P	Hydrocarbon loss and product formation
P + OH	?	$b$$RO_2$ + loss	Product loss
P + hn	?	$c$$RO_2$ + loss	Product photolysis
RO_2 + NO	?	NO_2 + loss	NO photooxidation
NO_2 + hn	?	NO + O_3	Photostationary state
Everything	?	loss	Dilution

In this mechanism, HO_2 radicals are lumped with RO_2, and, to a first approximation, all RO_2 are assumed to react with NO. This mechanism does not predict the OH concentration, taking instead the quantity k_1[OH] as an input hydrocarbon reactivity parameter. Clearly this mechanism is highly simplified, but it can predict the major features of ozone formation.

More recent developments take a number of approaches to the problem, based on a lumping of the organic species together according to a variety of classifications. These approaches have been reviewed by Seinfeld (1988). Two of the chemical schemes most widely used for modelling ground-level ozone formation employ:

- A lumped molecule approach; this mechanism was developed by Carter and co-workers (Lurmann *et al*, 1987; Carter, 1990; Carter and Lurmann, 1991) at the University of California Riverside and has been described as the SAPRC or LCC mechanism
- A lumped structure approach developed by Gery *et al* (1989), described as the Carbon Bond (CB) Mechanism; various updates have been produced with version 4, CB-IV, being widely used; recent developments and revisions have led to CB99 (see description at http://airsite.unc.edu/soft/cb4/cb4main.html)

These two approaches are widely used in urban airshed models, but it is recognised that further refinements and improvements are both possible and desirable. For example, Jeffries' group at UNC and Michael Gery, at Atmospheric Research Assoc., Boston MA (ARA) have created a new kind of representation for organic species in air quality model photochemical reaction mechanisms. In addition to the normal molecules that appear in such mechanisms, reaction entities that have dynamic character or properties throughout the simulation have been introduced; these new entities are called "morphecules" (see http://airsite.unc.edu/atmchemunc/morpho/intro.html for a description of this approach).

Systematic mechanism reduction techniques have also been applied to this problem. Drawing on techniques developed for the modelling of combustion systems, semi-automatic techniques based on sensitivity analysis and the quasi-steady-state approximation (QSSA) have been used to derive greatly simplified chemical schemes which accurately represent the behaviour of chosen key species. Heard *et al* (1998) have produced a mechanism containing 59 reactions and 23 species which predicts ozone with acceptable accuracy compared to CB-IV. Further developments using reduction techniques can be anticipated.

Another approach, developed by Johnson, Azzi and co-workers at CSIRO is based on semi-empirical techniques. Using smog chamber experiments a set of reactions was developed (the Generalised Reaction Scheme, or GRS) to predict ozone formation and NO disappearance in chamber experiments. In this part of the AAQFS project the GRS mechanism is further developed to address some shortcomings, and in order to provide more accurate predictions of ozone in Australian urban airsheds.

The GRS version 1 (GRS) mechanism

The GRS mechanism (Azzi *et al*, 1992) is a simplified chemical scheme for predicting the rate of photochemical smog formation. It was developed from smog chamber data and has been used extensively as a model for screening calculations. The major advantages of the model are:

- it is based on experimental data
- it requires far less computer run time and chemical detail than do other more explicit chemical schemes.

The GRS model consists of seven reactions among seven species. These are:

ROC+hν	?	ROC+RP	(1)
RP+NO	?	NO_2	(2)
NO_2	?	$NO+O_3$	(3)
$NO+O_3$	?	NO_2	(4)
RP+RP	?	RP	(5)
$RP+NO_2$	?	Stable Gaseous Nitrogen (SGN)	(6)
$RP+NO_2$	?	Stable non Gaseous Nitrogen (SNGN)	(7)

where ROC are reactive organic compounds and RP are reactive products. The GRS mechanism was introduced as a reduced reaction scheme to describe photochemical smog formation in contrast to the more detailed chemical kinetics of the Carbon Bond IV (CB-IV) model. Consequently reactions (1), (2), (5), (6) and (7) are descriptive in nature whereas reactions (3) and (4) refer to fundamental chemical processes.

The GRS model has been tested in three ways namely by

- comparison with outdoor smog chamber data
- comparison with estimates from more detailed photochemical mechanisms; and
- incorporation into urban airshed models (UAM and CIT) and applications to different oxidant episodes from different locations.

These studies have shown that in urban atmospheres the GRS model predictions compared well with those obtained from field and smog chamber data. In rural atmospheres GRS does not compare well with predictions from more detailed models, such as CB-IV, as GRS was not developed for these conditions. In addition, air pollution controls over the past decade have reduced HC/NO_x ratios to values as low as ~4 (ppmC/ppmV). Under these conditions GRS overestimates the ozone production by ~30%, while CB-IV underestimates this concentration by ~ 60%. GRS also has difficulties in reproducing the cross plume concentration patterns of NO_x and O_3 as NO-rich plumes are advected downwind and entrain ambient air. Consequently there is a need to extend the range of applicability of the GRS model.

The main reasons for the inability of GRS to cope with rural conditions are

- the different composition and reactivity of typical rural ROC compared to urban ROC
- the lack of a background radical production mechanism responsible for the initiation of photochemical smog production.

In urban atmospheres the main limitation of GRS is due to the description of radicals which are continuously produced as long as light is available. At low ROC/NO_x ratios the model may quickly consume the available NO_x and accelerate the production of ozone as has been observed in smog chamber data (equations (1), (2) and (3) above).

GRS2 development

In an attempt to overcome these limitations of GRS, an explicit treatment of key radical species has been added as well as direct ozone photolysis. The expanded model is referred to as the GRS2 model and consists of the reactions listed in Table 1.

The GRS2 model includes the main reactions for daytime ozone formation and the formation of OH radicals. The production of organic peroxy radicals RO_2, can be achieved by the oxidation reaction of hydrocarbons by OH. The product RO_2 would react with NO to produce NO_2, HO_2 and lower carbon hydrocarbons represented by RCHO.

Unlike the treatment of radical species in GRS where all radicals were lumped into one single radical named "RP", GRS2 has distinguished between the following major radical species OH, HO_2 and RO_2. The first two reactions from GRS have been expanded into reactions (1) to (5) in the GRS2 model. The photolysis reaction of NO_2 to produce O_3 and NO and the titration reaction of O_3 by NO were unchanged. Reactions (8), (9), (15) and (16) have been added to include ozone photolysis to produce OH radicals. These reactions that treat background ozone and OH are of great importance in rural conditions.

Reactions (6) and (7) in GRS have been written more explicitly as reactions (11), (12) and (13) to distinguish between formation of nitric acid, HNO_3, and the lumped peroxy nitrate species, PERNIT. The other chemical reactions were included to describe more fully the role of the radicals OH and HO_2.

Reactions (20) and (21) are gas phase decomposition reactions of the important toxic hydrocarbon, 1,3-butadiene. This species is emitted in motor-vehicle exhaust and from other industrial sources, and has a very high specific risk factor. However, it reacts relatively rapidly with both OH and O_3 and its atmospheric half-life is therefore short compared to that of other toxic species such as benzene. The AAQFS provides forecasts of the atmospheric concentrations of 1,3-butadiene based on the emissions inventory; hence inclusion of these reactions is essential to enable the atmospheric reactivity of 1,3-butadiene to be allowed for.

Atmospheric oxidation of sulphur dioxide is also important in predicting the concentrations of this criteria pollutant. Sulphur dioxide also plays an important role in secondary particle formation in the atmosphere, ultimately affecting PM_{10} and $PM_{2.5}$ concentrations. Reaction (22) was included to calculate the homogeneous oxidation of SO_2. This reaction proceeds by reaction of SO_2 with OH. It is recognised that atmospheric SO_2 oxidation is a more complex process than represented by reaction (22), involving both homogeneous and heterogeneous processes, but reaction (22) at least allows an estimate of the homogeneous pathway.

The GRS2 rate coefficients have largely been obtained from the literature and from those used in CB-IV, as noted in Table 1. The rate for reaction (1) was deduced from outdoor smog chamber experiments in a similar way to that previously used for GRS1. Reaction (2) represents the oxidation of NO by RO_2 to produce NO_2, together with fractional amounts (α and β respectively) of the radical and reactive species HO_2 and RCHO. The values of the coefficients α and β were chosen to reproduce the best GRS2 results for ozone, NO and NO_2 when compared to measurements from the selected smog chamber experiments.

To evaluate the GRS2 model performance a series of outdoor smog chamber experiments were selected to cover a wide range of urban atmospheric conditions. These experiments were performed in the CSIRO Outdoor Smog Chamber Facility at North Ryde. Details of the experiments have been reported elsewhere (Hess *et al* 1992; Johnson 1993). Briefly, a mix of hydrocarbon species was used for these experiments including an exhaust surrogate, and petrol and solvent components. The initial conditions are given in Table 2. ROC/NO_x ratios for these experiments varied in the range from 3.6–15.6. These conditions thus represent a very broad test of the model's ability to predict pollutant concentrations. Presently, most urban airsheds

would operate with ROC/NO_x ratios less than 9; this is certainly true for Sydney and Melbourne, the first two cities for which the AAQFS was demonstrated. The first evaluation of the performance of GRS2 compared to the smog chamber results for stable pollutant species, and to that of GRS and CB-IV for these species and other radical species for which no measurements are available, is given in Figures 1 to 8 below .

Table 1: GRS2 kinetic parameters (cm ^{3} molecule $^{-1}$ s $^{-1}$ units)

#	Reaction	A (units depend on order)	Ea/R	k_{298}	Comments
1	ROC + hv = HO2 + RO2 + ROC	k_6*FTT*tivity*2			Complex function derived from smog chamber experiments
2	RO2 + NO = NO2 + 0.1*HO2 + 0.5*RCHO	5.30E-12	-360	1.77389E-11	CB-IV_99; reaction rate for C2O3 + NO = NO2 + XO2 + HCHO + HO2; fitted values for HO2 and RCHO co-efficients
3	HO2 + NO = NO2 + OH	3.70E-12	-242	8.33458E-12	CBIV
4	ROC + OH = RO2	1.00E-11		1E-11	CBIV
5	RCHO + OH = C2O3	1.68E-11	559	2.5742E-12	Rate taken from Seinfeld (1986) for RH + OH + RO2 + H2O
6	NO2 + hv = NO + O3	radiation dependent			
7	NO + O3 = NO2	2.00E-12	1400	1.82272E-14	CB-IV 99
8	O3 + hv = O(1D)	radiation dependent			
9	O(1D)+ H2O = OH + OH	2.20E-10		2.20E-10	CB-IV
10	O3 + HO2 = OH	1.10E-14	580	1.5708E-15	CB-IV
11	C2O3 + NO2 = PERNIT	2.63E-12	-380	9.41356E-12	CB-IV; Rate for PERNIT=PAN
12	PERNIT = NO2 + C2O3	2.00E+16	13500	0.000423268	CB-IV; Rate for PERNIT=PAN
13	OH + NO2 = HNO3	1.00E-12	-713	1.09421E-11	CB-IV
14	HO2 + HO2 = H2O2	5.90E-14	-1150	2.79783E-12	CB-IV
15	O(1D) = O	1.92E-11	-126	2.93E-11	CB-IV
16	O=O3	6.0E-34 * ((1/T)$^{-2.3}$)			CBIV
17	H2O2=2OH	radiation dependent			
18	OH+H2O2=HO2	2.90E-12	160	1.70E-12	CBIV
19	RO2+HO2=ROOH	5.60E-12			Seinfield (1986)
20	C4H6+OH=P1	1.48E-11	-448	6.66E-11	
21	C4H6+O3=P2	1.34E-14	2283	6.31E-18	
22	SO2+OH=HOSO2	9.00E-13		9.00E-13	DeMore et al (1997)

Table 2: Summary of initial gas compositions for CSIRO smog chamber runs used to test GRS2 model performance

Experiment	Total HC (ppmC)	NO (ppmv)	NO_2 (ppmv)	HC (ppmC)/NO_x (ppmv)
102L	0.76	0.06	0.0016	12.3
102P	0.637	0.0665	0.0016	9.3
134L	1.176	0.121	0.002	9.6
134P	1.176	0.0721	0.0033	15.6
137L	1.176	0.116	0.0056	9.7
137P	0.588	0.163	0.0069	3.5
138L	1.176	0.118	0.004	9.6
138P	0.588	0.118	0.004	4.8

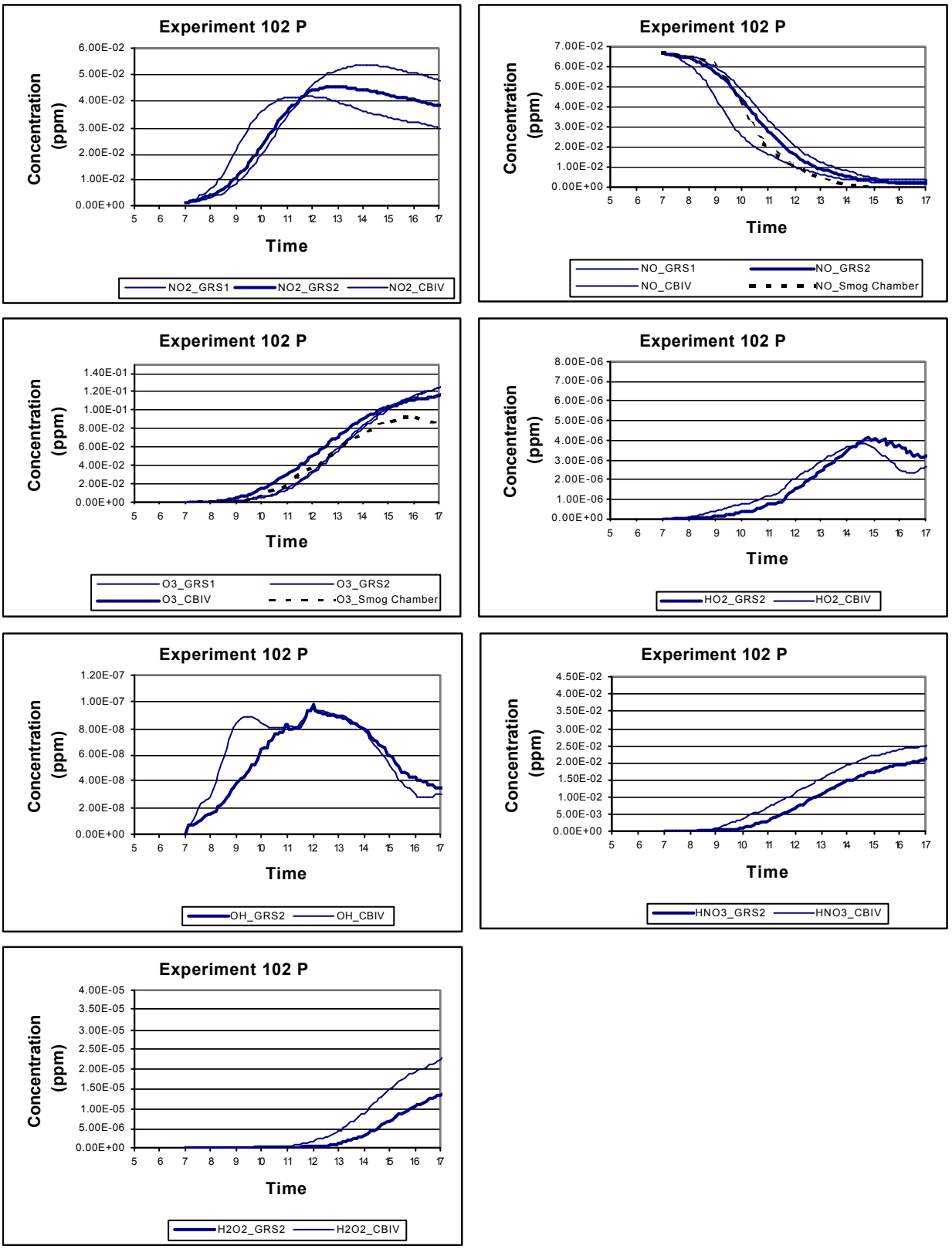

Figure 1: Comparison of measurements from smog chamber 102 P experiment with model predictions

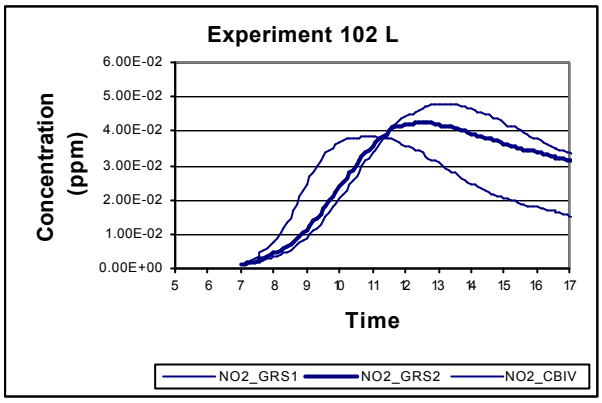

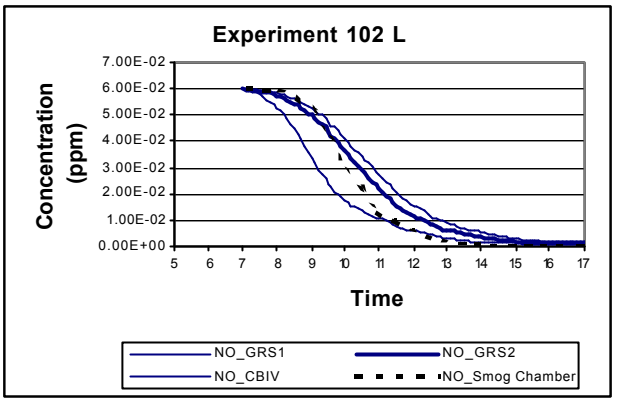

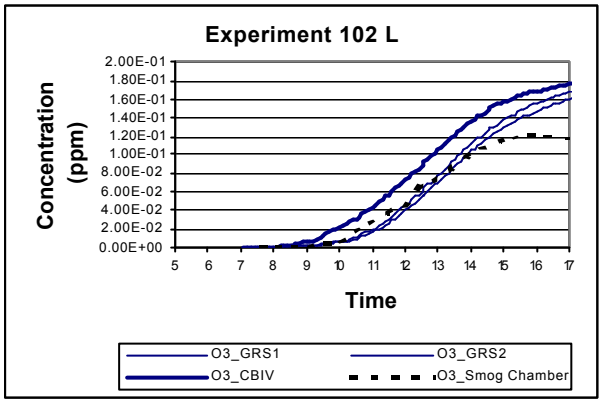

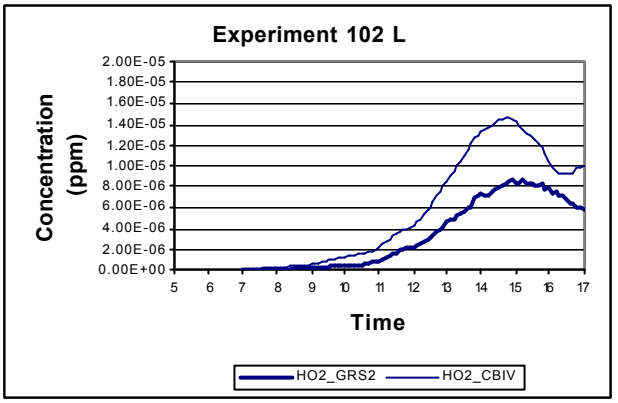

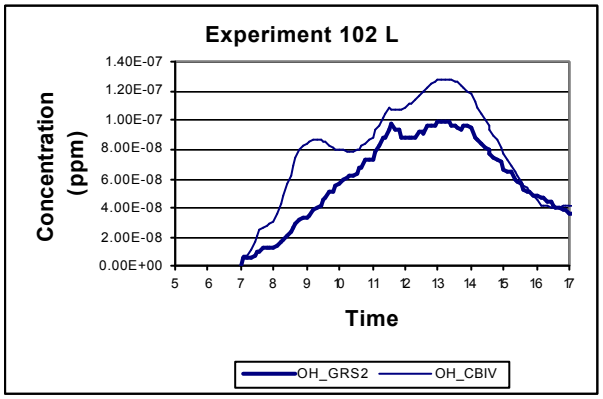

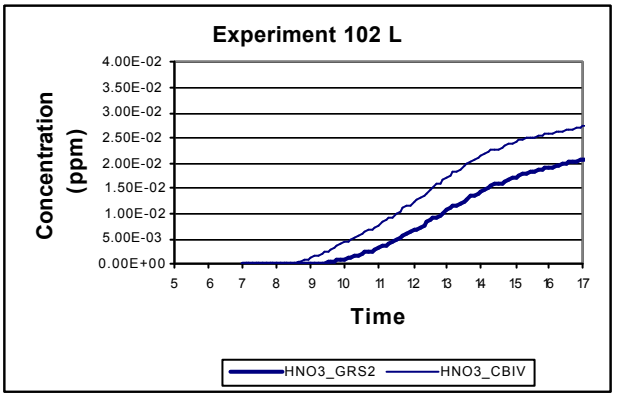

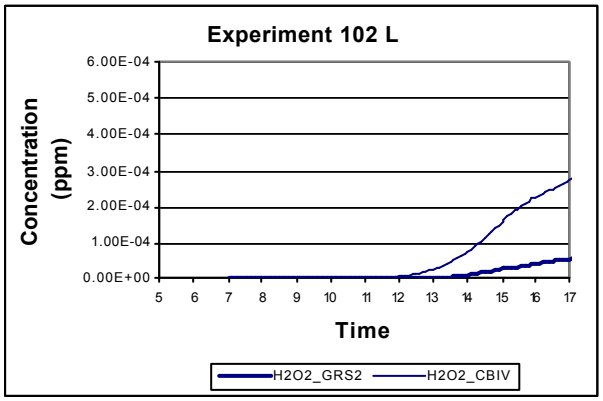

Figure 2: Comparison of measurements from smog chamber 102 L experiment with model predictions

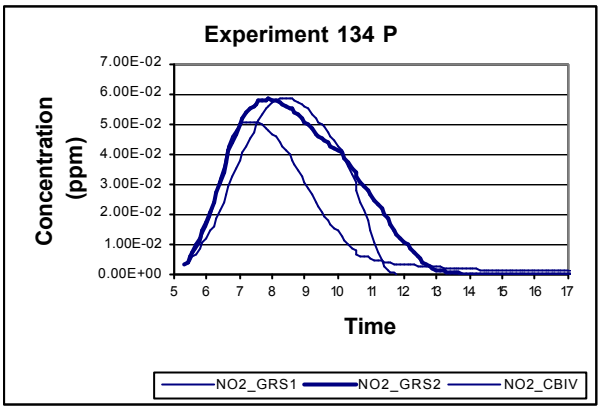

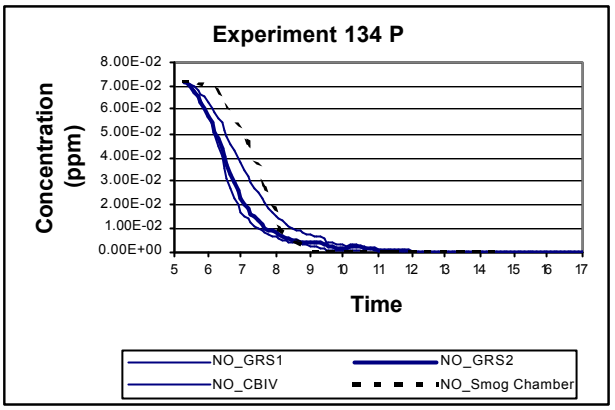

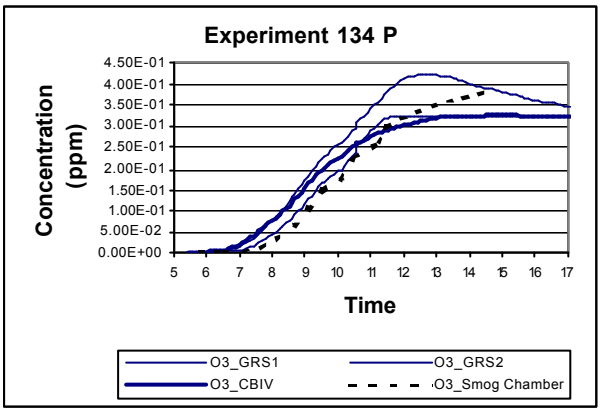

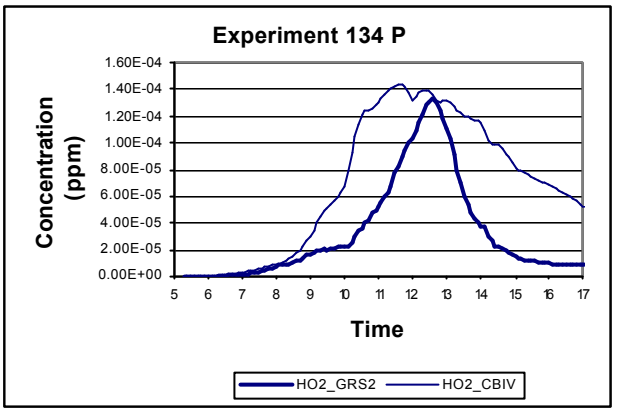

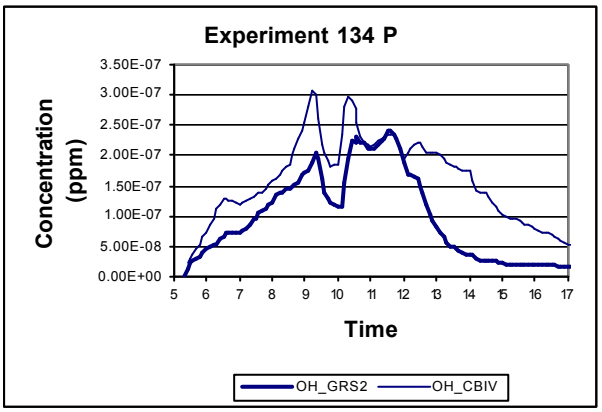

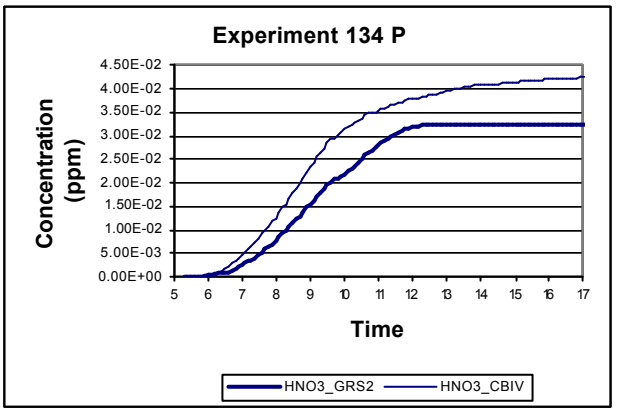

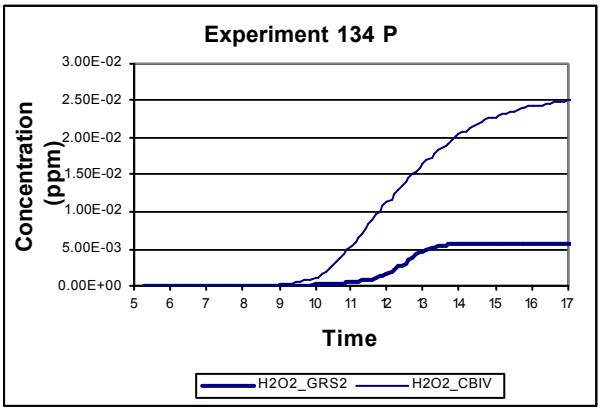

Figure 3: Comparison of measurements from smog chamber 134 P experiments with model predictions

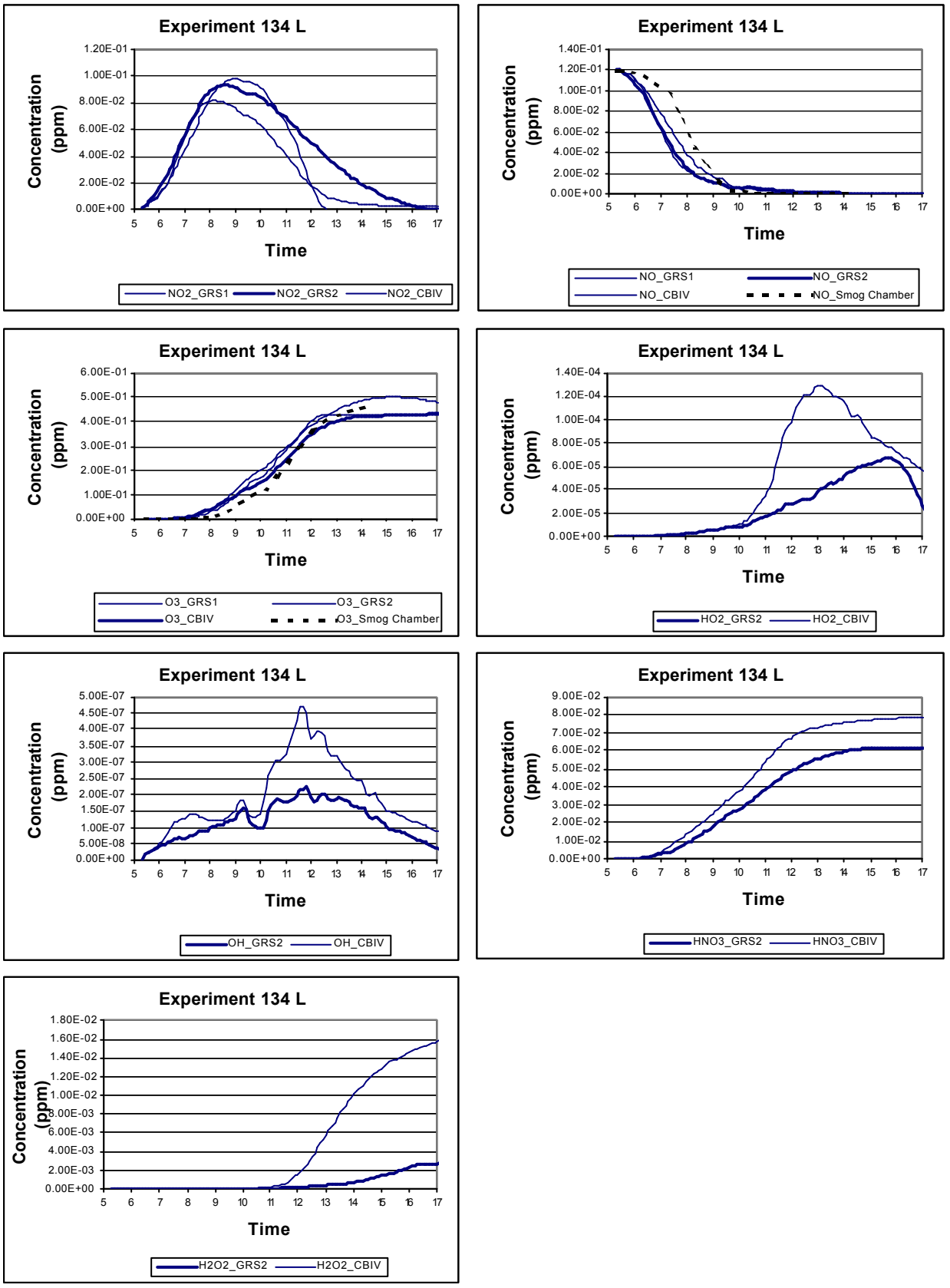

Figure 4: Comparison of measurements from smog chamber 134 L experiment with model predictions

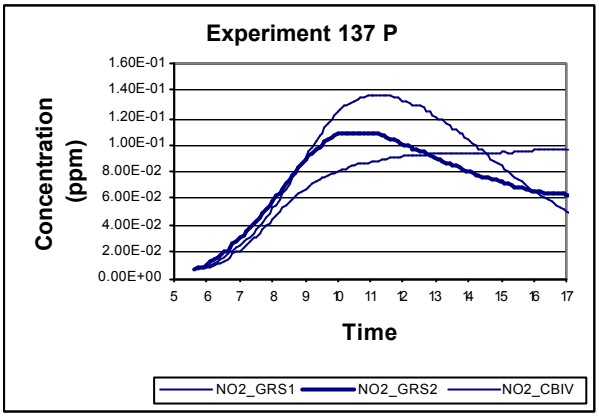

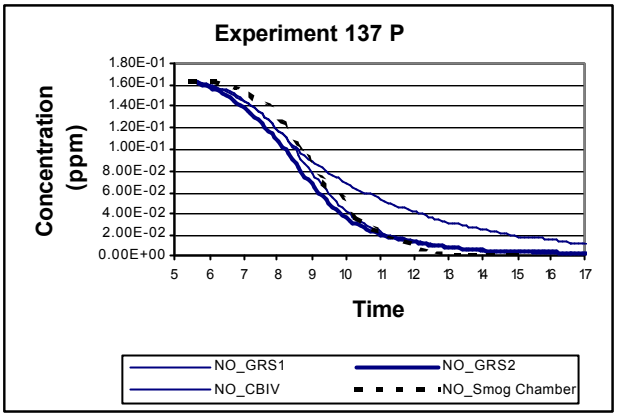

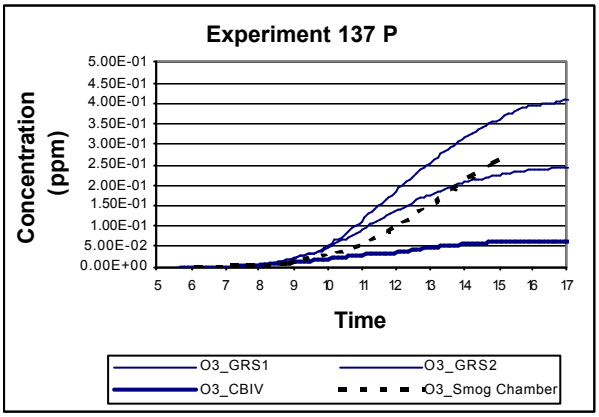

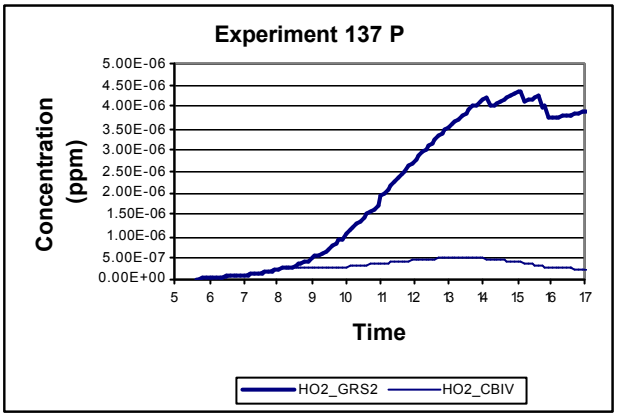

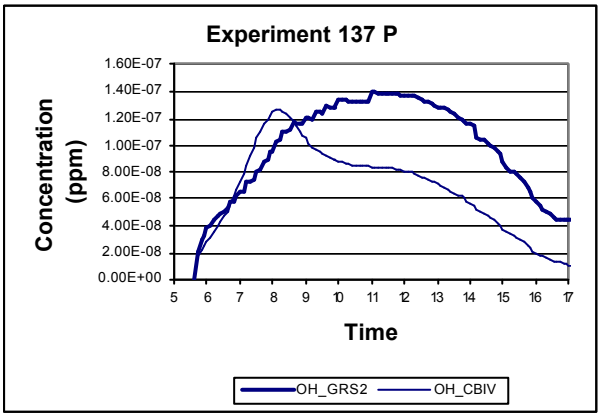

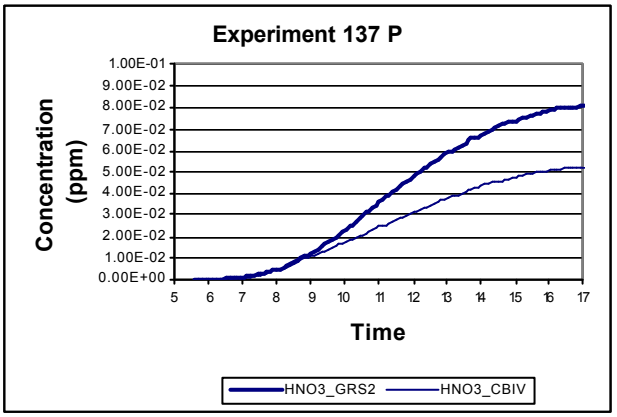

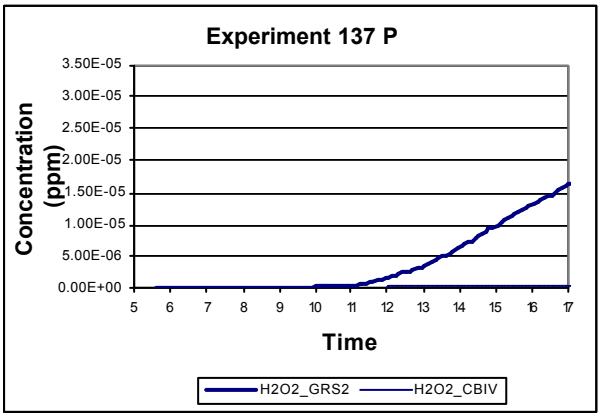

Figure 5: Comparison of measurements from smog chamber 137 P experiments with model predictions

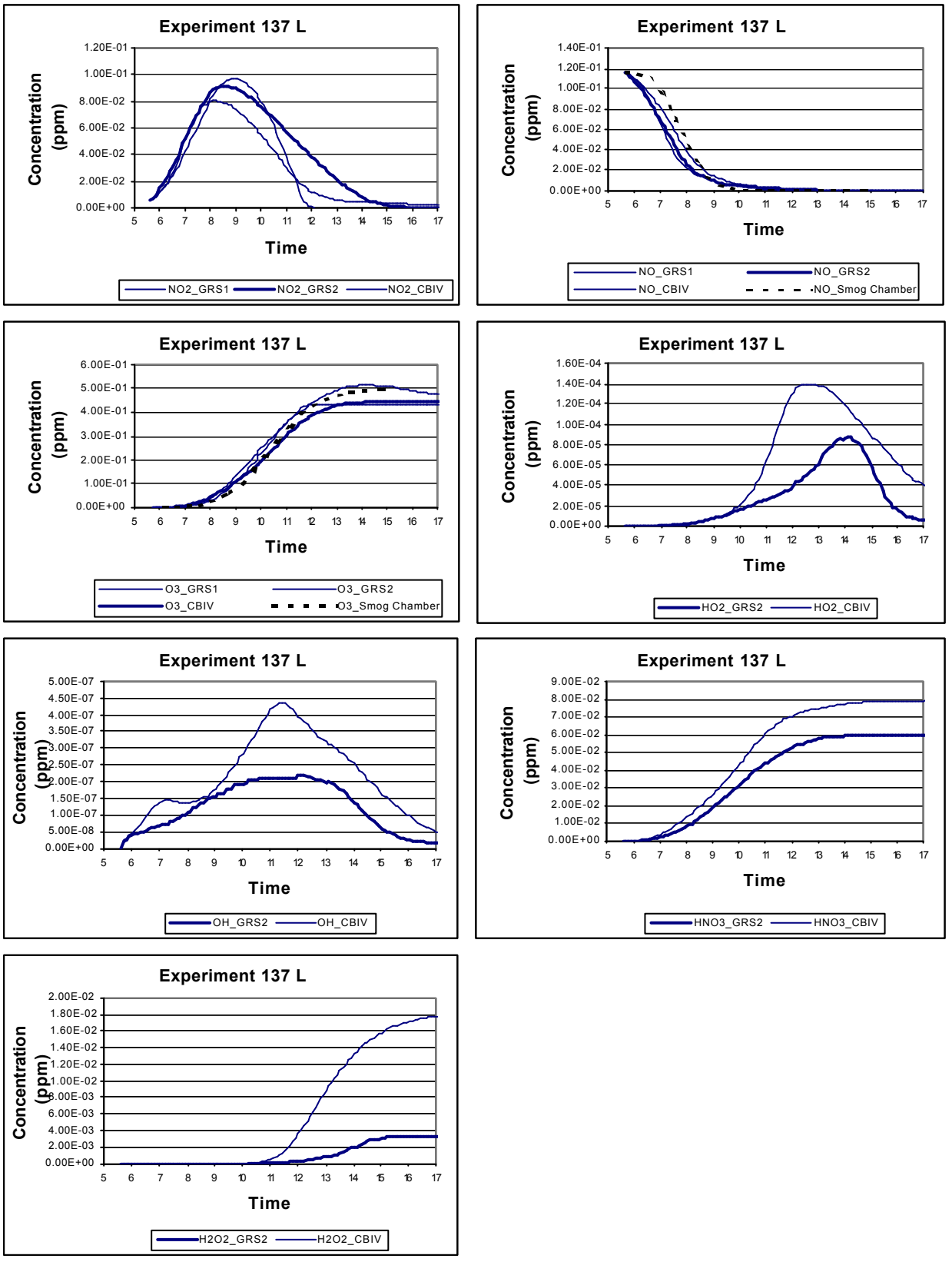

Figure 6: Comparison of measurements from smog chamber 137 L experiment with model predictions

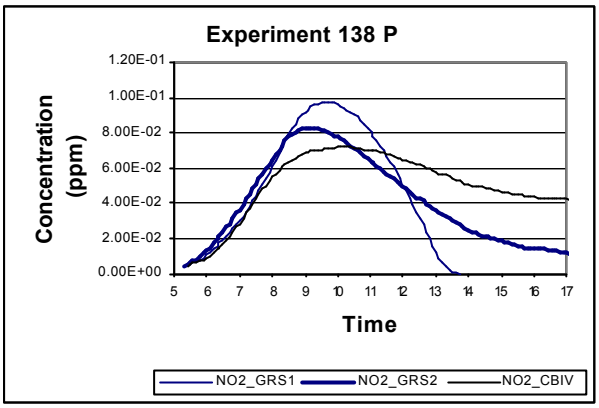

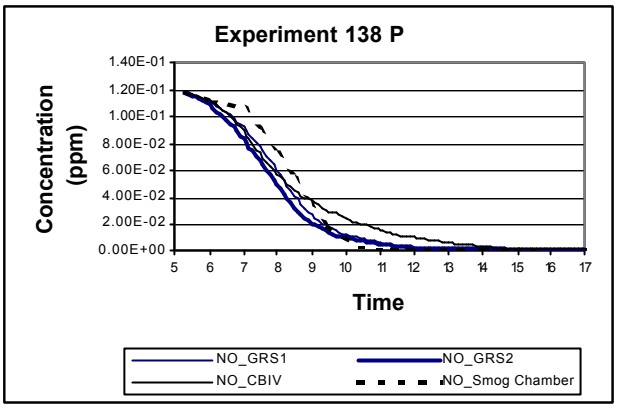

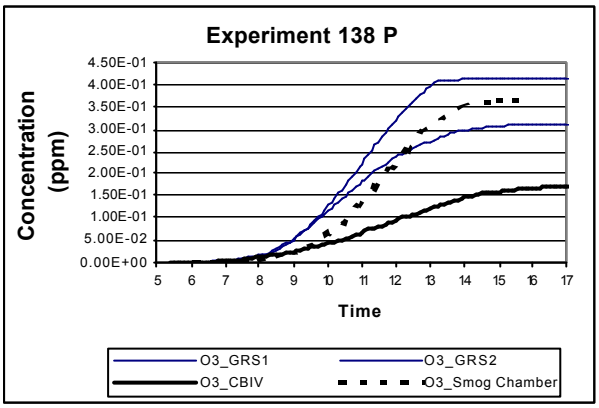

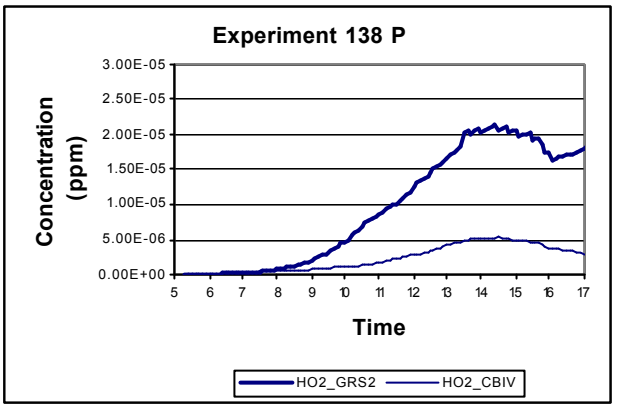

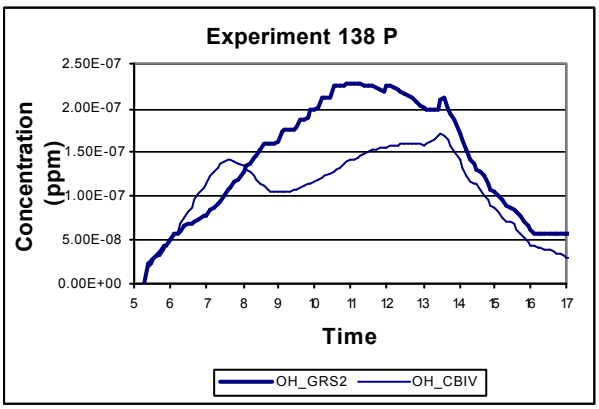

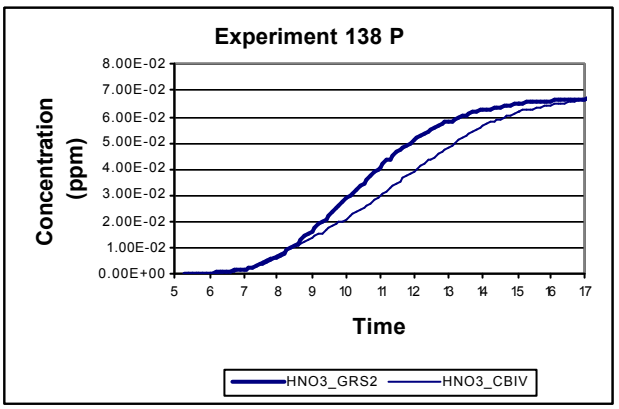

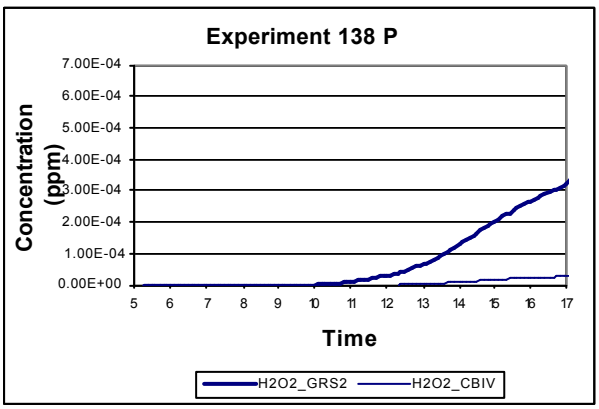

Figure 7: Comparison of measurements from smog chamber 138 P experiments with model predictions

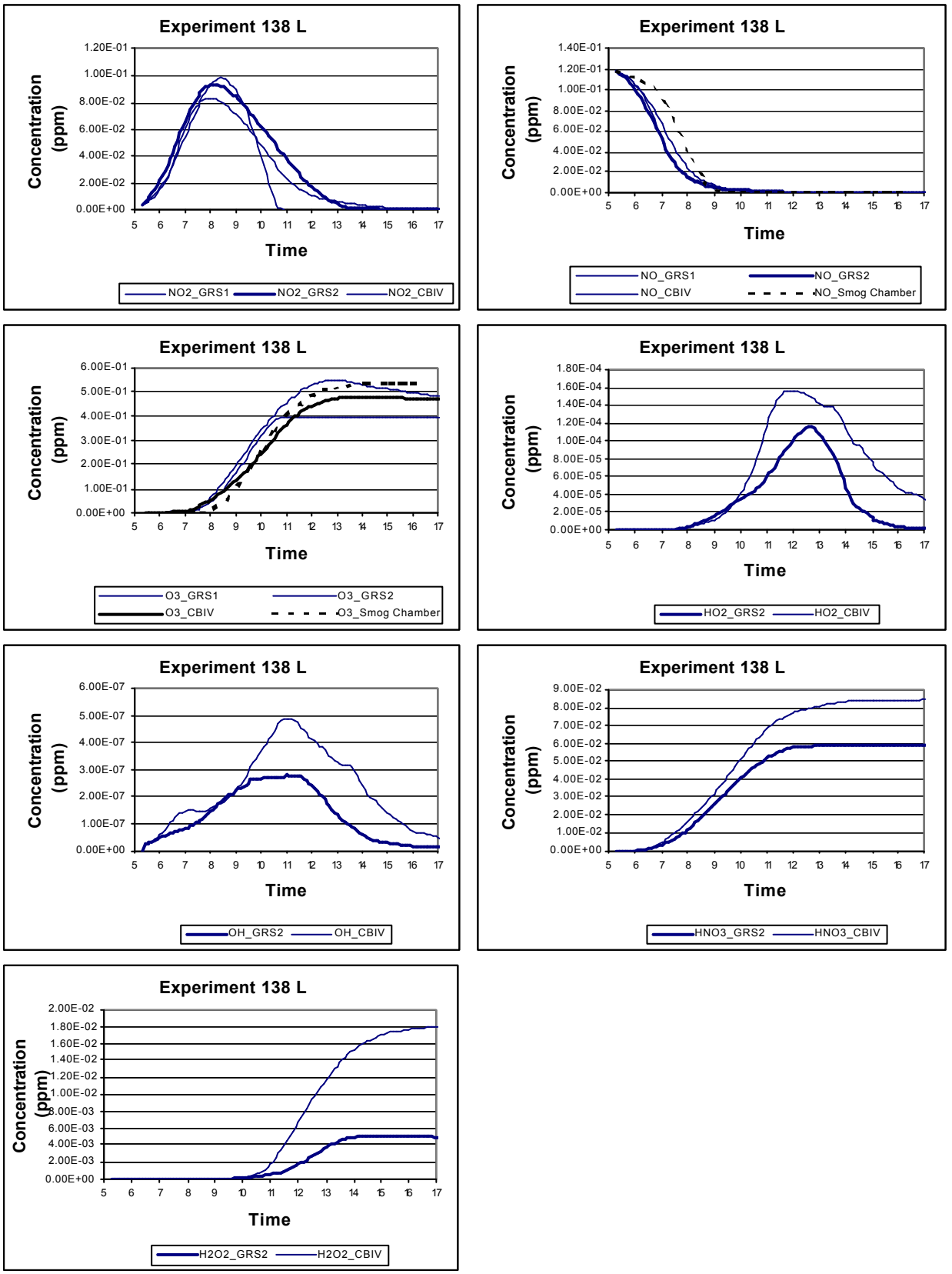

Figure 8: Comparison of measurements from smog chamber 138 L experiments with model predictions

In general GRS2 provides reasonable predictions for NO, NO_2, and O_3 when compared to the measurements made for the smog chamber experiments and to the predictions made for selected species by CB-IV. For O_3, the major indicator species for photochemical smog, peak concentrations calculated by GRS2 are within ±10-20% of measured concentrations when high concentrations of O_3 (~0.2 – 0.5 ppm) are formed. For lower O_3 concentrations of 0.1-0.2 ppm, GRS2 predictions are only within ± 40% or so of the measurements.

In some cases, the GRS2 predictions are in better agreement with the measurements than the estimates produced by the other models. For example, Figure 1 shows results obtained for the outdoor smog chamber Experiment 102 P, at an ROC/NO_x value of 12.3. Predictions for OH, HO_2, H_2O_2 and HNO_3 were in reasonable agreement with those of CB-IV. This agreement is perhaps not so surprising given the use of CB-IV rate constants for many of the reactions in GRS2.

At the higher ROC/NO_x value (15.6) of experiment 134 P, GRS2 appears to over-predict the ozone concentrations compared to the measurements and compared to the other models, but a more extensive series of comparisons would be required to confirm this. Concentrations of NO calculated by GRS2 decreased at a rate similar to the decrease predicted by CB-IV, but exceeded those observed in the experiments.

Two smog chamber experiments (137 P and 138 P) were carried out at low ROC/NO_x ratios of 3.5 and 4.8 respectively. Figures 5 and 7 illustrate modelling results obtained from CB-IV, GRS, GRS2 and smog chamber results. Ozone concentrations predicted by GRS2 for the selected experiments were in good agreement with the observations. Hence the performance of GRS2 appears to be reasonable for a wide range of ROC/NO_x ratios.

The performance of GRS2 with respect to some of the other species is not so encouraging. Compared to CB-IV, concentrations of OH, HO_2, and H_2O_2 can be over- or under-predicted by wide margins, suggesting that more work is required to refine the mechanism. The current version of the GRS model could be modified to include specific hydrocarbon species that would include selective reactivities that control radical production. However the difficulties in fitting a wide range of species for a range of initial conditions are probably a consequence of the empirical nature of the GRS approach, and present a limit to its applicability. Further refinements of reduced mechanisms for smog modelling are probably better pursued using the rigorous approaches developed elsewhere based on systematic examination of the sensitivity of predictions to specific reactions, and well-based mechanism reduction techniques.

Conclusions

A modified version of the Generalised Reaction Scheme, or GRS approach to the modelling of the chemistry of photochemical smog has been developed. The GRS scheme is a semi-empirical model which uses smog chamber data from the CSIRO outdoor smog chambers to develop reaction rates for ozone formation. The modified version, GRS2, extends this approach by including reactions which explicitly account for the formation and destruction of the key radical species, OH and HO_2. Inclusion of these reactions is necessary to more accurately predict background ozone formation in relatively clean atmospheres where NO concentrations control ozone production.

GRS2 also includes reactions to account for 1,3-butadiene decomposition and the heterogeneous oxidation of SO_2 by OH.

The performance of GRS2 has been compared with measurements made during a range of experiments in the CSIRO outdoor smog chambers, for ROC/NO_x ratios of 3.5-15.6. For O_3, the major indicator species for photochemical smog, peak concentrations calculated by GRS2 are within ±10-20% of measured concentrations when high concentrations of O_3 (~0.2 – 0.5 ppm) are formed. For lower O_3 concentrations of 0.1-0.2 ppm, GRS2 predictions are only within ± 40% or so of the measurements.

The performance of GRS2 with respect to some of the other species is not so encouraging. Compared to CB-IV, concentrations of OH, HO_2, and H_2O_2 can be over- or under-predicted by wide margins, suggesting that more work is required to refine the mechanism.

Further refinements of computationally efficient mechanisms for smog modelling are probably better pursued using a rigorous approach to mechanism reduction.

References

Azzi M. Johnson G.M. and Cope M. (1992) An introduction to the generic reaction set photochemical smog mechanism. In *proc. 11th Clean Air Conf. & 4th Regional IUAPPA Conf.,* Brisbane, Australia.

Carter W.P.L. (1990) A detailed mechanism for the gas-phase atmospheric oxidation of organics. *Atmos. Environ.* **24A**, 481-518.

Carter W.P.L. and Lurmann F.W. (1991) Evaluation of a detailed gas-phase atmospheric reaction mechanism using environmental chamber data. *Atmos. Environ.* **25A**, 2771-2806.

Gery M.W. Whitten G.Z. Killus J.P. and Dodge M.C. (1989) A photochemical kinetics mechanism for urban and regional scale computer modelling. *J. Geophysical Research* **94**, 12,925-12,956.

DeMore, W.B., Sander, S.P., Golden, D.M., *et al.* (1997) Chemical kinetics and photo-chemical data for use in stratospheric modelling. Evaluation number 12. NASA panel for data evaluation. *Jet Propulsion Laboratory Report*, 97–104.

Heard A.C. Pilling M.J. and Tomlin A.S. (1998) Mechanism reduction techniques applied to tropospheric chemistry. *Atmos. Environ*. **32**, 1059–1073.

Hess G. D., Carnovale F., Cope M., and Johnson G.M. (1992) Evaluation of some photochemical mechanisms- I. Temperature and initial concentration effects. Atmospheric Environment 26 A, 625-641

Johnson G.M. Compilation of CSIRO Dual Outdoor Smog Chamber Data. November, 1993. CSIRO Division of Coal and Energy Technology Investigation Report CET/IR192.

Lurmann F.W. Carter W.P.L. and Coyner L.A. (1987) A surrogate species chemical reaction mechanism for urban-scale air quality simulation models. Vol. I – adaptation of the mechanism. Final report, EPA contract No. 68-02-4104, Atmospheric Sciences Research laboratory, Research Triangle Park, NC.

Moshiri E. and O'Brien R.J. (1984) A concise hydrocarbon-specific photochemical ozone model. Presented at American Chemical Society Meeting, St Louis, MO, April 1984.

Seinfeld J.H. (1986) *Atmospheric Chemistry and Physics of Air Pollution,* Wiley-Interscience, New York, 738 + xxiii pp.

Seinfeld J.H. (1988) Ozone air quality models. A critical review. *JAPCA* **38**, 616-645.

Appendix 5.2 Demonstration of a Green Scenario

Proceedings of 10th International Symposium "Transport and Air Pollution"
17–19 September 2001 – Boulder, Colorado USA

The Australian Air Quality Forecasting System: Predicting the Impact of Motor Vehicle Emissions

Martin COPE[1,3], Dale HESS[2], Sunhee LEE[1], Peter MANINS[1], Kamal PURI[2], Kevin TORY[2], Neil WONG[4], John CARRAS[3] and Bill LILLEY[3]

[1]CSIRO Atmospheric Research, Aspendale Victoria, Australia
[2]Bureau of Meteorology Research Centre, Melbourne, Victoria, Australia
[3]CSIRO Energy Technology, North Ryde, NSW. Australia
[4]Environment Protection Authority of Victoria, Melbourne, Victoria, Australia

Abstract

The Australian Air Quality Forecasting System provides 24–36 hour, high-resolution, numerical air quality forecasts, twice daily, for New South Wales and Victoria. The system is described, and performance results for NO_y, NO_2, O_3 and PM10 for March 2001, and O_3 time series for a 4-day episode, 6–9 March 2001, are presented. The impact of motor vehicles is explored by computing the PM10 concentration and dosage for a commuter travelling 70 km to work between Geelong and Melbourne under 'business-as-usual' and 'green' scenarios.

Keywords: Air quality, forecasting, numerical, modelling, urban, motor vehicles.

Introduction

The Australian Air Quality Forecasting System (AAQFS) is a joint project between CSIRO Atmospheric Research, CSIRO Energy Technology, the Bureau of Meteorology (BoM), the Environment Protection Authority of Victoria (EPAVIC) and the Environment Protection Authority of New South Wales (EPANSW) to develop a high-resolution air quality forecasting system as a contribution to Australia's Natural Heritage Trust activities. Currently, twice-daily 24–36 hour, numerical air quality forecasts are issued for two regions: the airshed of Melbourne and Geelong (3.7 million people) in Victoria (see Fig. 1) and the airshed of Sydney (4 million people) in New South Wales (NSW). The principal AAQFS goal is to issue numerical forecasts to State EPAs in time for guidance and reference against current air quality forecasting procedures.

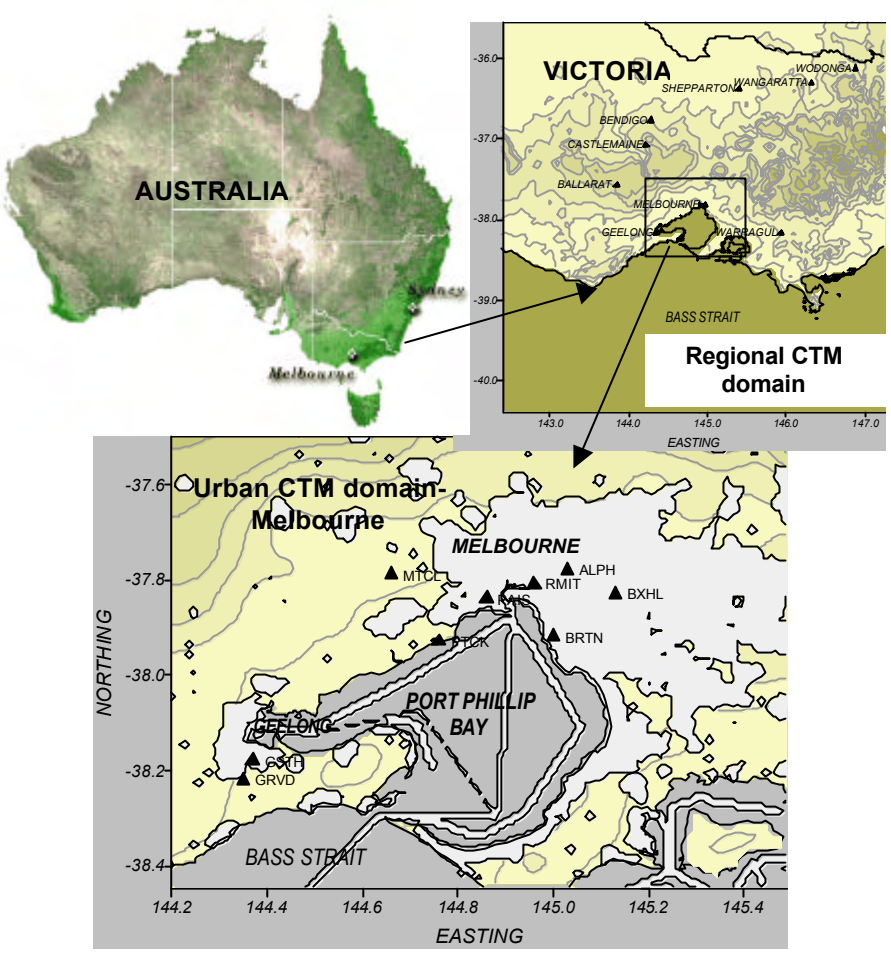

Figure 1. Location of CTM modelling domains for Victorian air quality forecast grids. The 98 x 98 point regional CTM grid has a horizontal spacing of 0.05° (~ 5 km). The 130 ´ 96 point urban CTM grid has a horizontal spacing of 0.01° (~ 1 km). Also shown on the urban grid are the locations of EPAVIC monitoring stations: ALPH–Alphington; BRTN–Brighton; BXHL–Box Hill; MTCL–Mt. Cottrell; PAIS–Paisley; PTCK–Pt. Cook; GSTH–Geelong South; GRVD–Grovedale. The main shipping channels are indicated in Port Phillip Bay and Western Port Bay (on the eastern side of the map). The topography and some emission regions are also shown.

1. AAQFS Objectives

In keeping with the AAQFS goal mentioned in the introduction, the primary objective has been the development of a state-of-the-art, flexible numerical system, able to forecast air quality for multiple pollutants over spatial scales ranging from intra-suburb to inter-regional (1–500 km). A secondary objective is the generation of a 'green' air quality forecast (with 25% reduction in motor vehicle emissions), in addition to the 'business-as-usual' forecast, to demonstrate the impact of a concerted public response to a forecast of potentially poor air quality.

2. Approach

The AAQFS consists of five tightly coupled components: (a) the Limited Area Prediction System (LAPS; Puri et al., 1998), one of BoM's operational weather forecasting systems, is used to generate forecasts of the transport fields at 0.05° (~5 km) horizontal grid spacing; (b) a hybrid offline/online emissions inventory module (EIM; Ng et al., 2000), which generates emission flux estimates for 60 chemical species from anthropogenic, biogenic and natural sources on horizontal grids with spacing of 0.01° (~1 km) for urban areas (i.e. Melbourne and Geelong; Sydney, Wollongong, Newcastle) and 0.05° for non-urban areas (i.e., remainder of Victoria, NSW). Emission totals for Melbourne are given in Table 1, where, in common with other modern cities, motor vehicles are seen to be the dominant source of air pollutants; (c) a chemical transport model (CTM), which generates air quality forecasts for 25 pollutants (including PM1, PM2.5, PM10, photochemical oxidants, formaldehyde, butadiene and benzene) on a horizontal grid spacing of 0.01° for the urban areas and 0.05° for the non-urban areas (Fig. 1). The CTM has been designed to run in either offline mode, (downstream of the LAPS forecast), or in online mode (as an interface, which is called within the time-marching loop of LAPS. Forecasts are undertaken using the highly condensed GRS mechanism (Azzi et al., 1992), thus enabling large domains to be simulated within the forecasting time window; (d) a validation system in which observed and forecast 1-hour time series of key meteorological variables and air quality species are compared on a daily basis using a range of graphical and statistical tools; (e) a data dissemination and archiving system which consists of an AAQFS web site, where graphical summaries of the daily forecasts are loaded for use by the EPAs, PC-based graphical display software for visualising forecast (and observed) meteorological variables and air pollutant species, and a platform-independent file-archiving system.

Table 1. Inventory breakdown of air pollutant emissions for the Melbourne/Geelong region for 1996. Motor vehicle vs non-motor vehicle component.

POLLUTANT	Motor vehicles (Mg/yr)	Other anthropogenic (Mg/yr)	Total (Mg/yr)	Motor vehicles % of total
oxides of nitrogen	37,920	35,868	73,788	51%
carbon monoxide	295,043	115,801	410,844	72%
volatile organics	47,099	95,158	142,257	33%
particles (PM10)	2,117	17,526	19,643	11%
1,3-butadiene	334	134	468	71%
benzene	2,633	908	3,541	74%
formaldehyde	612	365	977	63%

NB: 'Other anthropogenic' excludes road dust

3. Results and Discussion

System Performance. Following the commencement in early August 2000 of the AAQFS in full demonstration mode, the performance of all system components has been carefully evaluated. Performance has been assessed for the meteorological and EIM forecasts in isolation and for the coupled LAPS-EIM-CTM system. In the case of the former, observed and modelled hourly profiles of wind vectors, dry-bulb temperature, and dew-point temperature, and estimates of mixing depth, and daily ventilation factors have been used in the evaluation. The performance of the EIM has been assessed through comparison of observed and modelled pollutant ratios. In the case of the coupled system, performance evaluation has been carried out in two ways:

a. Air quality forecasts have been compared to daily observations and the resultant bias statistics have been used to identify trends in system performance over an extended period of time. Here the purpose is to ascertain the ability of the system to reproduce the observed meteorological and air quality over a large dynamic range of meteorological, emission and air quality conditions. For example, Fig. 2 shows scatter plots of observed and modelled 50th, 90th, 95th, 99.5th, 99.9th and 100th percentile 1-hour concentrations of NO_y, NO_2, O_3 and PM10 for March 2001 for a number of monitoring stations in the Melbourne/Geelong region (see Fig. 1 for list of localities).

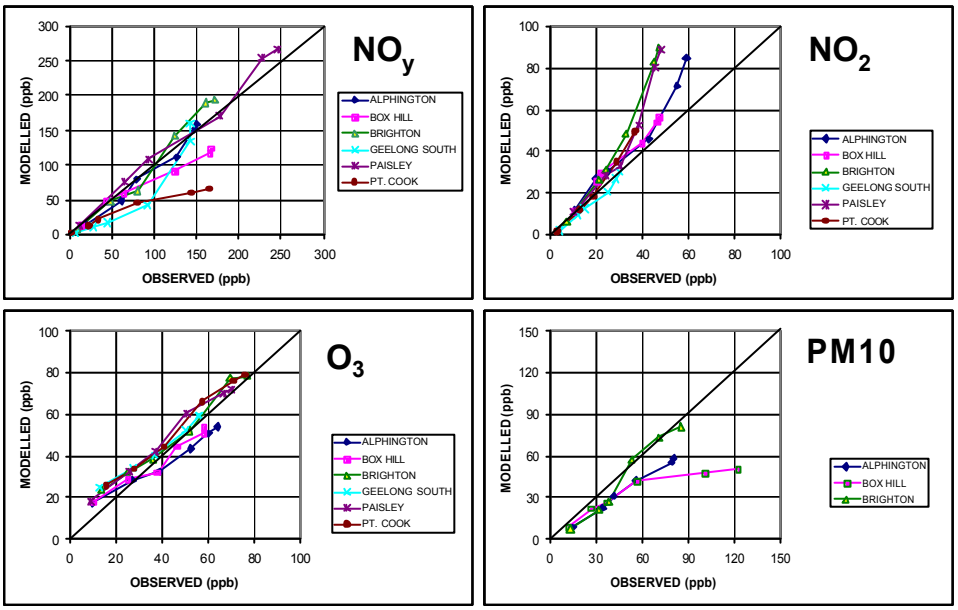

Figure 2: Scatter plots of observed and modelled 50th, 90th, 95th, 99th, 99.9th and 100th percentile concentrations for selected pollutants for March 2001 for the Melbourne/ Geelong region (see Fig. 1 for localities).

It can be seen that (1) the distribution of NO_y is well predicted at all monitoring stations except for the semi-rural Pt. Cook monitoring site. Further investigation suggests that the cause of the under

prediction at this site is a small angular error in the trajectory of the urban plume; (2) NO_2 is increasingly over-predicted at the higher percentiles. In this case the cause is likely to be a systematic over- estimate of the initial reactivity of the urban air mass by the highly condensed GRS photochemical mechanism; (3) O_3 is predicted with little bias at the higher percentiles but is increasingly overestimated at the lower percentiles. The cause is a 5–10 ppb over-prescription of the background O_3 concentration in unpolluted maritime flows (25 ppb vs. 15–20 ppb). The reason again appears to lie with the GRS mechanism — ozone destruction under conditions of low NO_x and high H_2O is not modelled by the mechanism; (4) the observed PM10 percentiles at Brighton monitoring station have been well reproduced by the system. All percentiles are slightly under-predicted by the system at Alphington and strongly under-predicted at the 99.9 and 100^{th} percentile at Box Hill monitoring station. In the latter case the cause is an isolated (single pollutant) PM10 one-hour event, which is likely to be the result of a short-term, local, un-inventoried source.

b. Outputs from the system have been examined in detail for selected pollutant episodes. Clearly, acceptable model performance during pollutant episodes is of paramount importance if the system is to be used in a forecast mode. The Melbourne/Geelong region experienced one moderate photochemical smog event during the month of March. Over the period 6–9 March, peak 1-hour ozone concentrations at all monitoring stations were above the local background concentration of 15–30 ppb, with peaks of up to 80 ppb observed at Pt. Cook and Brighton monitoring stations (see Fig. 1 for station locations). The concentrations of other pollutants were also observed to be elevated. Time series plots of observed and forecast 1-hour ozone concentration are displayed in Fig. 3 for selected monitoring stations in the Melbourne/Geelong region. The distribution of ozone shows good skill over the four-day period, with the only significant discrepancy being the over-prediction of ozone associated with the arrival of the sea breeze on 7 March (hours 36–42) at Pt. Cook, Brighton and Paisley.

Motor vehicle impacts. Because of the dominant contribution made by motor vehicle emissions to urban air pollution in Australia (Table 1), two key objectives of the AAQFS have been (1) to comprehensively model the impact of motor vehicles, including the emissions, transport and transformation — at the regional scale, at the urban scale, and, potentially, at the street scale; (2) to forecast and disseminate to the general population, the impact of a concerted reduction in motor vehicle usage on the daily air quality within the urban areas. An example of the latter is illustrated in Fig. 4, where there is a hypothetical 25% reduction in motor vehicle usage (the 'green' forecast scenario), following a concerted move by the commuting population away from single-occupant motor vehicle use in response to a forecast of potentially deleterious air pollutant levels.

In order to illustrate the cumulative impact of reduced motor vehicle usage, we consider a case in which a commuter travels each day from a home base in Geelong to a work place in Melbourne's CBD (Fig. 4a). In a 'business-as-usual' scenario, the commuter is assumed to spend 12 hours per day at home, 3 hours commuting by motor vehicle and 9 hours at work. Due allowance is made for in-car *vs*. near-road pollutant concentrations for vehicle-produced pollutants (Duffy and Nelson, 1997).

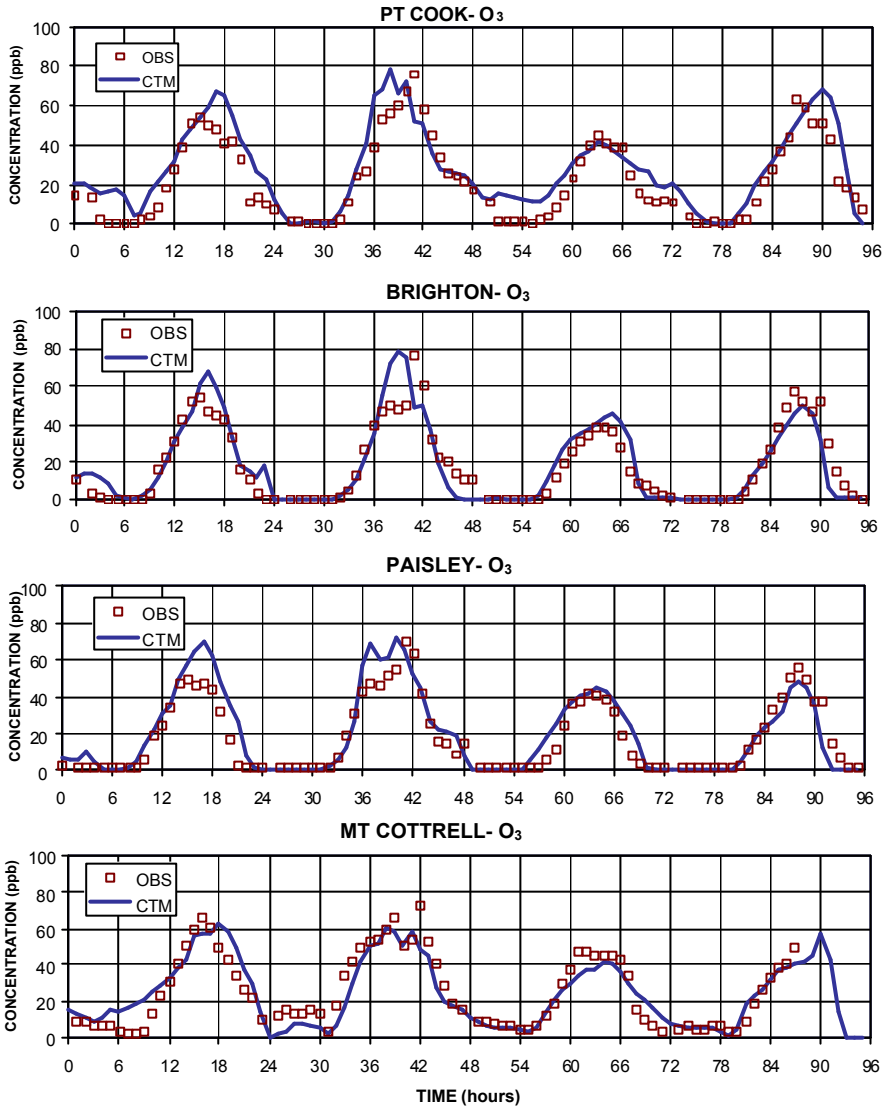

Figure 3: Time series plots of observed (OBS) and forecast (CTM) 1-hour ozone concentrations for monitoring stations in Melbourne region, 6-9 March 2001. Bilinear interpolation was used to interpolate modelled concentrations to the location of each monitoring station.

Forecasts of the commuter's running 24-hour average PM10 concentration, and PM10 cumulative dosage over the period 7–9 March are shown in Fig. 4b and Fig 4c respectively for 'business-as-usual'; a 'green' scenario, but still including motor vehicle transport; and a 'green' scenario and non-motor vehicle transport (e.g. train travel). In the 'business-as-usual' forecast, the commuter's running 24-hour PM10 concentration approached EPAVIC's air quality objective of 50 µg m^{-3} and the cumulative PM10 dosage reached 27000 µg m^{3} hr by the end of the third day. Under the 'green' scenario (but still travelling to work by motor vehicle), the commuter's peak 24-hour PM10 concentration was reduced by 20%, and the cumulative PM10 dosage by 23%. Replacing the motor vehicle by train as the transport mode results in even larger reductions in pollutant exposure: the peak 24-hour PM10 is reduced by 47% and the cumulative dosage by 33% relative to the 'business-as-usual' scenario.

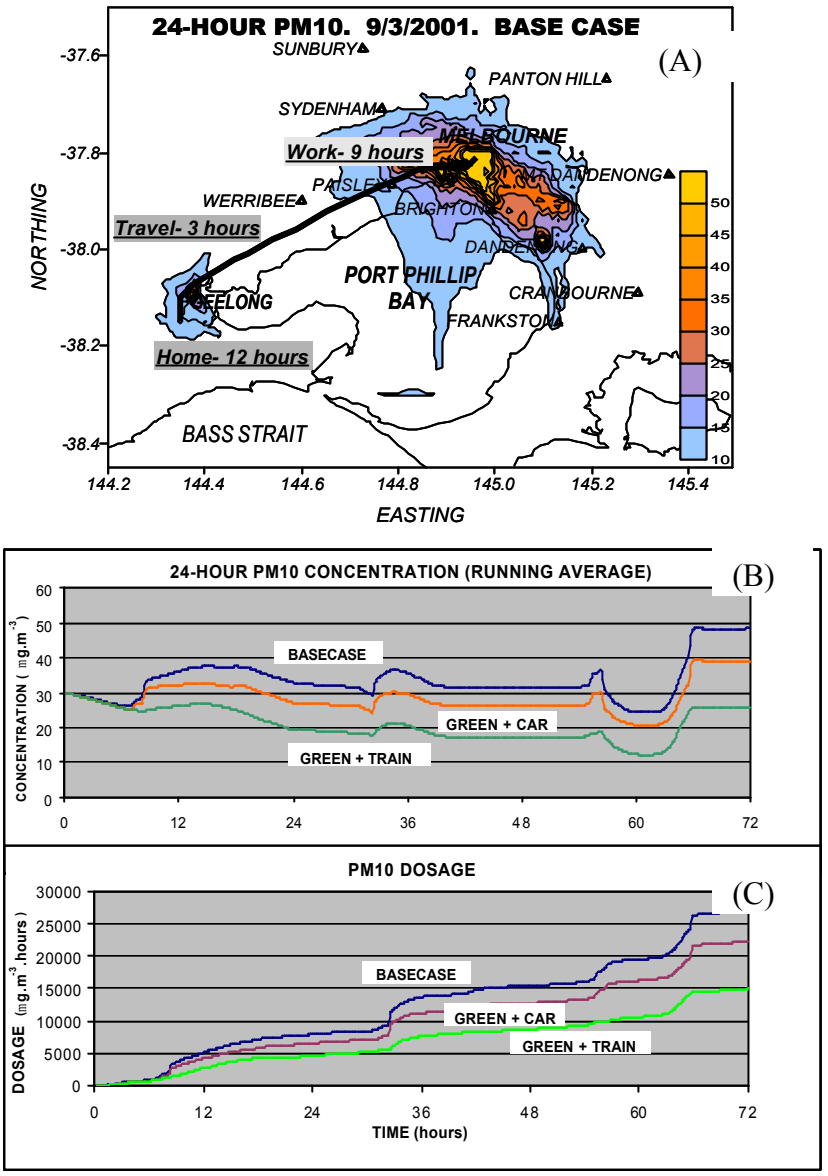

Figure 4: Example of a 'green' scenario forecast for 7–9 March 2001. (A) Forecast 24-hour PM10 concentration for 9 March 2001 and pathway taken by a person who daily commutes 70 km from Geelong to Melbourne. (B) Forecast 24-hour PM10 concentration (running average) and (C) forecast dosage experienced by the commuter for 3 scenarios ¾ 'business-as-usual' (base case), 25% reduction in motor vehicle emissions and commuter travels by car (green+car), 25% reduction in motor vehicle emissions and commuter travels by train (green+train).

Conclusions

This study has shown that the AAQFS, in general, is performing well. However several areas can be improved. Of particular importance is the implementation and testing of a subgrid-scale near-road model. This model will initially be run for selected regions in Sydney, and will relate emissions estimates to the instantaneous power expended by each vehicle (Williams et al. 1994), giving much finer resolution of roadside concentrations and impacts. Another improvement includes the replacement of the GRS photochemical mechanism with an upgraded mechanism—GRS2. GRS2 has a more comprehensive inorganic reaction set than GRS, including an explicit OH-HO_2 cycle and an explicit representation of nitric acid. Implementation of GRS2 will be followed by the development of an improved secondary aerosol mechanism. Additional work in progress includes online testing of the CTM module — operating within the time-marching loop of LAPS, and the development of a hybrid prognostic/diagnostic interpolation scheme for generating transport fields on the high-resolution urban grids.

Acknowledgments

AAQFS was developed under funding from by the Air Pollution in Major Cities Program, sponsored by Environment Australia.

References

Azzi, M., Johnson, G. J., and Cope, M., 1992. An introduction to the Generic Reaction Set photochemical smog mechanism. Proc. 11th International Clean Air Environment Conf., 5-9 July 1992, Brisbane, Clean Air Society of Australia and New Zealand, 451–462.

Duffy and Nelson 1997. Exposure to emissions of 1,3-butadiene and benzene in the cabins of moving motor vehicles and buses in Sydney, Australia. Atmos. Environ., 31 (23) 3877–3885.

Ng, Y. L., Walsh, S. and Wong, N., 2000. Emissions model for the Australian Air Quality Forecasting System. Proc. 15th International Clean Air Environment Conf., Vol. 1, 26–30 November 2000, Sydney, Clean Air Society of Australia and New Zealand, 275–280.

Puri, K., Dietachmayer, G., Mills, G. A., Davidson, N. E., Bowen, R. A., Logan, L. W., 1998. The new BMRC Limited Area Prediction System, LAPS. Aust. Met. Mag., 47, 203–213.

Williams, D. J., Shenouda, D.A. and Carras, J.N., 1994. Modelling air toxic emissions from motor vehicles. Proc. Air Toxics Conf., Clean Air Society of Australia and New Zealand, Vol. 2, 31-47.

Appendix 5.4 Power-Based Motor Vehicle Emissions

POWER-BASED MOTOR VEHICLE EMISSIONS MODELLING APPLIED TO THE SYDNEY REGION

W E Lilley, D J Williams and J N Carras

CSIRO ENERGY TECHNOLOGY
PO Box 136 North Ryde NSW 1670

JULY, 2001

TABLE OF CONTENTS

Summary

The use of VKT as a means of calculating emissions from motor vehicles has a number of limitations. Key among these is the inability to take into account in a detailed way, factors such as road grade, acceleration and deceleration and behaviour of vehicles at intersections. Vehicle emissions using instantaneous vehicle power as the independent variable, can in principle provide the flexibility required. However, power-based modelling has largely been untried in the Australian context.

The work presented in this report has refined and applied a power-based model of motor vehicle emissions to a reduced set of Sydney major roads. The emissions take into account road grade and the presence of intersections as well as the traffic flow rates. While simplifications and generalisations have been required the work presents the first application of power-based modelling to a city road network in Australia.

The need for a vast amount of data, while recognised at the outset, has nevertheless been highlighted by the application of the model to Sydney. Much of the data required for such modelling is simply not available in sufficient detail and many assumptions have been required.

The work described in this report is based on the synthesis of a large amount of data describing petrol- and diesel-vehicle emissions, vehicle fleet mixes, road traffic statistics, road networks and vehicle behaviour in free stream traffic and at intersections. Many of the data, particularly the emissions data and the driver behaviour data, show large variations from vehicle to vehicle. This highlights the need for continuing research and data for

- pollutant emission rates from motor vehicles
- traffic-flow data
- driver and vehicle behaviour, particularly at intersections.

These data are essential for approaches based on power modelling to be able to provide a more detailed and accurate motor vehicle emissions modelling inventory.

1. Introduction

The power-based approach to describing motor vehicle emissions derives the instantaneous rate of exhaust emissions as a function of the instantaneous power expended by the vehicle at any particular time. Integrating over time provides the overall exhaust pollutant emissions. This is in contrast to the VKT approach where emissions are assigned to motor vehicle classes using kilometres travelled and an emission factor derived from dynamometer studies. The major advantage of power-based modelling is that finer scale studies of motor vehicle emissions which take into account speed, acceleration and road grade can be made on a road, sub-link by sub-link. In addition, power-based modelling allows intersections to be modelled explicitly. The major disadvantage of power-based modelling is that it requires much more data than the VKT approach, in particular typical speed-time profiles of traffic being modelled. These profiles are not normally readily available. While the VKT approach is relatively easy to apply it does not readily capture detailed driving behaviour nor the presence of road grades or intersections.

2. Model Basis

Power-based motor vehicle emissions modelling is based on the fact that the emission rate of pollutants can be shown to depend on the instantaneous power expended by a vehicle. The approach is one that CSIRO has been developing for a number of years and builds on initial studies carried out by Sydney University and other Australian Institutions (see Kent *et al.* 1982 and Williams *et al*. 1994 for further information). An illustration of the model output is presented in Figure 1 compared with actual emission data from the recently completed NEPC funded project establishing diesel emissions for 80 in service diesel vehicles. (The project was carried out by Parsons Australia in collaboration with CSIRO Energy Technology and the project results are available from the NEPC website www.nepc.gov.au)

Figure 1 shows a plot of pollutant emission rate as a function of vehicle power as measured on a chassis dynamometer. It is clear that the emission rates of the pollutants are correlated with the power expended as measured by the chassis dynamometer. (Note that the persistence of the NO_x concentration and slight phase lags are due to sampling and instrument response time issues). Consequently it is anticipated that the instantaneous emission rate of pollutant can be expressed simply as a function of the total instantaneous power expended by a vehicle. Note that petrol-fuelled vehicles provide a similar dependence to that shown in Figure 1.

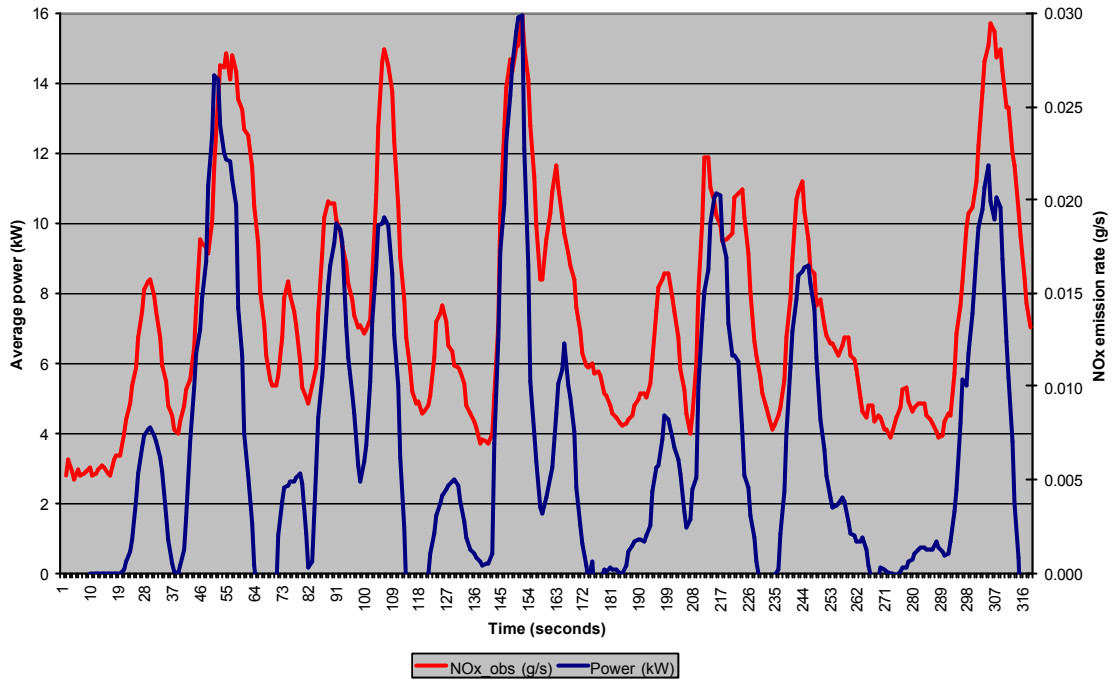

Figure 1: Plot of pollutant emission rate as a function of vehicle power

In order to provide an expression for the instantaneous power expended by a vehicle it is necessary to consider the power required to overcome the various resistances to the motion, *i.e.*

$$z_t = z_d + z_a + z_r + z_i + z_{ac} \quad (1)$$

where z_t is the total instantaneous power, z_d is the power required to overcome drive train resistance, z_a is the power required to overcome the aerodynamic drag, z_r the power to overcome tyre rolling friction, z_i is the power required to overcome inertial effects such as road grades or vehicle acceleration, and z_{ac} the power to run vehicle accessories such as air conditioning.

Each power component in equation (1) can be further expressed as follows

$$z_d = Av^2M$$
$$z_r = (Bv + Cv^2)\,M$$
$$z_a = D\,A_f\,C_d\,v^3$$
$$z_i = (a + g\sin\theta)\,Mv$$

where,

M = mass of the vehicle, C_d the drag coefficient, A_f the frontal area, a the acceleration, g the acceleration due to gravity, θ the road grade and *A, B, C* and *D* empirically derived coefficients. These coefficients have been derived from the results of Richardson (1982).

Calculation of the power from each of the above components for a vehicle mass of 1250 kg as a function of speed is shown in Figure 2a for three road grades (2%, 5% and 10%).

(2)

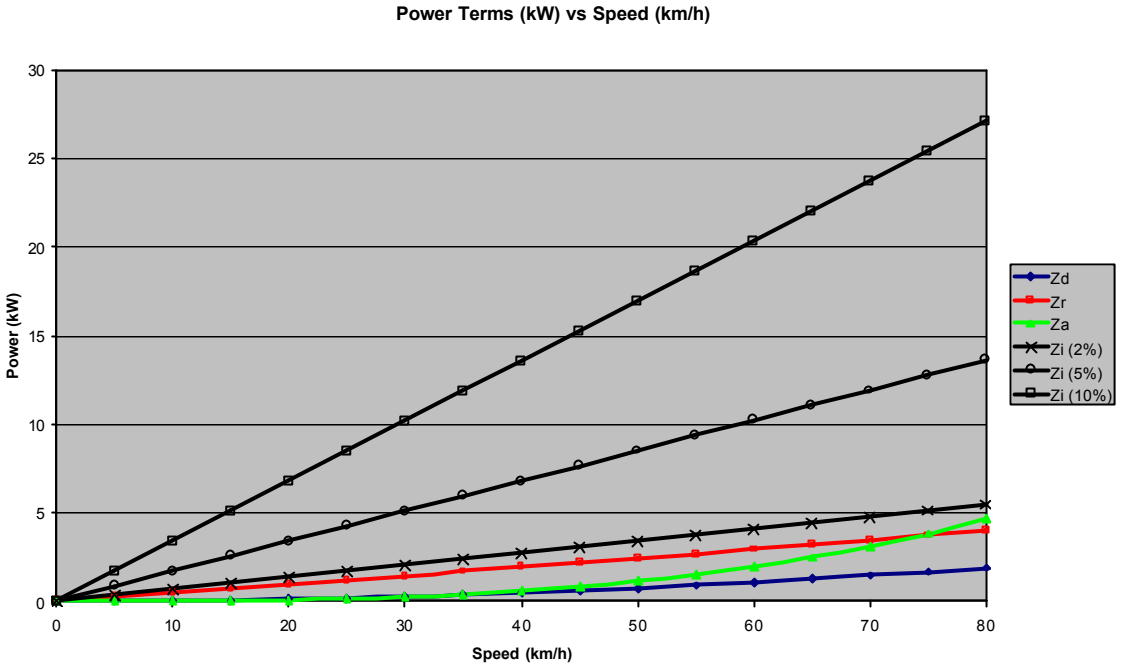

Figure 2a: Power components for various grades at constant speed.

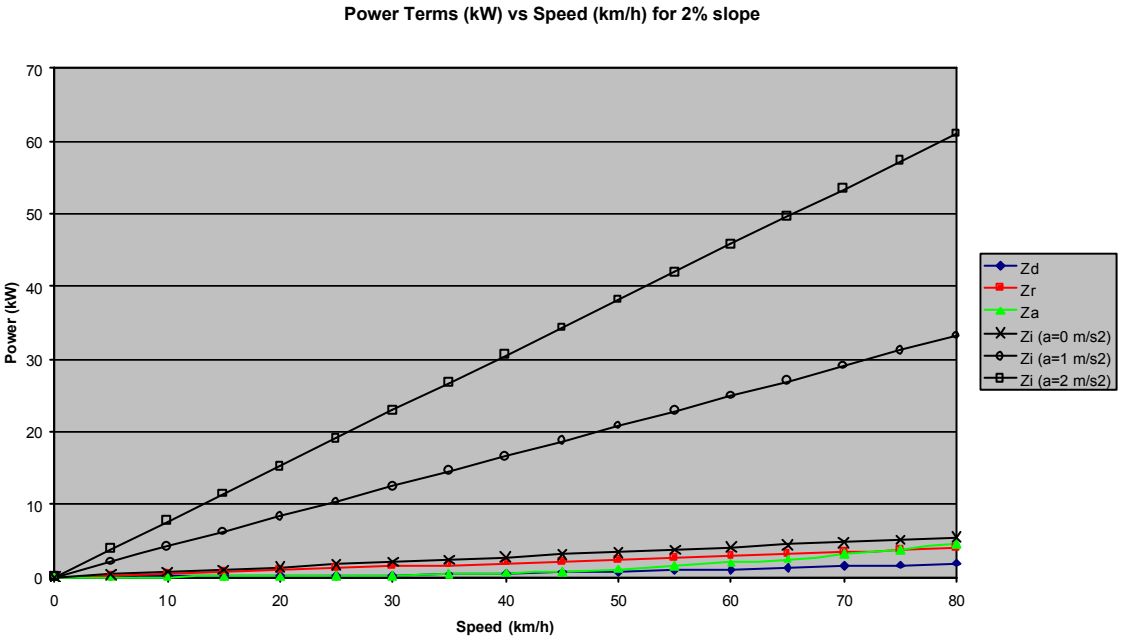

Figure 2b: Power components as a function of speed for various acceleration rates for a 2% slope.

It is clear from Figure 2(a) that as road grade increases, the power expended by a vehicle is dominated by that required to overcome gravity in climbing the hill. Similarly, the data in Figure 2(b) show that for a 2% slope the power is dominated by acceleration up the slope.

3. Emissions of pollutants

3.1 Petrol-fuelled vehicles

The FORS study (1996) measured emissions from 611 in-use spark ignition vehicles which were driven over an ADR 37 drive cycle. The drive cycle was broken into three parts namely cold start, hot transient and hot start. For each of these parts the motor vehicle exhaust emissions were captured in a bag which was subsequently measured for a suite of standard motor vehicle exhaust emissions. Each bag therefore represented the average emissions generated for that part of the drive cycle.

In describing the FORS emissions using power-based emission modelling we have assumed that for each vehicle class the instantaneous rate of emission can be expressed as a linear function of the instantaneous power exerted by the vehicle. This can be written

$$R = a\ E + b\ z_t \tag{2}$$

where R is the rate of pollutant emission, E is the engine capacity and a and b are empirical factors obtained by fitting the above expression to exhaust-emission data such as that provided by the FORS data set. The values of α and β are specific for each pollutant and for each class of vehicle exhaust control technologies.

In determining the appropriate values for α and β equation (2) was integrated over the speed-time profile of the ADR37 drive cycle for each vehicle tested in the FORS project. Due allowance was made for tyre rolling resistance in the dynamometer tests as well as the simulation of aerodynamic resistance. The calculated integrated emission of each pollutant was compared to the measured bag value. The best fit values of α and β derived from this process were taken to represent the emissions from spark ignition vehicles.

Table 1 shows a comparison of the average total emissions for each pollutant measured during the FORS study compared with the average emissions predicted from the power modelling approach. The FORS database includes vehicles equipped with 3-way and 2-way catalysts as well as vehicles without catalysts.

Table 1: Comparison of measured and predicted emissions from the FORS data set.

Catalyst	Bag 1 (g)			Bag 2 (g)			Bag 3 (g)			ADR37			
										FE	CO	HC	NOx
	CO	HC	NOx	CO	HC	NOx	CO	HC	NOx	L/100 km	g/km	g/km	g/km
3-way Predicted	87.03	7.67	9.81	50.88	3.91	6.45	40.42	3.72	8.23	13.41	9.98	0.86	1.37
3-way Measured	96.07	7.58	10.41	49.49	3.66	5.16	39.25	3.28	9.03	12.15	9.43	0.72	1.23
2-way Predicted	162.9	7.80	8.52	65.30	4.10	5.46	47.99	4.09	7.35	10.62	15.47	0.90	1.19
2-way Measured	151.3	8.11	9.98	68.16	3.94	6.70	58.86	3.64	9.71	10.38	13.94	0.79	1.38
none Predicted	179.1	14.53	16.24	153.4	11.77	13.63	107.4	10.31	16.24	11.72	24.63	2.05	2.58
none Measured	177.4	15.52	14.02	164.1	13.07	8.98	106.0	10.65	14.04	11.53	25.11	2.16	1.92

Inspection of the data in Table 1 shows that the measured and calculated averages are in good agreement.

Figures 3a and 3b illustrate the use of the power model for a catalyst-equipped vehicle of mass 1250 kg. Pollutant emission rates are shown as a function of vehicle speed for CO and NO_x for two values of the road grade.

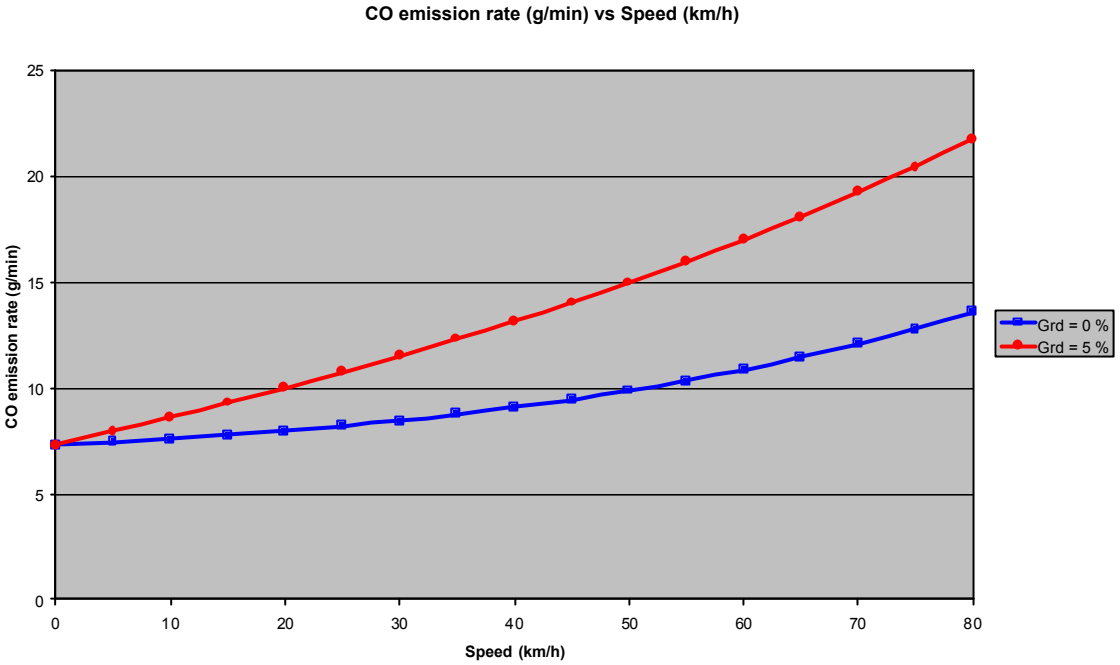

Figure 3a: Carbon monoxide emission rate as a function of constant speed and grade.

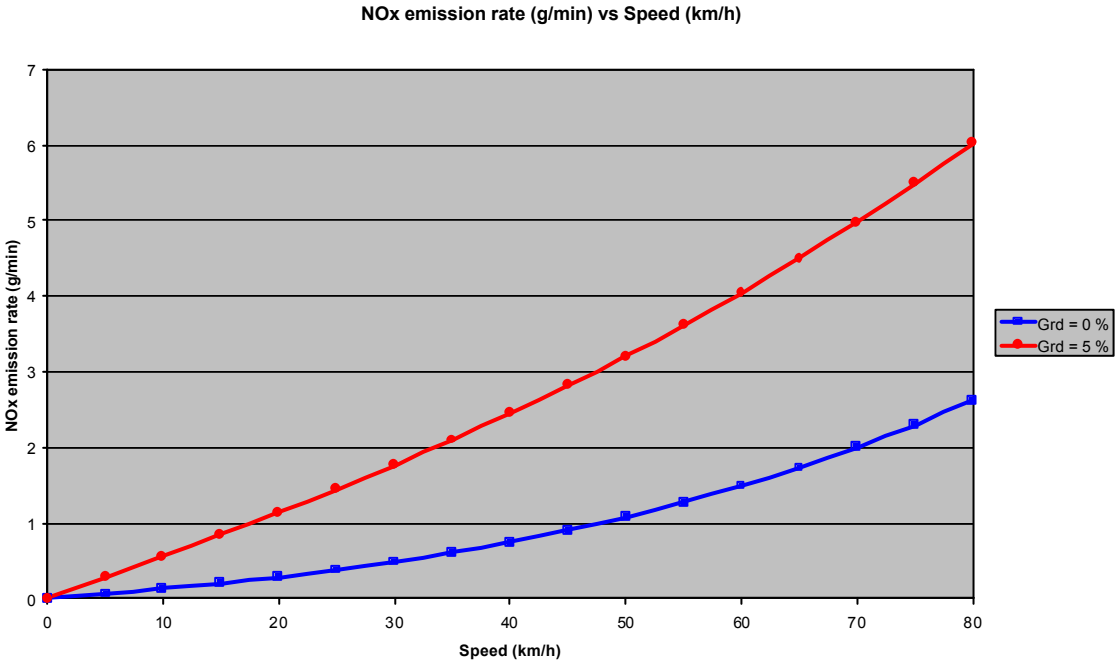

Figure 3b: Nitrogen oxide emission rate as a function of constant speed and grade.

3.2 Diesel-fuelled vehicles

For diesel vehicles, the data provided from the NEPC study are currently being processed to determine the best fit parameters for the data. However an illustration of the empirical basis of the power model is shown in Figures 4a, b and c where the measured and modelled emission rates (for NO_x, CO and hydrocarbons respectively), based on equations (1) and (2) above, are compared.

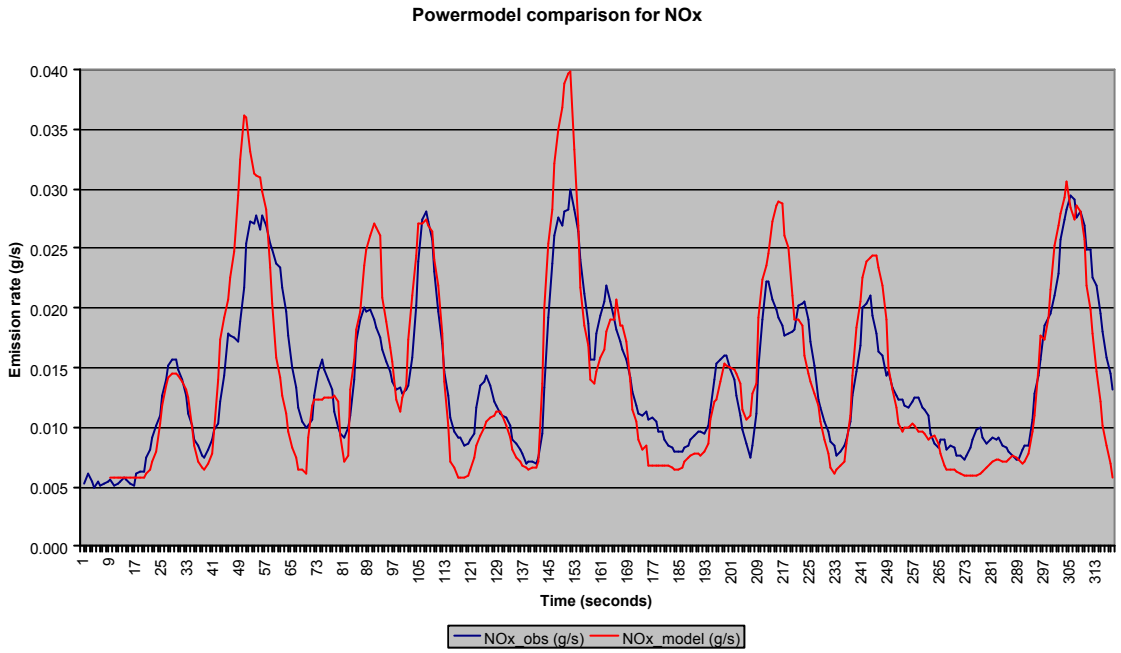

Figure 4(a): Plot of measured and modelled emission rates based on the power model for NO_x

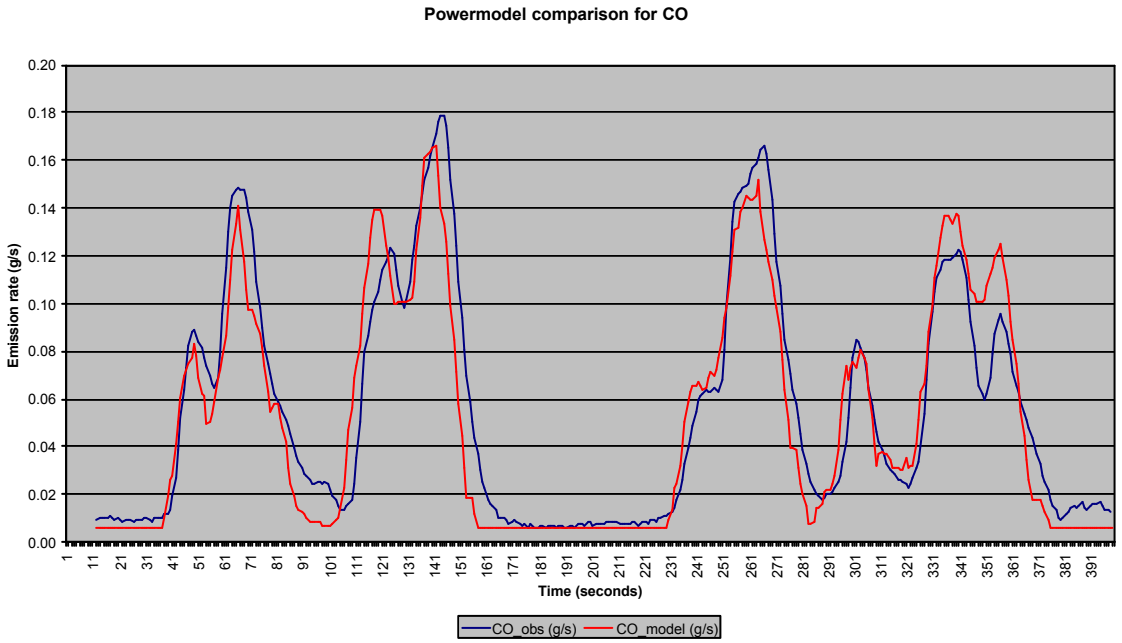

Figure 4(b): Plot of measured and modelled emission rates based on the power model for CO

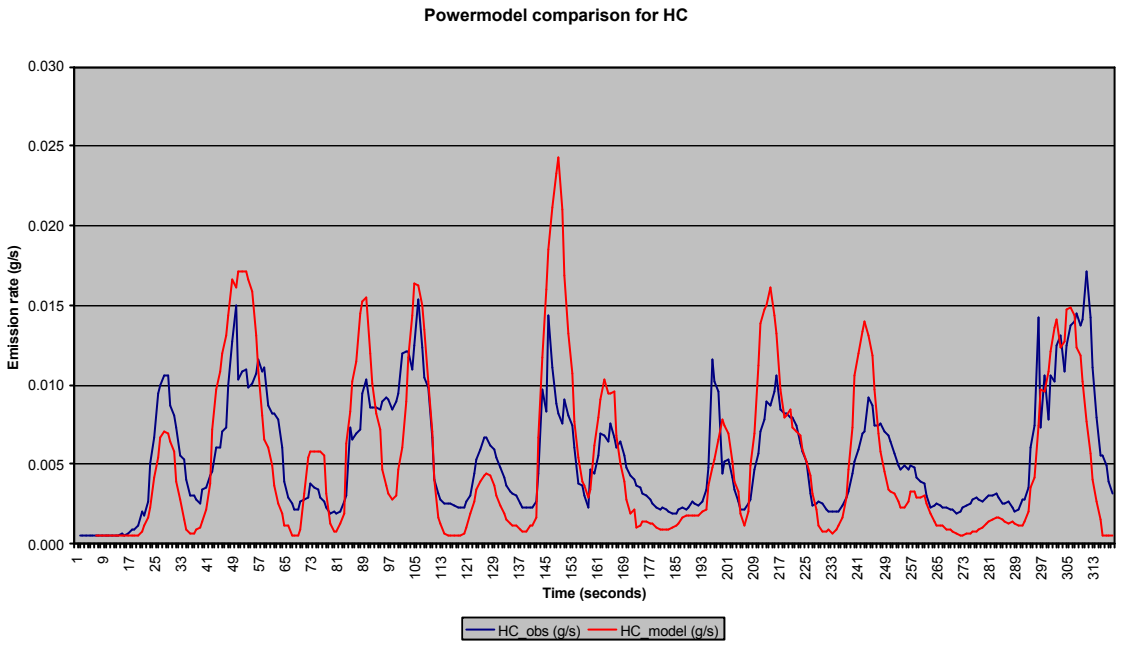

Figure 4(c): Plot of measured and modelled emission rates based on the power model for hydrocarbons

Further development of power modelling is part of continuing research being undertaken at CSIRO and when completed will be used to provide the most recent estimates of diesel emissions for use in the forecasting system.

As is evident from the data presented in this section the power-based approach to motor vehicle exhaust emissions allows great flexibility in modelling emission rates. This flexibility is not readily available from the VKT approach. However, in order to obtain maximum utility from this advantage, detailed knowledge of the road network and traffic flows is also required.

4. Road network data required for power modelling

From the above discussion it is apparent that in applying power modelling to a road network, detailed information over the entire network is needed in:

a) road grade
b) traffic flow rates in both directions
c) vehicle mix
d) intersection location and operational details

4.1 The Sydney road network

Road grades for the Sydney metropolitan region were determined by the following procedure. A surface contouring package was used to interpolate a 0.0025° resolution terrain map to a grid of 0.0001° resolution. The Sydney road network was then overlain. This is shown in Figure 5 where the major road network is shown against the major terrain features.

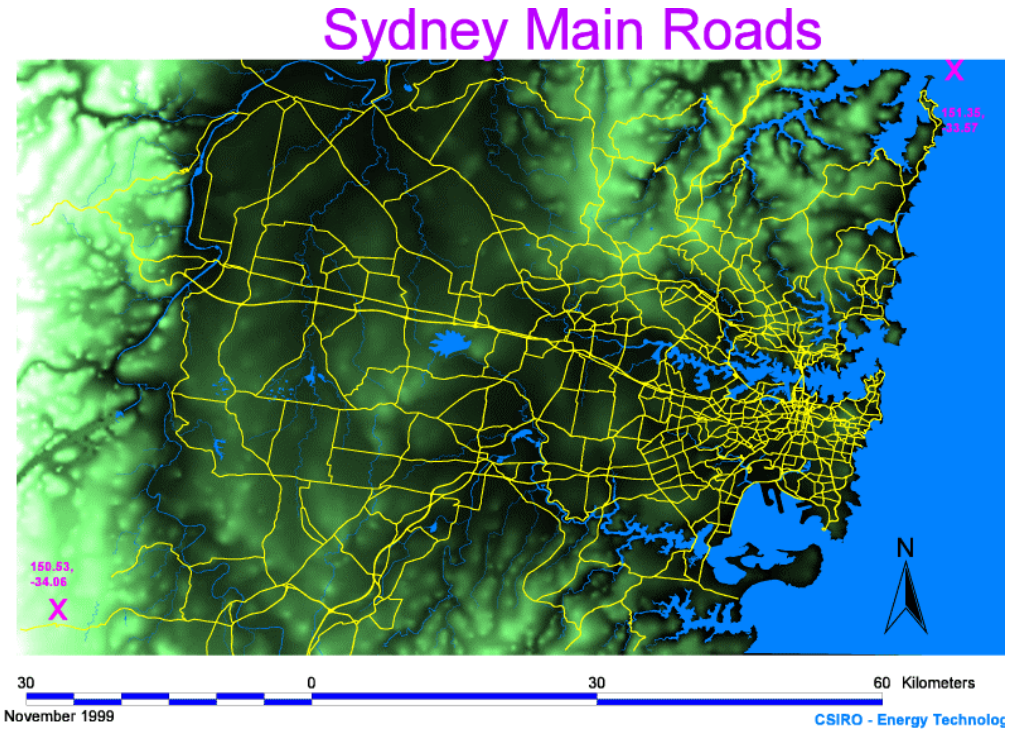

Figure 5: Sydney main road network.

From all the roads shown in Figure 5 a more tractable subset of major roads was derived. The choice was determined by the location of the routine traffic monitoring sites operated by the RTA. The subset of major roads is shown in Figure 6.

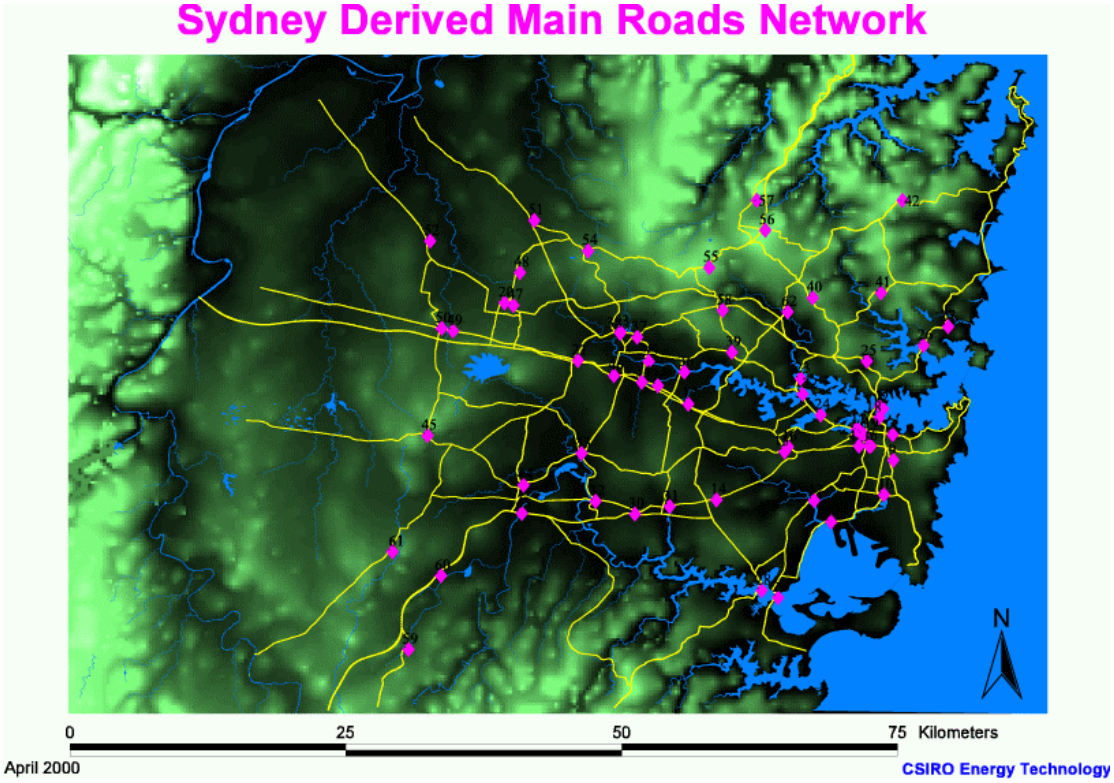

Figure 6: Derived Sydney main roads network

Software was then created to break the road network up into smaller sub-links with each sub-link being characterised by its start and end coordinates, the road grade, the direction of travel and intersection association. Using this procedure some 155,463 sub-links of approximately 10m lengths were produced to describe the derived main roads network.

These detailed data are illustrated in Table 2, which shows data for 30 of the 155,463 sub-links described above.

Table 2: Details of 30 sub-links for the Sydney derived main roads network

Sydmrd	Length	Long-1	Lat-1	Z1	Long-2	Lat-2	Z2	St_name	St_typ1	Suburb	St_hier	Direction	Intsec1	Intsec2	CellX	CellY
4157	8.749	151.079559	-33.771292	73.296	151.079651	-33.771273	73.526	CARLINGFORD	RD	EPPING	Highway	0	0	0	58	33
4158	8.749	151.079651	-33.771273	73.069	151.079742	-33.771254	73.296	CARLINGFORD	RD	EPPING	Highway	0	0	0	58	33
4159	8.749	151.079742	-33.771254	72.844	151.079834	-33.771234	73.069	CARLINGFORD	RD	EPPING	Highway	0	0	0	58	33
4160	8.749	151.079834	-33.771234	72.622	151.079926	-33.771215	72.844	CARLINGFORD	RD	EPPING	Highway	0	0	0	58	33
4161	8.749	151.079926	-33.771215	72.410	151.080017	-33.771195	72.622	CARLINGFORD	RD	EPPING	Highway	0	0	0	58	33
4162	8.749	151.080017	-33.771195	72.208	151.080109	-33.771176	72.410	CARLINGFORD	RD	EPPING	Highway	0	0	0	58	33
4163	8.749	151.080109	-33.771176	71.988	151.080200	-33.771157	72.208	CARLINGFORD	RD	EPPING	Highway	0	0	0	58	33
4164	8.749	151.080200	-33.771157	71.770	151.080292	-33.771137	71.988	CARLINGFORD	RD	EPPING	Highway	0	0	0	58	33
4236	8.741	151.080292	-33.771137	71.555	151.080383	-33.771118	71.770	CARLINGFORD	RD	EPPING	Highway	0	0	0	58	33
4237	8.741	151.080383	-33.771118	71.341	151.080475	-33.771099	71.555	CARLINGFORD	RD	EPPING	Highway	0	0	0	58	33
4238	8.741	151.080475	-33.771099	71.128	151.080566	-33.771080	71.341	CARLINGFORD	RD	EPPING	Highway	0	0	0	58	33
5236	7.830	151.080566	-33.771080	70.938	151.080648	-33.771061	71.128	CARLINGFORD	RD	EPPING	Highway	0	0	0	58	33
5237	7.830	151.080648	-33.771061	70.748	151.080729	-33.771042	70.938	CARLINGFORD	RD	EPPING	Highway	0	0	0	58	33
5238	7.830	151.080729	-33.771042	70.560	151.080811	-33.771023	70.748	CARLINGFORD	RD	EPPING	Highway	0	0	0	58	33
4230	6.582	151.080811	-33.771023	70.403	151.080879	-33.771008	70.560	CARLINGFORD	RD	EPPING	Highway	0	0	0	58	33
4231	6.582	151.080879	-33.771008	70.247	151.080948	-33.770992	70.403	CARLINGFORD	RD	EPPING	Highway	0	0	0	58	33
5229	8.648	151.080948	-33.770992	70.048	151.081039	-33.770977	70.247	CARLINGFORD	RD	EPPING	Highway	0	0	0	58	33
6229	6.037	151.081039	-33.770977	69.903	151.081100	-33.770958	70.048	CARLINGFORD	RD	EPPING	Highway	0	0	0	58	33
4121	7.180	151.081100	-33.770958	69.741	151.081177	-33.770947	69.903	CARLINGFORD	RD	EPPING	Highway	1	0	21	58	33
4442	8.670	151.081177	-33.770947	69.811	151.081197	-33.771023	69.741	BEECROFT	RD	EPPING	Metroad	1	21	0	58	33
4443	8.670	151.081197	-33.771023	69.881	151.081217	-33.771099	69.811	BEECROFT	RD	EPPING	Metroad	1	0	0	58	33
4444	8.670	151.081217	-33.771099	69.951	151.081238	-33.771175	69.881	BEECROFT	RD	EPPING	Metroad	1	0	0	58	33
5442	6.090	151.081238	-33.771175	69.998	151.081253	-33.771229	69.951	BEECROFT	RD	EPPING	Metroad	1	0	0	58	33
5443	6.090	151.081253	-33.771229	70.045	151.081268	-33.771282	69.998	BEECROFT	RD	EPPING	Metroad	1	0	0	58	33
6442	7.926	151.081268	-33.771282	70.081	151.081299	-33.771349	70.045	BEECROFT	RD	EPPING	Metroad	1	0	0	58	33
6443	7.926	151.081299	-33.771349	70.117	151.081329	-33.771416	70.081	BEECROFT	RD	EPPING	Metroad	1	0	0	58	33
7442	7.746	151.081329	-33.771416	70.186	151.081345	-33.771484	70.117	BEECROFT	RD	EPPING	Metroad	1	0	0	58	33
7443	7.746	151.081345	-33.771484	70.255	151.081360	-33.771553	70.186	BEECROFT	RD	EPPING	Metroad	1	0	0	58	33
8442	10.102	151.081360	-33.771553	70.334	151.081385	-33.771642	70.255	BEECROFT	RD	EPPING	Metroad	1	0	0	58	33
8443	10.102	151.081385	-33.771642	70.414	151.081409	-33.771730	70.334	BEECROFT	RD	EPPING	Metroad	1	0	0	58	33

Note that in Table 2 the columns named ‘CellX’ and ‘CellY’ refer to the grid used by the EPA Victoria to compile the emissions inventory for the Sydney Region.

4.2 Traffic flow rates

Traffic flow rates have been obtained from data published by the RTA NSW (RTA, 1996). These data are in the form of 15 minute counts for each traffic direction at selected locations around Sydney. Figure 7 shows an example of the form of the data.

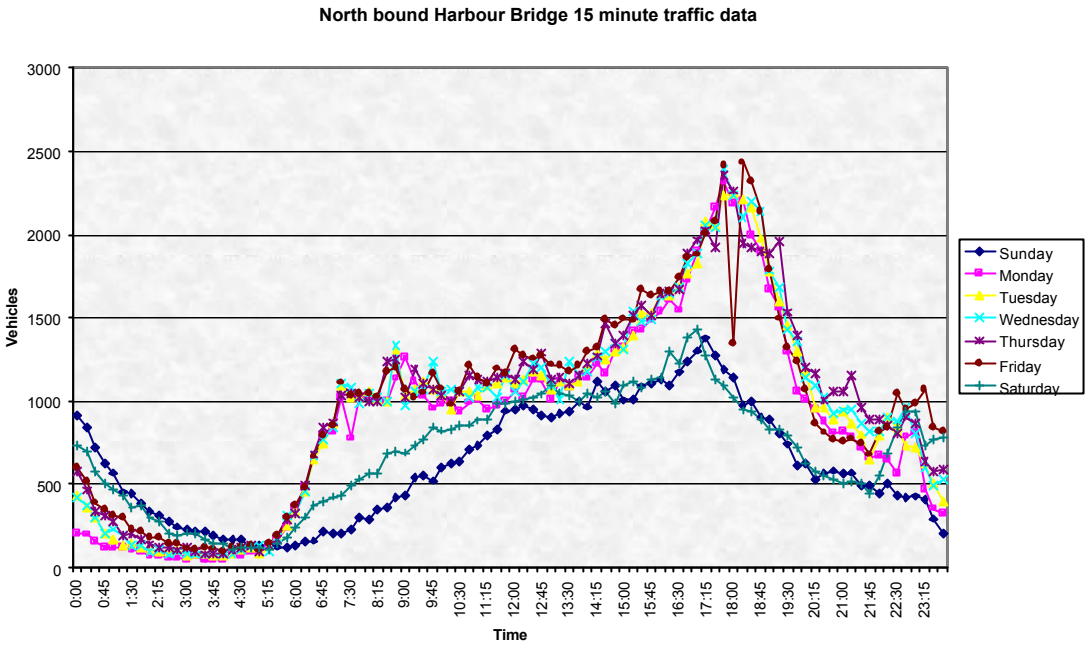

Figure 7: Example of RTA traffic count data.

The data show the clear difference between weekdays, Saturdays and Sundays. The coloured dots in Figure 6 show the location of similarly detailed data for the derived road network.

4.3 Intersection data

In addition to identifying the road traffic data, intersections must also be identified. This is because acceleration away from intersections can be a significant source of pollutant as shown in Figure 2b. Even though emission rates are relatively low when vehicles have stopped at intersections the total emissions can be relatively large as the vehicles spend considerably greater time in idle than when in free flow.

Software was developed to identify and mark each major intersection in the Sydney derived road network.

This is illustrated in Figure 8 which shows the major intersections for Epping Road a major link east west in the northern Sydney region and a road which carries maximum loads of ~ 15000 vehicles per hour.

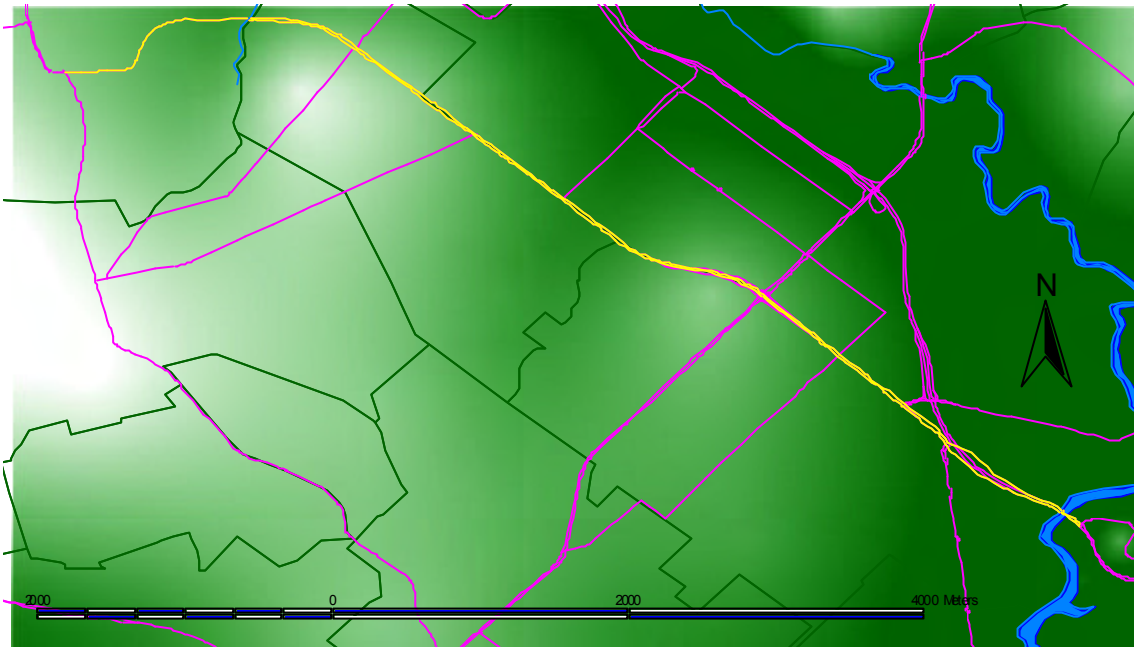

Figure 8: Detailed schematic view of Epping Road and adjoining roadways.

5. Application of power-based emissions modelling to Epping Road

In order to illustrate the concepts discussed above we have used a standard gaussian plume model, CALINE4, developed for motor vehicle emissions modelling (Benson, 1989). CALINE4 models a road as a series of sub-links and applies formulations for line source emissions. Full application of CALINE4 requires detailed knowledge of wind speed and direction. However in order to simplify and for purposes of illustration we have used a constant wind direction, constant wind speed, constant atmospheric stability and traffic vehicle mix. This allows the changes in emissions due to changes in road grade to be readily appreciated.

Figure 9 shows a 15 minute average output from CALINE4 for a vehicle travelling from Mowbray Road toward Midson Street along Epping Road. This is an actual simulation based on a CSIRO measured speed-time profile obtained by driving an instrumented vehicle, in traffic, along the route.

In Figure 9, the different colours define different zones of pollutant concentration. The regions of greatest concentration show the combined effects of road grade, acceleration and intersections. While the concentration profiles shown in Figure 9 are for one vehicle, and for purposes of illustration, they show clearly the great detail that can be provided by power-based emissions modelling.

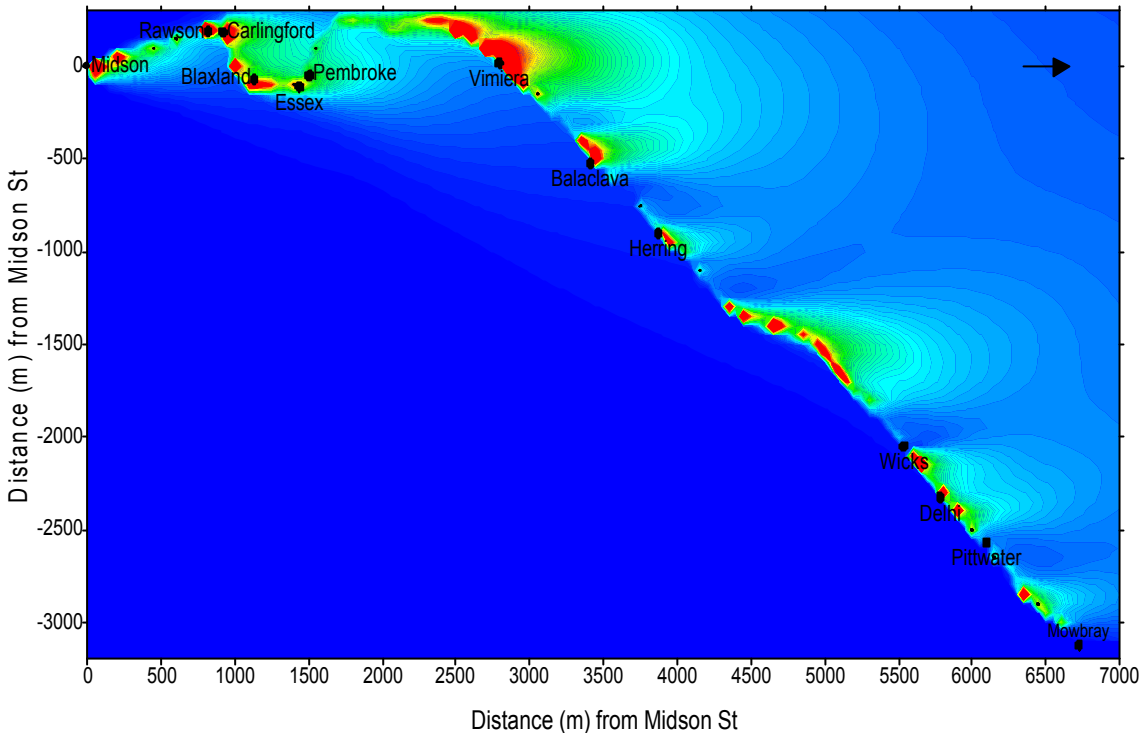

Figure 9: Indicative pollutant concentration profiles for a vehicle travelling in traffic along Epping Road.

6. Application of power-based modelling to an intersection

In addition to the example outlined above the detailed power model has been applied to intersections. This is illustrated below for the intersection layout shown in Figure 10.

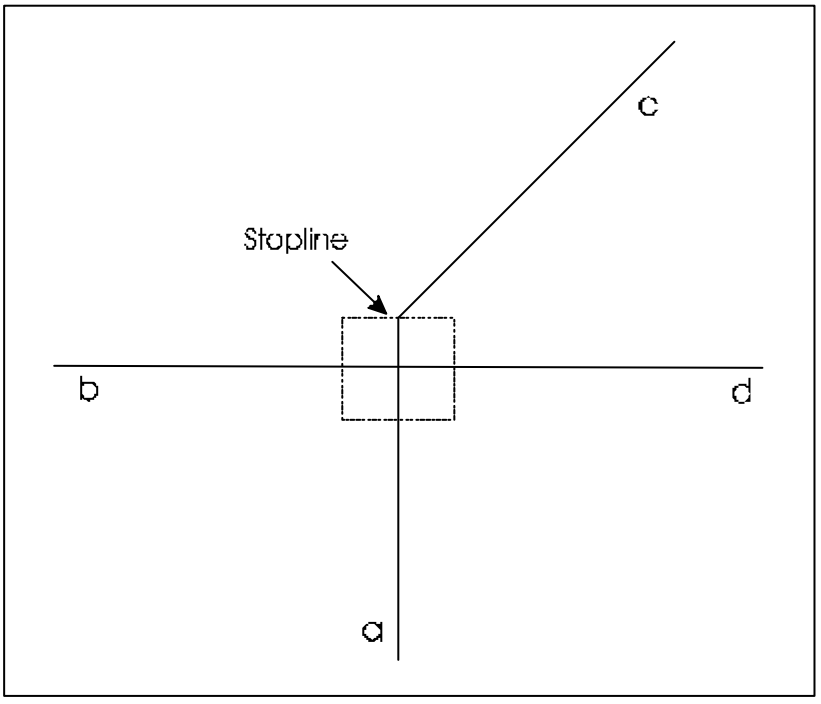

Figure 10: Layout of modelled intersection

Table 3: Details of road grade and traffic flow. (Note numbers are for purposes of illustration only).

Direction	Grade (Start ® Stopline)	Grade (Stopline ® End)	Cars per cycle	Queue	Max idle time (s)
a ® b	4°	0°	17	13	45
a ® c	4°	0°	40	10	30
c ® b	0°	0°	10	8	60
c ® a	0°	-4°	30	5	30
d ® b	4°	0°	10	8	120

For this model intersection, traffic from 'a' travels uphill to the intersection stopline. Traffic flow from the stopline in the 'b' and 'c' directions is on a level grade, while traffic flow from the stopline toward 'a' is downhill. We also have assumed that the traffic flow from 'd' is one-way, and that the free-stream speed for turning vehicles is significantly slower than for straight-through traffic. Thus non-delayed turning vehicles slow down on approaching the intersection and accelerate away after completing the turn. These characteristics are summarised in Table 3.

In order to apply the emissions power modelling approach, information on the rates of deceleration and acceleration from intersections as well as the statistics of traffic flow in individual lanes is required. Rates of acceleration and deceleration were obtained from CSIRO field measurements at intersections in Sydney.

Calculation of the emission rates for the intersection were run using the above information, the traffic light cycle shown in Table 3 and a model of vehicle motion based on kinematic considerations which tracks each vehicle explicitly at the intersection. The emission rates for CO and NO_x averaged over a full 15 minute period are shown for each part of the intersection in Figure 11.

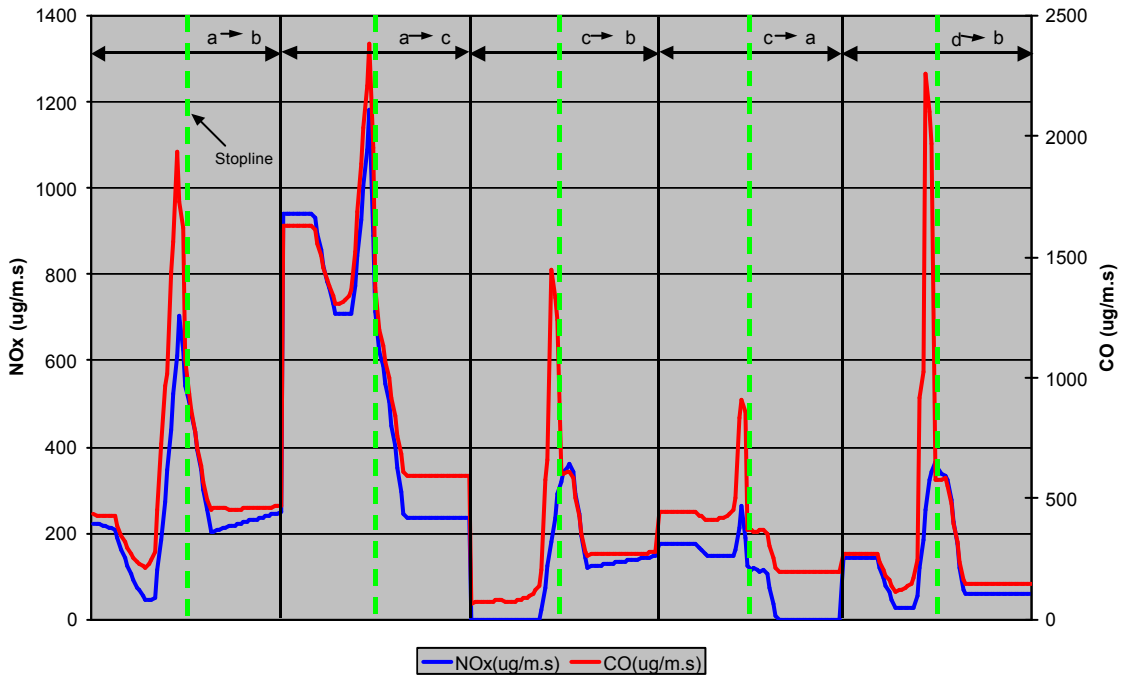

Figure 11: Average emission rates (15min) for the intersection defined by Figure 10 and the data in Table 3

The emissions data in Figure 11 show the complex nature of the emission profile even for constant traffic flow motion when the complicating features of vehicle deceleration, acceleration and idle at traffic lights are included. The stop lights are indicated by the vertical dashed lines.

Figure 12 shows an enlarged section of Figure 11 for the route 'a' to 'c'.

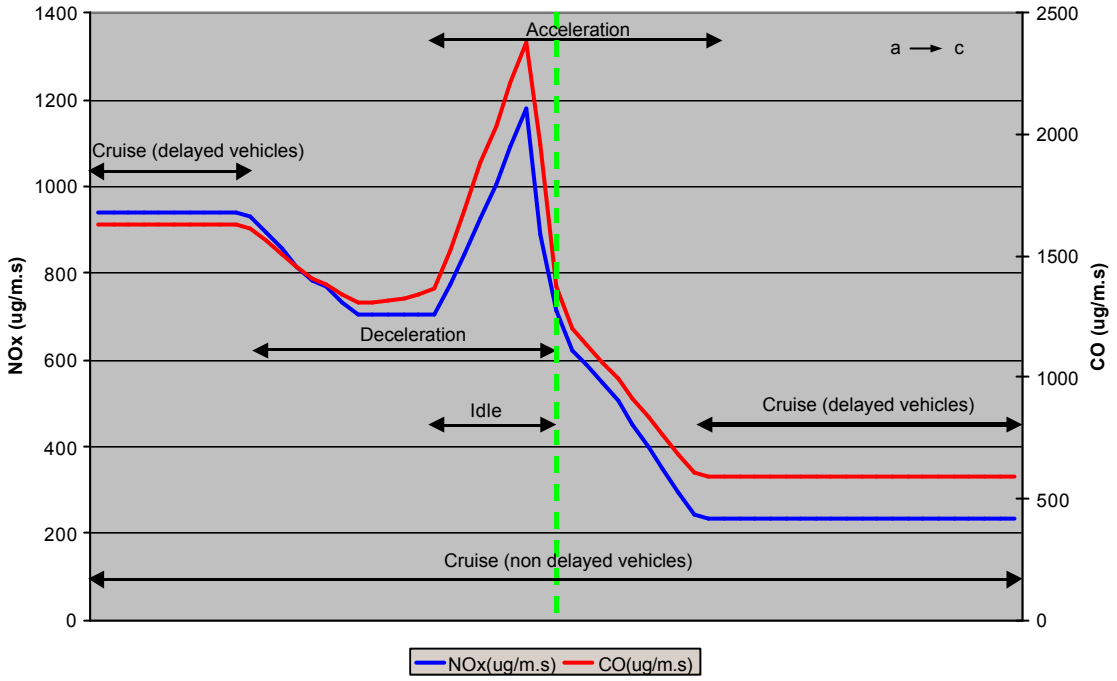

Figure 12: Enlarged section of Figure 9.

The route includes an uphill section, with either direct travel through the intersection onto the region of zero grade if the traffic light is green, or deceleration and stop for a red light. Once the light is green the vehicles accelerate toward 'c' in flat terrain after they have passed the stopline until they achieve the constant cruise speed. The peak in average emission near the stopline is due to acceleration of the vehicles away from the intersection and the added time the vehicles are stationary at this location due to a red light. The combination of all these factors produces a complex average emission rate signature.

Figure 13 shows the calculations of NO_x concentration emitted during stable meteorological conditions (Pasquill category F) from CALINE4 for a constant traffic fleet mix and flow rate.

Similar calculations for CO are shown in Figure 14.

In Figures 13 and 14 there are clearly zones of acceleration and deceleration. Notable differences however are observed between the overall CO and NO_x emission profiles. Referring to Figures 3a and 3b it is apparent that there is a higher emission rate during stopped (idle) conditions for CO than there is for NOx. This is clearly observed in Figure 14 with an accumulation of emissions within the vicinity of the stopline.

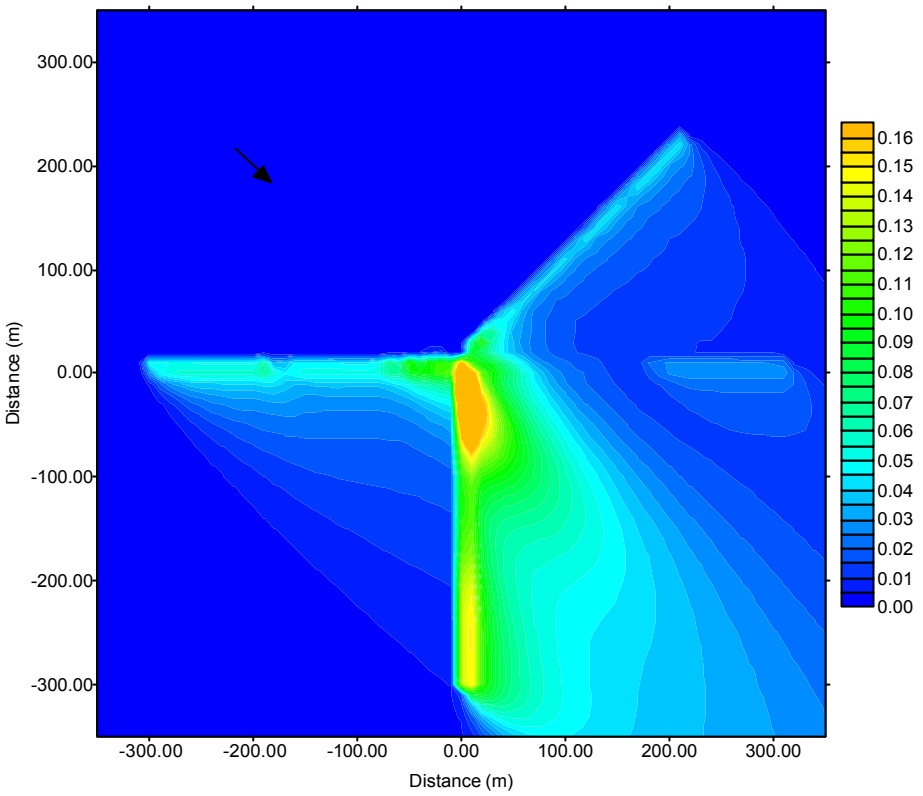

Figure 13: Calculations of NO_x concentrations for the intersection of Figure 8 using CALINE4 and the emissions profiles shown in Figure 12.

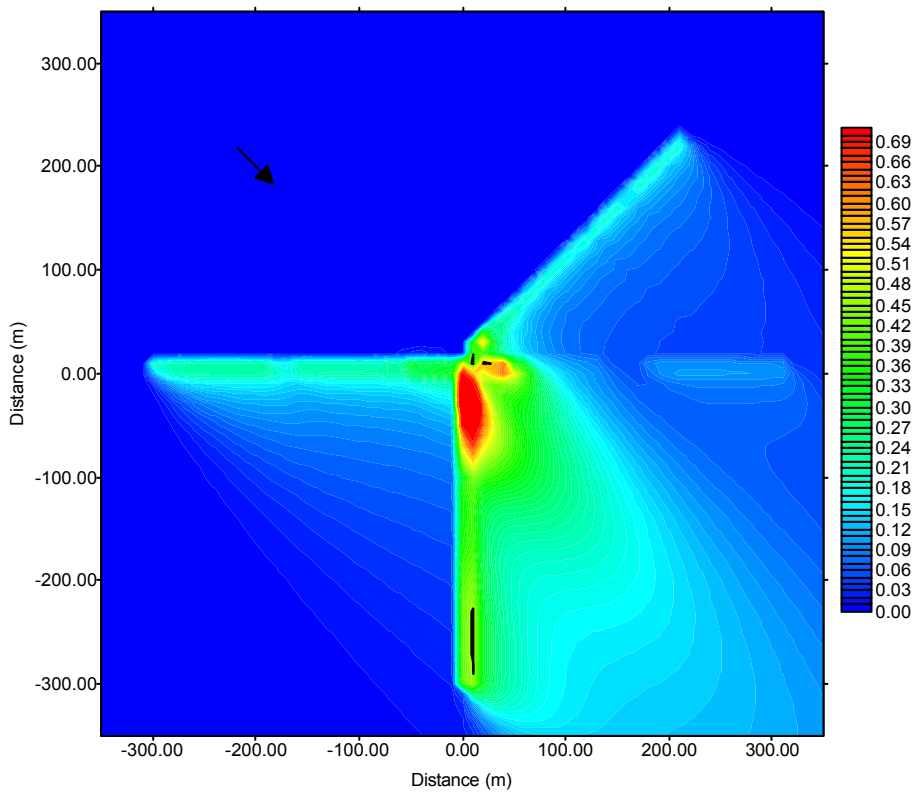

Figure 14: Calculations of CO concentrations for the intersection of Figure 10 using CALINE4 and the emissions profiles shown in Figure 12.

7. Generalisation to the road network

In order to generalise the above considerations to an entire road network, albeit a simplified one as developed here, a number of further assumptions are required concerning traffic flow. Data are limited and this highlights one of the major limitations that needs to be overcome in order to obtain maximum use of power-based modelling schemes.

The RTA road statistics provide vehicle counts for a limited number of roads in the reduced Sydney road network developed here. Consequently a number of generalisations of the data available to (and obtained) during the current study have been required.

Key among these is traffic flow at intersections. A number of assumptions have been required to relate intersection traffic flow properties to average traffic count data available from the RTA published data. These assumptions were derived from CSIRO field measurements in conjunction with RTA data at a limited number of intersections from a major Sydney road. Time dependent variables for the number of cars per cycle, number of cars delayed per cycle, maximum stop time and average intersection speed were developed as a function of total vehicle count as displayed in Figure 15.

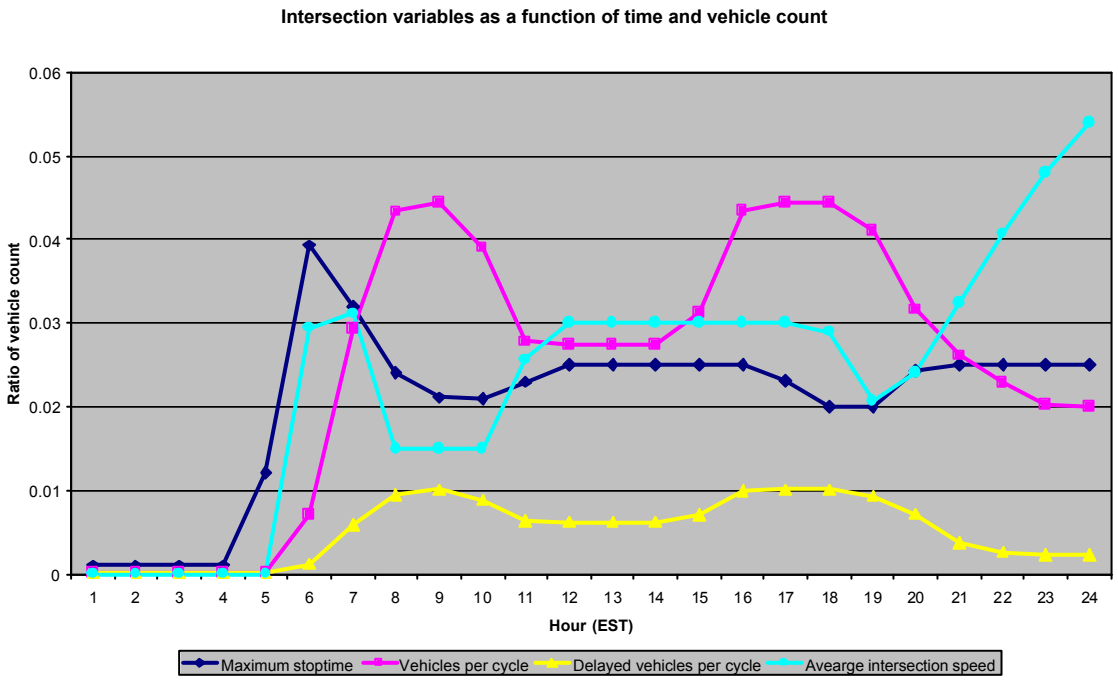

Figure 15: Traffic details for generalised intersection.

Average intersection speed from 12am to 5am was assumed to be equal to the free-stream speed.

Free-stream traffic speed was based on road hierarchy using the assumed speeds shown in Table 4.

Table 4: Assume speeds for free flowing traffic for different road classes.

Hierarchy	Free-stream speed (km/h)
Avenue	60
Drive	60
Expressway	80
Freeway	80
Highway	60
Motorway	80
Parade	60
Road	60
Street	60
Way	60
Unknown	60

Acceleration rates for cars, light-duty diesels and heavy-duty diesels were obtained from CSIRO measurements at varying distances from the intersections. Average values employed in this study were 1.6 m/s^2 for cars, 1.3 m/s^2 for light duty diesels and 0.7 m/s^2 for heavy duty vehicles. Deceleration rates were assumed to be 80% of the acceleration rate. These data were assumed to be representative for all intersections in the Sydney main road network.

In addition to the intersection variables, a number of other traffic related properties were also required. These include an estimate of the vehicle traffic mix, the proportion of vehicles by age and catalyst type and average vehicle properties for the four classes of vehicle modelled (spark-ignition vehicles, spark-ignition catalyst-equipped vehicles, light duty- and heavy duty diesel vehicles).

Average vehicle traffic mix was derived from CSIRO field measurements detailed above. These data are represented in Figure 16.

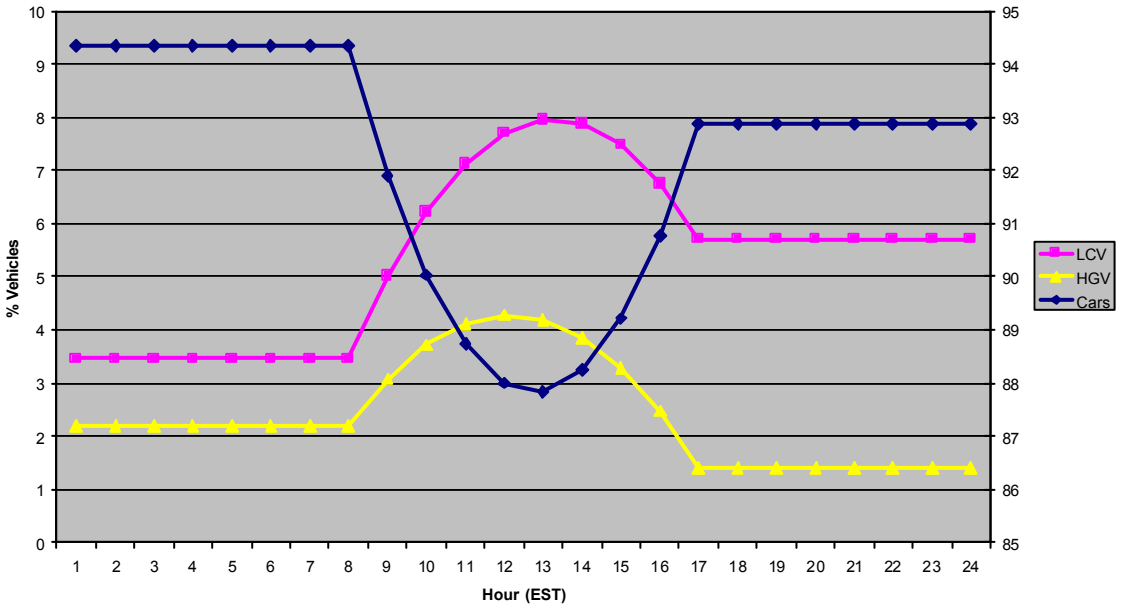

Figure 16: Average traffic mix as a function of time.

Data for hours before 8 am were assumed equal to the measurements at 8am and data after 6 pm were assumed equal to those taken at 5:30 pm. As was the case for the intersection data, these data were applied to all modelled intersections. Again based on CSIRO data 2/3 of the LCV's were assumed to be petrol vehicles and 1/3 were assumed to be diesel.

Vehicle proportions as a function of age expressed in 5-yearly brackets were derived from the National Greenhouse Gas Inventory Workbook (NGGI 1998). The same age distributions were assumed for diesel vehicles. Average catalyst proportions for the entire fleet were also derived from the NGGI Workbook (1998), adjusting for total vehicle count.

In addition to the traffic flow data, it was also necessary to generalise the parameters used in the power modelling for each class of vehicle.

Average vehicle class properties for mass and engine capacity were derived assuming vehicles measured in the FORS and the NEPC study for diesel vehicles were representative of the total vehicle fleet. These are shown in Table 5.

Table 5: Shows the average values for vehicle characteristics used in this study.

Vehicle type	Drag coefficient	Frontal area (m^2)	Mass (kg)	Engine capacity (L)
SI catalyst	0.35	2.0	1285	2.6
SI non catalyst	0.40	2.0	1200	2.5
LDD	0.80	4.0	4400	3.5
HDD	0.80	10.0	25000	9.0

For occasions when calculated power requirement exceeded a prescribed power output a maximum value was assumed in order to minimize unacceptably high emission rates. These values are shown in Table 6.

Table 6: Maximum power for each type of vehicle.

Vehicle type	Maximum power (kw)
SI catalyst	150
SI non catalyst	150
LDD	150
HDD	300

8. Comparisons with VKT data

A simple comparison was made with VKT estimates using the methodology adopted by EPA Victoria. Estimates of emission rates quoted below for EPA Victoria data set are based on exhaust emissions only. VKT adjustment factors used were 1.10 for a weekday (Monday), 0.73 for a weekend day, a monthly adjustment factor of 1.0 (October) and an ambient temperature of 20 ºC. Percentage comparisons are given in Table 7 below.

Table 7: Comparison between VKT and power model outputs

Day	VKT	NOx (diesel)	NOx (petrol)	CO (diesel)	CO (petrol)	HC (diesel)	HC (petrol)
Weekday	38 %	73 %	35 %	12 %	17 %	12 %	22 %
Saturday	50 %	102 %	47 %	16 %	22 %	17 %	29 %
Sunday	43 %	86 %	41 %	14 %	19 %	14 %	25 %

In Table 7 the VKT comparison highlights the smaller road network employed for the detailed modelling.

The data in Table 7 also show that, for example, on a weekday the power model would account for 73% of the total NO_x emitted for the entire grid based on the VKT/emission factor approach even though the reduced road network only accounted for 38% of the VKT. Similarly for the other pollutants shown. The difference between the EPA Victoria estimates may reflect the uncertainty in the pollution emissions factors used in the two approaches, which may also reflect the fact that road grade and acceleration is more explicitly dealt with in this power model.

While the comparisons shown in Table 7 are interesting there are too few data to draw any clear conclusions at this stage. This remains an issue for continuing research.

9. Conclusion

This work has refined and applied the power-based model of motor vehicle emissions to a reduced set of Sydney major roads. The emissions take into account road grade and the presence of intersections as well as the traffic flow rates. Although simplifications and generalisations have been necessary, the work presents the first application of power-based modelling to a city road network in Australia.

The need for a vast amount of data, while recognised at the outset has nevertheless been highlighted by the application of the model to Sydney. Much of the data required for such modelling is simply not available in sufficient detail and many assumptions were required.

The work described in this report is based on the synthesis of a large amount of data describing petrol- and diesel-vehicle emissions, vehicle-fleet mixes, road-traffic statistics, road networks and vehicle behaviour in free stream traffic and at intersections. Many of the data, particularly the emissions data and the driver behaviour data, show large variations from vehicle to vehicle. This highlights the need for continuing research and data for

- pollutant emission rates from motor vehicles
- traffic-flow data
- driver and vehicle behaviour, particularly at intersections.

These data are essential for approaches based on power modelling to be able to provide a more detailed and accurate motor-vehicle emissions modelling inventory.

Acknowledgment

The authors wish to acknowledge the cooperation of EPA Victoria and the RTA of NSW during the course of this work.

References

Benson, P.E., et al., (1989). Caline4 - A dispersion model for predicting air pollutant concentrations near roadways. Final report No FHWA/CA/TL-84/15. California Department of Transport, Sacramento, California, USA.

Kent, J.H., Post, K. and Tomlin, J.A. (1982) Second Conference on Traffic, Energy and Emissions, 19-20 May 1982 at National Science Centre, Melbourne.

Richardson, A.J. 1982 Stop-start fuel consumption rates. Second Conference on Traffic, Energy and Emissions, 19-20 May 1982 at the National Science Centre, Melbourne.

Williams, D.J., Shenouda, D.A. and Carras, J.N. (1994) Modelling air toxic emissions from motor vehicles. 1994 August, Proceedings Air Toxics Conference Vol 2: pp31-47.

FORS (1996) Motor vehicle pollution in Australia. Report on the national in-service vehicle emissions study. Federal Office of Road Safety.

NEPC (2000) In-Service Emissions Performance – Phase 2: Vehicle Testing. National Environment Protection Council Service Corporation 2000.

NGGI (1998) Workbook for Transport Mobile Sources. National Greenhouse Gas Inventory Committee. Workbook 3.1. Canberra.

RTA (1996) Traffic volume data for Sydney region 1996. Volume2.

Appendix 7.1 Melbourne 3-Day Photochemical Smog Event

K. J. Tory[1], G. D. Hess[1], M. E. Cope[2,3] and S. Lee[2]

[1]Bureau of Meteorology Research Centre,
[2]CSIRO Atmospheric Research, [3] CSIRO Energy Technology

1. Background

During 7–9 March 2001 elevated ozone concentrations were recorded at a number of Melbourne air quality monitoring stations. The synoptic situation is presented in Figure 1. On the morning of 7 March (11 am EDT) the pressure gradient over Melbourne was particularly weak (Figure 1a). A broad trough covered much of northern and western Australia punctuated by a series of low-pressure centres. Pressure increased gradually to the south of the continent (except southwest of Western Australia) which suggests a light easterly gradient wind over southeastern Australia was present. Twenty-four hours later the pressure had increased over the Tasman Sea and coastal southeastern Australia, with the approach of a cold front from the south (Figure 1b). This led to a slight rotation and an increase in the pressure gradients there, which resulted in a rotation to northeasterly and strengthening of the gradient wind. In the next 24 hours ridging over the Tasman Sea became more pronounced and the gradient wind became more northerly in direction over southeastern Australia (Figure 1c). Figure 1d shows a trough and cold front approaching. Northerly winds, enhanced by this approaching front, led to greater ventilation, which contributed to low-ozone concentrations on the following few days. During the three-day period of elevated ozone, the local scale meteorology was influenced by the diurnal heating and cooling cycle, and the development of bay and sea breezes. The ozone cycle in the immediate Melbourne area (e.g., the monitoring sites) can be explained largely in terms of precursor transport and ventilation. However, complex ozone circulation patterns were present over much of Victoria due to ozone transported by winds that varied significantly in space and time.

2. Mesoscale Meteorology and AAQFS Performance

Throughout the three-day period the atmosphere was strongly stable above 750 hPa. This can be seen in the time versus height profiles of the atmosphere at Melbourne Airport presented in Figure 2. The stable layer acted to trap pollutant species vertically and thus inhibited vertical dilution. Compared with other high-ozone days this stable layer was relatively deep, which might partly explain why the observed maximum ozone levels were high rather than extreme (i.e., greater dilution). The observed structure (Figure 2a) was constructed from data collected by domestic aircraft as they take off from Melbourne Airport. The equivalent profile generated from LAPS data is presented in Figure 2b. Note Figure 2b is constructed from three consecutive LAPS forecasts. The vertical lines mark the division between model runs. A comparison of Figures 2a and b show the model forecast captured the strong diurnal pattern of low-level nocturnal cooling followed by surface heating, and the development of a daytime mixed layer that extended to 800 hPa on the first and third days, and about 850 hPa on the second day. On each day the forecast depth of the mixed layer (yellow line) compares very well with that observed. The changing direction of the low-level winds was also well represented. On the first day the low-level winds were northerly between 1900 and 2300 UTC (due, in the model, to drainage flow and downstream turning of the upstream northeasterly winds flowing parallel to the Great Dividing Range (GDR)) and shifted to southerly by about 0100 UTC (midday) in both the model and observations. The model southerly winds were due to the arrival of the bay breeze and later the sea breeze, and were reinforced by larger-scale southeasterly winds that continued throughout the night and into the next day. The same pattern was evident in the observations, although the observed southerlies had more of an easterly component. We show below that the southerly winds played an important role in advecting ozone that had formed over Port Phillip (the bay) northwards over

suburban Melbourne. Between 1900 and 0300 UTC on the final day both model and observations show stronger northerly winds (due to the strengthening northerly gradient winds, Figure 1b). After this time Figure 2a shows a bay/sea breeze arrived at the Airport (see the wind shift to southeasterly and an accompanying drop in temperature after about 0500 UTC 9 March (4 pm EDT), Figure 2a). The model bay/sea breeze did not penetrate as far as the Airport (although the northerlies did weaken due to the close proximity of the wind shift further south). We show below that the model bay breeze penetration was hampered by the synoptic northerlies and stopped just short of the Alphington monitoring station. Thus, higher concentrations of ozone carried by the bay breeze did not reach Alphington, which explains a model under-prediction on that day. Finally both the model and the observations show the northerlies re-intensified between 1900 and 2300 UTC, 9 March (6 and 10 am, 10 March EDT) as the cold front approached from the west.

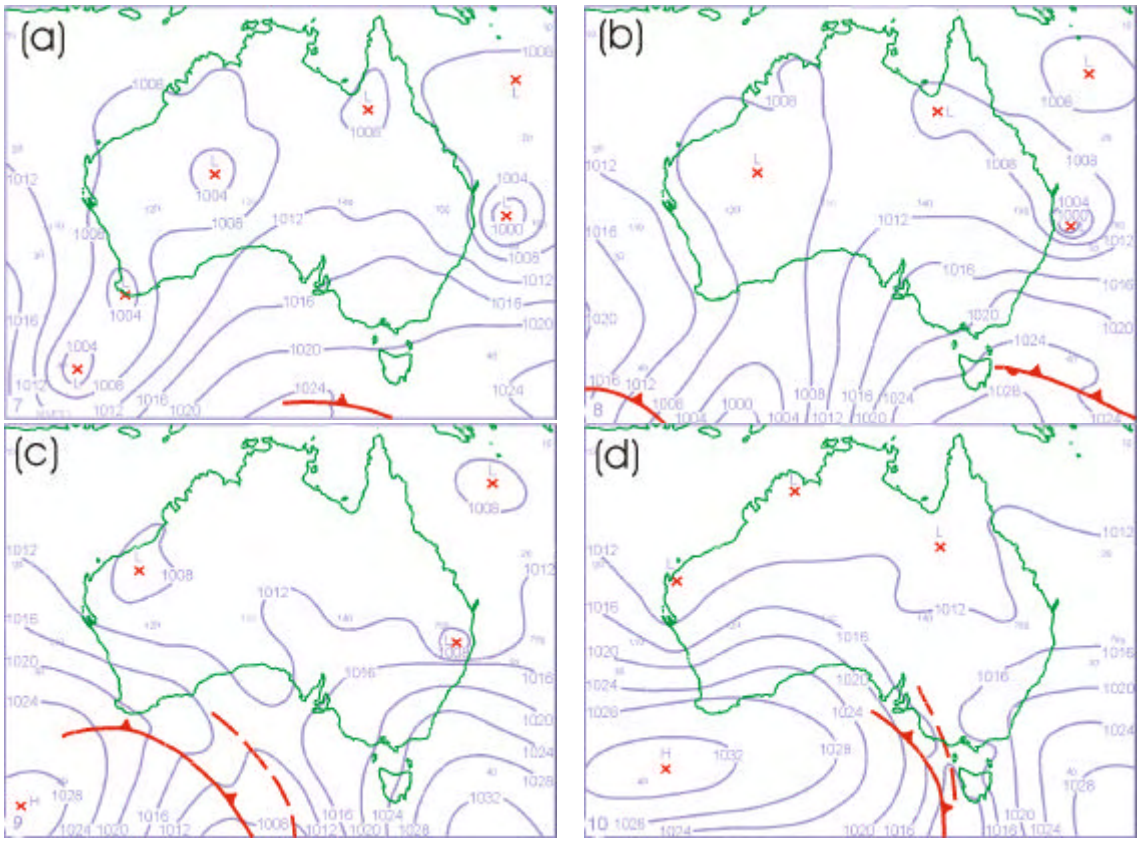

Figure 1. Synoptic pressure charts at 0000 UTC on (a) 7, (b) 8, (c) 9 and (d) 10 March 2001. Contour interval = 4 hPa. Cold fronts are depicted as full red lines with triangles, and the trough as a dashed red line.

3. Ozone

On the morning of the first day ozone precursors were advected over the bay by drainage flow. This is illustrated in Figure 3, which shows precursor concentrations (shaded) with observed (yellow) and modelled (white) wind vectors overlayed. Converging drainage winds and the light synoptic easterly winds in the south of the domain led to the formation of an eddy over the bay just offshore of Geelong (Figures 3a and b). See the rotation of the Melbourne and Geelong precursor plumes. A bay breeze began to develop at 1100 EDT (Figure 3c) at which time the precursor concentrations were at a maximum, with the highest concentrations to the north and east of the bay and over the eastern half of the bay. Two hours later (Figure 3d), the bay breeze had become well established and the precursors were advected radially out from the bay in the north and northeast, and westward across the bay.

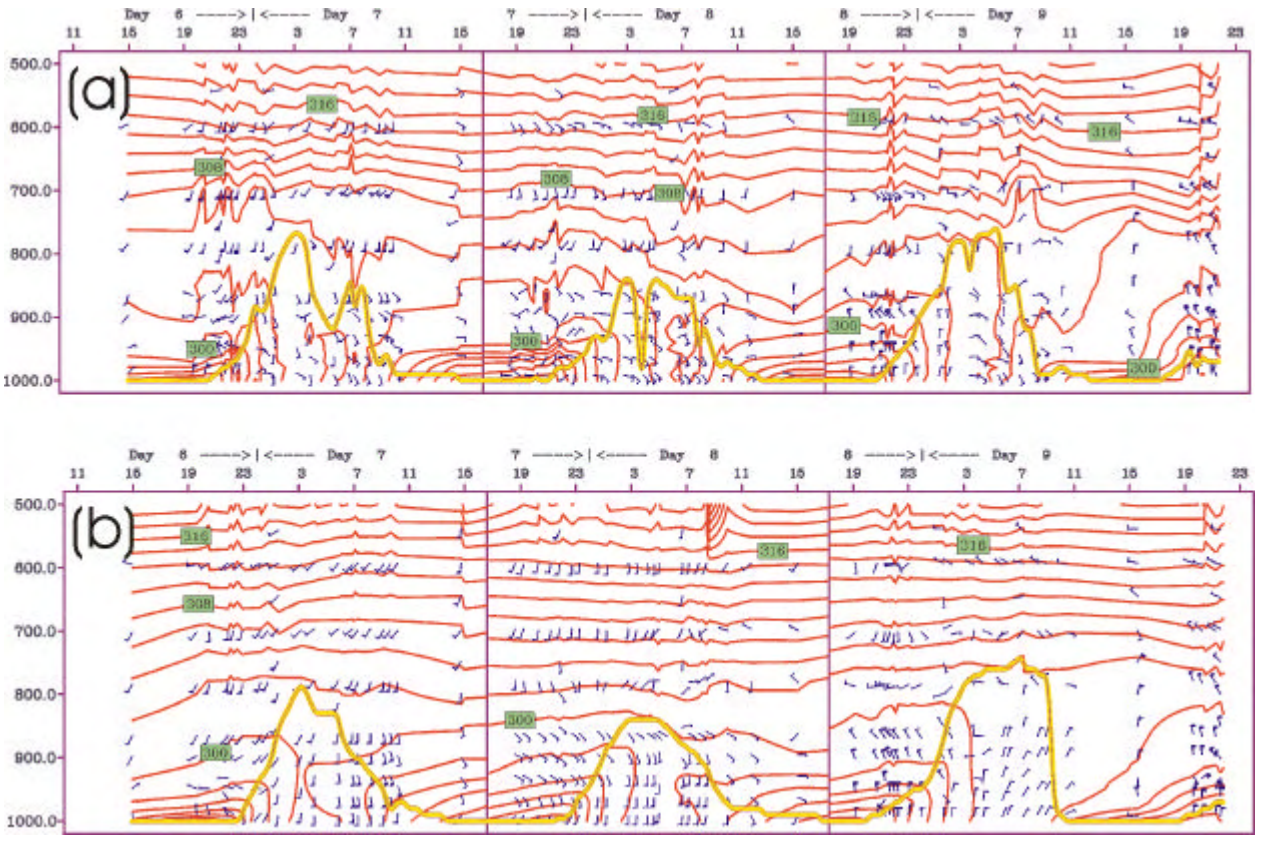

Figure 2. Time-height profiles of potential temperature (contour interval 2 K) and winds (full barb = 10 knots), for the 84-hour period following 1100 UTC 7 March 2001 at Melbourne Airport. The yellow line marks the approximate position of the top of the mixed layer, determined by the level at which the atmosphere is first 1 K warmer than the 10-m potential temperature. Image (a) was constructed from data collected by commercial aircraft as they take-off from Melbourne Airport, and (b) from LAPS data interpolated to the flight paths.

By midday on Day 1 the ozone concentrations began to increase semi-uniformly across the Melbourne airshed. Four hours later concentrations over the bay were considerably greater than the surrounding areas. This is evident in Figure 4a, which shows the forecast surface ozone concentrations. About 750 m above the surface the pattern was largely reversed; the greater concentrations surrounded the bay and the concentrations over most of the bay were close to background levels. A vertical section through longitude 145.0° (passing through Brighton and relatively close to RMIT and Alphington) is presented in Figure 4c. Potential temperature contours were included to illustrate the stability of the atmosphere on this section. There was a clear correlation between stable layer depth and ozone concentrations. Over the bay the stable layer was considerably lower than the surrounding area, and the ozone was trapped below about 700 m. Heating of the land surface generated turbulent mixing that diluted the ozone over a depth of about 2400 m (Figure 4c). In other words, ozone concentration was proportional to the ventilation. The eight monitoring stations that recorded ozone during this period (Box Hill, Mt. Cottrell, Alphington, RMIT, Geelong South, Paisley, Pt. Cook and Brighton) are all located relatively close to the bay (approximately 15, 15, 10, 5, 5, 1, 1 and 1 km respectively). All stations are located near the northern parts of the bay except Geelong South, which is close to the western extreme of the bay. The southerly flow, evident in Figure 4a, advected the cooler, ozone-rich bay air beyond the northern stations before the mixed layer growth had become significantly deep, and each station experienced maximum ozone concentrations within about 50-70 ppb. Time-series of observed and modelled ozone concentrations are presented in Figure 5 for the 3-day period at the eight stations mentioned above. The model performed well at each station on this day, with a maximum error of about a 15 ppb under-prediction at Mt. Cottrell. Even at these small distances from the bay

there is a clear correlation between modelled maximum concentration and proximity to the bay at the northern stations (Figure 5). At the stations closest to the bay (Paisley, Brighton and Pt. Cook) maximum concentrations were about 70 ppb. Mt. Cottrell experienced a modelled maximum of about 60 ppb compared with 50 ppb at the further stations of Alphington, RMIT, and Box Hill. Although Geelong South is relatively close to the bay it experienced lower readings since it was not located down-wind of the ozone-rich bay air. Later in the afternoon when the ozone production began to slow the southerly flow advected the remaining ozone inland and clear of the Melbourne area.

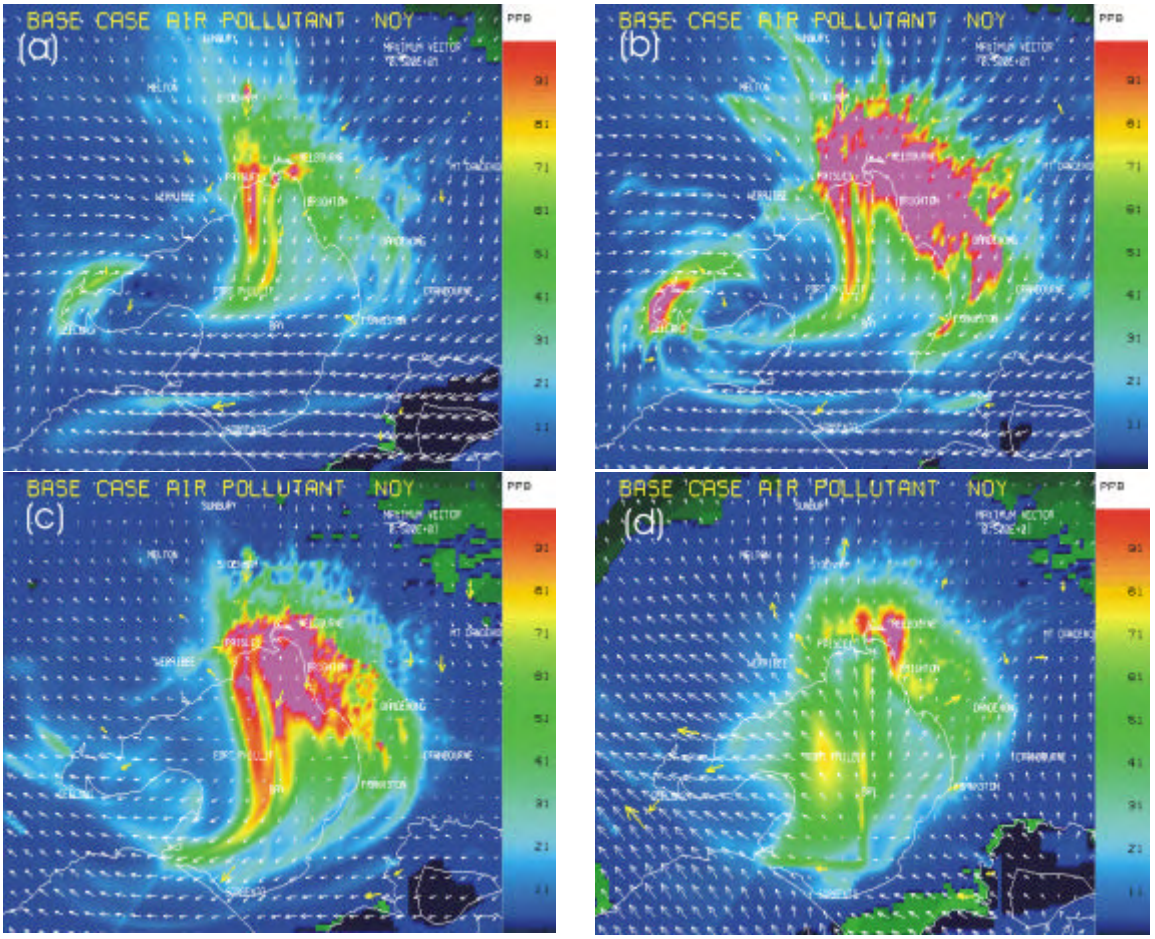

Figure 3. Ozone Precursors on the morning of Day 1 at (a) 0500, (b) 0700, (c) 1100 and (d) 1300 EDT. Drainage flow advected precursors over the bay (a) and (b). Converging drainage winds and the light synoptic easterlies to the south led to the development of an eddy entered over the bay offshore of Geelong (a) and (b). (See the rotation of the Melbourne and Geelong precursor plumes.) The maximum precursor concentration over the bay occurred at 1100 EDT (c). At this time a bay breeze was beginning to develop, which advected the precursors northward and westward (d). Note in (d) the east-west line through the heads and the perpendicular north-south line in the middle of the bay. These lines reflect emissions from shipping channels.

On the second day the synoptic wind strength increased (consistent with the gradient winds indicated in Figure 1c). Turning of the northeasterly winds downwind of the GDR led to east-southeasterly winds over the southern part of the bay. The interaction of this stronger synoptic flow with the weak drainage flow led to the formation of an eddy northeast of Melbourne. This is evident in Figure 6a, which shows ozone precursors and observed and modelled winds (same as Figure 3) at 0500 EDT on Day 2. The synoptic east-southeasterly winds ensured the bay remained largely precursor free (Figure 6b). The precursors were contained within the eddy to the north of Melbourne (Figure 6c) and remained there for a number of hours (Figure 6d). Thus, unlike the previous day when significant

concentrations of precursors were advected over the bay, the bay remained largely precursor free for all of Day 2.

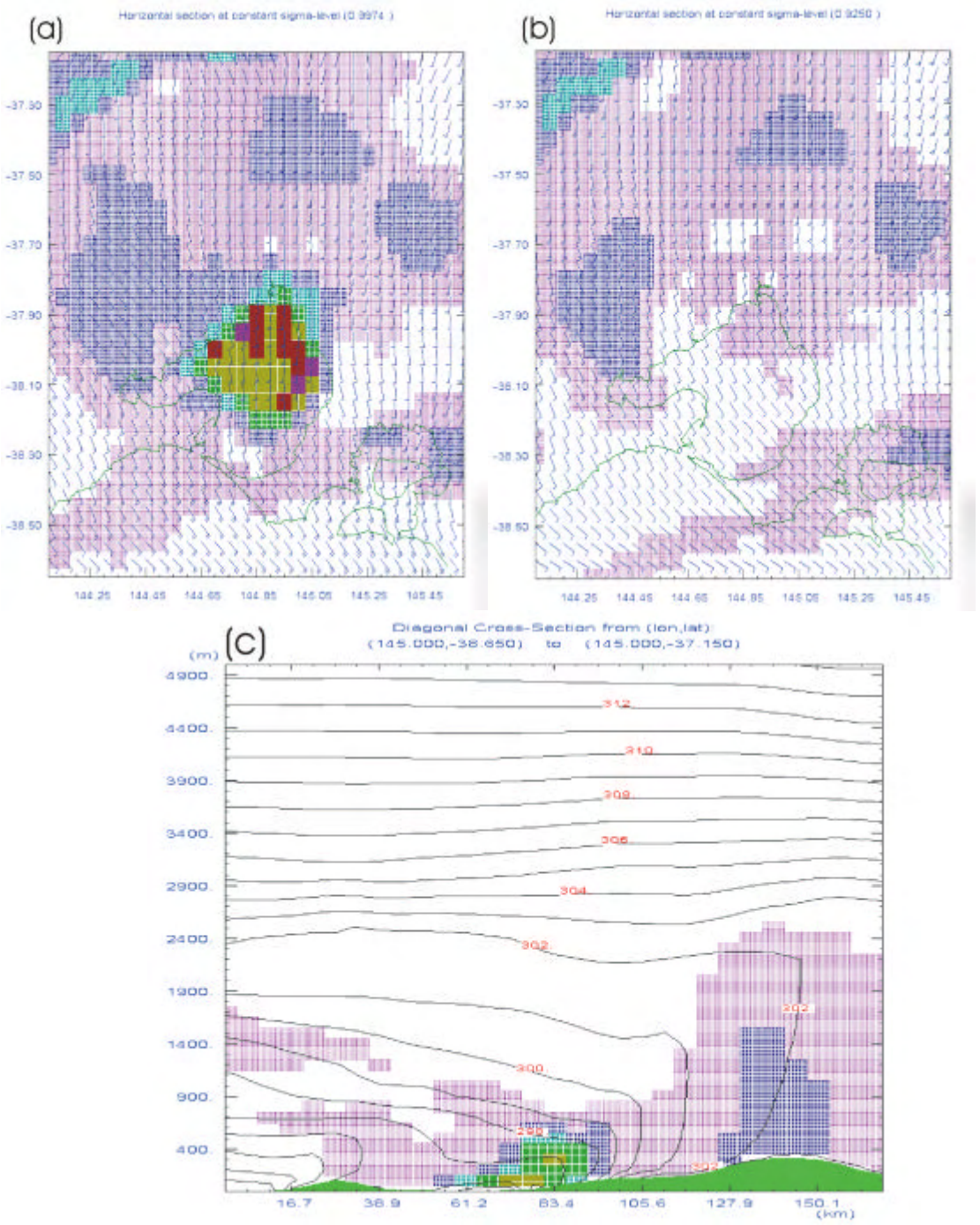

Figure 4. Ozone (shaded) at 4 pm on Day 1 (0500 UTC, 7 March 2001). Concentrations increase by 10 ppb with each colour from magenta through to red and magenta again, beginning with the range 40-50 ppb. Horizontal winds (full barb = 6 knots) are included in (a) and (b) at the surface and about 750 m respectively. Potential temperature is added to (c) (contour interval, 1 K), a north-south vertical section that passes close to the Brighton, RMIT and Alphington monitoring stations (longitude 145.0°). These images illustrate the shallow mixed layer with relatively high ozone concentrations over the bay, and the deeper mixed layer further north over the land, with weaker ozone concentrations.

The pattern of ozone formation and dissipation on Day 2 was similar to Day 1 due to similar daytime meteorology. The maximum ozone concentrations tended to be 10–20 ppb lower due to a combination of reduced precursor concentrations over the bay and a 400 m deeper mixed layer over the bay (not shown). This led to reduced ozone formation over the bay and increased ozone dilution due to mixing over a greater depth. The observed and modelled mixed layer depth over the land was shallower than the previous day (Figure 2). The ozone forecasts were excellent at all stations except Alphington (Figure 5). The Alphington forecast was under-predicted by about 15 ppb and Box Hill was not operating. Once again the region was dominated by southerly winds in the afternoon. The model showed higher (lower) ozone concentrations over the land (bay and a few km downwind) than the previous day. This can be largely explained by the difference in precursor distribution between the two days, and differences in vertical dilution related to the deeper bay mixed layer and the shallower land mixed layer. Once again the ozone cleared in the late afternoon, advected northward by the southerly winds, and again Geelong South experienced lower maximum ozone concentrations than other stations to the north of the bay due to the wind direction.

On the evening prior to the third day the winds shifted to a northerly direction (Figure 1c, Figure 2). In the early hours of the morning of Day 3, the model low-level winds were decoupled from the synoptic northerly winds above (nocturnal jet effect), and drainage flow advected precursors from Melbourne over the bay in a pattern very similar to Day 1. By mid-morning, when the mixed layer had begun to grow over the land, the synoptic northerly winds had mixed back down to the surface to the north of Melbourne. The drainage and synoptic northerlies transported ozone precursors over the bay in a similar manner to Day 1 (not shown). The developing bay and sea breezes opposed the northerly flow a few hours later. By midday modelled ozone was beginning to develop over the bay and to the north the air was relatively clean. Over the bay area the winds had a greater easterly component than at the Airport which, when the bay breeze began to develop a couple of hours later, produced a stronger bay breeze on the western side of the bay (not shown). By 5 pm the bay breeze had been replaced by a stronger sea breeze blowing from the south-southeast, and a delicate balance between it and the synoptic northerlies existed. The more highly concentrated ozone, below the shallow stable layer of the sea breeze, was carried inland by the sea breeze (Figure 7a). In the model the penetration of the ozone-rich bay/sea breeze stopped just short of Alphington, Box Hill and RMIT, which explains the under-prediction at these stations (Figure 5). The model bay/sea breeze did arrive at the other three stations where the forecast maximum ozone concentrations were excellent. The model ozone cleared to the west (high concentrations passed between Melbourne and Geelong) during the evening, as the sea breeze continued turning to the left due to inertial rotation (Figure 7b). That night the northerly winds redeveloped and strengthened throughout the following day as the cold front approached (Figure 1d). The increased ventilation due to stronger winds reduced the potential for ozone accumulation over the next few days.

Although the Melbourne ozone cycle was governed by relatively simple dynamics, the same cannot be said for the greater Victorian region, where re-circulation, vertical transport, ozone plume shearing, and fumigation all played significant roles in ozone transport that contributed to concentrations in excess of 80 ppb as far away as Cape Otway, King Island and south of Wilsons Promontory (170–250 km away). Figure 8a shows ozone transported towards Cape Otway and King Island on two fronts (i) over Bass Strait from Melbourne and (ii) offshore further west at 2 pm on Day 3. The latter source originated from the previous days ozone that had been advected inland by the southerly flow, which rotated through 180° counter-clockwise throughout the night. The easterly flow through Bass Strait transported the ozone to King Island and Cape Otway and reinforced the sea breeze transport inland east of Cape Otway. Figure 9 shows a very different flow structure about 2000 m above the surface on Day 3. The winds were predominantly northwesterly over Melbourne and shifted to northerly south of Wilsons Promontory. Figure 9a shows remnant ozone from the previous day being advected over Melbourne at 8 am, where Melbourne precursors mixed upwards were lifted into the northwesterly air stream and carried away to the southeast. Throughout the day the ozone concentrations increased until levels in excess of 80 ppb were reached about 100 km south of Wilsons Promontory. Thus, at 2000 m maximum ozone concentrations were present in the southeast corner of the domain (Figure 9b), and closer to the surface the maximum concentrations were near the southwest corner of the domain (Figure 8b). This 'shear' is illustrated in Figure 10a, which shows ozone on an east-west vertical section at a latitude of −39.7° (through northern King Island) at 8 pm. The plume

had been sheared over 400 km through a depth of 2500 m. Figure 10b illustrates the shear earlier in the day (midday, Day 3) on an east-west section at a latitude of –38.7° (through a point just north of Cape Otway). At this early time the plume was predominantly a remnant of the previous day. Fumigation at Cape Otway is evident.

4. Summary of the Melbourne 3-Day Event

For the 3-day photochemical smog event over Melbourne, the ozone cycle depended on the interaction of light synoptic flow and mesoscale bay and sea breeze circulations. The AAQFS performed very well in forecasting the ozone cycle on all three days, during which precursor transport and ventilation played important roles in determining the ozone concentrations. On Days 1 and 3 concentrations were greatest (weakest) over the bay and immediate surrounding areas (inland) where the mixed layer was relatively shallow (deep). In the early morning ozone precursors were advected out over the bay, and in the afternoon ozone that had developed over the bay was advected inland with the bay and sea breezes. On Day 2 precursors were confined to an area north of Melbourne and limited ozone production occurred over the bay. This resulted in lower maximum ozone concentrations at the monitoring stations than Days 1 and 3. On Day 3 the sea breeze penetration was slightly under-predicted by the model leading to under-predictions of maximum ozone at Alphington.

The transport dynamics for the greater Victorian region were more complex than the region immediately surrounding Melbourne. The larger scale ozone transport highlights the considerable distances high concentrations of pollutants, such as ozone and its precursors, can be transported. It shows also that pollution originating in the Melbourne area can be of regional as well as local concern. This example demonstrates that the AAQFS can offer guidance to pollution forecasters outside the current EPA forecast areas, although without monitoring stations the results cannot be verified.

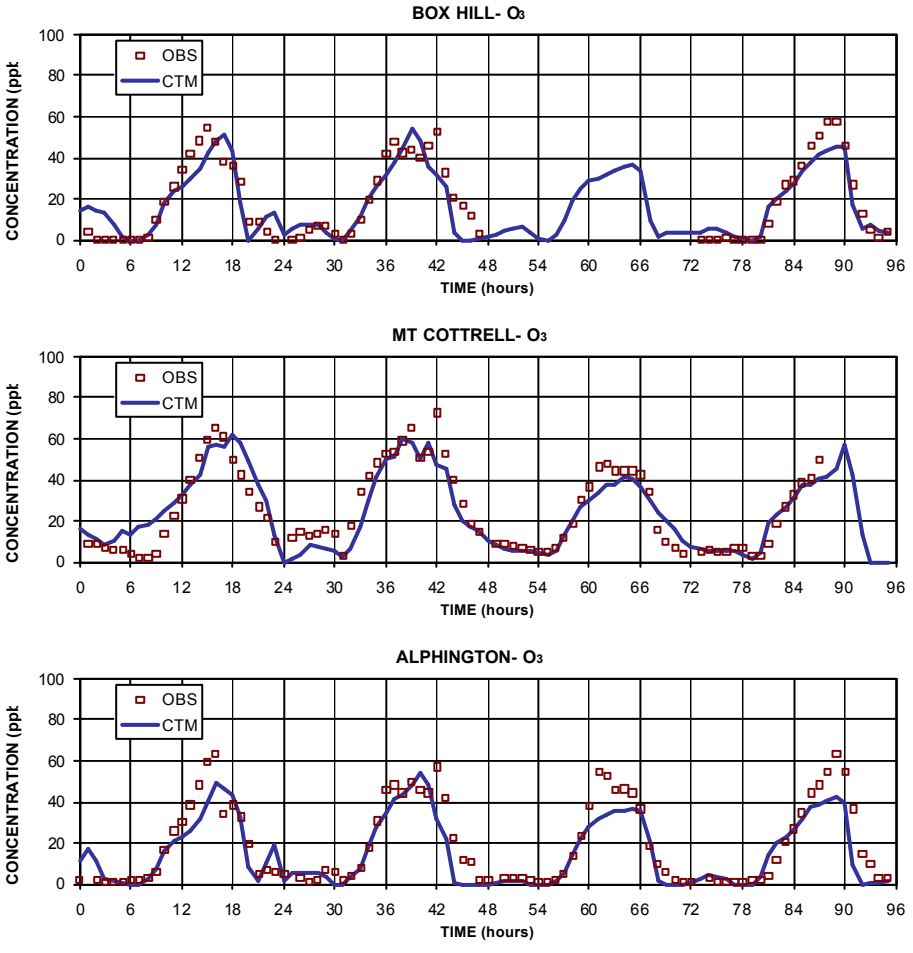

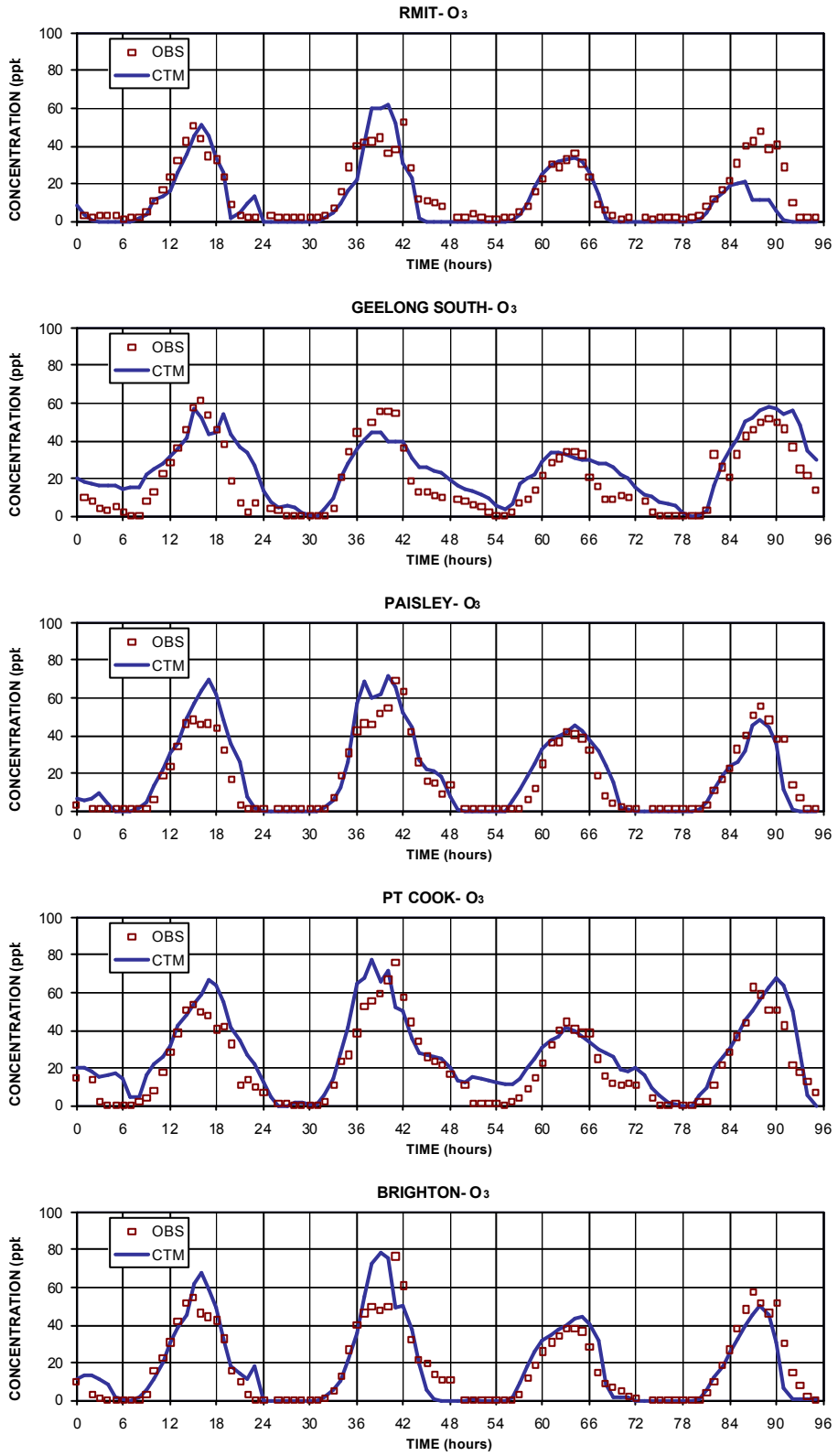

Figure 5. Observed and forecast ozone concentrations at Box Hill, Mt. Cottrell, Alphington, RMIT, Geelong South, Paisley, Pt. Cook and Brighton, from 0000 7 March to 0000 10 March 2001 (EDT).

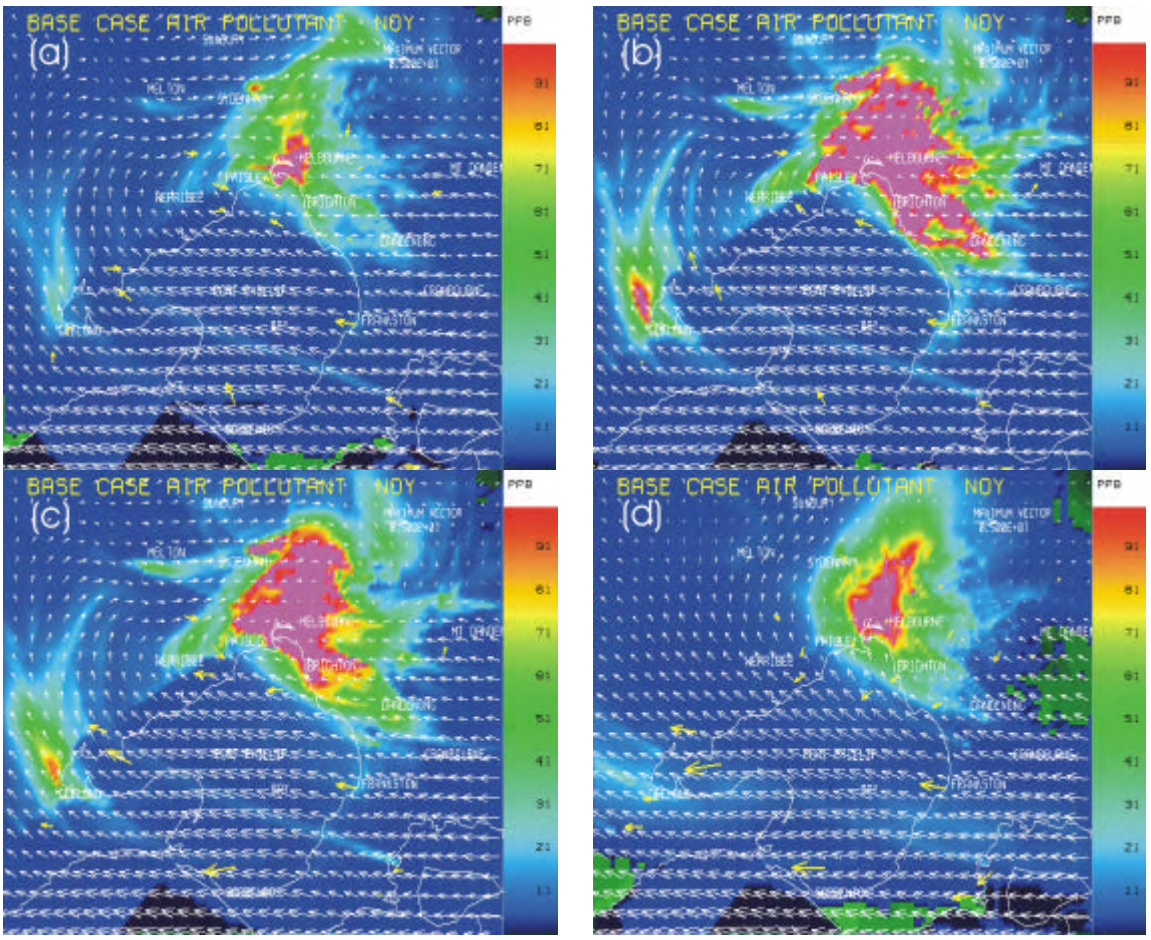

Figure 6. Same as Figure 3, except at (a) 0500, (b) 0700, (c) 0800 and (d) 1000 EDT on Day 2. The stronger ESE synoptic winds interacted with weak drainage flow to generate an eddy centred northeast of Melbourne (a). These synoptic winds ensured most of the bay remained free of precursors (b). The precursors are contained within the eddy to the north of Melbourne (c) and remains there hours later (d).

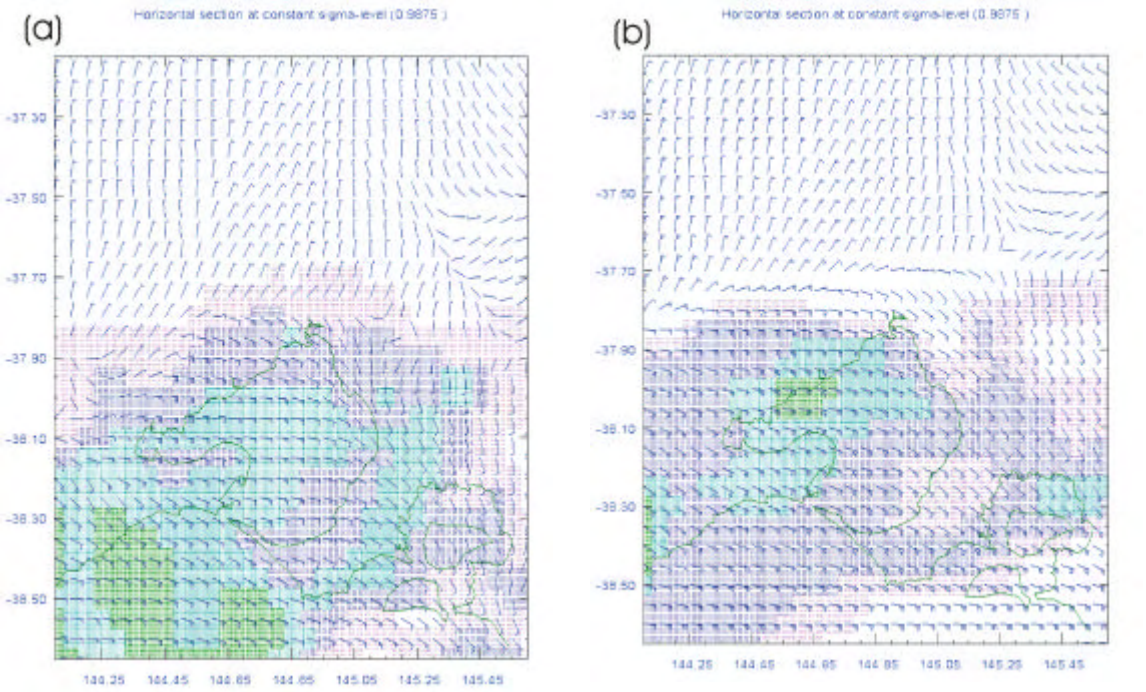

Figure 7. Ozone (shaded) and winds (full barb = 6 knots) at (a) 5 pm and (b) 8 pm near the surface on Day 3 (0600 and 0900 UTC, 9 March 2001). Ozone concentrations increase by 10 ppb with each colour from magenta through to red, beginning with the range 40-50 ppb. The extent of the sea breeze penetration is evident in (a), marked by the converging wind barbs. Note the higher concentrations of ozone in the sea breeze air mass. Three hours later the ozone clears to the west as the sea breeze turns counter-clockwise due to inertial rotation.

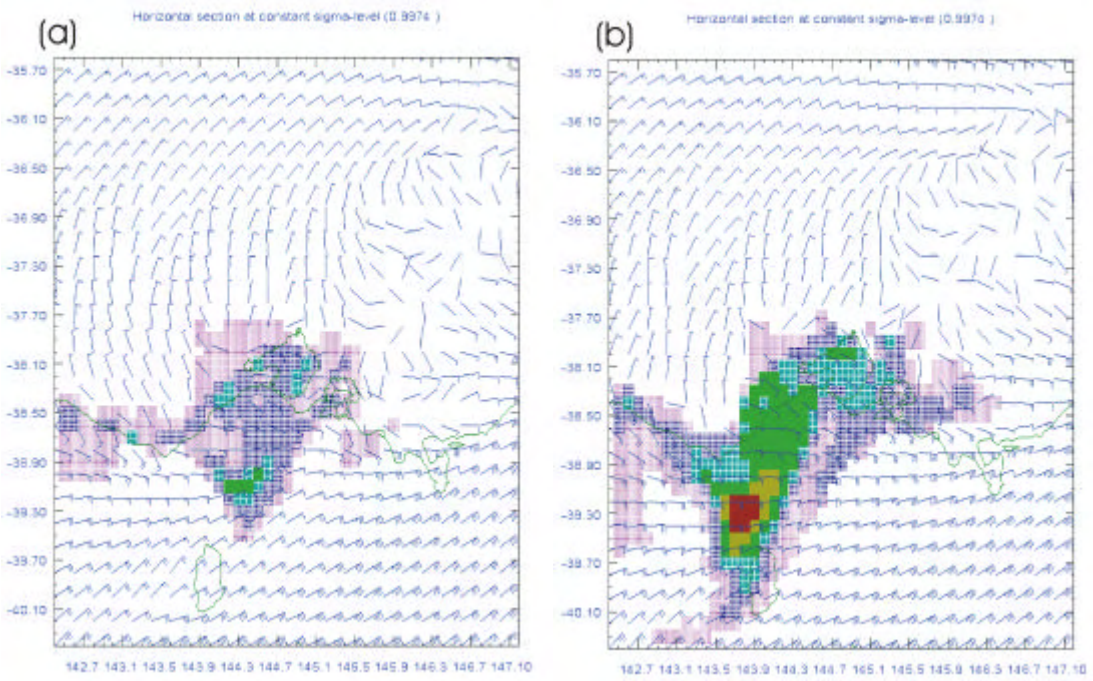

Figure 8. Surface ozone (shaded) and winds (full barb = 6 knots) on Day 3 at (a) 3 pm and (b) 6 pm. Ozone concentrations increase by 10 ppb with each colour from magenta through to red, beginning with the range 40-50 ppb (red = >90 ppb). These two images illustrate the transport of ozone from the Melbourne area (and ozone pre-cursors, not shown) over Bass Strait (a) and then westward (b). In addition, remnant ozone, that was carried inland (north of Melbourne) with the sea breeze from the previous day, followed a circular path over night which turned counter clockwise through 180° until transported offshore at Cape Otway (a). The two sources combined, and further development produced the high concentrations evident in (b) that extend as far south as King Island. High concentrations were advected inland between Cape Otway and Geelong with the sea breeze.

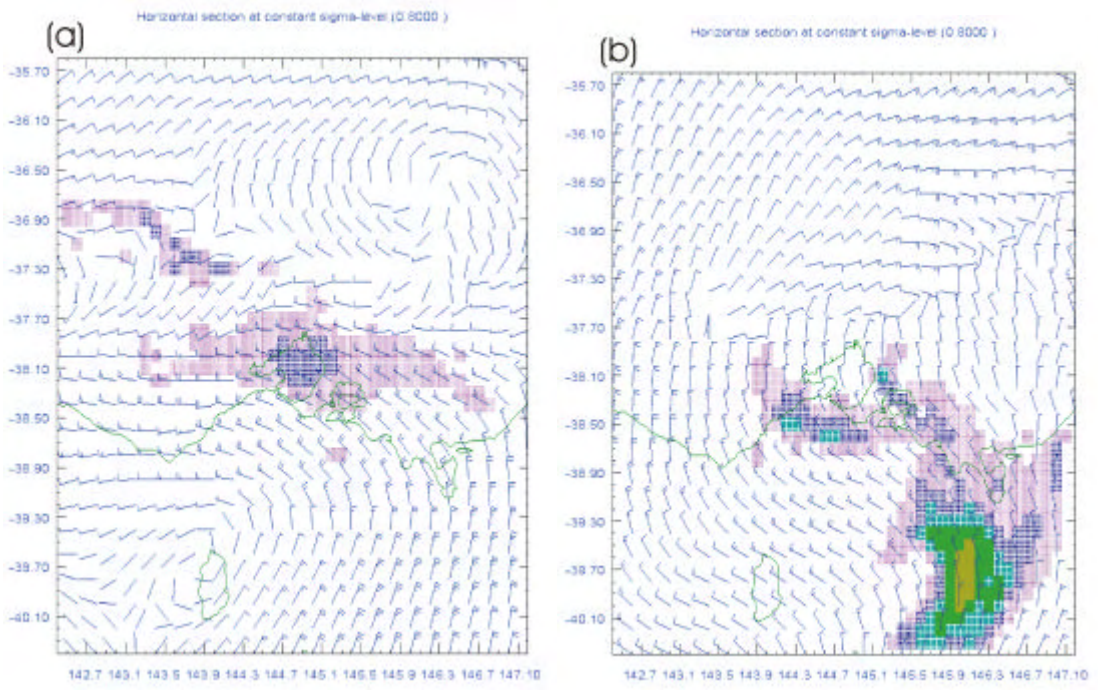

Figure 9. Same as Figure 6 accept at an elevation of about 2000 m above the surface and at (a) 9 am and (b) 9 pm. Remnant ozone from the previous day is advected to the southeast over Melbourne (a) and beyond to south of Wilsons Promontory (b). While passing over Melbourne surface pre-cursors and recently formed ozone were mixed up into this elevated air stream leading to growing ozone concentrations that peaked near 8 pm.

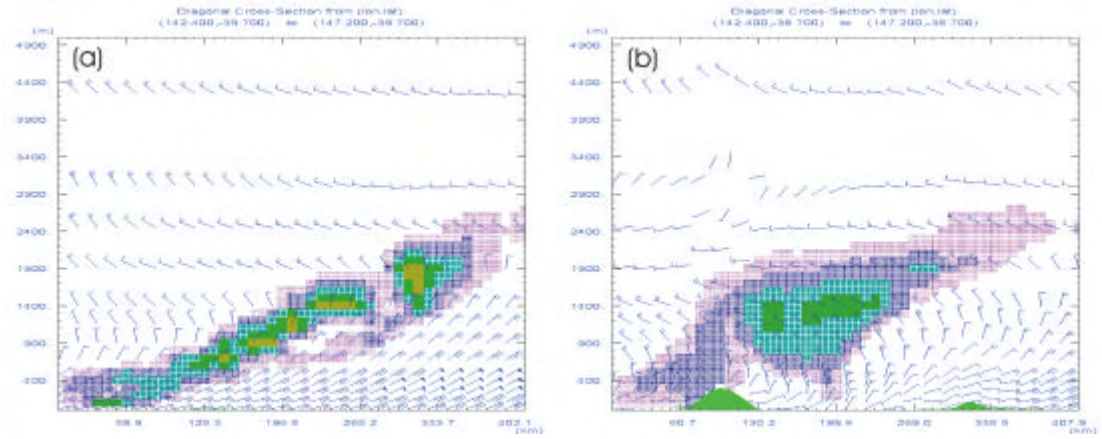

Figure 10. Vertical sections on Day 3 illustrating the greatly sheared ozone plume through (a) latitude =-39.7° at 9 pm, and (b) latitude = -38.7° at 1 pm. Ozone concentrations increase by 10 ppb with each colour from magenta through to red, beginning with the range 40-50 ppb. The plume is sheared over a distance of 400 km through a depth of just 2500 m (a). Significant concentrations of remnant ozone are present between 900 and 1900 m east of Cape Otway (green hill near 100 km), and fumigation is evident over Cape Otway (b).

Appendix 7.2 Sydney 7-Day Photochemical Smog Event

K. J. Tory[1], G. D. Hess[1], M. E. Cope[2,3] and S. Lee[2]

[1]Bureau of Meteorology Research Centre,
[2]CSIRO Atmospheric Research, [3] CSIRO Energy Technology

1. Background

In January 2001 the Sydney region experienced a prolonged period, lasting seven days, of high ozone concentrations (greater than 80 ppb). This was the worst photochemical event for this region for the oxidant season of 2000–2001, and for this reason it was chosen as a case study. At the time of the original forecasts, the CTM was still undergoing development. However, once the development was completed the CTM was run in a 'hindcast' mode for this period, using the original LAPS forecast meteorological fields as input.

This study will illustrate a number of features of the AAQFS: the ability to forecast extreme events, the ability to model the impact of re-circulation and fumigation of pollutants, the complexity of the flow in Sydney region, and the high demands that this made on the modelling system.

The synoptic conditions at 0000 UTC 20–27 January 2001 (1100 EDT) are depicted in Figure 1. The dates are shown in the lower left-hand corner of each map. The solid lines with barbs indicate cold fronts; the dashed lines indicate trough lines. The trough line across the north of Australia indicates the position of the monsoonal trough. During the summer period cold fronts move from west to east but tend to remain south of the Australian mainland. Wind shifts and temperature changes are often associated with propagating trough lines in the mid-latitudes, analysed on these charts. Unlike the analysed cold fronts, they tend to be dry and cloud-free. Such wind shifts and temperature changes frequently affect the Sydney area during the warmer months. They are often shallow and short-lived, and are not always analysed on the synoptic charts.

The first day shown (20 January 2001) is the day prior to the event. On this day a cold front was oriented northwest-southeast located west of Tasmania with a pre-frontal trough ahead of it. A high-pressure cell, which remained quasi-stationary for the period, was located in the Tasman Sea southeast of Sydney. The gradient wind in the Sydney region was from the northeast. By the next day (21 January, the start of the event) the southern cold front moved east of Tasmania. The pre-frontal trough line moved up the east coast of Australia to the Sydney region. The weak gradient wind rotated counter-clockwise to north-northwest. The high-pressure cell in the Tasman Sea strengthened on the second day of the event (22 January), as did the gradient wind from the north-northwest. New cold fronts developed to the southwest of Australia, but passed to the south of the mainland. On the third day (23 January) the high-pressure cell moved eastward, the gradient wind rotated further counter-clockwise to a northwesterly direction, and the cold front to the south of the mainland reached Tasmania. By the next day (24 January) the gradient wind weakened. Trough lines are present on the map between Melbourne and Adelaide and just west of the Australian Bight. The map for Day 5 (25 January) shows that a trough line moved up the east coast. It reached Wollongong near midnight. The trough line passed through the Sydney region on Day 6 (26 January) and then dissipated. The map for the last day of the event (27 January) shows low pressure to the north of Sydney and a high-pressure cell southeast of Tasmania; over the Sydney region the gradient is very weak. The model shows, and wind observations confirm, a wind shift developed and passed through Sydney at 1100 EDT and continued up the coast past Newcastle. No associated trough line was analysed on the synoptic chart. The southerly winds swept the pollutants away from the Sydney region.

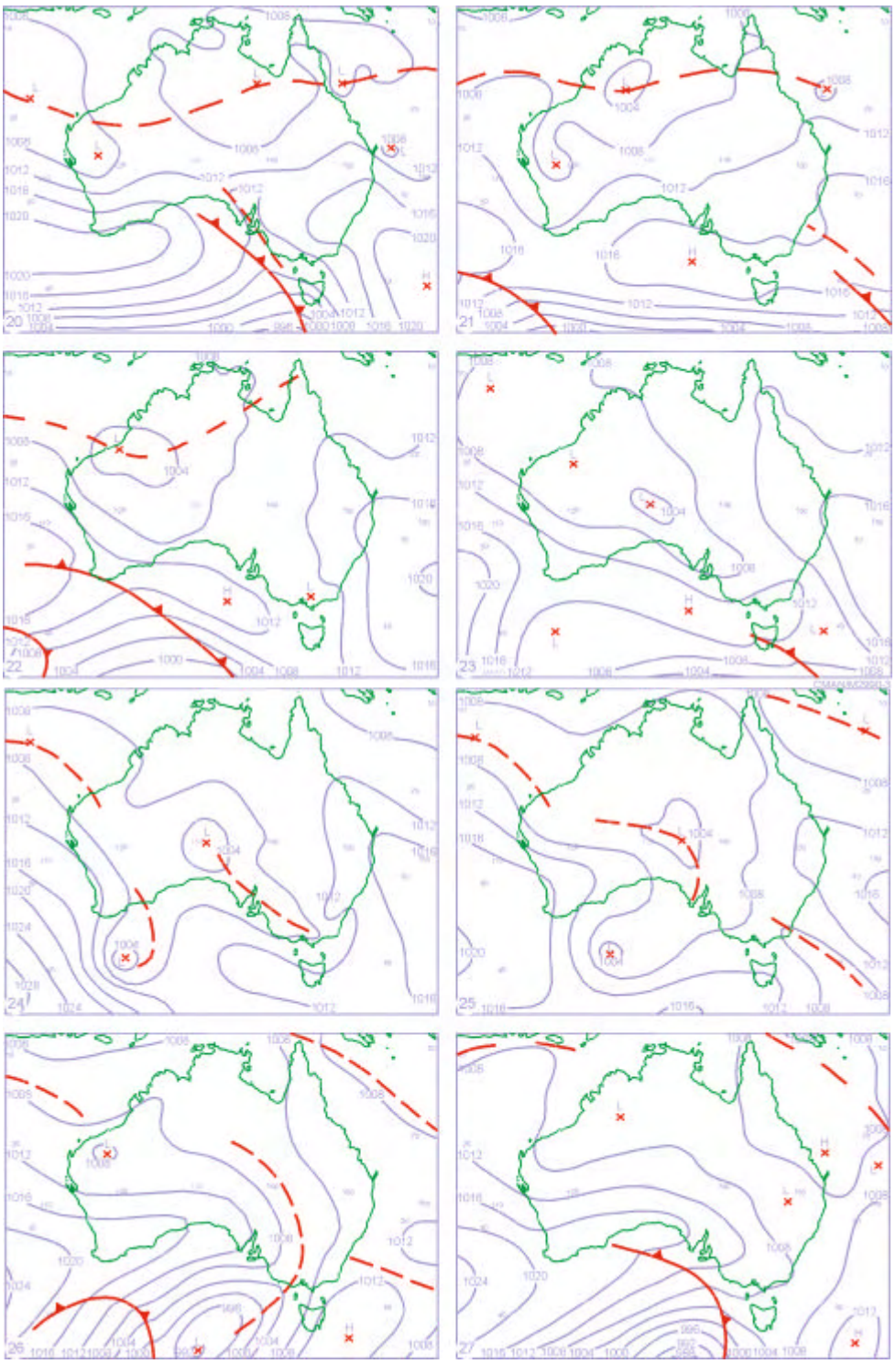

Figure 1. Synoptic charts at 0000 UTC for the day prior to and those days of a 7-day photochemical smog event in Sydney. The date is shown in the lower left-hand corner of the maps (20–27 January 2001). In local time, the charts are at 1100 EDT. The solid lines with barbs indicate cold fronts; the dashed lines indicate trough lines; the contours show the mean sea-level pressure in hPa with a contour interval of 4 hPa.

2. Mesoscale meteorology and AAQFS performance

The first day of the 7-day event illustrates a number of the features often found in ozone events in the Sydney region. Nocturnal cooling of a shallow layer of air near the surface in the near-coastal region led to the formation of drainage (katabatic) flow. This westerly flow, occurred between 0400 and 0800 EDT, and is seen in Figure 2 in a region between Sydney and Wollongong, bringing precursors into the urban areas and out over the sea. In the northeast corner of the domain the winds are northwesterly. Just north of Newcastle the winds are northerlies. Figure 2 also shows the observed winds at 0600 EDT and the agreement between the modelled and observed winds is good. In Figure 2 we also plot the concentration of the NO_y at 0600 EDT. Note the high concentrations of NO_y found in the Hunter Valley (from the power stations there) and in the Sydney area. We will return to this observation later.

In terms of the meteorology the two main quantities that need to be correctly forecast for air quality applications are the wind field and the planetary boundary layer (PBL) height. In Figure 3 we show a comparison of the predicted and observed PBL height, based on AMDAR (commercial aircraft) observations for 22–28 January 2001. Particularly important are the values of the PBL height at the times of the early morning traffic peak (0800–1000) and the maximum diurnal height. The plots show severely limited growth of the PBL height during the event period (because of the strong stratification). Data were not available for 21 January.

Between 0800 and 1000 EDT the winds over land near the coast were nearly calm while over the sea northerly winds were maintained. As the land surface heated up, the temperature difference between the land and sea built. By 1100 EDT the temperature difference was great enough for the sea breeze to begin to come onshore. The arrival of the sea breeze transported the pollutants back inland that had previously been carried offshore by drainage flow.

On this particular day, in addition to the mesoscale circulation of the sea breeze, a synoptic-scale trough line travelled northwards up the east coast of Australia (Figure 1). By 0600 EDT the edge of the southerly wind change, associated with the trough line, is just visible at the southernmost part of the domain (Figure 2). Figure 4 shows the convergence of this southerly wind surge and the onshore flow of the sea breeze just south of Wollongong at 1200 EDT. The low values of the PBL height near the coast (shown in green) indicate the penetration of the sea breeze in the northern part of the domain, the combined flow of the southerly wind surge and the sea breeze near Wollongong, and the penetration of the surge of cool air behind the wind shift south of Wollongong. The cooler air (implied by lower PBL heights) and the beginnings of the penetration of the sea breeze up the Hunter Valley can also be seen. In Figure 5 the flow pattern at 1600 EDT shows the advance of the sea-breeze front and the combined sea breeze-southerly wind surge front (which is found significantly further inland). Comparison of the modelled winds with the observations gives very good agreement. The ozone pattern at 1600 EDT is show in Figure 6. The existence of two centres of NO_y precursor concentrations led to two centres of ozone production, one at Sydney and a second near Muswellbrook. The location of the Sydney centre was now at the leading edge of the combined sea breeze-southerly wind surge front (cf. Figure 5, near Lithgow); the location of the northern centre was to the west of Muswellbrook due to advection from the onshore flow up the Hunter Valley. Figure 7 presents a vertical section oriented perpendicularly to the sea breeze front and going through the northern ozone maximum. Note the ozone was carried inland at the leading edge of the sea breeze (indicated by the region of strongest horizontal potential temperature gradient), and the larger and more highly concentrated ozone plume further inland (west of Muswellbrook).

The ozone maxima continued to be advected to the west as the sea breeze and southerly wind surge penetrated further inland. At 2200 EDT both centres began to dissipate. The relative strength of the sea breeze compared to the southerly wind surge was such that the surge did not advance beyond Sydney.

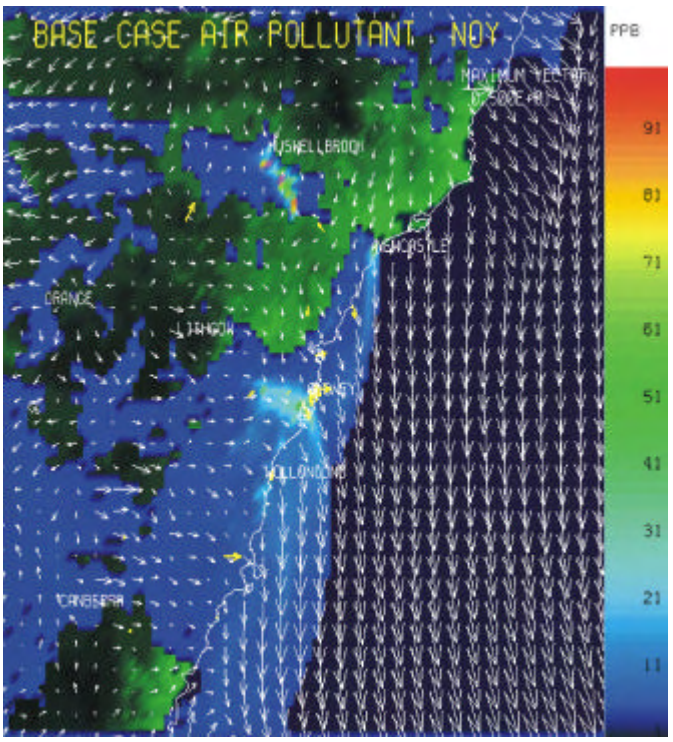

Figure 2. The wind pattern, showing the drainage flow, and precursor NO_y concentrations at 0600 EDT on 21 January 2001 (Day 1). The wind observations are shown by yellow vectors.

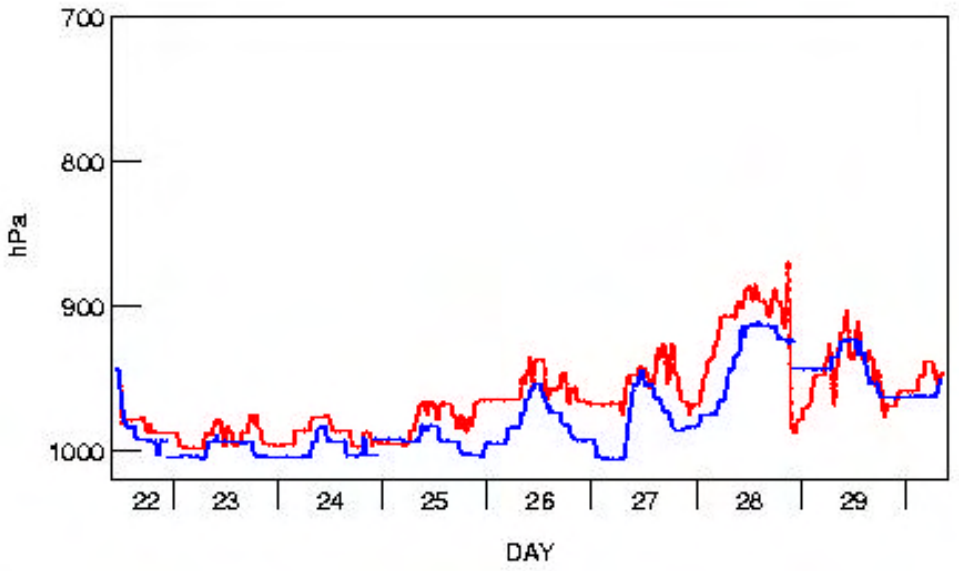

Figure 3. Comparison of the forecast planetary-boundary layer height (in blue) and the observed PBL height in red, based on measurements from commercial aircraft (AMDAR). The agreement between predicted and observed, in general, is very good.

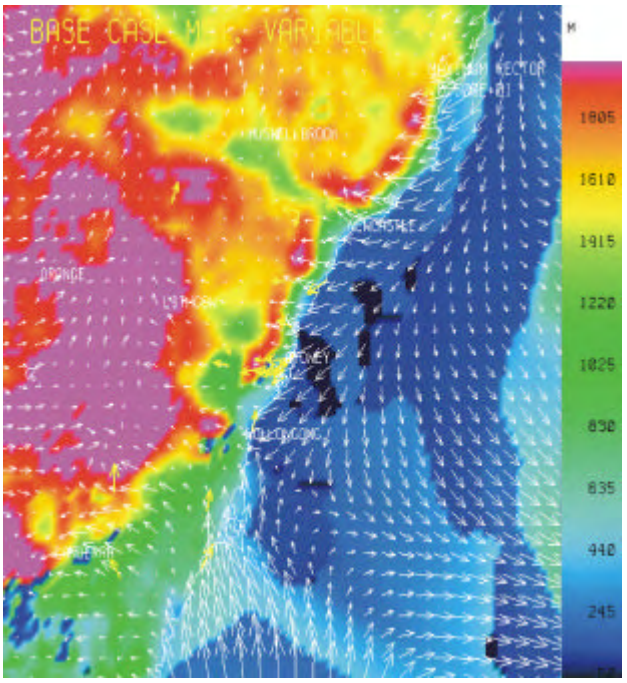

Figure 4. The wind field and the PBL height patterns at 1200 EDT 21 January 2001 (Day 1), showing the arrival of the sea breeze (in green near the coast). The wind observations are shown by yellow vectors.

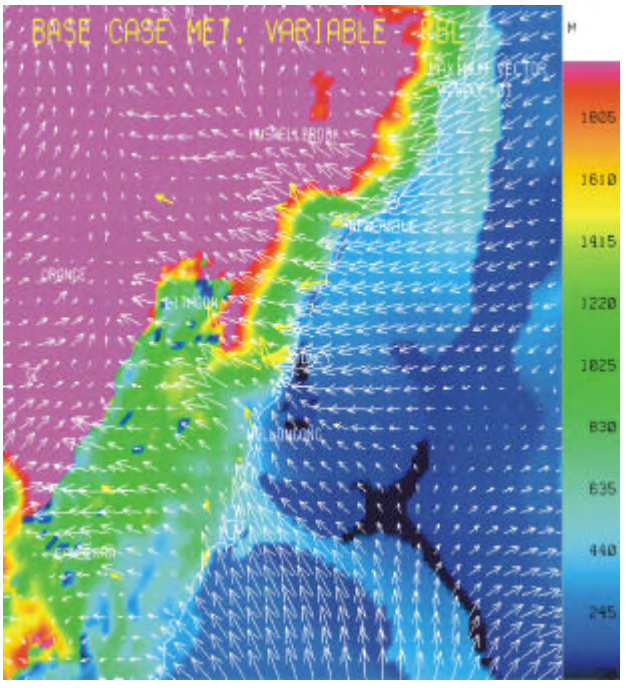

Figure 5. The wind field and the PBL height patterns at 1600 EDT 21 January 2001 (Day 1), showing the location of the sea breeze front (the edge of the green area progressing inland from the coast). Note that the combined southerly wind surge and sea breeze flow penetrates further inland. The wind observations are shown by yellow vectors.

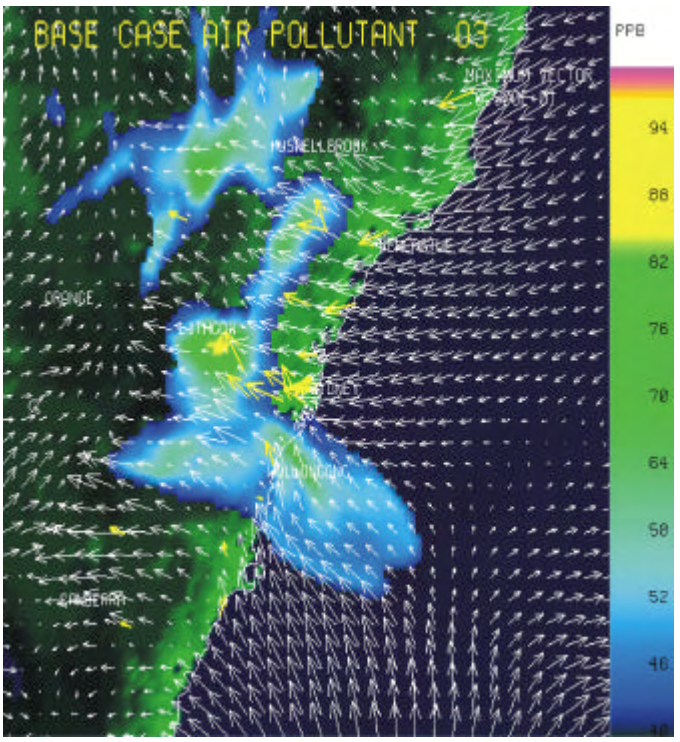

Figure 6. Wind field and ozone concentration patterns at 1600 EDT 21 January 2001 (Day 1). The wind observations are shown by yellow vectors.

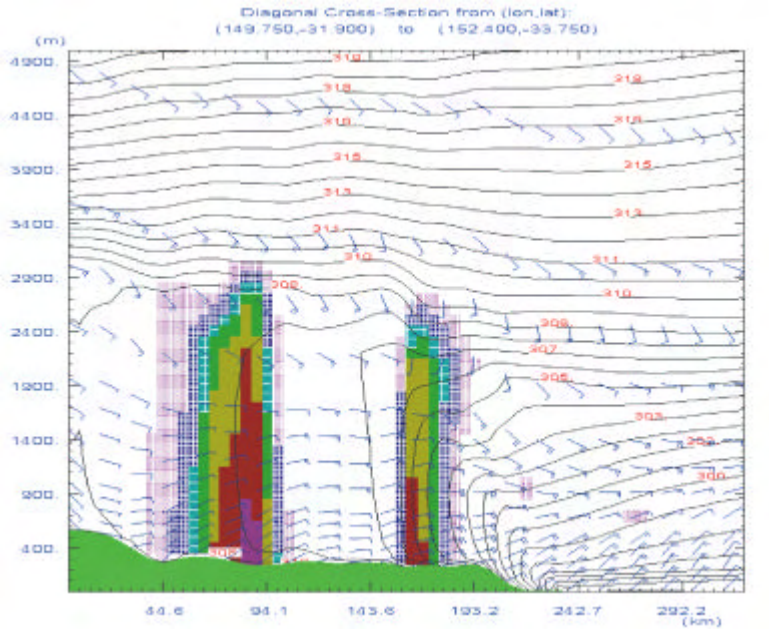

Figure 7. Vertical section perpendicular to the sea-breeze front through the ozone maximum west of Muswellbrook in Figure 6 at 1600 21 January 2001 (Day 1). Concentrations increase by 5 ppb with each colour from magenta through to red, beginning with the range 40-45 ppb. Potential temperature is contoured (interval, 1 K) and horizontal winds are represented by wind barbs (full barb = 6 knots) . Downward (upward) pointed barbs represent flow out of (into) the page.

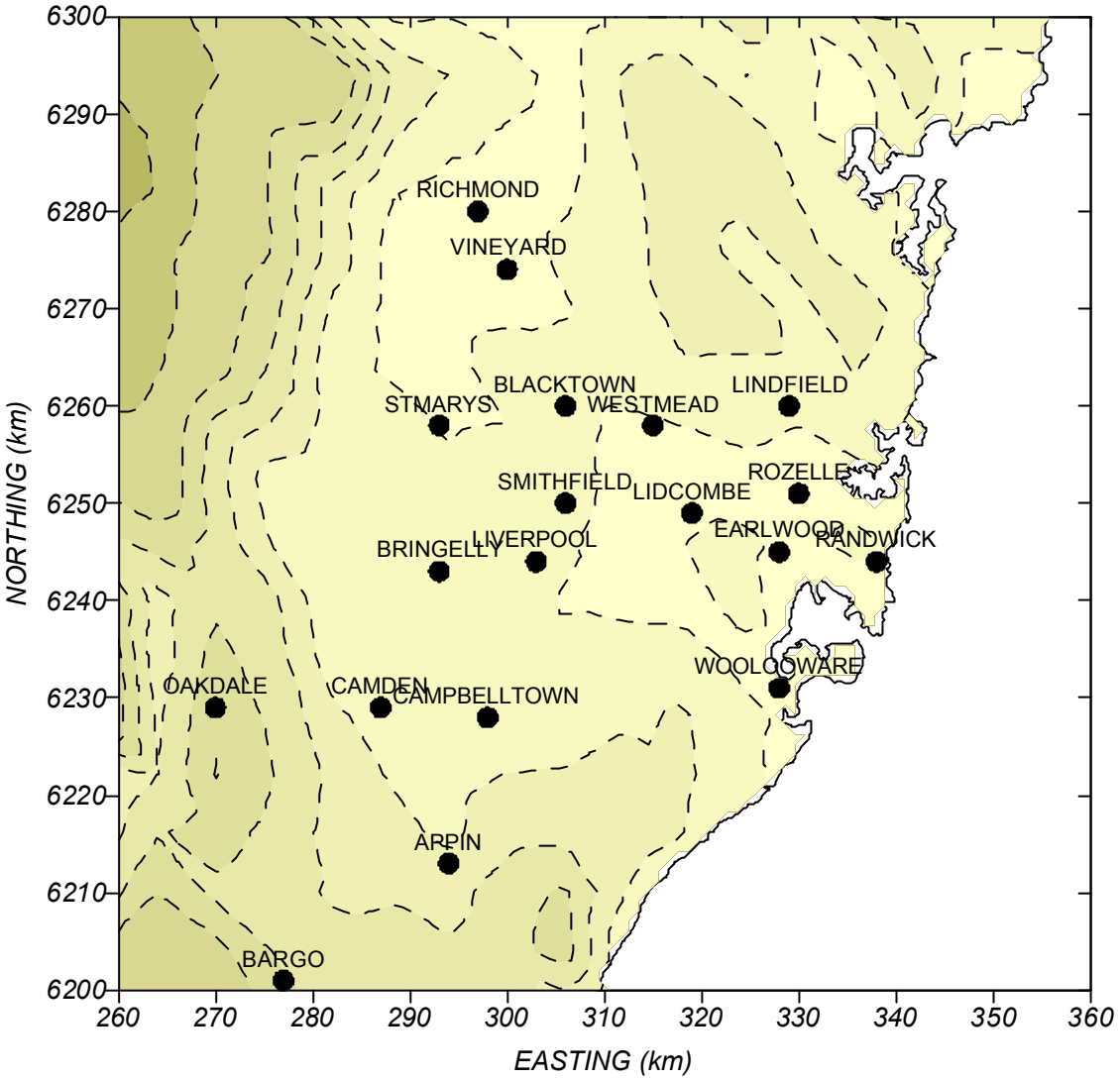

Figure 8. Map of the NSW region showing the location of the EPA monitoring station.

We now turn our attention to examining the time series from 15 ozone monitoring stations in order to evaluate the performance of the AAQFS, recognising that this is a very sensitive measure of the system performance and that it places very high demands on the accuracy of the entire system: the emissions inventory, meteorology and photochemistry. Figure 8 shows location of the monitoring stations and Figure 9 shows the time series for predicted and observed ozone concentrations for the entire 7-day period. We plot both the modelled value interpolated to the location of the monitoring station and the best modelled value from the nearest four grid points (i.e. within a radius of 1–2 km).

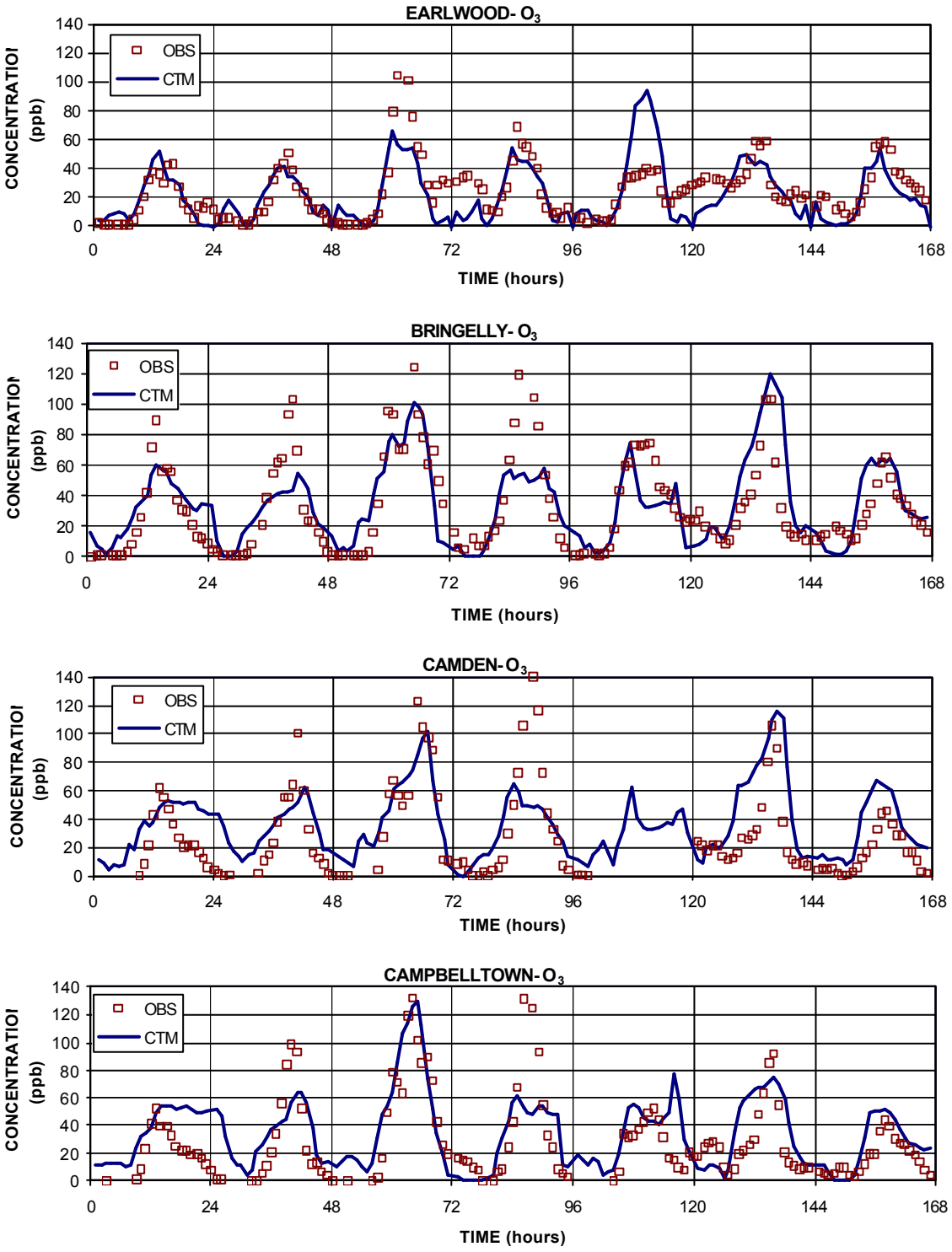

Figure 9. Time series of predicted and observed ozone concentrations at the EPA NSW monitoring stations for the period 21–27 January 2001.

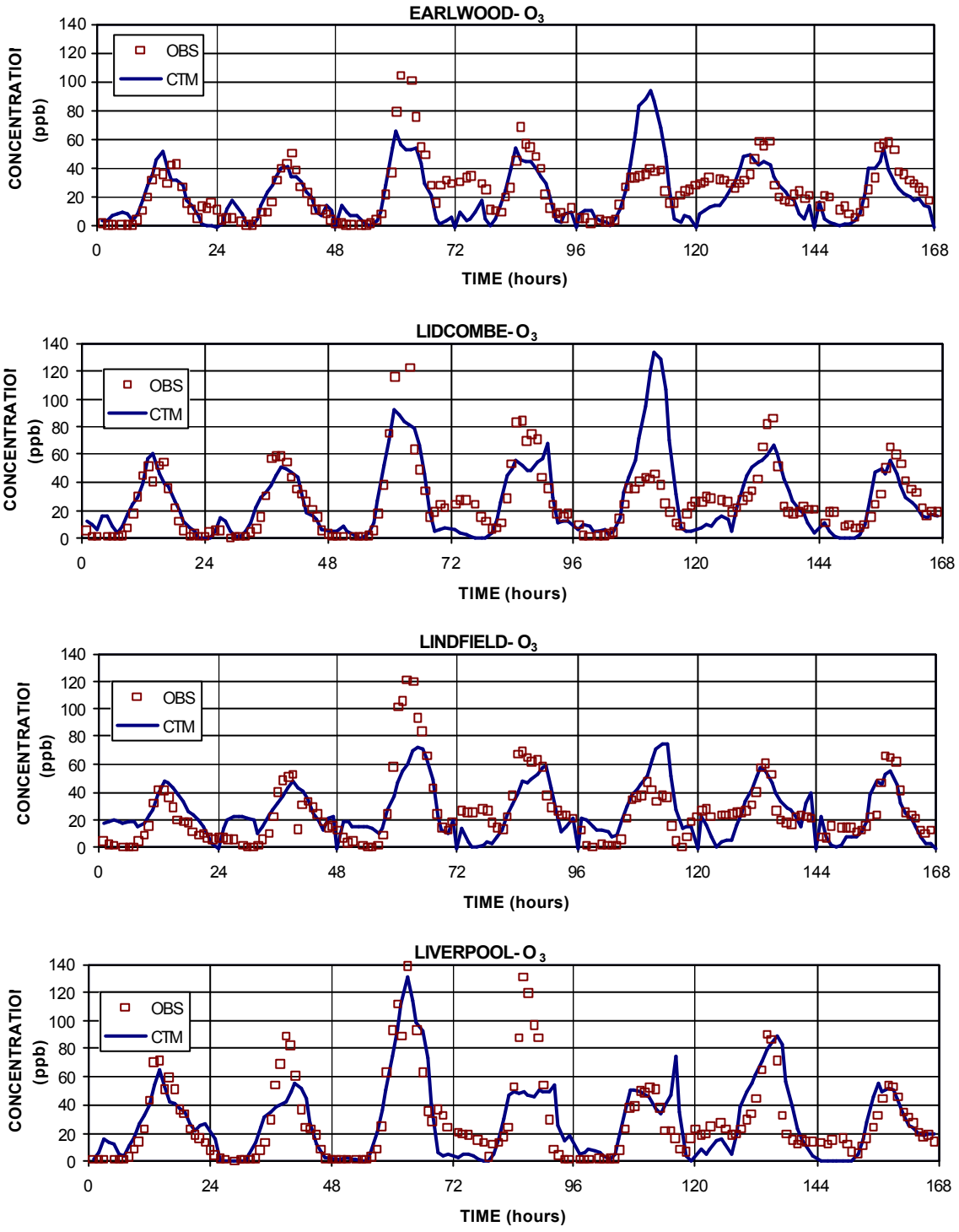

Figure 9. Continued.

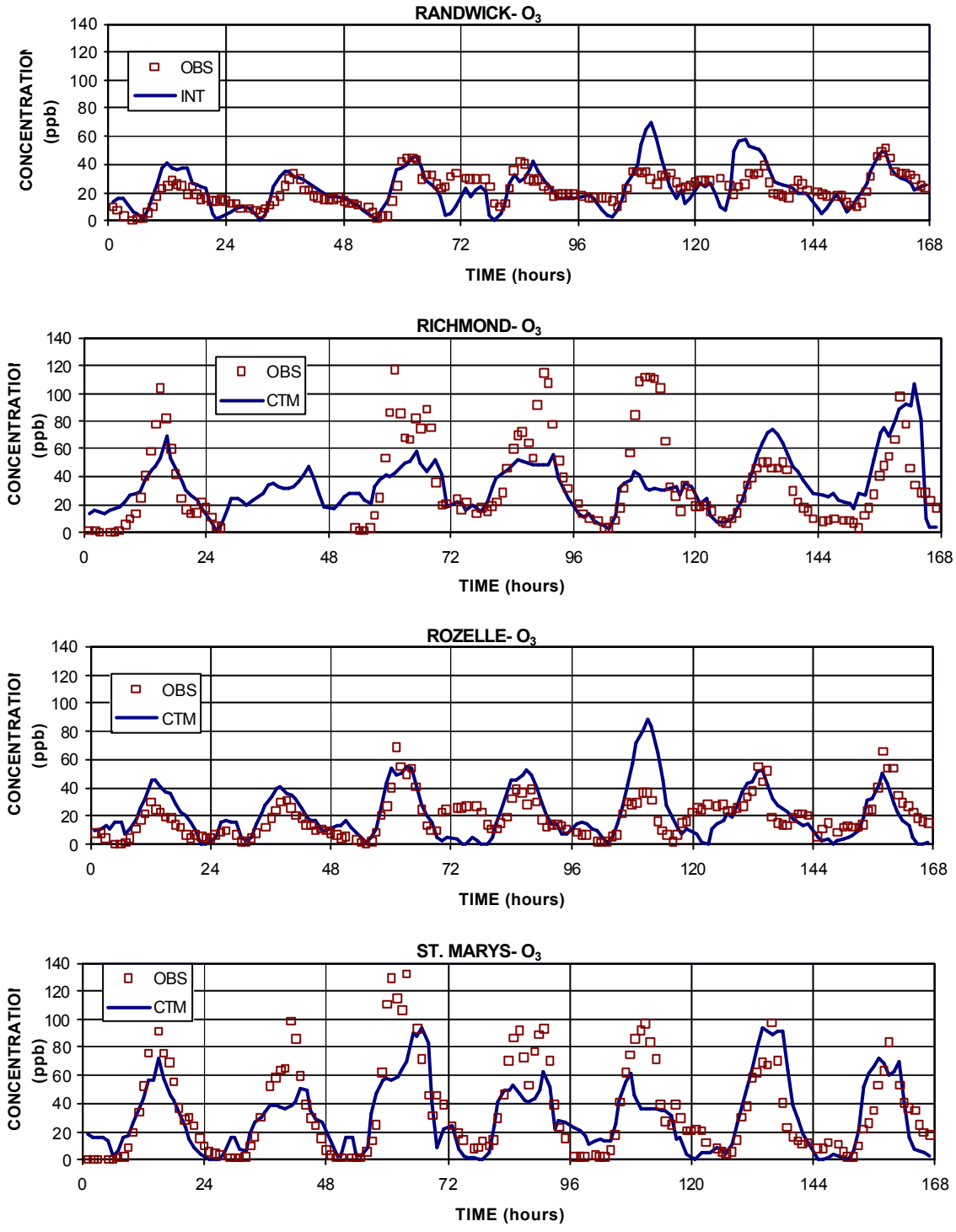

Figure 9. Continued

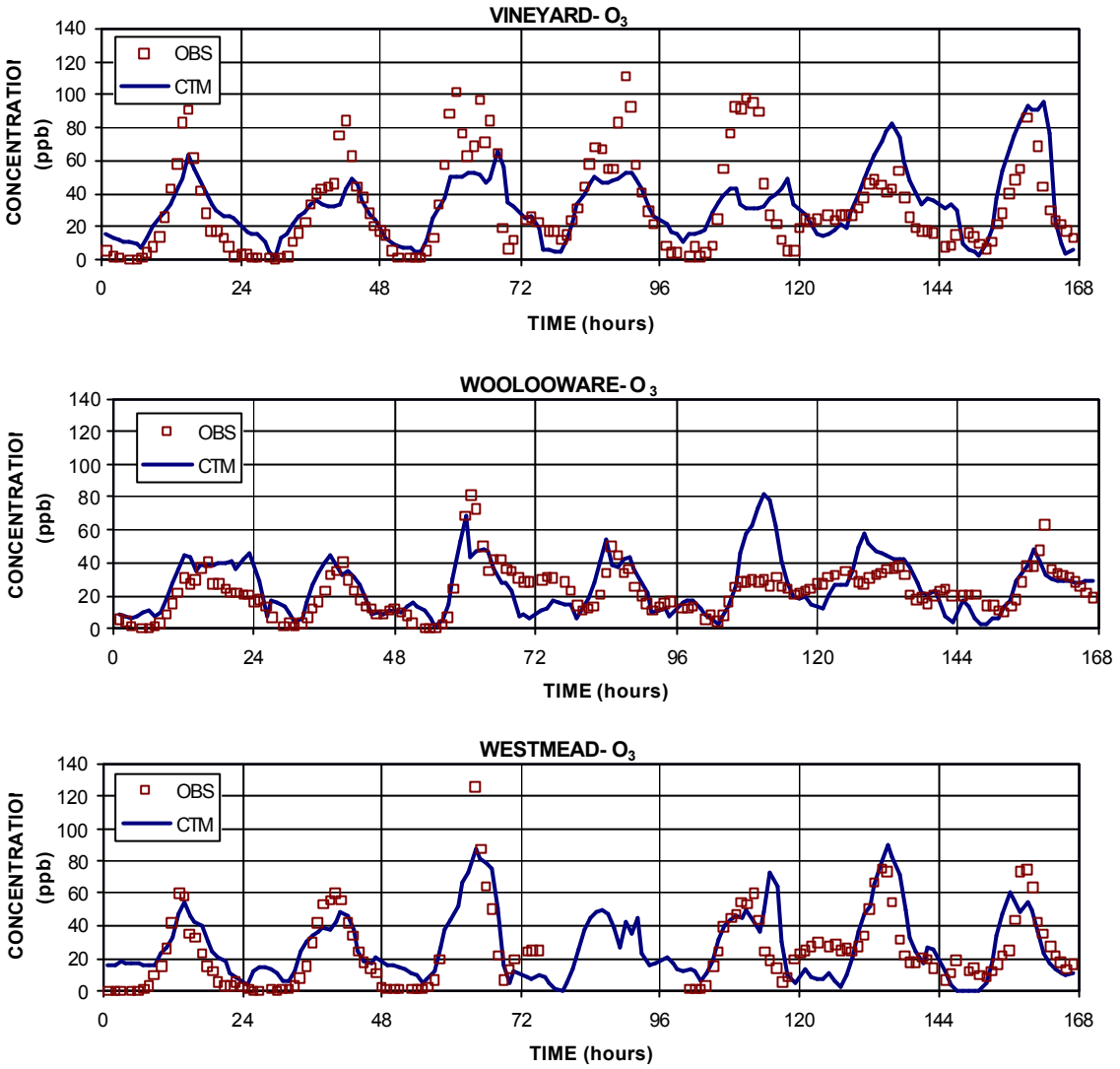

Figure 9. Continued.

The results of the comparison for the first day (21 January 2001) show that the AAQFS gives very good agreement with most of the observations. There is, however, a slight tendency for the northern most stations, Richmond, Vineyard, St. Marys and Blacktown, to be underestimated. The cause of this discrepancy is not known. It may be that the PBL height is overestimated in these inland regions, or it may be due to emissions uncertainties or to the simplicity of the chemical mechanism.

The second day began with high concentrations of precursors left over from the previous day. Figure 10 shows the NO_y concentrations at 0000 EDT on 22 January 2001. There are NO_y centres near Wollongong and Sydney, and between Newcastle and the Hunter Valley. The onshore wind pattern blows the NO_y away from the urban areas. Several hours later the early morning drainage flow pattern became established (Figure 11) and the pattern was similar to the first day drainage flow pattern. The winds were again well predicted. The NO_y precursors in Figure 11 are concentrated between Sydney and Wollongong because of the drainage flow, and the onshore flow near Newcastle generated a plume extending from Newcastle to the power stations in the Hunter Valley. The Sydney precursor plume was transported south of Sydney and by midday (Figure 12) was located south of Wollongong. The Hunter Valley centre was relatively stationary, but the Newcastle plume was transported southeastward down the coast. The sea breeze had just begun to come onshore by midday (Figure 13, indicated by the low values of the PBL height). The advance of the sea breeze was not directly opposed by westerly flow; there was a buffer zone of northerly flow in between these two regimes. By

1700 EDT the sea breeze had penetrated inland as seen by the green areas of the PBL heights in Figure 14. The ozone was distributed along the sea-breeze front (Figure 15) and over a wide area southeast of Canberra. The Hunter Valley precursors, evident in Figures 11 and 12, were responsible for the large ozone area between Muswellbrook and Newcastle. The observations show that the wind patterns were well forecast.

The AAQFS predicts the ozone very well at many of the stations (Figure 9) on this day, but underestimates the peak ozone values at the inland stations (Blacktown, Bringelly, Camden, Campbelltown, Liverpool, St. Marys, and Vineyard). The observed and predicted PBL height based on aircraft take-offs from Sydney Airport is shown in Figure 3. Unfortunately no early morning AMDAR flights were available. However, the available data show good agreement between the model predictions and the measurements, indicating a PBL height of 500–600 m during the morning traffic peak. Other uncertainties in the modelling have previously been indicated.

The NO_y concentrations at 0000 EDT on the third day (23 January 2001) are shown in Figure 16. Precursors cover the Sydney – Wollongong area, and are visible in the Hunter Valley and along the coast extending south from Newcastle. A wind shift moved up the coast and is just visible in the southern part of the domain shown in Figure 16. By 0600 EDT the drainage flow was well established and the wind shift had reached Nowra (Figure 17). Ahead of the wind shift a mesoscale cyclonic eddy formed. Between 0600 and 1000 EDT this circulation and the northerly coastal flow to the north of it drew the precursors southward and out over the sea to the southeast of Wollongong (see Figure 18, which shows the NO_y concentrations at 0800 EDT and the precursors drawn into the eddy leading the wind shift). The presence of significant amounts of re-circulated precursors over the land led to early formation of ozone (Figure 19) at 1000 EDT. At this time two maxima of ozone were present; however shortly afterwards the northerly flow merged the northern centre with the coastal ozone centre. By midday there was convergence of flow on the Sydney ozone centre from four directions, synoptic westerlies approaching from the west, the southerly change from the south, the sea breeze coming from the east and weak northerly flow from the north (Figure 20). At this time the southerly wind shift had rotated inland due to the low pressure over the land because of surface heating, and the opposing northerly component of the sea breeze ahead.

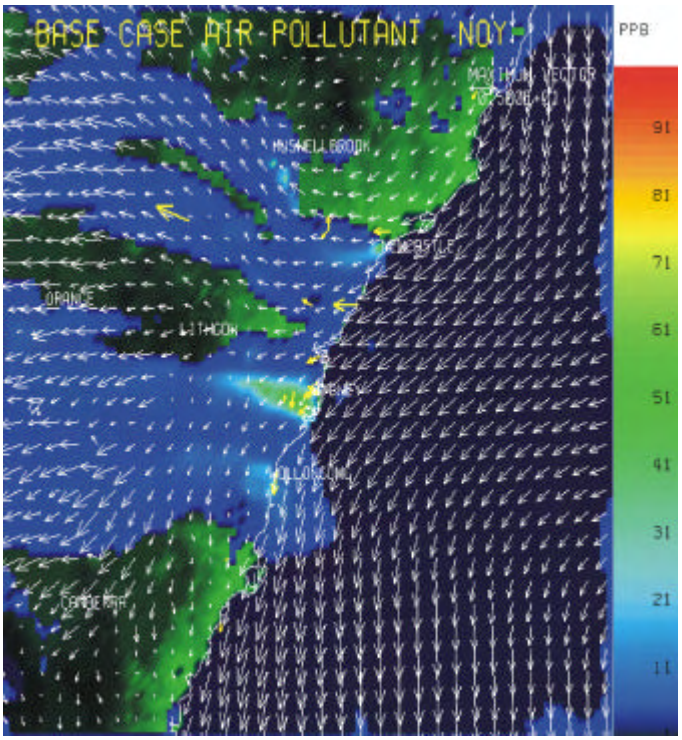

Figure 10. The wind field and precursor NO_y concentration patterns at 0000 EDT 22 January 2001 (Day 2). The wind observations are shown by yellow vectors.

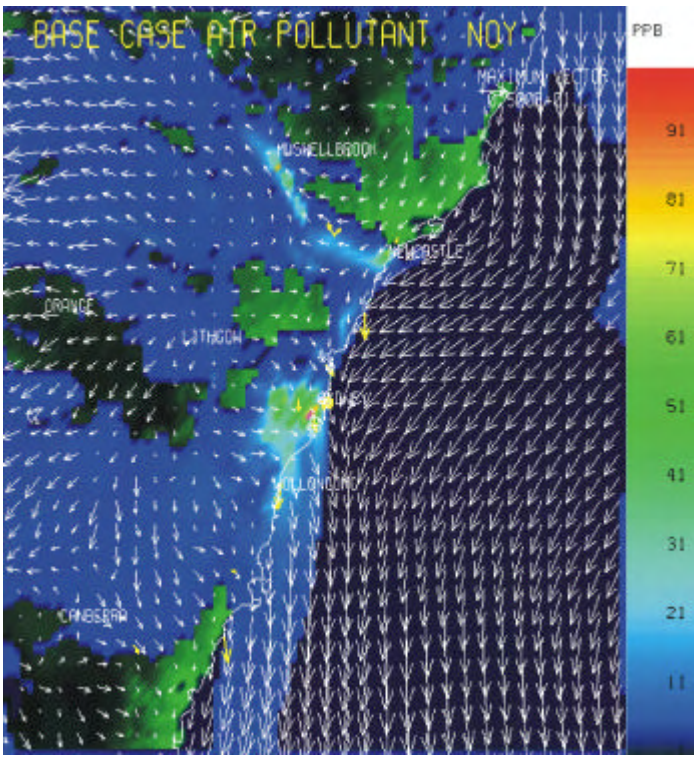

Figure 11. The wind field and precursor NO_y concentration patterns at 0600 EDT 22 January 2001 (Day 2). The wind observations are shown by yellow vectors.

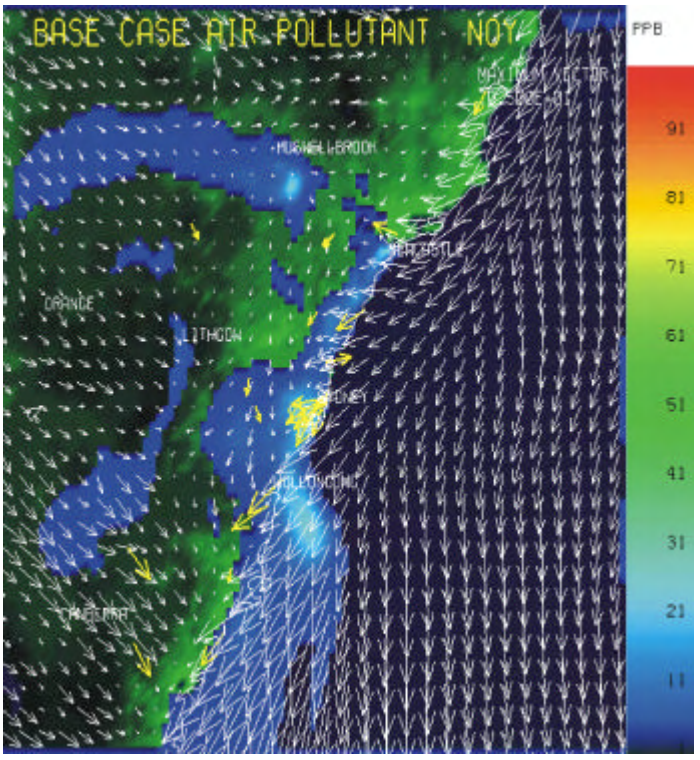

Figure 12. The wind field and precursor NO_y concentration patterns at 1200 EDT 22 January 2001 (Day 2). The wind observations are shown by yellow vectors.

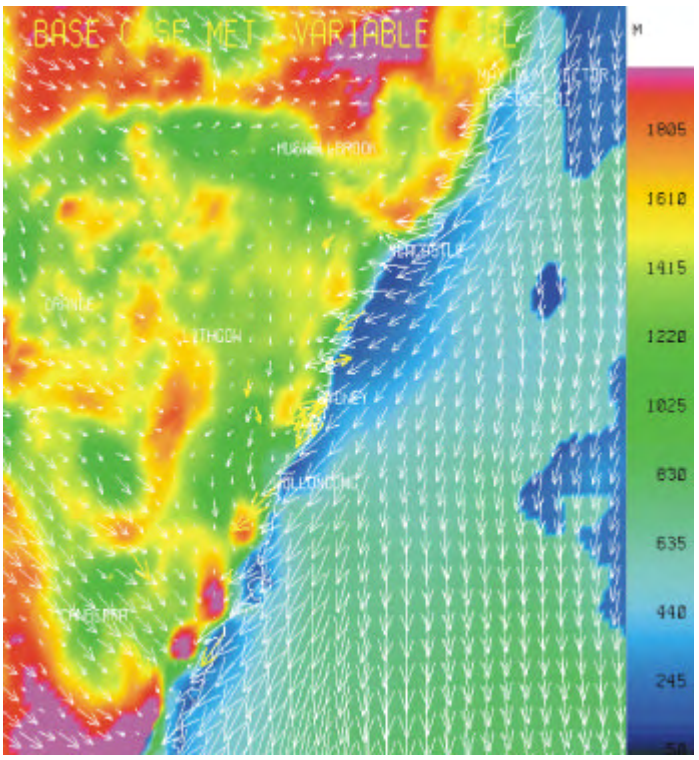

Figure 13. The wind field and the PBL height patterns at 1200 EDT 22 January 2001 (Day 2). The wind observations are shown by yellow vectors.

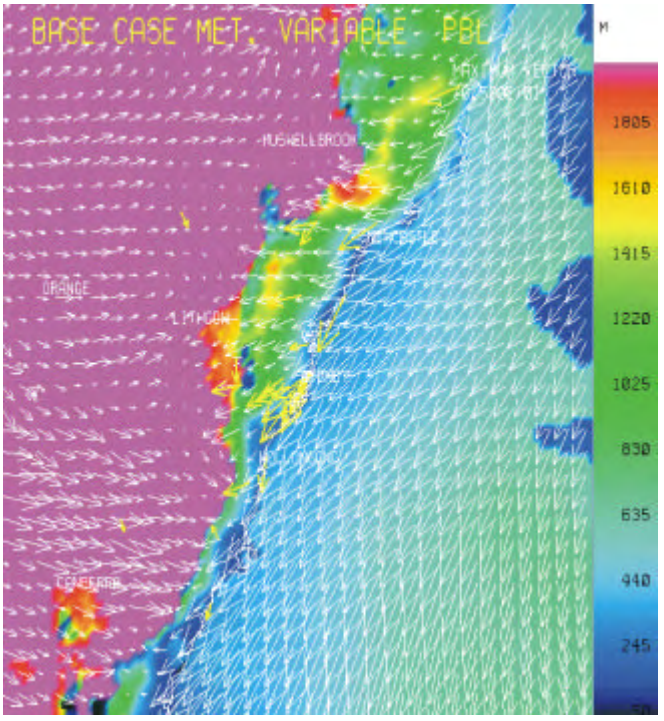

Figure 14. The wind field and the PBL height patterns at 1700 EDT 22 January 2001 (Day 2). The green are shows the advance of the sea breeze. The wind observations are shown by yellow vectors.

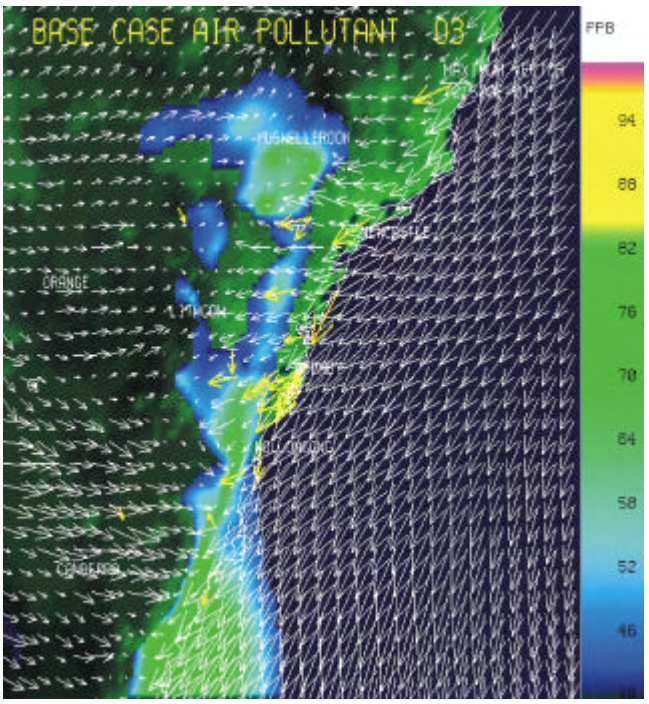

Figure 15. The wind field and the ozone concentration patterns at 1700 EDT 22 January 2001 (Day 2). South of Newcastle the ozone arrives with the sea breeze front. The peak south of Muswellbrook is due to a separate mechanism, the precursors in the Hunter Valley. The wind observations are shown by yellow vectors.

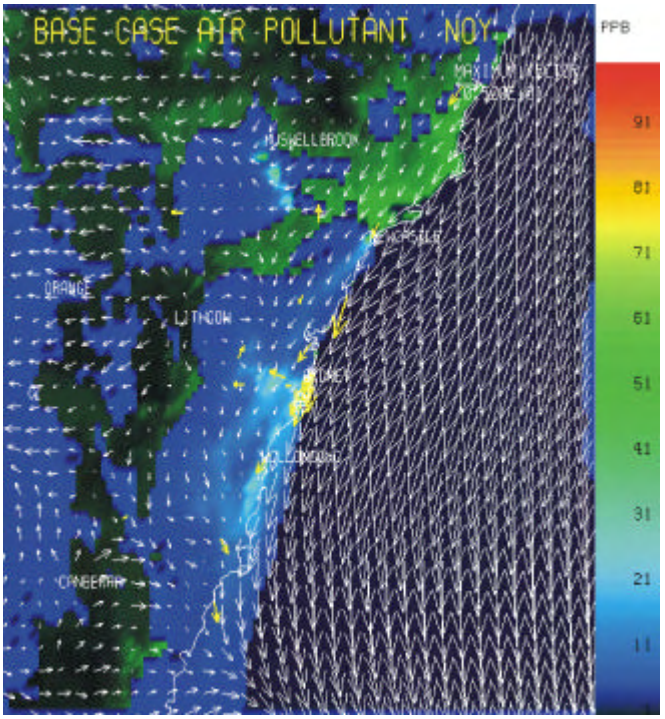

Figure 16. The wind field and precursor NO_y concentration patterns at 0000 EDT 23 January 2001 (Day 3). The wind observations are shown by yellow vectors.

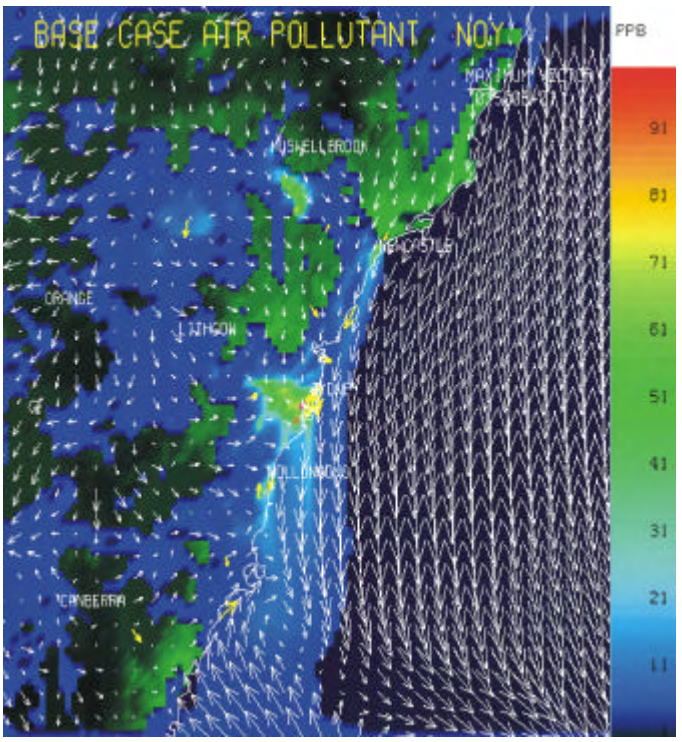

Figure 17. The wind field and precursor NO_y concentation patterns at 0600 EDT 23 2001 January (Day 3). The wind observations are shown by yellow vectors.

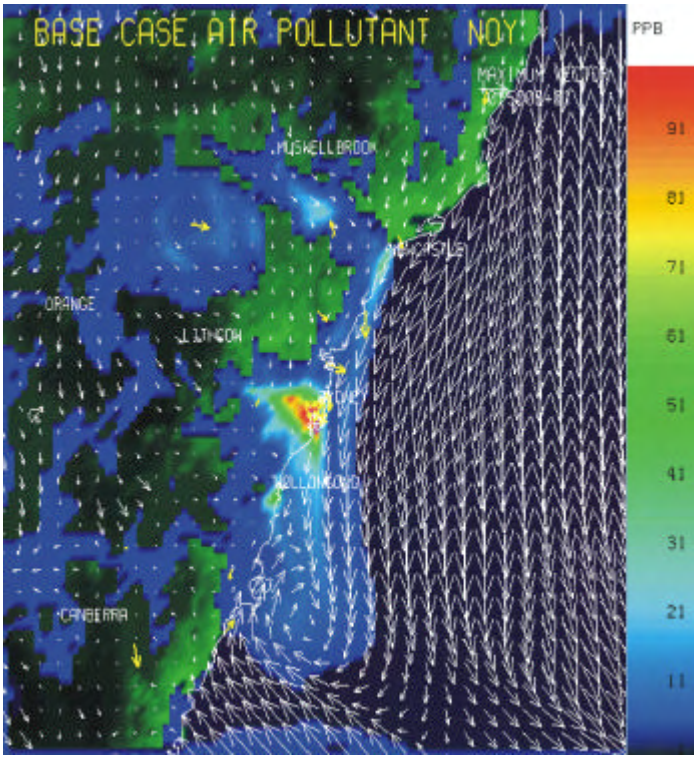

Figure 18. The wind field and precursor NO_y concentration patterns at 0800 EDT 23 January 2001 (Day 3). The wind observations are shown by yellow vectors.

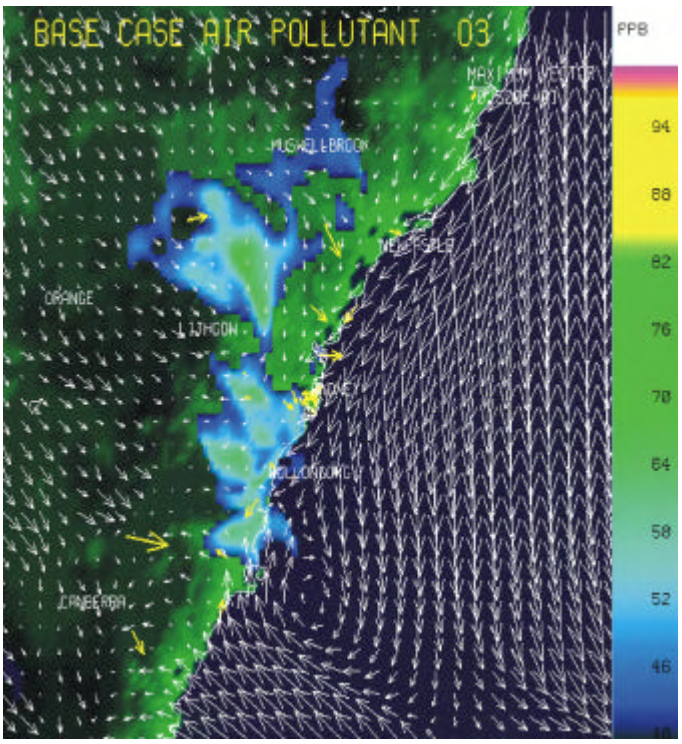

Figure 19. The wind field and ozone concentration patterns at 1000 EDT 23 January 2001 (Day 3). The wind observations are shown by yellow vectors.

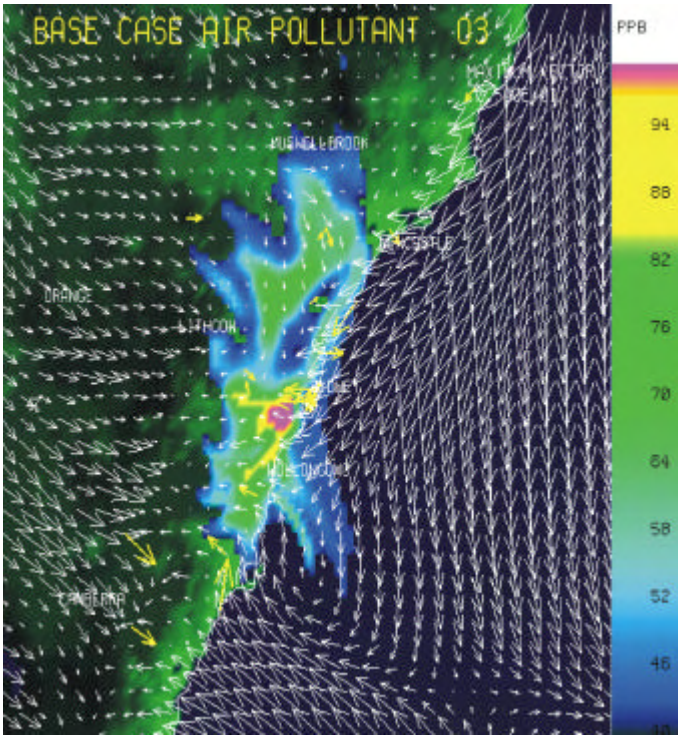

Figure 20. The wind field and ozone concentration patterns at 1200 EDT 23 January 2001 (Day 3). The wind observations are shown by yellow vectors.

The ozone progressed inland with the sea-breeze front. Figure 21 shows the ozone spatial distribution at 1800 EDT.

Comparison of the predicted PBL heights with the AMDAR data (Figure 3) for 23 January shows that they are well predicted. The time series of predicted ozone concentrations in general corresponds well with the observations (Figure9). It is particularly noteworthy that AAQFS correctly predicted the high values (> 100 ppb at Camden, > 130 ppb at Campbelltown, and > 140 ppb at Liverpool). The system substantially underestimated the peaks at some of the stations (Blacktown, Earlwood, Lindfield, Richmond, St. Marys and Vineyard). Some of the inland stations exhibit a double peak (e.g. Bringelly), both in the observations and in the forecasts. This appears to occur because the strong thermal stratification limited the early morning growth of the PBL height and the ozone concentration increased with time. At the surface heating continued to increase during the course of the morning, until a point was reached when the dry convection was strong enough to break through the limiting stratification and the PBL grew in height. This growth was accompanied by a dilution of the ozone concentration, creating the trough between the peaks in Figure 9. The second ozone peak occurred when the sea breeze arrived and brought with it higher ozone concentrations. For stations located closer to the coast the sea breeze arrived before the ozone trough occurred, and consequently the time series shows only a single peak.

Days 4 and 5 were only partially successfully modelled by AAQFS. The reason is the same for both days. The meteorological dynamics for the western transport of ozone depends on a delicate balance between the synoptic wind field and the mesoscale sea breeze circulation. In the case of 24 and 25 January 2001 the synoptic westerly flow was too strong compared to the incoming sea breeze.

On Day 4 (24 January 2001) there is a significant ozone remnant at the surface and aloft left over from the previous day. Figure 22 shows the surface pattern at 0300 EDT. Note that the concentrations reach values > 80 ppb south of Lithgow and east of Canberra. Between 0300 and midday these plumes are advected southeastward and southward along the coast.

Up until about 1400 EDT the winds are well forecast. But then the balance between synoptic flow and mesoscale flow changed. The advance of the sea breeze was blocked by the synoptic flow between 1400 EDT and 2100 EDT (Figure 23 shows the predicted and observed wind pattern and the ozone spatial distribution at 1400 EDT). Some of the ozone ahead of the sea breeze front appeared to be transported aloft and rode over the top of the sea-breeze boundary layer. This is illustrated in Figure 24, which shows a vertical section oriented NW-SE (perpendicularly to the coast), passing through Sydney. The consequence of the stalled sea breeze front and lifting of the ozone is seen in Figure 9. Stations on the coastal side of the blocked sea breeze front (Earlwood, Lidcombe, Linfield, Randwick, Rozelle, and Wooloowaare) are predicted very well. Stations inland of the blocked sea breeze front (Blacktown, Bringelly, Camden, Campbelltown, Liverpool, Richmond, St. Marys and Vineyard) are underestimated.

The advance of the sea breeze was blocked on the next day (25 January 2001) also. Strong synoptic northwesterlies and westerlies not only prevented the sea breeze from coming inland, but south of Wollongong advected the ozone out to sea (the ozone spatial distribution at 1700 EDT is shown in Figure 25). Some of the stations (Earlwood, Lidcombe, Lindfield, and Rozelle) appeared to be located right where the modelled sea breeze was stalled. The AAQFS overestimated the ozone concentrations for these stations (Figure 9). Other stations (Blacktown, Richmond, St. Marys, Vineyard and Wooloowaare) are further inland and consequently AAQFS underestimated the ozone concentrations there because the ozone associated with the sea breeze had not arrived in time. The system did well at the remaining stations (Bringelly, Campbelltown, Liverpool, Randwick, and Westmead).

A wind shift moved up the coast late on 25 January 2001 and by 0000 EDT 26 January 2001 reached the area between Wollongong and Sydney. The southerly winds behind the wind shift prevented the ozone precursors from being advected offshore; however, remnant ozone from the previous day (with concentrations > 80 ppb) was found between Wollongong and Canberra at 0100 EDT (Figure 26). As the land heated up and the vertical mixing increased fumigation occurred in this region.

The general flow pattern is similar to the first event day, except in this case the sea breeze brings in clean air. The pollutants were transported from the coast ahead of the sea breeze. The incoming sea breeze reinforced the southerly wind surge. The balance between the synoptic flow and the mesoscale

flow was restored and there is good agreement with the forecast winds and observations for the entire day. The ozone time series give good agreement at all of the monitoring stations, including the inland stations (Figure 9). Values of ozone concentrations > 100 ppb at Bringelly, Camden and St. Marys are well forecast (Figure 27 shows the ozone distribution at 1700 EDT).

On the last day of the event (27 January 2001) another wind shift travelled up the coast. The flow patterns were also similar to the first event day. Figure 28 shows the drainage winds at 0600 EDT and the high levels of NO_y concentrations near Sydney and in the Hunter Valley. Because the southerly wind surge was stronger it pushed beyond Newcastle and the ozone merged into a single plume ahead of the surge as it turned inland (Figure 29 shows the ozone distribution at 1700 EDT). Behind the trough line the southerly winds brought in clean air. Comparison of the forecast and observed ozone time series gives good agreement at all stations (Figure 9).

3. Summary of the Sydney 7-day event

The 7-day Sydney event demonstrated the ability of AAQFS to forecast situations involving re-circulation of precursors and remnant ozone, fumigation and complex meteorological dynamics. The forecasting system was able to successfully predict high values of ozone, although sometimes the peak concentrations for the inland stations were underestimated. The dynamics for the Sydney region require a sensitive balance between the synoptic flow and the mesoscale flow. On two occasions the system forecast a synoptic flow that was too strong. This resulted in blocking of the inland advancement of the sea breeze and only partial success in forecasting the correct values of ozone on those occasions.

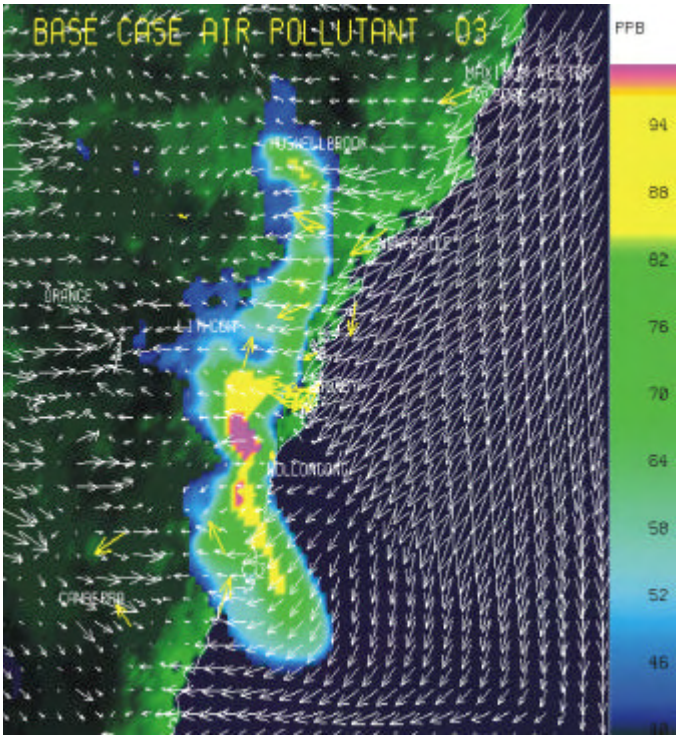

Figure 21. The wind field and ozone concentration patterns at 1800 EDT 23 January 2001 (Day 3). The wind observations are shown by yellow vectors.

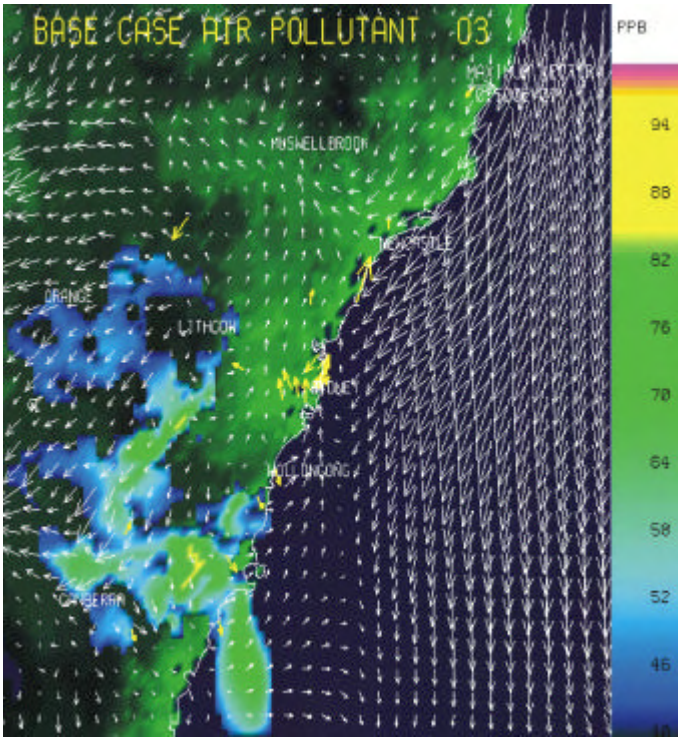

Figure 22. The wind field and ozone concentration patterns at 0300 EDT 24 January 2001 (Day 4). The wind observations are shown by yellow vectors.

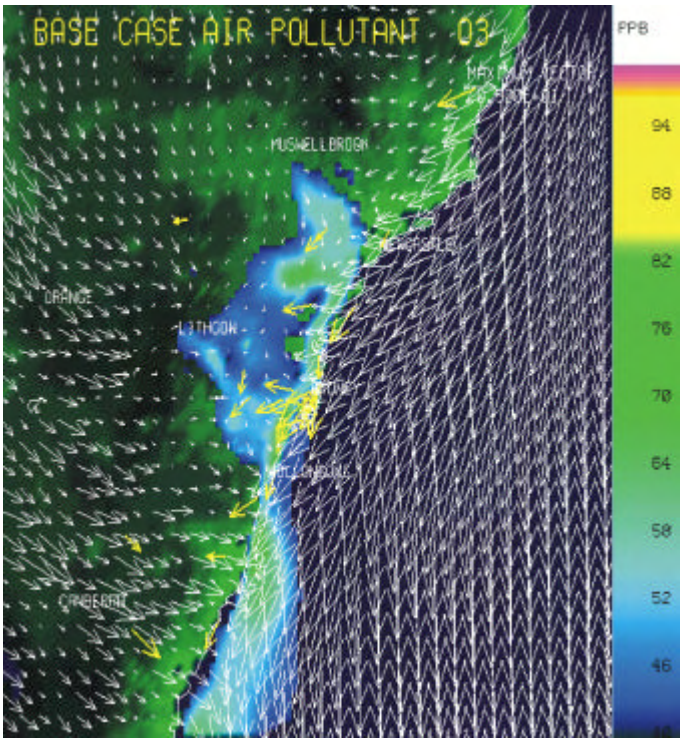

Figure 23. The wind field and ozone concentration patterns at 1400 EDT 24 January 2001 (Day 4). The wind observations are shown by yellow vectors.

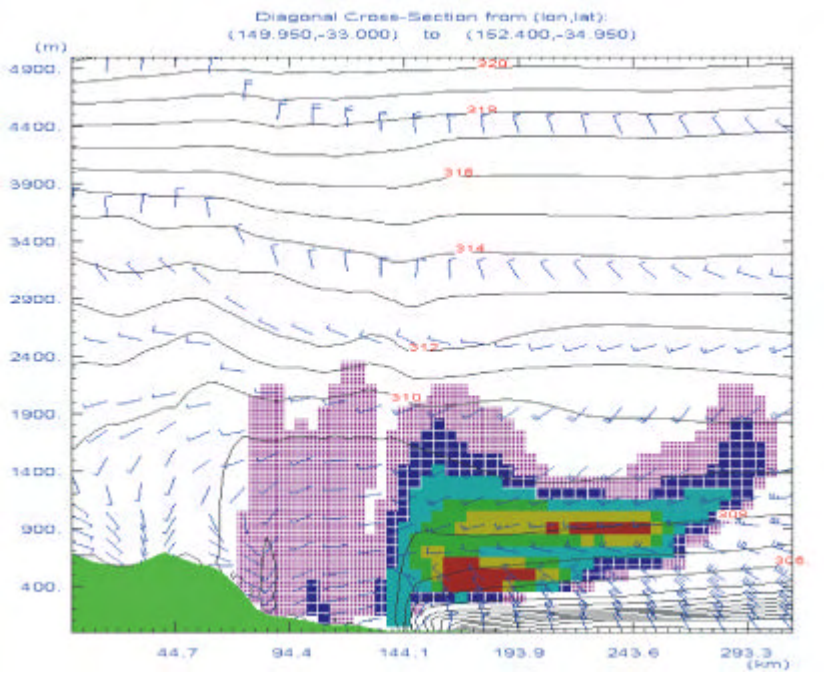

Figure 24. Ozone lifted up over the sea-breeze at 1700 EDT 24 January 2001 (Day 4). The section is oriented NW-SE (perpendicular to the coast) and passes through Sydney. Concentrations increase by 10 ppb with each colour from magenta through to red, beginning with the range 40-50 ppb. Potential temperature is contoured (interval, 1 K) and horizontal winds are represented by wind barbs (full barb = 6 knots) . Downward (upward) pointed barbs represent flow out of (into) the page.

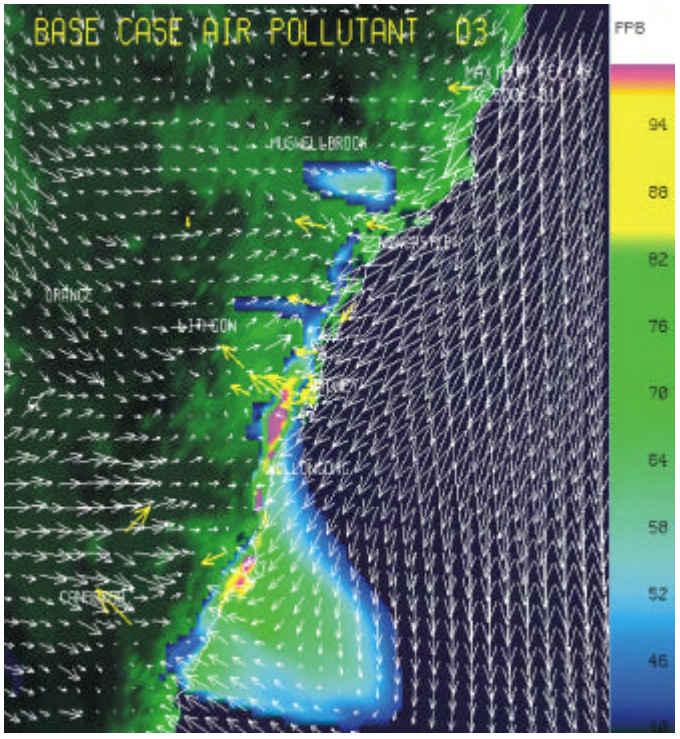

Figure 25. The wind field and ozone concentration patterns at 1700 EDT 25 January 2001 (Day 5). The wind observations are shown by yellow vectors.

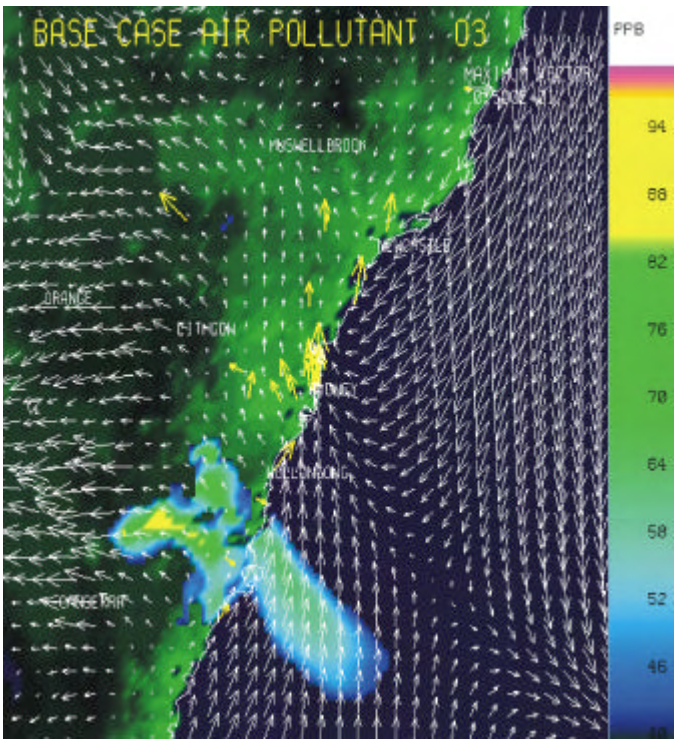

Figure 26. The wind field and ozone concentration patterns at 0100 EDT 26 January 2001 (Day 6). The wind observations are shown by yellow vectors.

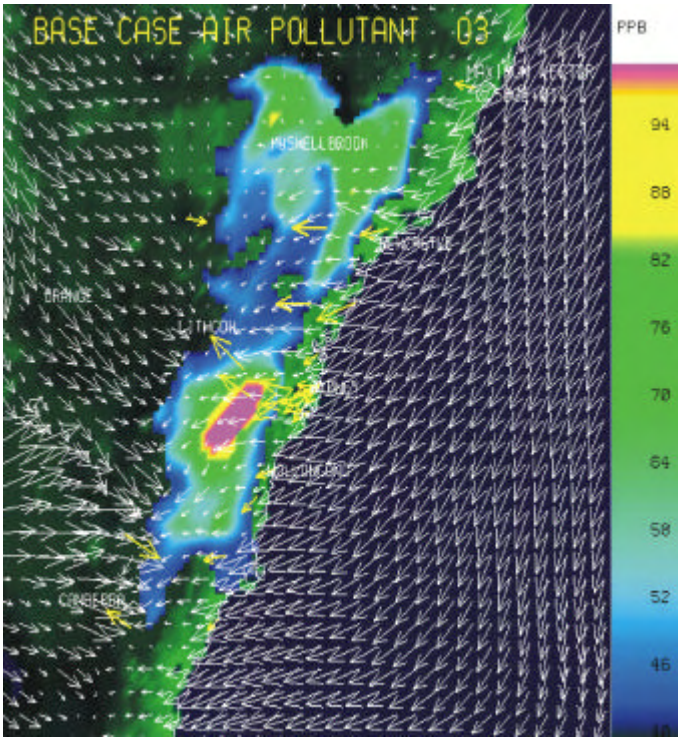

Figure 27. The wind field and ozone concentration patterns at 1700 EDT 26 January 2001 (Day 6). The wind observations are shown by yellow vectors.

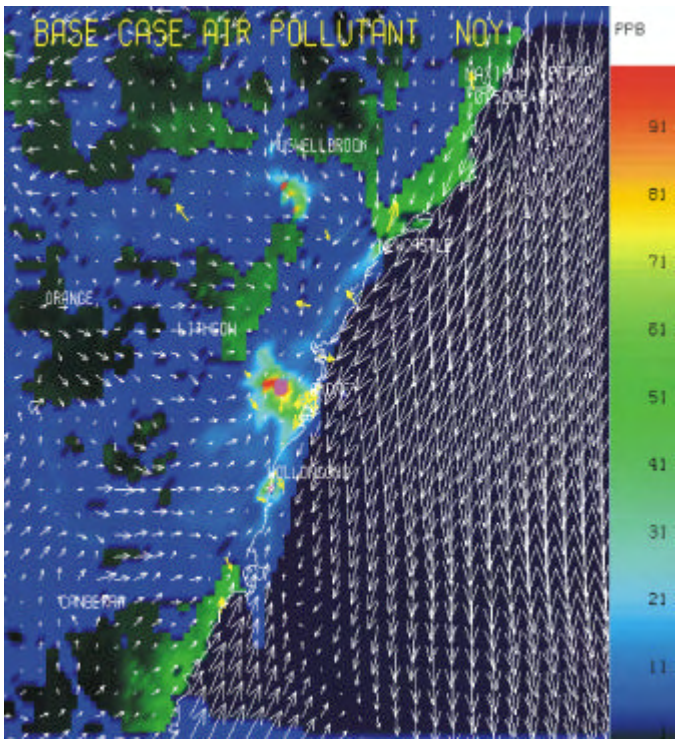

Figure 28. The wind field and precursor NO_y concentration patterns at 0600 EDT 27 January 2001 (Day 7). The wind observations are shown by yellow vectors.

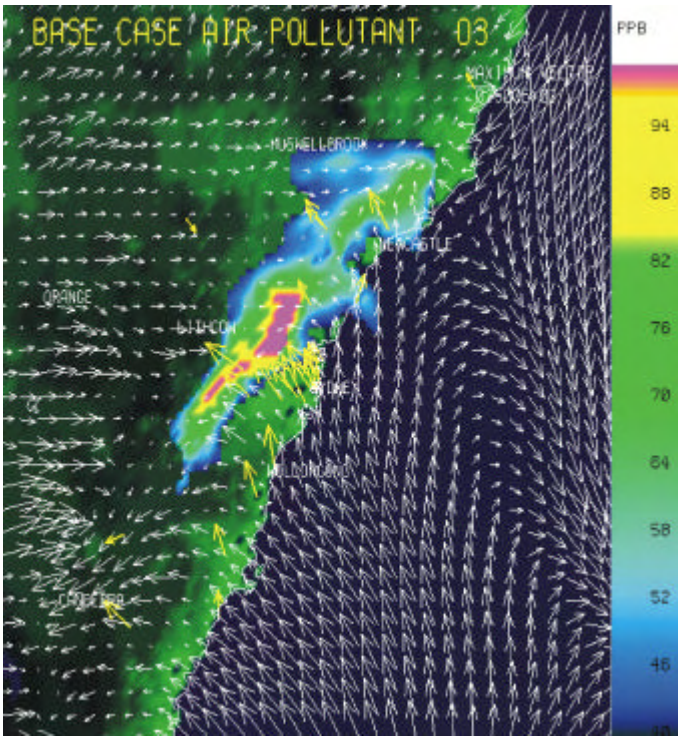

Figure 29. The wind field and ozone concentration patterns at 1700 EDT 27 January 2001 (Day 7). The wind observations are shown by yellow vectors.

Appendix 7.3 King Island Bushfire Smoke

K. J. Tory[1], G. D. Hess[1], M. E. Cope[2,3] and S. Lee[2]

[1]Bureau of Meteorology Research Centre,
[2]CSIRO Atmospheric Research, [3] CSIRO Energy Technology

1. Background

On 11 January 2001 thick smoke was transported behind a cold front from King Island to the Melbourne area which led to the worst particle exceedences since the Ash Wednesday bushfires and the Melbourne Dust Storm of 1983. The smoke from the King Island fire arrived in the Melbourne suburbs during the evening. Earlier that afternoon smoke from a smaller fire at Winchelsea (100 km south-west of Melbourne) arrived with the cold front. The operational air quality forecasts at the time did not include irregular emission sources such as bushfire smoke. To demonstrate the ability of AAQFS to model such an event the system was re-run at a later date with particle tracer sources added at the fire locations. A comparison of this 'hindcast' with the available observations, showed the AAQFS was capable of reproducing the smoke transport with considerable skill in both space and time.

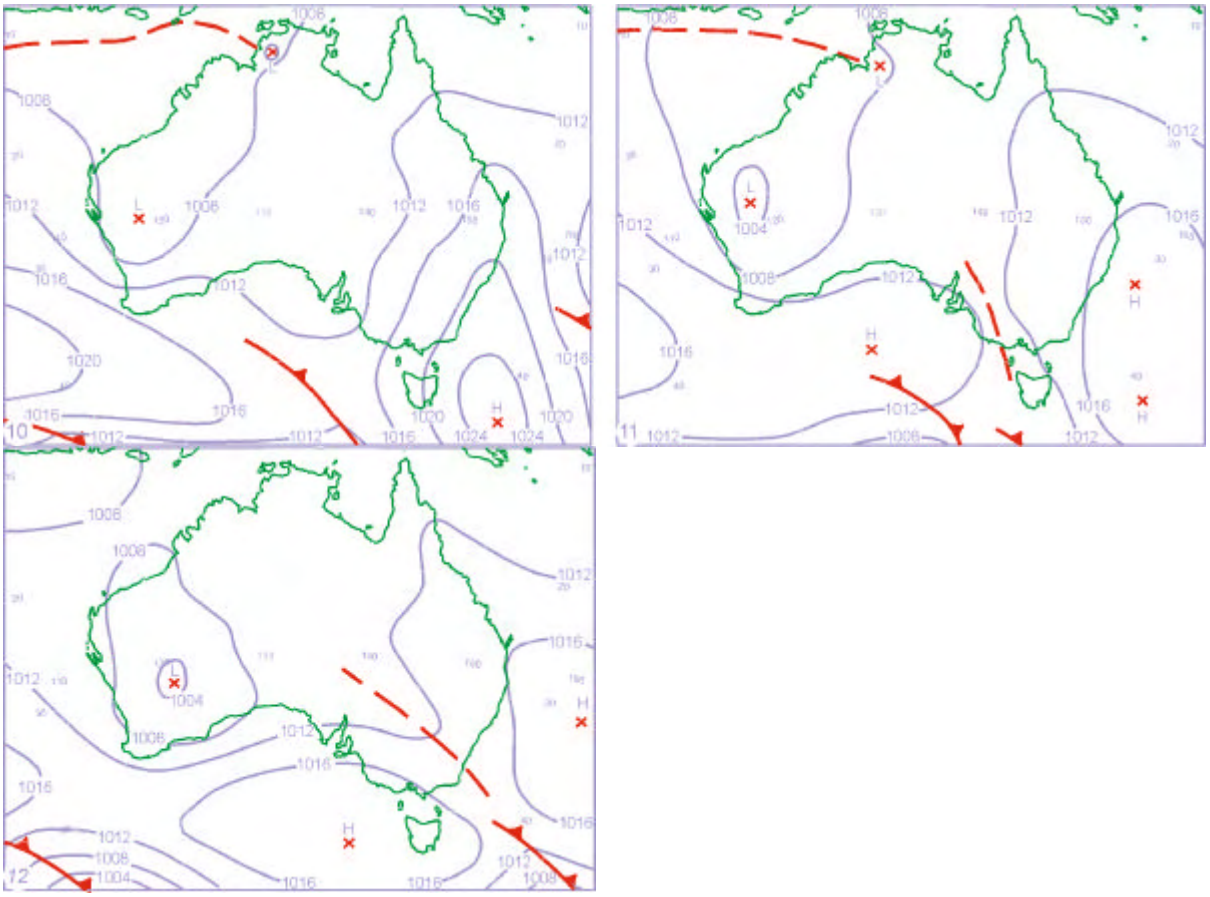

Figure 1. Synoptic pressure charts at 0000 UTC on (a) 10, (b) 11 and (c) 12 January 2001. Contour interval = 4 hPa. Cold fronts are depicted as full red lines with triangles, and the trough is depicted as a dashed red line.

The synoptic conditions at 0000 UTC 10, 11 and 12 January are depicted in Figure 1a–c respectively. Figure 1a shows a high-pressure system east of Tasmania directing a north-north-easterly gradient wind over most of Victoria and King Island. Figure 1b illustrates the pressure gradients were particularly weak in the southeastern Australian region, approximately six hours prior to the arrival of the cold front in Melbourne, with weak high pressure systems to the east and west. A trough is analysed (dashed line) running from the west of King Island through western Victoria and eastern South Australia. The trough propagated from west to east with time. Prior to the trough arrival (at a particular location) the gradient wind was from the northwest and shifted to the southwest when the trough passed. The actual wind shift was particularly shallow and there was insignificant associated cloud, which may explain why it was not analysed as a front. We show below that despite being shallow and dry the wind shift and associated temperature change was sufficiently large and abrupt to be considered frontal, and will be termed the 'King Island front' from here on. Figure 1c shows a broad weak high-pressure system to the south of the mainland which directed the south-easterly gradient winds over Melbourne that was responsible for flushing the Melbourne area clean of smoke.

2. Mesoscale Meteorology and Model Performance

To the southwest and north of Melbourne the model wind shift arrived 1–2 hours earlier than that observed, and southeast of Melbourne the timing was close to coincident. Compare Figures 2a and 2b (west and east of Melbourne respectively) which show time-series of observed and modelled wind temperature and dewpoint temperature at Laverton and Moorabbin. The frontal arrival is marked by the drop in temperature, the rise in air moisture (represented by the rise in dewpoint temperature) and the shift in wind direction. This is considered to be a good forecast since the cold front arrival is particularly sensitive to the balance between the weak synoptic northerlies and the development of sea and bay breezes. The latter winds can enhance the frontal structure, and accelerate or stall the larger scale wind change, which further complicates the frontal forecast. In this case the model sea/bay breeze influence differed on either side of the bay.

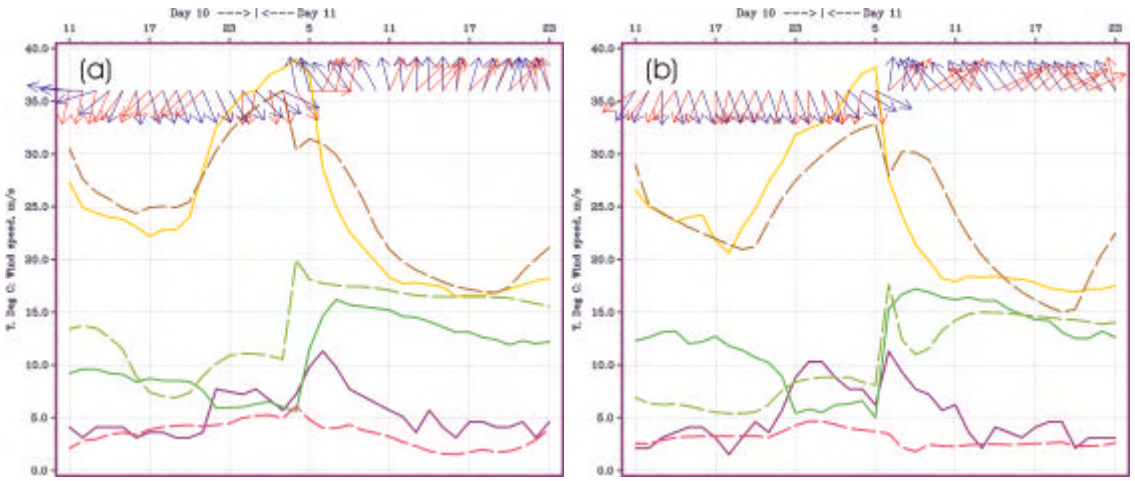

Figure 2. Time series of surface temperature (yellow=observed, brown=LAPS), dewpoint temperature (green full line=observed, green dashed=LAPS), wind speed (purple=observed, pink dashed=LAPS) and wind direction (red vectors=observed, blue vectors=LAPS) over the 36-hour period following 1100 UTC 10 January at (a) Laverton and (b) Moorabbin. See Figure 4 for locations. The arrival of the cold front is evident in the drop in temperature, rise in dewpoint temperature, and shift in wind direction between 4 and 6 UTC (3-5 pm) in (a) and near 6 UTC (5 pm) in (b).

The vertical structure of the observed front is depicted in Figure 3a which shows a time versus height profile of the temperature and wind structure from data collected by commercial aircraft as they take-off from Melbourne airport. The development of a well-mixed layer is evident in Figure 3a (yellow line) that extends to 850 hPa after 2100 UTC (8 am EDT) with winds from the north-northwest. After 0500 UTC (4 pm EDT) the wind shifted to southerly and the temperature dropped significantly below 950 hPa, as the colder southerly flow arrived behind the front. Note the very stable layer that formed between the lower-level cold air and the remaining warmer air above. This stable layer effectively put a lid on the smoke and helped maintain the high particle concentrations by inhibiting vertical dilution. An equivalent LAPS chart (Figure 3b) was constructed by interpolating the gridded model data to the flight paths. This shows the model vertical structure was well forecast. The timing of the change and depth of the cold air is in very good agreement with Figure 3a. The diagnosed PBL height (yellow line) is over-predicted during the day due to slightly cooler temperatures between 800 and 900 hPa. Other differences are largely due to limitations of the model grid resolution. This shows up in the less abrupt frontal leading edge and stable layer, and the more gradual wind shift from north to south.

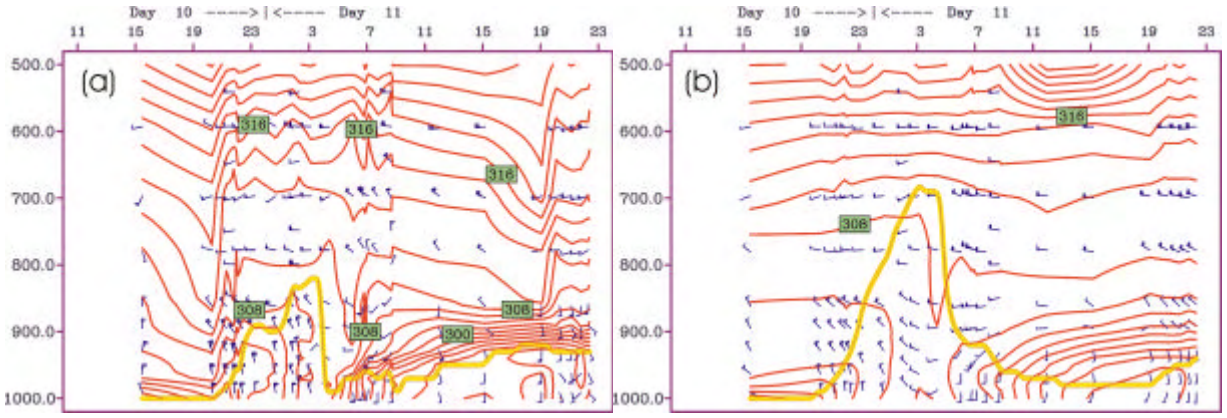

Figure 3. Time-height profiles of potential temperature (contour interval 2 K) and winds (full barb = 10 knots), for the 36-hour period following 1100 UTC 10 January 2001. The yellow line marks the approximate position of the top of the mixed layer, determined by the level at which the atmosphere is first 1 K warmer than the 10-m potential temperature. Image (a) was constructed from data collected by commercial aircraft as they take-off from Melbourne airport, and (b) from LAPS data interpolated to the flight paths. The cold front arrival (determined from the wind barbs) occurred near 6 and 5 UTC (5 and 4 pm EDT) in (a) and (b) respectively.

The horizontal flow structure of the model front, as it crossed Port Phillip, is illustrated in Figure 4 (1 pm EDT). Since the model front arrived about 1–2 hours early to the north and south-west of Melbourne, we have superimposed the observed winds from a time two hours later, to show the good agreement between the model and observed frontal structure.

3. Smoke Plumes

The King Island bushfire was burning for a number of days prior to the arrival of the cold front that transported the smoke to Melbourne. This is evident in Figure 5 which shows satellite images at 7:32 am and 12:32 pm on 10 January, and 12:32 pm and 3:25 pm (EDT) on 11 January respectively. During this period the winds shifted from north-easterly to north-westerly (consistent with the gradient winds implied from Figure 1) which generated a smoke plume that extended to the south-west and rotated with time to the south-east just prior to the arrival of the frontal wind change. The fire intensified when the winds picked up as the front approached. The southwesterly change advected the plume to the northeast and the most recently emitted smoke began to form a plume directed to the northeast.

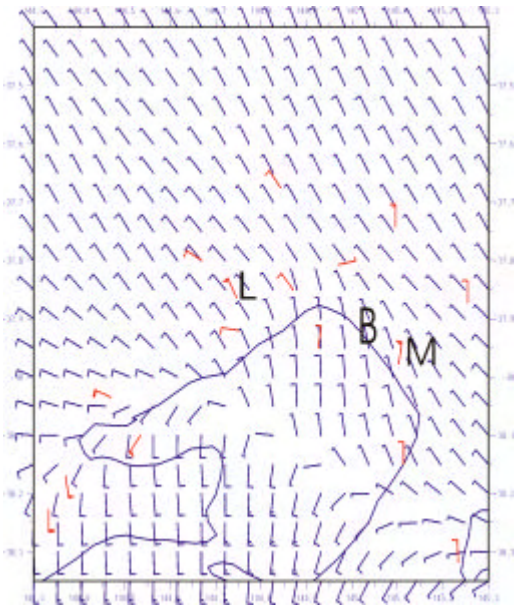

Figure 4. LAPS surface winds (blue barbs) at 0200 UTC 11 January (1 pm EDT), with observed winds two hours later overlayed (red barbs). The letters 'L' and 'M' mark the locations of Laverton and Moorabbin (neighbouring red barbs) re ferred to in the text, and 'B' marks the location of the Brighton EPA monitoring station. The cold front crossing the bay is defined by the line of converging wind barbs.

This produced the dog-leg shape evident in the last Figure 5 image and in Figure 6. Figure 6 shows the plume at 6:31 pm beginning to be obscured by cloud. Figure 7 shows the model plume at a similar time to Figure 6. Note the good agreement between the two plumes. The model dog-leg is less sharp due to the less abrupt model frontal change (mentioned above). It was difficult to distinguish smoke from cloud in all later images. From this time on we rely on the model hindcast and emission observations at metropolitan observing stations to understand the smoke transport.

The Winchelsea fire began on the afternoon of 11 January. Smoke from this fire was transported to Melbourne by the cold front and arrived at the same time as the wind change. The smoke from the Winchelsea fire was not visible in the satellite images, and the particle levels measured at the Brighton monitoring station were significantly less than the King Island plume, which suggests the Winchelsea event was secondary to the King Island event. The remaining analysis will concentrate mostly on the latter event.

The model winds rotated from southwesterly to southerly during the night and consequently the King Island plume rotated counter-clockwise and swept over Melbourne from the southeast. This is evident in Figure 8 which shows the surface plume at midnight, 4 am, 9 am and midday, 12 January. Figure 8a shows the most concentrated part of the plume entering Port Phillip at midnight (note also the Winchelsea plume to the north). The plume had swept across the bay by 4 am (Figure 8b) and cleared the eastern metropolitan and bay regions by 9 am (Figure 8c). However, three hours later these regions were once again consumed by smoke. This was due to fumigation as daytime turbulent mixing began to transport smoke down to the surface from above.

The vertical structure of the plume showed considerable variation with height due to the vertical variation of the frontal structure. The wind change arrived first at the surface (typical of cold fronts) that led to a lag in the plume rotation with height. The more gradual wind rotation from southwesterly to southerly that followed also lagged with height. The lag is evident when Figure 9 (same as Figures 8c,d but ~1000 m higher) is compared with Figure 8c and 8d. This lag caused the plume to be sheared over more than one hundred km in the lowest 1000 m of the atmosphere by the time it arrived in Melbourne. As a result, after the smoke had cleared in the eastern suburbs of Melbourne (Figure 8c), the plume remained not far above the surface (Figure 9a). Later in the morning, after a few hours of

solar heating, turbulent mixing began to transport the elevated smoke back down to the surface (fumigation) and eastern Melbourne and the bay were once again consumed by smoke (Figure 8d).

Since there were no satellite images available with visible smoke after 6:30 pm, the only smoke verification possible is from particle data collected by the EPA monitoring stations. Data from the Brighton monitoring station (see Figure 4 for location) is presented as a time-series in Figure 10. Model data from vertical north-south cross sections through Brighton are presented in Figure 11, at 5 pm 11 January, 1 am, 9 am and midday 12 January. A comparison of these four Figures, shows good consistency between the timing of the observed peaks and troughs and the model plume arrivals, plume clearing, and fumigation. The initial peak in Figure 10 (5-8 pm EDT) was associated with the Winchelsea plume (see Figure 11a). The midnight to 6 AM peak represents the King Island plume (see Figure 11b), the trough near 8 AM is the clearing that occurred before fumigation (Figure 11c) and the 9 am to midday peak resulted from the fumigation (Figure 11d). After this time the model smoke was cleared by easterly winds (implied in Figure 1c). The final peak evident in Figure 10 is believed to be due to sea-spray, and industrial and motor vehicle sources. (These other sources were not included in Figures 7–10 to ensure clarity of the smoke plume.)

4. Summary of the King Island Event

On the afternoon and evening of 11 January 2001 a cold front transported smoke from the Winchelsea and King Island bushfires to Melbourne. The meteorology was particularly complex owing to the delicate balance between the bay/sea breeze and the synoptic northerlies, and the effect these small-scale systems can have on the timing and spatial structure of the arriving cold front. Despite these difficulties LAPS produced an excellent forecast of the meteorology, which, when re-run with smoke sources added, showed the AAQFS is capable of producing high quality forecasts of smoke transport from bushfire events.

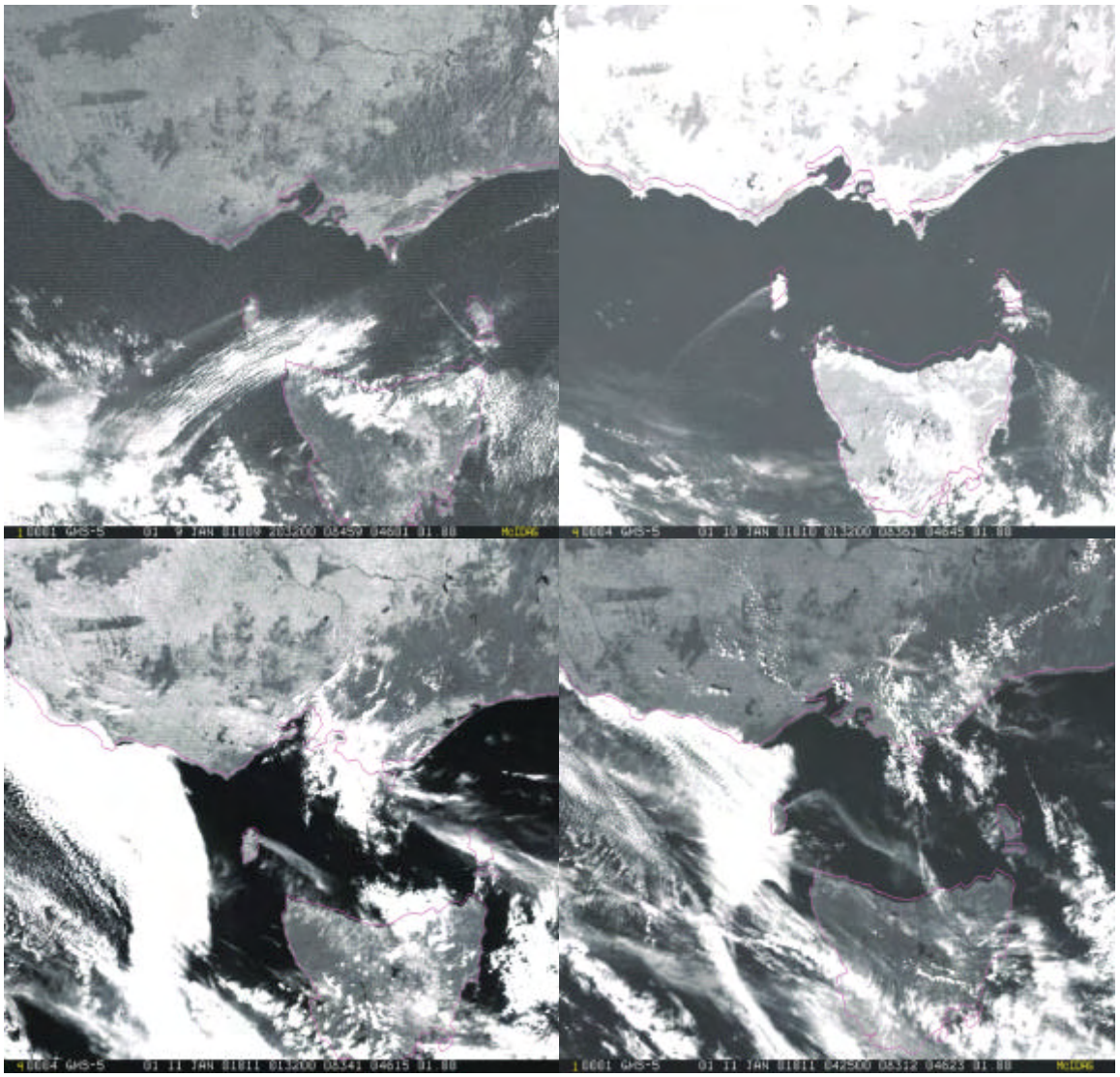

Figure 5. Satellite images illustrating the changing direction of the smoke plume from the King Island bushfire at 7:32 am, 12:32 pm EDT 10 January (upper images) and 12:32 pm, 3:25 pm 11 January (lower images).

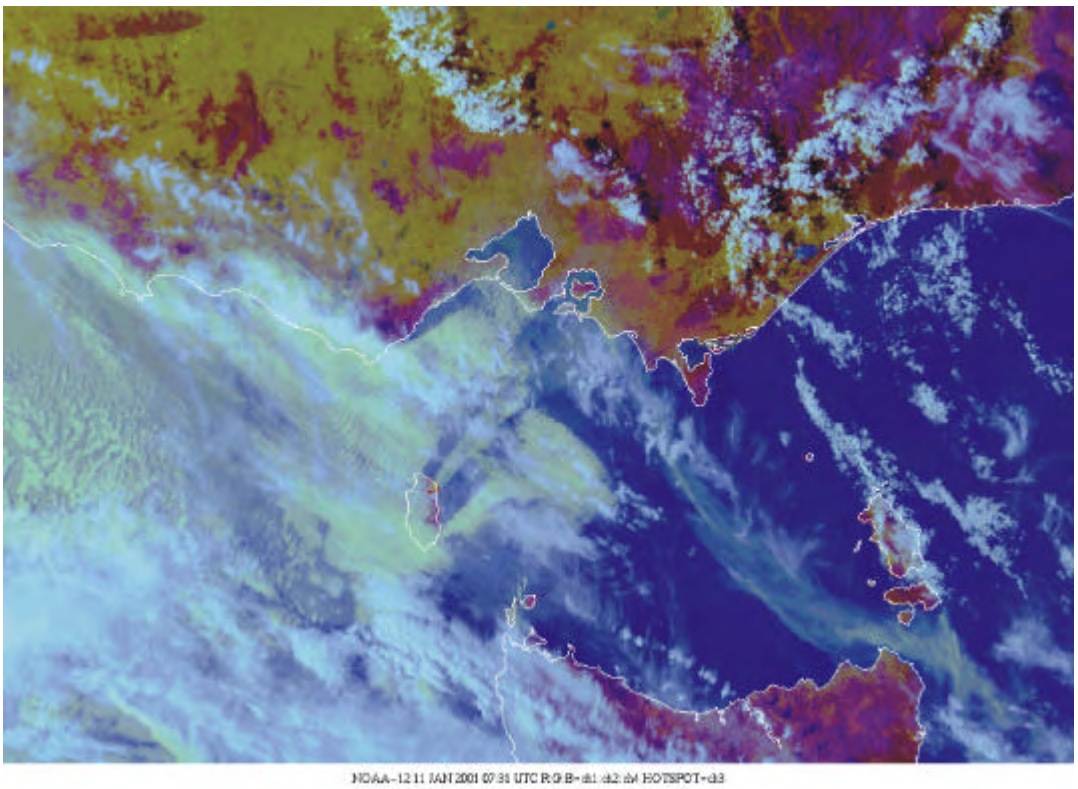

Figure 6. Satellite image enhanced to highlight the King Island smoke plume 0731 UTC 11 January (6:31 pm EDT). At this time cloud is beginning to obscure the plume, which extends from King Island to near Phillip Island and then curves back to the south-east corner of the image.

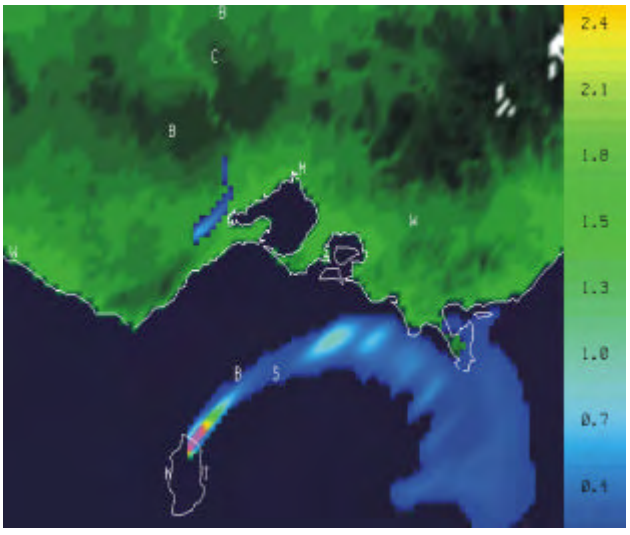

Figure 7. Equivalent AAQFS smoke plume to Figure 6.

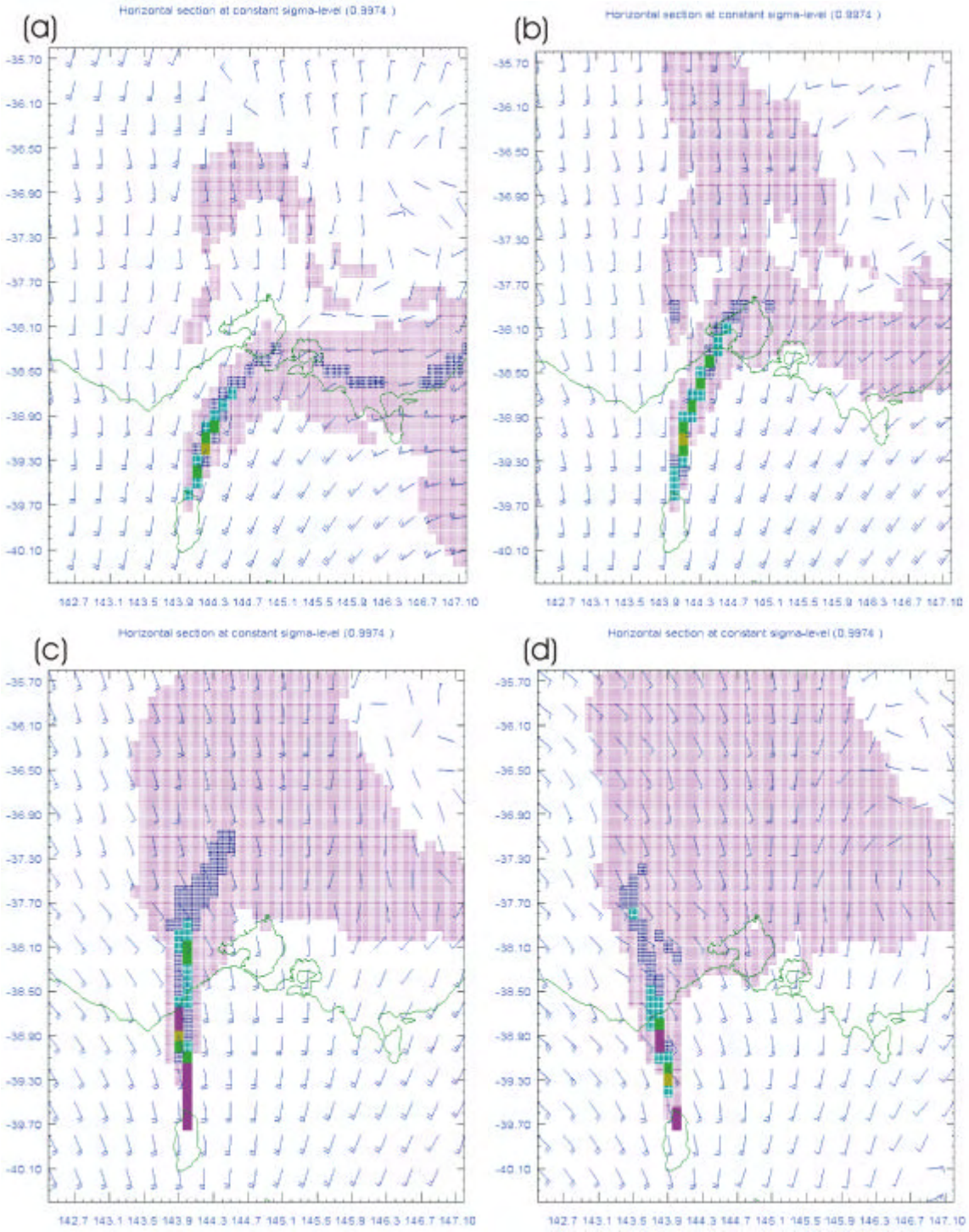

Figure 8. LAPS smoke plume with wind barbs overlayed (~30 km spacing, full barb = 6 knots) at (a) midnight, (b) 4 am, (c) 9 am and (d) midday EDT 12 January. The plume swept across Melbourne and the bay from the southeast (a and b) and had mostly cleared by 9am (c). Fumigation returned smoke to the surface over the bay and most of metropolitan Melbourne by midday (d).

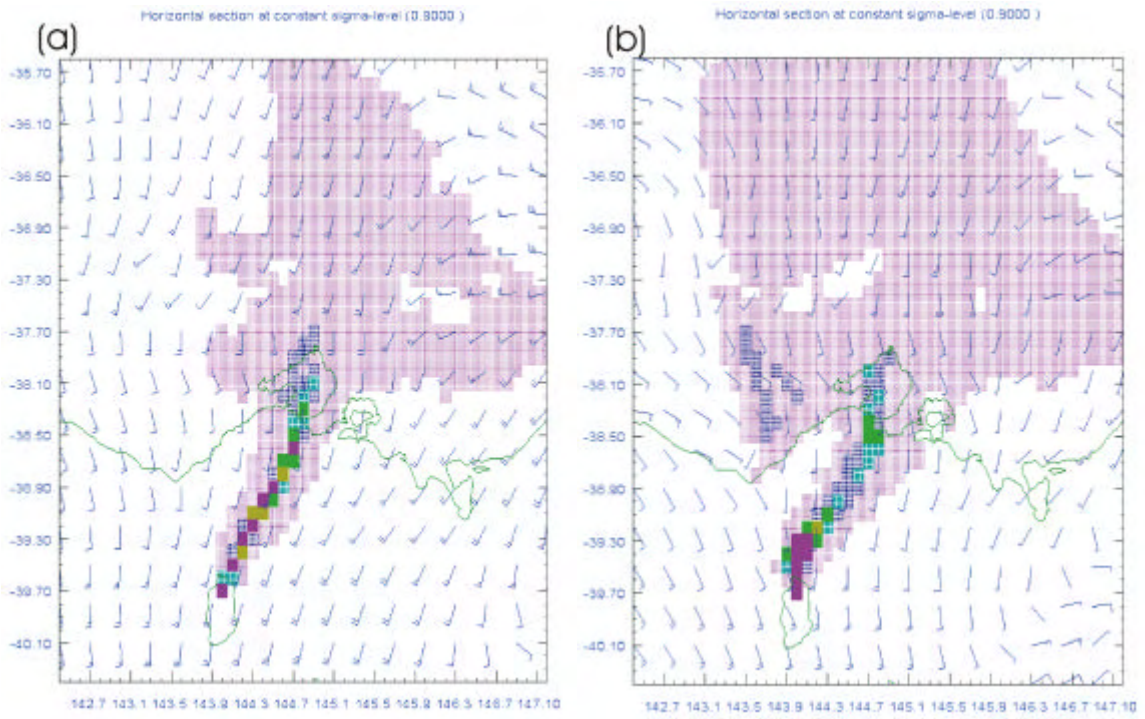

Figure 9. Same as Figures 8c and 8d respectively except ~1000m above the surface. Comparisons with Figures 8c and 8d show the lag of the smoke plume with height.

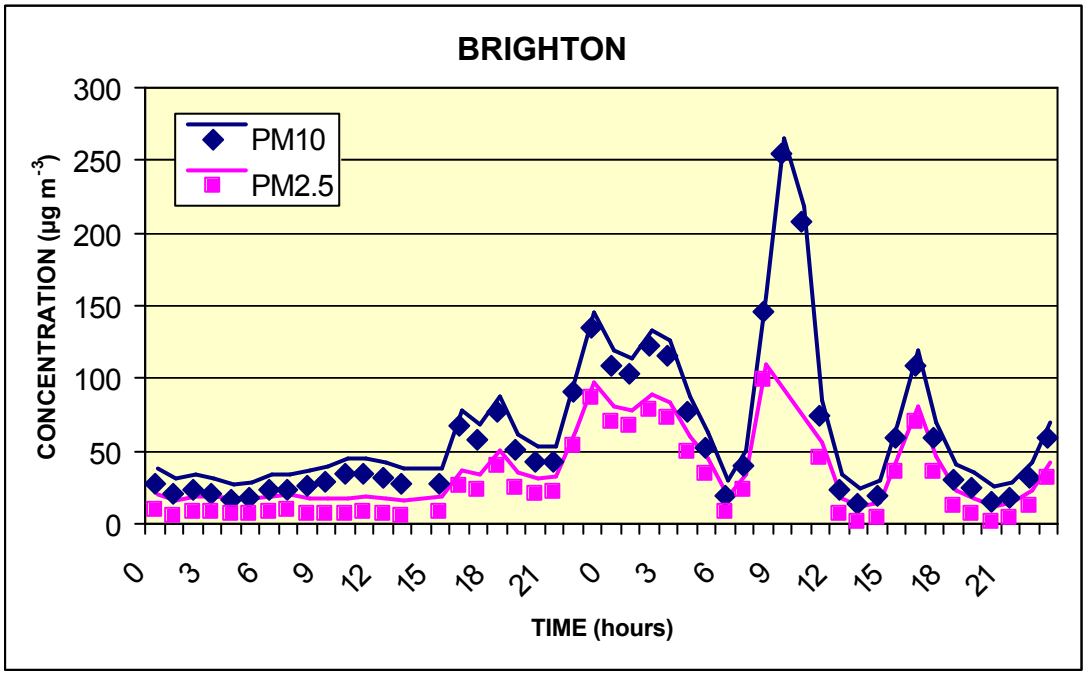

Figure 10. Time-series of observed particle concentrations at Brighton during 11-12 January 2001. Times are in local Summer time (EDT).

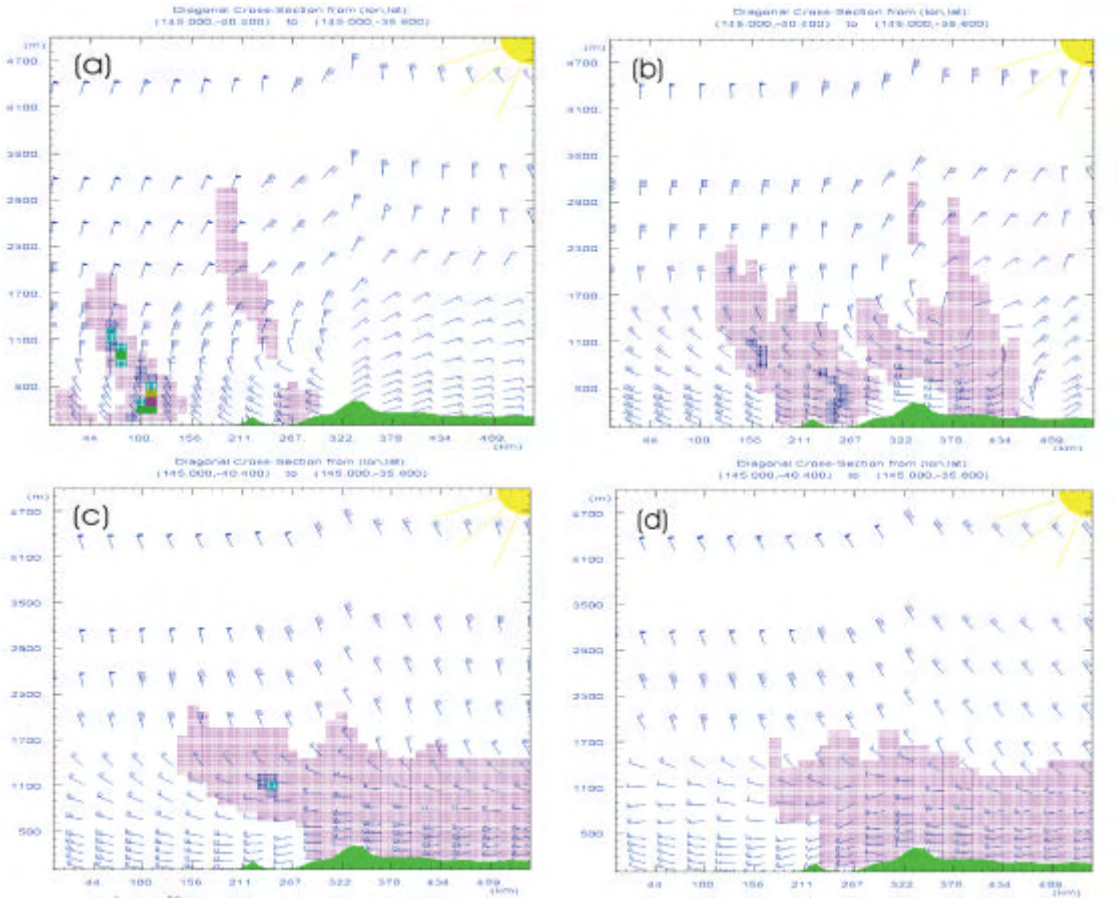

Figure 11. Vertical north-south section of the King Island smoke plume through Brighton (near 267 km on the horizontal axis, see Figure 4 for the location). The horizontal winds are overlayed (blue barbs, full barb = 6 knots, flag = 30 knots). Downward (upward) pointing barbs represent wind flowing out of (into) the page. The Winchelsea plume arrived at Brighton near 5 pm (a) accompanied by the cold front (see converging wind barbs). The King island plume is located about 120 km behind. The King Island plume arrived at Brighton near 1 am (b). The two plumes had merged by 9 am (c). Note the clear air south of about 280 km and below 600 m in (c), with smoke above. Note also the return of smoke to the surface in (d) as far south as 250 km, due to fumigation, three hours later (midday).

Appendix 7.3a A Severe Smoke Event in Melbourne

25th NATO/CCMS; International Technical Meeting
on Air Pollution Modelling and its Application,
15-19 October 2001, Louvain-la-Neuve, Belgium.

THE AUSTRALIAN AIR QUALITY FORECASTING SYSTEM: MODELLING OF A SEVERE SMOKE EVENT IN MELBOURNE, AUSTRALIA

Sunhee Lee, Martin Cope, Kevin Tory, Dale Hess, and Yuk L. Ng*

1. INTRODUCTION

The Australian Air Quality Forecasting System (AAQFS) is a joint project between CSIRO Atmospheric Research, CSIRO Energy Technology, the Bureau of Meteorology (BoM), the EPA Victoria and the EPA of New South Wales to develop a high-resolution air quality forecasting system. Currently, numerical air quality forecasts are issued twice daily for two regions: the airshed of Melbourne and Geelong in Victoria (see Figure 1) and the airshed of Sydney in New South Wales. The principal AAQFS role is to issue numerical forecasts to State EPAs in time for guidance and reference against current air quality forecasting procedures.

The AAQFS consists of five tightly coupled components: (a) the Limited Area Prediction System (LAPS, Puri et al., 1998), one of the BoM's operational weather forecasting systems, is used to generate forecasts of the transport fields at 0.05° (~5 km) horizontal grid spacing; (b) a hybrid offline/online emissions inventory module (EIM, Ng et al., 2000), which generates emission flux estimates for 53 chemical species from anthropogenic, biogenic and natural sources on horizontal grids with spacing of 0.01° for urban areas and 0.05° for non-urban areas; (c) a chemical transport model (CTM; Cope et al., 1999), which generates air quality forecasts for 25 pollutants (including PM1; PM2.5; PM10; photochemical oxidants, formaldehyde, butadiene and benzene) on a horizontal grid spacing of 0.01° for the urban areas and 0.05° for the non-urban areas. Forecasts are undertaken using the highly condensed GRS mechanism (Azzi et al., 1992), thus enabling large domains to be simulated within the forecasting window; (d) a validation system in which observed and forecast 1-hour time series of key meteorological variables and air quality species are compared on a daily basis using a range of graphical and statistical tools; (e) a data dissemination and archiving system which consists of an AAQFS web site displaying graphical summaries of the daily forecasts for use by the EPAs, a PC-based graphical display software for visualising air pollutant species, forecast and observed meteorological variables, and a platform-independent file-archiving system.

* Sunhee Lee, CSIRO Atmospheric Research, Aspendale VIC Australia, Martin Cope, CSIRO Atmospheric Research and Energy Technology, North Ryde NSW, Kevin Tory and Dale Hess, BMRC Melbourne VIC Australia, Yuk L. Ng, Victoria EPA, Melbourne VIC Australia

On 11-12 January 2001, Melbourne experienced the worst visibility episode since the Ash Wednesday bushfire and the Melbourne Dust Storm in 1983. The episode was caused by thick smoke emitted from bushfires on King Island (some 300 km south of Melbourne) and Winchelsea (100 km south-west of Melbourne). Smoke from the Winchelsea fire arrived immediately behind a cold front in the afternoon of 11 January; smoke from the King Island fire first arrived in the Melbourne area during the evening and continued to cross the region throughout the following day.

This paper describes a study in which the AAQFS was used to simulate the severe smoke event of 11-12 January.

Figure 1. The location of the AAQFS Victorian (0.05° horizontal grid spacing) and Melbourne (0.01° horizontal grid spacing) domains. Note that Winchelsea and King Island are in the Victorian domain.

2. CHARACTERISTICS OF THE KING ISLAND AND WINCHELSEA FIRES

The King Island fire started on 3 January 2001. Over the next 7 days the fire burnt 2000-3000 ha of vegetation; the fire was thought to be under control by 10 January. On 11 January, a strong south-west wind came through and the fire was re-ignited and burnt 4500-5000 ha of tea-tree forest, sage-land and heath-lands. The Winchelsea fire started at 15:55 EDT (Eastern Daylight Saving Time), 11 January and was contained by 18:00 EDT, though smouldering continued for another two days. The area burnt was 320 ha of grass-land. The times stated in this paper are all in EDT.

Figure 2 shows GMS-5 satellite images of smoke from the King Island fire at 7:32 and 12:32 on 10 January and 12:32 and 15:25 on 11 January. During this period the winds shifted from north-easterly to north-westerly, which generated a smoke plume that extended to the south-west and rotated with time to the south-east just prior to the arrival of the frontal wind change. The fire intensified when the winds picked up as the front approached. The south-westerly change advected the plume to

the northeast and the most recently emitted smoke began to form a plume directed to the northeast. Smoke from the Winchelsea fire was transported to Melbourne by the cold front and arrived at the same time as the wind changes. The Winchelsea fire was relatively small compared to the King Island fire and the smoke from the fire was not visible in satellite images. The King Island smoke plume was not clearly discernable in the satellite images after 18:30, because of the presence of clouds.

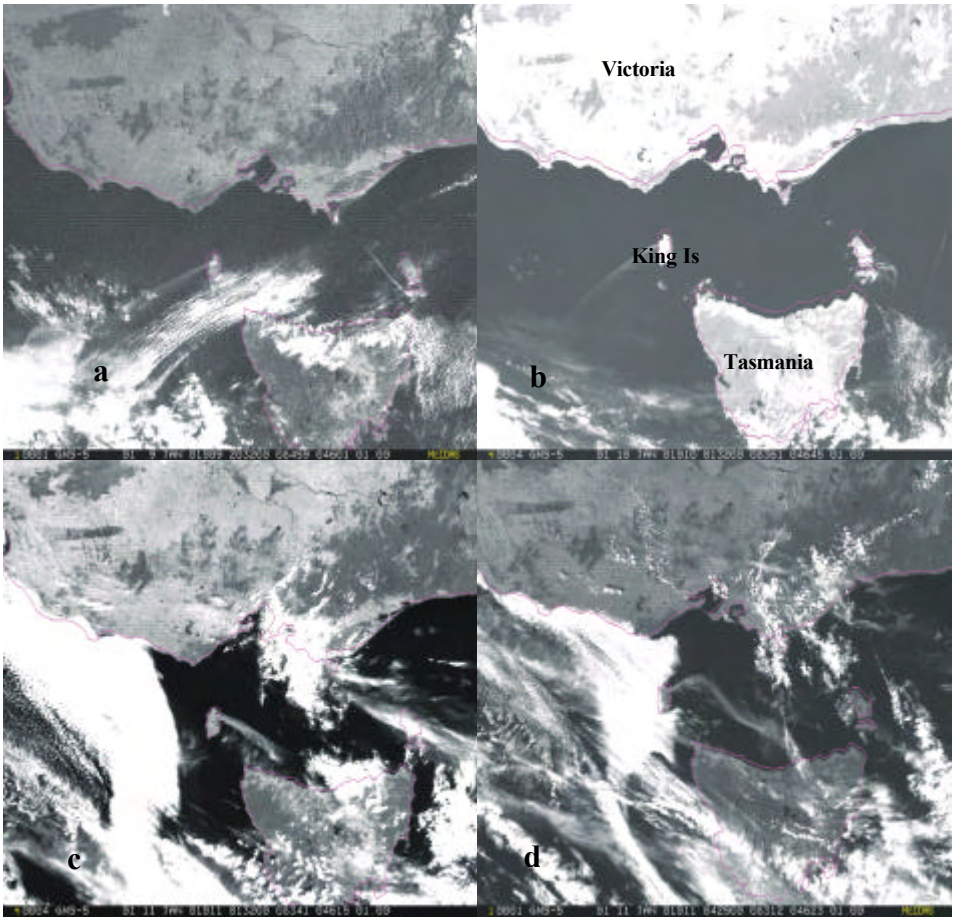

Figure 2. GMS-5 satellite images illustrating the changing direction of the smoke plume from the King Island wildfire. The upper images (a) and (b) are at 7:32 and 12: 32 EDT on 10 January. The lower images (c) and (d) are at 12:32 and 15:25 EDT on 11 January

3. THE AAQFS-LAPS METEOROLOGICAL PREDICTION

A comparison of observed and modelled winds indicated that the cold front was predicted to arrive 1-2 hours earlier than was observed to the southwest and north of Melbourne, while for southeast of Melbourne the timing was close to coincident. Figure 3(a) and 3(b) show time-series of observed and modelled wind temperature and dewpoint temperature at Laverton, west of Melbourne, and at Moorabbin, east of Melbourne, respectively (see Figure 1). The frontal arrival is shown by the drop in temperature, the rise in air moisture (represented by the rise in dewpoint temperature) and the shift in wind direction. This is considered to be a good forecast since the cold front arrival is particularly sensitive to the balance between the weak synoptic northerlies and the development of sea and bay breezes. The latter winds can enhance the frontal structure, and accelerate or stall the larger scale wind change, which further complicates the frontal forecast. In this case the model sea/bay breeze influence differed on either side of the bay.

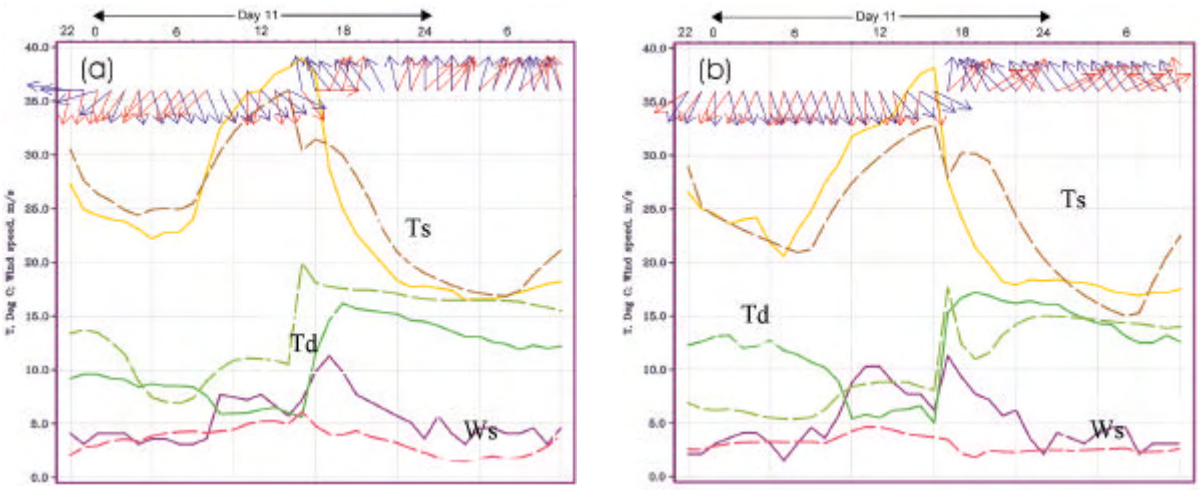

Figure 3. Time series of surface temperature (Ts), dewpoint temperature (Td), and wind speed (Ws) for a period from 22:00 10 January to 10:00 12 January, at (a) Laverton and (b) Moorabbin. The dashed (solid) lines represent LAPS (observed) Td, Ts and Ws, while dark (light) arrows represent LAPS (observed) wind direction.

Figure 4(a) shows the vertical profile of observed temperature and wind structure obtained from data collected by commercial aircraft as they took-off from Melbourne airport. It shows a well-mixed layer extending to 850 hPa after 8:00 11 January with winds from the north-northwest. After 16:00, the wind shifted to southerly and the temperature dropped significantly below 950 hPa, as the colder southerly flow arrived behind the front. A very stable layer formed between the lower-level cold air and the remaining warmer air above. This stable layer effectively put a lid on the smoke and helped maintain the high particle concentrations by inhibiting vertical dilution. A similar vertical profile in Figure 4(b) was constructed by interpolating the gridded model data to the flight paths. The timing of the change and depth of the cold air is in very good agreement with the observed profile. The diagnosed PBL height is over-predicted during the day due to slightly cooler temperatures between 800 and 900 hPa. Other differences are largely due to limitations of the model grid resolution.

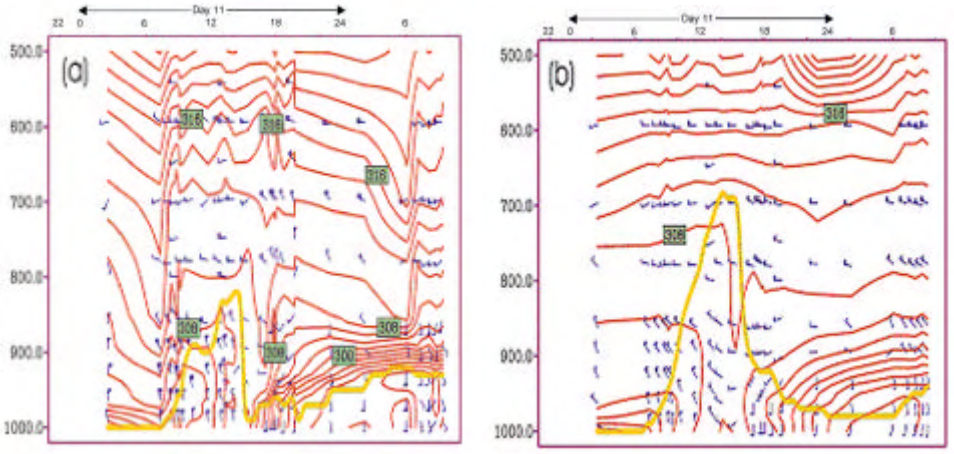

Figure 4. Time-height profiles of potential temperature (contour interval 2K) and winds (full barb = 10 knots), for the 36 hour period following 22:00 10 January 2001. The thick line marks the approximate position of the top of the mixed layer, determined by the level at which the atmosphere is first 1 K warmer than the 10-m potential temperature. Image (a) was constructed from data collected by commercial aircraft as they took off from Melbourne airport, and (b) from LAPS data interpolated to the flight paths. The cold front arrival (determined from the wind barbs) occurred near 17:00 in (a), and 16:00 in (b).

4. THE AAQFS-CHEMICAL TRANSPORT MODELLING

To investigate the suitability of the AAQFS for forecasting the impact of severe smoke events, a series of hindcasts were carried out. A simple fire emission model was developed to calculate hourly emission of PM10, carbon monoxide, butadiene, reactive organic carbon, and oxides of nitrogen using a constant fuel consumption rate. Emission factors were obtained from studies of USEPA (1995) and SAFARI-92 (Andreae et al., 1997). For the Winchelsea fire, the fire size and fuel loading were assumed to be 320 ha and 5.6 tonnes per ha, respectively. For the King Island fire, the fuel loading was assumed to be 45 tonnes per ha and fire size to be 5000 ha. Table 1 lists the emissions values used in the hindcast.

Table 1. The emissions are in g/s. For the Winchelsea fire, the emission values are for the flaming phase, 16:00 to 18:00 EDT. For smouldering phase after 18:00, emission values are reduced by 2/3.

	PM10	CO	NOy	ROC	BTD
King Island	38887	182028	5200	27563	247
Winchelsea	3733	17474	499	2646	24

4.1. Basecase

A basecase simulation was generated by integrating the AAQFS for a 36-hour period commencing 10:00 11 January. The King Island plume was released uniformly between the surface and 1000 m, in accordance with visual observations. For the Winchelsea fire, emissions were uniformly placed between the surface and 500 m. Because there is some uncertainty associated with the release heights, a number of sensitivity runs were undertaken to assess the impact on the spatial and temporal distribution of the PM10 plumes (see Section 4.2).

Shown in Figure 5(a) is the ground level PM10 plume as predicted for 12:00 on 11 January. At this time the plume is still within a north-westerly flow. The location of the predicted plume is in good agreement with the observed (see Figure 2c).

Following the passage of the cold front after 17:00, both observed and modelled winds backed from south-westerly to southerly, causing the King Island plume to rotate counter-clockwise. The plume reached the southern edge of Port Phillip Bay at midnight and swept over Melbourne from the southeast at 2:00 12 January (Figure 5b). The eastern edge of the plume had cleared Port Phillip Bay by 6:00 (Figure 5c), and had cleared the eastern metropolitan area by 7:00. However, this region was again affected by smoke between the hours 10:00 to 11:00 inclusive. The simulation suggests that this second impact was caused by fumigation of PM10 from an elevated air mass, in response to convective boundary-layer growth.

Three air quality monitoring stations in eastern Melbourne recorded PM10 measurements during this smoke event. The observed PM10 measurements from these stations showed a similar pattern; three major peaks occurred at 17:00 11 January (60-80 $\mu g\ m^{-3}$), from midnight to 3:00, 12 January (120-140 $\mu g\ m^{-3}$), and 9:00 to 10:00, 12 January (170-220 $\mu g\ m^{-3}$). The initial peak represented the Winchelsea plume and the major peaks were from the King island plume and fumigation. The AAQFS simulation, as described above, agreed well with the observed timing of peak occurrences, however, the observed maximum concentrations of PM10 were under-predicted.

4.2. Sensitivity Studies

In order to investigate sensitivity of plume distribution and timing with respect to release height, two sensitivity runs were carried out.

In the first run, emissions from King Island were allocated with an effective plume height of 1000 m. In the case of Winchelsea, the effective plume height was set to 500m.

The effect of locating all of the plume mass at these heights was seen in both the timing and the magnitude of the PM10 impacts on Melbourne. For example, the smoke plume was now predicted to reach Port Phillip Bay at 2:00 (two hours later than the basecase) and to sweep over Melbourne at 5:00 (three hours later than basecase). On the other hand, the fumigation event occurred two hours earlier (commencing at 9:00 instead of 11:00) and resulted in considerably higher (by up to 100 $\mu g\ m^{-3}$) PM10 concentrations as shown in figure 6(a). Figure 6(b) displays the basecase PM10 concentrations for the Melbourne grid at 11:00 12 January.

In the second sensitivity run, emissions were allocated with an effective plume height of 500 m for King Island and of 250 m for Winchelsea. In this run, the plume reached Port Phillip Bay at 23:00 11 January (one hour earlier than the basecase) and reached Melbourne at 2:00 12 January. It cleared eastern Melbourne then moved slightly back eastward at 9:00 before completely clearing the Melbourne area. This run did not feature strong fumigation.

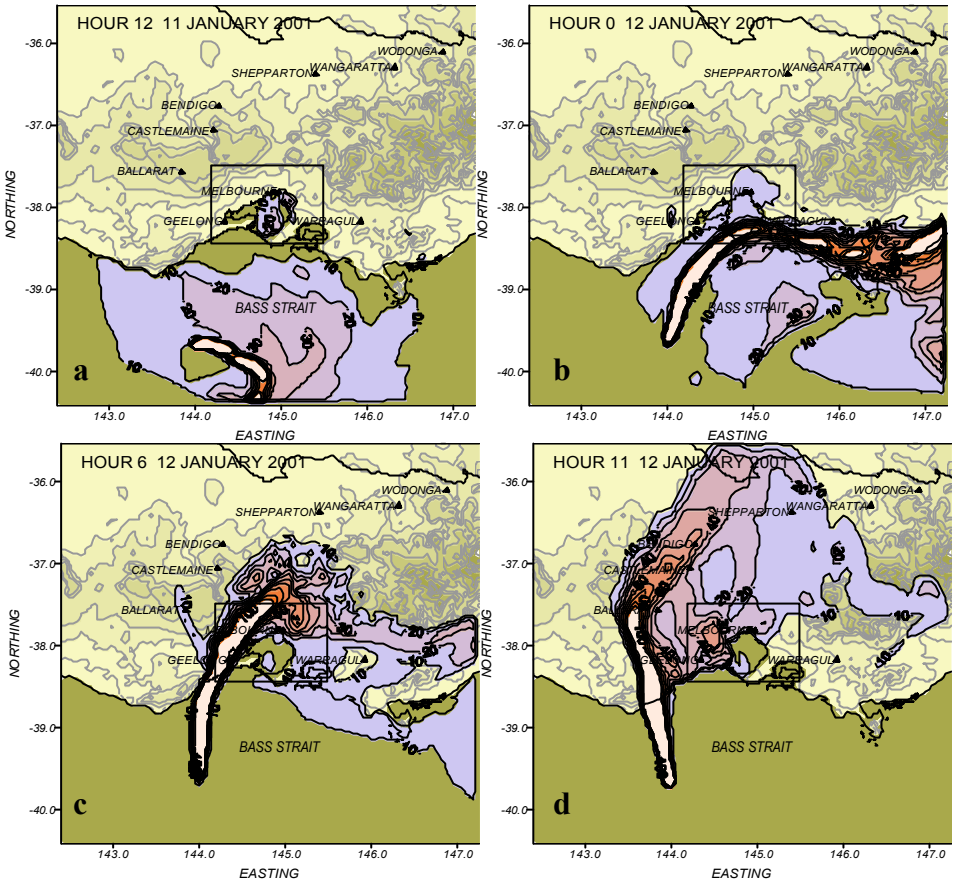

Figure 5. The AAQFS smoke plume from the King Island fire covering period from 12:00 11 January to 11:00 12 January when fumigation started.

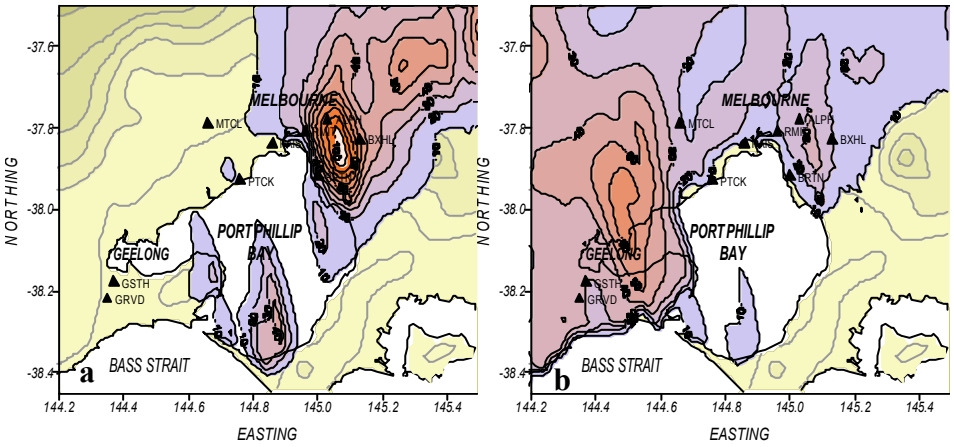

Figure 6. (a) The PM10 concentrations of a sensitivity run with all the emissions at 1000 m height at 11:00 12 January. (b) The same as (a), except for the base case.

The impact of using different emissions factors and fire size in the simulation was also investigated. The resultant effects on plume distribution and magnitude were insignificant compared to those of using different plume release heights.

The impacts of other air quality species emitted by the wildfires, e.g. NO_2, SO_2, C_6H_6, CH_2O and C_4H_6, were also modelled and found to have a reduced level of influence compared with PM10.

5. SUMMARY

The AAQFS currently issues twice daily 24-36 hour numerical air quality forecast for the Melbourne and Sydney regions for Victoria EPA and NSW EPA in time to provide reference and guidance for air quality forecasting. One of the potential usages of the AAQFS is to provide guidance in the management of prescribed burns and in alerting the public of smoke impacts on air quality.

On 11 January 2000, Melbourne experienced the worst visibility episode since 1983 due to thick smoke from the King Island and Winchelsea bushfires. A series of the AAQFS simulations were carried out to model the severe smoke event and determine the sensitivity to emissions factors, fire size and plume height.

The AAQFS demonstrated that the modelled distribution and transport of smoke plume were qualitatively in good agreement with the observation from the satellite and monitoring stations, with regard to the timing of plume arrival, dissipation, and fumigation. Additional tests showed that the PM10 plume development and magnitude were sensitive to the plume release heights, while they were relatively insensitive to emissions factors and fire size.

6. ACKNOWLEDGMENT

The AAQFS was developed under funding from the Air Pollution in Major Cities Program, sponsored by Environment Australia.

7. REFERENCE

Andreae, A., Atlas, E., Cachier, H., Cofer, W., Harris, G., Helas, G., Koppmann, R., Lacaus, J., and Ward, D., 1977, Trace gas and aerosol emissions from savanna fires, in: *Biomass Burning and Global Change* Vol **1**, J. Levine, ed., MIT press, Cambridge, pp. 278-295.

Azzi, M., Johnson, G. J., and Cope, M., 1992. An introduction to the Generic Reaction Set photochemica smog mechanism. Proc. 11th International Clean Air Environment Conf., 5-9 July 1992, Brisbane, Clean Air Society of Australia and New Zealand, 451-462.

Cope, M., Hess, D., Lee, S., Azzi, M., Carras, J., Wong, N., and Young, M., 1999. Development of the Australian Air Quality Forecasting System: Current status. Proc. International Conf. Urban Climatology, 8-12 November 1999, Sydney, 595-600.

Ng, Y. L., Walsh, S. and Wong, N., 2000. Emissions model for the Australian Air Quality Forecasting System. Proc. 15th International Clean Air Environment Conf., Vol. 1, 26-30 November 2000, Sydney, Clean Air Society of Australia and New Zealand, 275-280.

Puri, K., Dietachmayer, G., Mills, G. A., Davidson, N. E., Bowen, R. A., Logan, L. W., 1998. The new BMRC Limited Area Prediction System, LAPS. Aust. Met. Mag., **47**, 203-213.

USA EPA, Compilation of air pollutant emission factors, Vol 1, Stationary point and area sources, AP-42, 1995.